DEVELOPMENT OF UNIFIED EQUATIONS FOR DESIGN OF CURVED AND STRAIGHT STEEL BRIDGE I GIRDERS

by

Donald W. White
Associate Professor

Abdul H. Zureick
Professor

Narin Phoawanich
Research Assistant

and

Se-Kwon Jung
Research Assistant

Final Report

Prepared for
American Iron and Steel Institute Transportation and Infrastructure Committee
Professional Service Industries, Inc.
and
Federal Highway Administration

School of Civil and Environmental Engineering
Georgia Institute of Technology
Atlanta, GA 30332-0355

October 2001

DEVELOPMENT OF UNIFIED EQUATIONS FOR DESIGN OF CURVED AND STRAIGHT STEEL BRIDGE I GIRDERS

Donald W. White, Abdul H. Zureick, Narin Phoawanich and Se-Kwon Jung

School of Civil and Environmental Engineering
Georgia Institute of Technology

This research examines analytically and computationally the maximum strength behavior of curved and straight steel I-girders subjected to uniform vertical bending, high shear and low vertical bending moment, and high-shear and high-vertical bending moment, combined with lateral bending due to torsion and/or applied design loads. The theoretical and practical background, qualities, and limitations of existing design predictor equations are outlined. Key existing equations and new predictor equations developed as part of this research are evaluated based on the results of a reasonably comprehensive finite element parametric study, as well as the data from and finite element analyses of prior experimental tests. Based on consideration of the maximum strength predictions as well as pre- and post-peak load-deflection results, a unified set of strength equations is recommended that can be applied to both curved and straight I-girders for all loading conditions, including lateral bending and torsion.

Keywords:

Steel, bridges, plate girders, horizontal curvature, lateral bending, torsion, flexural strength, shear strength, moment-shear interaction

ACKNOWLEGEMENTS

The authors express their sincere thanks to the American Iron and Steel Institute (AISI), Professional Service Industries, Inc. (PSI) and the Federal Highway Administration (FHWA) and for their support of this work. This research was funded by AISI, through the AISI Transportation and Infrastructure Committee, and by FHWA, through a subcontractor arrangement with Professional Service Industries, Inc. Mr. Camille Rubeiz is the technical contact at AISI, Dr. Mohammad S. Kahn is the technical contact at PSI, and Mr. William Wright is the technical contact at FHWA. Also, many helpful comments have been received from members of the AISI Bridge Task Force and AASHTO T-14, and from Professor Roberto Leon of Georgia Tech. The research funding from AISI and FHWA/PSI and the assistance from the AISI Bridge Task Force, AASHTO T-14 and Prof. Leon are gratefully acknowledged. This report is based in part on the doctoral dissertation research by Narin Phoawanich. The opinions, findings and conclusions expressed in this report are those of the authors and do not necessarily reflect the views of the individuals and groups acknowledged here.

TABLE OF CONTENTS

TABLE OF CONTENTS
(continued)

TABLE OF CONTENTS
(continued)

TABLE OF CONTENTS
(continued)

TABLE OF CONTENTS
(continued)

TABLE OF CONTENTS
(continued)

TABLE OF CONTENTS
(continued)

TABLE OF CONTENTS
(continued)

TABLE OF CONTENTS
(continued)

LIST OF FIGURES

LIST OF FIGURES
(continued)

LIST OF FIGURES
(continued)

LIST OF FIGURES
(continued)

LIST OF FIGURES
(continued)

LIST OF FIGURES
(continued)

LIST OF FIGURES
(continued)

LIST OF FIGURES
(continued)

LIST OF FIGURES
(continued)

LIST OF FIGURES
(continued)

LIST OF FIGURES
(continued)

LIST OF FIGURES
(continued)

LIST OF FIGURES
(continued)

LIST OF FIGURES
(continued)

LIST OF FIGURES
(continued)

LIST OF FIGURES
(continued)

LIST OF FIGURES
(continued)

LIST OF FIGURES
(continued)

LIST OF FIGURES
(continued)

LIST OF TABLES

LIST OF TABLES
(continued)

LIST OF TABLES
(continued)

LIST OF TABLES
(continued)

LIST OF TABLES
(continued)

LIST OF TABLES
(continued)

LIST OF TABLES
(continued)

LIST OF TABLES
(continued)

LIST OF TABLES
(continued)

LIST OF TABLES
(continued)

LIST OF TABLES
(continued)

LIST OF TABLES
(continued)

LIST OF TABLES
(continued)

LIST OF TABLES
(continued)

LIST OF TABLES
(continued)

LIST OF TABLES
(continued)

LIST OF TABLES
(continued)

CHAPTER I

INTRODUCTION

1.1 BACKGROUND

Due to the need to augment the traffic capacity of urban highways, restrictions on existing land use, and consideration of aesthetics, there has been a steady growth in the use of curved steel bridges in the past twenty-five years. Nevertheless, accurate prediction of the performance of these structures is a task of tremendous complexity. The behavior of curved steel bridges still is not clearly understood.

1.1.1 Current American Specifications for Design of Curved I Girder Bridges

The *AASHTO Guide Specifications for Horizontally Curved Highway Bridges* (AASHTO 1993) are the current (May 2001) basis for design of curved steel I girder bridges within the United States. These specifications are predominantly the result of research by the Consortium of University Research Teams (CURT) within the early 1970s (Culver and Frampton 1970, Culver and Nasir 1971, McManus 1971, Culver 1972, Culver et al. 1972a, b and c, Culver et al.1973, Mariani et al. 1973, and Mozer et al. 1970, 1971 and 1973), as well as subsequent research extending this work to Load Factor Design by Galambos (1978), although a number of their provisions have been updated since their original publication in 1980.

Recently, Hall and Yoo (1998) have developed the *Recommended Specifications for Steel Curved-Girder Bridges*. These specifications are the result of NCHRP Project 12-38. They reflect the state-of-the-art as of December 1998. Hall et al. (1999) provide an extensive discussion of the findings of NCHRP Project 12-38, the background to the provisions in the Recommended Specifications, and design examples involving the use of these specifications. This project focused on a thorough review of the literature, existing guidelines, laboratory testing, analytical studies, and experience with state-of-the-art design and construction of curved steel bridges in the United States. Its primary goal and scope was to synthesize the state-of-the-art into updated design provisions.

The developers of the Recommended Specifications recognized limits within the state of knowledge and practice, and key recommendations for new research were forwarded (Hall et al. 1999). However, execution of new research to repair flaws and to liberalize conservative equations and procedures was outside the scope of their effort. In a number of areas, Hall et al. (1999) state that the provisions in the Recommended Specifications are likely to be conservative, but that restrictive rules are implemented due to lack of complete knowledge of the underlying behavior and/or the broad implications on curved bridge performance. Some of the key limitations of the strength equations within the

Recommended Specifications are outlined below. A more comprehensive evaluation of various resistance equations for straight and curved I girders is provided in Chapter II.

1.1.2 Design Equations for Flexural Strength

It is important to recognize that the design equations within the current American specifications for curved steel bridge design (AASHTO 1993; Hall and Yoo 1998) represent significant engineering achievements. However, if fundamental improvements are to be sought, it is essential to understand their weaknesses. The equations for the flexural strength of I girders in these specifications are based largely on the research by McManus (1971). These equations have a number of limitations including:

- They are incompatible with current AASHTO LRFD (2001) straight-girder design equations, that is, they do not reduce to the current AASHTO straight-girder equations in the limit that the radius of curvature goes to infinity.

- They exhibit some minor anomalies as the radius of curvature approaches infinity.

- They predict a significant discontinuity in the flexural strength of sections depending on whether the compression flange is classified as compact or noncompact.

- Although they are believed to be adequate and safe for design of unsymmetrical noncomposite and composite girders, they are based predominantly on research focused only on doubly symmetric noncomposite steel I sections. The modifications to the base formulas aimed at addressing the strength of singly symmetric sections are simple and ad hoc. It is likely that the strength of unsymmetric I girders can be quantified in a simple but more rigorous fashion.

- They focus only on the flexural strength of girders subjected to uniform vertical bending along their unbraced lengths; the potentially significant increases in flexural strength due to moment gradient for girders with intermediate to large unsupported lengths are not accounted for. It should be noted that the 2001 interims of the AASHTO LRFD Specifications (AASHTO 2001) detail a practical and conservative procedure that allows the engineer to account for moment gradient in straight bridge girder design, based on the use of moment envelopes.

- They do not separate the analysis problem, i.e., the estimation of internal moments or stresses, from equations for the design resistance; as a result, these equations depend on a combination of several strength reduction factors that are difficult to understand and properly apply.

- The above mentioned strength reduction factors are based on approximate second-order elastic analyses, which at the time of their development involved quite innovative research, but which subsequently have been shown to contain a number of interpretations that lead to significantly over-conservative estimates of the true second-order elastic stresses.

- They restrict the web flexural stresses to the elastic bend buckling stress under all loading conditions. This restriction may not be necessary when checking the maximum strength limit state.

Hall et al. (1999) state in their discussion of new recommended research, "Better definition of local flange buckling is needed." For curved I girders, the implications of flange slenderness values larger than the traditional plastic design compactness limit ($b_f/t_f = 14$ for $F_{yc} = 345$ MPa (50 ksi)) are not fully understood. This compactness limit was developed in straight-beam research to allow large inelastic flange strains in flexure (i.e., inelastic rotations in straight beams with compact webs up to the onset of strain hardening at approximately 10 to 15 times the yield rotation (ASCE/WRC 1971, Salmon and Johnson 1996)) prior to the onset of significant stability effects. Much of the prior curved I girder research has migrated essentially to this straight-girder limit as a requirement for avoiding the influence of local buckling on the strength, e.g., (Culver and Nasir 1971; Kitda 1986). However, the detrimental influence of exceeding such a limit, for whatever b_f/t_f value at which a nonnegligible reduction in the maximum strength due to local buckling occurs, is certainly not that suddenly the flange can only support loadings up to first yield in vertical and lateral bending. This simplification was adopted in McManus's (1971) research. With new research and the use of modern research tools, it should be possible to quantify girder strengths more accurately and with greater simplicity. The influence of flange slenderness on both the strength as well as the extent and magnitude of the pre-peak nonlinear response and the post-collapse unloading characteristics of curved I girders needs to be better understood.

1.1.3 Design Equations for Shear Strength

In addition to the above limitations of the flexural strength equations within the Recommended Specifications, these specifications place significant restrictions on the web proportions of curved I girders. Due to the lack of test data on shear capacity of curved I girder webs with slenderness (D/t_w) greater than about 70, the web slenderness is limited to 100 for curved girders with unstiffened web panels and a radius of curvature less than 213.5 m (700 ft). Also, the Recommended Specifications restrict the panel aspect ratio to $d_o/D \leq 1$ for girders designed with stiffened web panels. Hall et al. (1999) state in their discussion of recommended new research,

> **"Relief from this requirement [the limit of $d_o/D \leq 1$] for some curvatures can be justified with additional testing. Neither fatigue behavior nor strength of curved-girder webs is well understood at this time, and it would be risky to reduce the stiffening requirements without further analytical and experimental research.... Reduction of required web stiffening is one area where gains are possible.... Investigation of various types of web stiffening should be expanded for bending, shear, and combined bending and shear conditions.... The effect of stiffener spacing on the bend-buckling strength of curved girders with varying details is needed."**

1.1.4 Design Equations for Moment-Shear Interaction

In research on moment-shear interaction in straight hybrid and nonhybrid I girders (Aydemir 2000), parallel to the research presented in this report, it has been shown that:

- It is incorrect to use the moment at a minimum of (D/2, d_o/2) from the maximum moment location in a web panel for checking moment-shear interaction, as suggested by Basler (1961c). The proper location for checking the flexural strength *for conditions of low shear* is the peak moment location. At regions subjected to high shear and high bending moment, the moment drops rapidly as we move away from this position. This drop is required for satisfaction of equilibrium, and is not due to M-V interaction. Therefore, use of the moment at a minimum of (D/2, d_o/2) to quantify the strength of regions that have high shear, and the maximum moment for definition of the strength in regions of low shear, leads to a false magnification of the true M-V interaction response.

- Although some moment-shear interaction is evident at combined levels of high shear and high moment, the interaction between the moment and shear strengths is rather mild if the value of M at the maximum moment location in the panel is always used for the design check. In many cases, the conservatism of the nominal moment and/or shear strength design equations is such that the strengths from experimental tests and from refined finite element models exceed the controlling predicted flexure or shear strength, *without the consideration of any moment-shear interaction effects*. If the data from high-shear low-moment, high-shear high-moment and low-shear high-moment tests and refined analyses is plotted in its entirety, it is evident that the maximum unconservative errors associated with neglecting M-V interaction are similar in magnitude to the maximum unconservative errors associated with approximations in the current AASHTO and in recommended modified AASHTO shear strength formulas in high-shear low-moment tests. In fact, the statistical distribution of the strength ratios (i.e., the "actual" divided by the controlling predicted nominal design strengths), neglecting any M-V strength interaction, is somewhat more conservative for the high-shear high-moment data than for the high-shear low-moment data.

Therefore, Aydemir (2000) recommends that, pending further experimental and analytical confirmation, the requirements for checking of moment-shear interaction in transversely-stiffened I girders may be eliminated from the AASHTO design specifications. This would simplify the design of new bridges, and it would lead to significant reduction in effort for rating of bridges containing girders subjected to high moment and high shear. The complexity associated with M-V interaction in the rating of bridges is highlighted in an eight-page section on handling of these checks for the AASHTO *Manual for Condition Evaluation of Bridges* recently prepared by Grubb and Ibrahim (2001).

By a strict interpretation, correct checking of M-V interaction requires calculation of the concurrent shear and bending moment. This is not practical for the engineer to do

within most design contexts; rather, most designs are checked based on the maximum envelope values for both the moment and the shear. It is expected that the minor unconservative error that occurs in some cases, due to neglecting M-V interaction, is more than offset by the use of the maximum envelope values for the moment and shear. Furthermore, in composite I girders, there is an incidental contribution from the bridge deck to the shear strength. This contribution is generally not included in steel I girder design, but its influence on the shear strength can be significant. Experimental tests are underway at the University of Missouri at Columbia and at the University of Nebraska at Lincoln to validate Aydemir's findings in the context of straight bridge I girders.

The Recommended Specifications currently do not require the checking of moment-shear interaction. This is largely due to the fact that these specifications restrict the web stresses such that neither shear nor bend buckling can occur under *all* the design loading conditions, thus neglecting potentially significant reserve strength associated with web postbuckling response. If the provisions of the Recommended Specifications are to be liberalized, Aydemir's research needs to be extended to curved steel bridge I girders to ascertain the moment-shear interaction behavior in curved girder web panels.

1.1.5 Recent Research on Steel I Girder Bridge Behavior and Design

There has been a large amount of research activity on curved steel I girder bridge behavior and design within the last ten years. Much of this research has centered around or has involved off-shoots from a comprehensive on-going multiyear Federal Highway Administration (FHWA) research program on horizontally-curved steel I girder bridges (Duwadi et al. 1994; Davidson 1996; Davidson and Yoo 1996; Davidson et al. 1996, 1999a, 1999b, 1999c, 2000a, 2000b and 2000c; Grubb et al. 1993; Grubb and Hall 2001; Hall 1994 and 2000; Hall et al. 1999; Hall and Yoo 1995 and 1998; Hartmann and Wright 2001; Kang and Yoo 1994a and 1994b; Lee and Yoo 1998, 1999a and 1999b; Linzell 1999; Linzell et al. 1999; Phoawanich et al. 1999a, 1999b and 1999c; SSRC 1991 and 1998; Yadlosky 1993; Yoo et al. 1993 and 1996; Yoo and Davidson 1997; Zureick et al. 1993; Zureick and Naqib 1999; Zureick et al. 2000 and 2001; Zureick and Kim 2000), although separate research by Galambos et al. (1996, 1999 and 2000), Hajjar et al. (1999), Huang (1996), Rudie (1997), Shanmugam et al. (1995), Simpson (2000), Simpson and Birkemoe (1997a and 1997b), and Thevendran et al. (1997, 1998, 1999 and 2000) has provided important contributions. Kitada et al. (1993) summarize some of the latest key research findings leading to development of design provisions for horizontally-curved steel bridges in Japan. The above-mentioned FHWA research program is referred to in this report as the Curved Steel Bridge Research Project, or the CSBRP.

The primary objectives of the FHWA-CSBRP are to conduct fundamental research on the behavior of curved I girders in flexure and shear and to directly address significant constructibility issues associated with curved I girder bridges. The initial task of the project was to develop a synthesis of all the available published research on horizontally-curved girders. This synthesis by Zureick et al. (1993) contains approximately 750 references. Publications on subsequent research conducted directly within the CSBRP and in related projects are listed above.

One of the significant decisions within the CSBRP was that the fundamental behavior of horizontally curved girders should be tested by inserting specimens within a complete bridge structure that resists vertical loads and torsion as a system. The bridge itself serves as the test frame. It was felt that this approach would provide the most representative idealization of boundary conditions that could exist on an actual critical unbraced length of a curved bridge I girder. All the previous tests on horizontally curved component specimens in the United States and Japan, except for the two-girder tests conducted by Mozer et al. (1973), did not accurately represent the behavior of the component within an actual bridge system (Hall et al. 1999). After extensive studies of alternative approaches, the FHWA project team decided that the testing of I girder component specimens within a full-scale, curved, three-girder test frame was the most rational and safest approach. Zureick et al. (2000) and Grubb and Hall (2001) discuss the design of these experiments.

At the current time (May 2001), eight noncomposite I girder specimens have been inserted one at a time in the center of the convex outermost girder of the bridge test frame, and have been subjected to nearly uniform vertical bending up to and beyond their maximum strength. These tests have been conducted at the FHWA Turner-Fairbank highway research facility. It is expected that the results of this research will be published in various forms within the near future.

In separate research as part of the CSBRP, tests of four single girders in high shear and low bending are being conducted at the Georgia Institute of Technology. These tests are discussed in (Zureick et al. 2001). Also, researchers at the Turner-Fairbank laboratory are about to commence with the testing of several high-moment high-shear test specimens within the overall bridge test frame. Further investigations are planned to extend prior efforts within the CSBRP by Linzell (1999) and others regarding the erection of curved steel I girder bridges (Wasserman 2000). Finally, a concrete deck will be cast onto the frame, and the composite bridge system will be tested to failure (Wasserman 2000).

Recently, NCHRP Project 12-52 has been initiated to prepare specifications for the design and construction of horizontally-curved steel bridges (for both I and box girders) in a calibrated load and resistance factor design format that can be recommended to AASHTO for adoption. These specifications are to be based on the Recommended Specifications developed under NCHRP 12-38, which are in a load factor design format, supplemented by the results of the FHWA large-scale curved I girder tests as they become available. This will greatly facilitate the design of curved steel I girder bridges, since at the present time (May 2001), the engineer often needs to use straight-girder provisions for certain portions of the structure and curved girder provisions for other portions of the same bridge.

1.2 PROBLEM STATEMENT AND RESEARCH SCOPE

This research investigates the maximum strength behavior of straight and curved steel I girders under a reasonably comprehensive range of loading and boundary conditions.

The primary focus is on the maximum strength of curved I girders. However, the strength of straight I girders subjected to both vertical and lateral bending is also addressed. The ultimate goal of this work is to provide updated resistance equations that can be merged with the provisions of the Recommended Specifications developed within NCHRP 12-38, and subsequently incorporated into the development of updated LRFD provisions for both straight and curved steel I girder bridges within NCHRP 12-52.

One requirement established at the onset of this research was that the recommended design equations should, to the maximum extent possible, take a unified approach to the prediction of the maximum strength of both straight and curved I girders. That is, the equations should apply to curved girders, but also they should reduce to appropriate design equations for straight girders in the limit that the radius of curvature goes to infinity. Furthermore, it was desired for the design equations to be able to handle the effects of lateral bending in the flanges of bridge I girders due to any source, including lateral bending and torsion due to horizontal curvature or to skew of the bridge (straight or curved), as well as torsion due to sources such as eccentricity of the deck weight on overhang brackets, deck forms, screed rails, sound barriers, utilities and sign posts, and lateral bending from sources such as wind loading on facia girders. Finally, it was required that both noncomposite and composite I girder design should be addressed within this research effort.

Many detailed issues regarding the behavior and design of curved steel I girders have been addressed in prior research. However, prior investigations often have involved either a limited range of boundary and/or loading conditions, or in many cases, local behavioral issues have been addressed using simplified models in which these conditions have been heavily idealized. Also, although very realistic boundary conditions can be mimicked in tests such as the eight uniform vertical bending tests recently completed within the FHWA-CSBRP, such tests only represent a sparse sampling of the range of boundary conditions that may exist on critical unbraced lengths of curved I girders within actual bridges. This research seeks to test the strength of complete curved steel I girder assemblies under a wide range of representative loading and boundary conditions.

This research focuses predominantly on issues pertaining to the maximum resistance of I girders in uniform vertical bending, high shear with low vertical bending moment, and high shear and high vertical moment, combined with lateral bending within the flanges due to torsion and lateral loading. The fatigue behavior and strength of curved-girder webs is an important consideration that needs further research (Hall et al. 1999). The current state-of-the-art regarding web slenderness limits to avoid fatigue design problems is summarized, but consideration of fatigue behavior and strength is beyond the scope of this work.

Furthermore, many of the issues that make the design of curved bridges challenging are associated with the overall analysis to determine the design forces on individual components within the bridge. The current study focuses on the maximum strength behavior, the development of new resistance equations, and the evaluation of these new equations as well as the most promising and well-known strength predictor equations that

have been proposed in prior research. This research assumes that first-order elastic forces or stresses within the subject unbraced length of an I girder have been evaluated accurately, and that appropriate amplification factors have been applied to these forces or stresses where necessary to estimate the corresponding amplified second-order elastic values. It is noted that only a first-order elastic analysis of the bridge superstructure is practical and necessary within the design of typical I girder bridges. Use of second-order elastic (i.e., geometric nonlinear) analysis generally would require extensive additional work since the analysis results for different loadings cannot be superposed. However, in order to remove the issue of analysis accuracy from the evaluation of design predictor equations, rigorous second-order shell finite element analyses are used for calculation of the design analysis elastic stresses in the majority of this research (unless the design predictor equations require first-order stresses). This allows the qualities and limitations of the equations for prediction of the design resistances to be evaluated directly, independent of the accuracy of the bridge analysis.

Given the accurately determined second-order elastic design forces or stresses (or the first-order stresses if the design equations are based on these quantities, as in the case of the flexural resistance equations of the Recommended Specifications), this research evaluates the accuracy of the various strength predictor equations. Some information is provided about the magnitude of the second-order elastic amplification of lateral bending stresses obtained from rigorous geometric nonlinear finite element analyses. Also, simple equations are recommended for estimating the maximum second-order flange lateral bending stresses in uniform vertical bending cases, given the first-order stresses computed based on the moments at the cross frames. However, evaluation of the accuracy of various methods for estimating the elastic design analysis stresses in curved I-girder bridge superstructures is beyond the scope of this work.

Prismatic unstiffened and transversely-stiffened steel bridge I girders are addressed in this research; no consideration is given to the design of longitudinally-stiffened I girders or to curved steel box or tub girders. Furthermore, the current research is focused on homogenous girders composed of Grade 345 steels (F_y = 345 MPa (50 ksi)). The performance of girders fabricated with high-performance steels of grades 480W or 690W, and the behavior of hybrid I girders are not addressed, although it is likely that many attributes of the maximum strength behavior will be similar for these girder types. The maximum limit on the subtended angle between the cross-frame locations of $L_b/R = 0.10$, as specified in the Guide Specifications (AASHTO 1993) and in the Recommended Specifications (Hall and Yoo 1998), is assumed. McManus (1971) explains that this value represents a practical upper limit for a range of curved bridges surveyed by an ASCE task subcommittee on curved girders (ASCE 1971)[1].

[1] Actually, one set of experimental tests in which the web is effectively hybrid is reviewed and analyzed in this research. Also, several experimental tests in which L_b/R is greater than 0.10 are reviewed and analyzed. However, this research is focused predominantly on homogeneous I girders with L_b/R less than or equal to 0.10.

1.3 OVERALL RESEARCH APPROACH

Experimental testing is an essential component of research to determine the maximum strength of structures. However, at the present time (May 2001), full nonlinear shell finite element analysis (FEA) has been established as a reliable tool for quantifying the complete elastic and inelastic stability limit-states behavior of a wide range of steel structures and components. The design of the pure vertical bending, shear, and high-moment high-shear tests that have been completed and are on-going in the FHWA-CSBRP has been accomplished with the extensive use of refined full nonlinear finite element models. The use of these tools was essential for the design of the three-girder bridge test frame utilized at the Turner-Fairbank laboratory. Preliminary assessment of the test data has indicated excellent correlation between the FEA predictions and the experimental test results.

Because of the expense of experimental tests, generally only a few key geometric and material configurations, loadings, and boundary conditions can be physically tested out of the extensive range of possible field conditions. However, due to the accuracy of carefully developed modern full nonlinear FEA models, researchers currently have an unprecedented opportunity to investigate the influence of a wide range of important design variables via numerical parametric studies. Experimental tests can be conducted to verify the predicted behavior and the accuracy of the finite element models for targeted benchmark cases, and subsequently the FEA models can be used to extend the test results to address more completely the parametric effects of different design variables.

This report focuses on the design and execution of a large finite element parametric study to establish base maximum strength data for curved and straight steel I girders subjected to uniform vertical bending, high shear with low vertical bending moment, and high-shear with high-vertical bending moment, combined with lateral bending due to torsion and/or applied loads. This data is then utilized to assess various design strength predictor equations, including new equations that have developed as part of this research. Extensive interpretation of the experimental data from the tests conducted within the FHWA-CSBRP, and correlation of the data from these experimental tests with the results from refined finite element analyses, is to be addressed in other reports to be published by the CSBRP team. However, in order to provide some confirmation of the accuracy of the specific finite element models developed in this research, one chapter of this report is devoted to a comparison between analysis predictions and basic responses determined from preliminary reduction of the experimental test data for seven of the eight bending specimens tested at the FHWA Turner-Fairbank laboratory. Furthermore, this chapter compares the analysis predictions to the experimental results for a number of other representative tests conducted in recent and in prior curved steel bridge research within the United States. In addition to the comparisons between the data from full nonlinear analyses and experimental tests, the various strength predictor equations are evaluated against the results of the CSBRP and prior experimental tests. Based on the maximum strength data from the parametric study, as well as data from the experimental tests, a unified set of strength equations is recommended that can be applied to both curved and straight I girders for all loading conditions, including lateral bending and torsion.

1.4 KEY CONCEPTS IN THE DEVELOPMENT OF UNIFIED FLEXURAL STRENGTH DESIGN EQUATIONS

1.4.1 Focus on Flange Vertical Bending Stress

The Recommended Specifications focus solely on the stress conditions in the flanges for checking the flexural strength of curved I girders. Hall and Yoo (1995) state that by taking this approach,

> **"... the proposed curved girder specifications permit a unified approach to noncomposite and composite sections. Girders may be unsymmetrical and noncomposite for some dead load and composite for some dead load and live load. If a doubly symmetric noncomposite girder bridge is designed, it is simply a special case and no separate provisions are needed. Stresses for noncomposite and composite cases are always additive. Thus, the section may be evaluated at the top and bottom at any time using provisions that apply to the state of the flange at that time."**

This basic concept or approach is applied in the current research for the development of modified (AASHTO 2001) flexural strength equations that accommodate lateral flange bending associated with girder lateral bending moments and/or torsion.

For composite noncompact girders in negative bending, the standard flexural strength equations in AASHTO LRFD (2001) are currently written in terms of the flange elastic bending stresses. Noncompact girders are defined as those for which the slenderness of the compression flange ($b_f/2t_f$) and/or the web ($2D_{cp}/t_w$) and/or the lateral brace spacing are not sufficient for the girder to be able to develop the plastic moment capacity M_p. In this case, the AASHTO LRFD equations for checking the lateral stability of the compression flange are based on the fundamental lateral-torsional buckling equation of an I beam, but with the contribution of the St. Venant torsional stiffness taken as zero. This results in the following simple expression for the basic elastic lateral buckling capacity, in terms of the compression flange vertical bending stress:

$$F_n = C_b R_b R_h \frac{\pi^2 E}{(L_b / r_t)^2} \le R_b R_h F_{yc} \qquad (1\text{-}1)$$

where F_n is the nominal strength, C_b is the moment-gradient modifier, R_b is the load shedding factor associated with web bend buckling, R_h is the hybrid girder factor, F_{yc} is the yield strength of the compression flange, r_t is the radius of gyration of a notional section composed of the compression flange plus one-third of the depth of the web in compression, L_b is the laterally-unsupported length, and L_b/r_t is the lateral-torsional buckling slenderness parameter.

Equation (1-1) can be obtained by starting with the fundamental elastic lateral-torsional buckling equation for a doubly-symmetric noncomposite I-beam, multiplying by

R_b and R_h, setting the St. Venant torsional stiffness parameter J equal to zero, and making the approximation that the distance between the mid-thickness of the flanges (h) is approximately equal to the total depth of the section (d) as well as the depth of the web (D). This is reviewed in Chapter II, and a proof is given that the proper definition of r_t is indeed as specified above. Also in Chapter II, it is shown that this equation can be applied to accurately estimate the lateral-torsional buckling capacity of nonsymmetric I girders, if r_t is still defined as the radius of gyration of the compression flange plus one-third of the depth of the web in compression. In summary, the current (AASHTO 2001) equations for the lateral-torsional buckling strength of composite girders (in negative bending) are based on the strength of an equivalent all-steel girder that has the same depth of web in compression (D_c). The beneficial effect of any torsional restraint from the bridge deck is neglected.

For noncomposite I girders that are not longitudinally-stiffened and in which the web load-shedding factor due to bend buckling (R_b) is less than one at $f_b = F_{yc}$, the current AASHTO LRFD Specifications (AASHTO 2001) effectively check the lateral stability of the compression flange based on Eq. (1-1)[2,3]. However, for these types of sections, the flexural capacity is expressed in terms of the vertical bending moment instead of the flange stress, and the Specifications define r_t as just the radius of gyration of the compression flange r_{yc}. The definition of $r_t = r_{yc}$ for this case appears to be an error, since it is evident that the composite and noncomposite equations are based on the same fundamental lateral-torsional buckling relationship, and since the use of $r_t = r_{yc}$ leads to a prediction that the lateral-torsional buckling strength of a composite girder is less than that of the corresponding equivalent all steel girder. By including one-third of the depth of the web in compression in computing r_t, and by the subsequent use of this r_t within the slenderness parameter for lateral-torsional buckling ($\lambda = L_b/r_t$), the lateral destabilizing effect that the compressed portion of the web has on the compression flange is always accounted for. Equation (1-1) can be viewed as a check of the compression flange plus a portion of the web as an equivalent axially compressed column.

A linear transition equation is provided in (AASHTO 2001) for calculation of the inelastic lateral buckling strength of composite and transversely-stiffened noncomposite girders with $R_b \leq 1$ at $f_b = F_{yc}$, i.e., noncomposite slender-web sections. This equation can also be shown to be identical for both composite and noncomposite girders, and can be written in terms of the flange vertical bending stress.

In noncomposite longitudinally-stiffened I girders, and in noncomposite transversely-stiffened I girders when $R_b = 1$ at $f_b = F_{yc}$, the current AAHSTO LRFD Specifications (2001) specify the lateral-torsional buckling strength as the fundamental lateral-torsional buckling equation for an I beam with the St. Venant torsional constant J included. Chapter II shows that this equation also can be written in a very simple and useful form in terms of the compression flange stress. The logic behind the approximation of J=0 for

[2] The term f_b is the flange stress due to vertical bending moment, computed by an elastic design analysis.

[3] These types of girders are typically referred to as "slender-web" sections (AISC 1999).

other noncomposite situations is that, if the girder is not longitudinally stiffened or if web bend buckling occurs prior to development of the design condition, web distortion is likely to significantly degrade the lateral buckling resistance. It can be argued that if $R_b = 1$ at $f_b = F_{yc}$ for a noncompact composite girder in negative bending, J should be included within the calculation of its lateral-torsional bending resistance. It appears that the Specifications assume $J = 0$ for all cases involving noncompact composite girders in negative bending for reasons of simplicity of the design provisions. An alternative simple set of design equations is proposed in this research that allows the use of $J > 0$ for straight nonslender web composite I girders in negative bending.

In summary, all the AASHTO LRFD (2001) formulas for the lateral stability of the compression flange can be expressed in terms of the flange vertical bending stress. In Chapter II, it is shown that this facilitates a unified treatment of composite and noncomposite beams subjected to combined vertical and lateral flange bending.

1.4.2 Approximate Equivalency Between the Flanges of an I Girder and a General Beam-Column for Checking of Strength

For a horizontally-curved I girder with a constant radius of curvature R, subjected to uniform vertical bending, if we assume that the horizontal curvature due to the initial geometry plus the girder deformations is small, then its effect can be expressed as an equivalent distributed lateral loading on the flanges of

$$q \cong \frac{f_b A_f}{R} \tag{1-2}$$

where A_f is the area of the flange and f_b is the average normal stress in the flange, computed from the vertical bending moment as

$$f_b = \frac{M(h/2)}{I_x} \tag{1-3}$$

where I_x is the moment of inertia, which can be approximated as

$$I_x \cong \frac{A_f h^2}{2} \tag{1-4}$$

and h is the distance between the mid-thickness of the flanges. Furthermore, if we consider an internal unbraced segment of the curved girder and assume that the flange rotations are effectively fixed at the cross-frame locations due to approximate symmetry end-conditions, we can approximate the flange end lateral moments as

$$M_\ell \cong \frac{qL_b^2}{12} \tag{1-5}$$

where M_ℓ is the lateral bending moment in the flange at the support. Then, by substituting Eqs. (1-2) through (1-4) into Eq. (1-5), we obtain

$$M_\ell \cong \frac{ML_b^2}{12Rh} \tag{1-6}$$

This formula is a well-known approximate expression for the lateral flange bending moment in curved I girders, commonly referred to as the V-Load equation (Poellot 1987; Fiechtl et al. 1987; Hall and Yoo 1998). The corresponding distribution of the flange lateral bending moments along the girder unsupported length is illustrated in Fig. 1.4.1. It should be noted that based on the above simple model, the moments within the top and bottom flanges of an I girder both have the distribution shown in this figure, but they are in opposite directions. The moments within the compression flange are associated with an increase in its horizontal curvature whereas the moments within the tension flange are associated with a straightening of its geometry.

For the purposes of the discussion here, the important point is not the result of Eq. (1-6), but rather that the horizontal-curvature effects can be approximated by the equivalent horizontal load q given by Eq. (1-2). Conceptually, the flange may be designed approximately as an equivalent beam-column subjected to this loading as well as the constant flange axial force due to the equal and opposite bending moments applied at the ends of the unbraced length. This equivalent beam-column is loaded predominantly within the plane of the flange plate, and is effectively restrained by the remainder of the I girder in the direction of the plane of the web. The influence of any torsional shear stresses within the flange is neglected, and it is assumed that the overall torsion on the complete I girder cross-section is resisted entirely by lateral bending (or warping) of the flanges.

If the vertical bending moment is not constant along the unbraced length due to the presence of vertical shear in the girder, then the effective loading on the compression flange is more complex. The influence of the horizontal curvature may still be represented approximately by Eq. (1-2) at any section along the length of the girder. However, due to the shear flow transferred between the web and the flange, the flange is also loaded effectively by a distributed tangential load along its length. Therefore, the corresponding equivalent beam-column is similar to that for the uniform vertical bending case, but the axial force varies along the length of the member.

For a general straight or curved, composite or noncomposite I girder subjected to vertical bending as well as torsion and/or lateral bending from whatever the source (geometry and/or applied loading), it is assumed in this research that the elastic vertical bending stresses (f_b) and lateral bending stresses (f_ℓ) within a steel flange can be computed accurately based on the analysis model selected by the engineer, e.g. from an approximate analysis equation (such as Eq. (1-6)) or from a direct elastic analysis of the bridge superstructure. The term "steel flange" is used here to distinguish the flanges that are unattached to the bridge deck from the top flange of a composite girder. It may be

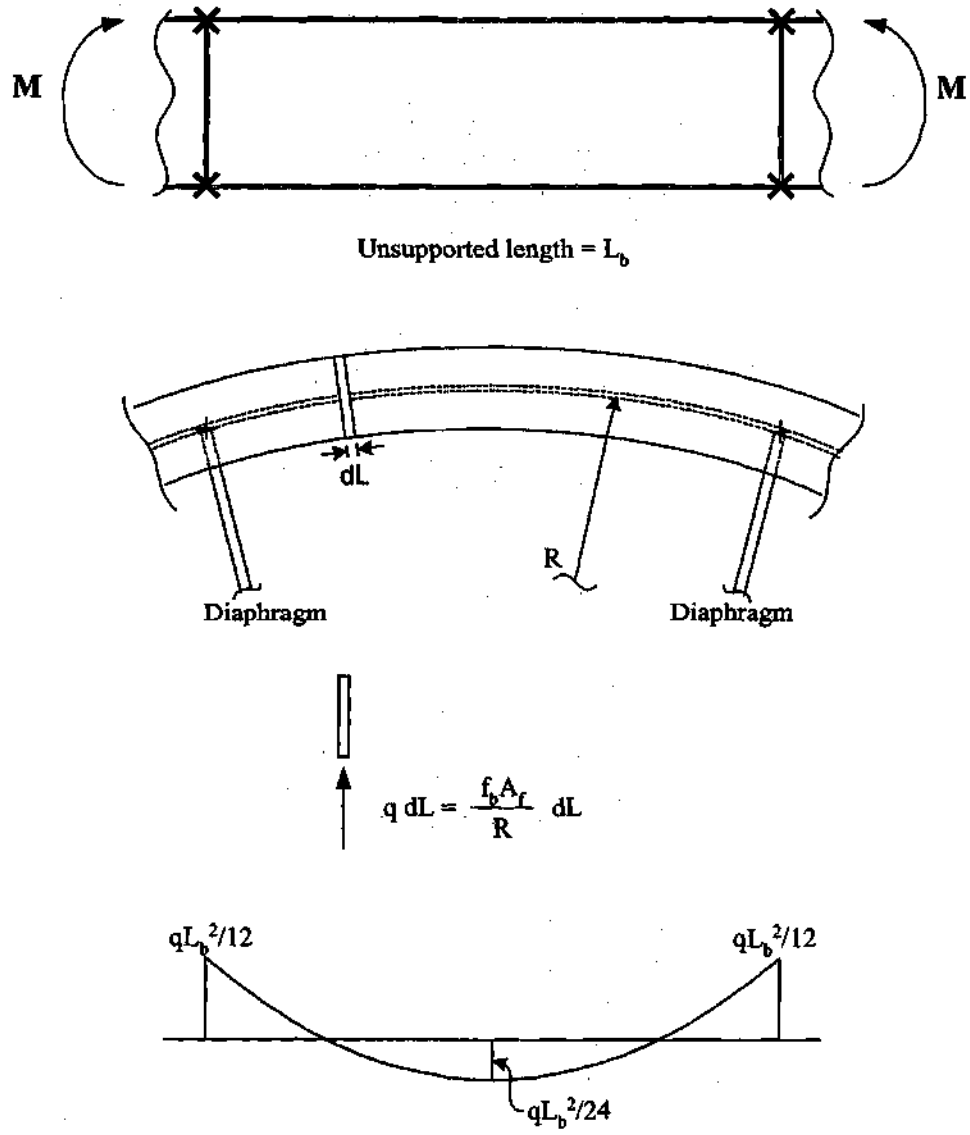

Figure 1.4.1. Distribution of flange lateral bending moments along a girder unsupported length due to uniform vertical bending moment, based on the V-Load method.

assumed that the lateral bending is taken predominantly by the slab at the top flange of composite girders. Therefore, after the structural integrity of the deck is established, the top flange of a composite girder can be checked simply for the vertical bending stress f_b.

In the above general cases, it is assumed for the purposes of conducting a strength check that any steel flanges, loaded in tension or compression, can be considered as a general two-dimensional beam-column subjected to distributed axial and/or lateral forces as well as applied end axial forces and moments. Furthermore, it is assumed that if the flange stresses are amplified significantly due to second-order effects, an accurate estimate of the second-order elastic amplification has been determined within the analysis (typically by application of amplification factors to the first-order elastic stresses).

If the above equivalent beam-column concept is accepted, then it is possible that the AASHTO LRFD (2001) beam-column interaction equations, which are the same as the beam-column interaction equations specified in the AISC LRFD Specification (1999), can be used for checking a flange subjected to a combined axial and lateral loading. Of course, these beam-column interaction equations are not directly intended for cases in which the axial force varies along the length of the member. This is handled within the conceptual approach suggested here by the inclusion of the moment gradient modifier C_b. Furthermore, an appropriate (and the most transparent) way of visualizing the effect of the hybrid (R_h) and load shedding (R_b) factors in the design of I girders is that the estimated actual flange stress is equal to $f_b / R_h R_b$. That is, the effect of making the web hybrid and/or slender is that the flange stresses (or the applied axial loads on the equivalent beam-column representing the steel flange) are increased.

It can be shown that in certain cases, the (AASHTO 2001) and (AISC 1999) beam-column interaction equations are a conservative representation of the strength. For example, if we consider a member loaded in tension and lateral bending, the theoretical full-plastic strength of the cross-section would give us a better representation of the member strength (ignoring any strength reduction due to holes within the cross-section or due to the introduction of the tension force to the member). This is illustrated for a beam-column with a rectangular cross-section, i.e., for the beam-column equivalent of the girder flanges, in Fig. 1.4.2.

Furthermore, it can be shown that in certain cases involving weak-axis bending and axial compression of I or rectangular shapes, the slope of the actual beam-column interaction strength data in the vicinity of the maximum axial load capacity (i.e., for small lateral bending moments) is significantly smaller (flatter) than the slope of the (AASHTO 2001; AISC 1999) interaction curve. Finally, a local buckling mode of failure of a compression flange would be analogous to the failure of a beam-column member in a torsional or torsional-flexural mode. It is possible that the strength in this mode of failure may also be represented conservatively by the (AASHTO 2001; AISC 1999) interaction curves. Therefore, a more liberal approximation of the effect of lateral bending on the axial strength of the flange, and hence on the vertical bending strength of an I girder, may be possible than simply a strict application of the (AASHTO 2001; AISC

1999) beam-column interaction curve to the equivalent beam-column. This issue is addressed further in Chapter II, and in the parametric investigations of this research.

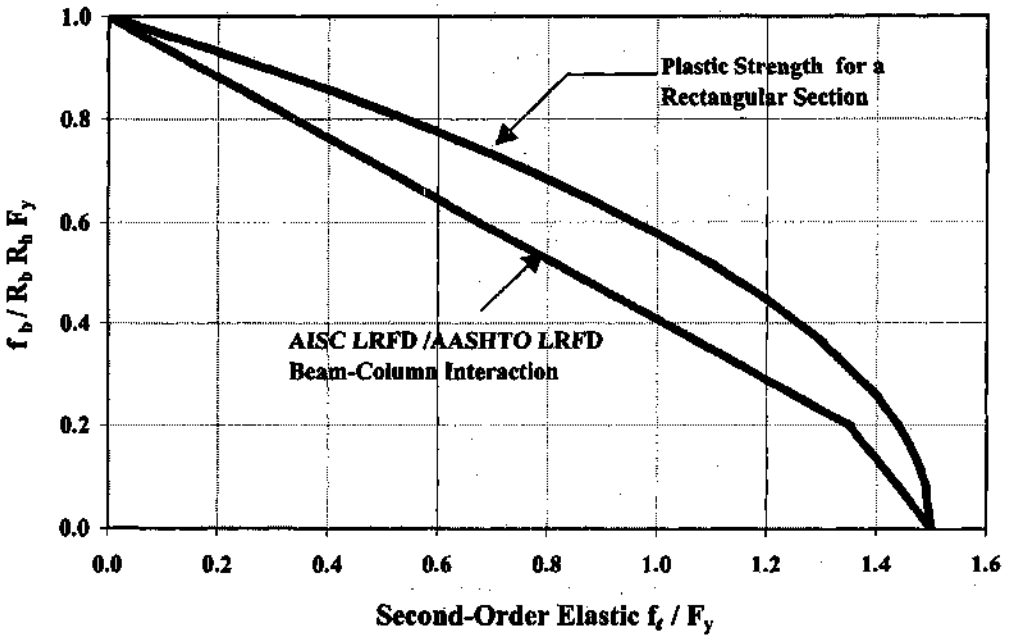

Figure 1.4.2. Comparison between the AISC LRFD/AASHTO LRFD beam-column interaction and the theoretical full plastic strength curves for a rectangular section.

As a final note regarding the concept of treating the steel flanges as an equivalent beam-column, one quality of the (AASHTO 2001; AISC 1999) beam-column interaction equations is significant and should be discussed. The developers of these equations specified explicitly that the input to the design equations should be the *maximum second-order elastic moment* (or equivalently, the maximum second-order elastic lateral bending stress) (Yura 1988; ASCE 1997). By doing this, they separated the analysis problem of determining the second-order forces within the system from the problem of checking the design resistances. This in turn allowed them to quantify the beam-column design resistances by the simple bi-linear relationship shown in Fig. 1.4.2. This philosophy is also adopted within the present research. It is assumed that the appropriate second-order elastic stresses are obtained within the analysis of the bridge system (typically by the use of a first-order elastic analysis along with appropriate amplification factors).

The equivalent beam-column approach obviously is of limited validity for highly curved members in which the subtended angle between the lateral bracing locations is large. However, within the maximum limit of $L_b/R = 0.10$ adopted in this study (and based on limit studies, also significantly beyond this limit), it is believed that the equivalent beam-column analogy serves as a useful and accurate design approximation.

1.4.3 Use of All-Steel Tests for Quantifying the Strength of Composite I Girders

Although the strength of the bottom flange in the negative moment region of a composite I girder may receive some benefit due to the torsional restraint provided by the bridge deck, this torsional restraint is neglected in this research. It is assumed that the steel flange strength in such a case (i.e., the strength of the bottom flange) can be represented sufficiently by studying an equivalent all-steel girder with the same depth of web in compression (D_c). This assumption is consistent with the approach for checking the steel flange stability in the AASHTO LRFD (2001) straight-girder strength provisions, and it is consistent with the approach taken in the Recommended Specifications (Hall and Yoo 1998) for handling the strength check of curved steel I girders (see Section 1.4.1).

1.5 ORGANIZATION

Chapter II provides a summary of a wide range of design equations for flexural strength, shear capacity and moment-shear interaction from current design standards as well as from prior research. The intent is to: (1) summarize the strength predictor equations in a consistent notation, such that the different equations can be easily compared, and (2) discuss the background and important qualities and limitations of the different equations. Also, this chapter summarizes the design predictor equations that are recommended based on this research. The studies leading to these recommendations, which include the evaluation of the most promising and well known existing equations as well as the recommended design equations, are then addressed within the subsequent chapters of the report.

Chapter III explains the details of the finite element models developed in this research. The various modeling assumptions and decisions, including the definition of stress-strain properties, initial geometric imperfections and residual stresses are discussed.

In Chapter IV, the capabilities of the finite element models (as detailed in Chapter III) as well as the most promising and well known design equations from Chapter II are evaluated versus experimental test results from prior and on-going research (Mozer et al. 1970, 1971, and 1973; Zureick and Kim 2000; Hartmann 2000; Hartmann and Wright 2001; and Zureick et al. 2001).

In Chapter V, the overall design of the parametric studies conducted in this research is presented. These studies are utilized to evaluate the accuracy of the various strength predictor equations summarized in Chapter II as well as attributes of the maximum strength limit states behavior, particularly the extent and magnitude of the pre-peak nonlinearity and the post-collapse load-shedding characteristics as a function of the girder geometry.

Chapter VI presents a sample of detailed results from the finite element parametric studies. The results for uniform vertical bending, high-moment low-shear, and high-

moment high-shear cases are considered with an emphasis on synthesis of the overall pre- and post-peak load-deflection characteristics, and the assessment of the deformed geometries and girder cross-section distortions at the peak load levels. Subsequently, Chapters VII and VIII focus on the synthesis of the parametric study results pertaining to the flexural and shear strengths of steel I girders. The analysis solutions for the maximum strength are evaluated and compared to selected design predictor equations described in Chapter II.

Chapter IX investigates the interaction between flexural and shear strengths for high levels of combined bending (vertical and lateral) and shear, in which case, the magnitude of shear force may cause some reduction in the flexural capacity or vice-versa. This chapter deviates from the other chapters in that the elastic design analysis stresses are calculated using a curved first-order open-walled section beam finite element. By using this approach for calculation of the elastic design stresses, the implications of potentially neglecting second-order amplification and web distortion effects in the context of the proposed design rules are highlighted. By neglecting these effects in the elastic design analysis, the elastic lateral bending stresses are somewhat smaller, and therefore the capacities predicted by the recommended resistance equations are somewhat larger. First and second-order elastic design analysis stresses are computed using shell finite element models in all the other studies within this research, such that any effects of web distortion are accounted for.

Chapter X provides summary observations and discusses further research needs.

Appendices A, B and C provide detailed information from all of the individual parametric analyses conducted in this research. The intent of these appendices is to provide the data necessary for engineers and researchers to verify the design equation results presented in Chapters V through IX, and also to provide the data such that researchers can use the analysis results from this research to evaluate other potential design predictor equations. Appendix A provides detailed analysis and design results from the parametric studies that focus on flexural strength (Chapter VII), and Appendix B provides this information for the shear strength studies (Chapter VIII). Appendix C summarizes the key analysis results associated with the moment-shear interaction plots in Chapter IX.

Appendix D summarizes parameters pertaining to the modeling of initial geometric imperfections in the full nonlinear finite element studies, and Appendix E details the Gauss point residual stresses defined for each of the cross-sections considered in this research.

Finally, detailed miscellaneous cross-section plate lengths and thicknesses for the parametric test specimens studied in this research are summarized in Appendix F, while Appendix G provides the stiffener dimensions of all of the individual parametric study girders.

CHAPTER II

OVERVIEW OF DESIGN EQUATIONS

This chapter provides a summary of a wide range of design equations for flexural strength, shear capacity and moment-shear interaction from current design standards as well as from prior research. The intent is to: (1) summarize the different resistance equations within a consistent notation, such that the different approaches can be easily compared, and (2) discuss the background and important qualities and limitations of the various equations. This chapter also summarizes design predictor equations that are recommended based on this research. The research leading to these recommendations, which largely involves the evaluation of the recommended as well as the most promising and well known existing design equations, is then addressed within the subsequent chapters of the report.

Section 2.1.1 gives an overview of a slightly modified form of the current AASHTO LRFD (2001) flexural design equations for straight I girders. The current AASHTO LRFD equations for design of composite and noncomposite I girders against lateral buckling are implicitly the same fundamental equations, but are expressed in different formats within separate sections of the Specifications. The straight-girder equations presented in this section are a unified and simplified statement of the AASHTO LRFD equations, consistent with the fundamental base lateral-torsional buckling formulas. Several modifications are suggested to ensure a more consistent application of the lateral-torsional buckling formulas to all types of composite and noncomposite I girders.

Furthermore, the proposed modified equations include a change in the flange local buckling (FLB) resistance formulas. This change makes the recommended FLB equations consistent with beam and plate girder strength equations within the AISC LRFD (1999) Specification, and provides significant improvements relative to the accuracy of the current AASHTO LRFD (2001) formulas. The AASHTO LRFD FLB equations are grossly conservative compared to experimental and analytical data for cases in which the flanges are close to the (AASHTO 2001) fabrication limit of $b_f/2t_f \leq 12$. Furthermore, the shape of the current AASHTO FLB curve (F_n versus $b_f/2t_f$) is concave, whereas the trend in the data from analytical and experimental studies tends to be convex. The AISC LRFD (1999) Specification provides a more accurate linear transition curve for flange inelastic buckling strength.

After the presentation of the proposed modified AASHTO straight-I girder equations, an extensive summary of key existing flexural design equations for curved steel I girders is provided. This summary includes the equations from the Recommended Specifications (Hall and Yoo 1998) and from recent comparable Japanese design standards (Hanshin

1988), as well as various key design equations that have been proposed in prior research. The qualities and limitations of the various equations are discussed.

With the discussion of the qualities and limitations of all the above equations as a background, Section 2.1.9 gives the motivation for and summarizes a set of proposed extensions to the modified AASHTO straight I girder design formulas to account for lateral flange bending due to torsion and/or applied lateral loading. The recommended flexural strength equations can be studied by reading only Sections 2.1.1 and 2.1.9.

Section 2.2 summarizes the shear strength equations and associated concepts from the Recommended (Hall and Yoo 1998) and the current AASHTO LRFD (2001) Specifications. Also, shear strength formulas recently proposed by Lee and Yoo (1998) are discussed, and a simple modification of the current AASHTO LRFD (2001) shear strength expressions, based on the research by Lee et al. (1996), is proposed. The recommendations of the current research regarding the calculation of shear capacity are summarized at the end of this section.

Finally, Section 2.3 summarizes how potential interaction between the bending and shear strengths is addressed within the Recommended (Hall and Yoo 1998) and AASHTO LRFD (2001) Specifications, and explains the conclusions from this research regarding the consideration of moment-shear interaction within the context of the proposed flexure and shear strength equations.

2.1 VERTICAL BENDING STRENGTH

2.1.1 Modified AASHTO LRFD (2001) Equations for Straight Girders

The proposed modified AASHTO LRFD (2001) equations for straight girders can be expressed in a simple succinct form as summarized below. Equations for the capacity of straight composite girders in positive vertical bending are not listed here. These equations should be the same as or similar to those specified in the current Specifications (AASHTO 2001). All of the flexural strength equations are written in terms of the elastic flange stresses due to vertical bending. As discussed in Chapter I, this facilitates the usage of the design equations for both composite and noncomposite design.

2.1.1.1 General Equations

For flanges subjected to tension and for compression flanges that meet compactness requirements for local and lateral buckling, the girder strength can be represented as

$$\frac{f_b}{R_b R_h} \le F_y \qquad (2\text{-}1)$$

where F_y is the yield strength of either the compression flange (F_{yc}) or the tension flange (F_{yt}). Furthermore, if the girder slenderness λ for either lateral-torsional or compression

flange local buckling falls between the compact limit (λ_p) and the limit associated with the transition from inelastic to elastic buckling (λ_r), i.e., if $\lambda_p \le \lambda \le \lambda_r$, then the strength can be expressed by the following inelastic buckling linear transition equation:

$$\frac{f_b}{R_b R_h} \le C_b \left[1 - \frac{(F_{yc} - F_L)}{F_{yc}} \left(\frac{\lambda - \lambda_p}{\lambda_r - \lambda_p} \right) \right] F_{yc} \le F_{yc} \qquad (2\text{-}2)$$

where F_L is the flexural stress corresponding to the onset of significant inelasticity, taken as the smaller of ($F_{yc} - F_{rs}$) or F_{yw}, and F_{rs} approximates the effect of residual stresses within the compression flange. For general application of the AASHTO flexural strength equations to plate girders with F_{yc} up to 690 MPa (100 ksi), $F_{rs} = 0.5\ F_{yc}$ is recommended. This makes Eq. (2-2) consistent with the comparable equation for plate girder design within the AISC LRFD Specification (1999). However, the authors have found in this research that slightly better correlation with finite element and experimental test results is obtained if F_{rs} is assumed equal to 114 MPa (16.5 ksi). This value of F_{rs} is consistent with the provisions in (AISC 1999) for welded beams. For checking of rolled beams, F_{rs} = 69 MPa (10 ksi) is recommended, which is consistent with the AISC LRFD Specifications (1999) for checking of rolled I sections. All the AASHTO LRFD based evaluations in this research are conducted with F_{rs} = 114 MPa (16.5 ksi) and F_{yc} = 345 MPa (50 ksi). For homogeneous Grade 345 girders, the use of $F_{rs} = 0.5F_{yc}$ makes Eq. (2-2) a maximum of less than two percent conservative for the local flange buckling checks and a maximum of approximately nine percent conservative for checking of lateral-torsional buckling relative to the use of F_{rs} = 114 MPa (16.5 ksi).

For slenderness values large enough such that the strength is governed by elastic buckling, i.e., for $\lambda \ge \lambda_r$, the strength may be expressed in terms of the compression flange stress as

$$\frac{f_b}{R_b R_h} \le F_e \le F_{yc} \qquad (2\text{-}3)$$

where the symbol F_e represents the elastic vertical bending stress corresponding either to lateral-torsional or local flange buckling.

Generally, Eqs. (2-1) through (2-3) must be applied to check both the local and lateral-torsional buckling strengths. The nominal design strength is taken as the smaller of these separate checks.

2.1.1.2 Flange Local Buckling Parameters

For checking of local flange buckling, Eqs. (2-2) and (2-3) are expressed in terms of the compression flange slenderness

$$\lambda = b_f / 2t_f \qquad (2\text{-}4)$$

and the compact and noncompact flange slenderness limits are

$$\lambda_p = 0.382\sqrt{\frac{E}{F_{yc}}} \tag{2-5}$$

and

$$\lambda_r = 1.90\sqrt{\frac{E}{F_L\sqrt{\frac{2D_c}{t_w}}}} \tag{2-6}$$

Equation (2-5) is the current compact-flange slenderness limit specified in both (AISC 1999) and (AASHTO 2001). Equation (2-6) is the current noncompact flange slenderness limit provided in (AISC 1999), if F_L is taken as 0.5 F_{yc}, and if the AISC flange buckling coefficient is expressed as[1]

$$k_c = \frac{4}{\sqrt{2D_c / t_w}} \tag{2-7}$$

Equation (2-6) is derived simply by setting the flange elastic local buckling strength, with the buckling coefficient k_c specified by Eq. (2-7), equal to F_L. Implications regarding the usage of Eq. (2-7) are discussed below. Finally, for checking of flange local buckling

$$C_b = 1 \tag{2-8}$$

since C_b is the modifier that accounts for the effect of moment-gradient on lateral-torsional buckling. The effect of moment gradient on flange local buckling (FLB) strength can be significant for cross-sections with highly compact flanges and webs, resulting in reliable maximum strengths as high as $0.5(F_u/F_y + 1)M_p$ (Lay and Galambos 1967). However, the influence of moment gradient on the FLB strength of I sections with noncompact or slender webs is not well understood, and to the authors' knowledge, is not considered in any of the major international steel design standards.

Figures 2.1.1 and 2.1.2 compare the flange local buckling strength as predicted by Eqs. (2-1), (2-2) and (2-3) with F_{rs} = 114 MPa (16.5 ksi), to a CRC-type FLB strength equation proposed by Johnson (1985) based on experimental tests of symmetrical I-beams with D/t_w ratios ranging up to 245, and to the AISC LRFD (1999) and current AASHTO LRFD (2001) flange strength equations. Figure 2.1.1 shows the comparison for a web slenderness of $2D_c/t_w$ of 140, and Figure 2.1.2 compares the flange strength predictions for $2D_c/t_w$ = 163. The value $2D_c/t_w$ = 163 is the maximum web slenderness allowed for transversely stiffened Grade 345 girders in AASHTO (2001).

[1] AISC LRFD (AISC 1999) places upper and lower limits on k_c of 0.763 and 0.35 as explained subsequently.

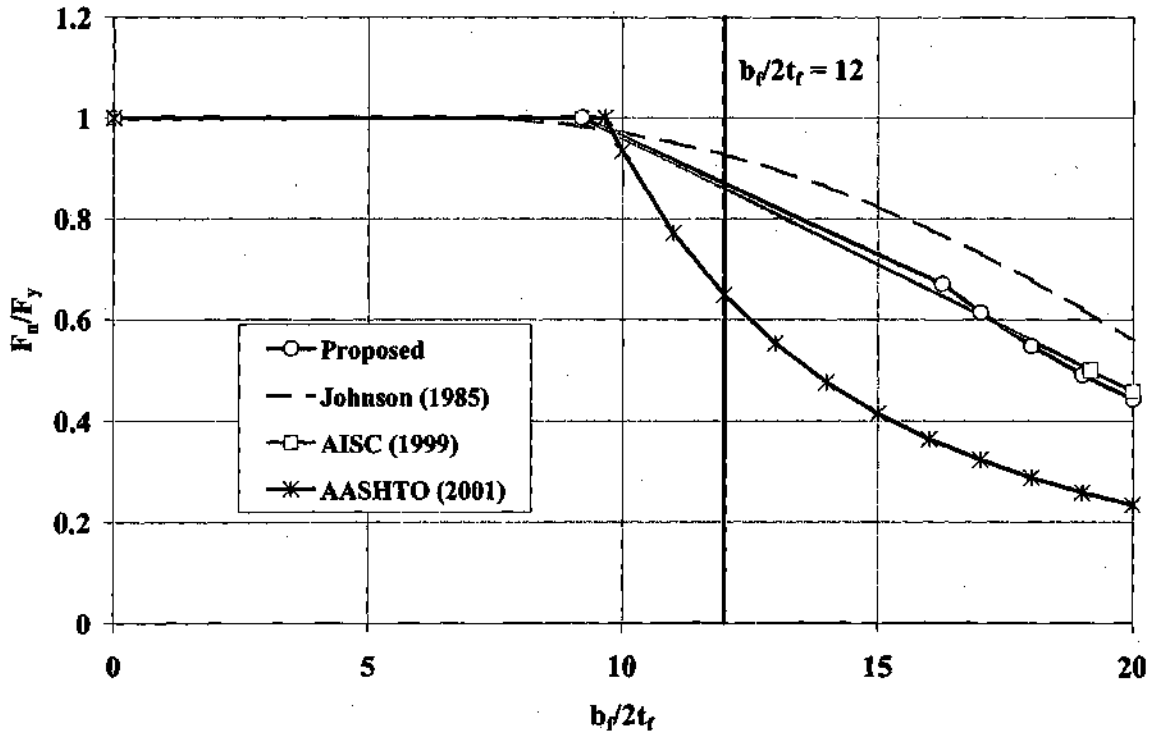

Figure 2.1.1. Straight flange local buckling strengths ($2D_c/t_w = 140$, $F_{yc} = 345$ MPa).

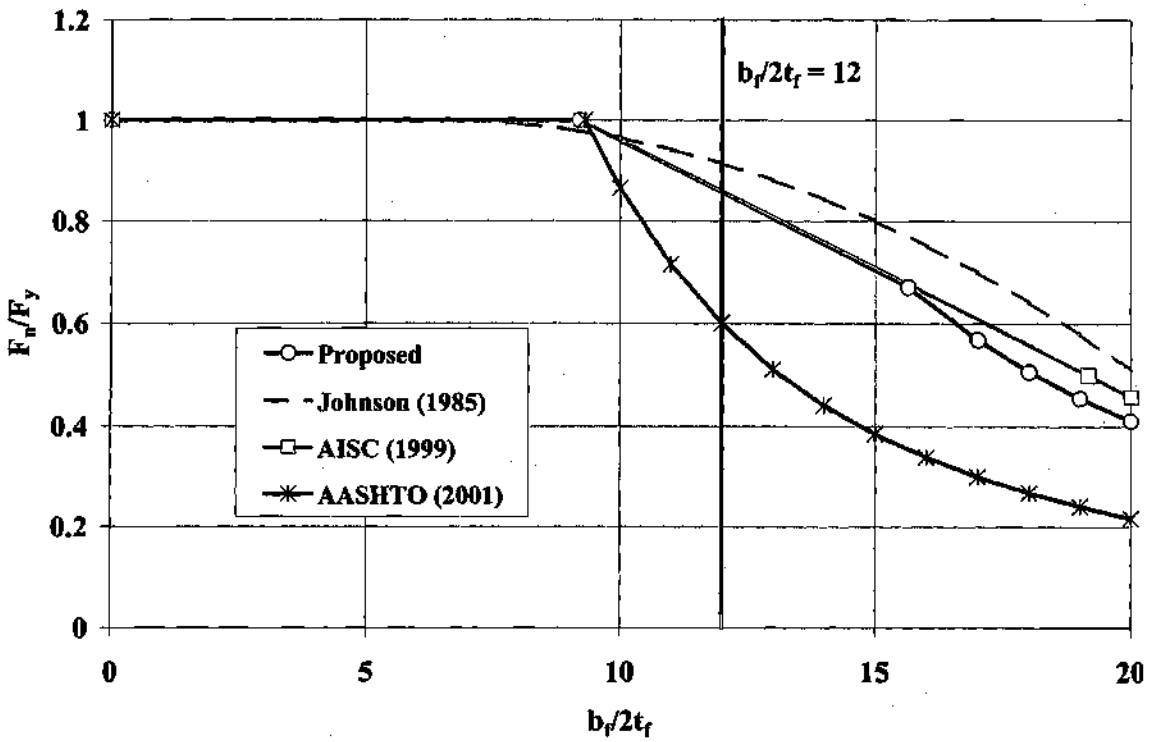

Figure 2.1.2. Straight flange local buckling strengths ($2D_c/t_w = 163$, $F_{yc} = 345$ MPa).

It can be observed that the AASHTO LRFD (2001) flange local buckling strengths are quite conservative relative to the other strength curves. This is due to the fact that the current AASHTO strength equation is based on Eq. (2-6) but with F_L equal to $1.9F_{yc}$. Equation (2-6), with $F_L = 1.9F_{yc}$, gives a reasonable *compact* flange slenderness limit that includes an approximation of the influence of the web on the flange stability. However, to obtain an expression for the flange local buckling strength, AASHTO sets F_{yc} in the resulting equation to the actual applied stress under the design loading, f_b, and then solves the resulting equation for f_b. This amounts to a requirement that the compression flange slenderness needs to satisfy a *compactness* limit based on the assumption that f_b is the flange yield strength. However, if f_b is less than F_{yc}, the flange does not need to be subjected to this strict of a requirement on its slenderness, since lesser inelastic straining is required to reach f_b than F_{yc}. As a result, the AASHTO LRFD expression for the flange strength is quite conservative for $\lambda = b_f/2t_f$ values approaching the maximum fabrication limit of 12 allowed by (AASHTO 2001).

It should be noted that for $F_{yc} \leq 480$ MPa (70 ksi), the flange local buckling strengths specified by the proposed as well as the AISC LRFD (1999) equations are never controlled by elastic buckling (for flanges that satisfy the requirement of $b_f/2t_f \leq 12$). Nevertheless, the flange elastic local buckling strength can be specified as

$$F_e = \frac{k_c \pi^2 E}{12(1-\nu^2)(b_f/2t_f)^2} \tag{2-9}$$

The AISC LRFD (1999) strength curves shown in Figs. 2.1.1 and 2.1.2 are approximately equal to the strength curves obtained based on Eqs. (2-1) through (2-7). The only differences are that the AISC LRFD strength curve is based on the equation

$$k_c = \frac{4}{\sqrt{D/t_w}}, \quad 0.35 \leq k_c \leq 0.763 \tag{2-10}$$

rather than Eq. (2-7), and F_{rs} is taken as $0.5F_{yc}$ rather than 114 MPa (16.5 ksi). The differences between the k_c values from the two equations for $2D_c/t_w = D/t_w = 140$ are practically negligible. However, for $2D_c/t_w = D/t_w = 163$, Eq. (2-7) gives $k_c = 0.31$ while Eq. (2-10) limits k_c to 0.35. This causes a minor shift in the inelastic transition curve in Fig. 2.1.2; $\lambda_r = 15.6$ by Eq. (2-6) whereas $\lambda_r = 19.2$ by the comparable AISC LRFD (1999) equation with k_c defined by Eq. (2-10). The lower limit of $k_c = 0.35$ specified in Eq. (2-10) is approximately the minimum value of k_c that can be back-calculated from Johnson's (1985) experimental data. The web slenderness has to be smaller than $D/t_w = 27.5$ for the upper limit of $k_c = 0.763$ in Eq. (2-10) to control. Therefore, the upper limit on k_c in Eq. (2-10) applies for many of the heavy rolled beam and column wide flange shapes in (AISC 1993); however, this limit does not control for any practical welded plate girder sections. The AASHTO LRFD Specifications (2001) disregard these limits and use Eq. (2-7) implicitly in several of their equations.

It is useful to compare Eqs. (2-7) and (2-10) to the equation

$$k_c = \frac{4.05}{(D/t_w)^{0.46}} \tag{2-11}$$

developed by Johnson (1985) based on curve-fitting to k_c values back-calculated from his experimental tests. Johnson's back-calculation of k_c values is based on equating the strength predicted by the CRC-based equation

$$F_n = F_{yc}\left[1 - 0.55\left(\sqrt{\frac{F_{yc}}{F_e}} - 0.46\right)^{1.92}\right] \tag{2-12}$$

where F_e is given by Eq. (2-9), to the computed elastic flange stress $f_{bmax} = M_{max} / S_{xc}$ determined from the maximum bending moment M_{max} achieved within his tests. Third-point loading through gusset plates attached to the bottom flange, producing uniform bending moment within the center third of the span, was employed in one set of Johnson's tests, and the beams were loaded with four concentrated loads through gussets attached to the bottom flange in a second set of tests.

Figure 2.1.3 compares Johnson's equation for k_c (Eq. 2-11) to the corresponding explicit AISC LRFD and implicit AASHTO LRFD equations, Eqs. (2-10) and (2-7) respectively, and to the values for k_c back-calculated from Johnson's data using Eqs. (2-11) and (2-12). It can be observed that the AASHTO and AISC equations are accurate to conservative relative to Johnson's data. If $2D_c/t_w = D/t_w$ values less than 27.5 are neglected as being unrealistic for checking of flange local buckling in bridge beams and girders, then it can be argued that the simpler Eq. (2-7) implicitly utilized in (AASHTO 2001) is a suitable conservative representation of Johnson's test data.

The above equations for k_c are simple expressions that consider neither the influence of the compression flange slenderness, $b_f/2t_f$, nor the influence of the relative area of the compression flange to the area of the web. These parameters are certain to affect the flange local buckling stability coefficient in general. Formulations are available for calculating the "exact" elastic k_c values, e.g., (Zureick and Shih 1995 and 1998). However, preliminary studies indicate that such formulations do not provide an improvement in the correlation with the test data for girders within the flange slenderness limits currently given in the AASHTO bridge-design specifications. In general, the local buckling limit state at the current flange slenderness limit of $b_f/2t_f = 12$ in the AASHTO Specifications always involves inelastic response (at least for $F_{yc} \leq 480$ MPa (70 ksi)). It can be stated that Eq. (2-7) gives an estimated lower-bound effect of interaction between the web and the compression flange on the flange local buckling resistance.

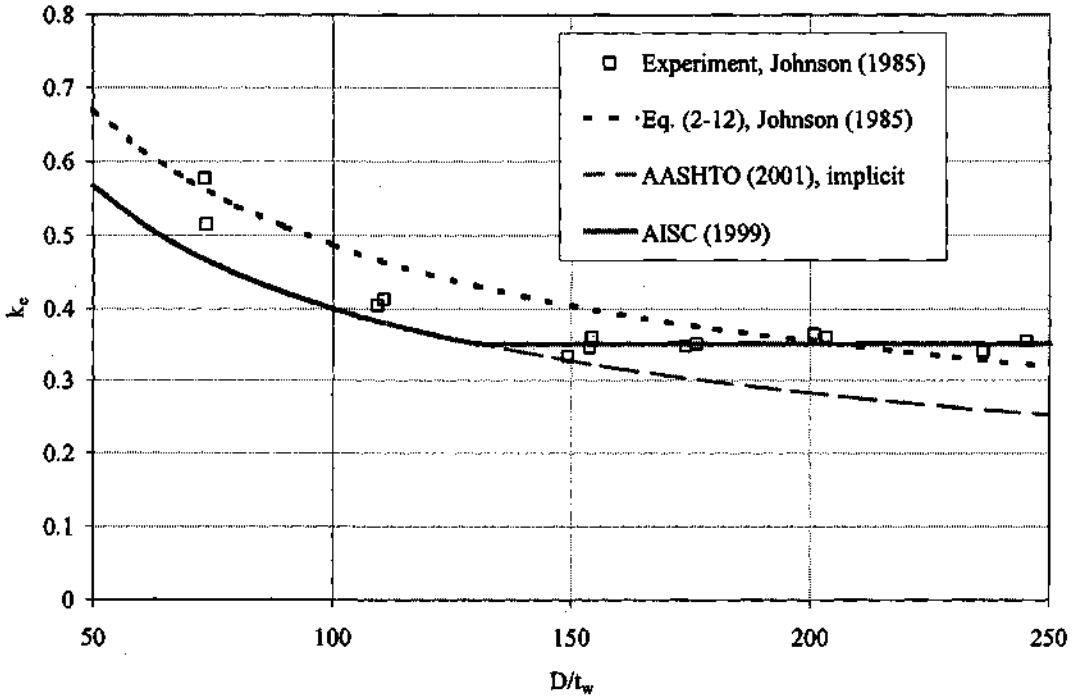

Figure 2.1.3. Straight flange local buckling stability coefficient, k_c.

2.1.1.3 Base Lateral-Torsional Buckling Equations

For checking of lateral-torsional buckling, Eqs. (2-2) and (2-3) are expressed in terms of the slenderness parameter

$$\lambda = L_b/r_t \tag{2-13}$$

where as discussed below, r_t should be computed as the radius of gyration of a notional section comprised of the compression flange plus one-third of the depth of the web in compression, taken about the vertical axis. The compactness limit for lateral-torsional buckling is taken as

$$\lambda_p = 1.76\sqrt{\frac{E}{F_{yc}}} \tag{2-14}$$

Equation (2.14) is the base compact lateral bracing limit (for uniform vertical bending and $C_b = 1$) specified in AISC LRFD (1999) for plate girders, and it is the base compact lateral bracing limit for I-shaped members that do not satisfy the requirements for development of moment capacities larger than the yield moment M_y in the current AASHTO LRFD Specifications (2001). AISC LRFD (1999) uses the same limit

(Eq. (2-14)) for all other types of I sections as well, but with λ defined as L_b/r_y (which is generally greater than L_b/r_t). AASHTO LRFD (2001) specifies that members must satisfy the AISC LRFD (1999) plastic design lateral bracing limits as one requirement to be able to develop vertical bending capacities larger than the yield moment.

Prior to discussing the noncompact limit for lateral-torsional buckling (λ_r), it is useful to consider the fundamental elastic lateral-torsional buckling equation for a doubly symmetric I beam:

$$F_e = \frac{C_b}{S_{xc}} \frac{\pi}{L_b} \sqrt{\left(\frac{\pi E}{L_b}\right)^2 I_y C_w + E I_y G J} \tag{2-15}$$

where C_b is the magnifier which accounts for the effect of moment gradient on the lateral buckling capacity, S_{xc} is the elastic section modulus associated with the compression flange, I_y is the moment of inertia of the full cross-section about the vertical axis in the plane of the web, C_w is the cross-section warping constant, and J is the St. Venant torsional constant for the section. If we make the substitutions

$$I_y \cong 2\, I_{yc} \tag{2-16a}$$

$$G = \frac{E}{2(1+\nu)} \tag{2-16b}$$

$$C_w \cong \frac{I_y h^2}{4} \cong \frac{I_{yc} h^2}{2} \tag{2-16c}$$

and

$$S_{xc} = \frac{I_x}{(d/2)} \tag{2-16d}$$

where I_{yc} is the moment of inertia of the compression flange taken about the vertical axis of the web, h is the distance between the mid-thickness of the flanges, and d is the total depth of the cross-section, we obtain, after some algebraic manipulation

$$F_e = \pi E \frac{C_b}{S_{xc}} \frac{I_{yc}}{L_b} \sqrt{\pi^2 \left(\frac{h}{L_b}\right)^2 + \frac{1}{(1+\nu)} \frac{J}{I_{yc}}} \tag{2-17a}$$

or

$$F_e = C_b \frac{\pi^2 E}{L_b^2} \frac{I_{yc} hd}{2I_x} \sqrt{1 + \frac{1}{\pi^2 (1+\nu)} \frac{J}{S_{xc} h} \frac{2I_x}{I_{yc} hd} L_b^2} \tag{2.17b}$$

Also, we can write

$$\frac{I_{yc} hd}{2I_x} \cong \frac{(A_c b_f^2 / 12)\, hd}{2(A_c h^2 / 2 + A_w D^2 / 12)} = \frac{A_c b_f^2 / 12}{A_c h / d + A_w D^2 / 6\, hd} \tag{2.18a}$$

where D is the depth of the web plate. If we assume that h, d and D are approximately equal, Eq. (2-18a) is a close approximation of

$$r_t^2 \cong \frac{A_c b_f^2 / 12}{A_c + A_w / 6} \tag{2.18b}$$

where r_t is the radius of gyration of the compression flange plus one third of the depth of the web in compression. Therefore, if we make this substitution into Eq. (2-17b), we obtain

$$F_e = C_b \frac{\pi^2 E}{\lambda^2} \sqrt{1 + \frac{1}{\pi^2 (1+\nu)} \frac{J}{S_{xc} h} \lambda^2} \tag{2-19}$$

based on $\lambda = L_b / r_t$. This is a very useful, simple form of the fundamental elastic lateral-torsional buckling equation for a doubly-symmetric I section, expressed in terms of the flange vertical bending stress. All of the terms in this equation are well known in terms of their physical significance, and are commonly calculated as part of the design process.

It should be noted that separate equations are provided for the elastic lateral-torsional buckling strength of composite and noncomposite girders in the current AASHTO LRFD Specifications (2001). However, both of the AASHTO equations are based on the same fundamental equation, Eq. (2.15). They are simply written in different formats. For composite girders in negative bending and for noncomposite transversely-stiffened girders in which the web load-shedding factor R_b is less than one at $f_b = F_{yc}$, the current AASHTO provisions discount the contribution to the strength from St. Venant torsion. Therefore, the second term under the radical in Eq. (2-19) is taken equal to zero. The rationale for this approximation (in the case of noncomposite girders) is that, when R_b is less than one at $f_b = F_{yc}$, cross-section distortion is more likely and therefore the contribution from St. Venant torsion may tend to be heavily nullified. By taking $J = 0$ in Eq. (2-19), we obtain

$$F_e = C_b \frac{\pi^2 E}{\lambda^2} \tag{2-20}$$

Presently, the AASHTO LRFD (2001) Specifications effectively use this equation with r_t defined as the radius of gyration of the compression flange plus one-third of the depth of the web in compression for composite I girders. However, the same equation is used with $r_t = r_{yc}$, the minimum radius of gyration of the compression flange taken about the vertical axis, for noncomposite "slender-web" I-sections (i.e., sections for which R_b is less than one at $f_b = F_{yc}$). This obviously produces an opposite effect from the expected trend in the behavior, since if anything, the torsional restraint from the bridge deck would tend to increase the capacity of the composite girder in negative bending. Based on the above developments resulting in Eqs. (2-19) and (2-20), it can be argued that r_t should be calculated including the area from one-third of the depth of the web in compression. These equations are equivalent to the current AASHTO (2001) elastic lateral-torsional buckling equations.

2.1.1.4 Application of Lateral-Torsional Buckling Equations to Unsymmetric Girders

Although Eqs. (2-19) and (2-20) are derived strictly based only on a doubly-symmetric I section, they can be extended to apply to unsymmetrical noncomposite girders – and to composite girders in general – simply by calculating r_t as defined above. Figures 2.1.4 through 2.1.6 compare the ratio of the strengths obtained from Eq. (2-20) to the strengths obtained from more accurate but more complex formulas for the elastic lateral-torsional bucking capacity of unsymmetric noncomposite girders presented in (AISC 1999) and (Kitipornchai and Trahair 1980), versus the ratio I_{yc}/I_y. "Exact" versions of the (AISC 1999; Kitipornchai and Trahair 1980) formulas (SSRC 1998) are used with $J = 0$ in producing these plots, and $I_{yc} + I_{yt}$ is used as an accurate approximation of I_y.

The AASHTO LRFD Specifications (2001) explicitly restrict the use of their provisions for I girder design to $0.1 \leq I_{yc}/I_y \leq 0.9$. Also, the AASHTO provisions are strictly applicable only to I girders in vertical bending with negligible longitudinal axial compression. In contrast, the provisions for rolled and built-up I-sections within Appendix F of the AISC LRFD Specification (1999) address combined bending with axial tension or compression, although the plate girder provisions in Appendix G of the AISC LRFD Specification also do not apply to cases with axial loads.

It can be observed from Figs. 2.1.4 to 2.1.6 that, within the range of I_{yc}/I_y permitted by the AASHTO Specifications, Eq. (2-20) gives a conservative approximation of the buckling strength well within 10 percent of the exact formulas. In Fig. 2.1.4, the comparisons are made for girders with $2D_c/t_w = 139$, which is the transition point between the definition of a nonslender and a slender web in (AISC 1999). Also, the b_f/t_f values of both flanges are assumed to be the same in order to obtain practical girder proportions that meet (AASHTO 2001) restrictions. The curves are plotted for D/b_f values of 2 and 5 and b_f/t_f values of 10 and 24. These are intended as extreme or bounding values for all practical girder proportions. From Fig. 2.1.4, it can be seen that Eq. (2-20) is approximately two to five percent conservative compared to the exact equations even for $I_{yc}/I_y = 0.5$ (i.e., for a symmetrical girder). This is due to the

assumption of $d \cong h \cong D$ in Eq. (2-20). Figure 2.1.5 shows the result for the most conservative case in Fig. 2.1.4 ($2D_c/t_w = 139$, $D/b_{fc} = 2$, $b_{fc}/t_{fc} = b_{ft}/t_{ft} = 10$) when the "exact" equation (Eq. (2-18a)) is used for r_t^2. Figure 2.1.6 shows the ratio of Eq. (2-20) to the exact strengths for an upper bound web slenderness of $2D_c/t_w = 277$, corresponding to the limit based on AASHTO (2001) for a longitudinally stiffened girder, with $D/b_{fc} = 5$ and $b_{fc}/t_{fc} = b_{ft}/t_{ft} = 24$. Figures 2.1.4 through 2.1.6 are representative of the range of errors obtained for any girders with $2D_c/t_w$ from 139 to 277, D/b_{fc} from 2 to 5, and b_{fc}/t_{fc} = 10 to 24.

Figures 2.1.7 through 2.1.9 are similar plots to those discussed above, but with $J = \Sigma\, bt^3/3$ from all the cross-section plate components. AASHTO LRFD (2001) specifies that this value of the St. Venant torsional constant is to be included in the lateral-torsional buckling calculations for "nonslender web" girders, i.e., girders in which $R_b = 1$ at $f_b = F_{yc}$. When $J = 0$, the ratio of the approximate and exact equations is independent of the girder length; however, this ratio is not independent of the length for $J > 0$. Therefore, the curves in Figs. 2.1.7 – 2.1.9 are plotted at $\lambda = L_b/r_t = \lambda_r$.

The design parameters specified in Fig. 2.1.7 are the same as those for the curves in Fig. 2.1.4. It can be observed that when the St. Venant torsional constant J is included, the beam-theory based elastic lateral-torsional buckling strength for girders with small D/b_{fc} and I_{yc}/I_y values tends to be significantly underestimated by Eq. (2-19). This is due to the fact that the use of Eq. (2-19) with r_t based on one-third of the depth of the web in compression does not fully capture the torsional restraint offered by the large tension flange in these girders. Nevertheless, it can be argued that the girder proportions are somewhat unrealistic for the curves that show larger than ten percent conservative error in Fig. 2.1.7, and that for most practical girders, the errors are less than ten percent conservative. Fig. 2.1.8 parallels Fig. 2.1.5, and shows the errors if the "exact" r_t (Eq. 2.18a) is utilized. This curve shows the largest unconservative error (approximately two percent) for all the parameters studied. Lastly, Fig. 2.1.9 shows the results for the combination of D/b_{fc} and b_f/t_f from Fig. 2.1.7, i.e., $D/b_{fc} = 2$ and $b_f/t_f = 10$, but with a representative lower-bound value for the web slenderness $2D_c/t_w$ of 30. This case represents a practical upper bound for the conservative error of Eq. (2-19) with $J > 0$. It can be seen that the conservative error in this plot is approximately the same as the error in the curve for $2D_c/t_w = 139$, $D/b_{fc} = 2$ and $b_f/t_f = 10$ in Fig. 2.1.7.

For composite girders in negative bending and in which web distortion effects may nullify the contributions from St. Venant torsion, Eq. (2-20) can be applied conservatively to estimate the lateral buckling capacity of the compression flange. This is based on the logic that the composite girder can be replaced by an equivalent noncomposite girder with the same depth of the web in compression, and that for these equivalent girders, the composite girder would always possess greater strength due to the torsional restraint provided by the bridge deck to the tension flange of the member.

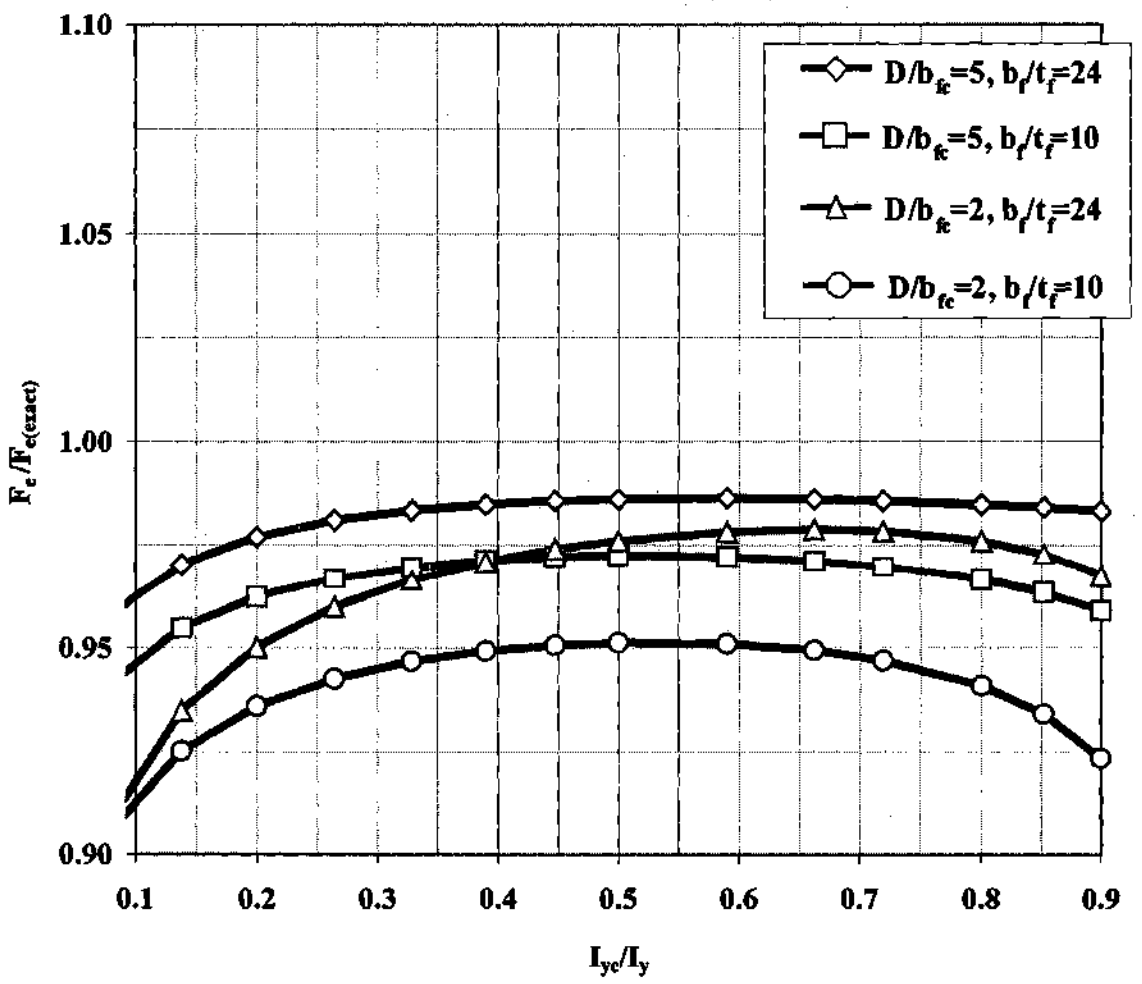

Figure 2.1.4. Ratio of the elastic lateral-torsional buckling capacity predicted by Eq. (2-20) to the capacity predicted by the "exact" beam lateral-torsional buckling equations with J = 0 (SSRC 1998), plotted as a function of I_{yc}/I_y ($2D_c/t_w = 139$, $b_{fc}/t_{fc} = b_{ft}/t_{ft}$).

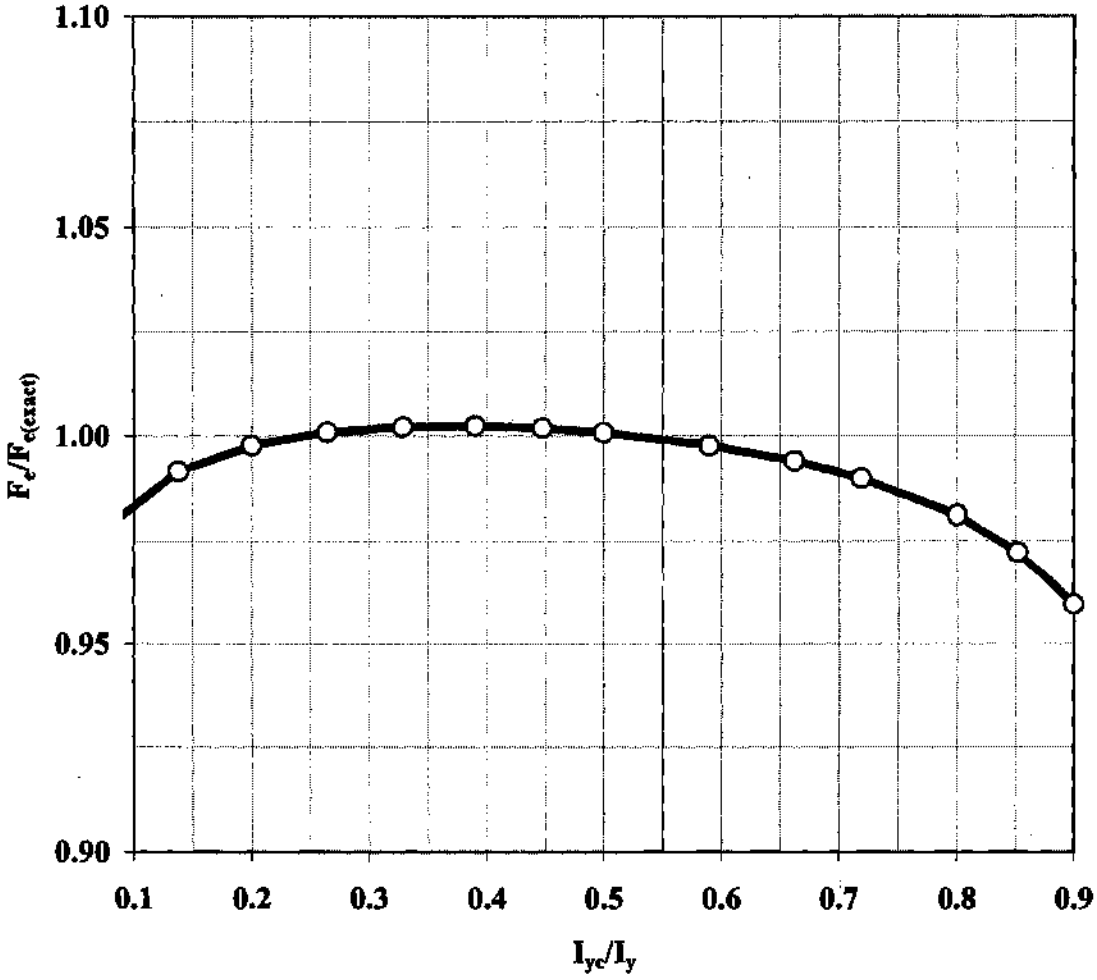

Figure 2.1.5. Ratio of the elastic lateral-torsional buckling capacity predicted by Eq. (2-20) using the "exact" r_t (Eq. (2-18a) to the capacity predicted by the "exact" beam lateral-torsional buckling equations with J = 0 (SSRC 1998), plotted as a function of I_{yc}/I_y ($2D_c/t_w = 139$, $b_{fc}/t_{fc} = b_{ft}/t_{ft} = 10$, $D/b_{fc} = 2$).

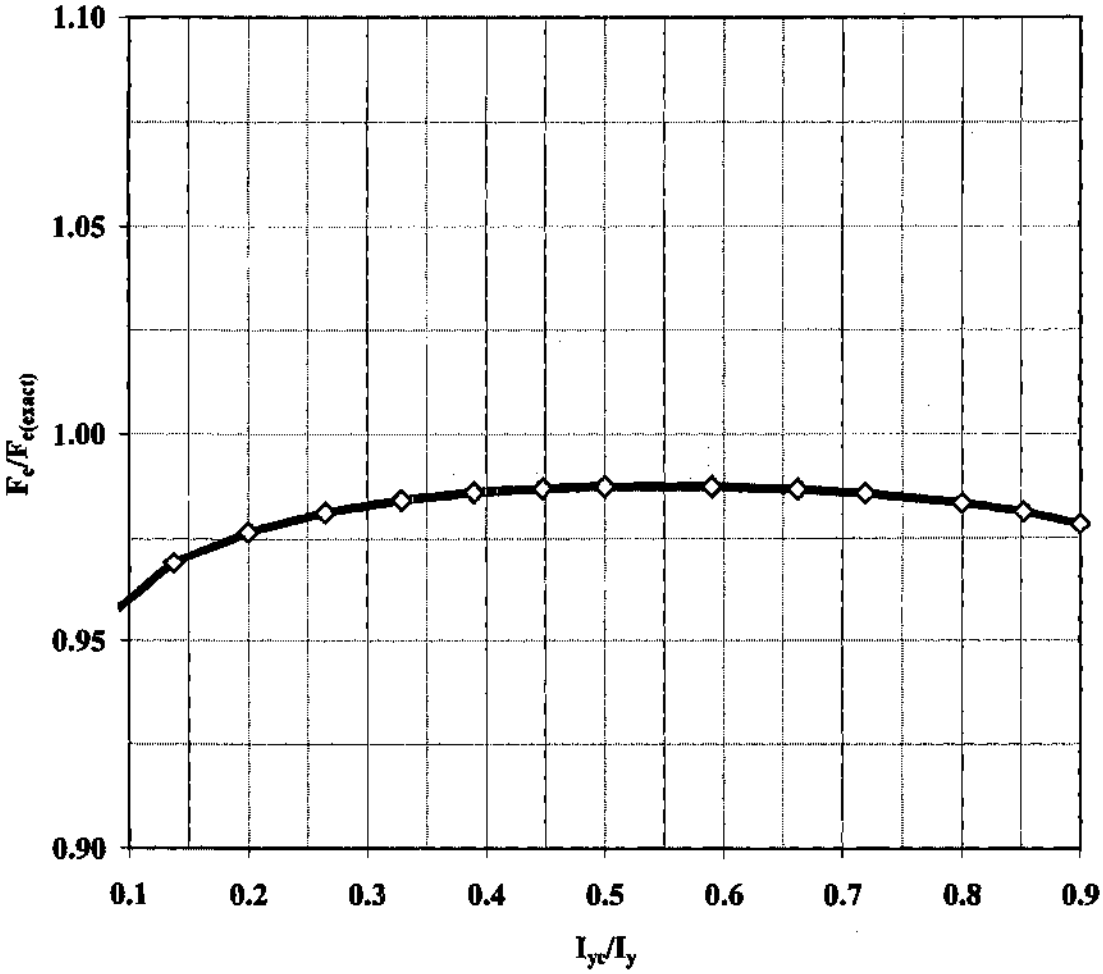

Figure 2.1.6. Ratio of the elastic lateral-torsional buckling capacity predicted by Eq. (2-20) to the capacity predicted by the "exact" beam lateral-torsional buckling equations with J = 0 (SSRC 1998), plotted as a function of I_{yc}/I_y ($2D_c/t_w = 277$, $b_{fc}/t_{fc} = b_{ft}/t_{ft} = 24$, $D/b_{fc} = 5$).

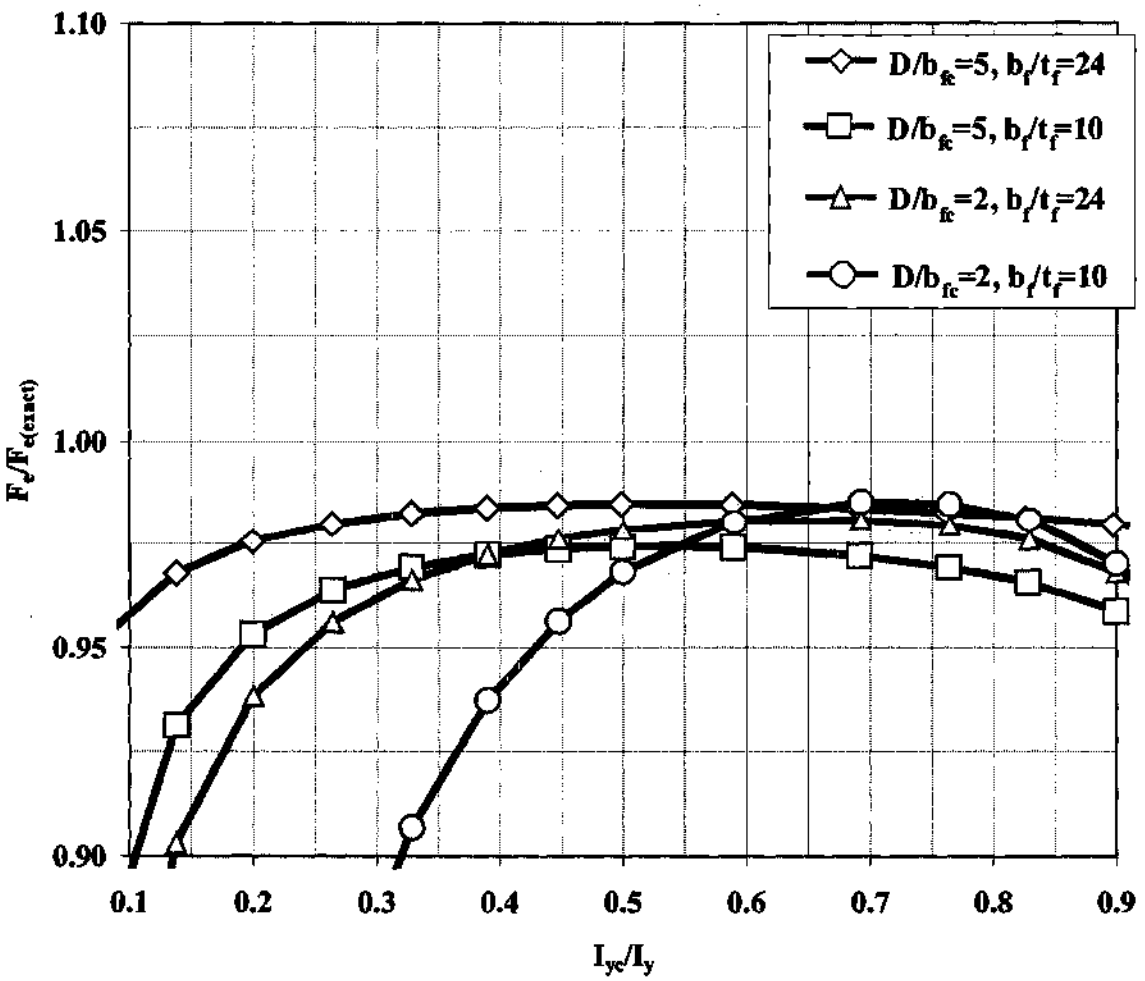

Figure 2.1.7. Ratio of the elastic lateral-torsional buckling capacity predicted by Eq. (2-19) to the capacity predicted by the "exact" beam lateral-torsional buckling equations with $J = \Sigma bt^3/3$ (SSRC 1998), plotted as a function of I_{yc}/I_y ($2D_c/t_w = 139$, $b_{fc}/t_{fc} = b_{ft}/t_{ft}$, $\lambda = L_b/r_t = \lambda_r$).

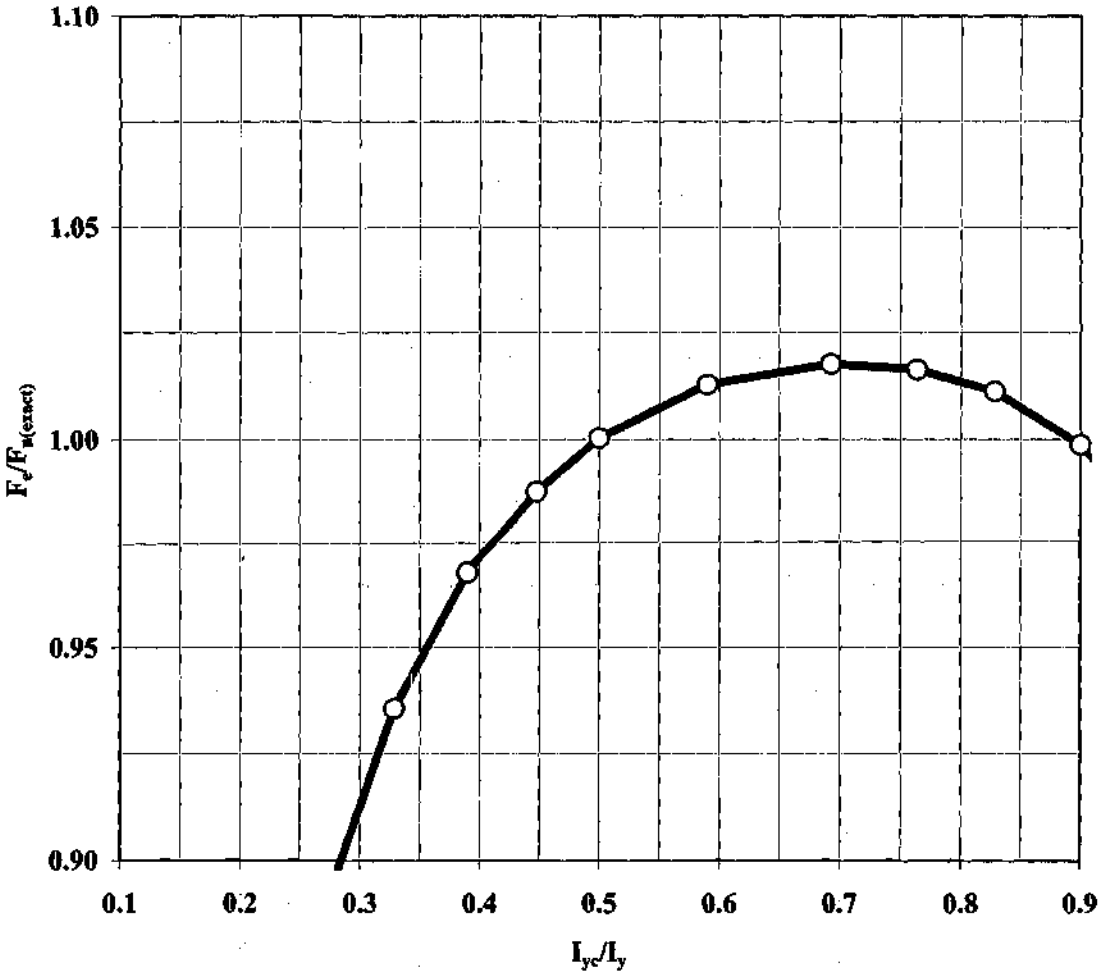

Figure 2.1.8. Ratio of the elastic lateral-torsional buckling capacity predicted by Eq. (2-20) using the "exact" r_t (Eq. (2-18a)) to the capacity predicted by the "exact" beam lateral-torsional buckling equations with $J = \Sigma bt^3/3$ (SSRC 1998), plotted as a function of I_{yc}/I_y ($2D_c/t_w = 139$, $b_{fc}/t_{fc} = b_{ft}/t_{ft} = 10$, $D/b_{fc} = 2$, $\lambda = L_b/r_t = \lambda_r$).

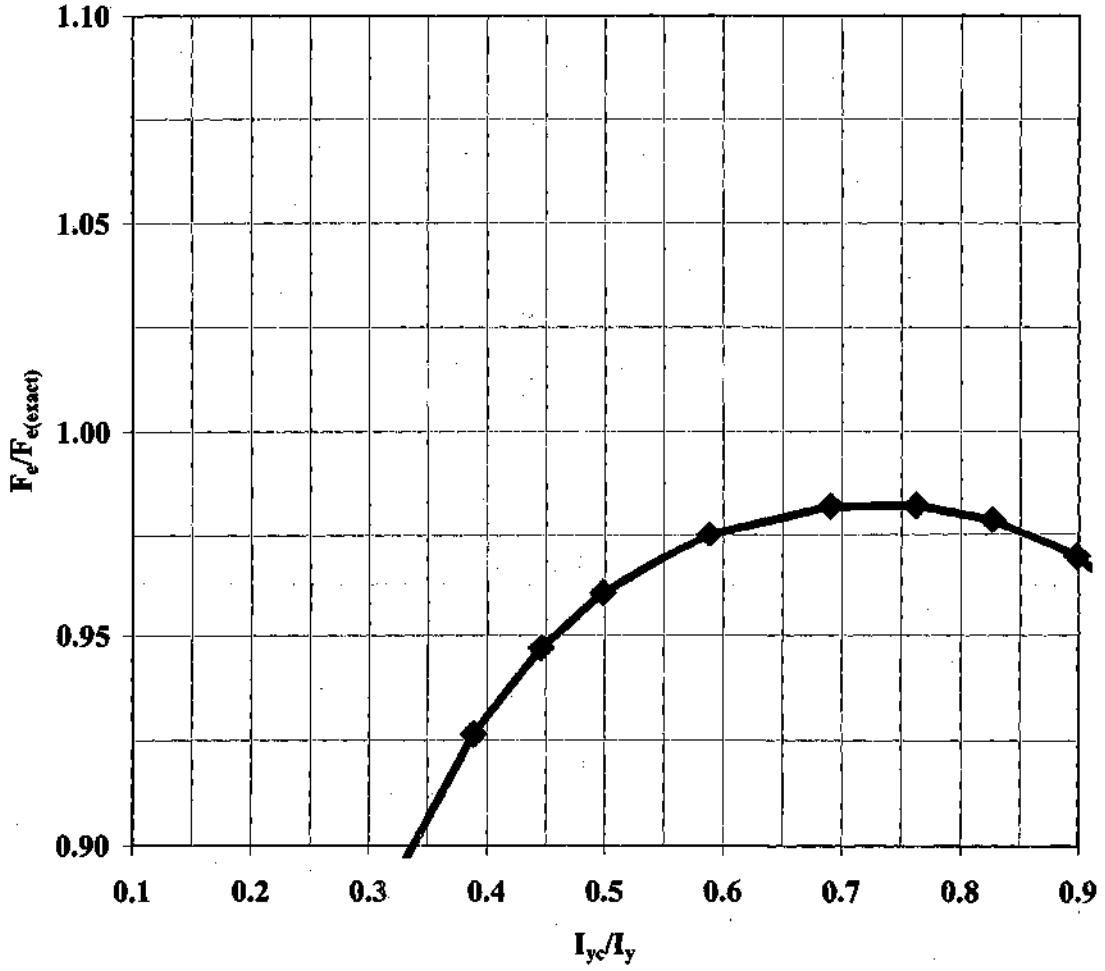

Figure 2.1.9. Ratio of the elastic lateral-torsional buckling capacity predicted by Eq. (2-19) to the capacity predicted by the "exact" beam lateral-torsional buckling equations with $J = \Sigma bt^3/3$ (SSRC 1998), plotted as a function of I_{yc}/I_y ($2D_c/t_w = 30$, $b_{fc}/t_{fc} = b_{ft}/t_{ft} = 10$, $D/b_{fc} = 2$, $\lambda = L_b/r_t = \lambda_r$).

2.1.1.5 Relationship of Lateral-Torsional Buckling Strength to L_b/b_f

If it is recognized that the radius of gyration r_t can be approximated as

$$r_t \cong r_{yc}\sqrt{\frac{1}{1+\frac{1}{6}a_r}} = \frac{b_f}{\sqrt{12(1+\frac{1}{6}a_r)}} \tag{2-21}$$

where

$$a_r = \frac{2D_c t_w}{b_{fc} t_{fc}} \tag{2-22}$$

is the ratio of two times the area of the web in compression to the area of the compression flange, utilized in the calculation of the web load-shedding factor R_b in (AASHTO 2001), Eq. (2-20) can be restated in a form that is more useful for understanding the influence of the compression flange geometric proportions:

$$F_e = C_b \frac{\pi^2 E}{(L_b/r_t)^2} = C_b \frac{\pi^2 E}{(L_b/b_f)^2} \frac{1}{12(1+\frac{1}{6}a_r)} \tag{2-23}$$

The relationship between this equation and rules stated in the Recommended Specifications (Hall and Yoo 1998) for the maximum allowable L_b/b_f in curved I girders is commented upon in the subsequent discussions. Equation (2-21) can be obtained by algebraic manipulation from Eq. (2-18b).

2.1.1.6 Lateral-Torsional Buckling Compact and Noncompact Bracing Limits

The compact bracing limit with respect to lateral-torsional buckling is specified by Eq. (2-14). If Eqs. (2-19) and (2-20) are accepted as appropriate expressions for the elastic lateral-torsional buckling capacity, then the associated noncompact lateral bracing limits can be determined as

$$\lambda_r = \frac{1.95E}{F_L}\sqrt{\frac{J}{S_{xc}h}}\sqrt{1+\sqrt{1+6.76\left(\frac{F_L S_{xc} h}{EJ}\right)^2}} \tag{2-24a}$$

and

$$\lambda_r = 3.14\sqrt{\frac{E}{F_L}} \tag{2-24b}$$

respectively. These equations are derived simply by equating the elastic lateral buckling strength given by Eqs. (2-19) and (2-20) to F_L. That is, λ_r is the slenderness L_b/r_t corresponding to the transition from the inelastic lateral buckling strength curve given by Eq. (2-2) to the elastic lateral buckling strength given by either Eq. (2-19) or (2-20). If $0.5F_{yc}$ is substituted for F_L, Eq. (2-24b) becomes the noncompact lateral-bracing limit for plate girders specified in (AISC 1999). Also, this equation with $F_L = 0.5F_{yc}$ is the noncompact lateral bracing limit for composite I girders within the current AASHTO LRFD Specifications (2001). For I-beams and girders in which the contribution from St. Venant torsion is included, Eq. (2-24a) is a close approximation to the noncompact limit stated in (AASHTO 2001) if F_L is taken as $0.5F_{yc}$. It is a close approximation to the noncompact limit stated in (AISC 1999) for general I-shapes with nonslender webs, if F_{rs} is taken as 114 MPa (16.5 ksi) for welded sections and 69 MPa (10 ksi) for rolled beams.

2.1.1.7 Summary Assessment of Proposed Lateral-Torsional Buckling Equations and Application of these Equations in this Research

Based on the precedent set by the Recommended Specifications (Hall and Yoo 1998) and discussions with engineers on AASHTO T14 and on the AISI Bridge Research Task Force advisory groups to this project, a decision was made early in this research to discount the beneficial effects of the St. Venant torsional stiffness J when checking the strength of I girders subjected to lateral bending and torsion. Therefore, all the design studies in this work involving the use of the modified AASHTO LRFD lateral buckling formulas utilize Eq. (2-20) or the equivalent Eq. (2-23) as the base elastic lateral buckling strength. The conservatism of this simplification, and the potential for use of Eq. (2-19) as the base elastic lateral buckling strength for certain cases is addressed within the discussion of the research results (see Chapter VII).

As noted previously, the use of $F_{rs} = 0.5F_{yc}$ is recommended in this work for general application of the AASHTO flexural strength equations to plate girders with F_{yc} up to 690 MPa (100 ksi). However, the value of $F_{rs} = 114$ MPa (16.5 ksi) is found to produce better correlation with the finite element and experimental test results for the homogeneous Grade 345 girders considered within this research than $F_{rs} = 0.5F_{yc}$. Therefore, $F_{rs} = 114$ MPa is utilized in the application of recommended design equations throughout this report. Based on further research, it may be possible to liberalize the $F_{rs} = 0.5F_{yc}$ limit for other grades of steel and for hybrid girders; however, this is outside of the scope of the present work.

Figures 2.1.10 and 2.1.11 show comparisons of the predictions of the resulting equations to other design predictor equations within the literature. It can be observed that the transition from inelastic to elastic buckling in the proposed equations occurs approximately at $L_b/b_f = 25$. Furthermore, it can be observed that the nominal strength limit on the flange stress obtained from traditional straight-girder lateral-torsional buckling equations, utilized within the Recommended Specifications (Hall and Yoo 1998), are slightly liberal compared to the proposed equations for L_b/b_f values close to this noncompact lateral-bracing limit. This is due to the fact that the traditional flange lateral strength equations are based on $r_{yc} = b_f / \sqrt{12}$. It should be noted that r_{yc} is the

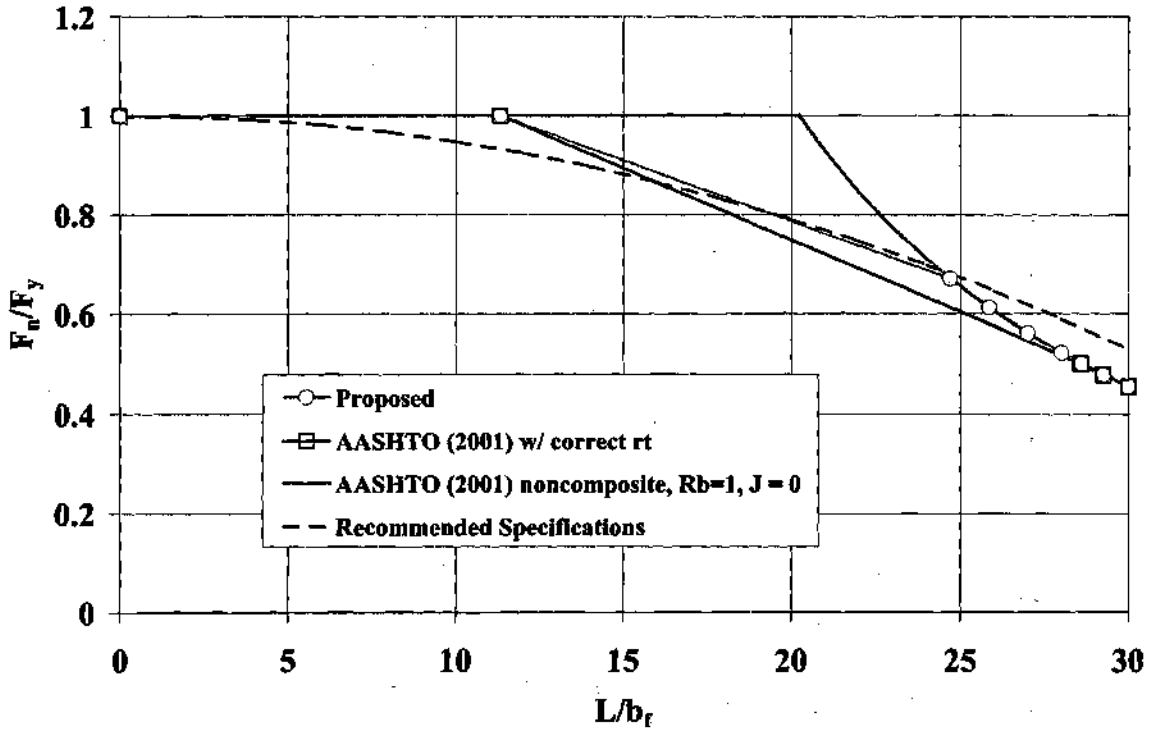

Figure 2.1.10. Straight girder lateral-torsional buckling curves ($a_r = 1$).

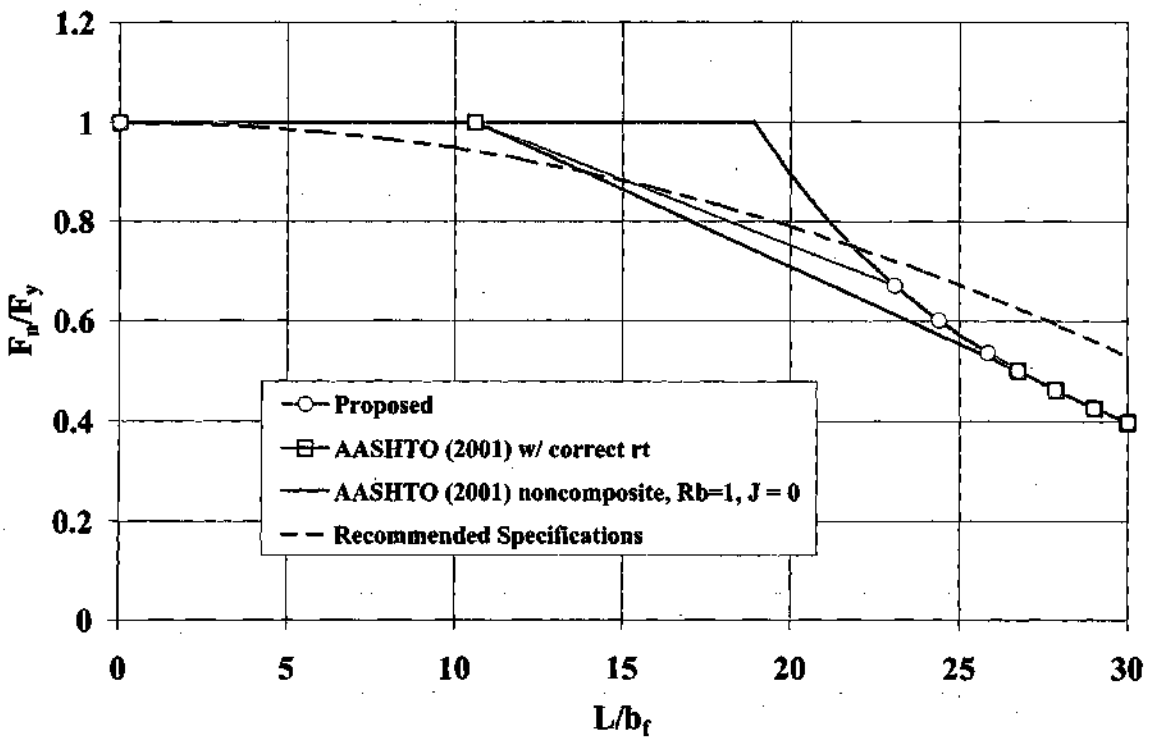

Figure 2.1.11. Straight girder lateral-torsional buckling curves ($a_r = 2$).

same for all girders that have the same flange width, regardless of the proportions of the tension flange and web. The term r_{yc} does not account for the potential destabilizing effects from compressive stresses in the web.

It can be argued that the potential conservatism involved with neglecting any St. Venant torsional stiffness contribution to the lateral buckling capacity, and due to restraint from the deck in composite girders, compensates for the liberal assumption of the use of r_{yc} in checking the lateral stability of the compression flange (rather than r_t). The proposed equations are slightly liberal relative to the traditional flange lateral buckling strengths for L_b/b_f values close to the compact bracing limit. This limit corresponds to L_b/b_f values of about 11 to 12 in the figures (depending on the value of a_r).

The lateral buckling strength predictions using the current AASHTO LRFD (2001) equations for noncomposite slender-web and composite girders, but with the proposed interpretation of r_t, are also shown within the plots in Figs. 2.1.10 and 2.1.11. As noted previously, these equations are based on $F_{rs} = 0.5\ F_{yc}$. Within the vicinity of the noncompact flange bracing limit (λ_r), the proposed equations are approximately a maximum of nine percent more liberal than the current AASHTO equations for homogeneous girders with $F_{yc} = 345$ MPa (50 ksi).

Lastly, the proposed equations are also compared to the current AASHTO (2001) equations for noncomposite transversely stiffened I sections with $R_b = 1$ and for noncomposite longitudinally stiffened I sections, but with J taken conservatively equal to zero. The AASHTO (2001) Specifications allow the engineer to include J in calculating the capacity of these types of girders, but currently, to avoid the complexity of equations such as Eq. (2-24a), these Specifications do not include an inelastic buckling transition region. As a result, the corresponding equations, as plotted in Figs. 2.1.10 and 2.1.11, are more than 20 percent liberal compared to the proposed lateral buckling strength curves for girders with L_b/b_f values close to 20. It can be shown that the corresponding equations also can be significantly liberal relative to the proposed equations when the St.Venant torsional stiffness parameter J is included. On this basis, the authors recommend that the AASHTO LRFD (2001) provisions for the flange lateral buckling capacity of longitudinally-stiffened girders and of transversely-stiffened girders with $R_b = 1$ should be modified to include the inelastic buckling transition region described by Eq. (2-2).

2.1.1.8 Consideration of the Moment Gradient Magnifier C_b for Bridge Design

The calculation of the moment-gradient magnifier C_b in bridge design merits some discussion. AASHTO LRFD (2001) specifies the following slightly modified version of the simple traditional definitions of this parameter:

- for unbraced cantilevers, or for members where the moment within a significant portion of the unbraced segment exceeds the larger of the segment end moments:

$$C_b = 1 \qquad (2\text{-}25)$$

- for all other cases:

$$C_b = 1.75 - 1.05\left(\frac{P_l}{P_h}\right) + 0.3\left(\frac{P_l}{P_h}\right)^2 \leq 2.3 \qquad (2\text{-}26)$$

where P_l is defined as the force in the compression flange at the brace point with the lower force due to the factored loading, and P_h is defined as the compression flange force at the brace point with the higher force due to the factored loading. For noncomposite I girders in single-curvature bending, or noncomposite I girders in reversed-curvature bending with $D_c = D/2$, Eq. (2-26) is the same as the traditional version of this equation specified in the commentary of (AISC 1999). However, for noncomposite I girders in reversed-curvature bending with $D_c > 0.5D$, Eq. (2-26) is more conservative than the traditional equation, and conversely, for these types of girders and $D_c < 0.5D$, Eq. (2-26) is liberal relative to the traditional equation. The rationale for use of P_l and P_h in Eq. (2-26) is that this better reflects the fact that the dead and live load vertical bending moments due to factored loads are applied to different sections in composite girders. Also, this modification of the traditional formulas is believed to better reflect the stability behavior of singly symmetric noncomposite girders (AASHTO 2001). Equation (2-26) is intended strictly only for application to girders in which the steel cross-section is prismatic along the unsupported length; also, this equation is valid strictly only for a linear variation of the flange force along the unbraced length.

The commentary of the AASHTO LRFD (2001) Specifications states, "It is conservative and convenient to use the maximum moment envelope at both brace points in this ratio or in computing P_l / P_h, although the actual behavior depends on the concurrent moments at these points." It is useful for the engineer to understand the proof of this statement.

Strict application of the C_b equation requires the calculation of the concurrent moments at adjacent brace points; that is, calculation of the governing value of P_h at the brace point with the higher force using the critical moment from the maximum moment envelope, along with the calculation of the value of P_l at the brace point with the lower force using the concurrent moment at that point. However, since concurrent moments are normally not tracked in bridge analysis, it is convenient and always conservative to use the worst-case moment envelope values in calculating P_l and P_h. The worst-case envelope value for calculation of P_h is the critical moment envelope value causing the largest P_h at the brace point with the higher force, and the worst-case envelope value used to calculate P_l is either the maximum or the minimum moment envelope value at the brace point with the lower force, whichever produces a lower value of C_b. The proof that the use of these worst-case moment values to compute P_l and P_h is always conservative is as follows.

Consider an example worst-case distribution of flange force along a critical unbraced length, as defined above (see Fig. 2.1.12). Obviously, if both P_l and P_h are defined in the above way, the concurrent moment value at the location of P_l for the load combination

that produces P_h will always produce a value of C_b greater than or equal to that calculated based on the worst-case P_l/P_h. Therefore, it is obvious that the use of the worst-case moment envelope values for the moments at the brace points results in a conservative value of C_b and a conservative check of lateral-torsional buckling *for the specific load combination that produces the maximum P_h*. However, an important problem that must be considered is that in general, it is possible that a load combination may exist which produces a smaller force than P_h at the maximum moment location, but yet also has a concurrent value of the flange force at the location of P_l that results in a flatter moment gradient than in the above worst-case check (thus also producing a smaller value of C_b). It is possible that such a load combination may be more critical with respect to lateral-torsional buckling than the load combination that produces P_h. For purposes of the discussion below, we will denote the smaller flange force at the maximum moment location for such a potential more critical moment diagram by the symbol P_2.

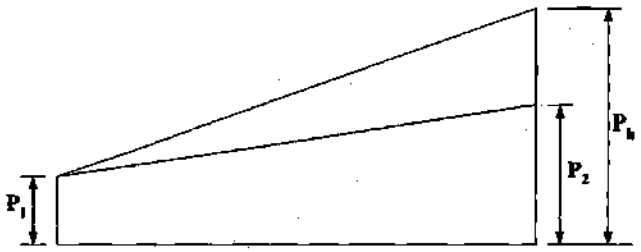

Figure 2.1.12. Worst-case flange force distribution (P_l to P_h) versus a conservative check of a potentially more-critical concurrent flange force distribution (P_l to P_2).

We can use the worst-case P_l, as defined above, along with the force P_2 as a conservative check of the above potentially more critical situation. Also, we assume a worst-case situation in which the unsupported length is long enough such that the increase in the member capacity due to C_b does not exceed the member strength based on Eq. (2-1). If we denote the value of C_b determined based on the envelope-based values P_l and P_h as C_{be}, if we denote the value of the moment gradient parameter based on P_l and P_2 as C_{b2}, and if we denote the flange bending stresses corresponding to P_h and P_2 as f_{bh} and f_{b2} respectively, then for the worst-case check using P_l and P_h to always control the design, we must have

$$f_{b2} \leq C_{b2} F_{e(Cb=1)} \tag{2-27}$$

Furthermore, if we assume that $f_{bh} = C_{be} F_{e(Cb=1)}$, we can substitute $F_{e(Cb=1)} = f_{bh}/C_{be}$ into Eq. (2-27) to obtain (after some minor algebraic manipulation)

$$\frac{f_{b2}}{f_{bh}} \frac{C_{be}}{C_{b2}} \leq 1 \tag{2-28}$$

If we assume only linear variations in the flange force between the two brace locations, we can show by varying P_l / P_h and f_{b2}/f_{bh} over a full range of their potential values that the above defined "worst case" check using the flange forces from the maximum and minimum design moment envelopes will always be conservative for any possible loading combination that the critical unsupported segment may see, including reversed-curvature bending.

The above development allows the engineer to account for moment gradient effects in the design, whenever he or she deems that the moments may be assumed to vary linearly along the unsupported length. A separate more refined equation for calculation of C_b developed by Kirby and Nethercot (1979) is provided within the commentary of the AASHTO LRFD (2001) Specification for handling of cases in which the moment diagrams are significantly nonlinear along the unsupported length. Based on reasoning similar to that of the above discussion, it can be shown that C_b also can be calculated conservatively from this equation, using worst-case values of the flange forces obtained from the maximum or the maximum and minimum moment envelopes. Other more refined formulas for C_b are discussed in (SSRC 1998). In this research, we utilize Eqs. (2-25) and (2-26) for the calculation of C_b with the exception of one set of studies involving internal loading within a curved I girder segment, in which case the Kirby and Nethercot (1979) equation is employed.

2.1.1.9 Summary

The proposed straight I girder equations defined in this section may be used as a base set of equations for defining the capacity of straight or curved I girders subjected to vertical bending combined with torsion and lateral moments. Additional modifications of these equations to achieve a unified set of I girder design equations, which address torsion and lateral bending, are discussed in Section 2.1.9. However, before motivating and presenting the development of these equations, it is important to first consider a number of other key design equations that have been developed in prior research for predicting the flexural capacity of curved I girders. Sections 2.1.2 through 2.1.8 provide a detailed discussion of existing strength predictor equations for curved I girders.

2.1.2 Flexural Strength Equations in the Recommended Specifications (Hall and Yoo 1998)

The vertical-bending strength equations for curved steel I girders in both the AASHTO Guide (AASHTO 1993) and the Recommended Specifications (Hall and Yoo 1998) are based on a modified form of predictor equations developed by McManus (1971). In his doctoral work, McManus (1971) conducted approximate second-order elastic analyses of a large suite of doubly symmetric curved I girders configured as shown in Fig. 2.1.13. These models are subjected to equal and opposite moments ($\overline{M}$) at their ends, producing near uniform vertical bending, as well as to end bimoments ($\overline{B}$), producing specified end flange moments ($\overline{M}_w = \overline{B}/h$) and warping stresses $\overline{f}_w$. The girders are simply supported, and the web is held vertical at the girder ends. In his

approximate second-order analysis, McManus computed the compression flange vertical bending stress as

$$\bar{f}_b = \frac{\overline{M}}{S_x} \tag{2-29}$$

where $\overline{M}$ is the applied end vertical bending moment and S_x is the elastic section modulus, and he calculated the *applied* end warping stress as

$$\bar{f}_w = \frac{\overline{B}\omega}{C_w} \cong \frac{\overline{M}_w h\left(\frac{h}{2}\frac{b_f}{2}\right)}{\left(\frac{I_{yc}h^2}{2}\right)} = \frac{\overline{M}_w \frac{b_f}{2}}{I_{yc}} \tag{2-30}$$

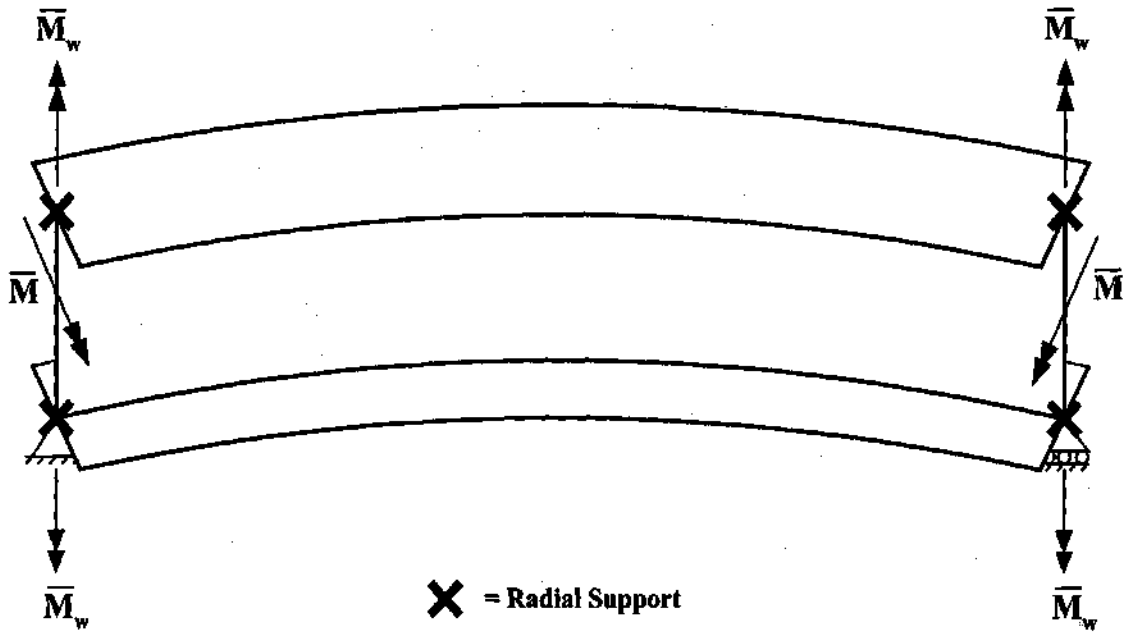

Figure 2.1.13. McManus's idealized single span model.

where $\overline{B}$ is the applied end bimoment, ω is the principal sectorial coordinate at the flange tips, C_w is the warping constant of the cross-section, $\overline{M}_w = \overline{B}/h$ gives the applied end lateral flange bending moments associated with $\overline{B}$, h is the distance between the mid-thickness of the flanges, b_f is the flange width, and I_{yc} is the moment of inertia of the individual flanges about a vertical axis through the web. McManus considered a wide

range of values for $\bar{f}_w / \bar{f}_b$ from –0.5 to +0.5. For purposes of discussion in this report, $\bar{f}_w / \bar{f}_b$ is taken as positive when $\bar{f}_w$ is compressive at the tip of the compression flange furthest away from the center of curvature of the beam. This is identical to the sign convention utilized for this ratio in the Guide and in the Recommended Specifications, but it is opposite to the sign convention utilized by McManus in his dissertation.

McManus conducted two sets of parametric studies aimed at the development of design strength predictor equations, one set based on the assumption of "compact" cross-section behavior and the other assuming "noncompact" cross-section response. In his compact-section studies, McManus defined the maximum strength as the minimum of: (1) the value of $\bar{f}_b$ at which a fully-plastic condition is developed in the cross-section at either the mid-length or at the ends of his model, whichever occurs first, or (2) the value of $\bar{f}_b$ associated with the parabolic CRC equation for inelastic lateral flange buckling that was in effect within the AASHTO straight girder design provisions at the time of his research. When the first of the above two conditions controlled, McManus assumed that the girder remains completely elastic until the fully plastic condition is developed at the critical cross-section. Furthermore, he considered the effects of estimated values for (1) internal *second-order elastic* bimoments, B_2, (2) internal *second-order elastic* radial (i.e., lateral) bending moments, M_{y2}, and (3) additional internal flange lateral bending moments due to distortion of the cross-section, $M_{\ell D}$, in addition to (4) the internal vertical bending moment $M \cong \overline{M}$ in determining the load level at which the full-plastic condition is reached at the most critical cross-section. In his noncompact section studies, McManus defined the maximum strength as the value of $\bar{f}_b$ at the first occurrence of yielding within the beam, either at the mid-length or at the ends of the member, based on the estimated second-order elastic internal moments listed above. The effect of internal residual stresses is not included within McManus's first-yield check.

Although he conducted other studies in which he considered a broader range of design parameters, for the specific development of his design predictor equations, McManus assumed the following values: F_{yc} = 250 MPa (36 ksi), A_w/A_f = 1.0, h/t_w = 150, b_f/t_f = 16.7, and t_w/t_f = 3. He explains that the above geometric parameters are close to average values of A_w/A_f = 1.3, h/t_w = 147, b_f/t_f = 17.2 and t_f/t_w = 3 determined from a survey conducted of 28 curved girder bridges. Furthermore, he restricted his studies for development of design equations to $0 \le L_b/R \le 0.1$, $L_b/b_f \le 25$, and $-0.5 \le \bar{f}_w / \bar{f}_b \le +0.5$.

2.1.2.1 Recommended Specification Compact Section Equations

McManus's resulting compact-section strength equations may be expressed as

$$\bar{f}_b \le F_{bs}\, \rho_{bc} \rho_{wc} \le F_{bs} \qquad (2\text{-}31)$$

where F_{bs} is the nominal vertical bending strength of the equivalent straight compression flange associated with inelastic lateral buckling, written in terms of the vertical bending stress $f_b = \bar{f}_b$. This strength is given by

$$F_{bs} = F_y\left[1 - 3\left(\frac{L_b}{b_f}\right)^2 \frac{F_y}{\pi^2 E}\right] \tag{2-32}$$

This is the traditional parabolic CRC inelastic column strength equation, which was in use for straight-girder design at the time of McManus's research. It should be noted that this equation is valid only for $F_{bs} \geq 0.5\ F_y$, i.e., for flanges in which the equivalent straight-girder capacity is limited by inelastic buckling; however, the potential of the flange being controlled by elastic lateral buckling is eliminated within the Recommended Specifications by a maximum limit on L_b/b_f of 25. If Eq. (2-32) is set equal to $0.5\ F_y$ and solved for L_b/b_f, we obtain $L_b/b_f = 30.9$ as the limit at which elastic lateral buckling would control the strength. The terms ρ_{bc} and ρ_{wc} are compact-section "strength reduction factors," which account explicitly for the effects of horizontal curvature and the applied end bimoments on the vertical bending strength, and account implicitly for the associated second-order elastic internal bimoments, radial bending moments, and amplified flange lateral bending moments due to cross-section distortion. McManus determined these factors by curve fitting to the strengths obtained from his parametric studies. The term ρ_{bc} in Eq. (2-31) is a correction factor that accounts for the effect of horizontal curvature in reducing the flange vertical bending strength *in the absence of any bimoment* at the ends of the girder unsupported length, i.e., $\overline{B} = 0$. This factor is specified as

$$\rho_{bc} = \frac{1}{1 + \frac{L_b}{b_f}\left(1 + \frac{L_b}{6b_f}\right)\left(\frac{L_b}{R} - 0.01\right)^2} \tag{2-33}$$

Finally, the term ρ_{wc} is a correction factor that accounts for the influence of the specified end bimoment $\overline{B}$, but expressed in terms of the ratio $\bar{f}_w / \bar{f}_b$. This term may be written as

$$\rho_{wc} = 0.95 + 18\left(0.1 - \frac{L_b}{R}\right)^2 + \frac{\bar{f}_w}{\bar{f}_b}\frac{\left(0.3 - 0.1\frac{L_b}{R}\frac{L_b}{b_f}\right)}{\rho_{bc}\frac{F_{bs}}{F_y}} \tag{2-34}$$

It should be noted that Eqs. (2-33) and (2-34) are expressed with respect to the terms L_b and b_f written in consistent units. The Recommended Specifications (Hall and Yoo 1998) include a conversion factor for the ratio L_b/b_f to convert L_b from feet to inches.

Also, it should be noted that Eq. (2-33) exhibits some minor anomalous behavior as L_b/R goes to zero. It is evident that this equation was intended to be applied for $L_b/R \geq 0.01$.

The proper calculation of $\bar{f}_w / \bar{f}_b$ for correlation with McManus's idealized girder configuration shown in Fig. 2.2.1 is clear. The value $\bar{f}_w / \bar{f}_b$ is the ratio of the end flange warping stress associated with the specified end bimoment $\bar{B}$ to the end vertical bending stress associated with the specified end moment $\bar{M}$. However, the meaning of the stress $\bar{f}_w$ in the context of the overall analysis of a curved bridge superstructure is somewhat ambiguous. McManus (1971) interprets $\bar{f}_w$ as the first-order lateral-bending stress in the compression flange, computed at the brace points (i.e., at the cross-frame locations) within the overall analysis of the bridge superstructure. However, Hall and Yoo (1998) assign a different meaning to this stress term. To understand the difficulty in the interpretation of $\bar{f}_w$ within the context of the analysis and design of a bridge, it is necessary to understand the details of McManus's approximate second-order elastic analysis procedure. However, before addressing this, it is useful to complete the discussion of McManus's strength predictor equations.

The Recommended Specifications utilize Eqs. (2-31) through (2-34), albeit with a different interpretation of $\bar{f}_w$ than adopted by McManus (1971). However, in the development of these specifications, it was recognized that in some cases Eq. (2-31) can exceed the theoretical plastic capacity of the compression flange in combined vertical and lateral bending, expressed in terms of the flange vertical bending force $\bar{P}_b = \bar{f}_b A_c$ and lateral bending moment $\bar{M}_w$, or the corresponding elastic stresses $\bar{f}_b$ and $\bar{f}_w$ (Hall et al. 1999). Therefore, Hall and Yoo (1998) require a separate check for this fully plastic flange force condition. This check is given by the simple equation

$$\bar{f}_b \leq F_y - \frac{1}{3}\left|\bar{f}_w\right| \tag{2-35}$$

and is referred to in this report as the compact-section based one-third rule. The basis for the one-third rule is discussed later in Section 2.1.8.

It should be noted that there are two basic reasons why Eq. (2-35) can be violated by Eq. (2-31): (1) Equation (2-31) is an approximate curve fit to McManus's parametric study results and (2) McManus assumed plastification of the *full* cross-section, not just the compression flange. Furthermore, one other subtlety regarding Eqs. (2-31) and (2-35) should be noted. Equation (2-31) implicitly accounts for an estimated second-order amplification of the member internal forces both at the ends of the unbraced length as well as at the middle of the unbraced length, and is based on full plastification at either of these locations, whichever is more critical as per McManus's second-order elastic solution. However, Eq. (2-31) focuses only on the cross-sections at the *ends* of the subject unsupported segment, and by the use of the stresses $\bar{f}_b$ and $\bar{f}_w$ – which the

Recommended Specifications specify as being determined based on a first-order analysis of the bridge superstructure – this equation does not account for any potential second-order amplification of the flange lateral bending moments at the cross-frame or mid-length locations.

2.1.2.2 Recommended Specification Noncompact Section Equations

For cross-sections that are defined as behaving noncompactly, McManus (1971) derived the following first-yield strength predictor equation

$$\bar{f}_b \le F_{bs}\rho_b\rho_\ell \tag{2-36}$$

where F_{bs} is the nominal vertical bending strength of the equivalent straight compression flange as previously defined by Eq. (2-32). The terms ρ_b and ρ_w are noncompact section strength reduction factors, which work similarly to the previously defined factors ρ_{bc} and ρ_{wc}, but are based on the reduction in the strength defined by the first-yield limit. In the above equation, the strength reduction *in the absence of any end bimoment*, i.e., for $\bar{B} = 0$, may be written as

$$\rho_b = \frac{1}{1+\frac{L_b}{R}\frac{L_b}{b_f}} \tag{2-37}$$

and the correction factor, which accounts for the specified end bimoment through the ratio $\bar{f}_w / \bar{f}_b$, may be expressed as

$$\rho_w = \min\left(\frac{1}{1-\frac{\bar{f}_w}{\bar{f}_b}\left(1-\frac{L_b}{75b_f}\right)}, \frac{0.95+\frac{\frac{L_b}{b_f}}{30+8000\left(0.1-\frac{L_b}{R}\right)^2}}{1+0.6\frac{\bar{f}_w}{\bar{f}_b}}\right) \tag{2-38a}$$

when $\bar{f}_w / \bar{f}_b \ge 0$ (i.e., compression due to $\bar{f}_w$ at the brace point compression flange tips furthest from the center of curvature), and as simply

$$\rho_w = \frac{1}{1 - \frac{\bar{f}_w}{\bar{f}_b}\left(1 - \frac{L_b}{75 b_f}\right)} \qquad (2\text{-}38b)$$

when $\bar{f}_w / \bar{f}_b$ is negative (i.e., compression due to $\bar{f}_w$ at the brace point compression flange tips closest to the center of curvature). Equation (2-37) is actually a simplification of McManus's original equation for ρ_b, specified in (Hall and Yoo 1998). McManus (1971) included an additional term in this equation that is for all practical purposes equal to 1.0 for $L_b/b_f \leq 25$. For $\bar{f}_w / \bar{f}_b = 0$, Eq. (2-38a) can potentially give a value less than one, but for all practical purposes, this equation equates to 1.0 for $\bar{f}_w / \bar{f}_b = 0$. Similar to the treatment in Eqs. (2-33) and (2-34), Eqs. (2-37) and (2-38) are expressed with respect to the terms L_b and b_f written in consistent units.

Equations (2-36) through (2-38) are employed within the Recommended Specifications (Hall and Yoo 1998), again with a different interpretation of $\bar{f}_w$ than adopted by McManus (1971). Furthermore, Hall et al. (1999) recognized in the development of these specifications that Eq. (2-36) could actually exceed a direct check of the cross-section first-yield strength based on the stresses $\bar{f}_b$ and $\bar{f}_w$ at the brace points. Also, for small L_b/R and L_b/b_f and negative $\bar{f}_w / \bar{f}_b$ (i.e., compression due to $\bar{f}_w$ at the brace point compression flange tips closest to the center of curvature), $\rho_b \rho_w$ can potentially be greater than one. Therefore, the Recommended Specifications limit the stress $\bar{f}_b$ to the value associated with first yield within the compression flange, based on the magnitude of $\bar{f}_w$, i.e.,

$$\bar{f}_b \leq F_y - \left|\bar{f}_w\right| \qquad (2\text{-}39)$$

Similar to the attributes discussed previously for Eq. (2-35), this equation focuses only on the cross-sections at the ends of the subject unbraced length, and by the use of the first-order stresses $\bar{f}_b$ and $\bar{f}_w$, it does not account for any potential second-order amplification of the flange lateral bending moments at the cross-frame or mid-length locations.

2.1.2.3 Trends in the Compact and Noncompact Section Predicted Strengths

It is important for the engineer to understand the trends in the predicted strengths specified by the compact section Eqs. (2-31) through (2-35) and by the noncompact section Eqs. (2-36) through (2-39) as a function of $\bar{f}_w / \bar{f}_b$. If $\bar{f}_w / \bar{f}_b$ is positive (i.e., compression due to $\bar{f}_w$ at the brace point compression flange tips furthest from the center of curvature), the compact section Eq. (2-31) predicts that the girder has a greater capacity with increasing $\bar{f}_w / \bar{f}_b$. However, for this situation, the noncompact section Eq. (2-36) can predict either an increase or a decrease in the girder capacity with increasing

$\bar{f}_w / \bar{f}_b$. Conversely, if $\bar{f}_w / \bar{f}_b$ is negative (i.e., compression due to $\bar{f}_w$ at the brace point compression flange tips closest to the center of curvature), the compact section Eq. (2-31) always predicts a decrease in the capacity with increasingly negative $\bar{f}_w / \bar{f}_b$, and the noncompact section Eq. (2-36) always predicts an increase in the capacity with increasingly negative $\bar{f}_w / \bar{f}_b$. This trend for noncompact sections is apparently due to the fact that the first yield, according to McManus's approximate second-order elastic calculations, is always delayed further by an increasingly negative $\bar{f}_w / \bar{f}_b$. The trend in the behavior of the compact section equations is more intuitive in that, if $\bar{f}_w / \bar{f}_b$ is positive, the compression flange lateral bending moment at the brace points ($\overline{M}_w$) counters the tendency of the flange to bend outward from the center of curvature, whereas if $\bar{f}_w / \bar{f}_b$ is negative, the moments $\overline{M}_w$ tend to bend the flange in the same direction of the flange displacements due to the horizontal curvature.

2.1.2.4 Recommended Specification Provisions for Singly-Symmetric I Sections

For unsymmetrical I girders, the Recommended Specifications require the compression flange width to be taken as $0.9b_f$ in Eq. (2-32). Hall et al (1999) explain that the factor 0.9 applied to the flange width was prescribed for singly symmetric sections in the AASHTO Specifications at the time of McManus's research, but was omitted in the Guide Specifications (AASHTO 1993). Therefore, Hall and Yoo (1998) decided to restore this factor in the Recommended Specifications. Furthermore, the Recommended Specifications specify a separate tension flange strength check to address singly symmetric girders. Since McManus focused on doubly symmetric sections, tension flanges were not specifically addressed in his research. This check is the combination of Eqs. (2-31) and (2-35), but with F_{bs} set to F_y. This is conservative for tensile $\bar{f}_b$ since the tension flange tends to straighten rather than increase in curvature.

2.1.2.5 Recommended Specification Design Limits

The Recommended Specifications specify the following limits of applicability for the above "modified McManus" design strength equations:

$$\bar{f}_w \leq 0.5\, F_y \tag{2.40a}$$

$$|\bar{f}_w / \bar{f}_b| \leq 0.5 \tag{2.40b}$$

$$L_b/b_f \leq 25 \tag{2.40c}$$

and

$$L_b/R \leq 0.1 \tag{2.40d}$$

2.1.2.6 Assessment of McManus's Approximate Second-Order Elastic Analysis Approach

As noted in the above discussions of McManus's compact and noncompact section strength predictor equations, the meaning of the stress term $\bar{f}_w$ in the context of the overall analysis of a curved bridge superstructure is somewhat ambiguous. McManus (1971) interprets $\bar{f}_w$ as the first-order lateral-bending stress in the compression flange, computed at the brace points (i.e., at the cross-frame locations) within the overall analysis of the bridge superstructure. However, Hall and Yoo (1998) assign a different meaning to this stress term. To understand the difficulty in the interpretation of $\bar{f}_w$ within the context of the analysis and design of a bridge, it is necessary to understand the details of McManus's approximate second-order elastic analysis procedure. This sub-section summarizes the essential attributes of McManus's second-order elastic analysis approach. The next sub-section then addresses the question of the appropriate calculation of $\bar{f}_w$ from a bridge analysis.

Given the girder shown in Fig. 2.1.13 with the applied end moments $\overline{M}$ and bimoments $\overline{B}$ as outlined in the above discussion, McManus calculates the vertical bending stress simply via Eq. (2-29) and assumes that this stress is constant along the length of the girder. However, he computes four separate contributions to the *second-order elastic* lateral bending stress ($f_{\ell 2}$) or the internal bending moment ($M_{\ell 2}$) within the compression flange in his approximate analysis procedure. The variation of each of these contributions along the length of the girder, at the compression flange tip furthest away from the center of curvature, is illustrated in Fig. 2.1.14.

McManus's four contributions to $f_{\ell 2}$ are:

1. The stress $f_{\ell 2\overline{M}}$ due to the bimoment induced by the vertical bending moment $\overline{M}$ and the effect of the horizontal curvature of the beam (see Fig. 2.1.14a). This stress and its associated bimoment are largest at the middle of the unbraced length and are equal to zero at the ends the member (based on the assumption of torsionally-simple end boundary conditions). McManus applies an approximate amplification factor AF (detailed below) to his computed first-order internal bimoments and the associated warping stresses to account for geometric nonlinear effects, i.e., to account for the effect of changes in the geometry, due to the applied loads, on the internal forces required for equilibrium. That is, we can write $f_{\ell 2\overline{M}} = AF\, f_{\ell 1\overline{M}}$, where $f_{\ell 1\overline{M}}$ is the first-order warping stresses calculated based on the internal bimoments determined by linear curved-beam theory for a simply-supported beam with the applied end vertical bending moments $\overline{M}$ and torsionally-simple end conditions.

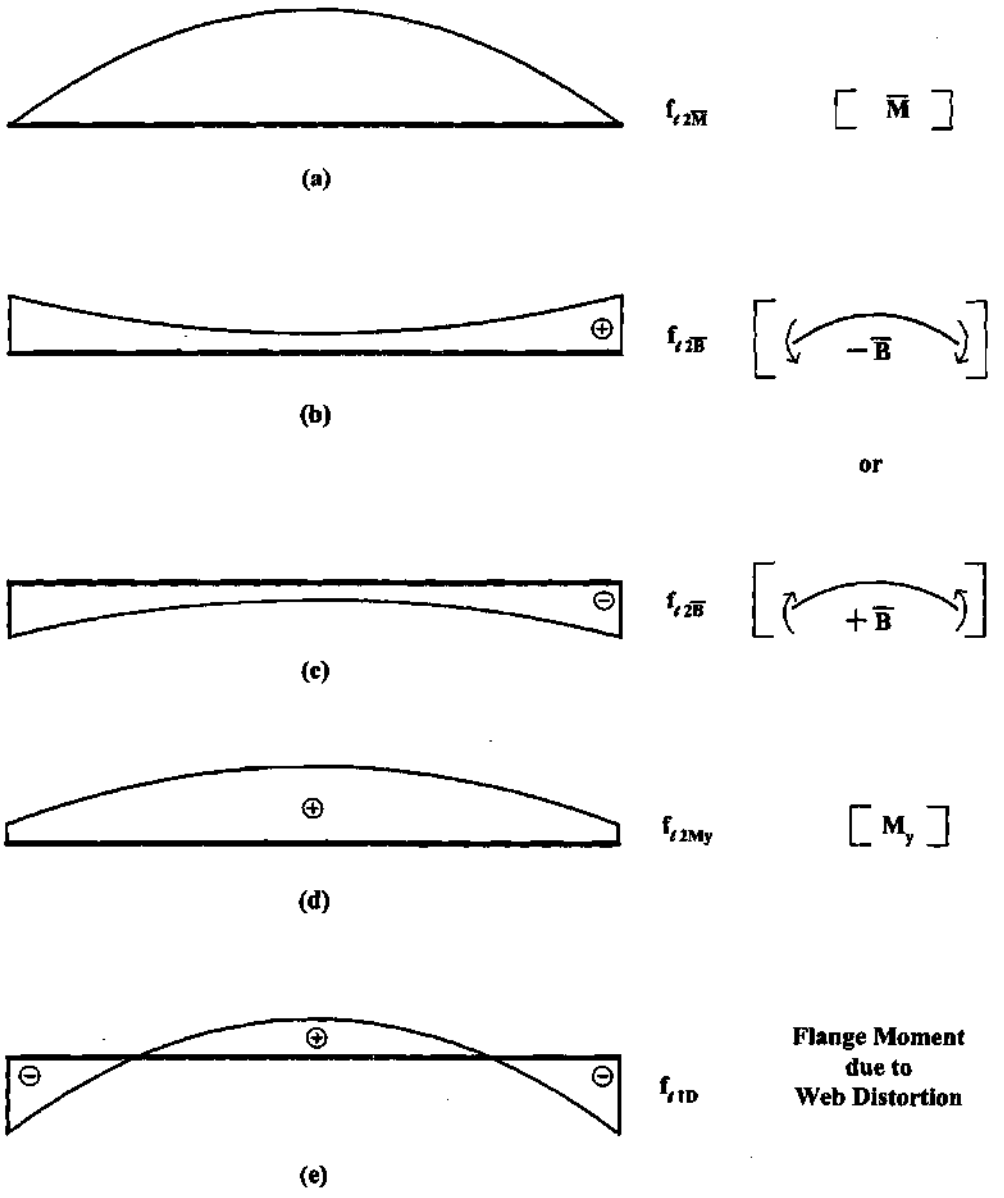

Figure 2.1.14. Variation of second-order elastic lateral bending stress contributions along the length of the girder at the compression flange tip furthest away from the center of curvature.

2. The stress $f_{\ell 2\bar{B}}$ due to the applied end bimoments (see Fig. 2.1.14b and c). By first-order curved-beam theory, these stresses are largest at the ends of the unbraced span and they are slightly smaller within the girder's unbraced length due to the effects of the horizontal curvature. McManus states that he also applies his amplification factor AF to these stresses, i.e., $f_{\ell 2\bar{B}} = AF\, f_{\ell 1\bar{B}}$. It is not apparent whether AF was applied only to the mid-span stresses or to both the mid-span stress and the stresses at the end of the beam. Application of AF to the stresses at the member ends is conservative, since $f_{\ell 2\bar{B}}$ should be equal to the specified $\bar{f}_w$ at the ends of the girder.

3. The stress $f_{\ell 2My}$ due to the internal second-order "radial bending" moment (see Fig. 2.1.14d). The radial bending moment is an internal moment about the vertical axis of the girder cross-section (M_y) caused by the internal vertical bending moment M acting through the twist of the girder plus the internal torque T acting through the girder rotation associated with vertical bending. This moment is approximated by McManus as

$$M_y = -M\,\phi_1 - T\,dv_1/dx \qquad (2\text{-}41)$$

where ϕ_1 is the first-order estimate of the girder twist, T is the internal torque, and v_1 is the first-order estimate of the vertical displacement at the cross-section under consideration. The stress $f_{\ell 2My}$ is largest at the middle of the unsupported length and is equal to $-\bar{T}\,d\bar{v}_1/dx$ at the girder ends, where the overbars indicate end values of the torque and of the slope due to vertical bending. McManus applies his amplification factor AF to the first term in Eq. (2-41), but not to the second term. Torsionally simple end conditions are assumed also in the calculation of these stresses.

4. The stress $f_{\ell 1D}$, which is McManus's (first-order) estimate of the increase in the lateral flange bending stress due to cross-section distortion, i.e., due to the potential lack of ability of the web to maintain its original straight shape within the cross-section profile. McManus uses the V-load equation (Eq. 1-6) to calculate this estimate at the member ends. The stress at the mid-span based on the simple V-load model is of opposite sign and has a magnitude equal to one-half of the magnitude of the corresponding stress at the member ends (see Fig. 2.1.14e). McManus does not apply his amplification factor AF to these stresses. It should be noted that McManus effectively assumes torsionally fixed end conditions for the calculation of $f_{\ell 1D}$.

The result of the above four contributions to the second-order elastic compression flange lateral bending stress are that, at the member ends, the computed lateral bending stress is

$$f_{\ell 2} = f_{\ell 2\bar{B}} + f_{\ell 2My} + f_{\ell 1D} \qquad (2\text{-}42a)$$

(since $f_{\ell 2\overline{M}}$ in McManus's calculations is equal to zero at the member ends) whereas at the middle of the unsupported length,

$$f_{\ell 2} = f_{\ell 2\overline{M}} + f_{\ell 2\overline{B}} + f_{\ell 2My} + f_{\ell 1D} \qquad (2\text{-}42b)$$

It should be noted that at the member ends, the stress contributions $f_{\ell 2\overline{B}}$ and $f_{\ell 1D}$ are of opposite sign if $\bar{f}_w / \bar{f}_b$ is negative (i.e., compression due $\bar{f}_w$ at the brace point compression flange tips closest to the center of curvature), but that they are additive if $\bar{f}_w / \bar{f}_b$ is positive. The contribution $f_{\ell 2My}$ is always opposite to $f_{\ell 1D}$ at the member ends. Furthermore, at the middle of the unsupported length, all the contributions are additive, unless $\bar{f}_w / \bar{f}_b$ is positive, in which case $f_{\ell 2\overline{B}}$ is opposite in sign to the other stresses. Equations (2-42) and the above descriptions also can be stated in the form of the second-order internal flange lateral bending moment $M_{\ell 2}$.

It is inconsistent to calculate the stress contribution $f_{\ell 1D}$ based on the assumption of end fixity while the other stress contributions are calculated based on torsionally simple end conditions. McManus appears to acknowledge this when he states that his estimate of $f_{\ell 1D}$ is intended to be conservative. Upon close inspection of McManus's procedure, it is apparent that by including both $f_{\ell 2\overline{M}}$ and $f_{\ell 1D}$ in his calculation of the lateral bending stress (or the flange lateral bending moment) at the middle of the girder unbraced length, McManus is indeed double counting the action of the end moments $\overline{M}$ on the curved beam. The stress $f_{\ell 2\overline{M}}$ is due to the torsion induced by the horizontal curvature and the application of $\overline{M}$ as per curved beam theory, and the stress $f_{\ell 1D}$ is due to the same effect but is an estimate based on the assumption that the torsion is effectively taken entirely by lateral bending in the flanges. However, $f_{\ell 2\overline{M}}$ is the beam-theory based stress that occurs on a simply-supported span, whereas $f_{\ell 1D}$ is actually just a first-order V-load method estimate of the stress on a span in which torsionally-fixed or symmetry boundary conditions are assumed at the brace locations. As a result, McManus effectively obtains a first-order estimate of the lateral bending stress at the brace points due to $\overline{M}$ based on a model with torsionally-fixed end conditions (since the stress $f_{\ell 2\overline{M}}$ is zero at the member ends), and a significantly over-estimated (double-counted) estimate of the lateral bending stress at the mid-span of his model.

Furthermore, by assuming torsionally-simple end conditions in calculating $f_{\ell 2\overline{M}}$, $f_{\ell 2\overline{B}}$ and $f_{\ell 2My}$, McManus's mid-span lateral bending stresses are significantly higher than they would be if the end restraint from adjacent segments of an internal unsupported length of a curved bridge I girder were considered. In fact, the maximum $f_{\ell 1\overline{M}}$ stress associated with torsionally-fixed or symmetric boundary conditions by beam theory is approximately three times smaller than the value calculated based on torsionally-simple end conditions. Therefore, it can be argued that in some cases McManus could be as

much as quadruple counting in his calculation of the lateral bending stress due to torsion at the middle of the unsupported length. Of course, it is important to consider the various potential boundary conditions (force and/or displacement) that may exist at the ends of an arbitrary unsupported segment within a curved bridge I girder. However, in the view of the authors, the nature of McManus's calculations is much too approximate and conservative to provide a reasonable representation of reality. Hall et al. (1999) observe a number of anomalies that are produced by these approximations in Fig. B-1 of their report.

In addition to the calculation of his first-order stress contributions $f_{\ell 2\overline{M}}$, $f_{\ell 2\overline{B}}$ and $f_{\ell 2My}$ based on torsionally simple end conditions, McManus derives his amplification factor AF also based on these conditions. McManus's amplification factor is

$$AF = \frac{1 - 0.86\frac{M}{M_{cr}} + 0.4\left(\frac{M}{M_{cr}}\right)^2}{1 - \frac{M}{M_{cr}}} \qquad (2\text{-}43)$$

where $M_{cr} = F_e S_{xc}$ is the elastic buckling moment determined based on Eq. (2-15). McManus determines this equation by curve fitting to the results of more rigorous, but still approximate, second-order beam-theory solutions that he develops within the early portions of his thesis. Due to the effects of continuity between adjacent unbraced lengths, and due to the tendency of the compression flange to bend outward from the center of curvature within each segment, the amplification of the lateral flange moments and stresses would tend to be smaller in nearly all practical design situations.

2.1.2.7 Interpretation of $\bar{f}_w$ and Assessment of Implications on Predicted Strengths

It should be noted that based on the calculations summarized in the previous sub-section, McManus's estimated second-order elastic lateral flange bending stress at the member ends, given by Eq. (2-42a), is incompatible with his specified flange end warping stress $\bar{f}_w$. Equivalently, his estimated internal flange lateral bending moment $M_{\ell 2}$ at the member ends is different than the specified end flange moment $\overline{M}_w$ (see Eq. (2-30)). This leads to some difficulty in interpreting how $\bar{f}_w$ should be determined from the results of a first-order analysis of a bridge superstructure. McManus (1971) interprets that $\bar{f}_w$ is the calculated flange lateral bending stress at the cross-frame locations from a first-order bridge analysis. However, in recognizing that McManus's approximate analysis calculations involve some double counting, Hall et al. (1999) state that $\bar{f}_w$ (denoted by f_m in their report and in the Recommended Specifications) should be the actual calculated lateral bending stress at the bracing locations from the bridge analysis, minus the contribution to this stress due to the horizontal curvature. This conclusion is logical in the sense that it can be argued that the first-order lateral bending

stress due to the end moments $\overline{M}$ is estimated reasonably well by the V-load equation for internal unbraced lengths of girders subjected approximately to uniform bending, and in which the brace spacing is approximately uniform along the full girder length. Therefore, if (1) the stress contribution $f_{\ell 2My}$ at the member ends is ignored, (2) it is assumed that $f_{\ell 2\overline{B}} = \bar{f}_w$, and (3) it is recognized that McManus's calculated value of $f_{\ell 1D}$ at the member ends is the lateral bending stress from the V-load equation, then Eq. (2-42a) can be re-written as

$$\bar{f}_w = f_{\ell 2} - f_{\ell 1D} \tag{2-44}$$

If we then assume that $f_{\ell 2}$ is approximated sufficiently based on the lateral flange bending moment determined at the brace points within a first-order analysis of the bridge superstructure, we arrive at the procedure that Hall and Yoo (1998) propose for calculation of $\bar{f}_w$ (denoted as f_m within the Recommended Specifications and in (Hall et al. 1999)).

Hall et al. (1999) state that the above interpretation of $\bar{f}_w$ leads to an improved prediction of the ultimate strength of curved test specimens. However, Tables B-5 and B-7, and Tables B-6 and B-8, of their report show that the predictions of the compact-section equations of the Recommended Specifications are actually made worse by the use of this interpretation compared to the use of McManus's original interpretation. The results using the noncompact section equations of the Recommended Specifications are slightly improved; however, the average ratio of the predicted and the test strengths (M_n/M_{test}) is 0.49 with a standard deviation of 0.18.

Even for the test girders considered that have b_f/t_f values above 20, the average reported M_n/M_{test}, using the noncompact section equations, is 0.57 with a standard deviation of 0.10 (Hall et al. 1999). For these same girders, the compact section equations with McManus's original interpretation of $\bar{f}_w$ give an average M_n/M_{test} of 0.98 with a standard deviation of 0.06. It is likely that McManus's conservative calculation of the girder internal forces compensates for the unconservative nature of assuming compact section behavior for these test girders. The Mozer-Culver test girders evaluated by Hall et al. (1999) and the implications of the different interpretations of $\bar{f}_w$ with respect to the Recommended Specification equations are studied further in Chapters IV and VII of this report.

2.1.2.8 Compact and Noncompact Classification of Cross-Sections

The Recommended Specifications (Hall and Yoo 1998) utilize McManus's compact-section equations for I girders with $b_f/2t_f \leq 9$. This limit is liberalized from the corresponding limit suggested by McManus (1971) and specified in the Guide Specifications (AASHTO 1993) of

$$\frac{b_f}{2t_f} \le 0.297\sqrt{\frac{E}{F_y}} \qquad (2\text{-}45)$$

which gives a value of 7.15 for F_y = 345 MPa (50 ksi). Equation (2-45) is the traditional plastic design flange-slenderness limit for I sections, which theoretically permits inelastic flange deformation in flexure up to the onset of strain-hardening in straight beams (i.e., inelastic rotations in vertical bending of straight beams and girders with compact webs of approximately 10 to 15 times the yield rotation (ASCE/WRC 1971, Salmon and Johnson 1996)) prior to loss of strength due to local buckling. Culver and Nasir (1971) studied the behavior of curved I girder flanges analytically, and concluded that the influence of curvature is small for $1 \times 10^6 < b_f/R < 0.01$. Based on the requirement that full yielding of the compression flange is necessary, such that flange strength equations which do not account for the effects of local flange buckling can be utilized, they recommended that the flange slenderness limits would need to be similar to those required for traditional plastic design. However, they suggest that if the flange stresses are limited, more liberal flange slenderness limits might be utilized.

The new b_f/t_f limit specified in the Recommended Specifications corresponds approximately to the compact flange slenderness limit in the AASHTO LRFD straight-girder Specifications (2001) given by Eq. (2-5) (for F_{yc} = 345 MPa). Equation (2-5) is based largely on the straight I-beam research by Lukey and Adams (1969). Lukey and Adams (1969) showed that I sections that satisfy this limit, and which also satisfy certain limits on the web slenderness and lateral brace spacing are able to develop a rotation capacity

$$R_{ult} = \frac{\theta_{ult}}{\theta_e} - 1 \qquad (2\text{-}46)$$

of three, where θ_{ult} is defined as the maximum total rotation at which the resisting moment decreases back to the plastic moment M_p on the descending portion of the moment-rotation curve, and θ_e is the total rotation at which a line extended through the linear-elastic portion of the curve intersects the M_p ordinate. Barth et al. (2000) review this and other plastic design slenderness limits that have been developed in prior research. Although the traditional plastic design flange slenderness limits include consideration of members subjected to uniform moment, the Lukey and Adams (1969) studies focus entirely on beams subjected to moment gradient. The implications of more liberal flange compactness limits, such as that of Eq. (2-5) need to be better understood for I girders subjected to uniform bending, particularly for curved I girders, which in the region near the middle of an unsupported length may be subjected to both near uniform vertical bending as well as lateral flange bending moments (Hall 2000b). Both the strength and the post-peak unloading characteristics of I girders with various flange slenderness values need to be investigated. These issues are addressed further in this report within Chapters IV and VI.

Nevertheless, it is clear from evaluation of the predictions by McManus's noncompact section equations versus test results, such as that conducted by Hall et al. (1999), that there is no sudden dramatic drop in the girder flexural strength when the flange slenderness is increased beyond a certain compactness limit, regardless of what that limit is.

The Recommended Specifications (Hall and Yoo 1998) utilize McManus's noncompact section equations for girders with

$$18 < \frac{b_f}{t_f} \le 1.02\sqrt{\frac{E}{(\bar{f}_b + \bar{f}_w)}} \le 23 \qquad \text{(2-47a)}$$

The third term in this expression is based on the compactness limit of

$$\frac{b_f}{2t_f} \le \left(0.951\sqrt{\frac{Ek_c}{F_y\left(\frac{F_e}{F_y}\right)}} = 0.557\sqrt{\frac{E}{F_y}} = \frac{95}{\sqrt{F_y}} \right) \quad \text{for } F_y \text{ in units of ksi} \qquad \text{(2-47b)}$$

with $k_c = 0.70$ and $(F_y/F_e) = 0.49$. This limit is required in (AISC 1999) for flanges of general I-shaped sections to be able to develop the yield stress F_y in uniform compression. The third term in Eq. (2-47a) is obtained by replacing F_y by $\bar{f}_b + \bar{f}_w$ in Eq. (2-47b) and by factoring this equation by approximately 0.9. The 0.9 factor is consistent with the traditional practice in AASHTO of setting slenderness limits 10 percent smaller than the corresponding AISC limits.

Equation (2-5) is a more rational limit than Eq. (2-47b) for ensuring that the flanges can develop their yield strength F_y in uniform compression prior to significant local buckling. A similar compact flange limit that explicitly includes an estimate of the effect of the web on the flange stability can be obtained by setting $F_L = 2F_y$ in Eq. (2-6), which gives

$$\frac{b_f}{2t_f} \le 1.34\sqrt{\frac{E}{F_y\sqrt{\frac{2D_c}{t_w}}}} \qquad \text{(2-47c)}$$

Equations (2-5) and (2-47c) are the same at a web slenderness, $2D_c/t_w$, of 150.

If it is desired for the flange to be able to develop uniform compression at a stress less than F_y, then Eqs. (2-2) and (2-9) are a more rational means of achieving this goal (see

Figs. 2.1.1 and 2.1.2 and the discussion regarding the current AASHTO LRFD (2001) flange local buckling strength equations in Section 2.1.1.2).

Of course, the compression flange of a curved I girder is subjected to both vertical and lateral bending stresses. In other words, the compression flange generally has a gradient in the longitudinal normal stress and the longitudinal normal strain across its width. Based on established research on compactness limits and deformation capacity of plates (ASCE/WRC 1971; Salmon and Johnson 1996; SSRC 1998), it is expected that the existence of such a gradient across the flange width is beneficial to the strength and deformation capacity. That is, since the stress $\bar{f}_b + \bar{f}_w$ at elastic buckling of the flange plate is increased as $\bar{f}_w$ is increased, it is expected that the longitudinal strain at the flange tip at the onset of significant inelastic local buckling, due to vertical and lateral bending, is increased with larger $\bar{f}_w$. However, the elastic vertical bending stress $\bar{f}_b$, i.e., the elastic stress at the web flange juncture, is reduced due to the existence of lateral bending stresses $\bar{f}_w$, and correspondingly, the vertical bending moment and any inelastic vertical bending deformations at the onset of significant inelastic local buckling of the compression flange are expected to be reduced due to increased lateral bending. It is expected that the third term in Eq. (2-47a) accounts for this detrimental effect conservatively, since it applies the traditional limit of Eq. (2-47b) as discussed above based on the maximum flange tip compression $\bar{f}_b + \bar{f}_w$, as if the flange were subjected to uniform axial compression at this value of the elastic stress. Furthermore, some benefit is expected due to the reduced compression and potential elastic unloading within the flange on the opposite side of the web from the peak compression. Section 2.1.9.3 reviews several methods that have been proposed to account for the stress gradient across the flange width, due to lateral flange bending, on the elastic buckling capacity of the compression flange, expressed in terms of the vertical bending stress $\bar{f}_b$.

The limit of 23 on b_f/t_f in Eq. (2-47a) is based on experimental observations by Mozer et al. (1970) and analytical observations by Culver and Nasir (1971). Culver and Nasir (1971) observed that flange local buckling starts to have a significant detrimental effect on the strength in the vicinity of this limit. Mozer et al. (1970) tested two heat-curved and two cut-curved I girders with $b_f/t_f = 23$, and concluded that this limit was adequate if both vertical bending and lateral flange bending stresses are considered and the capacity is limited to initial yielding at the flange tips. The ratio $b_f/t_f = 23$ was the approximate limit within the AASHTO straight-girder specifications for $F_y = 250$ MPa (36 ksi) in effect at the time of Mozer's research.

The current AASHTO LRFD (2001) Specifications limit b_f/t_f to a maximum value of 24 "to avoid potential excessive distortion of the flange due to welding." Also, this limit may help to prevent damage to the flange during construction operations. This research investigates the implications of extending the b_f/t_f limit for curved girders up to the current maximum straight-girder limit.

2.1.2.9 Web Stress Limits

Hall et al. (1999) evaluated the prior research on fatigue of curved I-girder webs, and concluded that fatigue problems do not occur if the web stresses are maintained below the elastic buckling strength (Hall 2000). There is precedent for limiting the web stresses to the elastic buckling stress to avoid fatigue issues in straight I girder webs (Patterson et al. 1970, Galambos et al. 1977, Fisher et al. 1979, Montgomery 1987, and Nowak et al. 1993). The theoretical web elastic bend buckling stress can be expressed as

$$f_{bw} \le \left[\frac{\pi^2 Ek}{12(1-\nu^2)\left(\frac{D}{t_w}\right)^2} = \frac{0.9Ek}{\left(\frac{D}{t_w}\right)^2} \right] \le F_y \tag{2-48}$$

where

$$k = 7.2\left(\frac{D}{D_c}\right)^2 \ge 7.2 \tag{2-49}$$

for unstiffened webs and

$$k = 9\left(\frac{D}{D_c}\right)^2 \ge 7.2 \tag{2-50}$$

for stiffened web panels. Also, the Recommended Specifications require $d_o/D \le 1$ for a panel to be defined as stiffened. The multiplier 7.2 in Eq. (2-49) results in a bend-buckling coefficient of 28.8 for doubly symmetric girders. This is close to the theoretical value of k = 24 for webs with $D_c = D/2$ and simply supported boundary conditions on their longitudinal edges. The multiplier 9 in Eq. (2-50) gives a k of 36 for a doubly symmetric girder, which is approximately 80 percent of the difference between the buckling coefficient for simply supported and fully restrained longitudinal edge conditions. Equation (2-49) is used implicitly in the current AASHTO LRFD (2001) Specifications for representation of the bend-buckling resistance within the load-shedding parameter R_b for sections with $D_c > D/2$, and Eq. (2-50) gives the bend-buckling coefficient implicitly used within R_b for sections with $D_c \le D/2$. Hall et al. (1999) explain that the smaller bend-buckling coefficient is used for unstiffened webs in the Recommended Specifications to account conservatively for potential moment-shear interaction effects. Also, they explain that the more liberal value is utilized for stiffened web panels since the reserve postbuckling strength of the panel in bending and in shear is currently ignored. The lower limit of 7.2 on the value of k is approximately equal to the theoretical buckling coefficient for a web plate under uniform compression assuming clamped boundary conditions at the flanges (SSRC 1998).

Daniels and Herbein (1980) conducted the most recent experimental research regarding fatigue of curved steel I girder bridge elements. Based on this research, the following equation was proposed for load factor design (Daniels et al. 1980):

$$\frac{D}{t_w} = 6.78\sqrt{\frac{E}{F_y}}\left[1 - 4\frac{d_o}{R}\right] \leq 192 \qquad (2\text{-}51)$$

If the web strength provisions in the Recommended Specifications are liberalized, this equation, or a modified form of this equation based on new investigations, might be adopted to address fatigue issues. If Eq. (2-51) were adopted directly, the result is that the web slenderness D/t_w would be restricted significantly relative to the requirements for strength. Alternately, it may be possible to avoid fatigue issues by restricting the web stresses to the elastic buckling stress only under fatigue loading conditions, at least up to some horizontal curvature limit. However, this type of limit would be significantly more liberal than the Daniels equation or the approach of the Recommended Specifications. It should be noted that the Recommended Specifications currently restrict the web stresses to the elastic buckling stress under all loading conditions. Both shear and bend buckling would likely need to be considered if fatigue issues were to be controlled based on an elastic buckling limit under fatigue loading conditions only. However, it is expected that moment-shear interaction would not need to be addressed in the calculation of web buckling if the current buckling coefficients for both shear and bending are employed. This is because the current AASHTO shear buckling equations are based on the assumption of simply supported boundary conditions at the web-flange juncture.

The current AASHTO LRFD (2001) Specifications limit the web stresses in straight I-girders under fatigue loading conditions to the elastic bend buckling stress. The Recommended Specifications require that the web stresses should be maintained below the bend-buckling stress for all loading conditions. The Recommended Specifications also restrict the web slenderness D/t_w of unstiffened girders (i.e., girders with $d_o/D > 1$) to 100 for $R \leq 213.5$ m (700 ft) and 150 for $R \geq 610$ m (2000 ft), with a linear transition in D/t_w between these limits. The $D/t_w \leq 150$ limit is the maximum slenderness specified to facilitate the handling of straight girders with unstiffened webs in (AASHTO 2001). The Recommended Specifications do not place any other limit on the web slenderness for transversely stiffened webs, but d_o/D is limited to a maximum value of one for these types of girders.

For $d_o/D \leq 1$, the limit on D/t_w based on Eq. (2-48), applied to all loading conditions, is typically more restrictive than the Daniels et al. (1979) equation (Eq. 2-51). However, for $d_o/D > 1$, the Daniels et al. equation can be more restrictive than the Recommended Specification limits on D/t_w. The reader can verify these observations by assuming $f_{bw} = F_y$ under the maximum strength loading conditions along with Eq. (2-48), and comparing the result to Eq. (2-51).

2.1.2.10 Summary

In summary, the flexural strength predictor equations in the Recommended Specifications (Hall and Yoo 1998) have the following limitations:

- They are incompatible with current AASHTO straight-girder design equations, that is, they do not reduce to the current AASHTO straight-girder equations in the limit that the radius of curvature goes to infinity.

- They exhibit some minor anomalies as the radius of curvature approaches infinity.

- They predict a significant discontinuity in the flexural strength of sections depending on whether the compression flange is classified as compact or noncompact.

- Although they are believed to be adequate and safe for design of unsymmetrical noncomposite and composite girders, they are based predominantly on research directed only at doubly symmetric noncomposite steel I girders. The modifications to the base formulas aimed at addressing the strength of singly symmetric sections are simple and ad hoc. It is likely that the strength of unsymmetric curved I girders can be quantified in a simple but more rigorous fashion.

- They focus only on the flexural strength of girders subjected to uniform vertical bending along their unbraced lengths; the potentially significant increases in flexural strength due to moment gradient for girders with intermediate to large unsupported lengths are not accounted for.

- They do not separate the analysis problem, i.e., the estimation of internal moments or stresses, from the statement of the design resistance; as a result, these equations depend on a combination of several strength reduction factors that are difficult to understand and properly apply.

- The above mentioned strength reduction factors are based on approximate second-order elastic analyses, which at the time of their development required quite innovative research, but which involve a number of approximations that lead to significantly over-conservative estimates of the true second-order elastic stresses.

- They restrict the web flexural stresses to the elastic bend buckling stress under all loading conditions. This restriction may not be necessary when checking the maximum strength limit state.

Therefore, it is worthwhile to investigate alternative approaches that can alleviate these shortcomings.

2.1.3 Fukumoto and Nishida's Equation

Fukumoto and Nishida (1981) established a second-order elastic analysis solution based on beam theory for simply-supported horizontally-curved I beams subjected to three loading conditions: (1) equal and opposite vertical end bending moment, (2) a mid-span concentrated transverse vertical load, i.e., a three-point bending test configuration, and (3) a uniformly distributed transverse loading. Torsionally simple boundary conditions were assumed at the ends of the beams, and rigid lateral (radial) supports were provided only at the ends. No end bimoments or flange lateral bending moments were applied. Fukumoto and Nishida (1981) also determined a second-order rigid-plastic strength curve for these types of beams, based on the assumption of fully-plastic compact section behavior under combined internal vertical bending moment, radial bending moment, and bimoment. They then derived an equation for the strength of their beams by determining the point of intersection of the second-order elastic and second-order rigid-plastic solutions. The effect of load height was not included within their formulation. The resulting flexural strength predictor equation may be written as

$$\left(\frac{M_p}{M_e}\right)^2\left(\frac{M_n}{M_p}\right)^4-\left\{\left[1+\frac{P_e(d-t_f)}{4M_p}\frac{L_b}{R}\frac{L_b}{b_f}\right]\left(\frac{M_p}{M_e}\right)^2+1\right\}\left(\frac{M_n}{M_p}\right)^2-\frac{1}{2}\frac{L_b}{R}\frac{L_b}{b_f}\left(\frac{M_n}{M_p}\right)+1=0 \tag{2-52}$$

where

$$P_e = \pi^2 EI_y/L_b^2 \tag{2-53}$$

$$M_e=\sqrt{\left[\left(1-\frac{1}{\pi^2}\left(\frac{L_b}{R}\right)^2\right)\left(\frac{\pi^2 EI_y}{L_b^{\,2}}\right)\left(GJ+\frac{\pi^2 EC_w}{L_b^{\,2}}\right)\right]} \tag{2-54}$$

M_p is the plastic vertical bending capacity of the section, and M_n is the nominal moment capacity. It can be observed that Eq. (2-54) is the fundamental elastic lateral-torsional buckling strength equation with the modifier $1-(L_b/\pi R)^2$, which accounts for the effect of the horizontal curvature on the buckling strength. For practical values of $L_b/R \leq 0.1$, this modifier is effectively equal to 1.0.

Fukumoto et al. (1980) verified Eq. (2-52) against the results of experimental tests. This equation is useful for predicting the strength of compact section I-beams with torsionally simple end conditions. However, it is rare for bridge I girders to be laterally unsupported over the entire length of the bridge, and it is desirable to consider the potential benefits of continuity with adjacent unsupported lengths. Furthermore, Fukumoto and Nishida's equation is limited in that it does not address the potential reduction in strength due to inelastic lateral or local instability of the compression flange (which involves significant influence from residual stress effects and distributed yielding

through the cross-section and along the member length). This limitation can be important for typical unsupported lengths utilized in curved I girder bridges. Also, Fukumoto and Nishida do not consider the influence of load shedding from a thin web on the girder response. Therefore, Eq. (2-52) is not considered further in the current research.

2.1.4 Simpson's Method

Simpson (2000) proposed an improved and simplified (closed-form) expression for the strength of curved doubly symmetric I girders based on Fukumoto and Nishida's fundamental approach. He focused on the case of a simply supported beam subjected to pure vertical bending in his base equation development. Twisting is prevented at the member ends, but the section is free to warp at these locations. Simpson explained that he computes the flange lateral bending moment as the summation of three components: 1) that caused by warping (due to bimoment induced by the vertical bending acting through the horizontal curvature of the beam); 2) that caused by the applied vertical bending moment acting through the deflected (twisted) geometry; and 3) that caused by the internal moment about the vertical axis of the girder cross-section (M_y) induced by lateral bending of the beam. He solved the governing differential equations of the uniform vertical bending problem considered by Fukumoto and Nishida (1981) to obtain the second-order elastic responses. Based on this solution, the maximum lateral bending moment in the compression flange (M_f) can be written as

$$M_f = \left(\frac{EC_w}{D}+\frac{M}{2}\right)\left(\frac{U_0\frac{P_e}{M_p}\left(\frac{M_n}{M_p}\right)\left(\frac{M_p}{M_e}\right)^4}{1-\left(\frac{M_n}{M_p}\right)^2\left(\frac{M_p}{M_e}\right)^4}\right)+\frac{P_e}{2}\left(\frac{U_0\left(\frac{M_n}{M_p}\right)^2\left(\frac{M_p}{M_e}\right)^4}{1-\left(\frac{M_n}{M_p}\right)^2\left(\frac{M_p}{M_e}\right)^4}\right) \tag{2-55}$$

where D is the depth of the web, M is the applied vertical bending moment,

$$U_0 = \frac{L_b}{R}\frac{L_b}{b_{fc}} \tag{2-56}$$

P_e is the elastic flexural buckling capacity of the cross-section defined in Eq. (2-52), M_p is the plastic bending capacity of the cross-section, M_n is the vertical bending strength (to be determined), and M_e is the elastic lateral-torsional buckling capacity given by Eq. (2-54), except that Fukumoto's modifier that accounts for the effect of the horizontal curvature on the buckling strength is not included by Simpson.

Simpson derived the following relationship to define the plastic flange lateral bending capacity (M_{nf}) as a function of plastic vertical bending capacity of the beam (M_p) and the applied vertical bending moment (M):

$$M_{n\ell} = \frac{b_{fc}}{4M_p D}\left(M_p{}^2 + M^2\right) \tag{2-57}$$

By equating Eqs. (2-55) and (2-57), and taking $M = M_n$, Simpson obtained the following expression, which can be solved to obtain the vertical bending strength M_n:

$$\left(\frac{M_p}{M_e}\right)^4\left(\frac{M_n}{M_p}\right)^4 - \left\{\left[1+\left(\frac{M_p}{M_e}\right)^4 + \frac{4D}{b_{fc}}\beta\right]\left(\frac{M_p}{M_e}\right)^2\right\} - \left(\frac{4EC_w\pi^2}{M_p b_{fc} L_b{}^2}\beta\right)\left(\frac{M_n}{M_p}\right)^2 + 1 = 0 \tag{2-58}$$

where

$$\beta = \frac{U_0 P_e}{M_p}\left(\frac{M_p}{M_e}\right)^4 \tag{2-59}$$

Simpson then simplified Eq. (2-58) by neglecting the St. Venant torsional stiffness (i.e., assuming $J = 0$) such that he can write

$$M_e = \frac{\pi^2 E I_y h}{2L_b{}^2} \tag{2-60}$$

where h is the distance between the centerline of the flanges,

$$\frac{M_p}{M_e} = \left(\frac{12F_y}{\pi^2 E}\left(\frac{L_b}{b_{fc}}\right)^2\right)^2 \tag{2-61}$$

and

$$\beta = \frac{24U_0\left(\frac{M_p}{M_e}\right)}{\kappa h} \tag{2-62}$$

The term κ in Eq. (2-62) is a slenderness parameter, and can be written as

$$\kappa = \frac{F_y}{\pi^2 E}\left(\frac{L_b}{b_{fc}}\right)^2 \tag{2-63}$$

By substituting Eqs. (2-60) through (2-63) into Eq. (2-58), a simplified form of Simpson's equation is obtained as (Simpson 2000):

$$144\kappa^2\left(\frac{M_n}{M_p}\right)^4 - \left[1 + 144\kappa^2 + 96\chi\kappa\right]\left(\frac{M_n}{M_p}\right)^2 - 4\chi\left(\frac{M_n}{M_p}\right) + 1 = 0 \qquad (2\text{-}64)$$

where

$$\chi = \frac{1}{8}\frac{L_b}{R}\frac{L_b}{b_{fc}} \qquad (2\text{-}65)$$

Simpson (2000) applied a nonlinear regression analysis to Eq. (2-64), to further simplify this equation to the following form that can be used to compute the vertical bending capacity directly:

$$\frac{M_n}{M_p} = (1 + \kappa^{c_1})^{c_2} + c_3 \qquad (2\text{-}66)$$

where

$$c_1 = 0.0164\ln^3(\chi) + 0.1957\ln^2(\chi) + 0.2061\ln(\chi) + 0.6996 \qquad (2\text{-}67)$$

$$c_2 = (1.312\chi^2 - 1.767\chi - 0.00547)^{-1} \qquad (2\text{-}68)$$

$$c_3 = 2.125\chi + 0.00253 \qquad (2\text{-}69)$$

Simpson (2000) states that the form of Eq. (2-66) was chosen because it resembles the column curve formula of CSA- S16.1 (1994) and because it is also suited for spreadsheet analysis.

The design limits of Eq. (2-66) are specified by Simpson (2000) as:

$$0 \le \kappa \le 0.15 \qquad (2\text{-}70a)$$

$$0 \le \chi \le 0.5 \qquad (2\text{-}70b)$$

$$L_b/b_f \le 25 \qquad (2\text{-}70c)$$

and

$$L_b/R \le 0.10 \qquad (2\text{-}70d)$$

It can be observed that Eqs. (2-70c and d) effectively prevent the limit of Eq. (2-70b) from being violated. That is, Eq. (2-70b) is redundant.

The above equations are developed based on the analysis of a simply supported beam subjected to uniform vertical bending. However, an internal segment within a curved bridge does not have this boundary condition. The warping restraint due to continuity with adjacent unbraced segments causes a flange moment to develop at the ends of the unsupported length. To account for this behavior, Simpson (2000) suggested that, in the calculation of the vertical bending strength, an approximate effective length of $L_{eff} = 0.6L_b$, should be used instead of the full unsupported length. Simpson explained his rationale for this decision as follows:

> **"Nakai showed that when a girder is changed from straight to curved, the lateral buckling mode changes from serpentine in shape to that resembling a fixed-fixed beam. A similar approach is considered here. If a girder's flange[s] are fixed against warping and the girder is subjected to a constant moment, the lateral flange bending moments distribute in the manner of the moments in a fixed-fixed beam subjected to a uniform load. Within the unbraced length, two points of inflection occur with respect to lateral bending. Between these two inflection points, the girder is loaded as assumed in the Fukumoto and Nishida, and Simpson equations, i.e., the strong axis bending moment is constant along the length of the beam and the end bimoments are equal to zero. Therefore, rather than use the entire beam length for the estimate of strength, the length between the points of inflection is used. For a fixed-fixed condition the distance between the points of inflection is equal to 0.577L, but for simplicity an approximate effective length, $L_{eff} = 0.6L_b$ has been adopted."**

It should be noted that the correct effective length for a girder in which warping is fully restrained at its ends is $0.5L_b$. Although Simpson's developments provide significant improvements with respect to the ease of use and technical rigor of the original approach taken by Fukumoto and Nishida (1981), it can be observed that Simpson's final strength relationship, given by Eqs. (2-66) through (2-69), still involves a number of somewhat long expressions that would complicate its use within design practice. Furthermore, Simpson's strength equation is far removed from the current AASHTO LRFD (2001) expressions for the strength of a straight girder.

Simpson (2000) concludes in his thesis that

> **"In the end, "the improved" equation (herein called the Simpson method) yields strength results similar to Fukumoto and Nishida's equation for all ranges of curvature and slenderness."**

This is to be expected since the fundamental concepts behind both Simpson's and Fukumoto and Nishida's equations are quite close. Similar to Fukumoto and Nishida's approach, Simpson's solution focuses on the behavior of compact-section beams and does not address the influence of flange inelastic local buckling and/or web bend buckling on the strength. As a result, Eq. (2-66) predicts approximately the same normalized vertical bending strength M_n/M_p in parametric study cases considered in this

research where significant differences in the capacities exist (see Chapter V for a detailed discussion of the design of the parametric studies). Figure 2.1.15 compares the results of Simpson's and Fukumoto's equations versus the capacities predicted within these parametric studies for specimens with $D/b_f = 2.75$, $D/t_w = 100$, $L_b/R = 0.05$ and 0.10, and target $f_c/f_b = 0.35$. It can be seen that Simpson's formulas and Fukumoto's equations give approximately the same prediction of the ratio of M_n/M_p for different b_f/t_f ratios. The FEA strengths for girders with $L_b/R = 0.05$ are smaller than those for $L_b/R = 0.10$ because these girders have a larger L_b associated with the target $f_c/f_b = 0.35$.

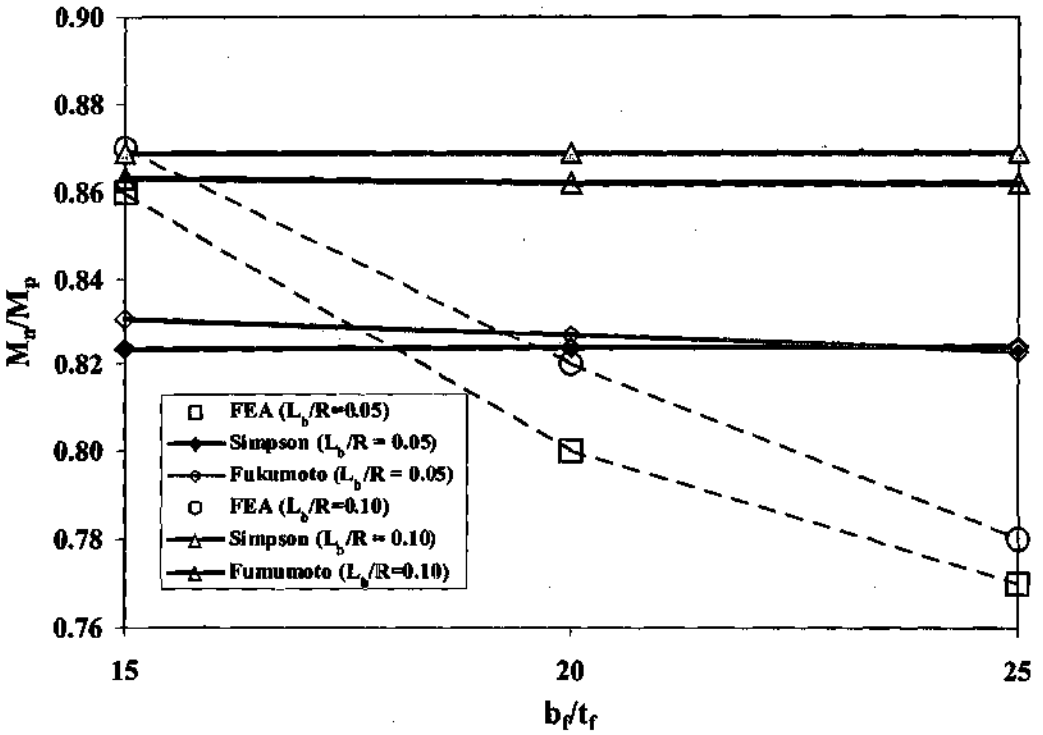

Figure 2.1.15. Comparison between Simpson's and Fukumoto and Nishida's equations for specimens with $D/b_f = 2.75$, $D/t_w = 100$, $L_b/R = 0.05$ and 0.10, and target $f_c/f_b = 0.35$.

Also, the handling of the flange inelastic lateral buckling capacity in Simpson's solution is based on the intersection between the second-order elastic load-deflection solution and an estimate of the cross-section plastic capacity. This approach is not capable of accurately capturing the lateral-torsional buckling strength behavior of I girders in the limit that the radius of curvature becomes large. Equation (2-64), upon which Simpson's final Eq. (2-66) is based, simplifies to $M_n/M_p = 1$ in the limit that the radius of curvature goes to infinity. Equation (2-66) becomes undefined for a straight girder.

Finally, the beneficial effect of a gradient in the vertical bending moment along the unsupported length is not addressed in Simpson's research, and Simpson's method does not accommodate lateral bending stresses from sources other than horizontal curvature. Therefore, Simpson's design predictor equation (Eq. 2-66) is not considered further within this research.

2.1.5 Nakai's Equation

Nakai et al. (1984a) proposed a simple design equation to predict the ultimate bending strength of horizontally-curved I girders based on curve fitting to the results from 19 experimental tests of compact section I beams with transverse stiffeners spaced at $d_o < D$. This equation is of the form

$$M_n = \left(1.92 + 0.357\frac{L_b}{R}\frac{L_b}{b_f}\right)M_{ns} \tag{2-71}$$

where M_{ns} is the nominal bending strength of a straight girder of equal unsupported length, as per Japanese design standards. Equation (2-71) is intended for curved I girders with a curvature parameter $d_o^2/8Rt_w \leq 1$. The term within the brackets of Eq. (2-71) is intended as a strength reduction factor. However, it can be seen that this term actually predicts that M_n is increased relative to the equivalent straight girder capacity as L/R increases. This is obviously counter-intuitive and incorrect. The SSRC Guide (SSRC 1998) shows example anomalous strength predictions using this equation. One possibility is that the sign within the strength reduction factor in Eq. (2-71) may be a typographical error. However, if this sign were intended to be negative, this equation still does not predict any reduction in the strength due to the horizontal curvature for practical L_b/R and L_b/b_f values less than or equal to 0.10 and 25 respectively. Equation (2-71) is not considered any further within the current research.

2.1.6 Hanshin Equations

In addition to the Guide Specifications (AASHTO 1993) and the Recommended Specifications (Hall and Yoo 1998), to the authors' knowledge, there is only one other design standard for horizontally curved steel bridges worldwide. This is the *Guidelines for the Design of Horizontally Curved Girder Bridges* (Hanshin 1988). This document was developed by the Hanshin Expressway Public Corporation in Japan. Hence it is referred to here as the Hanshin Guidelines. Nakai and Yoo (1988) provide a detailed discussion of the background research resulting in the design predictor equations contained within these guidelines. The strength provisions within the Hanshin Guidelines were developed in part based on inelastic finite element analyses and curve fitting.

The Hanshin Guidelines refer to the *Specifications for Highway Bridges* (Japan Road Association 1990) for their base requirements and primarily contain only provisions that pertain to the effects of horizontal curvature. Although these provisions, as well as the requirements in (Japan Road Association 1990) are written in an allowable stress

design format, the combined set of strength predictor formulas may be expressed in terms of a nominal maximum strength. These equations may be summarized as follows. The I girder strength predictor equation in the Hanshin Guidelines is a linear interaction equation relating the vertical bending stress (f_b) and the flange lateral bending stress (f_ℓ), i.e.,

$$\frac{f_b}{F_{bc}} + \frac{f_\ell}{F_y} \le 1.0 \tag{2-72}$$

where

$$F_{bc} = F_y \psi \tag{2-73}$$

is the vertical bending capacity in terms of the flange stress in the absence of any lateral flange bending, considering the potential reduction in strength due to lateral-torsional instability. It should be noted that if F_{bc} is equal to F_y, i.e., if ψ is equal to 1.0, then Eq. (2-72) amounts simply to a first yield check of the compression flange based on the vertical and lateral flange bending stresses, neglecting residual stresses. The term ψ is defined as

$$\psi = 1.0 \qquad \text{if } L_b/R < 0.02\alpha_s \tag{2-74a}$$

and

$$\psi = 1.0 - 1.05\sqrt{\alpha_c}\left(L_b/R + 4.52(L_b/R)^2\right) \qquad \text{if } 0.02\alpha_s \le L_b/R \le 0.2 \tag{2-74b}$$

where

$$\alpha_s = \frac{2}{\pi}\sqrt{3 + \frac{A_w}{2A_c}\frac{L_b}{b_f}\sqrt{\frac{F_y}{E}}} \tag{2-75}$$

and

$$\alpha_c = \gamma\, \alpha_s \tag{2-76}$$

The term γ in Eq. (2-76) is defined as

$$\gamma = 1.0 \qquad \text{if } L_b/R < 0.02\, \alpha_s \tag{2-77a}$$

and

$$\gamma = 1.0 - 1.97\,(L_b/R)^{1/3} + 4.25\,(L_b/R)^2 - 26.3\,(L_b/R)^3 \qquad \text{if } 0.02\,\alpha_s \le L_b/R \le 0.2 \tag{2-77b}$$

The application of the Hanshin equations is limited to girders with a compression flange slenderness satisfying the restriction

$$\frac{b_f}{t_f} \le 0.872\sqrt{\frac{E}{F_y}} \tag{2-78}$$

For F_y = 345 MPa (50 ksi), Eq. (2-78) limits b_f/t_f to 21.

Equation (2-72) with $F_{bc} = F_y$ could be used to check the tension flange of a general unsymmetrical girder; however, this check would tend to be very conservative relative to the true tension flange capacity. An equation based on the true flange plastic capacity might be more appropriate for this situation. Furthermore, it can be questioned that the linear interaction between $f_b = F_{bc}$ and $f_\ell = F_y$ may be somewhat conservative for the low values of f_ℓ that are encountered in US design practice, based on the lateral bending stress restrictions in the Guide Specifications (AASHTO 1993) and the Recommended Specifications (Hall and Yoo 1998). Equation (2-72) is conservative relative to the use of the AASHTO LRFD (2001) beam-column interaction equations for checking of the compression flange, and as discussed in Chapter I, the AASHTO LRFD (2001) beam-column interaction equations are likely to be conservative for checking of a rectangular flange in many cases (see Fig. 1.2). It should be noted that, based on Eqs. (2-74), F_{bc} in Eq. (2-72) is taken equal to F_y whenever $L_b/R < 0.02\alpha_s$. From the developments reviewed in Section 2.1.8.2, it can be observed that Eq. (2-72) is simply a nominal first yield limit in this situation (if f_ℓ and f_b are located at the same cross-section). Furthermore, Eq. (2-72) does not include any terms that would account for the beneficial effects of moment gradient within the curved girder unbraced length. Finally, Eq. (2-72) does not account for potential reduction of the flange strength due to local buckling. It would appear that the limit specified by Eq. (2-78) is related to the resulting need to prevent any influence of flange local buckling on the design strength.

In Chapter VII, the Hanshin Guidelines equations are evaluated in detail along with the predictor equations from the Recommended Specifications and new proposed equations that have been developed within the current research.

2.1.7 Simplified Equation Proposed by Yoo

Yoo (1996) and Yoo et al. (1996) propose a simple formula for determining the flexural capacity of a horizontally curved I girder that is based on the same general concept as that considered by Nakai et al. (1984a). This equation is referred to as a potential ultimate strength formula for design evaluation of curved I girders in Hall et al. (1999) (p. 82) and is compared versus other strength predictor equations in Yoo and Davidson (1997). Yoo et al. (1996) propose that the bending capacity of a horizontally-curved girder can be calculated based on the bending capacity of the equivalent straight girder of equal unsupported length L_b, multiplied by a strength reduction factor. Their proposed strength reduction factor is developed as the reduction in the elastic lateral-torsional buckling strength due to horizontal curvature, and is stated as a function only of

the parameter L_b/R. They obtain this reduction factor based on curve fitting to the results of a large number of elastic linear buckling analyses of curved I girders based on beam theory. The resulting proposed equation for the design strength can be written as

$$M_n = \left(1 - 0.1058\left(\frac{L_b}{R}\right)^{2.129}\right)^{2.152} M_{ns} \qquad (2\text{-}79)$$

where M_{ns} is the flexural capacity of the equivalent straight girder. Although the strength reduction factor in Eq. (2-79) is an accurate fit to the reduction in the elastic lateral buckling strength due to horizontal curvature, this reduction is less than 0.5 percent at the maximum L_b/R of 0.10 permitted in the AASHTO Guide Specifications (AASHTO 1993) and in the Recommended Specifications (Hall and Yoo 1998). Inspection of the available test and analytical data for the flexural strength of curved I beams and girders indicates that: (1) the horizontally-curved girder problem is generally a load-deflection problem in which the maximum strength is reached, even for girders with large unsupported lengths, well before the elastic lateral-torsional buckling capacity is achieved, (2) in most practical cases, the maximum capacity is associated with some degree of inelastic response, and (3) the reduction in the vertical bending capacity due to horizontal curvature is generally much larger than 0.5 percent. Because of these discrepancies between Eq. (2-79) and observed results, this equation is not considered further within this research.

2.1.8 Cross-Section Yield Interaction Equations Proposed by Yoo

Yoo (1996) and Yoo and Davidson (1997) have developed a family of 17 sets of yield interaction equations which quantify the maximum strength of general noncomposite and composite I girders subjected to vertical bending moment (M) and lateral flange bending moments due to torsion (M_ℓ), with second-order (i.e., geometric nonlinear) effects neglected. These interaction equations are based directly on the static equilibrium of the cross-section at the most critically loaded location along the member length. As stated by Yoo and Davidson (1997), these "formulations offer a theoretically pure starting point for defining the strength of curved composite sections and offer distinct advantages over works previously presented by others involving the strength of noncomposite curved girders." Yoo and his colleagues base their cross-section analysis on the beam-theory based assumption that the lateral flange moments due to torsion (M_ℓ) within a general doubly- or singly-symmetric I section are self-equilibrating. That is, it is assumed that at any given location along the length of an I girder, the lateral bending moments in the top and bottom flanges are equal and opposite. In general, this assumption may be violated due to (1) distortion of the web and (2) the existence of second-order radial bending moments within the girder. Also, in general, the flexural stresses within I girders may deviate somewhat from the predictions of beam theory, due to web bend buckling. However, all of the above deviations from first-order beam theory are likely to be small in many practical cases.

Yoo and his colleagues also include approximate analysis equations for the lateral flange bending moments due to the torsion induced by horizontal curvature. These approximate equations are of the same form as the V-load equation (Eq. 1-6), which predicts the maximum M_ℓ to be at the ends of the unbraced length, but the coefficient "12" in the denominator of the V-load equation is replaced by a variable constant. Yoo (1996) suggests that a value of 10 should be used for this coefficient, instead of 12, to indirectly account for the omission of the web in the V-load calculations. Yoo and Davidson (1997) find that a value of 14 gives somewhat better correlation with the actual maximum lateral flange bending moments in 18 hypothetical horizontally curved bridges.

It is important to note that the yield interaction equations developed by these researchers can be used more generally with the results of *any* bridge superstructure analysis that produces predicted values of the vertical and lateral flange bending moments, M and M_ℓ (or the vertical bending moments M and bimoments B). In general, it is important to separate the analysis solution from the resistance equations since the actual internal forces within many bridge structures can vary significantly from the predictions of the V-load type equation due to many factors, including bridge skew and applied loadings on the girders. Yoo's interaction equations can give an estimate of the girder flexural capacity for any set of computed elastic moments M and M_ℓ.

It is assumed implicitly in Yoo's cross-section strength analysis that the lateral (or radial) bending moment is equal to zero. Although this is a limitation of the existing yield interaction equations, this limitation can be removed by application of the basic principles established within Yoo's research. Yoo and Davidson (1997) state that

> **"... the assumed stress states may not appropriately represent the actual conditions of the composite or noncomposite curved girder system at either first yield or ultimate strength. Furthermore, secondary amplification effects, residual stress effects and fabrication and erection concerns may be significant."**

However, it is possible that these issues may turn out to be minor upon further investigations, or adjustments to Yoo's procedures may be possible to account for these effects where they are important.

2.1.8.1 Cross-Section Yield Interaction Equations for Composite Beams

Yoo and Davidson (1997) detail the yield interaction equations for composite beams. These equations may be particularly useful in quantifying the strength of curved composite I girders in positive bending, where it is expected that some of the limitations discussed above are particularly minor. For composite girders in positive bending, the maximum vertical bending strength is typically significantly larger than $R_h M_y$, where M_y is the moment capacity at first yield of the short-term composite section, not including residual stress effects. The AASHTO LRFD (2001) straight girder specifications permit flexural capacities up to the plastic moment capacity M_p, in simple spans and in continuous spans with compact sections in the negative flexural regions over the interior

supports. They specify a maximum capacity of $M_n = 1.3\,R_h\,M_y$ by the most commonly used approach for continuous-span girders with noncompact interior support sections. Yoo and Davidson's (1997) yield interaction equations provide a particularly useful means for extending the AASHTO LRFD (2001) formulas for composite I girders in positive bending to include the effect of lateral bending within the bottom flange. If curved composite girder system studies can demonstrate that the nonlinearity associated with the development of these capacities is not detrimental to the overall bridge performance, these equations will provide a significant advance over current strength equations in the Guide and Recommended Specifications, and in the Hanshin Guidelines, which limit the girder vertical bending capacity to a maximum of M_y.

2.1.8.2 Noncomposite Compact-Flange Section and Noncompact Section Formulas

In the current research, the authors focus on the development of unified I girder strength equations that are based on consideration of the bottom flange of a composite I girder as an equivalent steel beam-column. This approach is believed to be an accurate idealization for composite girders in negative bending. It is expected to be conservative for the maximum strength of isolated composite girders in positive bending. Within this context, the predictions of two of Yoo's noncomposite yield interaction equations are evaluated in the subsequent chapters. These are the yield interaction equations that Yoo (1996) and Yoo and Davidson (1997) define as the "noncomposite compact-flange section" and the "noncomposite noncompact section" equations. Compact-flange sections are defined as all-steel sections in which the compression flange behaves compactly (i.e., the flange slenderness is sufficiently low such that full plastification of the flange on one side of the web can be achieved), but in which the web is not capable of developing strengths beyond its first yield strength. Noncompact sections are defined as those in which neither the flange nor the web is capable of developing combined stress states beyond first yield.

As described in Chapter V, webs with $D/t_w = 160$, 130 and 100 and flanges with $b_f/t_f = 15$, 20 and 25 are considered in the parametric studies of this research. Yoo's compact flange section equations are utilized in this research to estimate the capacities of the I girders with $b_f/t_f = 15$, and his noncompact section equations are utilized for all the other cases. In the experimental tests discussed in Chapter IV, Eq. (2-5) is utilized to define the slenderness corresponding to the transition between the compact-flange and noncompact section equations.

Figures 2.1.16 and 2.1.17 illustrate the general states of internal stress that can exist within a noncomposite compact flange section and a noncomposite noncompact section respectively. The dark shaded stress blocks within the top and bottom flanges represent the stresses due to flange lateral bending and the white stress blocks correspond to the stresses due to vertical moment. The top flange is labeled as the compression flange in the figures; however, the section analysis is the same if the sign of the vertical bending moment is reversed.

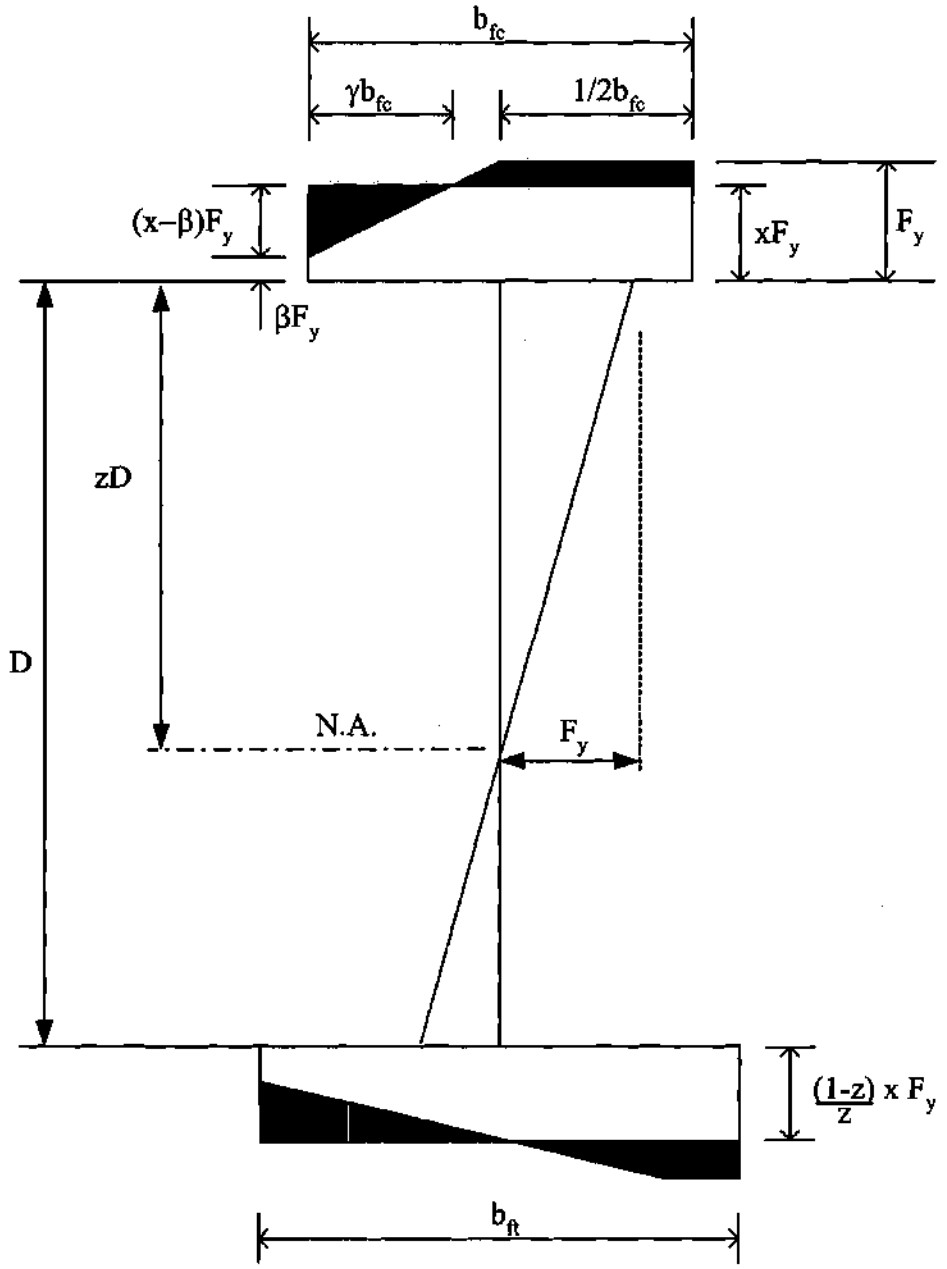

Figure 2.1.16. Stress distribution at strength limit of a noncomposite compact-flange I-section (Yoo 1996).

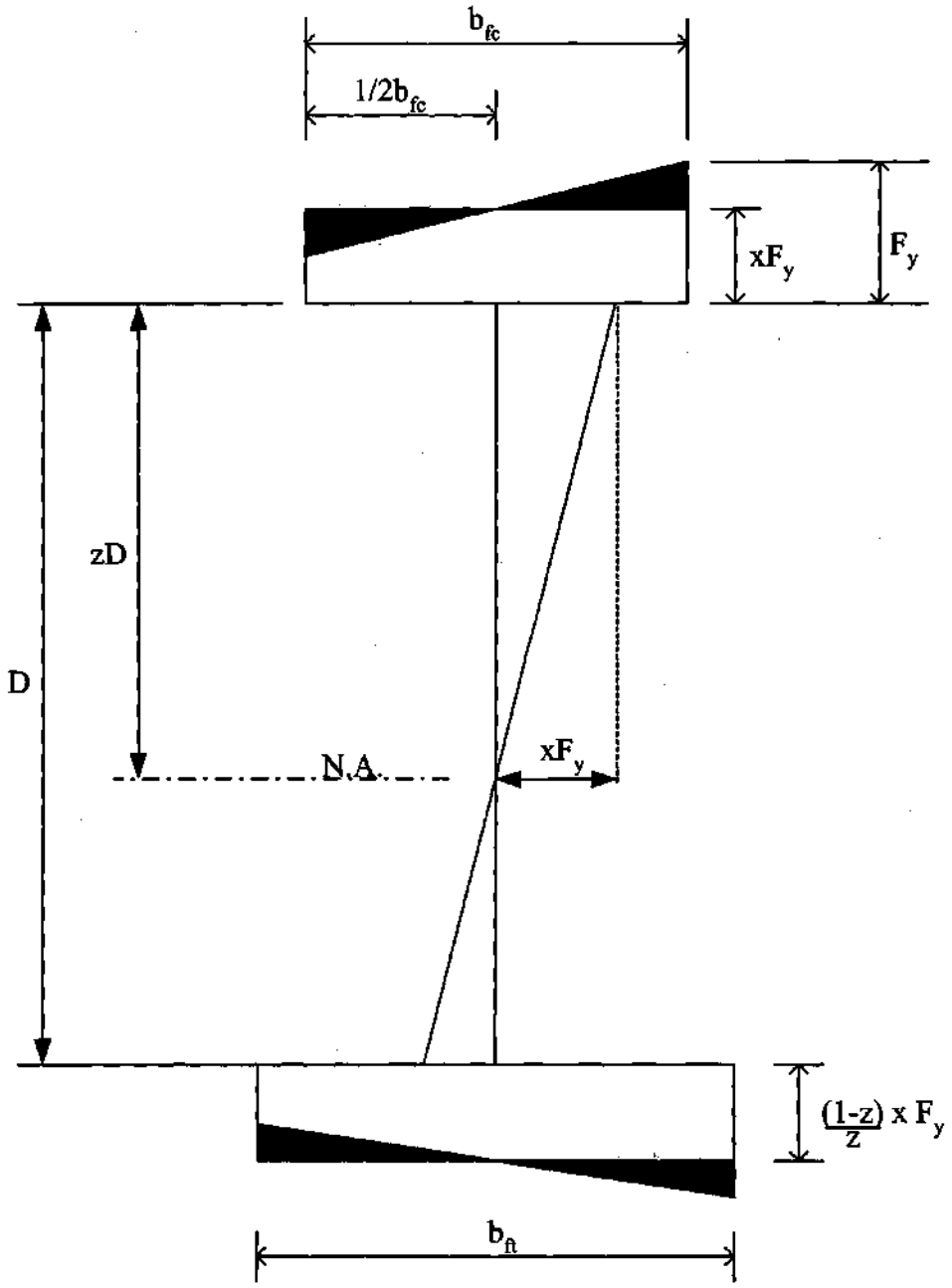

Figure 2.1.17. Stress distribution at strength limit of a noncomposite noncompact I-section (Yoo 1996).

For the compact flange section (see Fig 2.1.16), the lateral flange bending moment (M_ℓ) is calculated from static equilibrium, the fact that the net axial force due to the lateral flange bending stress blocks (shaded in black) must equal zero, and from similar triangles. Based on the these considerations, the lateral flange bending moment in the smaller top flange (M_ℓ) for the compact flange section is obtained as

$$M_\ell = \frac{65}{192}(1-x)\,b_{fc}A_{fc}F_y \tag{2-80a}$$

This equation can be written in terms of a flange elastic lateral bending stress by dividing through by the elastic section modulus of the flange to obtain

$$f_\ell = \frac{390}{192}(1-x)\,F_y \tag{2-80b}$$

This equation can in turn be solved for x, resulting in

$$x = 1 - \frac{192}{390}\frac{f_\ell}{F_y} \cong 1 - \frac{1}{2}\frac{f_\ell}{F_y} \tag{2-80c}$$

For noncompact sections, Yoo (1996) assumes that the cross-section cannot sustain any *nominal* yielding when subjected to the vertical and lateral flange bending moments obtained from the overall bridge analysis. That is, the combined stress state, neglecting initial residual stresses, is limited to first yield. Based on this limit and the consideration of static equilibrium, i.e., no net axial force in the flanges due to vertical bending moment, and the use of the classical elastic bending formulas, the lateral flange bending moment in the smaller top flange of the noncompact section is obtained as

$$M_\ell = \frac{1}{6}(1-x)b_{fc}A_{fc}F_y \tag{2-81a}$$

or if written in terms of a flange elastic lateral bending stress

$$f_\ell = (1-x)F_y \tag{2-81b}$$

If we solve this equation for x, we obtain simply

$$x = 1 - \frac{f_\ell}{F_y} \tag{2-81c}$$

It is important for the engineer to understand the meaning of the parameters "x", "z" and "β" shown in Figs. 2.1.16 and 2.1.17. Both of these figures illustrate a general singly symmetric I section in which the top flange is smaller than the bottom flange. Due

to the smaller top flange, the depth of the web in compression $D_c = zD$ is larger than D/2, i.e., $z > 0.5$.

In Fig. 2.1.16, the strength of the cross-section is defined as the loading at which the maximum flexural stress in the web, located at the top of the web in this case, becomes equal to F_y. Therefore, the strain at the top of the web is exactly equal to the yield strain ε_y at this state. Yoo and his colleagues assume in their cross-section analysis that the stresses and strains at the mid width of the I girder flanges are identical to the stresses and strains at the top or at the bottom of the web (i.e., the differences between the depth of the web D, the distance between the mid-thickness of the flanges h, and the total depth of the section d are neglected in their cross-section analyses). Therefore, based on the assumption of a homogenous I section, the top flange is also at incipient yielding at its mid width.

If we continue with the consideration of the effects of the lateral flange bending moments, it can be observed that due to the lateral bending within the top flange, and due to the top flange being at incipient yield at its mid width, the stresses on the right-hand side of the top flange are all equal to F_y. Also, due to the fact that the total axial force due to the lateral flange bending is zero, the total area under the dark shaded part of the stress distribution due to M_ℓ must integrate to zero. Therefore, if we assume that a certain fraction of the total stress at the mid width of the top flange xF_y is due to vertical bending, we can then calculate the corresponding stress βF_y that must exist at the left-hand tip of the top flange. Yoo and his colleagues assume that this flange tip does not yield, which is a sufficient assumption for practical values of x. Given the corresponding lateral bending stress distribution, shown in black within Fig. 2.1.16, we obtain Eq. (2-80a).

Based on the above cross-section analysis, it can be seen that the girder vertical bending capacity associated with the stress state in Fig. 2.1.16 can be approximated as

$$M_n \cong x\, M_y \tag{2-82a}$$

(the actual moment is slightly larger, due to the maximum stress in the web being larger than xF_y; however, the increase in the capacity resulting from these additional web stresses is small). In terms of an elastic vertical bending stress, the strength may be written as

$$F_n \cong x\, F_y \tag{2-82b}$$

These equations may be applied in design practice by determining x from Eq. (2-80c) based on a value of f_ℓ computed from an elastic analysis of the bridge superstructure.

The calculations pertaining to Fig. 2.1.17 are simpler to describe since there is no yielding anywhere within the cross-section. In this case, the strength is controlled by reaching F_y at the right-hand tip of the top flange (assuming additive compressive stresses

on this side of the top flange). If we then assume that the average stress in the top flange, which is equal to the stress at the flange mid width since the cross-section is elastic, is equal to xF_y, we obtain Eqs. (2-82) exactly for the vertical bending capacity, and Eqs. (2-81a) and (b) for the flange lateral bending moment or stress. Similar to the above developments for compact flange sections, Eqs. (2-82) may be applied in practice for noncompact sections by determining x from Eq. (2-81c) based on a value of f_ℓ computed from an elastic analysis of the bridge superstructure.

2.1.8.3 Implications With Respect to Hybrid I Girder Design

Yoo and Davidson (1997) state that there is little benefit to making the web hybrid in compact-flange and noncompact I girders. It appears that their reasoning on this issue is based on the cross-section analysis shown in Fig. 2.1.16. However, it is well known that in the design of hybrid I girders, the web is allowed to yield under the maximum design loading conditions, regardless of whether it is compact or not (Schilling and Frost 1964; Schilling 1968; ASCE 1968). The reduction in the flexural capacity due to web yielding and web bend buckling is accounted for within the hybrid R_h and load-shedding R_b factors of the AASHTO (2001) Specifications. The capacity of a hybrid girder does not need to be limited to first yielding of the web based on a beam-theory analysis.

Similarly, there is no reason why a noncompact or slender homogeneous I girder web needs to be limited to first yield under the loading conditions for maximum strength evaluation. It can be shown that generally, the overall contribution of the web to both vertical and lateral bending is relatively small compared to that of the flanges of an I girder. It should be possible to allow some yielding within a noncompact or slender web at the maximum load levels without any significant detriment to the overall girder vertical and/or lateral bending capacity. This issue is considered within the context of homogenous I girders in the parametric studies of this research.

For horizontally-curved hybrid I girders, the extent of yielding in the web at the maximum strength limit state will typically be less than in straight hybrid I girders, since part of the girder flexural capacity is "used up" by the lateral bending in the flanges. Therefore, the influence of a hybrid web on the girder flexural strength may be of lesser consequence in curved than in straight I girder design. The consideration of hybrid horizontally-curved I girders is beyond the scope of the current research. However, one set of experimental tests considered in Chapter IV involves I girders that are effectively hybrid.

2.1.9 Proposed Unified Vertical Bending Strength Equations for Design of I Girders Subjected to Vertical Bending, Lateral Bending and Torsion

2.1.9.1 Motivation

Section 1.4 explains the key concepts adopted in the current research for development of a set of unified vertical bending strength equations for design of I girders subjected to vertical bending, lateral bending and torsion. Briefly, these concepts are: (1) use of an

equation format based on the flange vertical bending stress in order to facilitate both composite and noncomposite I girder design, (2) focusing on the tension and compression flanges as equivalent beam-columns, subjected to loadings produced by horizontal curvature as well as other internal loadings induced by the geometry of the bridge superstructure or directly applied loadings, and (3) conservatively neglecting the torsional restraint provided to the top flange of the I girder from the bridge deck, thus permitting the development and verification of formulas by studies of all-steel girders.

Section 2.1.1 addresses modifications to the current AASHTO LRFD (2001) Specifications that significantly improve the accuracy of their flexural strength prediction equations for certain situations, and which improve the simplicity and ease of use of the associated AASHTO provisions.

This section provides further specifics on the logic behind, and the motivation for, the proposed extension of these equations to handle lateral flange bending. Section 2.1.9.2 then summarizes the proposed equations for handling of flange lateral bending moments due to lateral bending and torsion.

Flange Plastic Capacity

Consider one of the flanges of an I girder subjected to combined vertical and lateral bending. The lateral moment in the flange is related to the flange elastic lateral bending stress, f_ℓ, by the equation

$$M_\ell = \frac{f_\ell b_f^{\,2} t_f}{6} \tag{2-83}$$

If the flange behaves compactly, it can develop the strengths associated with the idealized fully plastic stress distribution shown in Fig. 2.1.18.

Within this idealized fully plastic stress distribution, the lateral moment is generated by the strips of width c at the tips of the flange, and the remaining width of the flange ($b_f - 2c$) develops the flange force associated with the vertical bending moment. By equating the elastic flange force due to vertical bending, $\hat{f}_b\, b_f\, t_f = f_b\, b_f\, t_f / (R_b\, R_h)$, to this fully plastic flange force, $F_y\, t_f (b_f - 2c)$, the elastic vertical bending stress associated with the flange plastic strength may be expressed as

$$\hat{f}_b = F_y \frac{b_f - 2c}{b_f} \tag{2-84}$$

where $\hat{f}_b = f_b / (R_b\, R_h)$ is the elastic flange vertical bending stress, accounting for load-shedding from the web due to hybrid and/or web bend-buckling behavior. Similarly, by equating the right-hand side of Eq. (2-83) to the lateral flange moment associated with Fig. 2.1.18, we obtain

$$\frac{f_\ell b_f^2 c}{6} = F_y c\,(b_f - c) \tag{2-85}$$

This quadratic equation can be solved for the width c shown in Fig. 2.1.18 to obtain

$$c = \frac{b_f}{2}\left(1 - \sqrt{1 - \frac{2}{3}\frac{f_\ell}{F_y}}\right) \tag{2-86}$$

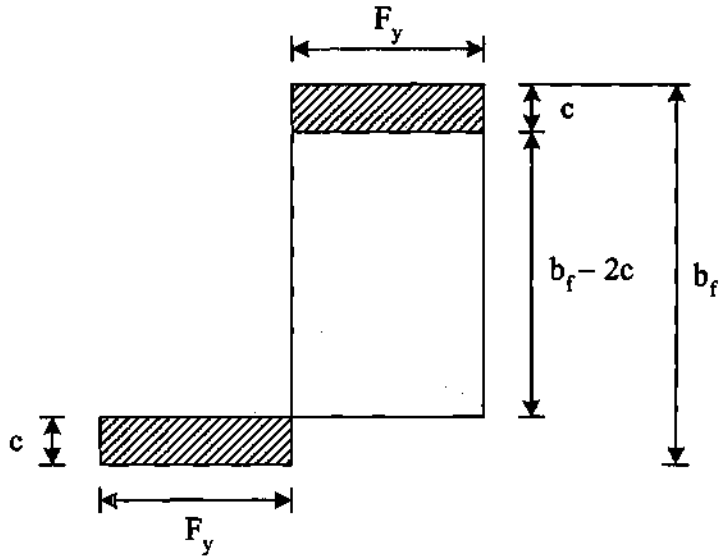

Figure 2.1.18. Idealized plastic stress distribution in a flange due to lateral and vertical bending.

Finally, by substituting Eq. (2-86) into Eq. (2-84), an expression for the elastic flange vertical bending stress ($\hat{f}_b$) associated with the plastic strength of the flange is obtained as a function of the elastic lateral bending stress at the flange tips (f_ℓ) as

$$\hat{f}_b = F_y\sqrt{1 - \frac{2}{3}\frac{f_\ell}{F_y}} \tag{2-87}$$

If we consider the practical design of bridge I girders, in which the elastic stress f_ℓ is generally much smaller than F_y, e.g., $f_\ell \le 0.5\,F_y$, Eq. (2-87) is accurately approximated by the following simple linear equation

$$\frac{f_b}{R_b R_h} = F_y - \frac{1}{3}f_\ell \tag{2-88}$$

The accuracy of this approximation is illustrated in Fig. 2.1.19. As noted in Section 2.1.2.1, Hall and Yoo (1998) originally developed this formula as a restriction on the flange capacity predicted by McManus's strength equations. However, if we neglect any conditions such as holes fabricated within the section for field splice connections, etc., this equation can potentially serve more generally as a specific limit for the vertical bending capacity of a *tension* flange subjected to whatever lateral bending moments (and corresponding elastic lateral bending stresses) are encountered within the overall analysis of a bridge superstructure. Equation (2-88) would need to be checked for the most critical combination of $\hat{f}_b$ and f_ℓ at any cross-section along the length of the girder, where $\hat{f}_b$ and f_ℓ are the computed *second-order elastic* stresses within the flange, including the effect of load-shedding from the web due to bend buckling. This is consistent with the AISC LRFD (1999) and AASHTO LRFD (2001) philosophies for checking of beam-columns loaded in tension. Furthermore, in practical design situations, it is commonly assumed that the above second-order elastic stresses are estimated sufficiently well based on a first-order elastic analysis of the structure, since axial tension tends to make the stresses smaller than the first-order elastic values. Equation (2-88) is referred to in this report as the compact-section based one-third rule.

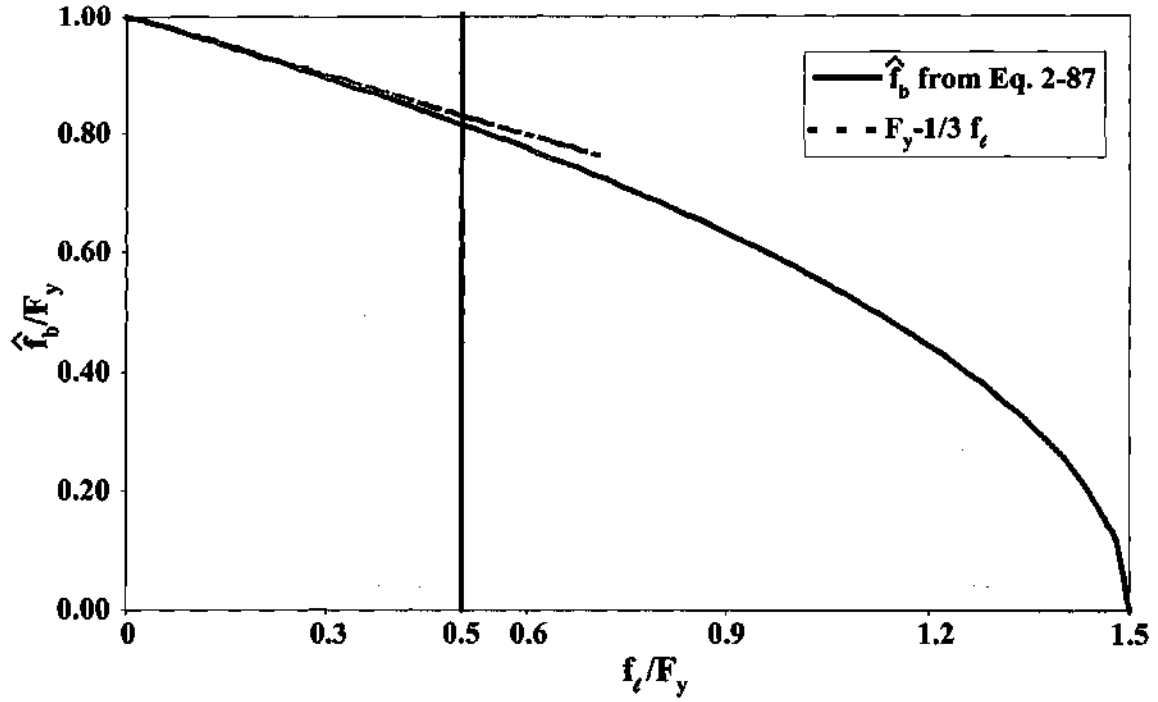

Figure 2.1.19. Comparison of the "exact" flange plastic strength and the compact-section based one-third rule.

Equation (2-88) would tend to give an upper-bound estimate of the strength of a *compression* flange as an equivalent beam-column, since the strength in compression

may be limited by local and/or lateral instability. The consideration of an appropriate representation of the effect of lateral bending on compression flange strength is discussed in the following sub-section.

Consideration of Flange Local and Lateral Stability

Obviously, the above compact-section based one-third rule does not account for the reduction in girder vertical bending capacity due to local flange or lateral-torsional buckling. However, as discussed in Section 1.4.2, it is expected that the compression flange of a curved I girder can be treated adequately as an equivalent beam-column. Therefore, based on this hypothesis, the (AISC 1999; AASHTO 2001) beam-column interaction equations should provide a conservative check of the compression flange strength, if the *maximum second-order elastic lateral bending moment* is utilized along with the compression flange axial force due to vertical bending. If the AISC (1999) and AASHTO (2001) beam-column checks are expressed in terms of the *second-order elastic* stresses f_b and f_ℓ (calculated based on a first-order analysis of the bridge superstructure along with appropriate approximate second-order amplification factors), and if the flange vertical bending strength from the straight girder specifications is taken as the *equivalent column strength*, then we obtain compression flange design strength interaction curves such as those illustrated in Fig. 2.1.20.

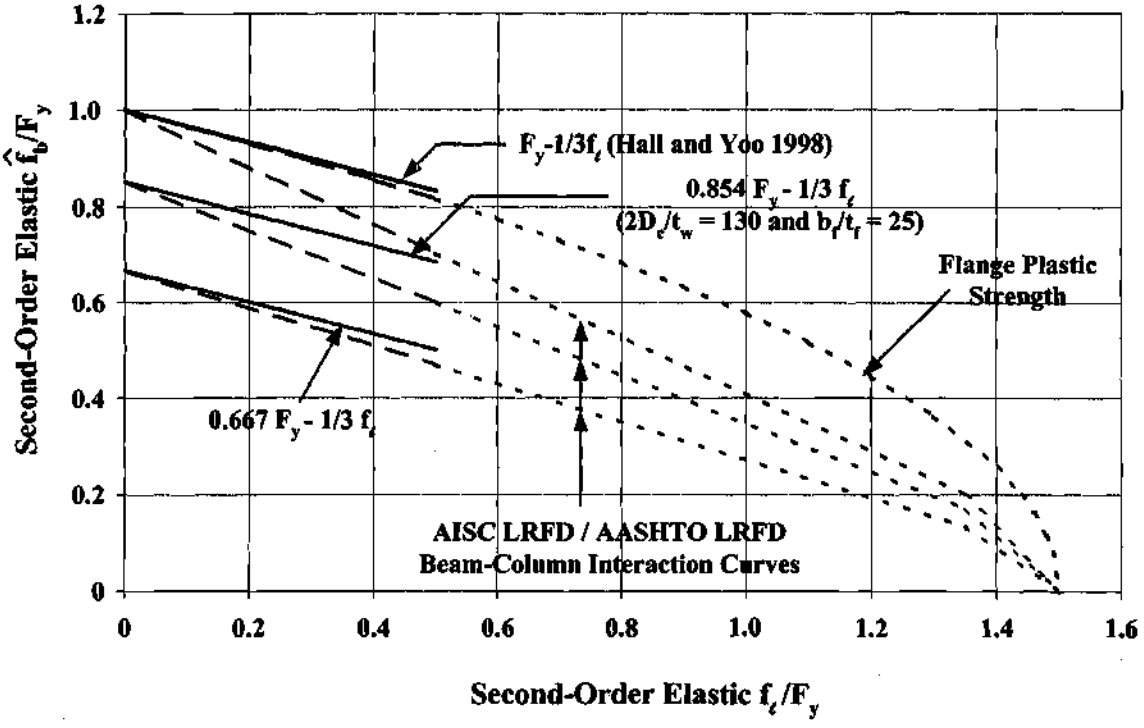

Figure 2.1.20. Comparison between the strengths predicted by the proposed one-third rule and the AISC LRFD (1999) - AASHTO LRFD (2001) beam-column interaction curves.

As noted in Chapter I, for small f_ℓ/F_y, the AISC LRFD (1999) and AASHTO LRFD (2001) beam-column strength interaction curves are often quite conservative for checking of I-shape members in weak-axis bending (ASCE 1997; Yura 1988), or more relevant to the case at hand in this research, beam-columns with rectangular or T shaped cross-sections. For a compact flange with an unsupported length such that the vertical bending strength of the compression flange is equal to or approximately F_y, it would be expected that the compact-section based one-third rule equation (Eq. 2-88) should work well as a design strength approximation. Furthermore, for a compression flange that is at the transition between the elastic and inelastic buckling strength, i.e., $F_n = 0.667\ F_{yc}$ in the straight-girder specification (for $F_{yc} = 345$ MPa (50 ksi) and $F_{rs} = 114$ MPa (16.5 ksi)), Fig. 2.1.20 shows that the one-third rule, with F_{yc} replaced by F_n, and the direct usage of the Specification beam-column interaction equations are nearly equivalent.

For the intermediate case, it can be observed from Fig. 2.1.20 that the one third rule – expressed as $F_n - 1/3\ f_\ell = 0.854\ F_y - 1/3\ f_\ell$ in the figure – is significantly liberal compared to the direct usage of the beam-column interaction equations. However, as explained above and in Chapter I, it is possible that this liberal estimate of the equivalent beam-column strength, relative to current AISC LRFD (1999) and AASHTO LRFD (2001) beam-column strength equations, is justified. Studies need to be conducted to verify this hypothesis. This is the subject of a large portion of this report. It should be noted that $F_n = 0.854\ F_y$ is obtained from the proposed modified AASHTO straight-girder strength equations based on the local buckling strength of a flange with $b_f/t_f = 25$ along with a corresponding web slenderness of $2D_c/t_w$ of 130 (see Sections 2.1.1.1 and 2.1.1.2). Also, this is the flange lateral buckling strength obtained from the proposed straight girder strength formulas for $L/b_f = 16.13$ at $a_r = 2$ and $L/b_f = 17.24$ at $a_r = 1$ (see Sections 2.1.1.1, 2.1.1.3 and 2.1.1.6).

It is interesting to note that, based on Yoo's (1996) yield interaction equations for a compact flange section (see Eqs. (2-80c) and (2-82b) and Fig. 2.1.16), it can be stated that web yielding will never occur in a non-hybrid member (based on the beam theory assumptions employed within the yield interaction equation derivations, neglecting the effect of residual stresses) if the flange vertical bending stresses are limited to

$$\frac{f_b}{R_b} = F_y - \frac{1}{2} f_\ell \tag{2-89}$$

It should be noted that this equation is a reasonably close approximation of the AISC LRFD (1999) - AASHTO LRFD (2001) interaction equations for $F_n = F_y$ in Fig. 2.1.20. Therefore, it can be stated that the use of the AASHTO LRFD (2001) beam-column interaction equations would limit the maximum *average* vertical bending *strain* within the compression flange approximately to the yield strain of the material ε_y (neglecting residual stress effects). However, Eq. (2-89), with F_y replaced by F_n, becomes significantly conservative relative to the use of the AASHTO LRFD (2001) beam-column interaction equations as F_n/F_y reduces below one. Nevertheless, all of the interaction relationships discussed here are significantly liberal relative to the simple linear

interaction equation specified by the *Hanshin Guidelines* (Japan Road Association 1990) (see Eq. 2-72). As noted previously, in many cases, this equation is equivalent to the use of Yoo's (1996) yield interaction equation for a noncompact section member (see Eqs. (2-81c) and (2-82b) and Fig. 2.1.17). In summary, the 1/3 rule (with F_y replaced by F_n) is proposed in this research because this rule gives the best correlation in general with the strength data from experimental tests as well as with the results of the parametric studies conducted by the authors (see Chapters IV through IX).

2.1.9.2 Recommended Equations

The one-third rule equations proposed in this research for handling the effects of lateral flange bending, based on a modification of straight-girder vertical bending strengths, can be expressed as follows:

- For flanges in tension, or for flanges in compression with $\lambda \le \lambda_p$

$$\frac{f_b}{R_b R_h} \le F_y - \frac{1}{3} f_\ell \tag{2-90a}$$

- For flanges in compression with $\lambda_p \le \lambda \le \lambda_r$

$$\frac{f_b}{R_b R_h} \le C_b \left[1 - \frac{(F_{yc} - F_L)}{F_{yc}} \left(\frac{\lambda - \lambda_p}{\lambda_r - \lambda_p} \right) \right] F_{yc} - \frac{1}{3} f_\ell$$

$$\le F_{yc} - \frac{1}{3} f_\ell \tag{2-90b}$$

where all of the parameters with the exception of f_ℓ are defined within the straight-girder design provisions (see Section 2.1.1). The term f_ℓ is the maximum second-order elastic flange lateral bending stress within the unsupported length under consideration. As in the straight-girder design provisions, the smaller of the local and lateral-torsional buckling strengths determined from these equations controls. Equations (2-90) are shown here in the form of a limit on the flange stresses due to vertical bending, amplified by the inverse of the factors R_b and R_h to account for load shedding from slender and/or hybrid webs. They may be written directly as flange vertical bending-lateral bending interaction equations simply by moving the term $f_\ell / 3$ to the left-hand side of these formulas.

The hybrid-girder factor R_h is included within Eqs. (2-90). However, hybrid girders are not specifically addressed within this research. Based on this and the fact that the Recommended Specifications do not permit the use of hybrid-curved girders, the authors do not recommend the use of these equations for hybrid curved I girders at the present time (May 2001). However, engineers need some way of checking lateral bending in

straight hybrid I girders. It is likely that the format of Eqs. (2-90a) and (2-90b) is applicable for these cases and for curved hybrid I girders, but there is a possibility that the form of the factor R_h might need to be modified. It should be noted that the Guide Specifications (AASHTO 1993) do permit the design of hybrid curved I girders, and that there has been some limited evaluation of these types of girders by Culver (1972). Several of the experimental tests considered with Chapter IV are effectively hybrid girders.

A one-third rule modification of elastic local and/or lateral buckling strengths is not shown in Eqs. (2-90). This is because, if the flanges are limited to a maximum b_f/t_f of 24, as is required in the current AASHTO LRFD (2001) Specifications, elastic flange local buckling never controls for $F_y \leq 480$ MPa (70 ksi). Furthermore, the corresponding elastic lateral-torsional buckling based equations are not shown either because it is expected that the lateral flange bending stresses will tend to be dramatically amplified by second-order effects for bridge girders designed beyond the inelastic-elastic lateral-torsional buckling transition limit. Therefore, in the view of the authors, it is wise to limit the design of bridge girders subjected to significant combined vertical and lateral flange bending to $\lambda \leq \lambda_r$ with respect to the straight-girder lateral-torsional buckling limit state. It is interesting that this corresponds approximately to the $L_b/b_f \leq 25$ limit required by McManus (1971), the AASHTO Guide Specifications (AASHTO 1993), and the Recommended Specifications (Hall and Yoo 1998).

It is possible that under construction loading conditions, I girders that have large unsupported lengths within the elastic buckling realm may need to be checked for combined vertical and lateral bending. In these cases, the elastic lateral-torsional buckling based one-third rule equation may be used. It is important to note that this equation is typically *more* restrictive than a first-yield check for these types of conditions, i.e., use of a first yield check with the results of elastic analysis can be significantly unconservative, unless an accurate second-order elastic analysis is employed that is capable of capturing the large amplification of the lateral bending stresses as the lateral-torsional buckling load is approached.

The proposed one-third rule equations are based on the following design limits:

$$b_f/t_f \leq 24 \tag{2-91a}$$

$$f_\ell \leq 0.5\, F_y \tag{2-91b}$$

$$L_b/R \leq 0.1 \tag{2-91c}$$

and

$$L_b/r_t \leq \lambda_r \tag{2-91d}$$

Figure 2.1.21 shows a sample comparison of the proposed one-third rule to results from the parametric studies conducted in this research for girders with $b_f/t_f = 25$, and in which the strengths are controlled by the inelastic flange-local buckling based design equations. Two design curves are shown in the figure, one corresponding to $2D_c/t_w = 130$ and one corresponding to $2D_c/t_w = 160$. The design strengths for these cases differ only slightly. Also, the values of $f_b/R_b/F_y$ corresponding to elastic flange buckling are shown for each of these cases. These curves are discussed within the next subsection. Furthermore, the limit on $f_b/R_b/F_y$ imposed by the current conservative AASHTO (2001) flange local buckling strength equation (see Figs. 2.1.1 and 2.1.2) is shown in the figure.

Figure 2.1.22 shows sample predictions relative to the results from parametric studies in this research for girders that are controlled by inelastic lateral-torsional buckling and which have $(\lambda - \lambda_p) / (\lambda_r - \lambda_p) \cong 0.4$ with respect to lateral-torsional buckling. Detailed discussion of the results of the parametric studies (with respect to the flexural capacity) is provided in Chapter VII.

The proposed equations do not utilize an effective length for girder lateral-torsional buckling. The actual unsupported lengths are to be used. It is expected that this leads to a conservative representation of the strength within interior unsupported segments of bridge girders, due to the continuity with adjacent unbraced segments. Also, this helps to prevent the second-order amplification of the flange lateral bending stresses from becoming large. However, for an unbraced length at the end of a bridge, it is possible that the physical boundary conditions at one end of the unsupported length may actually be close to torsionally simple. This type of situation is considered within the parametric studies of this research (see Section 5.11). It is expected that the use of the actual unsupported length within the design equations is conservative with respect to the use of an effective length for these cases as well.

2.9.1.3 Calculation of Flange Elastic Local Buckling Strengths

In addition to the results of the one-third rule based equations shown in Figure 2.1.21, the flange elastic buckling strengths are also shown. These strengths are based on Eq. (2-9) with the buckling coefficient given by Eq. (2-7), combined with a reduction coefficient developed by Davidson and Yoo (1996). This reduction coefficient accounts for the effect of lateral bending (due to horizontal curvature) on the elastic buckling capacity, and can be written as:

$$(F_e)_{cv} = (F_e)_{st}\left[1.0643 - \frac{0.15\, f_\ell}{0.35\, f_b}\right] \leq (F_e)_{st} \qquad (2\text{-}92)$$

where

$(F_e)_{cv}$ = elastic buckling stress of the curved plate

$(F_e)_{st}$ = elastic buckling stress of the equivalent straight plate

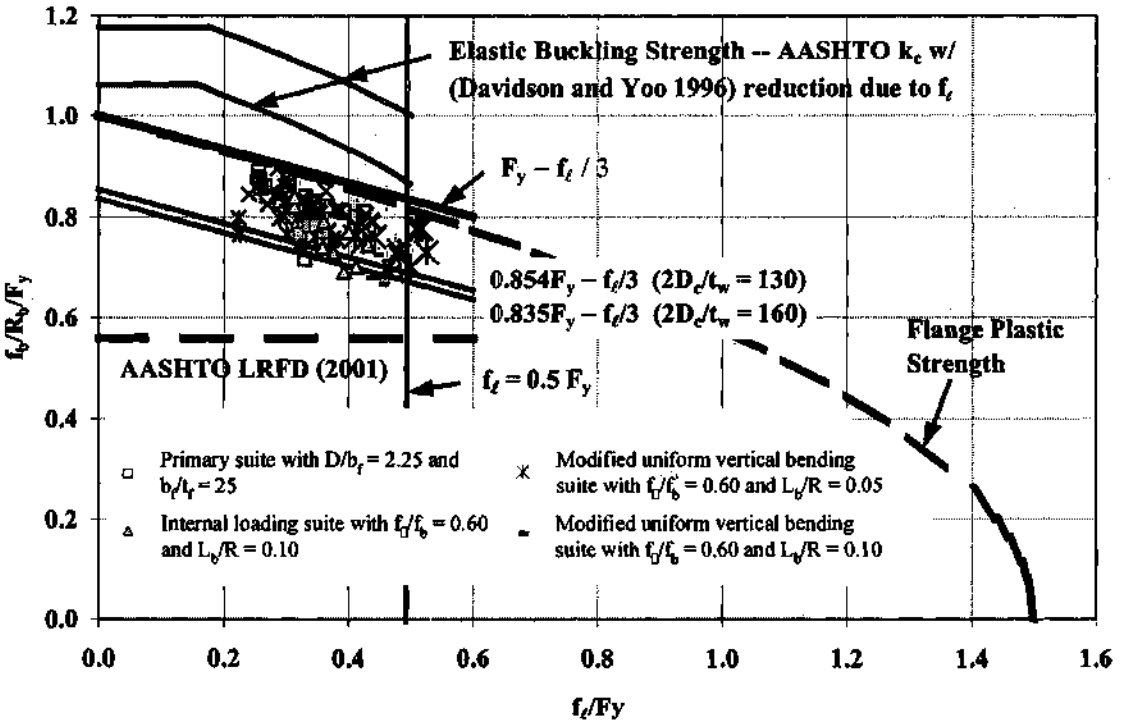

Figure 2.1.21. Local flange buckling strengths for b_f/t_f =25 ($2D_c/t_w$ = 130 and 160).

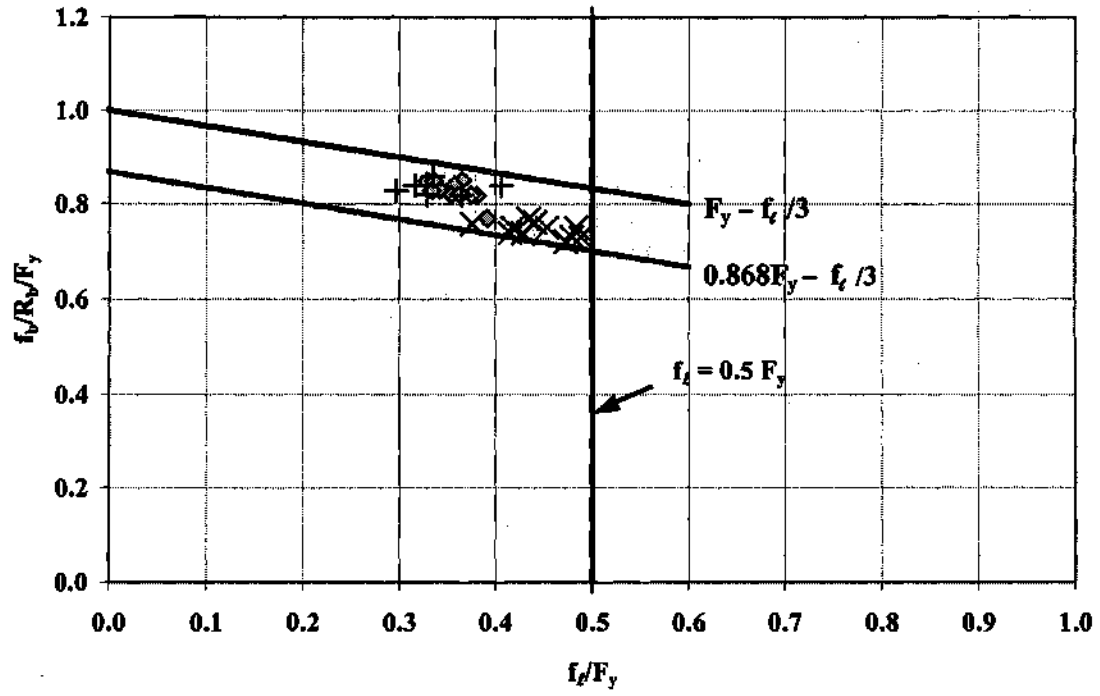

Figure 2.1.22. Lateral-torsional buckling strengths for $(\lambda_b - \lambda_p) / (\lambda_r - \lambda_p) \cong 0.4$.

It should be noted that these buckling stresses should be compared against the vertical bending stress at the web-flange juncture, f_b, not to the total longitudinal normal stress at the flange tip ($f_b + f_\ell$). Davidson and Yoo (1996) developed this equation as a lower-bound fit to finite element elastic buckling analysis results for a range of horizontal curvatures. It is interesting that the slope of the elastic buckling strength curves in Fig. 2.1.21, as per Davidson and Yoo's reduction formula, is slightly larger than the slope of the one-third rule curves.

The buckling of plates subjected to a gradient in stress is often written in terms of the maximum elastic stress. Eurocode 3 (CEN 1992) provides the following formula for the buckling coefficient corresponding to the flange tip stress in flanges subjected to longitudinal compression and a constant gradient in stress across the flange width:

$$k_{min} = 0.57 - 0.21\left(\frac{f_1}{f_2}\right) + 0.07\left(\frac{f_1}{f_2}\right)^2 \qquad \text{(2-93a)}$$

where $f_1 = f_b + f_\ell$ is the larger stress, located at the flange tip, and $f_2 = f_b$ is the smaller stress located at the web-flange juncture. This equation is based on the assumption of simply supported boundary conditions at the edge connected to the web. It is interesting to compare the result of this equation to the prediction determined by Davidson and Yoo's (1996) formula. The equivalent form of Eq. (2-93a) that corresponds to the stress at the web-flange juncture, $f_2 = f_b$, is obtained simply by multiplying this equation by f_2/f_1, and after some minor algebraic manipulation may be expressed as

$$k_{min} = 0.43 - 0.57\frac{f_\ell}{f_b + f_\ell} + 0.07\frac{f_\ell}{f_b} \qquad \text{(2-93b)}$$

Figure 2.1.23 compares (2-93b) to the corresponding flange buckling coefficient based on Eq. (2-92) combined with a buckling coefficient of 0.43 corresponding to simply supported conditions at the web-flange juncture. It should be noted that Davidson and Yoo (1996) do not provide any information about the actual buckling strengths calculated in their studies. They only provide information pertaining to the reduction in the elastic buckling capacity due to lateral bending associated with horizontal curvature.

2.1.9.4 Summary

The proposed one-third rule equations have the following advantages relative to other predictor equations that have been evaluated by the authors:

- They are very simple, but they also have a strong conceptual basis in that they allow the engineer to conceptualize the flexural strength of I girder based on the strength of the flanges as equivalent beam columns.

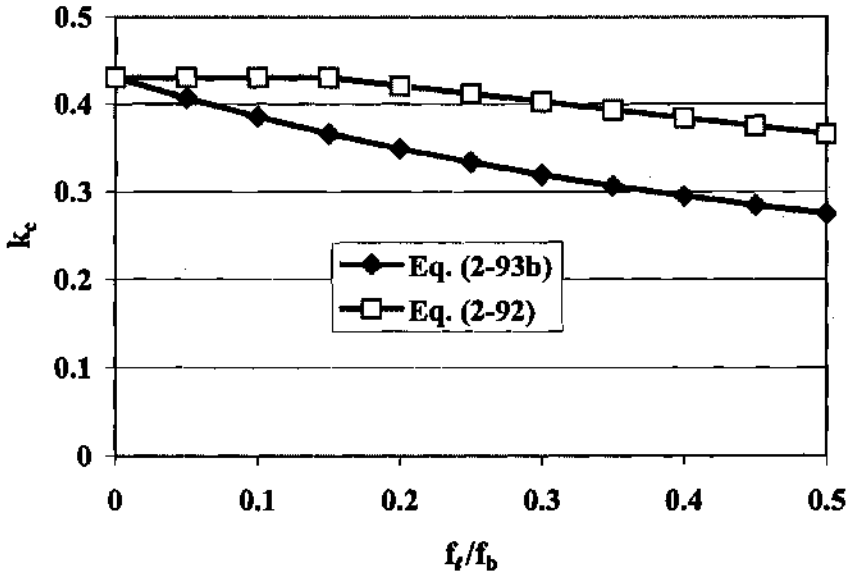

Figure 2.1.23. Flange elastic buckling coefficients based on simply supported conditions at the web-flange juncture versus f_f/f_b.

- They reduce to recommended AASHTO LRFD formulas for the strength of straight I girders in the limit that R approaches infinity. The recommended modifications to the AASHTO straight-girder design strength equations provide more rational and realistic limits for the local buckling strength of compression flanges, and are essentially the same equations as provided in the AISC LRFD (1999) Specification for doubly-symmetric noncomposite plate girders. Also, these equations provide a simpler and more consistent treatment of flange lateral stability for all types of composite and noncomposite I girders than the current AASHTO LRFD (2001) Specifications.

- They do not exhibit any anomalies as the radius of curvature of a curved I girder approaches infinity.

- They do not have any discontinuity in the predicted design strength at the transition between a compact and a noncompact flange, i.e., at $\lambda = \lambda_p$ pertaining to local flange buckling.

- They are applicable to doubly- and singly-symmetric as well as noncomposite and composite I girders, although as noted in Sections 2.1.1 and 2.1.8.1, other formulas based on cross-section plastic strength may provide a better characterization of the strength for straight and curved composite I girders in positive vertical bending. The proposed formulas adopt the same idealization as the current AASHTO LRFD (2001) approach with respect to composite I girders in negative bending, i.e., they neglect the potential beneficial effect of the torsional restraint provided to the tension flange from the bridge deck.

- They account for the potential increase in vertical bending strength due to gradients in the vertical bending moment.

- They allow flange b_f/t_f values up to 24, which is the limit on the flange slenderness in the current AASHTO (2001) straight-girder LRFD provisions. This may lead to significant advantages in terms of the overall economy of the design for resistance to lateral bending and torsion effects, since it allows the flanges to be made wider without increasing the amount of material to satisfy more restrictive b_f/t_f limits.

- They separate the structural analysis problem, i.e., the calculation of the elastic stresses f_b and f_ℓ, from the characterization of the structural resistance. This significantly improves the clarity and transparency of the formulas compared to approaches in which approximate analysis solutions have been "built inside" of the design resistance equations.

- They unify the AASHTO LRFD flexure equations for design of curved and straight I girder design, and handle lateral bending from all potential sources. Furthermore, they maintain a format of the design predictor equations that is close to that of the AISC LRFD (1999) Specification. This should make it easier for young engineers that first learn structural steel design with the AISC LRFD Specification to understand the background behind the fundamental strength prediction equations utilized for bridge design.

- In general, they offer significant improvements in the strength predictions compared to the other flexural strength predictor equations that are evaluated in this research (see Chapters IV, VII, and IX).

2.2 SHEAR STRENGTH

The shear strength of curved I girders has been studied in prior research both analytically and experimentally (Mozer et al. 1970, 1971 and 1975; Mariani et al. 1973, Abdel-Sayed 1973; Davidson 1996; and Lee and Yoo 1999b). It is generally agreed that horizontal curvature has an influence on both the elastic shear buckling strength as well as the maximum strength. The elastic buckling strength of a curved web panel is greater than that of a straight girder panel with the same aspect ratio, material properties, web slenderness ratio, and boundary conditions (Davidson 1996; Mariani et al. 1973; Abdel-Sayed 1973). Both the AASHTO Guide Specifications (AASHTO 1993) and the Recommended Specifications (1998) ignore this benefit and calculate the shear buckling strength based on the current AASHTO equations for straight girders.

Regarding the influence of horizontal curvature on maximum shear strength, results obtained from the experiments conducted by Mozer et al. (1970, 1971, and 1975) indicate that tension field action can indeed be developed in curved girder webs with transverse stiffeners. These investigators observed that the magnitude of the postbuckling strength is reduced by the curvature effects. However, they found that there appears to be no

significant reduction in the web shear strength for practical values of horizontal curvature (e.g., $L_b/R \leq 0.10$). Lee and Yoo (1999) have confirmed these observations. Similar observations have been made in experimental shear tests conducted under the Curved Steel Bridge Research Project (Zureick et al. 2001). It is apparent from these tests that significant postbuckling strength can be developed in web panels of curved I girders.

In this section, four methods of calculating the nominal shear strength of curved and straight steel I girders are discussed and a recommended approach is outlined. First, the method suggested in the Recommended Specifications (1998), which utilizes only the shear buckling strength based on research by Timoshenko (1910), Bergmann and Reissner (1932), Seydel (1933), Bleich (1952) and Basler (1961b), is presented in Section 2.2.1. Next, the approach adopted in the current AASHTO LRFD Specifications for straight girders (AASHTO 2001), which includes the postbuckling reserve strength from Basler's (1961b) tension-field theory in addition to the web buckling strength, is outlined in Section 2.2.2. This is followed by an explanation of ultimate shear strength equations recently proposed by Lee and Yoo (1998) in Section 2.2.3. In Section 2.2.4, a procedure is described that utilizes the shear buckling coefficients proposed by Lee et al. (1996) along with the fundamental shear buckling equations and Basler's tension-field theory for the postbuckling strength. This approach is referred to in this research as the modified AASHTO method. Finally, based on the current and prior research, equations for calculating the shear strength of straight and curved I girders are recommended.

2.2.1 Recommended Specifications (Hall and Yoo 1998)

The Recommended Specifications suggest that, based on prior experimental research on curved girders, Basler's (1961b) analytical model for the buckling strength of flat webs can be used safely for the design of curved webs within stated limitations. The Recommended Specification formulas for the web shear strength are the same as the shear strength equations in the AASHTO Guide Specifications (AASHTO 1993).

To calculate the web shear strength, the Recommended Specifications classify curved web panels into two categories, unstiffened and transversely stiffened. The maximum spacing of transverse stiffeners in stiffened webs is limited to the web depth D, which is the same as that specified in the AASHTO Guide Specifications (AASHTO 1993). Furthermore, the maximum stiffener spacing is limited to D/2 at simple supports. Apparently, this is intended to allow the girder to develop postbuckling shear strength, although this strength is not included in the shear capacity calculations. The web shear strengths for both stiffened and unstiffened girders are calculated based on shear buckling alone; the postbuckling reserve strength is ignored. The boundary conditions at the web-flange juncture are conservatively assumed to be simply supported. On this basis, the shear strength of a curved web panel, V_{cr}, can be calculated as:

$$V_{cr} = CV_p \tag{2-94}$$

where

$$C = 1.0 \quad \text{for} \quad \frac{D}{t_w} < 1.10\sqrt{\frac{Ek}{F_y}} \tag{2-95a}$$

$$C = \frac{1.10}{\left(\frac{D}{t_w}\right)}\sqrt{\frac{Ek}{F_y}} \quad \text{for} \quad 1.10\sqrt{\frac{Ek}{F_y}} \le \frac{D}{t_w} \le 1.38\sqrt{\frac{Ek}{F_y}} \tag{2-95b}$$

$$C = \frac{1.52Ek}{\left(\frac{D}{t_w}\right)^2 F_y} \quad \text{for} \quad \frac{D}{t_w} > 1.38\sqrt{\frac{Ek}{F_y}} \tag{2-95c}$$

and V_p is the web plastic shear strength

$$V_p = 0.58\, F_y\, D\, t_w \tag{2-95d}$$

Equation (2.95a) corresponds to a web that can develop the full plastic shear strength, Eq. (2-95b) gives the strength for a web that buckles inelastically, and Eq. (2.95c) is the web strength corresponding to elastic buckling. The elastic to inelastic buckling transition occurs at $0.8V_p$. The buckling coefficient in these equations (based on simply-supported edge conditions) is specified as

$$k = 5 \tag{2-96a}$$

for unstiffened webs and

$$k = 5 + \frac{5}{\left(\frac{d_o}{D}\right)^2} \tag{2-96b}$$

for transversely stiffened webs (i.e., webs with $d_o/D \le 1$). It should be noted that Eqs. (2-95) and (2-96) are also utilized to quantify the web shear buckling strength of straight I girders in the AASHTO LRFD (2001) Specifications. However, these specifications consider girders as transversely stiffened for $d_o/D \le 3$. Equations (2-96) are simplified from other approximate equations for the shear buckling coefficient utilized by Bleich (1952) and Basler (1961b).

2.2.2 Current AASHTO LRFD Equations

The current AASHTO LRFD equations (AASHTO 2001) subdivide the shear strength into the buckling resistance plus a contribution from postbuckling strength. The buckling resistance equations are the same as those in the Recommended Specifications. As noted

in the previous section, these strengths are based on the assumption of simply supported longitudinal edge conditions. The full set of AASHTO LRFD equations, which are based on the research by Basler (1961b), allow webs with a panel aspect ratio (d_o/D) up to three to be considered as stiffened. Basler initiates the development of his equations by assuming that the plate bending stiffness of the flanges is sufficiently small such that they are not capable of withstanding transverse normal stresses from the web. Based on this assumption, he postulates that the postbuckling strength is developed by constant additional normal stresses σ_t within the diagonal band shown in Fig. 2.2.1.

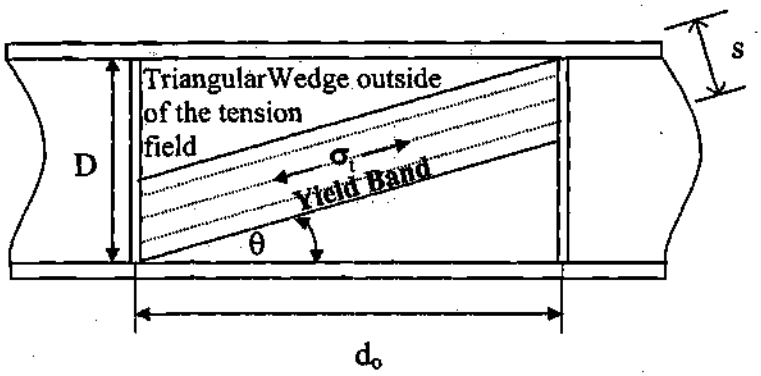

Figure 2.2.1. Assumed tension field in the original and true Basler solutions.

The corresponding contribution to the postbuckling shear resistance is therefore

$$V_{PB} = \sigma_t \, s \, t_w \sin\theta \tag{2-97}$$

where

$$s = D\cos\theta - d_o \sin\theta \tag{2-98a}$$

from the geometry of the panel. Basler then assumes that V_{PB} is maximized with respect to θ to obtain (Salmon and Johnson 1996)

$$\tan 2\theta = D/d_o \tag{2-98b}$$

After some trigonometric and algebraic manipulation, the sum of the buckling and postbuckling resistances may be written as

$$V_n = \tau_{cr} D t_w + \sigma_t \frac{D t_w}{2} \frac{1}{\sqrt{1+\left(\frac{d_o}{D}\right)^2} + \frac{d_o}{D}} \tag{2-99}$$

where τ_{cr} is the web shear buckling stress. This equation has become known as the "true" or "correct" Basler solution (Gaylord 1963; Porter et al. 1975; SSRC 1998). It implicitly assumes that the state of stress within the triangular wedges outside of the tension band remains constant at τ_{cr} once the shear buckling stress is reached.

However, in the next step of his derivation, Basler deviates from this assumption. He considers the free-body diagram shown in Fig. 2.2.2, which is extracted from the girder by making cuts at the mid-depth of the web and at the mid width of the web panels on each side of one of the transverse stiffeners. Based on the previous derivation, it can be shown that the mid-depth cut in this free-body diagram is always inside of the tension band, i.e., the tension band always intersects the transverse stiffeners at a position closer than D/2 from the flanges. Therefore, the horizontal shear force on the mid-depth cut, due to the tension field action, is $\sigma_t t_w d_o \sin\theta \cos\theta$. Basler neglects the increment in the web force F_w due to the girder shear or moment gradient, and assumes that the moment gradient effect is dominated by the increment in the flange force ΔF_f. Given these assumptions, Basler obtains the sum of the buckling and postbuckling contributions to the shear strength as

$$V_n = \tau_{cr} D t_w + \sigma_t \frac{D t_w}{2} \frac{1}{\sqrt{1+\left(\frac{d_o}{D}\right)^2}} \qquad \text{(2-100a)}$$

or

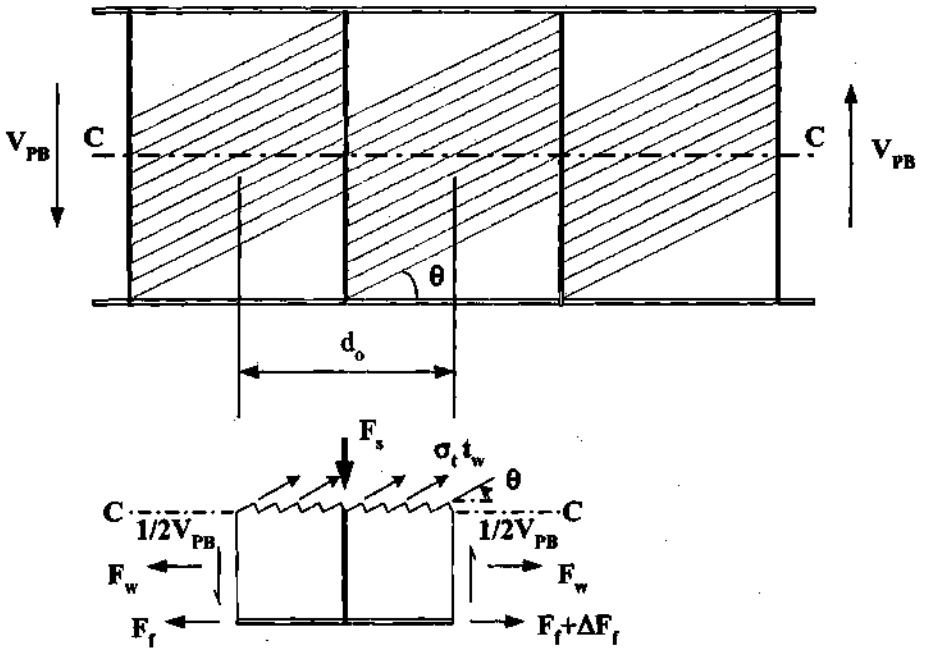

Figure 2.2.2. Free-body diagram at stiffener location.

$$V_n = \tau_{cr} D t_w + \sigma_t D t_w \sin\theta \cos\theta \qquad (2\text{-}100b)$$

where the postbuckling contribution is based on horizontal force and moment equilibrium of the free-body diagram in Fig. 2.2.2. Equations (2-100) are the basis for the (AASHTO 2001) shear strength formulas, and are referred to here as the "original" Basler shear strength. It is apparent from these equations that the panel aspect ratio d_o/D plays an important role in the development of tension-field action and postbuckling strength.

If one considers the possibility that the stresses σ_t can be developed over the full height of the web at any given location along the length of the girder, as shown in Fig. 2.2.3, the contribution of the tension-field membrane stresses to the postbuckling shear resistance is obtained as

$$V_{PB} = \sigma_t D t_w \sin\theta \cos\theta \qquad (2\text{-}101)$$

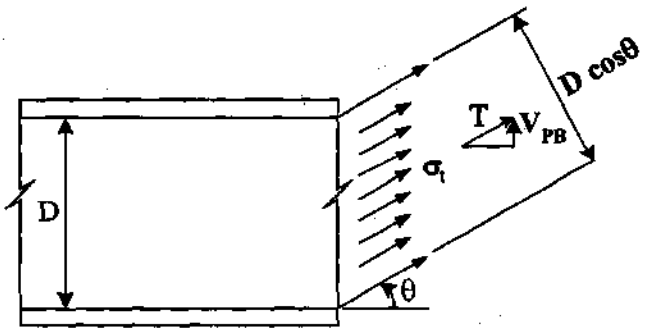

Figure 2.2.3. Membrane stresses associated with a complete tension field.

This postbuckling shear strength contribution is identical to the second term in Eq. (2-100b). In other words, based on the idealized free-body diagram shown in Fig. 2.2.2, Basler implicitly violates his initial assumption that the stresses σ_t are only developed within the tension band of width s. Basler's original shear strength equation is based on the optimum angle θ determined in the context of his initial assumption (Eq. 2-98b), but his final shear strength expression is implicitly based on the stresses σ_t being developed at this angle throughout the entire web panel. That is, Basler's original shear strength formula corresponds to a "complete" tension field. This fact was first noted by Gaylord (1963), and subsequently by Fujii (1968a) and Selberg (1973).

Porter et al. (1975) present an alternative tension field theory that has become known as the Cardiff model. This model explicitly accounts for the contribution of the flanges to the postbuckling resistance, and is possibly the most popular shear strength model outside of the United States. Porter et al. (1975) explain that if the contribution of the flanges to the resistance is neglected, the Cardiff model reduces to the true Basler strength equation, although there is a minor typographical error in the expression for the

true Basler strength in their paper. Therefore, it can be stated that Basler's original formula overestimates the postbuckling strength of a girder whose flanges are incapable of supporting lateral load from the tension field. Gaylord (1963) suggested that this partly explains the tendency of Basler's equations to overestimate his experimental shear strengths as the panel aspect ratio is decreased. Basler (1963) acknowledged Gaylord's observations, but indicated that the stress state in the triangular wedge outside of tension field does not exceed that of the primary tension field, which satisfies the yield condition.

To obtain a simple final solution, either for the original or the true Basler shear strength, it is necessary to make an additional conservative assumption that the angle θ is 45 degrees, such that a principal stress of $\sigma_t + \tau_{cr}$ can be assumed along the tension diagonal direction (which is still otherwise assumed to be oriented at the optimum value of θ) and such that the other principal stress can be assumed to be at $-\tau_{cr}$. Based on this estimate, along with a straight-line approximation of the Mises yield condition within the possible range of these principal stresses (Salmon and Johnson 1996), the tension field membrane stress is obtained as

$$\sigma_t = F_{yw}\left(1 - \frac{\tau_{cr}}{\tau_{yw}}\right) \tag{2-102}$$

where F_{yw} is the yield stress of the web plate and τ_{yw} is the shear yield stress, which is typically taken as $F_{yw}/\sqrt{3}$. By substituting Eq. (2-102) into Eq. (2-100a), the web shear strength equation is obtained in the following form stated with the AASHTO Specifications (2001):

$$V_n = 0.58F_{yw}Dt_w\left(C + \frac{0.87(1-C)}{\sqrt{1+\left(\frac{d_o}{D}\right)^2}}\right) \tag{2-103}$$

To clarify the shear strength predictions based on the original and true Basler solutions, Figs. 2.2.4 and 2.2.5 compare the ratios of these strengths to the web plastic strength, as a function of the web slenderness ratio, for $d_o/D = 1$ and 3 respectively. It can be seen that for $d_o/D = 1$, the ratio of the shear capacity based on the original Basler solution to that based on the true Basler solution varies from 1.04 to 1.30 as D/t_w varies from 100 to 160, whereas for $d_o/D = 3$, this ratio varies from 1.13 to 1.32.

Aydemir (2000) studies a practical range of straight hybrid I girders. He considers I shapes that are practical as bridge girders, but which have relatively small flanges. In his most extreme cases, his flanges have a slenderness $b_f/2t_f$ of 8.75 and the ratio of the area of the web to the average area of the flanges $2A_w/(A_{fc} + A_{ft})$ is equal to 2.4. It is believed that these parameters represent a reasonable extreme for practical bridge I girder design.

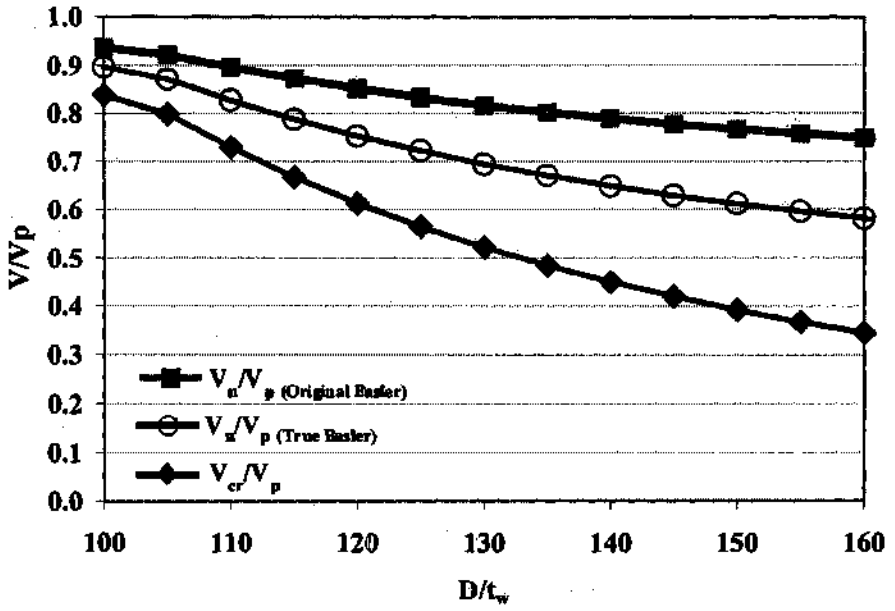

Figure 2.2.4. Shear strengths by Basler's original equations (equivalent to (AASHTO 2001)), the true Basler solution, and the web shear buckling formulas for girders with $d_o/D = 1$ -- shear buckling strength calculated by Basler's equations (Eqs. 2-95) with the (AASHTO 2001) buckling coefficients (Eqs. 2-96).

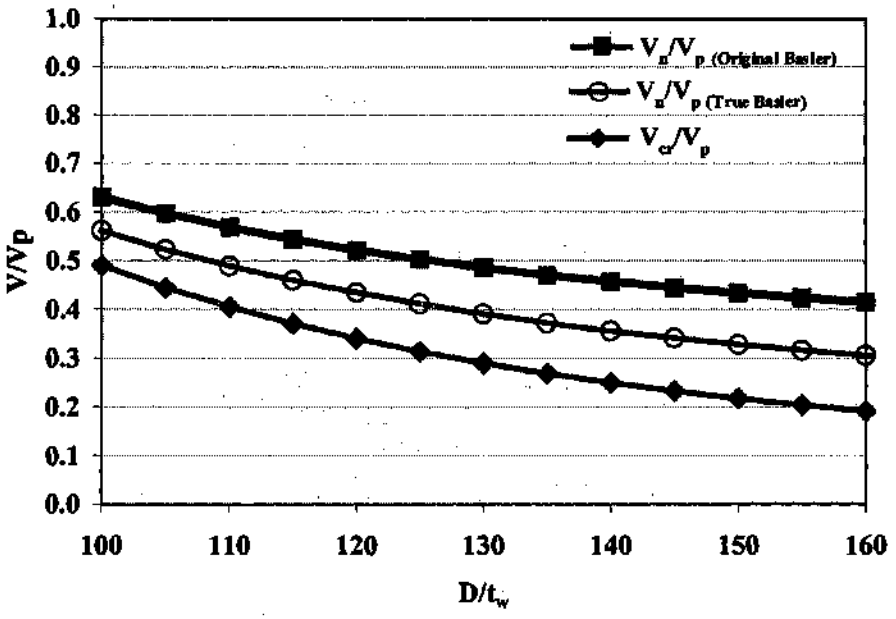

Figure 2.2.5. Shear strengths by Basler's original equations (equivalent to (AASHTO 2001)), the true Basler solution, and the web shear buckling formulas for girders with $d_o/D = 3$ -- shear buckling strength calculated by Basler's equations (Eqs. 2-95) with the (AASHTO 2001) buckling coefficients (Eqs. 2-96).

It is interesting to note that Aydemir observes the same trends in the behavior of Basler's original shear strength equation versus the results of refined full nonlinear shell finite element analyses that Basler (1961b) observes in comparisons to his experimental results. For web panels with large d_o/D, the shear strengths are predicted accurately to conservatively; however, for small d_o/D, Basler's original formula tends to overestimate the capacities somewhat. The maximum unconservative error in Eq. (2-103) observed by Aydemir is 6.2 % for low moment cases, i.e., $M < 0.75\ M_n$, and 10 % for high-shear high-moment cases. This supports Basler's claims that the results of his ten ultimate load tests in shear were sufficient to substantiate his equations, and justify their use within American design practice, e.g., (AISC 1999) and (AASHTO 2001). Basler's (1961b) maximum unconservative error for Eq. (2-103) versus his experimental shear test data is 12 %.

Since Basler (1961b), many alternative tension field theories have been proposed by various researchers (SSRC 1998). Although better accuracy is achievable with some of the alternative models, such as the Cardiff model (Porter et al. 1975), it can be argued that none of the other models retain the combined simplicity and accuracy of Basler's shear strength equations. The more accurate alternative models typically include explicit contributions from the girder flanges both in postulating the stress distribution (e.g., the extent of a tension field) in the web at failure, as well as in providing resistance due to frame action (i.e., plate bending of the flanges) after the web capacity is exhausted. These developments tend to complicate the strength prediction equations substantially.

2.2.3 Lee and Yoo's Equations (1998)

Lee and Yoo (1998) propose shear strength equations that are also based on the summation of an elastic buckling strength (V_{cr}) and a postbuckling strength (V_{PB}). However, they consider the restraint provided by the flanges in calculating the web elastic buckling strength by using simplified equations for the shear buckling coefficient developed by Lee et al. (1996)[2]. Lee et al. (1996) determine that the buckling restraint from the flanges can be quantified sufficiently based on the geometric parameters d_o/D and t_f/t_w. Lee and Yoo's (1998) representation of the postbuckling strength is explained later in this section.

Lee et al. (1996) studied the degree of restraint at the web-flange juncture numerically using elastic finite element models. Figure 2.2.6 shows an idealized model of a plate girder segment between two adjacent transverse stiffeners utilized by Lee et al. (1996) in their research. In order to simulate a state of pure shear, Lee et al. (1996) applied the shearing forces V and $V(D/d_o)$ as shown in figure. Also, they imposed the displacement boundary conditions illustrated in Fig. 2.2.6. The variables studied in their research include d_o/D, D/t_w, D/b_f, and t_f/t_w. Lee et al. (1996) found that the mode shapes of web panels with relatively low values of t_f/t_w are essentially identical to the mode shapes of a

[2] Lee and Yoo (1998) also use a form of the elastic shear buckling equation with the coefficient 1.55 rather than 1.52 as shown in Eq. (2-95c). The coefficient of 1.55 is obtained when τ_{yw} is taken as $F_{yw}/\sqrt{3}$ instead of $0.6\ F_{yw}$.

plate with simply supported boundary conditions at the web-flange juncture. However, as the value of t_f/t_w increases, the mode shapes change from the simply supported case toward that associated with fixed support at the web-flange juncture. They also found that the buckling characteristics are identical in models with the two extreme values of D/t_w examined in their study (D/t_w =80 and 200). Based on these results, Lee et al (1996) concluded that the boundary condition at the web-flange juncture is close to a fixed support for high t_f/t_w ratios, and that the web slenderness ratio does not affect the buckling coefficient significantly.

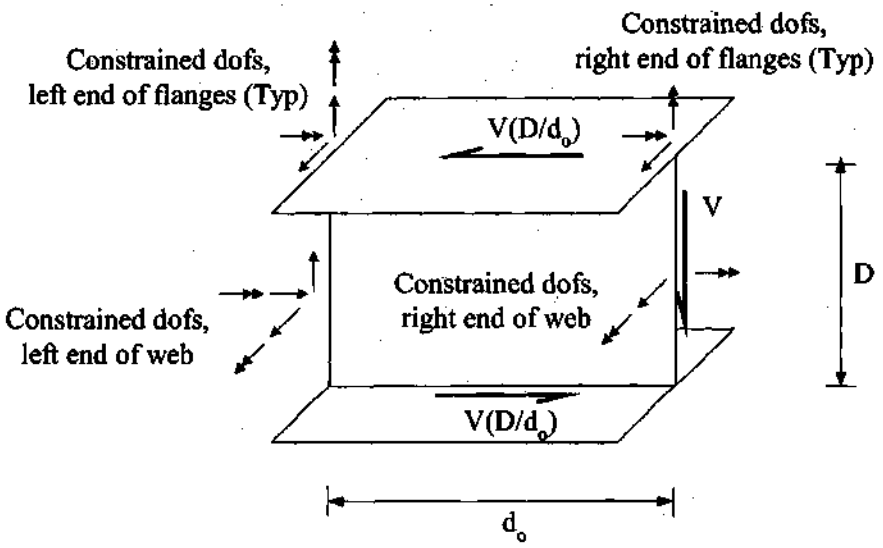

Figure 2.2.6. Typical segment of a plate girder web panel between two adjacent transverse stiffeners, subjected to pure shear edge loading and with zero displacement boundary conditions (Lee et al. 1996).

Lee et al. (1996) propose two equations to be used in the determination of the shear buckling coefficient. For $\frac{1}{2} \le \frac{t_f}{t_w} < 2$, they suggest

$$k = k_{ss} + \frac{4}{5}(k_{sf} - k_{ss})\left[1 - \frac{2}{3}\left(2 - \frac{t_f}{t_w}\right)\right] \qquad (2\text{-}104)$$

and for $\frac{t_f}{t_w} \ge 2$, they specify

$$k = k_{ss} + \frac{4}{5}(k_{sf} - k_{ss}) \qquad (2\text{-}105)$$

where k_{ss} and k_{sf} are the regression formulas for the shear buckling coefficient provided in (SSRC 1998) for a plate simply supported on all sides, and for a plate fully fixed on its longitudinal edges and simply supported on its transverse boundaries:

$$k_{ss} = 4 + \frac{5.34}{\left(\frac{d_o}{D}\right)^2} \qquad \text{for } \frac{d_o}{D} < 1$$

$$= 5.34 + \frac{4}{\left(\frac{d_o}{D}\right)^2} \qquad \text{for } \frac{d_o}{D} \geq 1 \tag{2-106a}$$

$$k_{sf} = \frac{5.34}{\left(\frac{d_o}{D}\right)^2} + \frac{2.31}{\left(\frac{d_o}{D}\right)} - 3.44 + 8.39\frac{d_o}{D} \quad \text{for } \frac{d_o}{D} < 1$$

$$= 8.98 + \frac{5.61}{\left(\frac{d_o}{D}\right)^2} - \frac{1.99}{\left(\frac{d_o}{D}\right)^3} \quad \text{for } \frac{d_o}{D} \geq 1 \tag{2-106b}$$

Bradford (1996) also studies the effect of restraint from the flanges on the web elastic shear buckling capacity, and develops charts for the shear buckling coefficient that give values very close to those predicted by Eqs. (2-104) through (2-106).

For the contribution from postbuckling strength, Lee and Yoo (1998) conclude that, when the plastic shear force (V_p) is greater than the elastic shear buckling strength (V_{cr}), the postbuckling strength (V_{PB}) is approximately equal to 40% of the difference between V_p and V_{cr}. Therefore, they suggest that the postbuckling strength can be predicted by

$$V_{PB} = 0.40\,(V_p - V_{cr}) \tag{2-107}$$

They then obtain the nominal shear strength by adding V_{PB} to V_{cr}. By introducing C, defined as the ratio of shear buckling strength to plastic shear strength (see Eqs. (2-94) and (2-95)), the base nominal shear strength equations proposed by Lee and Yoo can be expressed as

$$V_n = V_p(C + 0.4\,[1 - C]) \tag{2-108}$$

Lee and Yoo (1998) state that the above equation is applicable only for web panels with relatively small initial out-of-flatness (equal to D/120000). Furthermore, they observe that due to web initial out-of-flatness and the postbuckling response, significant plate bending occurs within the web prior to the development of the maximum shear

strength. They conclude that a significant limitation of prior web strength models is that these plate bending stresses are not considered, and that their effects should be accounted for directly. To account for these effects, Lee and Yoo evaluate the shear strengths via finite element analysis for web panels with an initial out-of-flatness equal to D/120, which is within the fabrication tolerances for transversely-stiffened girders specified by AWS/AASHTO (1996). They find from their analysis results that, when the elastic shear buckling strength is greater than the 80 percent of the shear yield strength (i.e., when the web slenderness is smaller than that associated with the elastic to inelastic buckling web transition from Eq. (2-95b), $D/t_w \le 1.10\sqrt{Ek/F_{yw}}$), the ultimate shear strength is reduced by approximately 20 percent due to initial out-of-flatness. On the other hand, the strength reduction due to initial imperfections for web panels with $D/t_w \ge 2.20\sqrt{Ek/F_{yw}}$ is found to be insignificant. Furthermore, for the range of web slenderness ratios between these two limits, Lee and Yoo report that the strength reduction varies almost linearly from 20 to zero percent. Therefore, they propose a reduction factor to represent the influence of initial imperfections as

$$R = 0.8 \qquad \text{for} \quad \frac{D}{t_w} < 1.10\sqrt{\frac{Ek}{F_{yw}}} \tag{2-109a}$$

$$R = 0.8 + 0.2\frac{\dfrac{D}{t_w} - 1.10\sqrt{\dfrac{Ek}{F_{yw}}}}{1.10\sqrt{\dfrac{Ek}{F_{yw}}}} \qquad \text{for} \quad 1.10\sqrt{\frac{Ek}{F_{yw}}} \le \frac{D}{t_w} \le 2.20\sqrt{\frac{Ek}{F_{yw}}} \tag{2-109b}$$

and

$$R = 1.0 \qquad \text{for} \quad \frac{D}{t_w} > 2.20\sqrt{\frac{Ek}{F_{yw}}} \tag{2-109c}$$

The final form of the shear strength equation proposed by Lee and Yoo (1998) is thus

$$V_n = R\,V_p(C + 0.4\,[1 - C]) \tag{2-110}$$

Based on the results of the current research, the authors find that the use of the shear buckling coefficient from Eq. (2-104) generally gives an improvement in the prediction of elastic shear buckling strength (see Section 8.2); however, Eq. (2-110) yields nonintuitive results for the postbuckling strength. Figure 2.2.7 plots V_{PB}/V_p and $(V_n - V_{cr})/V_p$ from Eqs. (2-107) and (2-110) versus the panel aspect ratio for an I girder with $F_{yw} = 345$ MPa (50 ksi), $D/t_w = 160$ and $t_f/t_w \ge 2$. It can be stated that V_{PB} in these equations is the unreduced postbuckling resistance, and that $(V_n - V_{cr})$ is the actual postbuckling resistance after the imperfection factor R is applied. It can be seen that Eq.

(2-107) predicts a slight increase in V_{PB} as the panel aspect ratio is increased, and that when the postbuckling strength is interpreted as $(V_n - V_{cr})$, this increase is accentuated.

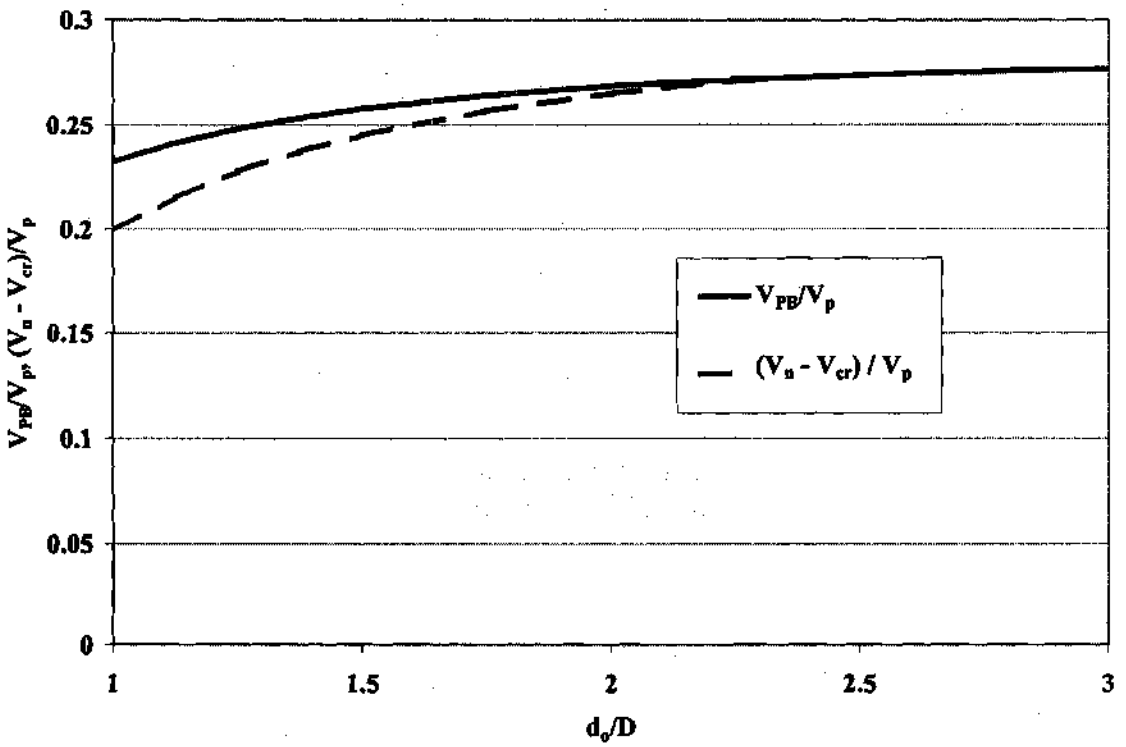

Figure 2.2.7. Predicted ratio of V_{PB}/V_p and $(V_n - V_{cr})/V_p$ from Eqs. (2-107) and (2-108) as a function of d_o/D for a girder with D/t_w =160 and $t_f/t_w \geq 2$.

Equation (2-107), i.e., the assertion that the postbuckling resistance V_{PB} is constant at 40 percent of the difference between the plastic shear and elastic buckling strengths, is simply a coarse approximation of the postbuckling strengths observed in full nonlinear finite element analyses of nearly flat web panels (out-of-flatness of D/120,000) with the idealized load and displacement boundary conditions shown in Fig. 2.2.6 (Lee and Yoo 1998). It does not have a theoretical basis. However, the buckling load V_{cr} generally decreases with increasing panel aspect ratio; therefore, the postbuckling resistance estimated by Eq. (2-107) (or based on $(V_n - V_{cr})$, with V_n obtained from Eq. (2-108)) tends to increase with increasing d_o/D. This is contradictory to prior experimental and analytical research (e.g., Basler 1961b and Porter et al. 1975) as well as results from this research presented in Chapter VIII. The correct contribution from the postbuckling strength tends to decrease as the panel aspect ratio is increased.

Nevertheless, the observation by Lee and Yoo (1998; 1999a) that significant plate bending exists in web panels at their shear strength limit state, and that these actions may influence the web shear capacity, are in the view of the authors important new developments. Furthermore, Lee and Yoo provide evidence in their papers that anchorage of a tension field by the flanges is not necessary for the development of

postbuckling strength. They observe in their finite element and experimental studies that the flange plate-bending stresses do not increase noticeably to any degree after the buckling strength of the web is exceeded. Furthermore, they show that at the maximum shear capacity of the web, the plate bending stresses in their flanges are typically small (i.e., much smaller than that required to initiate a flange plastic collapse mechanism), and that the flange rigidity appears to have little effect on the postbuckling strength of web panels.

Lee and Yoo provide the theoretical sketch shown in Fig. 2.2.8a to explain that, after buckling, additional shear stresses equal to $\tau - \tau_{cr}$ can equilibrate the diagonal tension, σ_t; therefore, there is no need for any anchoring system from the flanges. However, their argument via this sketch requires an equal compressive stress due to tension-field action on the other diagonal of the differential element. Conversely, additional diagonal membrane compressive stresses (if any) must be smaller than the incremental diagonal tension stresses after shear buckling occurs. Therefore, some transverse loading on the flanges would still be expected within the postbuckling range of the behavior based on this sketch.

Marsh and Ajam (1987) and Marsh et al. (1988) provide a more precise theoretical argument for development of postbuckling strength without anchorage from the flanges. Fig. 2.2.8b summarizes their explanation. Based on Mohr's circle, it can be concluded that significant diagonal tension, along with a smaller diagonal compression in the other principal direction, can be developed at the web-flange boundary without the development of any transverse loading on the flanges. Marsh and Ajam (1987) further explain that

> **"In practice, for an imperfect panel, the stress is never uniform and, as the panel distorts after the bifurcation stress is reached, the distribution is radically modified. The diagonal strips in compression are shorter the closer they are to the 'tension corner' and thus can sustain higher stresses before buckling. In the corner, where the strips are very short, the yield stress in shear can be resisted along the boundary. At this stage, in the corner, the principal tension and compression stresses are then equal to half the yield stress in tension [based on the Tresca yield criterion]. In this limiting condition, the shear stress varies along the boundary from a value close to the initial critical shear stress at one end, to the yield stress in shear at the other. The system is elastic and requires only that the flanges have axial rigidity, as no stress normal to the boundary is postulated.... For long panels with end stiffeners only, the direction of the principal stresses is rotated in such a manner that an increasing shear force can be sustained with a constant principal compressive stress equal to the critical shear stress...."**

Unfortunately, the strength prediction model proposed by Ajam and Marsh (1991) requires consideration of the flange proportions and loading due to vertical bending in order to attain good accuracy relative to experimental results.

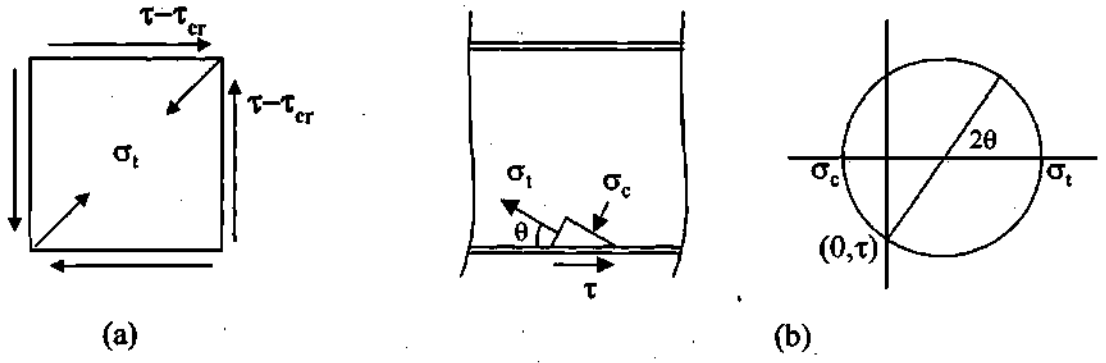

Figure 2.2.8. Diagonal tension and lack of a need for anchorage from the flanges: (a) Differential element in the web, at the web-flange juncture, after buckling (Lee and Yoo 1998) and (b) Stress state illustrated by Ajam and Marsh (1991).

It is clear from Lee and Yoo's (1999) experimental research that the failure of a web panel in shear can occur prior to the development of plastic hinges in the girder flanges. However, it should be noted that the girders studied experimentally by Lee and Yoo (1999a) have a small ratio of the area of the web to the average area of the flanges ($2A_w/(A_{fc} + A_{ft})$ in their ten experimental tests ranges from 0.60 to 1.23), four of these tests have quite stocky flanges with $b_f/2t_f \leq 5$, and seven have compact flanges with $b_f/2t_f \leq 6.65$. For girders with smaller and more slender flanges, the bending of the flanges may be more significant. Furthermore, Marsh and Ajam (1987), Marsh et al. (1988) and Ajam and Marsh (1991) show significant enhancement in the shear capacity due to frame action in girders with heavy flanges.

Lee and Yoo (1998) consider a wide range of flange sizes (i.e., flange rigidities) in numerical studies of the maximum shear strength of web panels. However, these studies are based on the idealized boundary conditions along the edges of the web panel shown in Fig. 2.2.6. It is suspected that their numerical results, particularly within the postbuckling range of the response, could be falsely skewed by the idealized applied pure shear loading along the web boundaries. This difficulty is circumvented within the current research by modeling complete girders with support and loading conditions exactly as would be utilized in experimental laboratory shear tests. Also, since the rotations are not restrained about a horizontal axis at the ends of the flanges in their finite element model (see Fig. 2.2.6), the development of frame action would be limited in their analysis predictions.

Basler (1961b) also recognizes the behavior discussed above regarding anchorage from the flanges. He states regarding his experimental results, "Strain gages mounted on the flanges of the test girders confirm that the plate bending effect prior to ultimate load is negligibly small." Furthermore, Basler argues that although Eq. (2-103) would indicate that the flanges in his tests would be loaded substantially beyond their yield stress in plate bending, his theory is still acceptable. Gaylord (1961) also states that,

"The good correlation between predicted values and experimental results cannot be dismissed. For this reason, the author's analysis may be an acceptable prediction of the postbuckling behavior of thin-webbed girders for the practicable range of parameters in civil engineering practice."

It should be noted that $2A_w/(A_{fc} + A_{ft})$ is relatively low also in Basler's ten shear tests (ranging from 0.72 to 1.09, including the area of cover plates welded to the flanges in two of the tests) (Basler et al. 1960), and all of his flanges have $b_f/2t_f \cong 8$. As noted in Section 2.2.2, Aydemir (2000) considers larger $2A_w/(A_{fc} + A_{ft})$ and $b_f/2t_f$ values in his finite element studies. These studies confirm the adequacy of Basler's (1961b) shear strength equations for straight girders up to $2A_w/(A_{fc} + A_{ft}) = 2.4$.

It should be noted that the shear strength equations proposed by Lee and Yoo (1998) are somewhat more complex than the corresponding current AASHTO LRFD (2001) equations, due to the calculation of the more accurate shear buckling coefficient, and due to the application of the imperfection factor R in the nominal capacity equations. Nevertheless, if these equations provide significantly more accurate results, their minor additional complexity may be merited. Unfortunately, the results of this research, the research reported in (Zureick et al. 2001), and Aydemir's (2000) research indicate that Eq. (2-110) does not perform as well as the current AASHTO LRFD (2001) equations.

2.2.4 Modified AASHTO LRFD Equations

It is desirable to maintain the simplicity of the current AASHTO equations as much as possible in considering any potential enhancements in predictors of the shear capacity. One possible approach considered in this research is the use of the shear buckling coefficient equations proposed by Lee et al. (1996) for calculation of the buckling strength, along with Basler's model for the postbuckling strength, within the present AASHTO shear strength equation (Eq. 2-103). As shown later in Chapter VIII, Lee and Yoo's shear buckling coefficient gives significantly improved predictions of the shear buckling load for the girders studied in this research, compared to the use of the current AASHTO shear buckling coefficient (Eqs. 2-96). The resulting shear strength equations are referred to here as the modified AASHTO equations. Also, Chapter VIII shows that, of the equations considered in this research, the best predictions of the maximum shear capacities are obtained from this approach.

It is interesting to evaluate the application of Lee and Yoo's shear buckling coefficient in conjunction with the true as well as the original Basler equations. Figures 2.2.9 and 2.2.10 compare the results for both of these models for panel aspect ratios (d_o/D) of 1 and 3. A value of $t_f/t_w \geq 2$ is assumed. These figures parallel Figs. 2.2.4 and 2.2.5 so that the effect of the modified shear buckling coefficient also can be ascertained. The term $V_{n(\text{Original Basler})}$ represents the modified AASHTO equations using Basler's original solution for tension field action, as adopted in the current AASHTO LRFD equations, whereas the term $V_{n(\text{True Basler})}$ represents the modified AASHTO equations using the true Basler solution for tension field action.

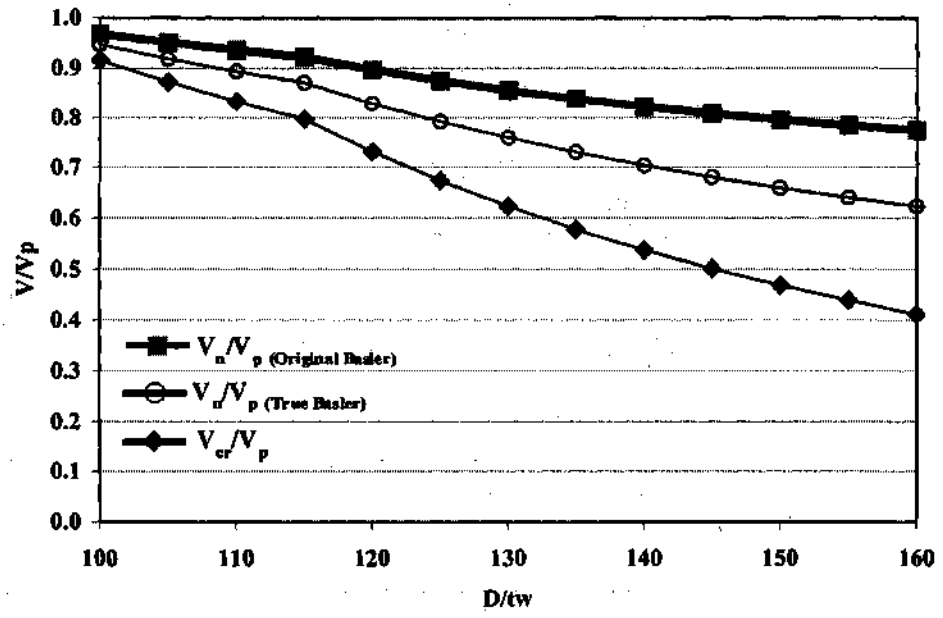

Figure 2.2.9. Shear strengths by Basler's original equations, the true Basler solution, and the web shear buckling formulas for girders with $d_o/D = 1$ and $t_f/t_w \geq 2$ -- shear buckling strength calculated by Basler's equations (Eqs. 2-95) using the shear buckling coefficients by Lee et al. (1996).

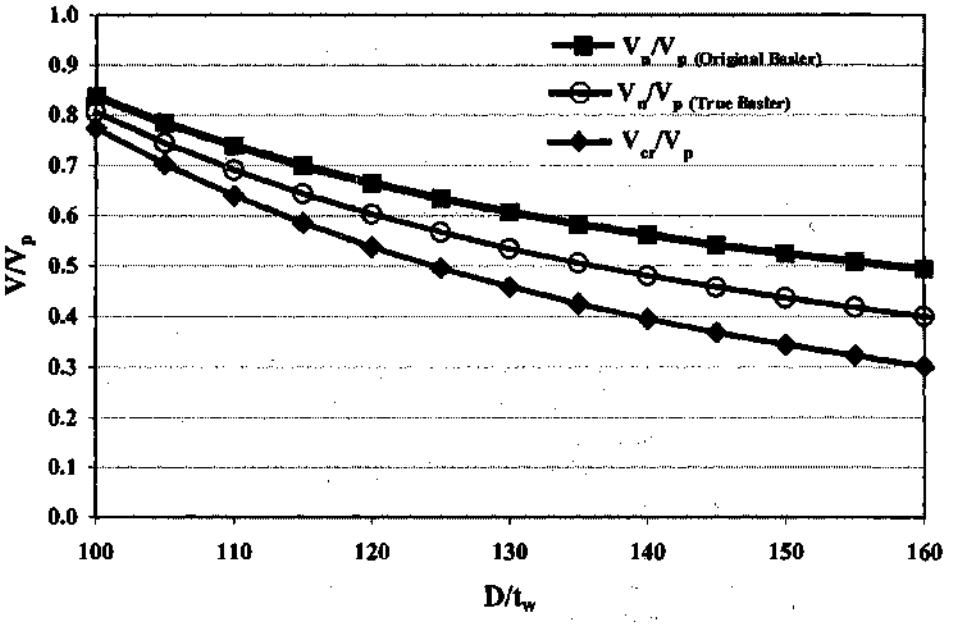

Figure 2.2.10. Shear strengths by Basler's original equations, the true Basler solution, and the web shear buckling formulas for girders with $d_o/D = 3$ and $t_f/t_w \geq 2$ -- shear buckling strength calculated by Basler's equations (Eqs. 2-95) using the shear buckling coefficients by Lee et al. (1996).

It can be observed that the modified AASHTO equations based on the true Basler solution yield significantly conservative predictions compared to the modified AASHTO equations with Basler's original tension field equation. The ratio of the shear capacity obtained from the modified equations using the original Basler solution to that using the true Basler strength ranges from 1.02 to 1.24 for $d_o/D = 1$ as D/t_w varies from 100 to 160, and from 1.04 to 1.24 for $d_o/D = 3$. Based on the significantly higher strengths associated with the original Basler solution, and based on the lack of significantly unconservative results with Basler's original equation (Eq. 2-103) relative to tests and finite element analyses considered in this research, only the original Basler postbuckling strength contribution is considered further in this research. However, both the corresponding AASHTO (2001) and modified AASHTO equations are evaluated.

By comparing the results based on the original Basler postbuckling strength in Fig. 2.2.9 to those in Fig. 2.2.4, it can be observed that the increase in the predicted shear capacities for $d_o/D = 1$ associated with the use of Lee and Yoo's (1996) shear buckling coefficient ranges only from 1.03 to 1.06. In other words, for small transverse stiffener spacing ($d_o/D \leq 1$), the difference in the maximum shear strengths predicted assuming simply-supported boundary conditions at the web-flange junctures versus assuming substantial restraint from the flanges is small. However, by comparing Figs. 2.2.10 and 2.2.5, it can be determined that the corresponding increase in capacities for $d_o/D = 3$ ranges from 1.33 (at $D/t_w = 100$) to 1.19 (at $D/t_w = 160$). These comparisons are shown for several values of d_o/D in Fig. 2.2.11.

2.2.5 Recommended Equations

Based on the results of this and other contemporary research, it is recommended that as a minimum the AASHTO LRFD (2001) equations, including tension-field action, should be adopted to quantify the maximum shear strength of both straight and horizontally-curved I girders. These equations provide a simple and acceptable prediction of the shear strength. From consideration of maximum strength alone (other issues are addressed below), the current research shows that the limits on the web slenderness and panel aspect ratios in the Recommended Specifications can be relaxed. The limit of $d_o/D \leq 3$ for designing girders as transversely stiffened, as required by the current AASHTO LRFD (2001) straight-girder Specifications, is found to be adequate also for curved I girders with $L_b/R \leq 0.10$. Since the shear strength data for transversely-stiffened I girders with a large ratio of the area of the web to the area of the flanges is very scarce, it is suggested that $2A_w/(A_{fc} + A_{ft}) = 2.4$ be taken as a practical upper limit for including the contribution of tension field action to the shear strength.

The modified AASHTO LRFD equations (see Section 2.2.4) are found to provide the best accuracy of the equations considered. The improvement in accuracy and the increase in the nominal shear strength relative to the current equations are minor for small d_o/D values, but they are significant for large panel aspect ratios. Therefore, the modified AASHTO equations should be given serious consideration. The current AASHTO LRFD (2001) shear strength equations tend to give liberal predictions for small d_o/D values (see Section 2.2.2). The modified AASHTO LRFD equations tend to give liberal strength

predictions for some cases with intermediate d_o/D values (see Section 8.1.1). When combined with appropriately derived resistance ϕ factors, it is expected that the factored design shear strengths with the modified AASTHO equations will be slightly more conservative than the current AASHTO equations for small d_o/D. However, the factored shear strengths will likely be significantly larger than the values predicted by the current AASHTO equations for large d_o/D values.

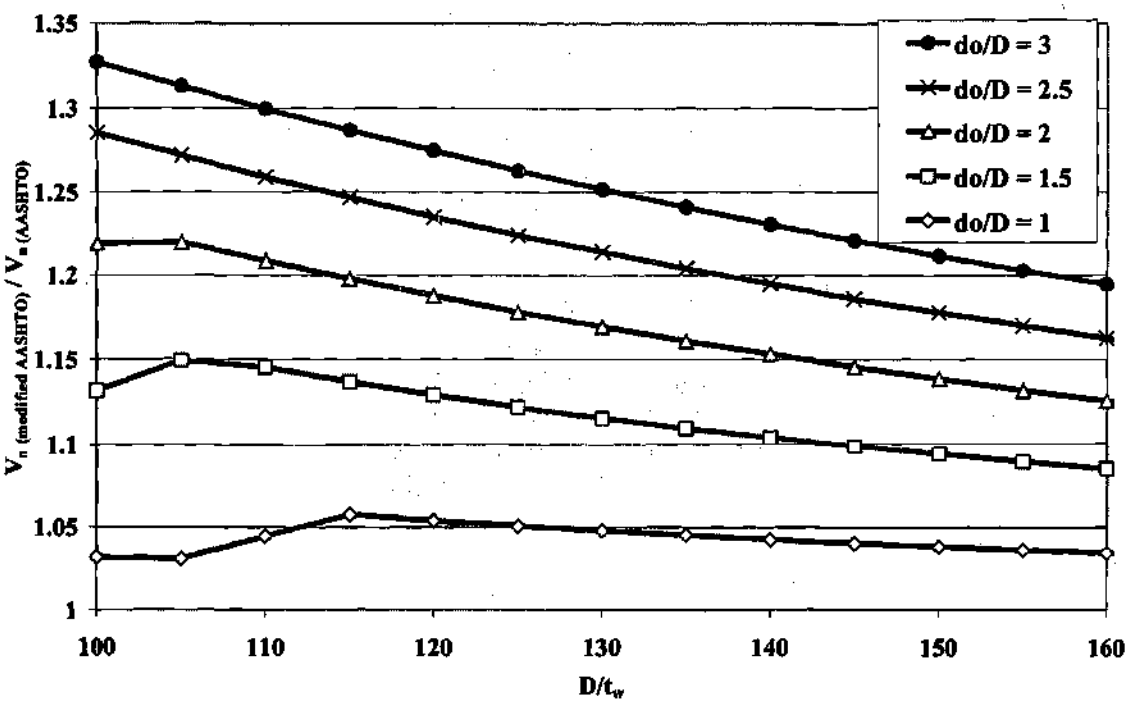

Figure 2.2.11. Ratio of V_n from modified AASHTO equations to V_n based on current AASHTO equations for girders with $t_f/t_w \geq 2$.

The above recommendations are focused on transversely stiffened I girders of Grade 345 steel, with D/t_w values up to 160. It should be noted that Lee and Yoo (1998) show substantial overprediction of the web shear capacity by Basler's (1961b) equations for larger web slenderness and $d_o/D < 1.5$. Further discussion of these recommendations is provided in Section 8.4.

There is one major issue that still needs to be addressed before the more accurate shear buckling coefficients from the research by Lee et al. (1986) can be adopted universally within the AASHTO LRFD (2001) Specifications. The current specifications restrict the shear stresses within I girder webs to the elastic buckling stress under fatigue loading conditions, based on the assumption of simply-supported boundary conditions at the flanges. Montgomery (1987) observed that girders tested under fatigue loading above the elastic shear buckling capacity – based on the current AASHTO LRFD (2001) equations – generated cracks along the welds connecting the web to the flange and also to

the stiffeners. The implications of the use of the more accurate shear buckling coefficients on this check needs to be investigated before these coefficients can be applied to these provisions. However, short of reinvestigating these fatigue limits, the shear buckling coefficients based on simply-supported boundary conditions at the flanges can be utilized for the fatigue provisions, and the more accurate shear buckling coefficients can be utilized for checking of maximum strength.

Prior to liberalizing the shear strength provisions as described above, further research on the fatigue strength of curved girder webs would be useful. As noted previously, the most recent experimental research regarding fatigue of curved I girder webs was conducted by Daniels and Herbein (1980). Based on this research, limits on web slenderness were proposed as summarized in Section 2.2.2 (see (Eq. 2-51)). If the Recommended Specification provisions for web design are liberalized, this equation, or a modified form of this formula based on further research, might be adopted to address fatigue issues. Alternatively, it is possible that checks based on web buckling under fatigue loading conditions might be sufficient up to some limit on the horizontal curvature. The reader is referred to Section 2.2.2 for a discussion of these issues.

2.3 MOMENT-SHEAR INTERACTION

2.3.1 Recommended Specifications

Interaction between moment and shear is not considered in the Recommended Specifications (Hall and Yoo 1998) for neither stiffened nor unstiffened curved I girders. This is also the practice in the AASHTO Guide Specifications (AASHTO 1993). Hall and Yoo (1998) explain that, for unstiffened webs, the bend-buckling coefficient is lowered to 7.2 to provide some conservatism for cases where unstiffened web panels are subjected to both high shear and high moment (note that (AASHTO 2001) also assumes $k = 7.2$ for calculation of R_b in girders with $D_c > D/2$). Also, for stiffened webs, the postbuckling strength in bending and shear is not included within the member design equations. As a result, there is no need to check moment-shear interaction for either stiffened or unstiffened webs.

2.3.2 AASHTO LRFD (2001)

The design strength curve for moment-shear interaction in the current AASHTO LRFD Specifications (2001) is shown in Fig. 2.3.1. This curve is based largely on the research by Basler (1961c). Reduction in the shear capacity due to bending moment is assumed to be negligible when $M \le 0.75\, M_n$. Similarly, the reduction in bending capacity resulting from coincident shear is ignored when $V \le 0.60V_n$,. However, when either of these limits is exceeded, plate girders with webs designed for tension-field action must satisfy the following flexure-shear interaction check:

$$\frac{M}{M_n} + 0.625\frac{V}{V_n} \le 1.375 \qquad (2\text{-}111)$$

For unstiffened girders and for other girders designed based only on the shear buckling strength, AASHTO LRFD (2001) does not require any moment-shear interaction check.

Equation (2-111) is a conservative fit to analytical moment-shear interaction curves developed by Basler (1961c), and to Basler's experimental test data. Basler bases his conclusions regarding moment-shear interaction largely on a theoretical lower-bound plastic analysis of the web, considering possible states of stress that are in equilibrium with the applied moment and shear, yet nowhere violate the yield condition. In this analysis, he assumes that the section can attain the plastic moment capacity in the absence of shear, and that the plastic flanges, by themselves, resist the moment at the maximum shear capacity of the section (associated with uniform shear yielding within the web). He takes the cross-section yield moment M_y as the design moment capacity.

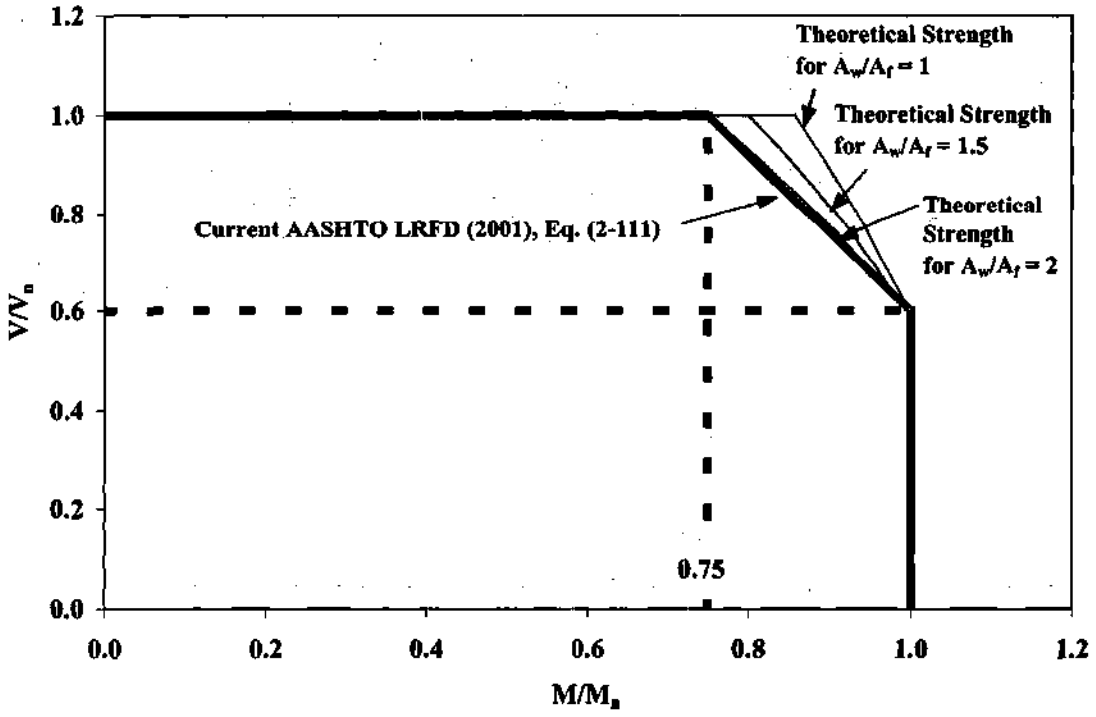

Figure 2.3.1. AASHTO LRFD (2001) moment-shear interaction for panels designed based on tension-field action versus theoretical M-V interaction curves from Basler's (1961c) developments.

Figure 2.3.2 shows the stress distributions associated with the moments used in Basler's derivation. Based on the assumption of a homogeneous doubly-symmetric I section, the moment resisted by the flanges when they are fully yielded is computed as

$$M_f = A_f F_y D \qquad (2\text{-}112)$$

Furthermore, Basler calculates the corresponding contribution of the web to the yield moment as

$$M_w = \frac{F_y A_w D}{6} \tag{2-113}$$

such that the yield moment can be approximated as

$$M_y = M_f + M_w = A_f F_y D\left(1 + \frac{1}{6}\frac{A_w}{A_f}\right) \tag{2-114}$$

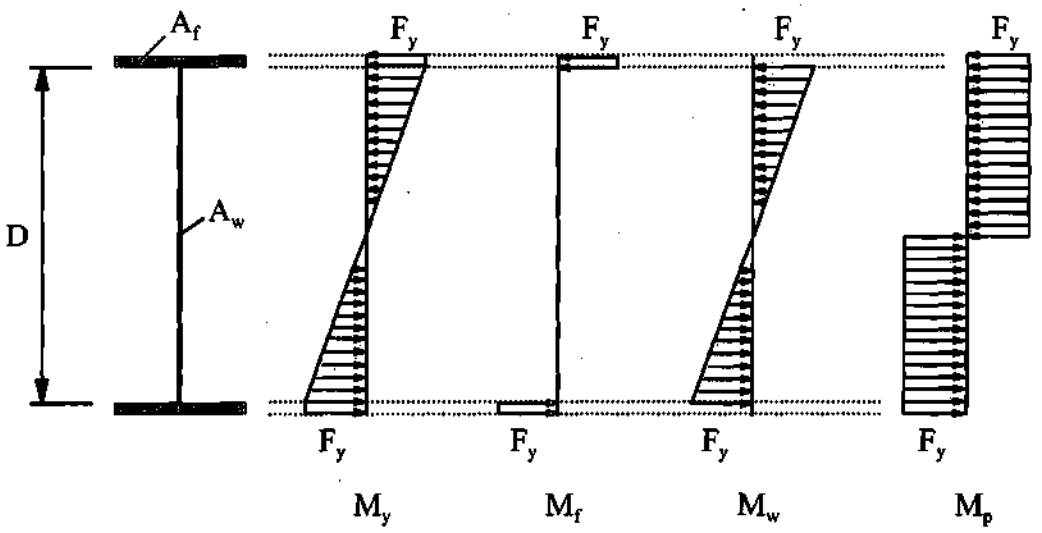

Figure 2.3.2. Reference moments utilized by Basler (1961c).

Basler develops his theoretical moment-shear interaction relationship by assuming that a central portion of the web of depth D_{wy} yields in shear as shown in Fig. 2.3.3. The remaining plastic section is assumed to be available to resist the moment. The nominal shear resisted by the middle portion of the web is taken as

$$V = D_{wy}\, t_w\, \tau_y \tag{2-115}$$

Therefore, Basler obtains

$$D_{wy} = \frac{V}{V_p} D \tag{2-116}$$

Basler's remaining flexural capacity is thus

$$M_n' = A_f F_y D + \left(t_w \frac{D}{2}\right) F_y \left(\frac{D}{2}\right) - \left(t_w \frac{D_{wy}}{2}\right) F_y \left(\frac{D_{wy}}{2}\right) \tag{2-117a}$$

which can be written as

$$M_n' = A_f F_y D \left[1 + \frac{A_w}{4A_f}\left(1 - \left(\frac{V}{V_p}\right)^2\right)\right] \tag{2-117b}$$

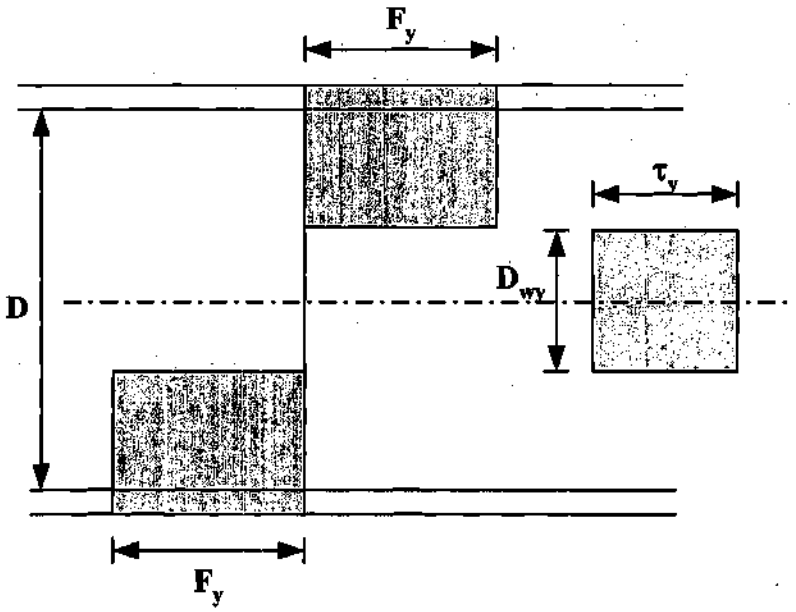

Figure 2.3.3. Shear and moment strengths under combined bending and shear.

Finally, if we divide Eq. (2-117b) by Eq. (2-114), we obtain

$$\frac{M_n'}{M_y} = \frac{1 + \frac{A_w}{4A_f}\left(1 - \left(\frac{V}{V_p}\right)^2\right)}{1 + \frac{1}{6}\left(\frac{A_w}{A_f}\right)} \tag{2-118}$$

Based on Eq. (2-118), it can be observed that the theoretical reduction in the moment capacity due to shear depends on the ratio of the applied web shear force to the web shear capacity (V/V_p) and on the ratio A_w/A_f. Basler then considers that for practical girders, A_w/A_f will be less than or equal to two. This analysis has subsequently been extrapolated to represent a theoretical M-V strength interaction curve for plate girders by

replacing M_y in Eq. (2-118) by the nominal moment capacity in the absence of shearing, $M_n \leq M_y$, and by replacing V_p in this equation by the nominal shear capacity (including the postbuckling strength) in the absence of bending moment, $V_n \leq V_p$. The resulting curves are shown in Fig. 2.3.1 for $A_w/A_f = 1$, 1.5 and 2. It can be seen that when $A_w/A_f = 2$, $M_n' = 0.75M_y$ at $V/V_p = 1$ in Eq. (2-118).

There are several places where potentially conservative assumptions are introduced in the above developments:

- In the lower-bound plastic analysis of the web. Basler (1961c) shows an alternative lower-bound solution that produces less severe moment-shear interaction for the compact-section assumptions utilized in his derivation.

- In the selection of $A_w/A_f = 2$ as a practical upper-bound value for substitution into Eq. (2-118). Note that for $A_w/A_f > 2$, Eq. (2-111) is unconservative relative to the theoretical M-V interaction equations.

- In setting V_p to V_n and M_y to M_n in Eq. (2-118). In a typical plate girder, V_n is significantly smaller than V_p and M_n is somewhat smaller than M_y. As a result, it is possible that the interaction effects are less severe than inferred by Basler's lower-bound plastic analysis. The actual stress state in the web of a slender-web plate girder subjected to high moment and high shear is of course very different than the simple stress-distribution assumed in Basler's derivation.

- In neglecting the potential benefit of localized strain-hardening within the web panel. For the only type of cross-section that Basler's analysis strictly applies (i.e., a compact web section), plastic design research has shown that the corresponding moment-shear interaction can be neglected (ASCE-WRC 1971).

- In approximating the lower-bound plastic analysis results for the moment-shear interaction by a linear equation (although it can be observed from Fig. 2.3.1 that a linear relationship between $0.6V_n$ and M_f represents Basler's theoretical predictions rather well).

- In the conservatism of the nominal design M_n and V_n values relative to the actual girder capacities for many (but not all) cases. In many girders, even though there is some small reduction in strengths due to high moment and high shear, all the data points for the strengths (M, V) fall outside of the rectangular box defined by the nominal girder moment and shear capacities.

Therefore, it is to be expected that in many practical situations, the actual strength under the action of high moment and high shear is significantly greater than implied by the AASHTO LRFD (2001) M-V interaction equation (Eq. 2-111).

Furthermore, as noted in Chapter I, Aydemir (2000) observes that Basler introduces conservative assumptions in comparisons of his experimental test data to his moment-shear interaction curves. Basler (1961c) discusses that, based on the fact that local buckling does not occur at the maximum moment location in his tests (due to the presence of a transverse stiffener at that location), the proper position for calculating the applied moment for the M-V interaction check is at a minimum of ($D/2$, $d_o/2$) from the maximum moment point. This interpretation is incorrect. The proper location for checking the flexural strength *for conditions of low shear* is the peak moment location. At regions subjected to high shear and high bending moment, the moment drops rapidly as we move away from this position. This drop is required for satisfaction of equilibrium, and is not due to M-V interaction. Therefore, by using the moment at min ($D/2$, $d_o/2$) for checking moment-shear interaction, Basler inadvertently introduces a false magnification of the M-V interaction behavior for high moment and high shear. Basler (1961c) shows data points on moment-shear interaction plots using both the moment at min($D/2$, $d_o/2$) and M_{max}. His data points based on the moment at min($D/2$, $d_o/2$) show only minor reduction in the moment capacity due to the presence of high shear, relative to the AASHTO LRFD (2001) bending strength M_n, and his data points based on M_{max} clearly show negligible M-V interaction.

Aydemir (2000) surveys the literature for other M-V interaction tests of transversely-stiffened girders and concludes that the available test data is sparse, but that of the tests in the literature, no significant moment-shear interaction is found if the maximum panel moment is used[3]. Aydemir then conducts refined finite element studies of a number of straight hybrid I girders, and shows that if the maximum panel moment is always used, the resulting finite element based capacities are reduced below the nominal design shear capacities – without consideration of any moment-shear interaction – by a maximum that is about the same magnitude as for the largest unconservative predictions associated with the shear strength equations (both with the current AASHTO (2001) and the modified AASHTO shear strength formulas). It can be shown that if the value of M at the maximum moment location in the panel is always used in the design checks, the statistical distribution of the strengths obtained in experimental and finite element based high-moment high-shear tests, relative to either the nominal moment capacity or the nominal shear capacity, whichever controls (*without the consideration of any moment shear interaction*), is actually better than the statistical distribution of the strengths relative to the nominal capacity predicted by the current AASHTO and recommended modified AASHTO shear strength formulas for high-shear *low-moment* tests. These conclusions are considered to be valid for girders with $2A_w/(A_{fc} + A_{ft})$ up to 2.4.

[3] Lee and Yoo (1999a) present results for one high-moment high-shear test (G10) that exhibits some of the largest strength reduction due to M-V interaction of the transversely-stiffened girder tests documented in the literature. They report a maximum shear strength in their test of 0.93 of the shear strength predicted by Basler's original equations, which is consistent with the observations by Aydemir. Based on the equations presented in this report and the material data reported by Lee and Yoo, the authors obtain a ratio of the shear strength in this experimental test to that predicted by the AASHTO LRFD (2001) equations of 1.03. The ratio of the measured test capacity to the predicted flexural strength from the modified AASHTO LRFD (2001) strength equations recommended in this research (see Section 2.1.1) is 1.00.

Based on Aydemir's work, it can be inferred that the M-V interaction effects might be absorbed into the calculation of the resistance factors in LRFD, thus eliminating the need for M-V interaction checks within the I girder design process. Unfortunately, Aydemir (2000) did not include residual stresses in many of his analyses pertaining to M-V interaction. His analyses with residual stresses included show slightly more rounding of the moment-shear strength interaction for high moment and high shear, and lower flexural strength. It can still be concluded from these analyses that M-V interaction in straight hybrid I girders is minor. However, further finite element studies are needed to consider the effect of residual stresses on the moment-shear interaction behavior for a wide range of girder geometries, and further experimental tests are needed to confirm the finite element predictions. In this research, a large number of finite element solutions are generated for curved homogeneous I girders, including the consideration of residual stresses.

One aspect of bridge design that should be factored into the consideration of the recommended potential changes is that in most (if not all) cases, engineers check M-V interaction based on maximum envelope values for the shear and moment. This introduces further conservatism into the M-V interaction check, since the true strength is influenced only by the concurrent values of the moment and shear. It is expected that the over-prediction of the combined moment and shear values based on the moment and shear envelopes more than compensates for the minor unconservatism that occurs for some cases due to neglecting M-V interaction. Furthermore, in composite I girders, there is an incidental contribution from the bridge deck to the shear strength. This contribution is generally not included in steel I girder design, but its influence on the shear strength can be significant.

2.3.3 Recommendations

Figure 2.3.4 summarizes the analysis results from all of the tests within the primary suite of the parametric studies conducted in this research (see Section 5.3). These studies include uniform vertical bending tests, shear strength tests with loadings applied to produce the maximum possible V/M within the test segment, and high-shear high-moment tests in which the ratio of V to M is reduced from that of the shear strength tests. All the girders in the primary test suite are doubly symmetric. Test results for monosymmetric I girders are discussed later in the report; these results are similar to those shown in the figure.

In Fig. 2.3.4, the nominal moment capacity based on the proposed one-third rule is used for M_n, and the nominal shear capacity based on the modified AASHTO shear strength equations (see Section 2.2) is used for V_n. The term V is the shear within the critical test length when the capacity of the specimen is reached, and M is the maximum vertical bending moment within the critical unsupported length at the limit load of the test, based on full nonlinear finite element analyses as specified in Chapter III.

Since in the one-third rule, M_n depends on the flange elastic lateral bending stress f_l, it is important to explain the procedure for determining the M/M_n values for the data

points in Fig. 2.3.4. Subsequent to the execution of the full nonlinear analyses to determine the capacities M and V, each of the specimens is subjected to a first-order elastic analysis with the same ratio of the applied loadings (as well as M/V) as employed within the corresponding full nonlinear analysis. An open-walled section curved beam finite element is utilized for these analyses[4]. These first-order elastic analyses are used to calculate the maximum ratio of f_ℓ/f_b within the test segment, which is a constant for all load levels in each test (since the analysis is first-order). This ratio is then substituted into Eqs. (2-90), and these equations are solved for the single unknown, f_b, corresponding to the nominal vertical bending strength. This value of f_b is then multiplied by the elastic section modulus to obtain M_n. The above design analysis lateral bending stresses are a lower-bound estimate of the second-order elastic stresses that would exist in the actual girders, including the effects of web distortion. Therefore, the vertical bending strengths M_n computed using these f_ℓ/f_b values tend to be liberal relative to the strengths computed with accurate second-order elastic stresses, and the M/M_n values within Fig. 2.3.4 tend to be slightly underestimated.

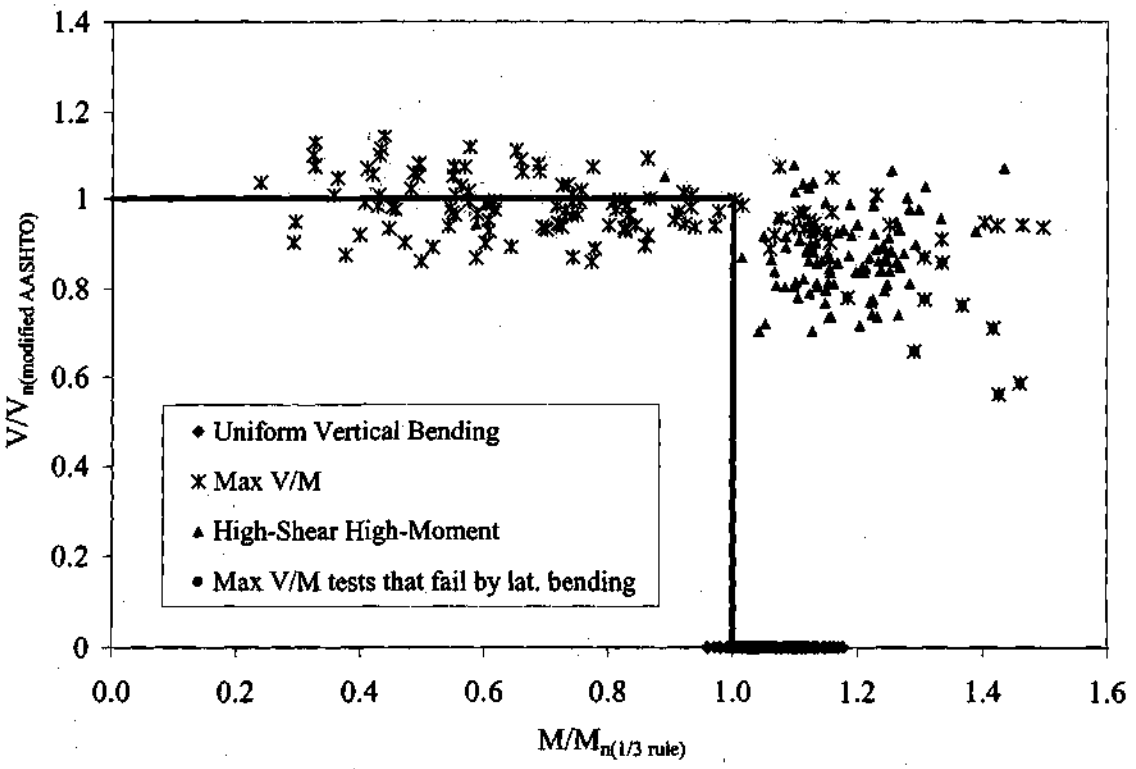

Figure 2.3.4. Moment-shear interaction results from the primary finite element parametric studies conducted in this research.

[4] As noted in Sections 1.2 and 1.5, second-order elastic shell finite element models are utilized for calculation of the elastic design analysis stresses in the majority of this research, to account for potential web distortion effects.

The lack of any significant moment-shear interaction is even more apparent here than in Aydemir's (2000) straight-girder studies. In fact, it can be seen that there is no evidence of any moment-shear interaction in Fig. 2.3.4, in spite of the use of first-order elastic design analysis to determine f_ℓ. This is not surprising once it is understood that the behavior in Fig. 2.3.4 actually corresponds to a three-way interaction: vertical bending moment, lateral flange bending moment, and vertical web shear. The combination of moment gradient (equal to the web shear force) and smaller flange lateral bending moments produces an increase in the flexural capacity in the high-shear high-moment loading cases. Also, the maximum moment occurs at a brace location in the high-shear high-moment tests, as well as in typical cases of high-shear high-moment in bridge structures.

Figure 2.3.4 illustrates that the one-third rule is generally conservative in predicting the maximum strength for the high-shear high-moment test cases. On this basis, pending experimental confirmation of these results, the authors recommend that moment-shear interaction does not need to be considered in horizontally-curved I girders. Also, as noted previously, based on Aydemir's research (2000) and parallel experimental and finite element studies at the University of Missouri at Columbia and at the University of Nebraska, it is expected that it may be possible to eliminate moment-shear strength interaction checks for a wide range of straight I girder proportions.

Figure 2.3.4 also shows significant scatter in the strengths for tests that are controlled by shear. However, the scatter in the shear strength predictions in this figure is reduced significantly compared to that associated with the current AASTHO LRFD (2001) shear strength equations. That is, the modified AASTHO shear strength equations give overall improved predictions of the shear strengths, although many of the data points for the shear tests are somewhat unconservative. The reader is referred to Chapter VIII for detailed discussions of these findings.

CHAPTER III

FINITE ELEMENT MODELING

3.1 OVERVIEW

The analysis studies in this research are conducted with the finite element software ABAQUS version 5.8-14 (HKS 1998a). The general-purpose shell element type S4R is used to model all of the plate components of the girders (i.e., the web, the top and bottom flanges, and the stiffeners) in the majority of the studies. This is a large strain shell element based on the exact geometric description of the large rotation kinematics. The element allows for transverse shear deformation, but the Kirchhoff thin shell assumption is matched as the shell thickness decreases (HKS 1998c) as would be expected physically. Five integration points and a trapezoidal integration rule are used through the thickness of the shell element. A J2 plasticity model (incremental flow theory) with multi-linear isotropic hardening is utilized in all the full nonlinear analyses. The B32OS curved beam element is employed for geometrically linear (i.e., first order) analyses to obtain elastic design analysis stresses in some of the studies. This element also allows for transverse shear deformation, and includes a seventh nodal degree of freedom at its two end nodes that accounts for warping of open-walled cross-sections.

The numerical solution provided by the finite element models tends toward the "exact" solution, for a given structural idealization, with increasing mesh density. However, high mesh refinement can significantly increase the solution time. Preliminary studies by the authors indicated that ten shell elements across the width of the flange and 20 elements through the depth of the web give converged results in the prediction of the girder capacities. However, a discretization of 20 elements across the width of the flanges and through the depth of the web is utilized in all the studies unless noted otherwise. The number of elements in the direction of the girder length is set to maintain an element aspect ratio of approximately one in the web panels. Somewhat larger aspect ratios are generally acceptable within the flanges because these components are subjected predominantly to longitudinal normal stresses.

Additional important modeling issues and details are described in the following sections. Section 3.2 explains the material stress-strain representations used within all the full nonlinear finite element analyses. In Section 3.3, the idealizations of the support conditions, the loading application, cross-frame or bracing members, and connectivity between web stiffeners and the flanges are explained. Next, in Section 3.4, the modeling of initial geometric imperfections is described. This is followed by a discussion of the residual stress idealization in Section 3.5. The chapter concludes with an explanation of the procedure employed for calculating the stresses in the elastic design analyses (Section 3.6).

3.2 STRESS-STRAIN REPRESENTATION

All of the parametric studies in this research are conducted based on idealized properties of A572 Grade 50 steel. Experimental data obtained from coupon tests of one of the bending specimens tested at the FHWA Turner-Fairbank Laboratory (Fig. 3.2.1) is used as a basis to develop representative stress-strain curves. The experimental engineering stress-strain data is converted to a multi-linear representation of a nominal true stress-strain curve, which is then input for the finite element analyses. This process is conducted as follows:

1. The ordinate of the experimental engineering stress-strain curve is scaled such that $F_y = 345$ MPa (50 ksi) (see Fig. 3.2.1).

2. The data from the above scaled curve is converted to true stress-strain using the following equations (HKS 1998b):

$$\varepsilon_{true} = \ln(1+\varepsilon_{eng}) \tag{3-1}$$

$$\sigma_{true} = \sigma_{eng}(1+\varepsilon_{eng}) \tag{3-2}$$

   where ε_{eng} is the engineering strain and σ_{eng} is the engineering stress. This is shown as the solid line curve in Fig. 3.2.2.

3. A multi-linear curve is then fit to the curve obtained in step 2 using an approximate (visual) least squares approach. This curve is indicated by the dashed curve with the labeled data points in Fig. 3.2.2.

The elastic modulus of the material is assumed at E = 200,000 MPa (29000 ksi). "Strain hardening" begins within the multilinear curve at a strain of 0.0209 mm/mm, which is 12.1 times the yield strain. The initial strain-hardening modulus of the multi-linear true stress-strain curve $(E_{st})_{true}$ is 2590 MPa (375 ksi). This is somewhat low compared to typical reported values for strain-hardening stiffness, and is a by-product of the scaling operation to normalize the yield strength to 345 MPa (50 ksi). The scale factor employed in step one above is 450/345 = 1.3. However, it should be noted that the scaled value for the ultimate engineering stress is 580/1.3 = 450 MPa (65 ksi) based on the curve shown in Fig. 3.2.1. Since 450 MPa (65 ksi) is specified as the minimum ultimate stress for A572 Grade 345 material, it is felt that the scaled nominal true-stress-strain curve developed here is an optimum representation of the nominal material characteristics. It is believed that typical reported values for the strain-hardening modulus are larger than the value of 2590 MPa typically because the actual ultimate stress is significantly higher than the ASTM minimum required value. Furthermore, by using $(E_{st})_{true} = 2590$ MPa for the strain-hardening modulus, it is felt that the effect of strain-hardening is represented in an approximate lower-bound sense.

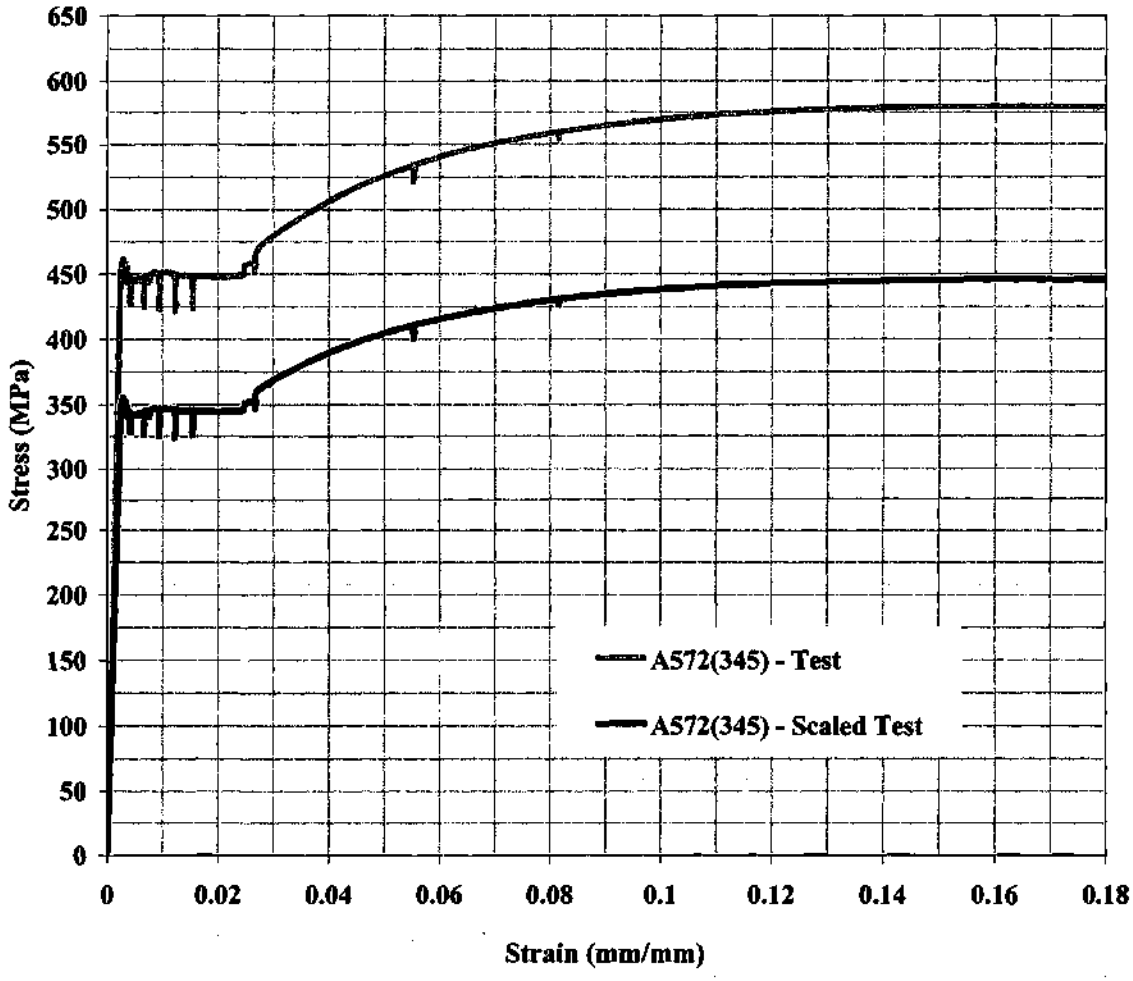

Figure 3.2.1. Typical engineering stress-strain curve for A572(345) steel and scaled form of this curve such that F_y = 345 MPa (50 ksi).

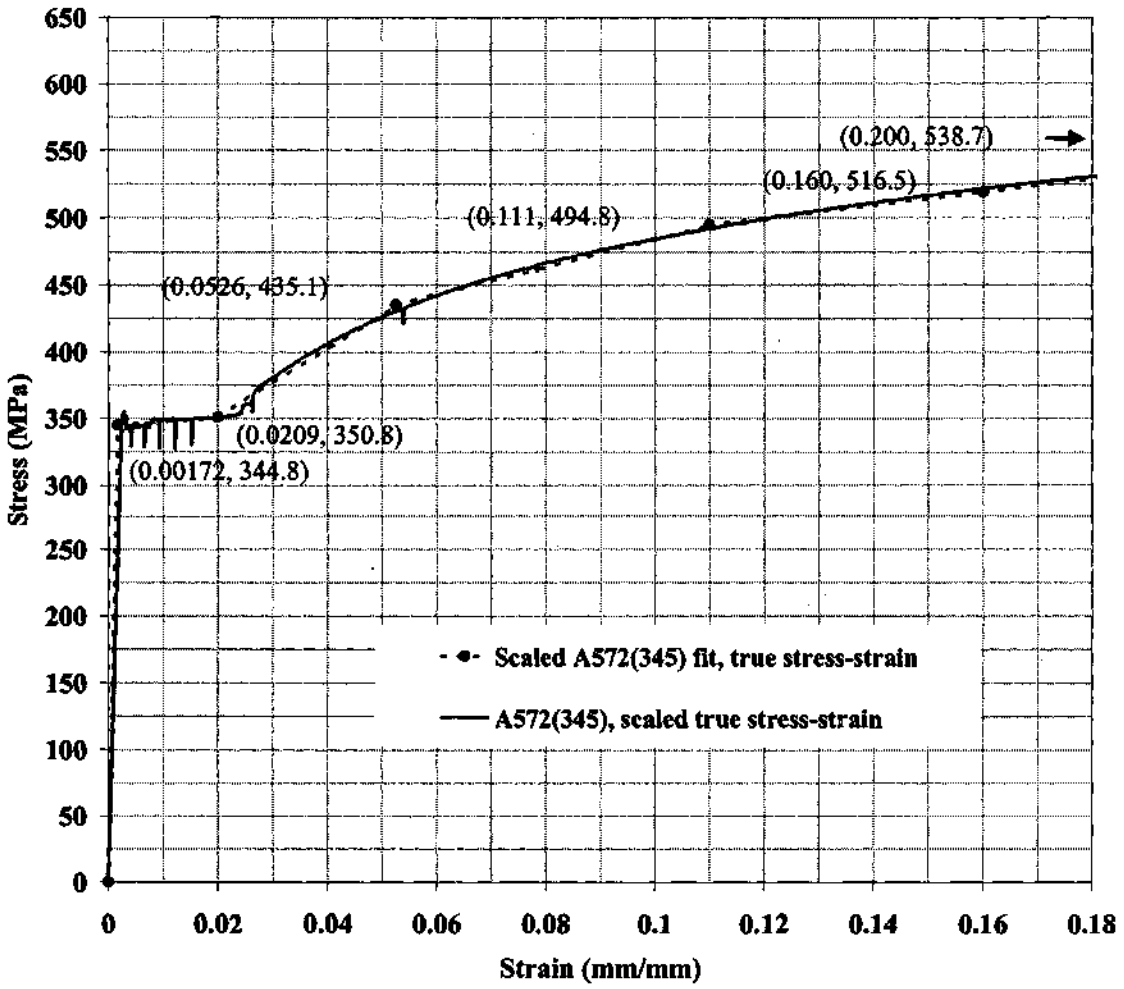

Figure 3.2.2. True stress-strain curve used in parametric studies.

Similar procedures are utilized to obtain representative engineering and true stress-strain curves for the analysis of experimental tests conducted in this research, as shown in Figs 3.2.3 and 3.2.4. However, the ordinate of the physical stress-strain curves is not scaled in these analyses.

Figure 3.2.3 shows typical multi-linear engineering and true stress-strain curves used in the analysis of the Mozer-Culver tests (Mozer et al. 1970, 1971 and 1973). Mozer et al. report only the yield and ultimate tensile strengths and the modulus of elasticity. Therefore a representative value of $\varepsilon_{st} = 0.014$ mm/mm and $E_{st} = 6200$ MPa (900 ksi) for A36 steel according to (Salmon and Johnson 1996) and (Brockenbrough and Johnston 1968) is assumed in this study. For these tests, a simple multi-linear representation of the engineering stress-strain response is employed: a flat yield plateau, followed by linear strain-hardening up to the ultimate strength, and a constant engineering stress subsequent to reaching the ultimate strength. This engineering stress-strain curve is converted to a true stress-strain curve for input to the analysis by application of the equations discussed previously to the data points shown in the figure.

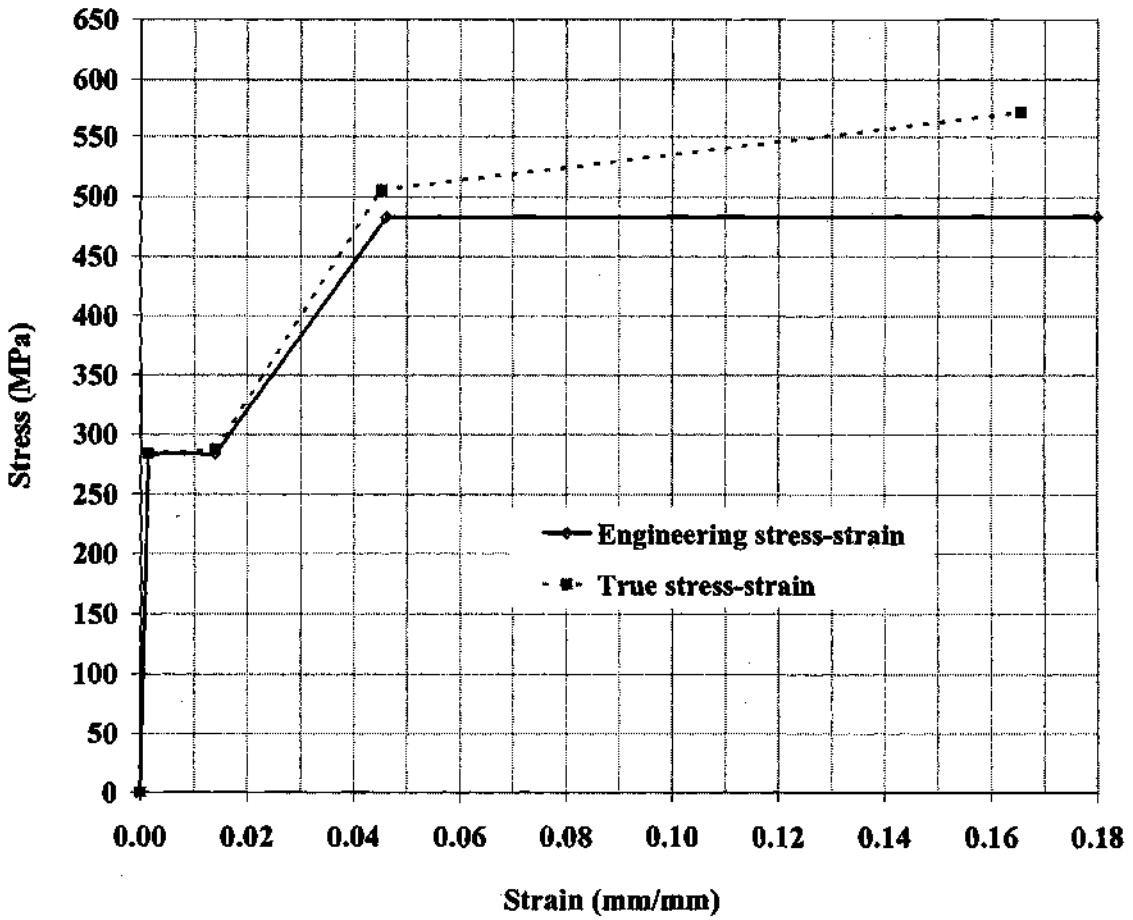

Figure 3.2.3. Typical engineering and true stress-strain curves used in the analysis of the Mozer et al. tests – flange of test L1-A.

Figure 3.2.4 shows typical engineering and true stress-strain curves used in the analysis of FHWA Turner-Fairbank Laboratory bending test specimens. The specific curves shown here are developed from coupon tests of the compression flange of specimen B1. In these analyses, two linear segments are utilized for representation of the strain-hardening region of the engineering stress-strain curves. The first segment starts at the strain-hardening strain ε_{st} and has a specified modulus equal to the initial strain-hardening modulus determined by Zureick and Kim (2000). The second segment starts at an engineering stress of $F_y + 0.667(F_u - F_y)$, and it connects this point on the first segment with the point (ε_u, F_u). This curve is then converted to the corresponding true stress-strain curve for input to the analysis in the same fashion as the curve in Fig. 3.2.3.

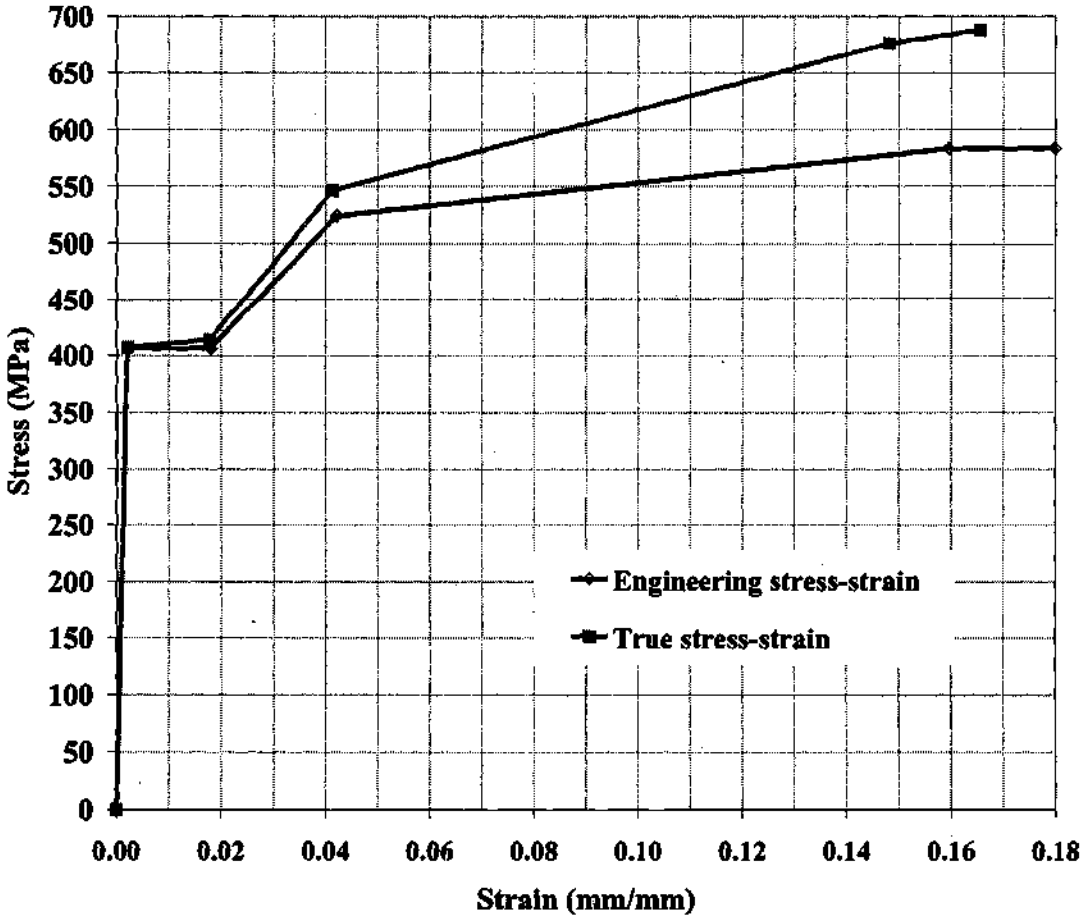

Figure 3.2.4. Typical engineering and true stress-strain curves for analysis of Curved Steel Bridge Research Project tests – compression flange of tests B1 to B4.

It should be noted that the effect of the differences in the multi-linear representation of the strain-hardening responses in Figs. 3.2.2, 3.2.3 and 3.2.4 is minor since the strain-hardening strain is typically not significantly exceeded except within very localized regions such as the folds of local buckles. Furthermore, these localized large strains typically do not occur until well into the post-peak response of the tests.

3.3 MODELING OF SUPPORTS, LOAD APPLICATION, CROSS-FRAMES OR BRACING, SPLICES AND STIFFENER-FLANGE CONNECTIVITY

With the exception of the analyses of the experimental shear tests conducted at the Georgia Institute of Technology (Zureick et al. 2001), the support idealizations utilized in this research are as follows:

- Vertical supports: Every node across the width of the bottom flange is restrained in the vertical direction, i.e., the vertical supports are modeled as a knife edge or roller.

- Tangential support: The node at the web-flange juncture at one of the vertical support locations is restrained in the direction tangent to the curved longitudinal axis of the girder to prevent rigid body rotation in the horizontal plane about the center of curvature.

- Radial supports: Unless noted otherwise, within the single girder studies, the nodes at the web-flange juncture on both the top and bottom flanges are rigidly restrained in the radial direction at every loading and support location. However, in a number of parametric studies, radial displacements are specified at some of the brace locations to simulate the effects of relative torsional rotations between the cross-frames in a bridge superstructure. The reader is referred to Chapter V for a discussion of these details.

The support idealizations for the shear specimens tested at the Georgia Institute of Technology (Specimens S1-0.10 and S1S-0.10) (Zureick et al. 2001) have the following attributes:

- Pin-ended bracing members, which frame in a radial direction from the girder to a massive reaction wall, are modeled directly within the finite element analysis. Spherical bearings were utilized at the brace ends, and therefore the pinned idealization is a close representation of the physical boundary conditions for these members. The braces were slightly inclined at the start of the physical tests, and rotate based on the girder displacements during the loading. The initial orientation of the braces, and the changes in this orientation during the loading are included in the analysis.

- The vertical support at one end (location 1) is modeled by restraining the displacements in the vertical direction along a line across the width of the bottom flange. This closely represents an actual roller support at this location.

- The vertical support at the interior support location (location 3, see Section 4.1) is assumed to be rigid in compressive contact over the full area of the bearing plate, but uplift is allowed at any location of the bottom flange that would tend to lift off of the bearing plate due to the deformations of the girder.

- Tangential displacements are assumed to be rigidly restrained along a line of nodes across the entire width of the bottom flange at location 3.

- Linear springs, oriented in the tangential direction, are provided across the flange width at location 2 to model the effect of the restraint provided by the actuator/loading frame against tangential movement. The total combined stiffness of these springs is estimated based on an elastic torsion analysis of the reaction beam of the test frame, and is specified as 43.8 kN/mm (250 kips/in) (Phoawanich et al. 1999a).

In all cases, with the exception of the internal loading test suite discussed in Section 5.10 and the eccentrically-loaded tests discussed in Section 4.1, concentrated loads are applied as a trapezoidal line load across the width of the bearing stiffeners as shown in Fig. 3.3.1. In the internal loading test suite, the concentrated load is applied as a distributed line load along the length of the web sufficient such that web yielding or web crippling due to the transverse load do not occur. The load location does not have a bearing stiffener in these tests. In the eccentrically loaded cases, a similar trapezoidal load with the required eccentricity is applied to the bearing stiffener. Self weight of the girders, bracing, cross-frames and bridge test systems is included in all the analyses as applicable, and is applied within the first step of the solution. In the redundant testing systems, potential stresses due to the sequence of erection are not considered.

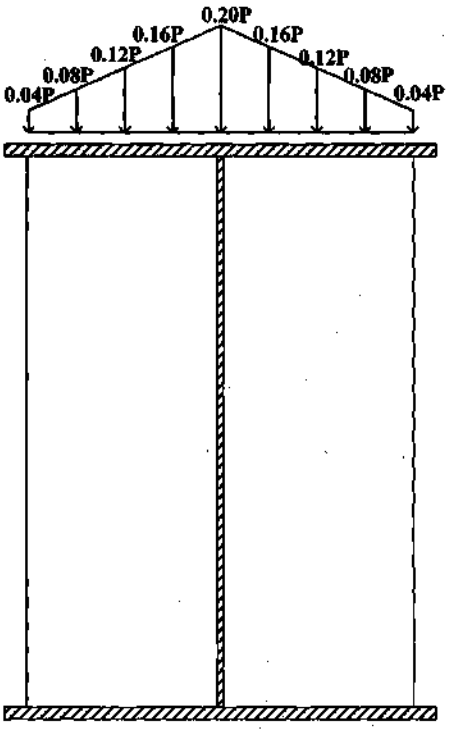

Figure 3.3.1. Typical line loading pattern at load locations.

The elements at the ends of bearing stiffeners (always two-sided) are constrained to the top and bottom flanges in all of the finite element studies within this research. Unless noted otherwise, the transverse stiffeners (one-sided) are stopped one element short of the tension flange, but are constrained to the compression flange.

In the analyses of the two- and three-girder system experimental tests (see Chapter IV), moment continuity of the cross-frame or diaphragm members with the girder connection plates is assumed within the finite element models. These members are modeled using five three-node quadratic-displacement beam elements (B32) between each joint of the cross-frame or diaphragm assemblies. The B32 element includes transverse shear deformation. The cross-sections of these elements are specified based on the type of member used in the physical tests, i.e., angle sections for the intermediate cross-frames and channel sections for the end diaphragms of the two-girder system tests, and pipe sections for the cross-frames in the three-girder system tests. The three-girder system tests also contain bottom chord WT bracing members near the ends of the bridge. The cross-frames within the three-girder system tests involve substantial connection plates that are not modeled explicitly within the finite element analysis. The joints are assumed to be infinitesimal in size, and the cross-frame, diaphragm and bracing members are assumed to frame concentrically into these joints in all of the finite element studies.

In the three-girder system tests, the splice connections of the component specimens to the bridge test frame are modeled by using multi-point constraints. The flange nodes at the juncture between the ends of the specimens and the girder G3 to which they are attached are constrained to deflect as if they are connected to a rigid bar across the width of each of the flanges. Aside from the attachment to the component and girder G3 flanges, these rigid bars are free to displace and rotate such that the flanges are able to warp at the splice connection. Direct nodal displacement and rotation compatibility is directly enforced at the web nodes of both the specimen and Girder G3 at the juncture between the components and the test frame. The above constraints do not explicitly model the splice plate connections between the bridge system and the components, but they are believed to adequately represent the overall behavior since the splices are located outside of the critical unsupported length of the specimens.

3.4 MODELING OF INITIAL GEOMETRIC IMPERFECTIONS

Three types of initial geometric imperfections are considered in the analyses conducted in this research: out-of-flatness of the web, tilt of the compression flange, and lateral sweep of the compression flange. With the exception of the definition of the imperfection magnitude, the modeling of these imperfections is handled in the same way for both the analyses of experimental tests as well as for the parametric studies.

For the parametric studies, the magnitude of the imperfections relative to the perfect horizontally curved geometry is based on the following AWS (1996) fabrication tolerances:

1. An initial out-of-flatness of the web of d/67 for panels of interior girders with one-sided stiffeners (where d is the least panel dimension) and D/150 for unstiffened girders. In this work, the d/67 limit is used for girders with panel aspect ratios d_o/D less than three whereas D/150 is used for the girders with $d_o/D = 3$.

2. A tilt of the flanges equal to the maximum of 1/100 of the flange width or 6.35 mm (¼ in).

3. A lateral sweep of the compression flange of $L_b/960$.

For the analyses of the experimental tests, measured values are used for the above quantities when this information is available. Otherwise, the above AWS (1996) values are assumed.

In both the analyses of the experimental tests as well as the finite element parametric studies, the displaced shape associated with the initial imperfections is established based on an elastic linear buckling analysis of the shell finite element model, or a form of the model modified as described below. The magnitude of the selected eigenmode (usually the first or fundamental buckling mode) is scaled up from zero until one of the above limits is satisfied. That is, a buckling mode shape is applied to the model as an initial displacement (with corresponding zero internal strains).

For the bending and high-moment high-shear tests, the flange tilt and the lateral sweep of the compression flange are expected to have the most significant effect on the girder strengths. However, for the girders that have thin webs, the first several buckling modes for these load cases are typically dominated by web bend buckling, or a combination of web bend and shear buckling. Therefore, the web is artificially thickened for the linear buckling analysis of these tests such that the buckling mode shape is dominated by flange deformations.

The specific procedure for generation of the initial imperfections is as follows:

1. An elastic linear buckling analysis is performed using the same loading as employed in the full nonlinear analysis. For most of the girders, the first three buckling modes are dominated by web local buckling if the actual girder geometry is employed.

    a. For shear capacity tests, the first buckling mode is used directly.

    b. For high-moment tests, it is well known that web imperfections have only a minor influence on the bending strength. Therefore, to obtain a mode shape that has a significant influence on the maximum strength, the web is thickened artificially for the linear buckling analysis to obtain a mode associated with flange local and/or lateral buckling within the test section. An artificial web D/t_w of approximately 100 is targeted for this analysis.

2. The computed buckling mode is scaled up until one of the AWS (1996) or experimentally measured limits is satisfied. This scaled buckling mode is then applied to the perfect horizontally curved geometry.

Example initial geometric imperfections for several of the experimental tests studied in this research are shown in Figs. 3.4.1-3.4.4. The artificially increased web thickness used within the linear buckling analyses is indicated within the figure captions as t_{wlb}, and the scale factors applied to the buckling modes (which are initially normalized such that they have a maximum nodal displacement of 1.0) are indicated by the parameter sf. The scale factor sf is set such that the dominant initial imperfection is at an AWS (1996) limit or actual measured imperfection for every model. The sf and t_{wlb} values are given in Chapter IV for the analyses of the experimental tests. For the parametric studies, this information is provided in Appendix D. It should be noted that the buckled shapes are magnified in Figs. 3.4.1 through 3.4.4 to illustrate the associated deformed geometry.

For the parametric study test specimens studied in this research, a set of sample specimens was first analyzed to assess the imperfection sensitivity of the models. Results from these preliminary analyses revealed that the combined effects of initial geometric imperfections and initial residual stresses can be significant for the uniform vertical bending and high moment-high shear loading cases. A maximum strength reduction of 15 percent was obtained, corresponding to several specimens with $b_f/t_f = 25$. In contrast, the inclusion of the initial geometric imperfections and residual stresses produced insignificant strength reduction for the maximum V/M loading cases (less than 4 percent in all the cases studied). Therefore initial geometric imperfections and residual stresses are introduced into the parametric study specimens for the uniform vertical bending and high moment-high shear loading cases only. Unless noted otherwise, the finite element shear strength predictions are based on the perfect horizontally curved geometry with zero residual stresses.

Sections 4.4 and 4.7 discuss the quality of the finite element predictions with and without initial residual stresses and geometric imperfections versus the experimental behavior of curved girders in high shear (Zureick et al. 2001), as well as for the uniform vertical bending tests conducted at the FHWA Turner Fairbank laboratory (Zureick and Kim 2000; Grubb and Hall 2001). The design of the parametric studies is presented in Chapter V.

Both full nonlinear finite element simulations, to predict the physical load-deflection response and maximum strength, and geometrically linear and nonlinear design analyses, to determine elastic stresses for use in design predictor equations, are conducted within this research. As noted previously in Chapter I, the elastic design analyses are conducted with the same shell finite element discretization as used for the full nonlinear simulations in the majority of the studies. Geometric imperfections and residual stresses are not included in the elastic design analyses. The calculation of elastic design analysis stresses is discussed in more detail in Section 3.6.

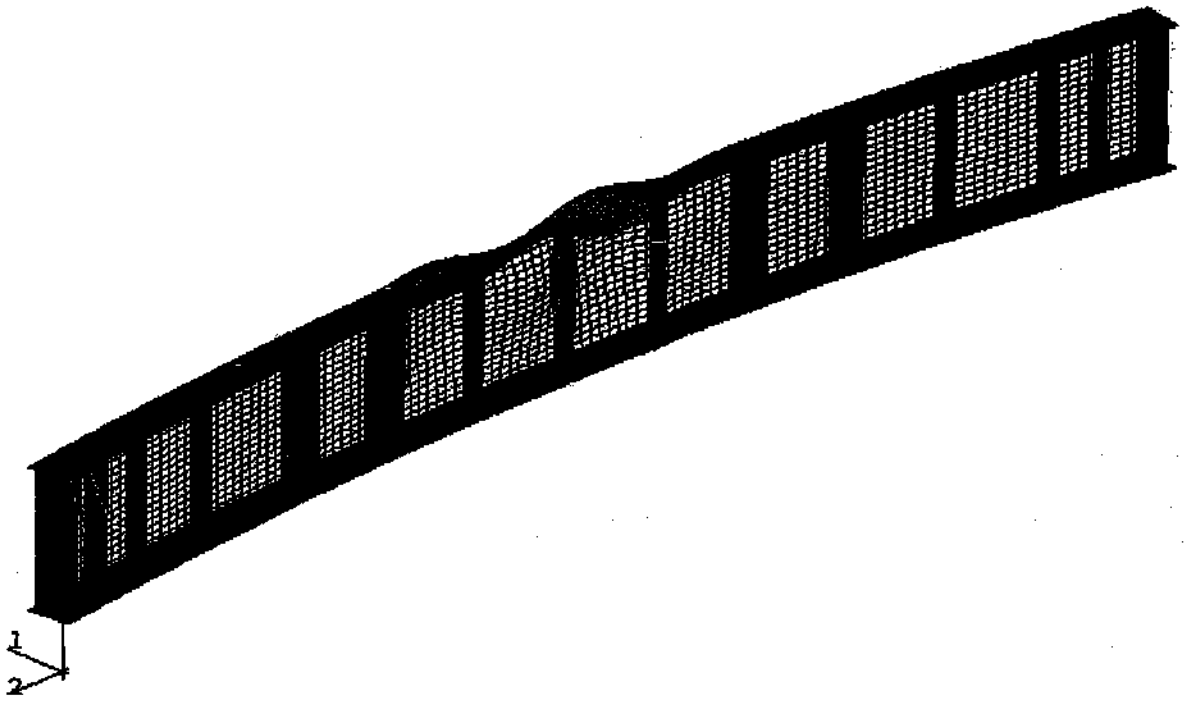

Figure 3.4.1. Assumed initial geometric imperfection for Mozer et al. (1971) test L1-A (t_{wlb} = 5.66 mm (0.223 in), sf = 0.295), magnification = 5.0.

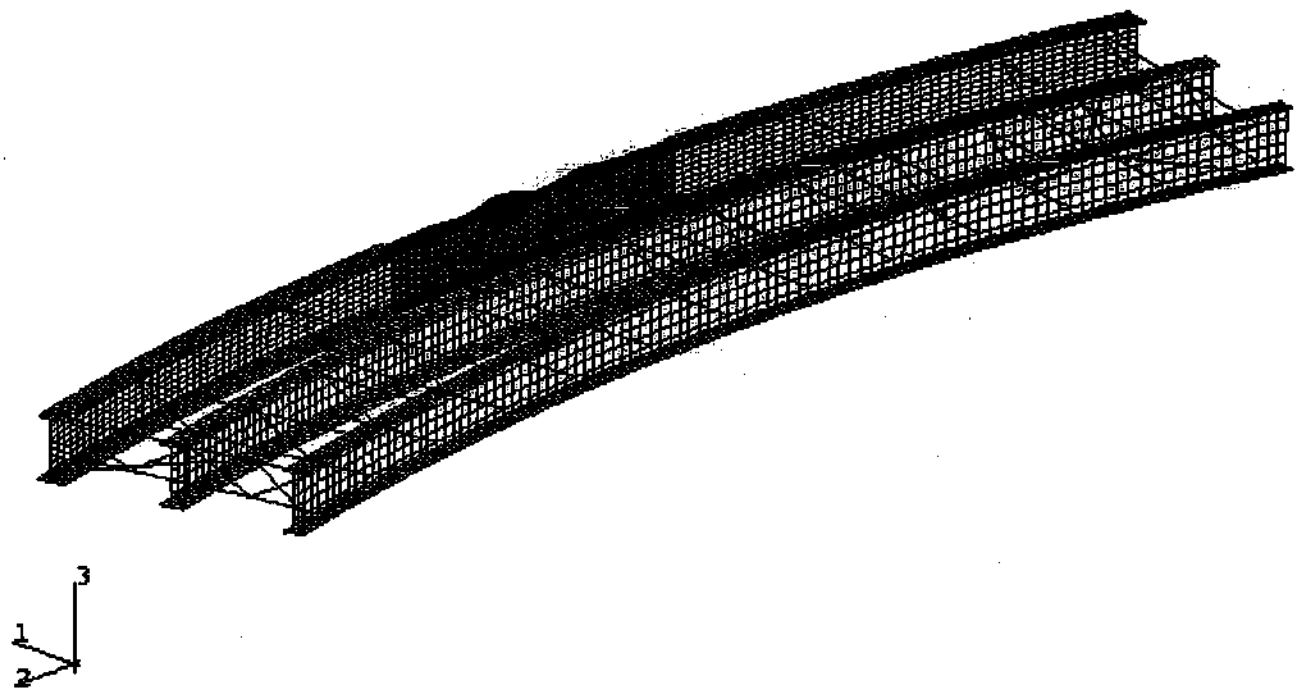

Figure 3.4.2. Assumed initial geometric imperfection for test B1 (Zureick and Kim 2000; Grubb and Hall 2001) (t_{wlb} = 12.2 mm (0.48 in), sf = 0.357), magnification = 5.0.

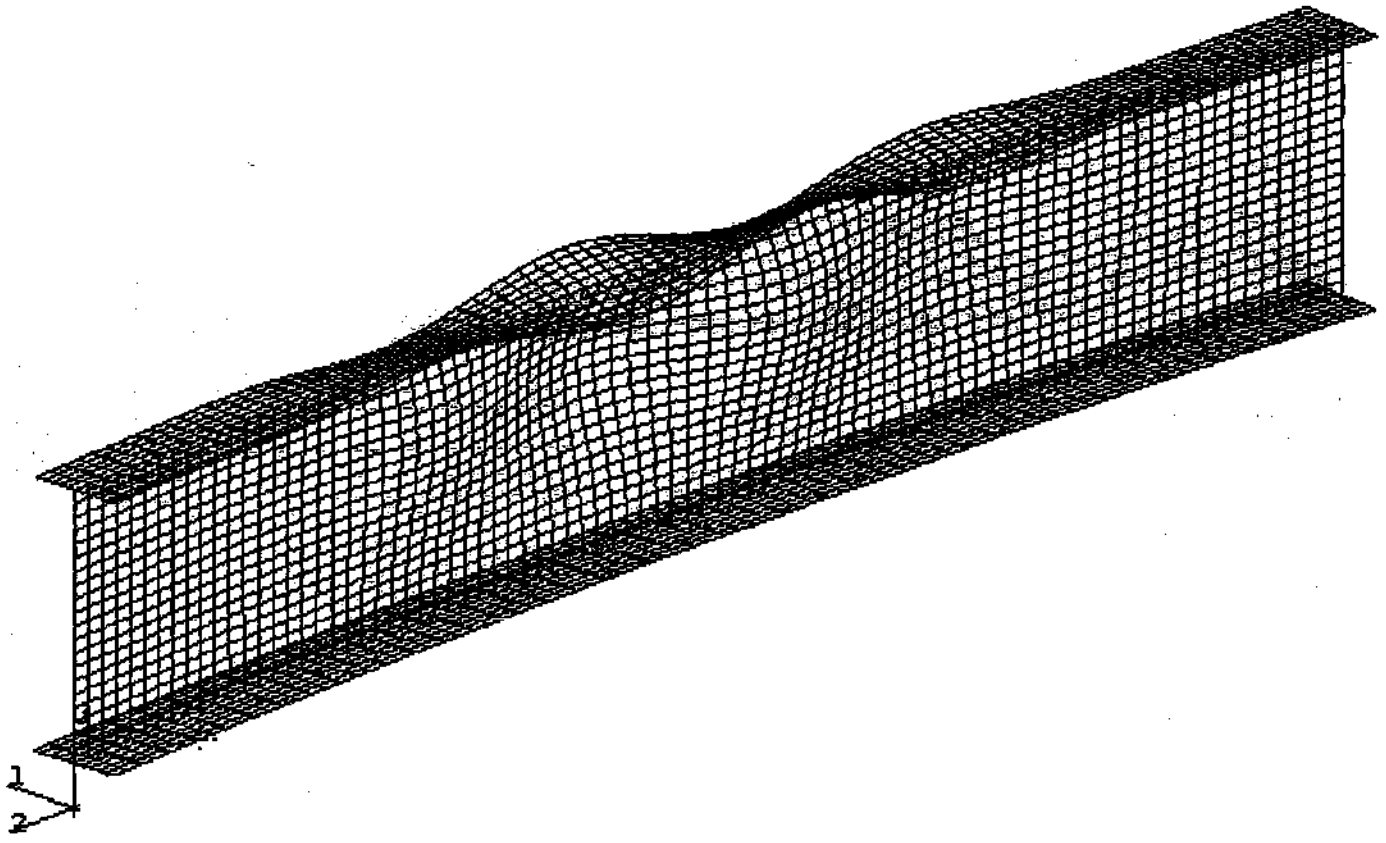

Figure 3.4.3. Close-up of assumed initial geometric imperfection in the component specimen for test B1 (Zureick and Kim 2000; Grubb and Hall 2001) (t_{wlb} = 12.2 mm (0.48 in), sf = 0.357), magnification = 5.0.

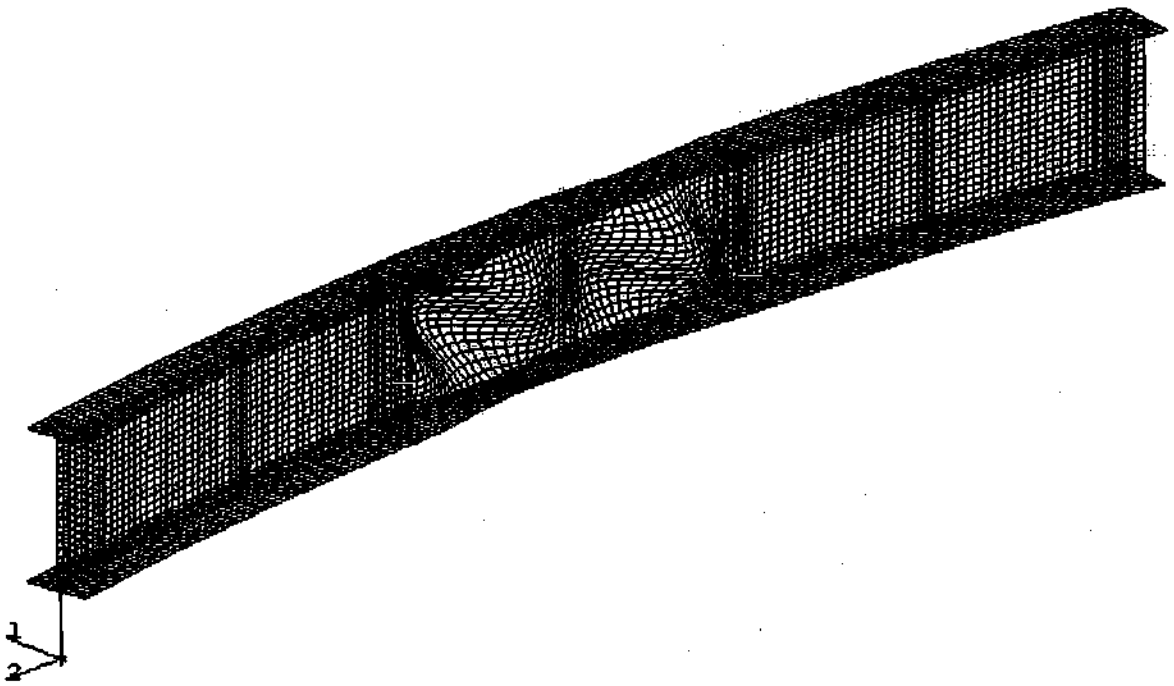

Figure 3.4.4. Assumed initial geometric imperfection for test S1-S-0.10 (Zureick et al. 2001) (t_{wlb} = 8.33 mm (0.328 in), sf = 0.369), magnification =20.0.

3.5 MODELING OF RESIDUAL STRESSES

It is well known that residual stresses can have a major impact on the stability and strength of steel structures. The nonlinearity in the response due to the presence of residual stresses can have a measurable impact on member pre-peak deflections and on the maximum load capacity.

Typically, in welded plate girders, the residual stresses are essentially equal to the yield stress of the material in tension within a small width at the heat affected zones, and a smaller near-constant self-equilibrating compression stress is developed within the other regions of the plates. In curved I girders, residual stresses can be introduced by flame cutting and welding as well as by heat curving. However, Hall (2000) suggests that heat curving is not used significantly in current practice due to difficulties in controlling the radius of curvature, making the process time consuming. Due to this deficiency of heat curving procedures, the sources of residual stress resulting from fabrication of curved girders at the present time (May 2001) are expected to be predominantly due to cut curving and welding. However, to obtain an estimate of the effect of heat curving on the ultimate strength of the test specimens, a selected set of test specimens is analyzed using a representative residual stress pattern developed by Culver and Nasir (1971). The results of these studies are compared to analysis predictions based on residual stresses due to cut curving and welding (see Section 7.13).

In this work, residual stress effects are represented by specifying initial stress conditions at the beginning of the analyses, in accordance with the following models:

- The (ECCS 1976) model, which estimates the residual stresses from welding and flame cutting.

- The Culver and Nasir (1971) model, which includes residual stresses from flame cutting, welding and heat curving.

The (ECCS 1976) model is explained in detail in Section 3.5.1 and the Culver-Nasir (1971) model is described in Section 3.5.2.

3.5.1 ECCS (1976) Model

The ECCS residual stress distribution is idealized based on the fact that when the section is free of external forces, the resultant forces due to the sum of the residual stresses over the entire cross-section must be zero. The stresses in the flanges and web are defined here in accordance with the equations of the *Manual on Stability of Steel Structures* (ECCS 1976), which address residual stresses due to both welding and flame cutting.

The idealized residual stresses are equal to the yield stress in a narrow strip of plate near the heat affected zones, and a smaller constant self-equilibrating compression stress

is generated within the other regions of the plate. ECCS (1976) specifies the width of the equivalent tension block (c_{fc}) for a plate that is flame-cut as

$$c_{fc} = \frac{1100\sqrt{t}}{F_y} \tag{3-3}$$

where t is the plate thickness in mm and F_y is the plate yield stress in MPa. In addition, based on the assumption of a continuous single pass weld between the web and the flange, the resulting tension block on each side of the centerline of the weld in the flange plates and at the top and bottom edges of the web plate is given by

$$c_{wld} = \frac{1200pA_{wld}}{F_y \sum t} \tag{3-4}$$

where p is the process efficiency factor, which depends on the welding process and is equal to 0.90 for submerged arc welding, A_{wld} is the cross-sectional area of the added weld metal in mm^2, and Σt is the sum of the plate thicknesses meeting at the weld in mm. Single pass submerged arc welds are assumed in this research. The residual stresses produced by an assumed single-pass weld are generally larger than those produced by a multiple-pass weld of the same size.

The combined effect of flame cutting and welding on the web does not result in the algebraic sum of the above tension block widths, since the processes are not concurrent and the weld heat tends to relieve the tension block formed due to cutting. The ECCS Manual (1976) suggests that the final tension block width ($c_{fc\text{-}wld}$) in the web can be calculated by

$$c_{fc\text{-}wld}^{\ 4} = c_{fc}^{\ 4} + c_{wld}^{\ 4} \tag{3-5}$$

where c_{fc} is the tension block width due to flame cutting alone and c_{wld} is the tension block width due to welding.

Based on the assumption that the web is fillet welded on each of its sides to the flange plates, ECCS (1976) proposes that the width of the tension block in the flanges on each side of the centerline of the web-flange juncture may be approximated as

$$c_2 = c_{wld} + 0.5\, t_w \quad \text{for } t_w \le 2c_{wld} \tag{3-6}$$

Given the widths that have stress equal to the yield stress (F_y) (c_{fc} and $2c_2$ at the edges and interior of the flange plates, and $c_{fc\text{-}wld}$ at both edges of the web plate), and neglecting the reduction in the residual stresses at the flange tips due to the compressive residual stresses caused by the welding, smaller constant self-equilibrating compressive stresses (F_{rcf} and F_{rcw}) can be calculated that exist within the majority of the plate areas based on

equilibrium of the longitudinal residual stresses. A nominal representation of the corresponding residual stress patterns for the flange and web plates is shown in Fig. 3.5.1.

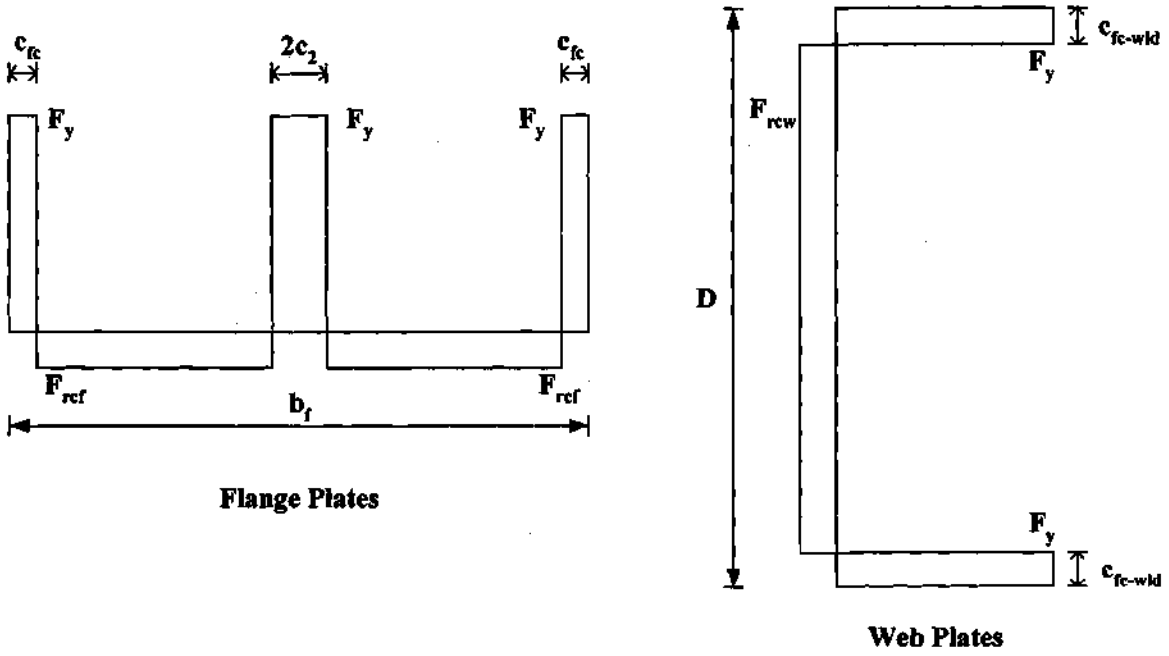

Figure 3.5.1. Idealized residual stress distribution in flange and web plates due to flame cutting and welding (ECCS 1976).

It should be noted that the current cutting technology is likely to produce smaller residual stresses than specified in ECCS (1976). Therefore, it is expected that the residual stress patterns computed in this work are conservative relative to girders fabricated in current practice.

The assumed fillet weld sizes are based on the minimum requirements according to the AASHTO LRFD Specifications (2001) as follows:

- 6.35 mm (1/4 in) for specimens having a material thickness of the thicker part joined of 12.7 mm to 19.1 mm (1/2 to 3/4 in), and

- 7.94 mm (5/16 in) for specimens having a material thickness of the thicker part joined greater than 19.1 mm (3/4 in).

For the shell finite element used in this research, i.e., the S4R element (HKS 1998c), one Gauss integration point location is employed within each element, with five integration points through the thickness at this location. The number of elements used in the finite element models is as follows:

- Twenty elements are used across the width of the top and bottom flanges as well as through the depth of the web for the specimens tested by Mozer et al. (1970, 1971, and 1973), and in all the parametric study tests. Therefore, there are 20 integration points across the width of both the top and bottom flanges and through the depth of the web for the girders in these tests.

- Ten elements are used across the width of the top and bottom flanges and 20 elements are used through the depth of the web for the bending component specimens tested in the Curved Steel Bridge Research Program at the FHWA Turner-Fairbank laboratory, and for the shear specimens tested at Georgia Institute of Technology (Zureick et al. 2001). Therefore, there are ten integration points across the width of both top and bottom flanges and 20 integration points through the depth of the web in these models.

Results from preliminary investigations by the authors revealed that ten elements across the width of both top and bottom flanges and twenty elements through the depth of the web provide converged results while minimizing the usage of computer resources and time to complete the analyses. However, to provide a refined representation of the Culver-Nasir (1971) residual stresses, and to eliminate any factors in comparing the results of these analyses with the results using the ECCS (1976) pattern, twenty elements are used across the width of both the top and bottom flanges as well as through the depth of the web in the tests listed above under item one, with both the Culver-Nasir (1971) and the ECCS (1976) residual stress patterns.

Based on the equations in (ECCS 1976), the width of the tension blocks is either wider or narrower than the width of an individual finite element. Thus, for the elements having residual stresses in both tension and compression, the total longitudinal force from the tensile and compressive residual stresses is divided by the cross-section area associated with the element to obtain the net residual stress at the integration point. Figures 3.5.2 to 3.5.4 show examples of the idealized Gauss point residual stresses, based on the ECCS (1976) residual stress patterns, utilized in analysis of three of the experimental tests. Complete illustrations of the self-equilibrating Gauss point residual stresses for all of the experimental and parametric study tests analyzed in this research are summarized in Appendix E.

3.5.2 Culver-Nasir Model (1971)

The Culver-Nasir (1971) residual stress pattern is utilized as an estimate of the residual stress effects due to heat curving. This pattern includes residual stresses from flame cutting and welding, as well as heat curving.

Figure 3.5.5 shows the idealized residual stress distribution in the flanges specified by Culver and Nasir. Figure 3.5.6 illustrates the self-equilibrating Gauss point residual stresses specified for the finite element analyses conducted in this study. The residual stresses in the web are assumed to be zero, as was assumed in the Culver and Nasir research.

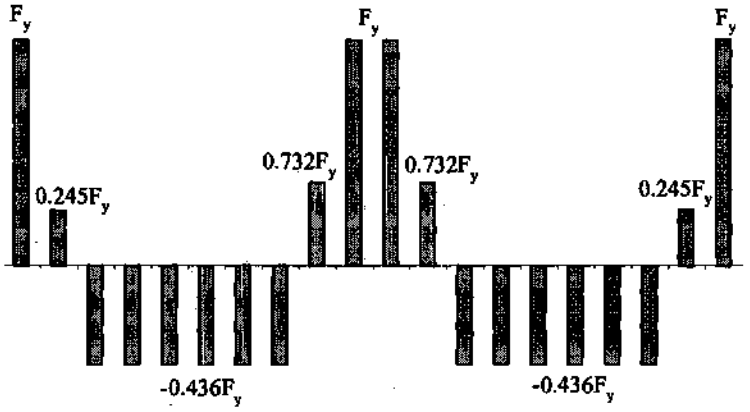

(a) Top and bottom flanges

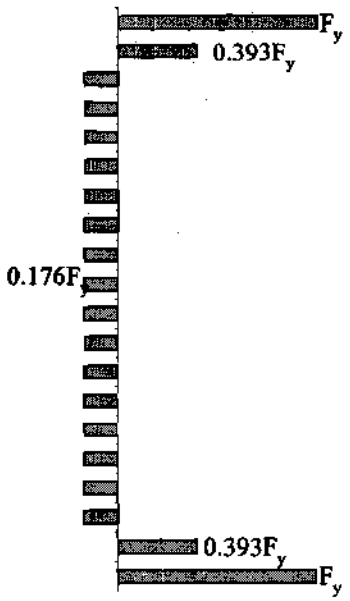

(b) Web

Figure 3.5.2. Assumed Gauss point residual stresses for Mozer et al. (1971) test L1-A.

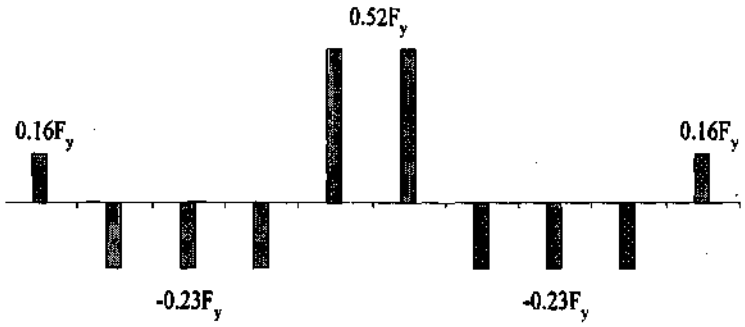

(a) Top and bottom flanges

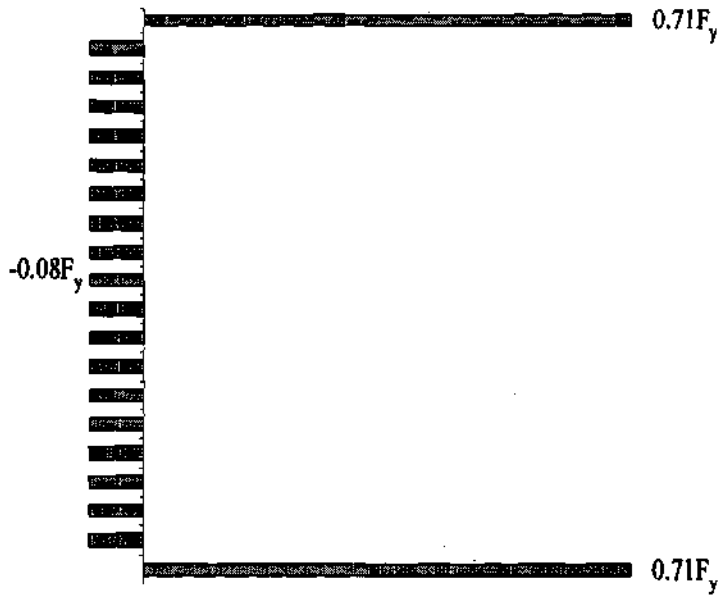

(b) Web

Figure 3.5.3. Assumed Gauss point residual stresses for Curved Steel Bridge Research Project bending test B1 (Zureick and Kim 2000; Grubb and Hall 2001).

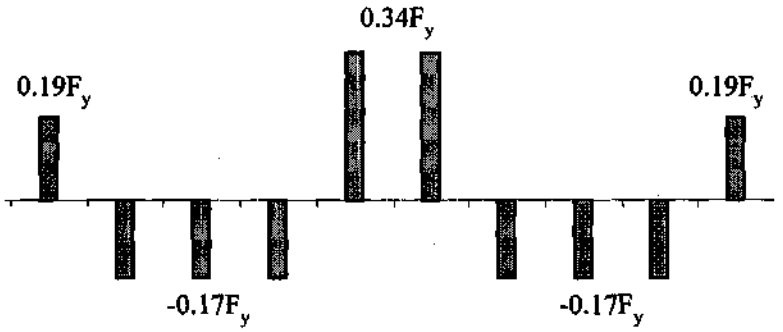

(a) Top and bottom flanges

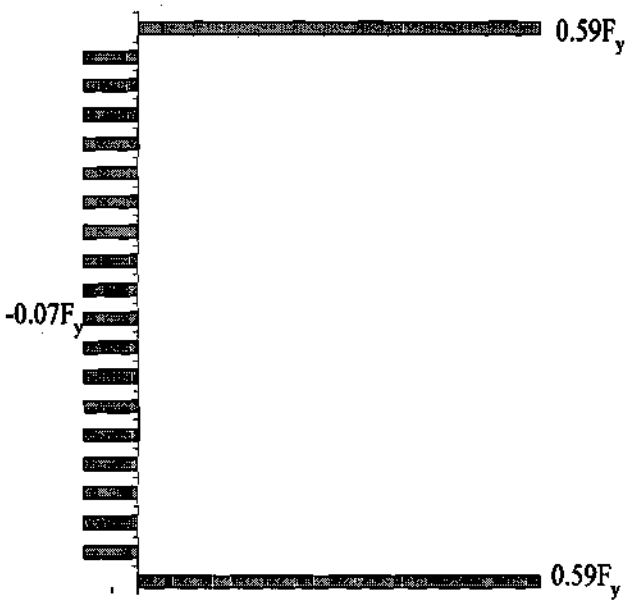

(b) Web

Figure 3.5.4. Assumed Gauss point residual stresses for Curved Steel Bridge Research Project shear tests S1-0.10 and S1S-0.10 (Phoawanich et al. 2001).

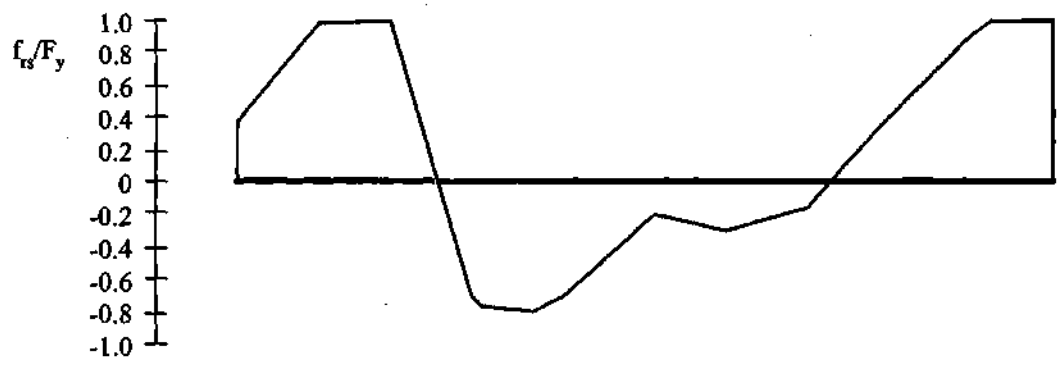

Figure 3.5.5. Idealized residual stress distribution in flanges due to heat curving (Culver and Nasir 1971).

3.6 CALCULATION OF ELASTIC DESIGN ANALYSIS STRESSES

As noted in Chapter I, the same shell finite element models are used for full nonlinear analyses and for calculation of elastic design analysis stresses in the majority of the studies in this research. Therefore, the effect of web distortion is directly included within the computed flange lateral bending stresses. Also, for the design predictor equations that are based on second-order elastic stresses, the second-order amplification of these stresses is estimated by the use of these models.

A cylindrical global coordinate system is employed for definition of the stresses in the finite element models. The elastic vertical and lateral bending stresses at a given location along the girder length, f_b and f_ℓ, are calculated from the shell finite element models in the following manner:

1. When the maximum vertical bending occurs at a support location, the element Gauss point tangential normal stresses in the shell elements at the flange tips and at the outermost integration points through the flange thickness (located at the extreme fibers of the flanges) are averaged between the shell elements on each side of the bearing stiffener at each flange tip. Otherwise, the maximum Gauss point stresses in the shell elements at the flange tips are obtained directly from the finite element model.

2. Since the above Gauss points are located at the mid-width of the flange tip shell elements, the above two flange tip Gauss point stress values are linearly extrapolated out to the actual flange tip position in each flange.

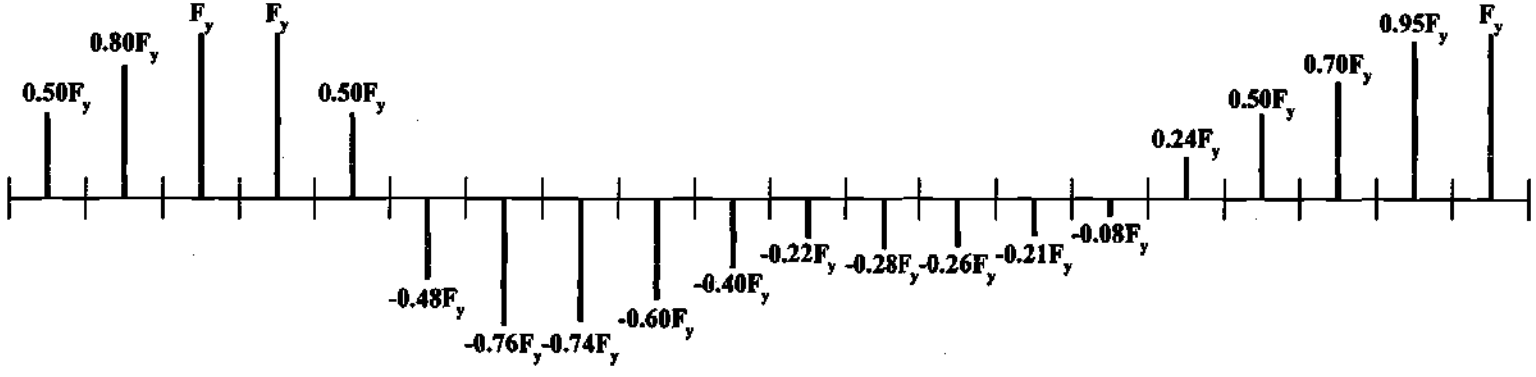

Figure 3.5.6. Idealized Gauss point residual stresses in flanges for analysis of heat-curved girders (Culver and Nasir 1971), e.g., Mozer et al. (1970) test C8-

3. The flange tip stresses obtained from step 2 are averaged to obtain f_b. The lateral bending stress f_ℓ is calculated as one-half of the difference between the stresses from step 2.

Generally, for the doubly symmetric test specimens, the f_ℓ values calculated in this way are slightly larger in the compression flange than in the tension flange at the maximum moment (or stress) locations along the girder length. These larger f_ℓ values are taken as the design analysis lateral bending stresses. As would be expected, the f_b values calculated in this way are approximately the same in the tension and compression flanges for the doubly symmetric specimens. Furthermore, for the tests that are statically determinant, the f_b values calculated in the above fashion are a close match to the f_b values that can be determined based on first calculating the vertical bending moment (M) at the corresponding cross-section by static equilibrium on the initial undeformed geometry, and then calculating f_b using the beam theory solution $f_b = M/S_x$.

The distribution of the shell element normal stresses in the direction tangent to the girder length is typically not perfectly linear across the width of the flanges. This is due predominantly to local flange plate bending effects. These local plate bending effects tend to be most significant at flanges corresponding to applied load positions (see Fig. 3.3.1 for a sketch of how the loads are applied at bearing stiffener locations). They are less significant at flanges corresponding to knife-edge or roller supports, and they are particularly minor at flanges that do not have any direct applied loading or support conditions. Nevertheless, in all cases, these local plate bending effects are small compared to the overall girder vertical and lateral bending effects.

The maximum values of the shell second-order elastic stresses f_b and f_ℓ within the critical unsupported length are utilized in all the design predictor equations considered in this work, with the exception of the Recommended Specification (Hall and Yoo 1998) equations. In the Recommend Specification equations, the maximum first-order elastic stress at the cross-frame locations is used.

In all cases in which second-order elastic design analysis stresses are obtained, the second-order elastic stresses are computed at the load level corresponding to satisfaction of the subject design strength equations. This presents a problem in that, in general, the values of f_b and f_ℓ and the ratio f_ℓ / f_b vary nonlinearly in the second-order elastic analysis. The appropriate values of f_ℓ and f_b are determined by incrementing the loads at less than one percent of that corresponding to the maximum strength in the full nonlinear analysis, and checking for a load level that satisfies the applicable design equations to within one percent. It should be noted that, in general, the design may be controlled either by flexure or by shear strength equations. The shear strength of course is checked directly against the maximum web shear force, whereas the flexural strength equations generally depend on both f_b and f_ℓ.

As noted in Sections 1.2, 1.5 and 2.3.3, the elastic design analysis stresses are calculated in some cases using a geometrically-linear (i.e., first-order) solution with an

open-walled section curved beam finite element. Specifically, the evaluation of moment-shear interaction in Chapter IX is conducted in this way. The calculation of f_ℓ and f_b is much simpler with these models. Since the analyses are first-order, the ratio f_ℓ / f_b is a constant and does not depend on the load level. Therefore, reference loads which have the same relative magnitudes to one another as the loads applied in the full nonlinear shell analyses may be applied to determine f_ℓ / f_b. Given a calculated bimoment B and vertical bending moment M, this ratio can be computed based on thin-walled beam theory as

$$\frac{f_\ell}{f_b} = \frac{B}{M}\frac{S_x}{S_{yf}}\frac{1}{h} \tag{3-7}$$

for a doubly-symmetric I girder, where S_{yf} is the elastic section modulus of the isolated flange corresponding to lateral bending, and h is the distance between the mid-thickness of the flanges. For monosymmetric I girders, the ratio of the flange lateral to vertical bending stress can be computed as

$$\frac{f_\ell}{f_b} = \frac{B}{M}\frac{\omega S_{xc}}{C_w} \tag{3-8a}$$

assuming that the compression flange is the smaller of the two flanges, where

$$\omega = y_{oc}\frac{b_{fc}}{2} \tag{3-8c}$$

is the sectorial coordinate at the tips of the compression flange,

$$y_{oc} = \frac{I_{yt}}{I_{yt} + I_{yc}} h \tag{3-8d}$$

is the distance from the shear center to the mid-thickness of the compression flange, I_{yt} and I_{yc} are the moments of inertia for the tension and compression flanges about a vertical axis within the plane of the web, h is the distance between the mid-thickness of the flanges, and

$$C_w = I_{yt}(h - y_{oc})^2 + I_{yc}y_{oc}^{\ 2} \tag{3-8e}$$

is the cross-section warping constant.

Once f_ℓ / f_b is calculated, it may be substituted into the flexural strength equation being evaluated to obtain the corresponding nominal flexural capacity. In general, the design may be controlled by flexural strength or by shear strength.

CHAPTER IV

COMPARISON TO EXPERIMENTAL RESULTS

This chapter presents comparisons between the results from prior experimental tests and finite element analyses conducted as prescribed in Chapter III, as well as between the experimental results and predictions of various design strength equations. These experiments include single curved girders (Mozer et al. 1970 and 1971), a test system with two curved girders (Mozer et al. 1973), and a test system with three curved girders (Zureick et al. 2000; Zureick and Kim 2000; Hartmann 2000; Grubb and Hall 2001; Hartmann and Wright 2001). Table 4.0.1 summarizes the types and objective parameters for each of these tests.

As noted in Chapter I, reduction and extensive interpretation of the experimental data from the prior and ongoing experiments conducted within Curved Steel Bridge Research Project (CSBRP), and correlation of the data from these experimental tests with the results from refined finite element analyses, is to be addressed in other project reports. However, to provide some confirmation of the accuracy of the finite element models developed in this research, this chapter is devoted to a comparison between analysis predictions and basic responses determined from this and other experimental test data. Also, key design predictor equations are compared to the experimental data.

The organization of this chapter is as follows. Section 4.1 summarizes the layout and the loading and displacement boundary conditions for all of the tests. The detailed geometric and material properties of the specimens are described in Section 4.2. Information about the geometric imperfections and residual stresses assumed within the finite element models is provided in Section 4.3. Next, the strengths obtained from physical tests are compared to the finite element predictions, as well as to the results of key design equations in Section 4.4. The one-third rule equations (Section 2.1.9), the flexural strength equations prescribed by the Recommended Specifications (see Section 2.1.2), and the yield interaction equations developed by Yoo (1996) (see Section 2.1.8) are evaluated. The Hanshin Guideline equations (Section 2.1.6) are evaluated with respect to the finite element parametric studies in Chapter VII. However, these equations are not considered here. The discussion of the various strength predictions is followed by Section 4.5, which provides example calculations to clarify how the design strengths are determined. Section 4.6 then discusses the effect of different interpretations regarding the calculated flange lateral bending stresses $\bar{f}_w$ on the predictions by the flexural strength equations in the Recommended Specifications (Hall and Yoo 1998). The reader is referred to Sections 2.1.2.6 and 2.1.2.7 for a thorough discussion of the background regarding these calculations. The load-vertical deflection data measured in the experimental tests are compared to the finite element predictions in Section 4.7. Finally,

Section 4.8 considers the measured and predicted specimen distortions from several of the tests.

Table 4.0.1. Types and objective parameters of girders examined experimentally.

Type	Specimen	Objective Parameter	Reference
Single Girder	C8-2	3-Point Bending	Mozer et al. (1970)
	C9-2	3-Point Bending	
	D13	3-Point Bending	
	D14	3-Point Bending	
	L1-A	4-Point Bending	Mozer et al. (1971)
	L2-A	4-Point Bending	
	L2-B	3-Point Bending	
	L2-C	3-Point Bending	
	S1-0.10	Shear	Zureick et al. (2001)
	S1S-0.10	Shear	
2-Girder System	GI-3	3-Point Bending	Mozer et al. (1973)
	GI-4	3-Point Bending	
	GI-5	4-Point Bending	
	GO-8	4-Point Bending	
3-Girder System	B1	Uniform Vertical Bending	Zureick et al. (2000)
	B2	Uniform Vertical Bending	Zureick and Kim (2000)
	B3	Uniform Vertical Bending	Grubb and Hall (2001)
	B4	Uniform Vertical Bending	Hartmann and Wright (2001)
	B5	Uniform Vertical Bending	
	B6	Uniform Vertical Bending	
	B7	Uniform Vertical Bending	Hartmann (2000) Grubb and Hall (2001) Hartmann and Wright (2001)

4.1 TEST CONFIGURATIONS

4.1.1 Single Girder Tests

Figures 4.1.1 through 4.1.6 illustrate the layout and the loading and displacement boundary conditions for the single girder tests studied herein. These tests include three-point bending (C8-2, C9-2, D13, D14, L2-B, and L2-C), four-point bending (L1-A and L2-A), and high shear-low moment configurations (S1-0.10 and S1S-0.10). All of the specimens except C8-2 are flame cut.

A schematic of the test setup for specimens C8-2, C9-2, D13 and D14 is presented in Fig. 4.1.1. In these tests, a single loading is applied eccentrically at the center of the 3.048 m (10 ft) simple span. Lateral and torsional restraints are provided at the end supports only. The eccentricity of the loading, e, is specified for each specimen such that the ratio of the lateral flange bending stress to the vertical flange bending stress (f_ℓ/f_b) is approximately equal to 0.30 based on the strains measured in the tests at an undefined low load level. The eccentricities actually utilized in the tests are not reported in (Mozer et al. 1970). Therefore, in the current research, e is first calculated for each test based on curved beam theory, and second-order elastic analyses of the perfect specimens are performed with this e to a load level of 25 percent of the maximum applied load attained in the experiments. Subsequently, e is varied in the second-order elastic analyses to obtain a close approximation of $f_\ell/f_b = 0.30$. It is found that a constant e of 45.72 mm (1.8 in) produces this value of f_ℓ/f_b to within $\pm$ 0.013, and therefore e = 45.72 mm is selected for all of these studies. The corresponding values of f_ℓ/f_b are listed in Table 4.1.1. The eccentric loading is applied as a trapezoidal distributed line load at the top of the bearing stiffener on the side of the web closest to the center of curvature.

Figures 4.1.2 to 4.1.4 show schematics of the setup of specimens L1-A, L2-A, L2-B, and L2-C. Each of these test specimens is flame cut to a nominal radius of 15.24 m (50 ft). Full-depth intermediate transverse stiffeners are used in specimen L1 (test L1-A) while the intermediate transverse stiffeners are cut-short in specimen L2 (tests L2-A, L2-B, and L2-C). This allowed Mozer et al. (1971) to compare the influence of stiffener types on the behavior and strength of the test specimens. The shaded areas in Figs. 4.1.2 and 4.1.3 represent the test panels.

Tests L1-A and L2-A are four-point bending tests with radial supports provided at all the loading and support locations. The loads are applied concentrically at the two middle bracing locations (see Fig 4.1.2). Tests L2-B and L2-C are three-point bending tests with lateral restraints at the support locations only. The loads are applied eccentrically to obtain specified ratios of lateral to vertical flange bending stress (f_ℓ/f_b). For test L2-B, an eccentricity of e = 43.43 mm is imposed to obtain a target ratio of $f_\ell/f_b = 0.50$ (computed by beam theory), and for test L2-C, an eccentricity of e = 49.78 mm (1.96 in) is specified to achieve a computed f_ℓ/f_b ratio of 0.25 (see Figs 4.1.3 and 4.1.4). These eccentric loads are modeled in a similar fashion to that described above for the Mozer et al. (1970) tests.

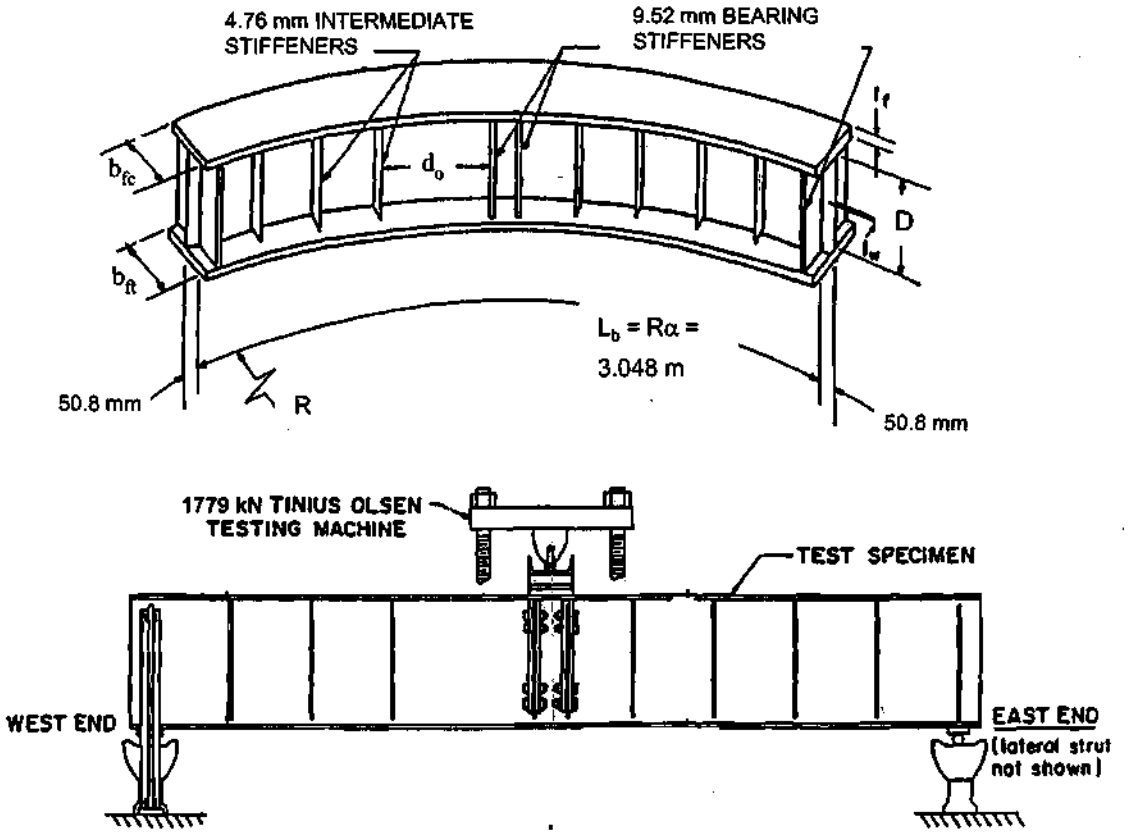

Figure 4.1.1. Tests C8-2, C9-2, D13 and D14 (Mozer et al. 1970).

Table 4.1.1. Values of the second-order elastic f_i/f_b at 25 percent of the experimental maximum load level utilized within the finite element models of the tests by Mozer et al. (1970), based on an eccentricity e of 45.72 mm (1.8 in).

Test	C8-2	C9-2	D13	D14
f_i/f_b	0.313	0.303	0.287	0.309

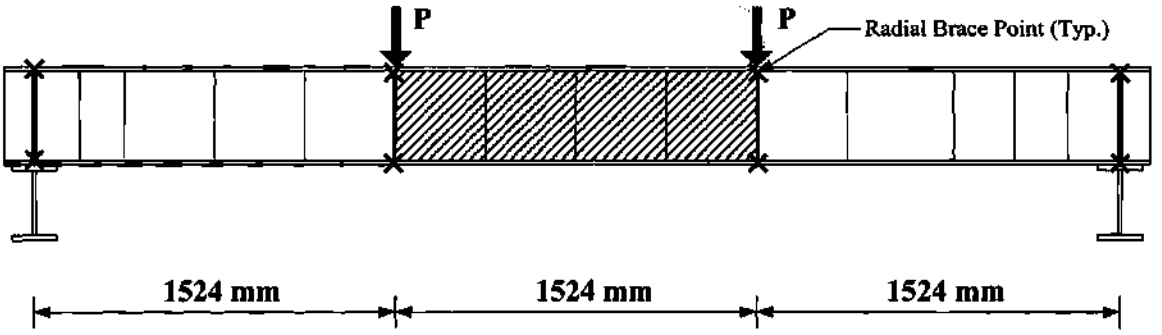

Figure 4.1.2. Mozer et al. (1971) tests L1-A and L2-A, side view.

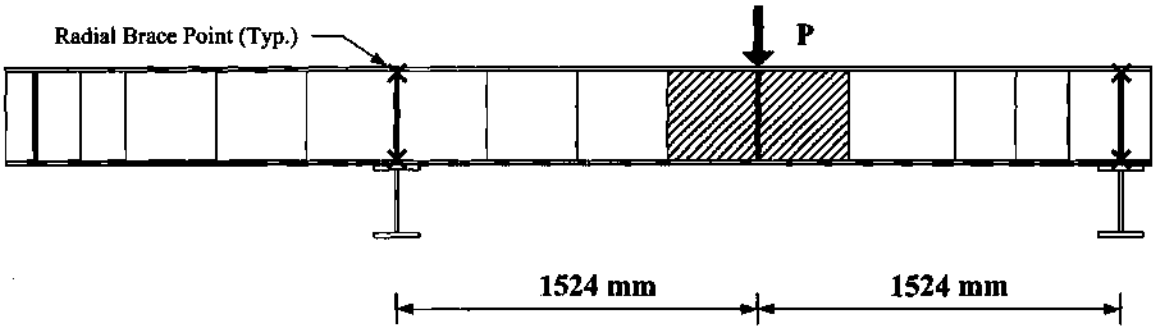

Figure 4.1.3. Mozer et al. (1971) tests L2-B and L2-C.

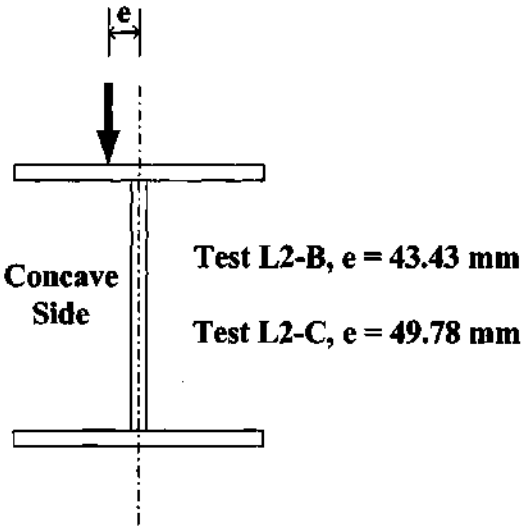

Figure 4.1.4. Load eccentricity of tests L2-B and L2-C (Mozer et al. 1971).

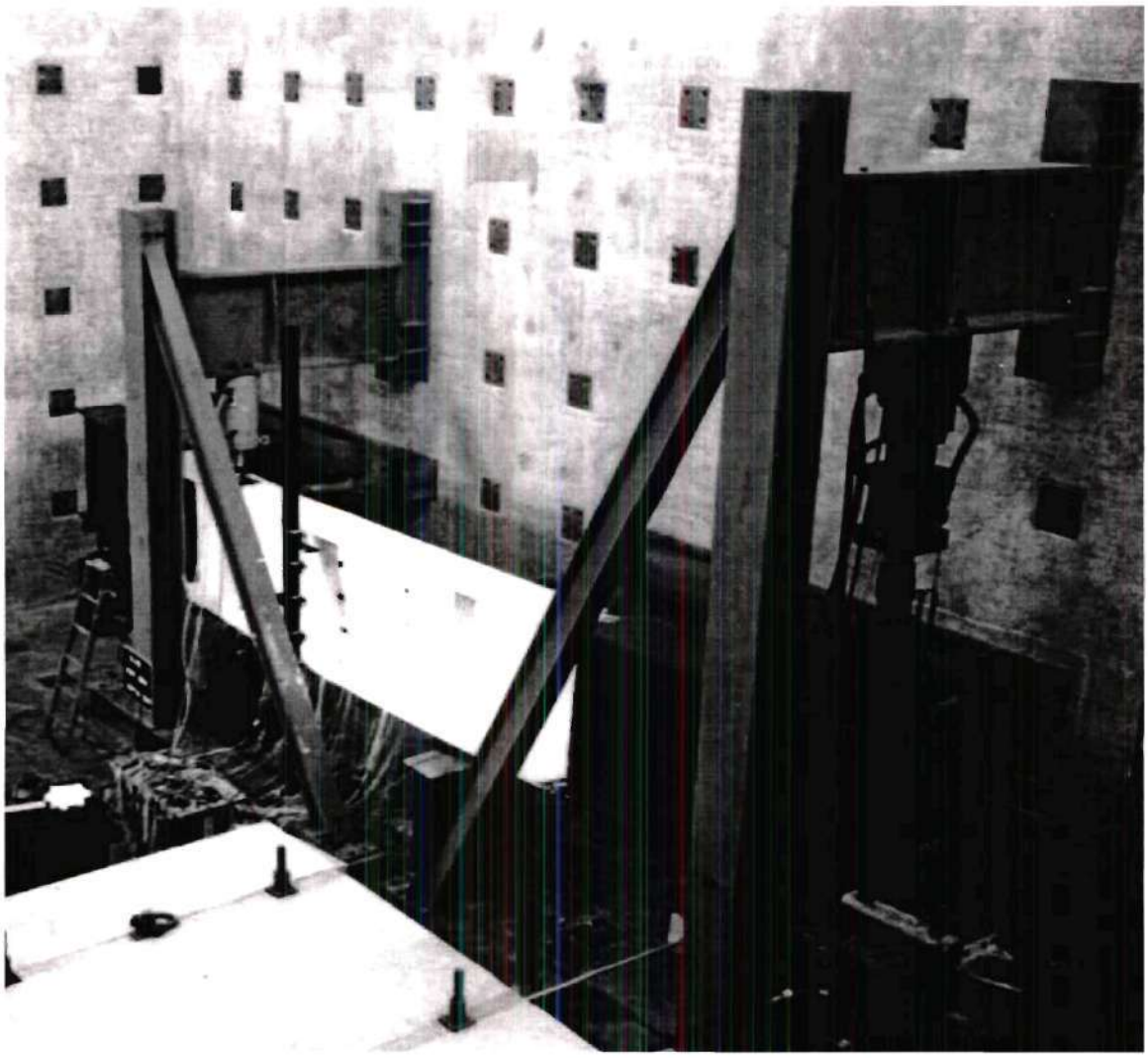

Figure 4.1.5. Test setup for specimens S1-0.10 and S1S-0.10 (Zureick et al. 2001).

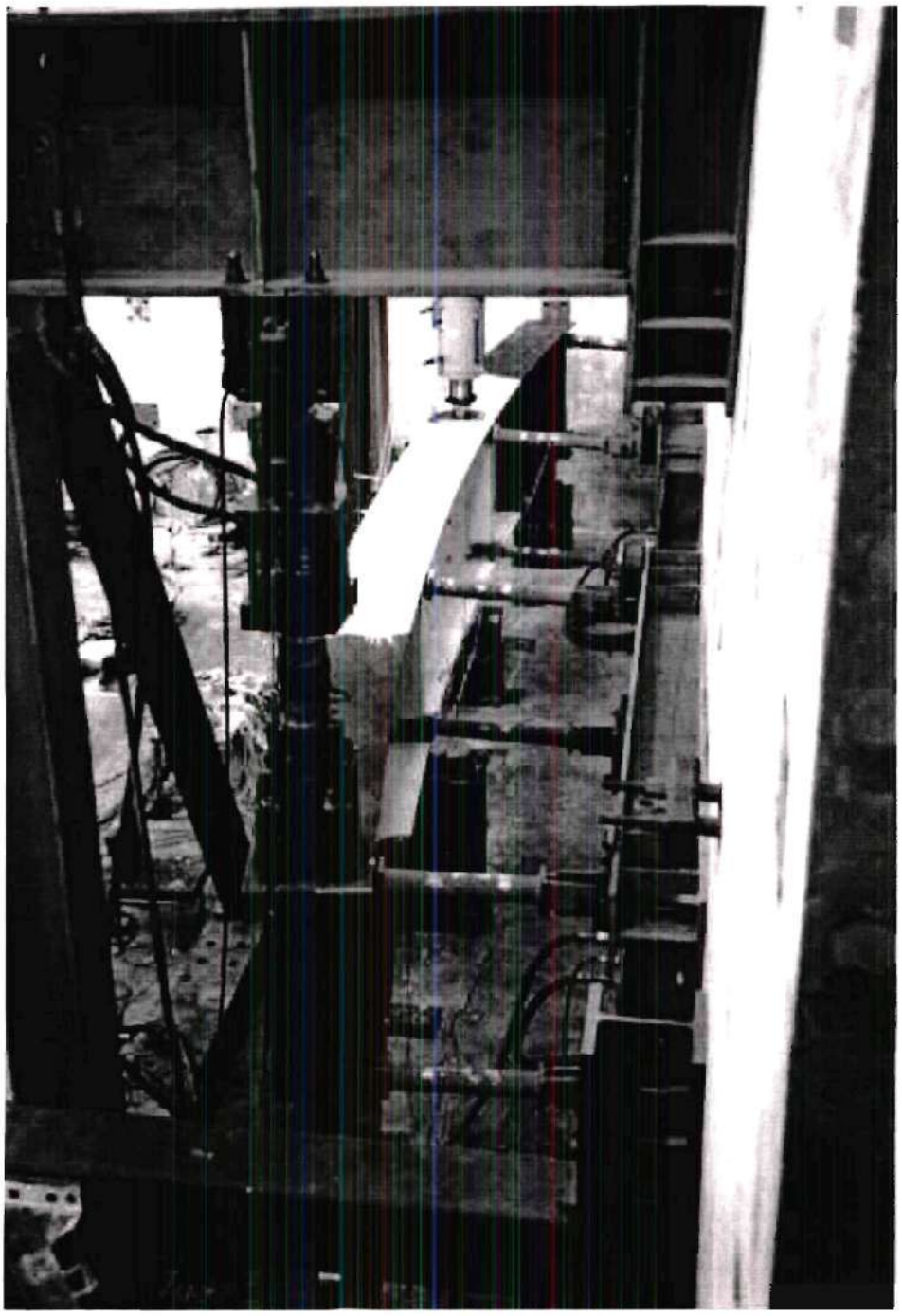

Figure 4.1.6. Test setup for specimens S1-0.10 and S1S-0.10 (Zureick et al. 2001).

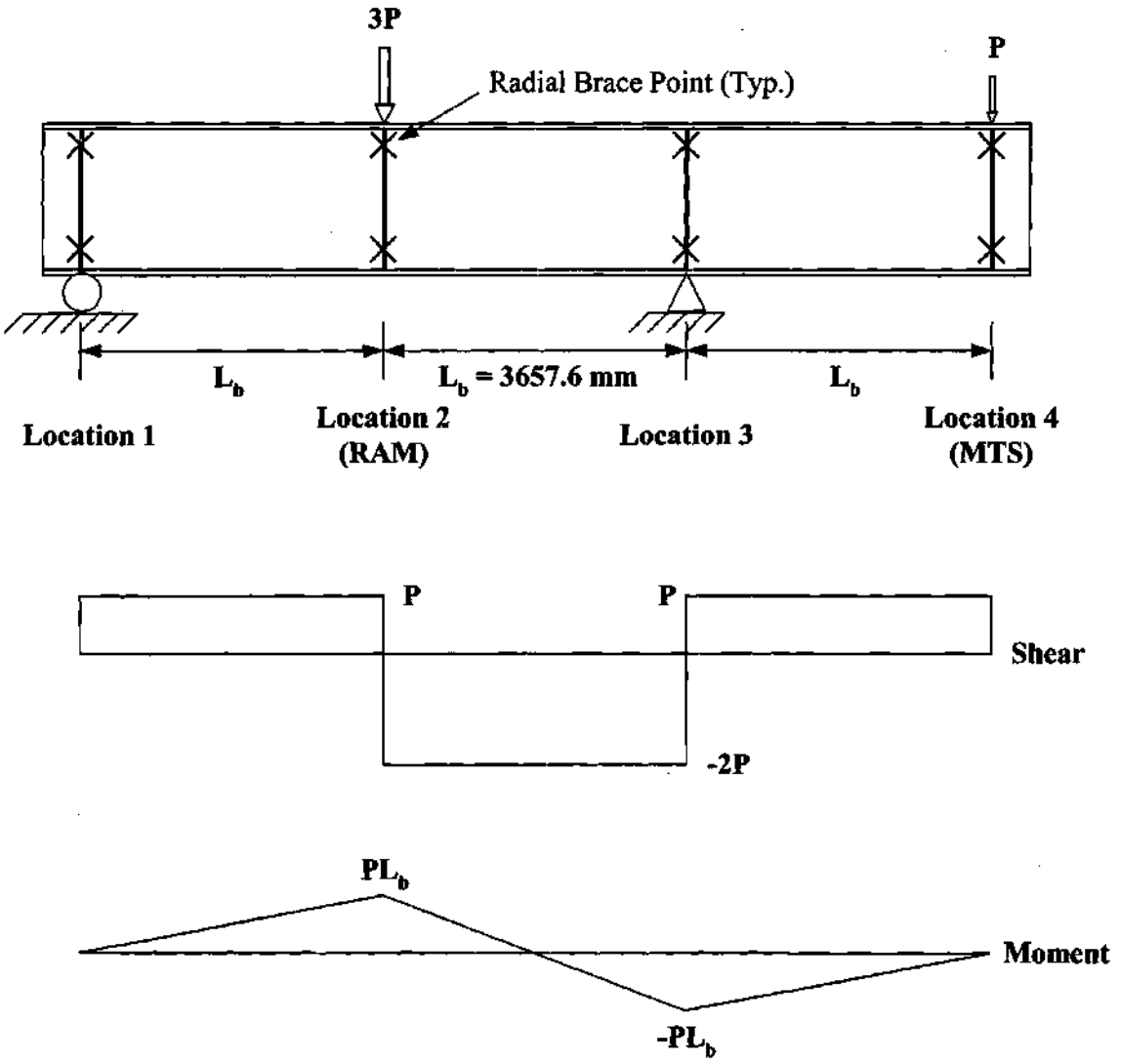

Figure 4.1.7. Loading scheme and the corresponding shear and vertical bending moment diagrams of specimens S1-0.10 and S1S-0.10 (Zureick et al. 2001).

Figures 4.1.5 and 4.1.6 show the setup for specimens S1-0.10 and S1S-0.10, and Fig. 4.1.7 shows the loading scheme and the corresponding approximate shear and vertical bending moment diagrams for these tests. A three-segment test configuration is utilized in which the center unsupported length (segment 2-3) contains the test panel(s). Vertical loads of 3P and P are applied at location 2 by a large capacity ram and at location 4 by an actuator, respectively. Vertical supports are positioned at locations 1 and 3. Radial bracing is provided at the supports and at the load locations. These braces have spherical bearings at both ends, to eliminate any restraint of displacements transverse to their line of orientation, and they are anchored to a massive reaction wall at their far ends.

The braces are inclined slightly upward at the beginning of the tests, such that they pass through a horizontal orientation at the loading locations prior to the end of the tests.

The downward loads of 3P and P at locations 2 and 4 produce a shear force of approximately 2P in the central test segment (the reactions at locations 1 and 3 are slightly different than P and 3P, due to the horizontal curvature of the girder; however, this difference is small). The moment is approximately zero at the center of the critical unsupported length, thus minimizing the influence of bending moment on the response.

Specimen S1-0.10 is an "unstiffened" girder with $L_b/R = 0.10$, $D/t_w = 146$ and $d_o/D = 3$. Relatively large flanges ($A_w/A_f = 0.81$) and small L_b/b_f (= 6.7) were used in these tests. Finite element studies conducted in the design of these experiments indicated that the girders were apt to fail by flange lateral bending rather than in web shear if the flanges were not sized appropriately. The selected flange proportions are practical, but smaller flanges are likely in many situations in practice. The problem is that with smaller flanges, the flange lateral bending stresses become larger. Consequently, the girder strength is controlled by lateral bending rather than by shear. These types of situations are considered within the finite element parametric studies of this research (see Chapters V and IX). Since the goal of the experimental tests is to investigate the existence of tension-field action in curved web panels, the girders were designed to ensure a web shear failure. Specimen S1S-0.10 is identical to S1-0.10 except an intermediate stiffener is added at the mid-length of the test segment (2-3) such that $d_o/D = 1.5$. Full details regarding the design of these tests are provided in (Zureick et al. 2001).

4.1.2 Two-Girder Test System

The test configurations in the two-girder test system studied by Mozer et al. (1973) are shown in Figs. 4.1.8 through 4.1.11. The critical panels are indicated by the shaded areas. The system is composed of two curved I girders, G-I and G-O, connected by end diaphragms and intermediate cross-frames (see Fig 4.1.8). The web of girder G-I is stiffened with single-sided, cut-short transverse stiffeners while the web of girder G-O is unstiffened between the bearing stiffeners. For tests GI-3 and GI-4, a single concentric load is applied at one-third of the length from the left and right ends of girder G-I, respectively (see Figs. 4.1.9 and 4.1.10.). For test GI-5, two equal concentrated loads are applied simultaneously at each of the one-third points of girder G-I, thereby producing a nearly constant moment region between the load points (see Fig. 4.1.11). In this test, the cross-frame ID-3 is removed, producing an L_b/b_f of 15 on the inside girder. Test GO-8 is conducted on the outside girder with the connected cross-frames ID-1, ID-3, and ID-5 removed. Concentrated loads are placed between the girders at the ¼ point nearest the outer girder to avoid uplift at the interior girder supports. The corresponding L_b/b_f for this test is approximately 10.

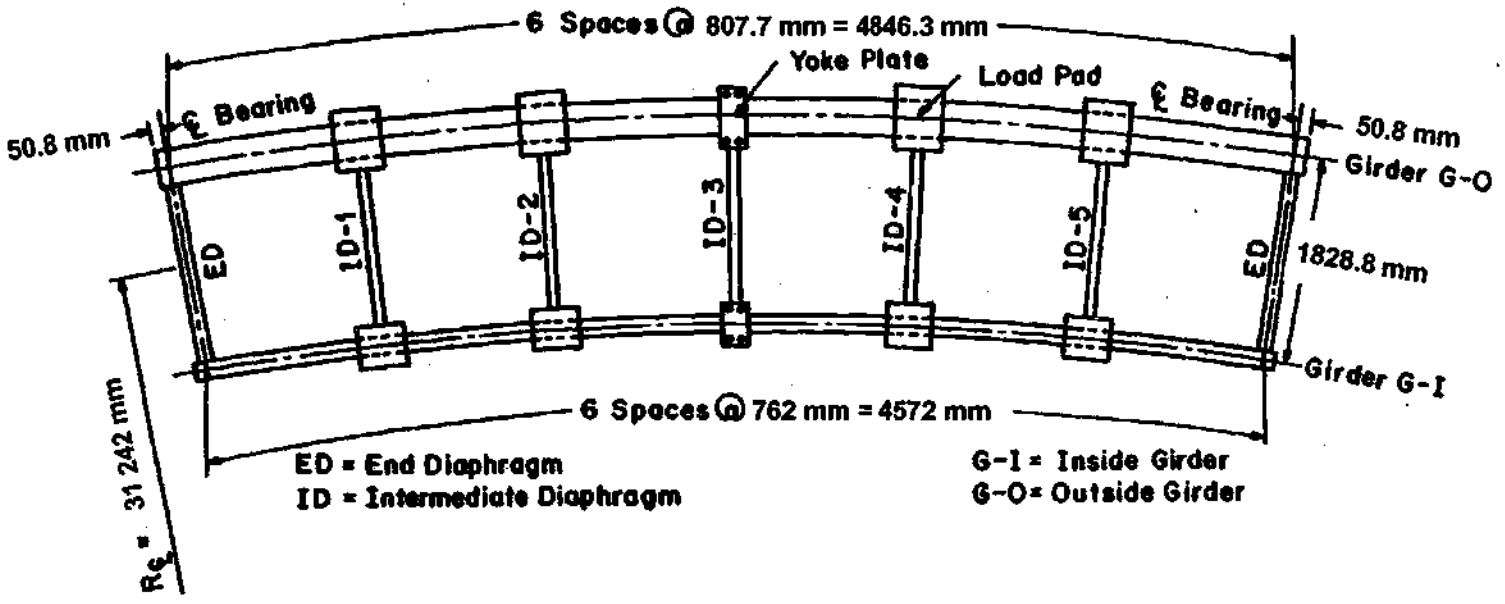

Figure 4.1.8. Framing plan of the test system for tests GI-3, GI-4, GI-5, and GO-8 (Mozer et al. 1973).

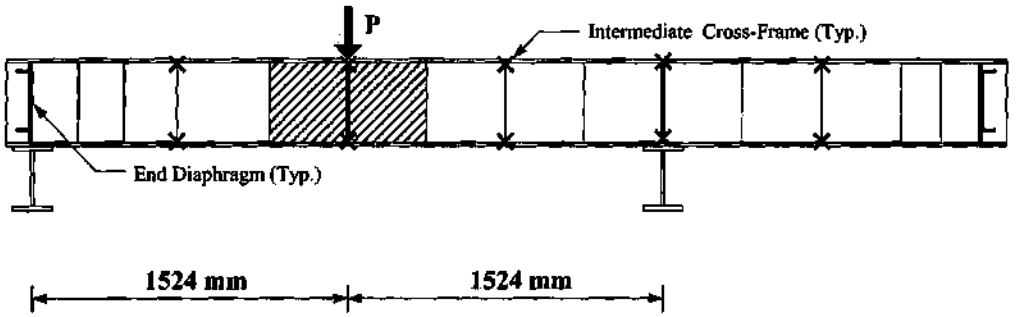

Figure 4.1.9. Loading scheme for test GI-3 (Mozer et al. 1973).

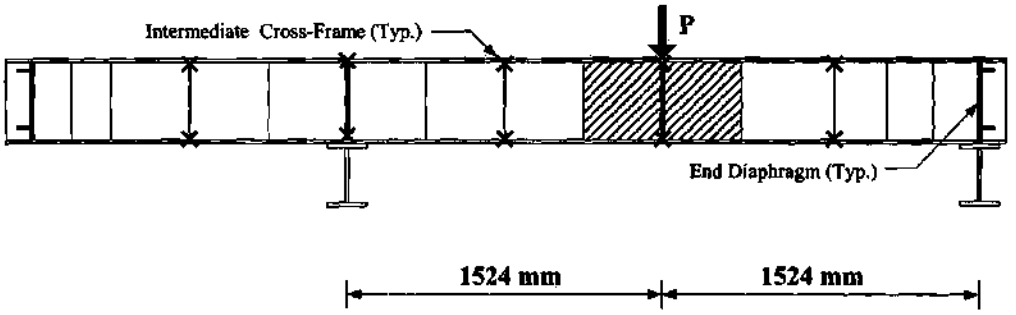

Figure 4.1.10. Loading scheme for test GI-4 (Mozer et al. 1973).

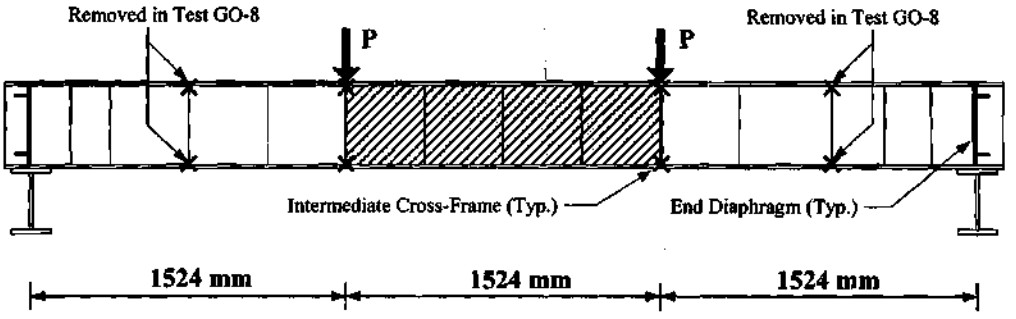

Figure 4.1.11. Loading scheme for tests GI-5 and GO-8 (Mozer et al. 1973).

4.1.3 Three-Girder Test System

Figure 4.1.12 is a picture of the overall configuration of the three-girder system utilized in the uniform vertical bending tests conducted at the FHWA Turner-Fairbank laboratory (Zureick et al. 2000; Zureick and Kim 2000; Hartmann 2000; Grubb and Hall 2001; Hartmann and Wright 2001). The simple-span bridge system used in these tests consists of three girders G1, G2, and G3 with respective radii of curvature of 58.29 m (191.25 ft), 60.96 m (200 ft), and 63.63 m (208.75 ft). The centerline span of girder G2 is 27.43 m (90 ft) measured along its arc length. Each of the component specimens in these tests are spliced into the center of the outside girder G3 and connected to this girder at a short distance outside of the closest cross-frames placed symmetrically about the middle of the bridge span. The specimens have a total arc length between the splice locations of 7.71 m (25.3 ft), with L_b = 4.57 m (15 ft) and L_b/R = 0.072 within the test length. The compression flange and web slenderness as well as the symmetry and non-symmetry of the cross-section are varied in the tests.

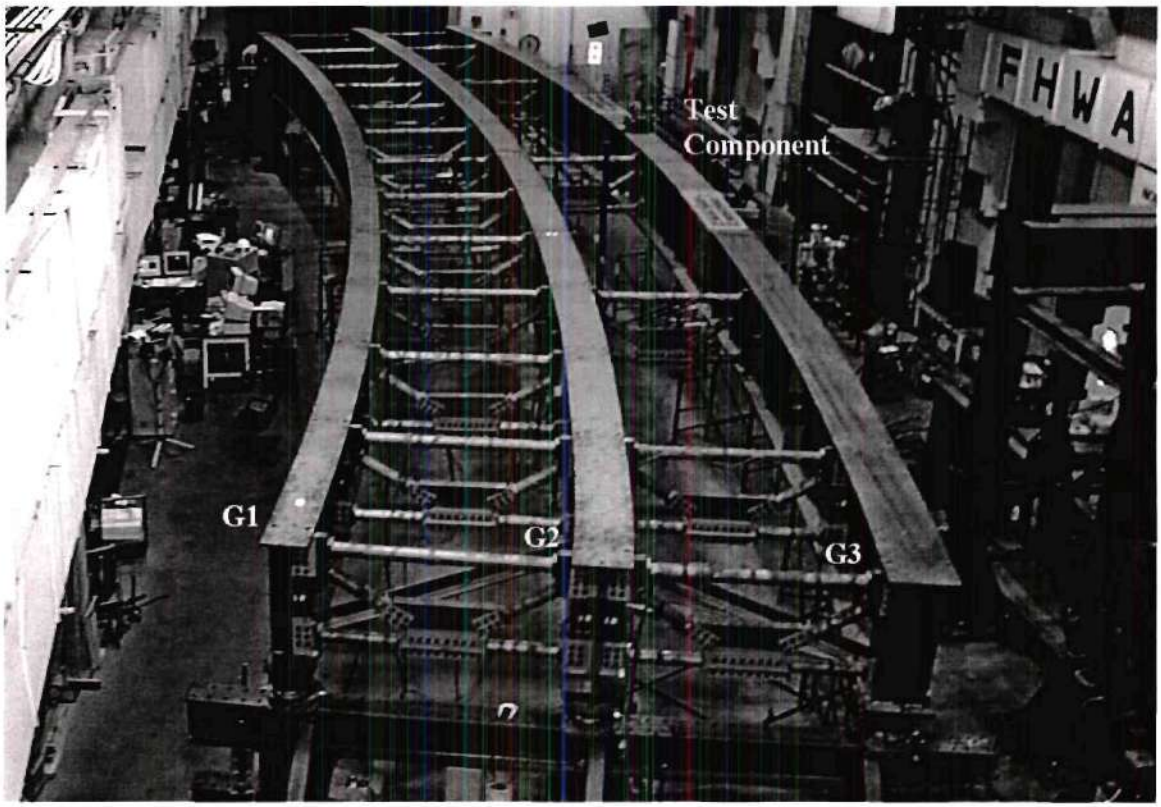

Figure 4.1.12. Overall test configuration, three-girder test system, FHWA Turner Fairbank laboratory (Hartmann 2000).

Equal loadings are applied to the bridge system approximately at each of the one-third points of all of the girders. Therefore, the test specimens are subjected to nearly constant vertical bending moment. These loadings are applied from assemblies that are positioned above the bridge and anchored to the test floor by four "tension column" dywidag bars (on each of their corners), which extend from the assemblies down to anchorages underneath the test floor (not shown in Fig. 4.1.12). This loading arrangement is designed to provide minimal constraint to the lateral movement of the bridge system at the load points. The reader is referred to Zureick et al. (2000), Zureick and Kim (2000), Grubb and Hall (2001) and Hartmann and Wright (2001) for a more detailed discussion of the loading and displacement boundary conditions of these tests.

Figure 4.1.12 shows the overall bridge system in a configuration slightly different than that utilized in the uniform vertical bending tests. In this figure, one cross-frame is connected to the component specimen at the center of the bridge span. Figure 4.1.13 shows a plan view of the actual cross-frame arrangement utilized in the uniform vertical bending experiments.

4.2 GEOMETRIC AND MATERIAL PROPERTIES

The geometric and material properties of the experimental specimens analyzed in this work are summarized in Tables 4.2.1 to 4.2.7. The as-built dimensions and material properties, and the nondimensional design parameters for the single-girder tests are summarized in Tables 4.2.1 and 4.2.2 respectively. This information is presented for the two-girder system tests in Tables 4.2.3 and 4.2.4, and for three-girder system tests in Tables 4.2.5 to 4.2.7. The tension and compression flange dimensions are essentially equal for the single-girder and two-girder system tests (i.e., the girder cross-sections are doubly symmetric).

All of the single-girder test specimens considered here have constant web slenderness ratios of approximately 150. This is the maximum web slenderness ratio permitted by the AASHTO Guide Specifications (1993) and is retained as a limit in the Recommended Specifications (Hall and Yoo 1998). The panel aspect ratio (d_o/D) ranges from 0.67 to 3.0 (see Table 4.2.2). The subtended angle L_b/R varies from 0.099 to 0.317. Several of these test specimens (specimens C9-2, D13, and D14) have subtended angles significantly greater than the maximum limit of $L_b/R = 0.10$ stated in the above two specifications. In addition, the single girder test specimens have flange slenderness ratios b_f/t_f ranging from 15.4 to 23.7, and L_b/b_f ratios ranging from 6.7 to 16.

It should be noted that girders L1-A, and L2-A, B and C are effectively hybrid girders ($F_{yf}/F_{yw} = 41.1/29.7 = 1.38$).

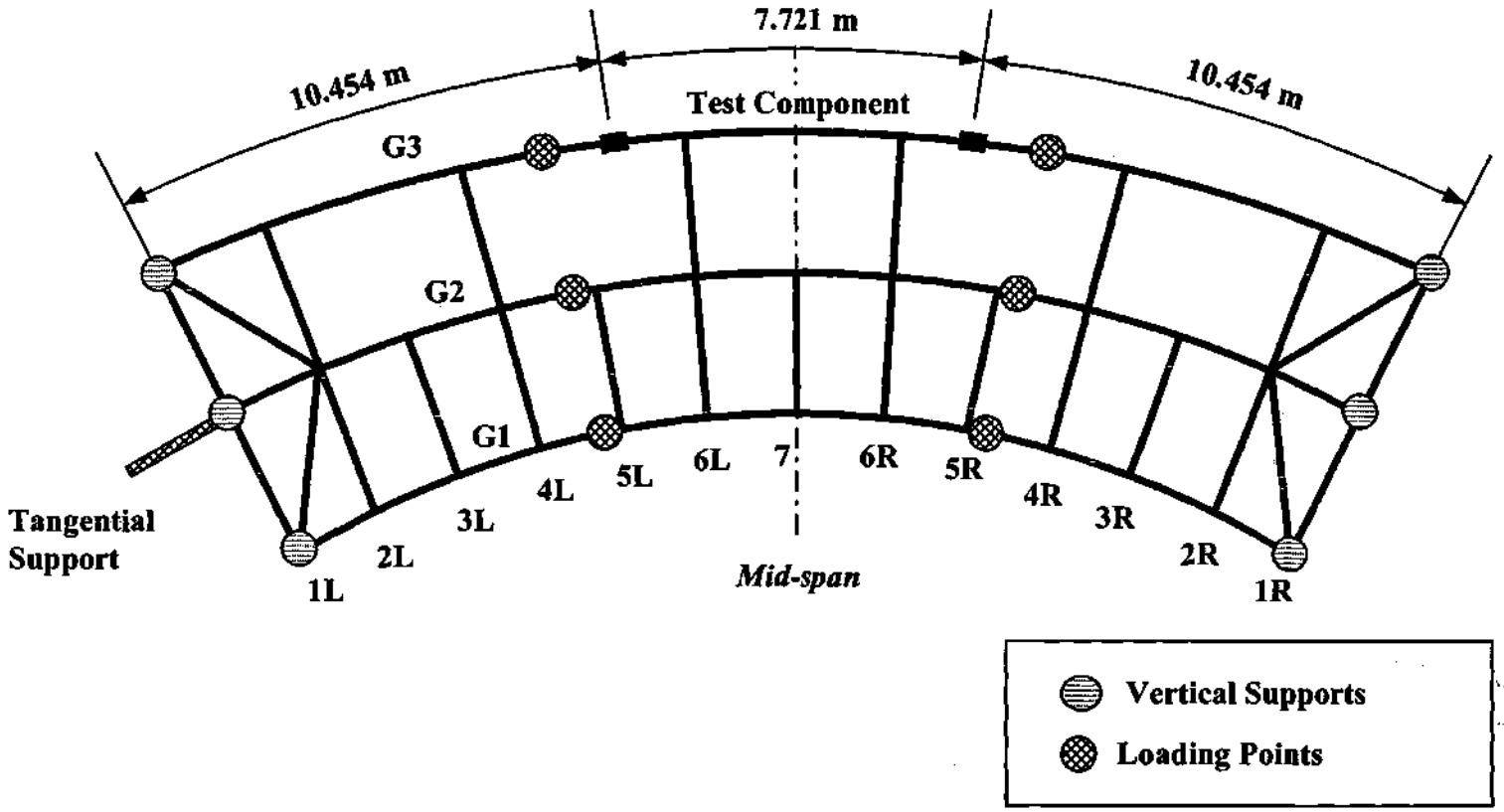

Figure 4.1.13. Plan view of test configuration utilized in the uniform vertical bending tests, three-girder test system (Zureick and Kim 2000).

Table 4.2.1. As-built dimensions and material properties, single-girder tests[1].

Test	L_b (mm)	R (m)	D (mm)	t_w (mm)	E_w (MPa)	F_{yw} (MPa)	F_{uw} (MPa)	b_{fc} (mm)	t_f (mm)	E_f (MPa)	F_{yf} (MPa)	F_{uf} (MPa)	References
C8-2	3048	28.27	456	3.23	197800	217	330	191	9.42	202100	285	401	Mozer et al. (1970)
C9-2	3048	9.60	457	3.05	207500	242	319	190	9.35	202700	239	365	
D13	3048	11.25	456	3.05	207500	242	319	217	9.35	202700	239	365	
D14	3048	11.23	457	3.05	207500	242	319	214	9.35	202700	239	365	
L1-A	1524	15.11	454	3.05	206200	205	345	151	9.91	205100	283	483	Mozer et al. (1971)
L2-A	1524	15.42	455	3.02	206200	205	345	152	9.91	205100	283	483	
L2-B	3048	15.42	455	3.02	206200	205	345	152	9.91	205100	283	483	
L2-C	3048	15.42	455	3.02	206200	205	345	152	9.91	205100	283	483	
S1-0.10	3658	36.58	1219	8.33	200100	397	563	545	23.01	205100	386	560	Zureick et al. (2001)
S1S-0.10	3658	36.58	1219	8.33	200100	397	563	545	23.01	205100	386	560	

[1]As noted in Section 3.2, the strain hardening material data is not reported by Mozer et al. (1970 and 1971). Values of ε_{st} = 0.014 and E_{st} = 6200 MPa (900 ksi), which are representative of A36 steel, are assumed for the web and the flanges. See Fig. 3.2.3 for the corresponding idealized uniaxial stress-strain curves. For the single-girder shear tests (Zureick et al. 2001), average measured values of ε_{stw} = 0.0232, E_{stw} = 3330 MPa (483 ksi) and ε_{uw} = 0.156 for the web and ε_{stf} = 0.0214, E_{stf} = 4010 MPa (581 ksi) and ε_{uf} = 0.152 are used for the flanges. The material properties used for S1-0.10 and S1S-0.10 are based on one set of approximately one-half of the tension coupons pulled for these tests (six flange tests and 12 web tests). The values reported in Zureick et al. (2001) are based on all of the tension coupons pulled for these tests.

Table 4.2.2. Nondimensional design parameters, single-girder tests.

Test	D/t_w	t_f/t_w	d_o/D	D/b_{fc}	$\frac{Dt_w}{b_{fc}t_{fc}}$	b_{fc}/t_f	L_b/R	L_b/b_{fc}	References
C8-2	141	2.92	1.34	2.39	0.82	20.3	0.108	16.0	Mozer et al. (1970)
C9-2	150	3.07	1.33	2.40	0.78	20.4	0.317	16.0	
D13	150	3.07	0.67	2.10	0.68	23.3	0.271	14.0	
D14	150	3.07	0.67	2.14	0.70	22.9	0.271	14.3	
L1-A	149	3.25	0.83	3.01	0.93	15.2	0.101	10.1	Mozer et al. (1971)
L2-A	151	3.28	0.83	2.99	0.91	15.4	0.099	10.0	
L2-B	151	3.28	0.83	2.99	0.91	15.4	0.099	10.0	
L2-C	151	3.28	0.83	2.99	0.91	15.4	0.099	10.0	
S1-0.10	146	2.76	1.5	2.24	0.81	23.7	0.10	6.7	Zureick et al. (2001)
S1S-0.10	146	2.76	3	2.24	0.81	23.7	0.10	6.7	

Table 4.2.3. As-built dimensions and material properties, two-girder system test components (Mozer et al 1973)[1].

Test	L_b (mm)	R (m)	D (mm)	t_w (mm)	E_w (MPa)	F_{yw} (MPa)	F_{uw} (MPa)	b_{fc} (mm)	t_f (mm)	E_f (MPa)	F_{yf} (MPa)	F_{uf} (MPa)
GI-3	762	15.24	457	3.05	209600	279	404	99.6	12.73	203700	232	435
GI-4	762	15.24	457	3.05	209600	279	404	99.6	12.73	203700	232	435
GI-5	1524	15.24	457	3.05	209600	279	404	99.6	12.73	203700	232	435
GO-8	1524	16.15	457	7.92	207200	267	472	152	9.65	209700	259	452

[1]Values of $\varepsilon_{st} = 0.014$ and $E_{st} = 6200$ MPa (900 ksi), which are representative of A36 steel, are assumed for the web and the flanges. See Fig. 3.2.3 for the corresponding idealized uniaxial stress-strain curves.

Table 4.2.4. Nondimensional design parameters, two-girder system test components (Mozer et al. 1973).

Test	D/t_w	t_f/t_w	d_o/D	D/b_{fc}	$\frac{Dt_w}{b_{fc}t_{fc}}$	b_{fc}/t_f	L_b/R	L_b/b_{fc}
GI-3	150	4.18	1.00	4.59	1.10	7.82	0.05	7.65
GI-4	150	4.18	0.83	4.59	1.10	7.82	0.05	7.65
GI-5	150	4.18	0.83	4.59	1.10	7.82	0.10	15.3
GO-8	57.7	1.22	3.33	3.01	2.47	15.7	0.094	10.0

Table. 4.2.5. As-built flange dimensions and material properties, three-girder system test components (Zureick and Kim 2000; Hartmann 2000); L_b = 4.57 m, R = 63.63 m, D = 1219 mm for all of the specimens.

Test	b_{fc} (mm)	t_{fc} (mm)	E_{fc} (MPa)	F_{yfc} (MPa)	ε_{stfc} (%)	E_{stfc} (MPa)	F_{ufc} (MPa)	ε_{ufc} (%)	b_{ft} (mm)	t_{ft} (mm)	E_{ft} (MPa)	F_{yft} (MPa)	ε_{stft} (%)	E_{stft} (MPa)	F_{uft} (MPa)	ε_{uft} (%)
B1	445	19.51	196100	406	1.802	4882	583	15.97	445	19.41	198200	401	2.094	4578	574	16.31
B2	445	19.43	196100	406	1.802	4882	583	15.97	445	19.43	198200	401	2.094	4578	574	16.31
B3	445	19.48	196100	406	1.802	4882	583	15.97	445	19.43	198200	401	2.094	4578	574	16.31
B4	445	19.46	196100	406	1.802	4882	583	15.97	445	32.44	204600	389	2.04	4854	564	16.78
B5	418	24.66	203500	390	2.210	4716	569	16.19	418	24.56	203500	390	2.21	4716	569	16.19
B6	411	30.96	213100	386	2.261	4171	569	16.19	411	31.04	213100	386	2.261	4171	557	16.79
B7	534	16.43	203500[1]	389	2.210[1]	4716[1]	569[1]	16.19[1]	445	19.41	198200	401	2.094	4578	574	16.31

[1] Data not available. The values reported in the table for Test B7 are assumed values based on the data from the other material tests.

Table 4.2.6. As-built web dimensions and material properties, three-girder system test components (Zureick and Kim 2000; Hartmann 2000) L_b = 4.57 m, R = 63.63 m, D = 1219 mm for all test components.

Test	t_w (mm)	E_w (MPa)	F_{yw} (MPa)	ε_{stw} (%)	E_{stw} (MPa)	F_{uw} (MPa)	ε_{uw} (%)
B1	8.20	197300	447	2.578	3468	592	16.44
B2	10.08	201600	395	2.576	3558	540	17.29
B3	10.19	200800	396	2.731	3599	541	16.87
B4	8.10	191400	445	2.835	3310	585	16.9
B5	8.46	204850	441	2.668	3461	585	15.27
B6	8.53	190600	441	2.604	3323	584	16.84
B7	8.20	197300	447	2.578	3468	592	16.44

Table 4.2.7. Nondimensional design parameters, three-girder system (L_b/R = 0.072 for all test components).

Test	$2D_c/t_w$	$\frac{(t_{fc} + t_{ft})}{2t_w}$	d_c/D	D_c/D	$2D_c/b_{fc}$	$\frac{Dt_w}{b_{fc}t_{fc}}$	b_{fc}/t_{fc}	L_b/b_{fc}	References
B1	149	1.95	1	0.5	2.74	1.15	22.8	10.3	Zureick and Kim (2000)
B2	121	1.93	1	0.5	2.74	1.42	22.9	10.3	
B3	120	1.91	3.9	0.5	2.74	1.43	22.8	10.3	
B4	188	2.77	0.98	0.625	2.74	1.43	22.8	10.3	
B5	144	2.91	0.98	0.5	2.92	1.00	16.9	11.0	
B6	143	3.63	0.98	0.5	2.96	0.82	13.3	11.2	
B7	149	2.19	1	0.498	2.28	1.14	32.5	8.6	Hartmann (2000)

For the two-girder system, all of the test specimens have stocky flanges, with a b_f/t_f of approximately 8 for GI-3, GI-4, and GI-5, and 16 for GO-8. These flanges are all considered to be compact according to both the Recommended Specifications (Hall and Yoo 1998) and the proposed one-third rule equations (see Sections 2.1.9.2 and 2.1.1.2). The subtended angles vary from 0.05 to 0.10 (see Table 4.2.4). Specimens GI-3 and GI-4 have L_b/R ratios of 0.05, and specimens GI-5 and GO-8 have an L_b/R approximately equal to 0.10. The significance of these values for the subtended angle is as follows. The L_b/R ratio of 0.05 is just below the limit of 0.06 at which the Recommended Specifications (Hall and Yoo 1998) suggest that the effect of curvature can be ignored in the calculation of vertical bending moments. In addition, $L_b/R = 0.10$ is the maximum limit on the subtended angle between the cross-frames as per the Recommended Specifications.

All of the test specimens utilized in the three-girder test system have the same unbraced length of $L_b = 4.57$ m and a constant radius of curvature of $R = 63.63$ m. This gives a constant subtended angle of $L_b/R = 0.072$ for all of the tests. These specimens, with the exception of B4, are doubly symmetric I girders with web slenderness ratios $2D_c/t_w$ ranging from 120 to149 and flange slenderness ratios ranging from $b_f/t_f = 13.3$ (specimen B6) to $b_f/t_f = 32.5$ (specimen B7) (see Table 4.2.7). Although the flange slenderness of Specimen B7 is beyond the limit of $b_f/t_f = 24$ permitted for straight bridge I girders in AASHTO LRFD (2001), this specimen provides valuable information about the flange stability behavior and potential degradation in the girder performance by making the compression flange too slender. The value of $b_f/t_f = 32.5$ is approximately at the limit λ_r associated with the transition from inelastic to elastic flange buckling in the proposed modified AASHTO flange buckling equations, based on $F_{rs} = 114$ MPa (see Section 2.1.1.2). Specimen B4 is a singly symmetric I girder with $2D_c/t_w = 188$ and $b_{fc}/t_{fc} = 22.8$. It should be noted that all of the L_b/b_f values of these test specimens are well within the limit of $L_b/b_f = 25$ stated in the AASHTO Guide Specifications (1993) and the Recommended Specifications (Hall and Yoo 1998), and the $\lambda \leq \lambda_r$ limit of the proposed one-third rule equations (see Section 2.1.9.2).

4.3 SPECIFIED GEOMETRIC IMPERFECTIONS AND RESIDUAL STRESSES

Representative initial geometric imperfections and residual stresses are specified for the finite element models of the experimental tests. The initial geometric imperfections are input as the scaled first mode obtained from an elastic linear buckling analysis of a modified form of the finite element models in which the web is artificially thickened (see Section 3.4). The first mode is scaled up from a magnitude of zero until the measured initial web out-of-flatness or flange tilt is achieved (where this information exists), or until one of the AWS (1996) fabrication tolerances described in Section 3.4 is reached in the cases where measured geometric imperfections are not available. Tables 4.3.1 to 4.3.3 summarize the web thicknesses of the test components (t_{wlb}) used in the linear buckling analyses and the scale factor (sf) applied to the first buckling mode to generate the initial displacements (with zero internal strain) relative to the perfect horizontally-curved geometries. It should be noted that the maximum nodal displacement in the first buckling mode, prior to multiplication by sf, is equal 1.0.

Table 4.3.1. Initial geometric imperfection parameters for single-girder tests.

Test	t_{wlb} (mm)	D/t_{wlb}	sf
C8-2	5.69	80	0.355
C9-2	5.72	80	0.295
D13	5.72	80	0.292
D14	5.72	80	0.291
L1-A	5.66	80	0.295
L2-A	5.69	80	0.296
L2-B	4.57	100	0.313
L2-C	4.57	100	0.314
S1-0.10	8.33[1]	146	0.369
S1S-0.10	8.33[1]	146	0.369

[1] $t_{wlb} = t_w$

Table 4.3.2. Initial geometric imperfection parameters for two-girder system tests.

Test	t_{wlb} (mm)	D/t_{wlb}	sf
GI-3	5.715	80	0.300
GI-4	5.715	80	0.299
GI-5	5.715	100	0.204
GO-8	7.925	100	0.209

Table 4.3.3. Initial geometric imperfection parameters for three-girder system tests.

Test	t_{wlb} (mm)	D/t_{wlb}	sf
B1	12.19	100	0.357
B2	12.19	100	0.368
B3	12.19	100	0.410
B4	12.19	100	0.353
B5	12.19	100	0.342
B6	12.19	100	0.351
B7	12.19	100	0.293

For the cut-curved specimens (all except Specimen C8-2), the ECCS (1976) equations are utilized to define a representative residual stress pattern (see Section 3.5.1). For Specimen C8-2, the Culver and Nasir (1971) residual stress pattern outlined in Section 3.5.2 is employed. The specific Gauss point residual stresses for each of the specimens are illustrated in Appendix E.

4.4 SUMMARY OF RESULTS

The experimental results from all the bending tests discussed in the previous sections are compared to the following predictors:

1. full nonlinear analysis – for the three-girder system tests, analyses both with and without residual stresses and initial geometric imperfections are considered,

2. the proposed one-third rule equations for the flexural strength (Section 2.1.9.2), based on second-order elastic stresses,

3. the proposed one-third rule equations, but based on first-order elastic stresses – these predictions can be compared to those of (2) to determine the significance of the design analysis second-order elastic amplification within the experimental tests,

4. the flexural strength equations of the Recommended Specifications (Hall and Yoo 1998) (Section 2.1.2), which are based on first-order elastic stresses obtained from the design analysis,

5. Yoo's (1996) cross-section yield interaction equations (Section 2.1.8.2), with the design analysis prediction of the flange lateral bending moment M_ℓ determined from Eq. (1-6)[1], i.e., based on the V-Load equation,

6. Yoo's (1996) cross-section yield interaction equations, but with the lateral flange bending moment M_ℓ determined from direct second-order elastic analysis, and

7. Yoo's (1996) cross-section yield interaction equations, with the lateral flange bending moment determined from a direct first-order elastic analysis – similar to (2) and (3), the results from this calculation can be compared to those of (6) to determine the significance of second-order elastic amplification within the experimental tests.

In addition, the experimental results from the shear tests (Zureick et al. 2001) are compared to the following predictors:

- full nonlinear analysis based on the measured initial imperfections along with representative residual stresses (i.e., full nonlinear analysis of the "imperfect" specimens),

[1] Yoo (2000) recommends that the coefficient of "12" should be utilized in the denominator of Eq. (1-6) for the calculation of M_ℓ rather than the values "10" or "14" discussed in Section 2.1.8. Equation (1-6) is based on a coefficient of 12.

- full nonlinear analysis with zero initial imperfections and zero residual stresses (i.e., full nonlinear analysis of the "perfect" specimens),
- the current AASHTO LRFD (2001) shear strength equations, including tension-field action (Section 2.2.2),
- Lee and Yoo's shear strength equation (Lee and Yoo 1998) (Section 2.2.3), and
- the modified AASHTO LRFD shear strength equations (Section 2.2.4).

4.4.1 Single-Girder Test Results

4.4.1.1 Bending Tests

Tables 4.4.1 through 4.4.3 present comparison results for the single-girder bending tests. From Table 4.4.1, it can be observed that the full nonlinear finite element models yield predicted values for the flexural strengths that vary from 13 percent conservative to one percent unconservative relative to the experimental results. The most conservative finite element predictions correspond to tests L1-A and L2-A. These are the uniform vertical bending tests conducted by Mozer et al. (1971) (see Fig. 4.1.2). The closest correlations between the finite element analysis and the experimental strengths are obtained for the tests in which there is a moment gradient. For the Mozer et al. (1970) tests (Fig. 4.1.1), the largest difference between the finite element and experimental strengths is only three percent. The most liberal finite element prediction is obtained for the heat-curved specimen, C8-2. However, the prediction of the experimental strength to within one percent for this test is considered to be excellent, given the coarse approximations associated with idealized residual stresses for this type of girder. The finite element prediction differs from the experimental strength by only four percent for test L2-B (Fig. 4.1.3), whereas for test L2-C the finite element solution predicts nine percent less strength than obtained in the experiment.

From Table 4.4.1, it can be seen that the one-third rule equations yield predicted strengths in flexure that are from two to 20 percent conservative relative to the experimental values for the single-girder tests, when based on second-order elastic flange lateral bending stresses. The most liberal prediction (two percent conservative) is obtained for the heat-curved specimen, C8-2. These equations are less than seven percent conservative relative to the experimental strengths for the Mozer et al. (1970) tests (C8-2, C9-2, D13 and D14, Fig. 4.1.1), and they are somewhat more conservative (17 to 20 percent) for the Mozer et al. (1971) tests (L1-A, L2-A, L2-B and L2-C, Figs. 4.1.2 and 4.1.3). The one-third rule results are essentially unchanged for these tests when the design calculations are based on a first-order elastic analysis; the predictions become one to 19 percent conservative relative to the experimental results, rather than two to 20 percent). This of course is due to the fact that the second-order effects are small in these tests.

The Recommended Specification equations significantly underestimate the strengths of tests C8-2, C9-2, D13, and D14 (see Table 4.4.2)[2]. The predicted strengths are only 13 to 39 percent of the strengths observed in the experiments (i.e., the predictions are 61 to 87 percent conservative). This is due in part to the fact that the L_b/R values for these tests are well beyond the limit of 0.10 that McManus (1971) established in the development of his equations. It should be noted that Hall et al. (1999) assume that the loading apparatus in these tests (see Fig. 4.1.1) braces the beams at their mid-span in their checks of these design equations. As a result, the predictions that they report are somewhat better than those shown here, although they are still significantly conservative. It is apparent from Tables 4.4.1 and 4.4.3 that this assumption is not necessary to obtain reasonable design predictions for the flexural strengths.

For specimens L1-A, L2-A, L2-B and L2-C, the Recommended Specification equations underestimate the strength by 18% to 26%. Other than the fact that these specimens fall within the L_b/R limits specified by McManus (1971), the significantly better predictions for them are due in large part to the fact that they have compact flanges as per the Recommended Specifications. The first four specimens in Table 4.4.2 are classified as noncompact sections. As discussed in Section 2.1.2.7, the studies by Hall et al. (1999) indicate that McManus's (1971) noncompact section equations yield significantly conservative results for the majority of the tests that they considered.

The cross-section yield interaction equations proposed by Yoo (1996), with M_ℓ calculated by Eq. (1-6), significantly underestimate the vertical bending strength of tests C8-2, C9-2, D13 and D14 (see Table 4.4.3). This is because Eq. (1-6) is not an accurate predictor for these tests, due to the eccentricity of the applied loading. When M_ℓ is calculated directly from a first or second-order elastic design analysis of the tests, the results are much improved. This underscores the important issue that the analysis and the design resistance calculations should generally be kept separate. Lateral flange bending can occur due to numerous effects other than horizontal curvature. When based on an accurate calculation of M_ℓ (or f_ℓ), Yoo's yield interaction equations are nine to 19 percent conservative relative to the experimental strengths. Similar to the one-third rule predictions, the most liberal strength estimate is obtained for the heat-curved specimen, C8-2. As would be expected based on the assessment of the one-third rule equations with and without the consideration of second-order amplification (in Table 4.4.1), the results for Yoo's yield interaction equations change little when they are based on first-order versus geometric nonlinear analysis (for these tests). It should be noted that girders C8-2, C9-2, D13 and D14 are assumed to be noncompact for calculation of the values reported in Table 4.4.3.

---

[2] In this section, McManus's (1971) interpretation of $\bar{f}_w / f_b$ is utilized in the calculations via the Recommended Specification equations. That is $\bar{f}_w / f_b$ is obtained directly from the calculated first-order flange lateral and vertical bending stresses at the cross-frame locations. Section 4.6 considers the implications of the alternative interpretation in the Recommended Specifications (Hall and Yoo 1998). See Sections 2.1.2.6 and 2.1.2.7 for a discussion of the background to these interpretations.

Table 4.4.1. Maximum load results, 1/3 rule equations versus experiment (Mozer et al. 1970 and 1971) and full nonlinear analysis, single-girder tests.

Test	[a] Experiment kN	[b] Full nonlinear analysis kN ([b]/[a])	[c] 1/3 rule w/ 2nd-order elastic analysis kN ([c]/[a])	2nd-order f_ℓ and f_b at strength limit	[d] 1/3 rule w/ 1st-order f_b and f_ℓ kN ([d]/[a])	1st-order f_ℓ and f_b at strength limit
C8-2	332	336 (1.01)	327 (0.98)	f_ℓ/F_{yf}=0.287 f_b/F_{yf}=0.907	330 (0.99)	f_ℓ/F_{yf}=0.284 f_b/F_{yf}=0.906
C9-2	266	263 (0.99)	246 (0.93)	f_ℓ/F_{yf}=0.276 f_b/F_{yf}=0.908	247 (0.93)	f_ℓ/F_{yf}=0.289 f_b/F_{yf}=0.909
D13	303	295 (0.97)	290 (0.96)	f_ℓ/F_{yf}=0.258 f_b/F_{yf}=0.890	293 (0.96)	f_ℓ/F_{yf}=0.256 f_b/F_{yf}=0.890
D14	287	283 (0.99)	272 (0.95)	f_ℓ/F_{yf}=0.280 f_b/F_{yf}=0.891	274 (0.95)	f_ℓ/F_{yf}=0.276 f_b/F_{yf}=0.892
L1-A	136	119 (0.87)	113 (0.83)	f_ℓ/F_{yf}=0.398 f_b/F_{yf}=0.868	115 (0.84)	f_ℓ/F_{yf}=0.378 f_b/F_{yf}=0.876
L2-A	136	121 (0.89)	115 (0.85)	f_ℓ/F_{yf}=0.385 f_b/F_{yf}=0.870	116 (0.86)	f_ℓ/F_{yf}=0.365 f_b/F_{yf}=0.880
L2-B	272	261 (0.96)	230 (0.84)	f_ℓ/F_{yf}=0.325 f_b/F_{yf}=0.894	231 (0.85)	f_ℓ/F_{yf}=0.306 f_b/F_{yf}=0.899
L2-C	288	263 (0.91)	231 (0.80)	f_ℓ/F_{yf}=0.327 f_b/F_{yf}=0.894	232 (0.81)	f_ℓ/F_{yf}=0.307 f_b/F_{yf}=0.899

Table 4.4.2. Maximum load results, Recommended Specifications versus experiment (Mozer et al. 1970 and 1971) and full nonlinear analysis, single-girder tests.

Test	[a] Experiment kN	[b] Full nonlinear analysis kN ([b]/[a])	[e] Rec. Spec. w/ 1st-order f_b and f_ℓ kN ([e]/[a]) (1)	1st-order f_ℓ and f_b at strength limit
C8-2	332	336 (1.01)	128 (0.39)	f_ℓ/F_{yf} =0.128 f_b/F_{yf} =0.404
C9-2	266	263 (0.99)	34.7 (0.13)	f_ℓ/F_{yf} =0.038 f_b/F_{yf} =0.125
D13	303	295 (0.97)	52.9 (0.17)	f_ℓ/F_{yf} =0.047 f_b/F_{yf} =0.165
D14	287	283 (0.99)	51.2 (0.18)	f_ℓ/F_{yf} =0.050 f_b/F_{yf} =0.161
L1-A	136	119 (0.87)	109 (0.80)	f_ℓ/F_{yf} =0.358 f_b/F_{yf} =0.831
L2-A	136	121 (0.89)	111 (0.82)	f_ℓ/F_{yf} =0.348 f_b/F_{yf} =0.838
L2-B	272	261 (0.96)	213 (0.78)	f_ℓ/F_{yf} =0.280 f_b/F_{yf} =0.823
L2-C	288	263 (0.91)	214 (0.74)	f_ℓ/F_{yf} =0.281 f_b/F_{yf} =0.824

(1) McManus's (1971) interpretation of $\tilde{f}_w / f_b$ is utilized in the calculations reported here. That is, $\tilde{f}_w / f_b$ is obtained directly from the calculated first-order flange lateral and vertical bending stresses (f_ℓ and f_b) at the cross-frame locations.

Table 4.4.3. Maximum load results, Yoo (1996) yield interaction equations versus experiment (Mozer et al. 1970 and 1971) and full nonlinear analysis, single-girder tests.

Test	[a] Experiment kN	[b] Full nonlinear analysis kN ([b]/[a])	[f] Yoo w/ $M_\ell = \frac{ML_b^2}{12Rh}$ kN ([f]/[a])	Approx. f_ℓ and f_b at strength limit	[g] Yoo w/ 2nd-order M and M_ℓ kN ([g]/[a])	2nd-order f_ℓ and f_b at strength limit	[h] Yoo w/ 1st-order M and M_ℓ kN ([h]/[a])	1st-order f_ℓ and f_b at strength limit	$\frac{M_\ell = \frac{ML_b^2}{12Rh}}{1^{st}\text{Order } M_\ell}$
C8-2	332	336 (1.01)	173 (0.52)	$f_\ell/F_{yf} = 0.499$ $f_b/F_{yf} = 0.501$	301 (0.91)	$f_\ell/F_{yf} = 0.240$ $f_b/F_{yf} = 0.759$	303 (0.91)	$f_\ell/F_{yf} = 0.238$ $f_b/F_{yf} = 0.762$	5.99
C9-2	266	263 (0.99)	72.1 (0.27)	$f_\ell/F_{yf} = 0.745$ $f_b/F_{yf} = 0.255$	194 (0.73)	$f_\ell/F_{yf} = 0.240$ $f_b/F_{yf} = 0.759$	195 (0.73)	$f_\ell/F_{yf} = 0.232$ $f_b/F_{yf} = 0.767$	8.94
D13	303	295 (0.97)	105 (0.35)	$f_\ell/F_{yf} = 0.683$ $f_b/F_{yf} = 0.317$	246 (0.81)	$f_\ell/F_{yf} = 0.225$ $f_b/F_{yf} = 0.775$	250 (0.82)	$f_\ell/F_{yf} = 0.224$ $f_b/F_{yf} = 0.776$	8.20
D14	287	283 (0.99)	102 (0.36)	$f_\ell/F_{yf} = 0.688$ $f_b/F_{yf} = 0.312$	241 (0.84)	$f_\ell/F_{yf} = 0.238$ $f_b/F_{yf} = 0.762$	247 (0.86)	$f_\ell/F_{yf} = 0.237$ $f_b/F_{yf} = 0.763$	8.25
L1-A	136	119 (0.87)	101 (0.74)	$f_\ell/F_{yf} = 0.463$ $f_b/F_{yf} = 0.772$	107 (0.79)	$f_\ell/F_{yf} = 0.374$ $f_b/F_{yf} = 0.816$	107 (0.79)	$f_\ell/F_{yf} = 0.355$ $f_b/F_{yf} = 0.825$	1.30
L2-A	136	121 (0.89)	103 (0.76)	$f_\ell/F_{yf} = 0.452$ $f_b/F_{yf} = 0.778$	109 (0.80)	$f_\ell/F_{yf} = 0.364$ $f_b/F_{yf} = 0.821$	109 (0.80)	$f_\ell/F_{yf} = 0.345$ $f_b/F_{yf} = 0.830$	1.31
L2-B	272	261 (0.96)	179 (0.66)	$f_\ell/F_{yf} = 0.592$ $f_b/F_{yf} = 0.709$	218 (0.80)	$f_\ell/F_{yf} = 0.309$ $f_b/F_{yf} = 0.848$	219 (0.81)	$f_\ell/F_{yf} = 0.291$ $f_b/F_{yf} = 0.857$	2.03
L2-C	288	263 (0.91)	190 (0.66)	$f_\ell/F_{yf} = 0.592$ $f_b/F_{yf} = 0.709$	219 (0.76)	$f_\ell/F_{yf} = 0.310$ $f_b/F_{yf} = 0.847$	220 (0.76)	$f_\ell/F_{yf} = 0.292$ $f_b/F_{yf} = 0.856$	2.03

The last four specimens in Table 4.4.3 are taken as compact-flange sections for application of Yoo's yield interaction equations. It can be observed that Eq. (1-6) gives a reasonably accurate prediction of the maximum flange lateral bending moment in these tests, and therefore column (f) is only 24 to 34 percent conservative for these specimens. However, the predictions by the yield interaction equations are again improved such that they are 20 to 24 percent conservative when M_ℓ (or f_ℓ) is based on an accurate first- or second-order elastic analysis.

4.4.1.2 Shear Tests

Table 4.4.4 shows the results of the different predictions for the single-girder shear tests (specimens S1-0.10 and S1S-0.10). It can be seen that there are no significant differences in the FEA predictions for the models with and without initial imperfections and residual stresses. The maximum difference between the two models is three percent. Also, all the finite element predictions are within three percent of the experimental maximum loads.

The ratio of the predicted to the measured physical strength based on the current AASHTO LRFD (2001) equations (see Section 2.2.2) is only one percent conservative for specimen S1S-0.10 ($d_o/D = 1.5$). However, these equations significantly underestimate the maximum shear strength (i.e., they are 17 percent conservative) for specimen S1-0.10, which has a larger d_o/D of three. These results are consistent with the trends observed from Basler's tests (Basler 1961b; Gaylord 1963) and from Aydemir's (2000) finite element parametric studies in that the predictions are less conservative for smaller panel aspect ratios (see Section 2.2.2). Since the flanges in these tests are relatively large, to accommodate lateral bending due to the horizontal curvature, the AASHTO (2001) equations are conservative for both of the tests. As noted previously in Section 2.2.2, these equations can give slightly unconservative predictions for girders with small flanges, although based on the straight-girder studies by Aydemir (2000), it can be concluded that they are adequate for practical bridge girder proportions with $A_w/A_f \leq 2.4$.

Table 4.4.4. Maximum shear strength predictions (kN) by various design equations versus experiment (Zureick et al. 2001) and full nonlinear analysis, specimens S1-0.10 and S1S-0.10.

Test	[a] Experiment	[b] Full nonlinear analysis, "*imperfect*" girders ([b]/[a])	[c] Full nonlinear analysis, "*perfect*" girders ([b]/[a])	[d] Current AASHTO ([d]/[a])	[e] Lee and Yoo ([e]/[a])	[f] Modified AASHTO ([f]/[a])
S1-0.10	1180	1150 (0.97)	1180 (1.00)	983 (0.83)	1380 (1.17)	1190 (1.00)
S1S-0.10	1460	1440 (0.99)	1450 (0.99)	1440 (0.99)	1410 (0.97)	1570 (1.08)

Lee and Yoo's (1998) equations (see Section 2.2.3) show a significant increase in the shear buckling strength, from 752 kN (169 kips) to 867 kN (195 kips) (not shown in Table 4.4.4), due to adding the transverse stiffener at the middle of the critical segment in Specimen S1S-0.10. As a result, their equations predict a significantly smaller postbuckling strength for this specimen, although it has a smaller d_o/D. The net effect is that these equations predict approximately the same strength for both the "unstiffened" and the "stiffened" shear specimens (V_n = 1380 kN (311 kips) versus 1410 kN (317 kips)).

The predicted shear strength obtained from the modified AASHTO equations (see Section 2.2.4) is approximately equal to the physical strength for specimen S1-0.10. However, for specimen S1S-0.10, the modified AASHTO equations overestimate the strength of the test specimen by about eight percent. Nevertheless, these are the best overall predictions of the three design strength predictors considered here. This trend is representative of the results for the shear strength predictions obtained within the finite element parametric studies detailed in Chapter VIII.

4.4.2 Two-Girder System Results

Tables 4.4.5 through 4.4.7 summarize the results for the two-girder system tests. It can be observed from Table 4.4.5 that the finite element models yield predicted vertical bending strengths that vary from 7 to 11 percent conservative relative to the experimental results.

The strengths predicted by the one-third rule equations (Section 2.1.9.2) are from 12 to 18 percent conservative relative to the experimental values, when second-order elastic stresses are calculated in the design analysis (see Table 4.4.5). These predictions become 9 to 17 percent conservative when the first-order elastic stresses are used, as shown in the table. Therefore, similar to the single-girder experiments discussed in the previous sub-section, it appears that the second-order elastic stress amplification is again insignificant for these tests.

The Recommended Specification equations yield predictions that are 9 and 11 percent conservative for specimen GI-3 and GI-4, respectively (see Table 4.4.6). However, they are 32 and 18 percent conservative for GI-5 and GO-8. It appears that these differences in accuracy are due to the fact that the L_b/R for girders GI-5 and GO-8 is at the maximum limit of 0.10. It is expected that the over-prediction of the second-order elastic stresses implicit within McManus's (1971) flexural strength equations (see Section 2.1.2.6) is highest for larger subtended angles between the cross-frames. Therefore, even though all of these girders have a flange slenderness b_{fc}/t_{fc} within the limits considered as compact by the Recommended Specifications, for which McManus's equations give the best correlation with experimental results, the correlation with the experimental strengths is relatively poor for GI-5 and GO-8. The design strength prediction for GI-5 is particularly low due to the fact that it also has a larger L_b/b_f.

Table 4.4.5. Maximum total load results, 1/3 rule versus experiment (Mozer et al. 1973) and full nonlinear analysis, two-girder test systems.

Test	[a] Experiment kN	[b] Full nonlinear analysis kN ([b]/[a])	[c] 1/3 rule w/ 2nd-order elastic analysis kN ([c]/[a])	2nd-order f_ℓ and f_b at strength limit	[d] 1/3 rule w/ 1st-order f_b and f_ℓ kN ([d]/[a])	1st-order f_ℓ and f_b at strength limit
GI-3	206	193 (0.93)	178 (0.86)	f_ℓ/F_{yf}=0.214 f_b/F_{yf}=0.933	178 (0.86)	f_ℓ/F_{yf}=0.202 f_b/F_{yf}=0.930
GI-4	211	193 (0.92)	178 (0.84)	f_ℓ/F_{yf}=0.213 f_b/F_{yf}=0.933	179 (0.85)	f_ℓ/F_{yf}=0.201 f_b/F_{yf}=0.931
GI-5	121	108 (0.89)	99.1 (0.82)	f_ℓ/F_{yf}=0.434 f_b/F_{yf}=0.862	101 (0.83)	f_ℓ/F_{yf}=0.363 f_b/F_{yf}=0.877
GO-8	186	173 (0.93)	164 (0.88)	f_ℓ/F_{yf}=0.345 f_b/F_{yf}=0.880	169 (0.91)	f_ℓ/F_{yf}=0.292 f_b/F_{yf}=0.905

Table 4.4.6. Maximum load results, Recommended Specifications versus experiment (Mozer et al. 1973) and full nonlinear analysis, two-girder test system.

Test	[a] Experiment kN	[b] Full nonlinear analysis kN ([b]/[a])	[e] Rec. Spec. w/ 1st-order f_b and f_ℓ kN ([e]/[a])[1]	1st-order f_ℓ and f_b at strength limit
GI-3	206	193 (0.93)	188 (0.91)	f_ℓ/F_{yf}=0.213 f_b/F_{yf}=0.982
GI-4	211	193 (0.92)	188 (0.89)	f_ℓ/F_{yf}=0.212 f_b/F_{yf}=0.980
GI-5	121	108 (0.89)	81.8 (0.68)	f_ℓ/F_{yf}=0.276 f_b/F_{yf}=0.667
GO-8	186	173 (0.93)	153 (0.82)	f_ℓ/F_{yf}=0.254 f_b/F_{yf}=0.787

[1] McManus's (1971) interpretation of $\bar{f}_w / f_b$ is utilized in the calculations reported here. That is $\bar{f}_w / f_b$ is obtained directly from the calculated first-order flange lateral and vertical bending stresses (f_ℓ and f_b) at the cross-frame locations.

Table 4.4.7. Maximum load results, Yoo's (1996) yield interaction equations versus experiment (Mozer et al. 1973) and full nonlinear analysis, two-girder test system.

Test	[a] Experiment kN	[b] Full nonlinear analysis kN ([b]/[a])	[f] Yoo w/ $M_\ell = \frac{ML_b^2}{12Rh}$ kN ([f]/[a])	Approx. f_ℓ and f_b at strength limit	[g] Yoo w/ 2nd-order M and M_ℓ kN ([g]/[a])	2nd-order f_ℓ and f_b at strength limit	[h] Yoo w/ 1st-order M and M_ℓ kN ([h]/[a])	1st-order f_ℓ and f_b at strength limit	$\frac{M_\ell = \frac{ML_b^2}{12Rh}}{1^{st}\text{Order } M_\ell}$
GI-3	206	193 (0.93)	165 (0.80)	$f_\ell/F_{yf}=0.208$ $f_b/F_{yf}=0.898$	171 (0.83)	$f_\ell/F_{yf}=0.206$ $f_b/F_{yf}=0.899$	173 (0.84)	$f_\ell/F_{yf}=0.196$ $f_b/F_{yf}=0.904$	1.06
GI-4	211	193 (0.92)	166 (0.79)	$f_\ell/F_{yf}=0.208$ $f_b/F_{yf}=0.898$	171 (0.81)	$f_\ell/F_{yf}=0.205$ $f_b/F_{yf}=0.899$	173 (0.82)	$f_\ell/F_{yf}=0.195$ $f_b/F_{yf}=0.904$	1.07
GI-5	121	108 (0.89)	79.6 (0.66)	$f_\ell/F_{yf}=0.636$ $f_b/F_{yf}=0.687$	90.7 (0.75)	$f_\ell/F_{yf}=0.404$ $f_b/F_{yf}=0.801$	91.2 (0.75)	$f_\ell/F_{yf}=0.343$ $f_b/F_{yf}=0.831$	1.85
GO-8	186	173 (0.93)	136 (0.73)	$f_\ell/F_{yf}=0.559$ $f_b/F_{yf}=0.725$	155 (0.83)	$f_\ell/F_{yf}=0.328$ $f_b/F_{yf}=0.838$	160 (0.86)	$f_\ell/F_{yf}=0.281$ $f_b/F_{yf}=0.862$	1.99

Yoo's (1996) cross-section yield interaction equations yield 20 to 34 percent conservative predictions relative to the experimental strengths when the lateral flange moments M_ℓ are calculated based on Eq. (1-6) (see Table 4.4.7). They yield 19 to 25 percent conservative predictions when M_ℓ (or f_ℓ) is calculated based on a direct second-order elastic analysis (18 to 25 percent conservative results when based on the moments or stresses from a first-order elastic design analysis). All the specimens listed in Table 4.4.7 are considered as compact-flange sections for application of the yield interaction formulas. It appears that the conservative nature of the above predictions is due to the definition of the maximum strength within these equations as the point at which the web first yields. As discussed previously in Section 2.1.8.3, it is expected that girders with noncompact and slender webs can develop strengths in excess of that associated with first yielding of the web. The flanges are the dominant contributor to the flexural strength. This is recognized within the current straight-girder provisions for straight hybrid I girders (AASHTO 2001).

4.4.3 Three-Girder System Results

4.4.3.1 Full Nonlinear Analysis Predictions

Comparison results for the three-girder system tests are shown in Tables 4.4.8 to 4.4.10. All of the full nonlinear analysis results reported in these tables include the estimated effects of initial geometric imperfections and residual stresses due to flame cutting and welding. It can be seen that the full nonlinear solutions yield predictions for the maximum total load (summed from the six equal loads applied to the bridge) that are only five percent conservative to one percent unconservative relative to the experimental results for tests B1 through B4 (see Table 4.4.8). These specimens all have flange slenderness values b_{fc}/t_{fc} of approximately 23. As a result, their maximum flexural strength is expected to be influenced significantly by flange inelastic local buckling.

The maximum load obtained in the finite element analysis of Specimen B7, which has the highly slender compression flange, is only four percent higher than the corresponding load in the experiment. As discussed later in Section 4.7, these strengths are associated only with a local limit point in the response, both in the experiment and in the finite element analysis. In this test, the total load drops a small amount after this limit load is reached, but subsequently the system continues to support increasing loads (although with relatively large vertical displacements). Both the experimental test as well as the finite element analysis are stopped at large vertical displacements in the component specimen, prior to reaching a second limit load. This is an important indicator of the potential for inelastic redistribution and reserve capacity even when the flanges of a critical girder are highly noncompact. Nevertheless, the three-girder system in these tests was designed such that it would not be damaged prior to the failure of the test components. That is, the girders and cross-frames of this system are heavier, relative to the component specimens, than would exist in an actual bridge. Therefore, it would be dangerous to infer from these results that large inelastic redistribution capacities would necessarily exist in an actual curved bridge. For these reasons, the total load at the first local limit point is taken as the maximum load in test B7.

Table 4.4.8. Maximum total load results, 1/3 rule versus experiment (Zureick and Kim 2000; Hartmann 2000) and full nonlinear analysis, three-girder test system.

Test $[2D_o/t_w, b_f/t_f, d_o/D]$	[a] Experiment kN	[b] Full nonlinear analysis[(1)] kN ([b]/[a])	[c] 1/3 rule w/ 2nd-order elastic analysis kN ([c]/[a])	2nd-order f_ℓ and f_b at strength limit	[d] 1/3 rule w/ 1st-order f_b and f_ℓ kN ([d]/[a])	1st-order f_ℓ and f_b at strength limit
B1 [149,23,1]	1350	1370 (1.01)	1240 (0.91)	f_ℓ/F_{yfc}=0.330 f_b/F_{yfc}=0.745	1290 (0.94)	f_ℓ/F_{yfc}=0.303 f_b/F_{yfc}=0.754
B2 [121,23,1]	1430	1400 (0.98)	1300 (0.91)	f_ℓ/F_{yfc}=0.340 f_b/F_{yfc}=0.758	1350 (0.94)	f_ℓ/F_{yfc}=0.317 f_b/F_{yfc}=0.764
B3 [120,23,4]	1500	1520 (1.01)	1290 (0.86)	f_ℓ/F_{yfc}=0.357 f_b/F_{yfc}=0.755	1340 (0.89)	f_ℓ/F_{yfc}=0.326 f_b/F_{yfc}=0.763
B4 [188,23,1]	1360	1290 (0.95)	1100 (0.81)	f_ℓ/F_{yfc}=0.384 f_b/F_{yfc}=0.726	1170 (0.86)	f_ℓ/F_{yfc}=0.315 f_b/F_{yfc}=0.736
B5 [144,17,1]	1830	1580 (0.86)	1550 (0.84)	f_ℓ/F_{yfc}=0.373 f_b/F_{yfc}=0.867	1600 (0.87)	f_ℓ/F_{yfc}=0.360 f_b/F_{yfc}=0.868
B6 [143,13,1]	2170	1890 (0.87)	1810 (0.83)	f_ℓ/F_{yfc}=0.378 f_b/F_{yfc}=0.876	1950 (0.90)	f_ℓ/F_{yfc}=0.370 f_b/F_{yfc}=0.873
B7 [149,33,1]	1130	1170 (1.04)	721 (0.64)	f_ℓ/F_{yfc}=0.223 f_b/F_{yfc}=0.498	730 (0.65)	f_ℓ/F_{yfc}=0.216 f_b/F_{yfc}=0.501

(1) Initial geometric imperfections and residual stresses included in the analysis.

Table 4.4.9. Maximum total load results, Recommended Specifications versus experiment (Zureick and Kim 2000; Hartmann 2000) and full nonlinear analysis, three-girder test system.

Test [D/t_w, b_f/t_f, d_c/D]	[a] Experiment kN	[b] Full nonlinear analysis[1] kN ([b]/[a])	[e] Rec. Spec. w/ 1st-order f_b and f_ℓ kN ([e]/[a])	1st-order f_ℓ and f_b at strength limit
B1 [148,23,1]	1350	1370 (1.01)	778 (0.58)	f_ℓ/F_{yfc}=0.205 f_b/F_{yfc}=0.541
B2 [120,23,1]	1430	1400 (0.98)	801 (0.56)	f_ℓ/F_{yfc}=0.212 f_b/F_{yfc}=0.538
B3 [119,23,4]	1500	1520 (1.01)	796 (0.53)	f_ℓ/F_{yfc}=0.219 f_b/F_{yfc}=0.533
B4 [188,23,1]	1360	1290 (0.95)	730 (0.54)	f_ℓ/F_{yfc}=0.225 f_b/F_{yfc}=0.526
B5 [144,17,1]	1830	1580 (0.86)	1610 (0.88)	f_ℓ/F_{yfc}=0.338 f_b/F_{yfc}=0.882
B6 [142,13,1]	2170	1890 (0.87)	1950 (0.90)	f_ℓ/F_{yfc}=0.334 f_b/F_{yfc}=0.878
B7 [149,33,1]	1130	1170 (1.04)	747 (0.66)	f_ℓ/F_{yfc}=0.198 f_b/F_{yfc}=0.583

[1] Initial geometric imperfections and residual stresses included in the analysis.

Table 4.4.10. Maximum total load results, Yoo's (1996) yield interaction equations versus experiment (Zureick and Kim 2000; Hartmann 2000) and full nonlinear analysis, three-girder test system.

Test [D/t_w, b_f/t_f, d_o/D]	[a] Experiment kN	[b] Full nonlinear analysis[(1)] kN ([b]/[a])	[f] Yoo w/ $M_\ell = \frac{ML_b^2}{12Rh}$ kN ([f]/[a])	Approx. f_ℓ and f_b at strength limit	[g] Yoo w/ 2nd-order M and M_ℓ kN ([g]/[a])	2nd-order f_ℓ and f_b at strength limit	[h] Yoo w/ 1st-order M and M_ℓ kN ([h]/[a])	1st-order f_ℓ and f_b at strength limit	$M_\ell = \frac{ML_b^2}{12Rh}$ / 1st Order M_ℓ
B1 [148,23,1]	1350	1370 (1.01)	1100 (0.81)	$f_\ell/F_{yfc} = 0.309$ $f_b/F_{yfc} = 0.709$	1070 (0.79)	$f_\ell/F_{yfc} = 0.303$ $f_b/F_{yfc} = 0.694$	1170 (0.86)	$f_\ell/F_{yfc} = 0.276$ $f_b/F_{yfc} = 0.726$	1.12
B2 [120,23,1]	1430	1400 (0.98)	1120 (0.78)	$f_\ell/F_{yfc} = 0.317$ $f_b/F_{yfc} = 0.700$	1100 (0.77)	$f_\ell/F_{yfc} = 0.304$ $f_b/F_{yfc} = 0.690$	1200 (0.84)	$f_\ell/F_{yfc} = 0.283$ $f_b/F_{yfc} = 0.720$	1.12
B3 [119,23,4]	1500	1520 (1.01)	1130 (0.75)	$f_\ell/F_{yfc} = 0.317$ $f_b/F_{yfc} = 0.701$	1100 (0.73)	$f_\ell/F_{yfc} = 0.319$ $f_b/F_{yfc} = 0.686$	1180 (0.79)	$f_\ell/F_{yfc} = 0.292$ $f_b/F_{yfc} = 0.711$	1.08
B4 [188,23,1]	1360	1290 (0.95)	974 (0.72)	$f_\ell/F_{yfc} = 0.309$ $f_b/F_{yfc} = 0.661$	1040 (0.76)	$f_\ell/F_{yfc} = 0.362$ $f_b/F_{yfc} = 0.693$	1094 (0.81)	$f_\ell/F_{yfc} = 0.300$ $f_b/F_{yfc} = 0.702$	1.03
B5 [144,17,1]	1830	1580 (0.86)	1450 (0.79)	$f_\ell/F_{yfc} = 0.187$ $f_b/F_{yfc} = 0.834$	1450 (0.79)	$f_\ell/F_{yfc} = 0.352$ $f_b/F_{yfc} = 0.827$	1520 (0.83)	$f_\ell/F_{yfc} = 0.323$ $f_b/F_{yfc} = 0.843$	1.18
B6 [142,13,1]	2170	1890 (0.87)	1780 (0.82)	$f_\ell/F_{yfc} = 0.186$ $f_b/F_{yfc} = 0.843$	1800 (0.83)	$f_\ell/F_{yfc} = 0.334$ $f_b/F_{yfc} = 0.835$	1860 (0.86)	$f_\ell/F_{yfc} = 0.320$ $f_b/F_{yfc} = 0.842$	1.18
B7 [149,33,1]	1130	1170 (1.04)	1100 (0.98)	$f_\ell/F_{yfc} = 0.269$ $f_b/F_{yfc} = 0.738$	1040 (0.92)	$f_\ell/F_{yfc} = 0.299$ $f_b/F_{yfc} = 0.706$	1160 (1.03)	$f_\ell/F_{yfc} = 0.254$ $f_b/F_{yfc} = 0.746$	1.06

(1) Initial geometric imperfections and residual stresses included in the analysis.

The full nonlinear analyses yield more conservative predictions (13 to 14 percent conservative) relative to the experimental maximum total load for tests B5 and B6. The component specimens in these tests have flange slenderness ratios b_{fc}/t_{fc} of 17 and 13 respectively. This result matches with the trends observed from the analyses reported in the previous two sub-sections. In all of the cases studied, the full-nonlinear analyses tend to give more conservative predictions relative to the experimental strengths for girders that have stocky flanges, whereas for the girders that have noncompact flanges (specimens C8-2, C9-2, D13 and D14 tested by Mozer et al. (1970) as well as tests B1 to B4 and B7 above), the finite element and experimental strengths are a closer match. As noted previously in Section 4.4.1, the existence of a moment gradient may also have some influence on the correlation between the physical and numerical strength values. Based on a comparison between the experimental and numerical results for tests L1-A and L2-A versus those for L2-B and L2-C, there is a mild indication that the finite element predictions are better for the tests with moment gradient (L2-B and L2-C) (see Table 4.4.1).

It is important to realize that the prediction of the actual specimen maximum vertical bending moment may be masked somewhat by various system effects, when the strength results are presented in terms of the total maximum load. However, the reduction of the experimental data to determine the maximum internal moments in the component specimens is only reported by Zureick and Kim (2000) at the present time, and is considered to be preliminary. Nevertheless, these results indicate that for B5 and B6, the maximum internal moments in the test specimens occur at the same time that the maximum total load is achieved on the complete bridge system.

The maximum values of M/M_y in these specimens, reduced from the experimental data as well as from the full nonlinear finite element analyses, are reported in Table 4.4.11. It can be observed that the M_{max}/M_y values reduced from the experimental data, including dead load effects, are nearly equal to one. Also, the M_{max}/M_y values computed from the full nonlinear analyses are significantly smaller than the corresponding experimental values; the ratio of the maximum moment determined by the analysis to that calculated from the experimental data is 0.72 for B5 and 0.76 for B6, when dead load effects are included in the experimental estimates (see column (c) of Table 4.4.11). The corresponding ratios between the predicted and the measured maximum total applied load on the bridge are 0.86 and 0.87 (see column (b) of Table 4.4.8). Conversely, the ratio of the maximum moment determined by the analysis to that calculated from the experimental data, excluding dead load effects, is 0.96 for both of these specimens (column (c) of Table 4.4.1). The ratio of the predicted total maximum load from the finite element analyses to that measured in these two tests is bracketed by the ratio of the maximum internal moments obtained with the dead load effects included and excluded. The authors believe that no conclusions should be drawn from this information until further detailed interrogation of the experimental data is conducted.

Table 4.4.11. Maximum internal vertical bending moments in specimens B5 and B6, reduced from the experimental (Zureick and Kim 2000) and the full nonlinear finite element data (initial geometric imperfections and residual stresses included).

Test	M_y (kN-m)	[a] M_{max}/M_y experiment, including dead load effects	[b] M_{max}/M_y experiment, excluding dead load effects	[c] M_{max}/M_y Full Nonlinear Analysis ([c]/[a]){[c]/[b]}
B5	5682	0.96	0.72	0.69 (0.72){0.96}
B6	6774	0.96	0.76	0.73 (0.76){0.96}

The calculation of the maximum moments M_{max} in Table 4.4.11 is conducted as follows. Based on the total load applied to the bridge system, including dead weight, the total internal moment about the horizontal axis for the entire bridge cross-section at the mid-span (Girders G1 and G2, and the component specimen) is determined statically. Next, the internal moment at the mid-span of Girders G1 and G2 is calculated based on their corresponding maximum elastic vertical bending stresses f_b, computed from the stresses at the extreme fibers of the flanges in the finite element models as detailed in Section 3.6, and determined from the measured flange strains in the experiment. Lastly, the moment in the component specimen is estimated by subtracting the moments in Girders G1 and G2 from the total internal moment evaluated in the first step. The influence of the bridge displacements and rotations on the internal moments is assumed to be negligible in these calculations.

Additional full nonlinear finite element predictions for the three-girder system tests, assuming "perfect" horizontally curved specimens, are reviewed subsequently and compared to the results discussed above. However, the predictions from the key flexural design equations are evaluated next, prior to considering these results.

4.4.3.2 Design Equation Predictions

The proposed one-third rule equations yield results that are from nine to 19 percent conservative relative to the experimental maximum total load capacity in tests B1 through B6, when based on second-order elastic stresses from the design analysis (see Table 4.4.8). These predictions become six to 14 percent conservative when the stresses f_ℓ and f_b are calculated based on a first-order elastic analysis. Therefore, it can be concluded once again that the effect of second-order elastic amplification of the stresses is quite minor for the girder geometries tested. The best predictions are obtained for girders B1 and B2, which have noncompact flanges ($b_f/t_f \cong 23$) and close transverse stiffener

spacing ($d_o/D = 1$). Otherwise, there are no discernable trends in the accuracy of the one-third rule equations for tests B1 through B6.

The one-third rule equations are 36 percent conservative relative to the experimental maximum load capacity for test B7. It is believed that this indicates that the base proposed modified AASHTO flange local buckling provisions (see Section 2.1.1.2 and Figs. 2.1.1 and 2.1.2) are conservative for a girder with a highly noncompact flange such as the one considered in this test. It is likely that at the strength limit, significant elastic unloading may be occurring on one side of the compression flange (the portion of the compression flange on the side away from the center of curvature in the case of a horizontally-curved girder) such that substantial restraint is provided to the other side along the line of the web-flange juncture. The assumed flange buckling coefficient k_c for Specimen B7 is 0.33 (see Eq. 2-7). Since this value is smaller than $k_c = 0.425$, corresponding to simply-supported boundary conditions along the web-flange juncture, the calculated design flange local buckling strength is based on the assumption of negative restraint, i.e., it is based on the assumption that the slender web in this test ($2D_c/t_w = 148$) is destabilizing the compression flange.

The Recommended Specification equations are again significantly conservative (36 to 47 percent) relative to the experimental strengths for the specimens that they classify as noncompact, i.e., for specimens B1 through B4 and B7 (see Table 4.4.9). As noted previously, this is due to the assumption that the girder strength is limited to first yield and due to the significant overestimation of the second-order elastic stresses implicit within these equations. The Recommended Specification equations give much better predictions for the compact-flange specimens B5 and B6 (10 and 12 percent conservative respectively).

Yoo's (1996) cross-section yield interaction equations are from two to 28 percent conservative for all the three-girder system tests in which the specimens are classified as noncompact (B1 through B4 and B7), when based on the approximate V-load equation (Eq. 1-6) (see Table 4.4.10). As can be observed from the last column of this table, the V-load equation provides a reasonably accurate estimate of the finite element based first-order elastic lateral flange bending moments for the three-girder system tests. Therefore, the results with these equations are only slightly improved when based on the direct design analysis (21 percent conservative to three percent unconservative relative to the experimental strengths, when based on a first-order elastic analysis). It is apparent that the first-yield limit is probably too restrictive for tests B1 through B4. Also, the fact that distributed plasticity effects are neglected in Yoo's first-yield equations, along with the fact that second-order effects are neglected in the first-order analysis, contributes to the slightly liberal estimate of the maximum total load capacity for test B7 in column (h) of the table (three percent unconservative).

The values for girders B5 and B6 in Table 4.4.10 are calculated based on Yoo's (1996) compact-flange yield interaction equations. As observed previously, the implicit limit of the maximum strength based on first yielding of the web in these equations appears to be too restrictive. The maximum total load capacity is limited to only 79 and

83 percent of the experimentally determined strength for these tests respectively (31 and 27 percent conservative).

4.4.3.3 Assessment of the Influence of Geometric Imperfections and Residual Stresses

The maximum applied loads attained in the three-girder system tests as well as the single-girder shear tests conducted under the FHWA Curved Steel Bridge Research Project are compared to the results predicted by the full nonlinear finite element models with and without residual stresses and geometric imperfections in Table 4.4.12. It can be observed that the combined effect of the residual stresses and geometric imperfections is a maximum of only three percent for the shear tests (specimens S1-0.10 and S1S-0.10). Also, their effect is relatively minor (a maximum of four percent) for the bending specimens B5 and B6, which have compact flanges. However, the influence of the specified geometric imperfections and residual stresses is significant for the other bending tests, with the exception of B3. This is expected, since the flanges in these tests are noncompact, i.e., their maximum strengths are limited by inelastic local buckling. It is well documented in the literature that inelastic buckling strengths are generally significantly influenced by the above attributes. The maximum predicted strength reductions due to the modeled residual stresses and geometric imperfections occur for specimen B4 (the unsymmetric girder) and for B7 (the highly noncompact specimen). The reduction in both of these tests is 12 percent.

Specimen B3 has a noncompact flange, and is of the same proportions as B2; however the intermediate transverse stiffeners are removed. It is possible that this may have had an effect on the lack of sensitivity to residual stresses and geometric imperfections in the finite element model (note that the finite element based strength only changes from 1.02 to 1.01 of the experimentally-determined strength when residual stresses and geometric imperfections are included), but the authors do not have a clear explanation for this behavior. It is intriguing that the maximum strength of B3 is larger than that of B2 both in the experimental test, and in the finite element analysis when residual stresses and geometric imperfections are included. However, the finite element analyses without imperfections and residual stresses predict a slight decrease in the capacity of B3 relative to B2.

From Table 4.4.12, it can be observed that the full nonlinear finite element predictions of the maximum total applied load range from 13 percent conservative to four percent unconservative relative to the experimental values, when initial geometric imperfection and residual stress effects are included in the analysis, versus 11 percent conservative to 16 percent unconservative when initial geometric imperfections and residual stresses are not included. Based on these results and the prior discussions, it can be concluded that the best and most reliable full-nonlinear predictions are obtained for the flexural strengths when residual stresses and geometric imperfections are included in the analysis. However, for the evaluation of shear strengths, the predictions are actually slightly improved relative to the experimental test results by neglecting these effects. The finite element models tend to under predict the experimental flexural strengths for the

compact flange girders B5 and B6. The behavior associated with these predictions is discussed further in Section 4.7.

Table 4.4.12. The maximum applied load attained in the physical tests and the predicted values obtained from finite element models with and without residual stresses and geometric imperfections.

Test	[a] Experiment kN	[b] Full nonlinear Analysis w/ residual stresses and geometric imperfections kN ([b]/[a])	[c] Full nonlinear Analysis w/o residual stresses and geometric imperfections kN ([c]/[a])
S1-0.10	1770	1720 (0.97)	1770 (1.00)
S1S-0.10	2190	2160 (0.99)	2180 (0.99)
B1	1350	1370 (1.01)	1490 (1.10)
B2	1430	1400 (0.98)	1550 (1.08)
B3	1500	1520 (1.01)	1530 (1.02)
B4	1360	1290 (0.95)	1460 (1.07)
B5	1830	1580 (0.86)	1650 (0.90)
B6	2170	1890 (0.87)	1940 (0.89)
B7	1130	1170 (1.04)	1300 (1.16)

4.5 EXAMPLE DESIGN CALCULATIONS

This section presents example design calculations for specimen B1 of the three-girder system tests and S1-0.10 of the single-girder shear tests. The design calculations for the proposed one-third rule equations, the flexural strength equations of the Recommended Specifications (Hall and Yoo 1998), and Yoo's (1996) cross-section yield interaction equations are shown for test B1. The one-third rule equations and the yield interaction equations are evaluated using the results from a second-order elastic design analysis, and the Recommended Specification equations are used with first-order elastic design analysis results. Furthermore, the calculations using the current AASHTO LRFD (2001) shear strength equations, the Lee and Yoo (1998) equations, and the modified AASHTO LRFD shear strength equations are shown for test specimen S1-0.10. These examples illustrate how the numerical values reported in Tables 4.4.1 through 4.4.10 are obtained. The corresponding equation numbers from Chapter II are shown for each of the calculation steps.

4.5.3 Flexural Strength Calculations for Specimen B1

The geometric and material properties utilized in the calculation of the flexural resistances are as follows[3]:

F_{yfc} = 406 MPa (58.9 ksi), E = 200,000 MPa (29000 ksi)

$F_L = F_{yfc} - F_{rs} = 406 - 114 = 292$ MPa (42.4 ksi)

b_{fc} = 445 mm (17.5 in), t_{fc} = 19.5 mm (0.768 in)

$D = 2D_c$ = 1219 mm (48 in), t_w = 8.20 mm (0.323 in)

L_b = 4572 mm (15 ft)

4.5.1.1 <u>One-Third Rule Equations</u>

a) Flange local buckling

$$\lambda = b_{fc}/2t_{fc} = 11.39 \quad (2\text{-}4)$$

$$\lambda_p = 0.382\sqrt{\frac{E}{F_{yc}}} = 8.48 \quad (2\text{-}5)$$

$$\lambda_r = 1.90\sqrt{\frac{E}{F_L\sqrt{\frac{2D_c}{t_w}}}} = 14.23 \quad (2\text{-}6)$$

$\lambda_p < \lambda < \lambda_r$

b) Lateral-torsional buckling

$$a_r = (2D_c t_w)/(b_{fc}t_{fc}) = 1.154 \quad (2\text{-}22)$$

$$r_t = \frac{b_f}{\sqrt{12\left(1+\frac{a_r}{6}\right)}} = 4.626 \quad (2\text{-}21)$$

$$\lambda = L_b/r_t = 38.91 \quad (2\text{-}13)$$

[3] The design strength equations in this chapter are all evaluated using E = 200,000 MPa (29000 ksi) rather than the values for E reported in Section 4.4, which are utilized in the full nonlinear and second-order elastic analyses. The maximum effect on the computed design resistances is approximately one percent.

$$\lambda_p = 1.76\sqrt{\frac{E}{F_{yc}}} = 39.05 \quad (2\text{-}14)$$

$$\lambda_r = 3.14\sqrt{\frac{E}{F_L}} = 82.11 \quad (2\text{-}24b)$$

$$\lambda < \lambda_p$$

Therefore, the vertical bending strength of specimen B1 is controlled by inelastic buckling of the compression flange.

c) Calculation of flexural capacity

$$\frac{f_b}{R_b R_h} \le \left\{ F_n = C_b\left[1 - \frac{(F_{yc} - F_L)}{F_{yc}}\left(\frac{\lambda - \lambda_p}{\lambda_r - \lambda_p}\right)\right] F_{yc} - \frac{1}{3} f_\ell \le F_{yc} - \frac{1}{3} f_\ell \right\} \quad (2\text{-}90b)$$

R_h = 1.0 (homogeneous girder)

C_b = 1.0 (uniform vertical bending)

$$R_b = 1 - \frac{a_r}{1200 + 300a_r}\left(\frac{2D_c}{t_w} - 5.76\sqrt{\frac{E}{f_{bc}}}\right) \le 1.0 \text{ (from AASHTO LRFD (2001))}$$

$$= 0.984 \quad (f_{bc} \text{ is conservatively assumed to be equal to } F_{yc}) \quad (4\text{-}1)$$

The one-third rule represents the interaction between the lateral and vertical bending strength through the term "$- f_\ell/3$." Therefore, the flexural capacity prediction of the one-third rule depends on the value of f_ℓ computed in the elastic design analysis. In general within this work, in order to find the load level that corresponds to the satisfaction of the second-order elastic stress based design resistance formulas, the loads in the test are incremented by a small fraction (less than one percent) of the maximum expected capacity, and the vertical bending resistance is checked against the applied vertical bending stress. At a load level of 1237 kN (278 kips), the maximum flange stresses obtained from the second-order elastic design analysis of the bridge system are $f_{b(analysis)}$ = 302.5 MPa (43.88 ksi) and $f_\ell = f_{\ell(analysis)}$ = 134.1 MPa (19.45 ksi). Upon substitution of the above values into Eq. (2-90b), we obtain

$$F_n = 1.0\left[1 - \frac{(406 - 292)}{406}\left(\frac{11.39 - 8.48}{14.23 - 8.48}\right)\right]406 - \frac{1}{3}134.1 = 303.8 \text{ MPa (44.07 ksi)}$$

Although $f_{b(analysis)}$ and $f_{\ell(analysis)}$ are obtained from a second-order elastic analysis, geometric imperfections and residual stresses are not included within this analysis. The second-order analysis theoretically accounts for web bend buckling, but the shedding of web stresses to the flanges may not be as large as might occur for a physical girder that contains the nominal initial geometric imperfections and residual stresses. Therefore, the load shedding factor R_b is applied with the second-order elastic analysis stresses. If both sides of Eq. (2-90b) are multiplied by R_b, we obtain

$$\left[f_{b(analysis)} = 302.5 \text{ MPa}\right] \cong \left[R_b F_n = (0.984)(303.8) = 298.7 \text{ MPa}\right]$$

Since these values are equal to within one percent, the corresponding load level of 1237 kN (278 kips) is accepted as the one-third rule prediction. This value is reported in column (c) of Table 4.4.8.

4.5.1.2 Recommended Specification Equations (Hall and Yoo 1998)

a) Flange compactness

$$18 < \left(b_{fc} / t_{fc} = 22.8\right) \cong \left\{\left(1.02\sqrt{\frac{E}{(f_b + f_\ell)}} \le 23\right) = 22.6\right\} \qquad (2\text{-}47a)$$

based on the assumption that $f_b + f_\ell = F_{yc}$. Therefore, the flange is noncompact.

b) Calculation of flexural capacity

At a load level of 778 kN (175 kips), $f_{b(analysis)} = 219.9$ MPa (31.89 ksi) and $f_{\ell(analysis)} = +83.29$ MPa (+12.08 ksi). Therefore

$$\rho_b = \frac{1}{1 + \frac{L_b}{R}\frac{L_b}{b_{fc}}} = 0.575 \qquad (2\text{-}37)$$

$$\rho_w = \min\left(\frac{1}{1 - \frac{\bar{f}_w}{\bar{f}_b}\left(1 - \frac{L_b}{75 b_f}\right)}, \frac{0.95 + \frac{\frac{L_b}{b_f}}{30 + 8000\left(0.1 - \frac{L_b}{R}\right)^2}}{1 + 0.6\frac{\bar{f}_w}{\bar{f}_b}}\right) \qquad (2\text{-}38a)$$

$$= \min(1.486, 1.005)$$

$$= 1.005$$

$$F_{bs} = F_{yfc}\left[1 - 3\left(\frac{L_b}{b_f}\right)^2 \frac{F_{yfc}}{\pi^2 E}\right] = 379.6 \text{ MPa } (55.06 \text{ ksi})$$

$$F_{cr1} = F_{bs}\rho_b\rho_w = 219.4 \text{ MPa } (31.82 \text{ ksi}) \quad (2\text{-}36)$$

$$F_{cr2} = F_{yfc} - |\bar{f}_w| = 322.9 \text{ MPa } (46.83 \text{ ksi}) \quad (2\text{-}39)$$

The flange vertical bending strength is taken as the minimum value from these two equations. As a result, we have

$$[f_{b(analysis)} = 219.9 \text{ MPa }] \cong [F_n = 219.4 \text{ MPa }]$$

Since these values are equal to within one percent, the corresponding load level of 778 kN (175 kips) is accepted as the Recommended Specification equation prediction. This value is reported in column (e) of Table 4.4.9. It should be noted that although the Recommended Specification flexure equations are based on the stresses from a linear analysis, the reduction coefficient ρ_w is nonlinear in the applied stresses; therefore, the applied loads are increased by small increments until the design equations are satisfied.

4.5.1.3 Yoo's (1996) Cross-Section Yield Interaction Equations

a) Flange compactness

$$(\lambda = b_{fc}/2t_{fc} = 11.39) > \left(\lambda_p = 0.382\sqrt{\frac{E}{F_{yc}}} = 8.48\right) \quad (2\text{-}4)$$

Therefore, the section is classified as noncompact.

b) Calculation of flexural capacity

At a load level of 1068 kN (240 kips), $f_{b(analysis)} = 282.0$ MPa (40.90 ksi) and $f_{\ell(analysis)} = 122.9$ MPa (17.82 ksi). Therefore

$$x = \left(1 - \frac{f_\ell}{F_{yc}}\right) = 0.6975 \quad (2\text{-}81c)$$

and

$$F_n = x\, F_{yc} = 283.2 \text{ MPa (41.08 ksi)} \qquad (2\text{-}82b)$$

As a result, we have

$$[f_{b(analysis)} = 282.0 \text{ MPa}] \cong [F_n = 283.2 \text{ MPa}]$$

Since these values are equal to within one percent, the corresponding load level of 1068 kN (240 kips) is accepted as the prediction from Yoo's (1996) equations. This value is reported in column (g) of Table 4.4.10.

4.5.4 Shear Strength Calculations for Specimen S1-0.10

The basic geometric and material properties utilized in the calculation of the shear resistances are as follows:

F_{yw} = 397.1 MPa (57.6 ksi), E = 200,000 MPa (29000 ksi)

b_{fc} = 544.6 mm (21.44 in), t_{fc} = 23.0 mm (0.906 in)

D = 1219 mm (48 in), t_w = 8.33 mm (0.328 in)

D/t_w = 146.3

d_o/D = 3.0

4.5.2.1 Current AASHTO LRFD (2001)

The AASHTO shear buckling coefficient, based on the assumption of simply supported boundary conditions at the web-flange juncture, is

$$k = 5 + \frac{5}{(d_o / D)^2} = 5.556 \qquad (2\text{-}96a)$$

The web slenderness satisfies the equation

$$\left(\frac{D}{t_w} = 146.3\right) > \left(1.38\sqrt{\frac{Ek}{F_{yw}}} = 73.0\right) \qquad (2\text{-}95c)$$

therefore, the ratio of the shear buckling strength to plastic buckling strength (C) is calculated as

$$C = \frac{1.52Ek}{\left(\frac{D}{t_w}\right)^2 F_{yw}} = 0.199 \qquad (2\text{-}95c)$$

The corresponding AASHTO LRFD (2001) shear strength, including tension-field action is then calculated as

$$V_n = 0.58F_{yw}Dt_w\left(C + \frac{0.87(1-C)}{\sqrt{1+\left(\frac{d_o}{D}\right)^2}}\right) = 983 \text{ kN (221 kips)} \qquad (2\text{-}103)$$

This value is reported in column (d) of Table 4.4.4.

4.5.2.2 Lee and Yoo's (1998) Equations

The shear buckling coefficient per Lee and Yoo's (1998) equations is interpolated from the (SSRC 1998) buckling coefficients for ideal simply supported and fully fixed boundary conditions at the web flange juncture:

$$k_{ss} = 5.34 + \frac{4}{(d_o/D)^2} = 5.784 \qquad (2\text{-}105)$$

$$k_{sf} = 8.98 + \frac{5.61}{(d_o/D)^2} - \frac{1.99}{(d_o/D)^3} = 9.530 \qquad (2\text{-}106)$$

The ratio of flange thickness to web thickness t_f/t_w is 2.76; therefore, the shear buckling coefficient (k) is calculated as

$$k = k_{ss} + \frac{4}{5}(k_{sf} - k_{ss}) = 8.781 \qquad (2\text{-}104)$$

The web slenderness satisfies the equation

$$\left(\frac{D}{t_w} = 146.3\right) > \left(1.38\sqrt{\frac{Ek}{F_{yw}}} = 91.8\right) \qquad (2\text{-}95c)$$

therefore, the ratio of the shear buckling strength to plastic buckling strength (C) is calculated as[4]

$$C = \frac{1.55Ek}{\left(\frac{D}{t_w}\right)^2 F_{yw}} = 0.321 \qquad (4\text{-}2)$$

The next step in determining the shear strength per Lee and Yoo (1998) is to calculate the reduction factor, which represents the influence of initial imperfections. Since

$$\left(1.10\sqrt{\frac{Ek}{F_{yw}}} = 73.1\right) \le \left(\frac{D}{t_w} = 146.3\right) \le \left(2.20\sqrt{\frac{Ek}{F_{yw}}} = 146.3\right)$$

the strength reduction factor R is calculated as

$$R = 0.8 + 0.2\frac{\frac{D}{t_w} - 1.10\sqrt{\frac{Ek}{F_{yw}}}}{1.10\sqrt{\frac{Ek}{F_{yw}}}} = 1.0 \qquad (2\text{-}109b)$$

Based on the above values for the shear buckling load and the strength reduction factor, the nominal shear strength is calculated as

$$V_n = 0.58F_{yw}Dt_wR(C + 0.4[1 - C]) = 1380 \text{ kN (311 kips)} \qquad (2\text{-}110)$$

This value is reported in column (e) of Table 4.4.4.

4.5.2.3 Modified AASHTO Equations

The proposed modified AASHTO LRFD shear strength equations (see Section 2.2.4) are based on the use of Lee and Yoo's (1998) shear buckling coefficient, as detailed in the previous subsection, for calculation of the shear buckling strength combined with Basler's tension-field strength formula, i.e.,

---

[4] In the calculation of the shear strength as per Lee and Yoo's (1998) equations, the traditional "English units" version of the AASHTO shear buckling equations is employed. The shear buckling strengths are stated in this fashion by Lee and Yoo (1998). When nondimensionalized, the coefficient of 1.55 is obtained with this equation, rather than 1.52 as reported in Eq. (2-95c) and specified in AASHTO LRFD (2001). The coefficient of 1.55 is obtained when τ_{yw} is taken as $F_{yw}/\sqrt{3}$ instead of 0.6 F_{yw}. This increases the calculated shear strength by approximately one percent for this example. Equation (4-2) is utilized in the calculations per Lee and Yoo's (1998) equations throughout this research.

$$k = 8.781$$

$$C = \frac{1.52Ek}{\left(\frac{D}{t_w}\right)^2 F_{yw}} = 0.314 \qquad (2\text{-}95c)$$

Therefore, based on Eq. (2-103), the nominal shear strength is

$$V_n = 0.58F_{yw}Dt_w\left(C + \frac{0.87(1-C)}{\sqrt{1+\left(\frac{d_o}{D}\right)^2}}\right) = 1190 \text{ kN (267 kips)} \qquad (2\text{-}103)$$

This value is reported in column (f) of Table 4.4.4.

4.6 EFFECT OF INTERPRETATION OF f_m ON RECOMMENDED SPECIFICATION PREDICTIONS

The application of the flexural strength equations of the Recommended Specifications (Hall and Yoo 1998) is hampered by the ambiguous nature of McManus's (1971) term for the applied flange lateral bending stress at the cross-frame locations, denoted by $\bar{f}_w$ in Section 2.1.2. This problem is due to the fact that the internal flange lateral bending stress at the cross-frames in McManus's approximate second-order elastic calculations is not equal to his specified applied flange lateral bending stress at the ends of his beam models (see Figs 2.1.13 and 2.1.14). McManus (1971) interprets $\bar{f}_w$ as the maximum lateral flange bending stress at the cross-frame locations, calculated by a first-order elastic analysis of the bridge superstructure. However, Hall et al. (1999) recognize that McManus double counted in calculating his elastic flange lateral bending stress contribution due to web distortion, and that this double counting can be partially compensated for by subtracting the warping stress due to curvature (determined based on the V-Load equation (Eq. 1-6)), from the lateral bending stress calculated in the analysis of the bridge superstructure (see Eq. 2-44) (Hall and Yoo 1998). They refer to the resulting lateral flange bending stress as the stress "due to effects other than horizontal curvature," and label this stress as f_m.

Table 4.6.1 summarizes the effect of the interpretation by Hall and Yoo (1998) versus McManus's (1971) original interpretation for all of the experimental tests evaluated in this chapter.

Table 4.6.1. Effect of interpretation of McManus's (1971) equations on Recommended Specification predictions.

Test	Experiment	Full Nonlinear Analysis	1st-Order Elastic Analysis	
			$\bar{f}_w = f_\ell$ McManus (1971)	$\bar{f}_w = f_m$ Hall and Yoo (1998)
	kN	kN	kN	kN
	[a]	[b] ([b]/[a])	[e] ([e]/[a])	[i] ([i]/[a])
C8-2	332	336 (1.01)	128 (0.39)	114 (0.34)
C9-2	266	263 (0.99)	34.7 (0.13)	43.6 (0.16)
D13	303	295 (0.97)	52.9 (0.17)	63.6 (0.21)
D14	287	283 (0.99)	51.2 (0.18)	61.8 (0.21)
L1-A	136	119 (0.87)	109 (0.80)	97.4 (0.72)
L2-A	136	121 (0.89)	111 (0.82)	99.6 (0.73)
L2-B	272	261 (0.96)	213 (0.78)	194 (0.71)
L2-C	288	263 (0.91)	214 (0.74)	195 (0.68)
GI-3	206	193 (0.93)	188 (0.91)	181 (0.88)
GI-4	211	193 (0.92)	188 (0.89)	181 (0.86)
GI-5	121	108 (0.89)	81.8 (0.68)	74.3 (0.61)
GO-8	186	173 (0.93)	153 (0.82)	142 (0.76)
B1	1350	1370 (1.01)	792 (0.58)	774 (0.57)
B2	1430	1400 (0.98)	801 (0.56)	801 (0.56)
B3	1500	1520 (1.01)	796 (0.53)	801 (0.53)
B4	1360	1290 (0.95)	730 (0.54)	747 (0.55)
B5	1830	1580 (0.86)	1610 (0.88)	1520 (0.83)
B6	2170	1890 (0.87)	1950 (0.90)	1850 (0.85)
B7	1130	1170 (1.04)	747 (0.66)	761 (0.68)

The results previously reported in Tables 4.4.2, 4.4.6, and 4.4.9 are based on McManus's interpretation, and are repeated in Table 4.6.1. Table 4.6.1 shows that in all but three cases (C9-2, D13 and D14), the interpretation specified within the Recommended Specifications (Hall and Yoo 1998) makes the predictions more conservative than when McManus's (1971) interpretation is employed. If girders C9-2, D13 and D14 are excluded from consideration, due to the fact that these girders have an L_b/R significantly larger than the maximum limit upon which McManus's equations were based, the Hall and Yoo (1998) interpretation gives an average ratio of the predicted to the experimental strength of 0.68 for the tests listed in Table 4.6.1, with a standard deviation of 0.15 and maximum and minimum values of 0.88 and 0.34. McManus's (1971) original interpretation gives an average ratio of the predicted to the experimental strength of 0.72, with a standard deviation of 0.16 and maximum and minimum values of 0.91 and 0.39.

4.7 LOAD-DEFLECTION PLOTS

4.7.1 Single-Girder Bending Tests

Figures 4.7.1 and 4.7.2 compare the finite element analysis predictions and experimental results for the applied load versus vertical displacement at the mid-span of specimens L1-A and L2-A. These are the single-girder four-point bending tests conducted by Mozer et al. (1971) (see Fig. 4.1.2 and Tables 4.2.1, 4.2.2, 4.3.1, and 4.4.1 through 4.4.3). They are selected for comparison of the numerical and experimental load-deflection results because, of all the single-girder tests, the least accurate finite element predictions relative to the experimental strengths are obtained for them.

One can observe from the plots in Figs. 4.7.1 and 4.7.2 that the pre-peak nonlinearity in the finite element predictions is less than that observed in the experiments. Furthermore, the finite element models predict a limit load at approximately 82 percent of the yield moment $M_y = F_{yf} S_{xc}$ in both of these tests, whereas the experiments are continued up to a load level corresponding to 93 and 94 percent of M_y respectively (with M_y calculated not including any effects from the flange lateral bending or from the hybrid web) before the loading is removed. The limit load in the finite element predictions corresponds to approximately 95 percent of the load level associated with the plastic flange capacity predicted by the compact-section based one-third rule, $f_b = F_y - f_\ell/3$ (see Fig. 2.1.19) where f_ℓ is obtained by elastic analysis of the system, whereas the experiment indicates a larger maximum load capacity than that given by this idealization. The continuation of the finite element predictions into the post-peak region of the response indicates a gradual shedding of the load from the girders.

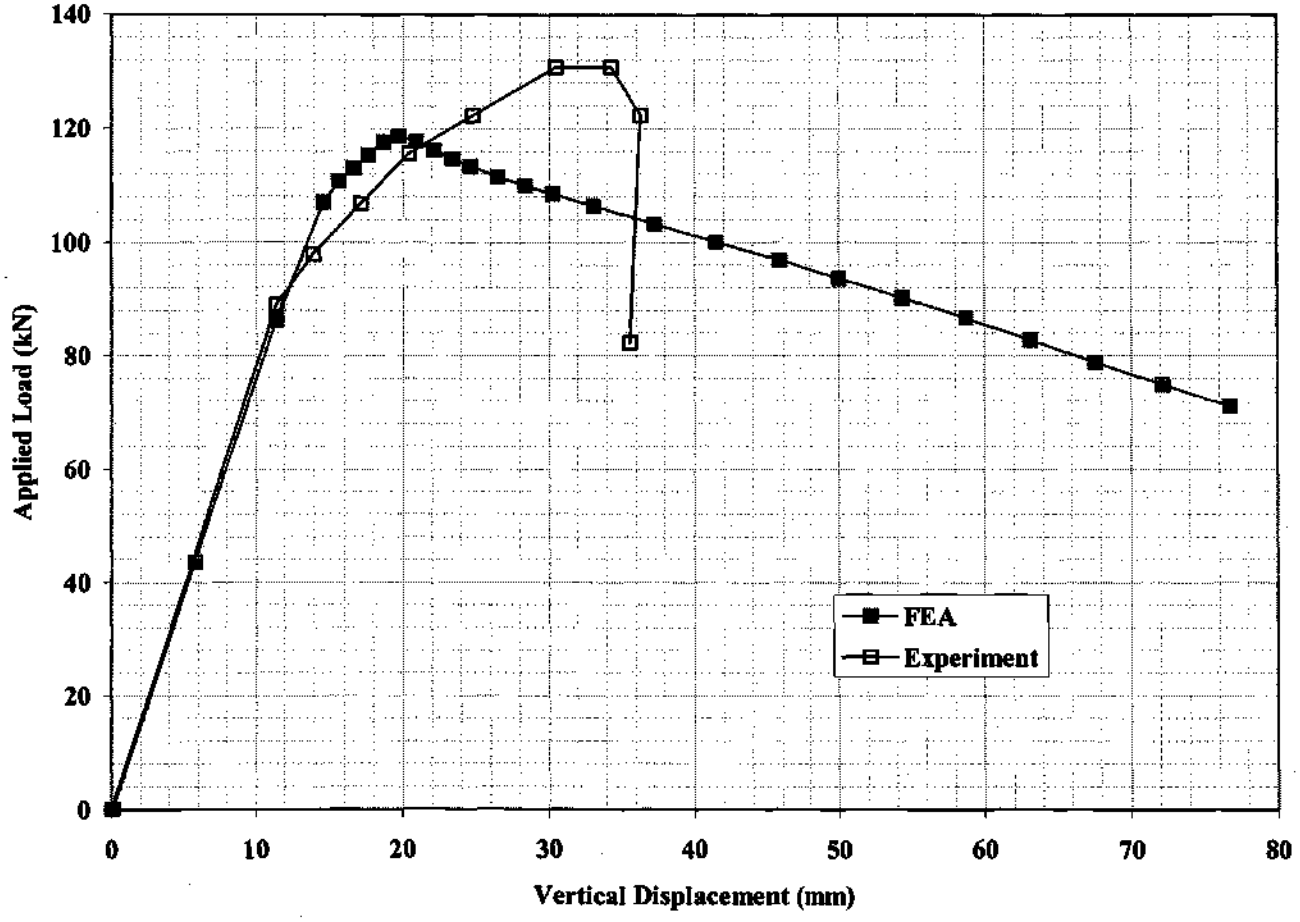

Figure 4.7.1. Applied load versus mid-span vertical displacement of Specimen L1-A.

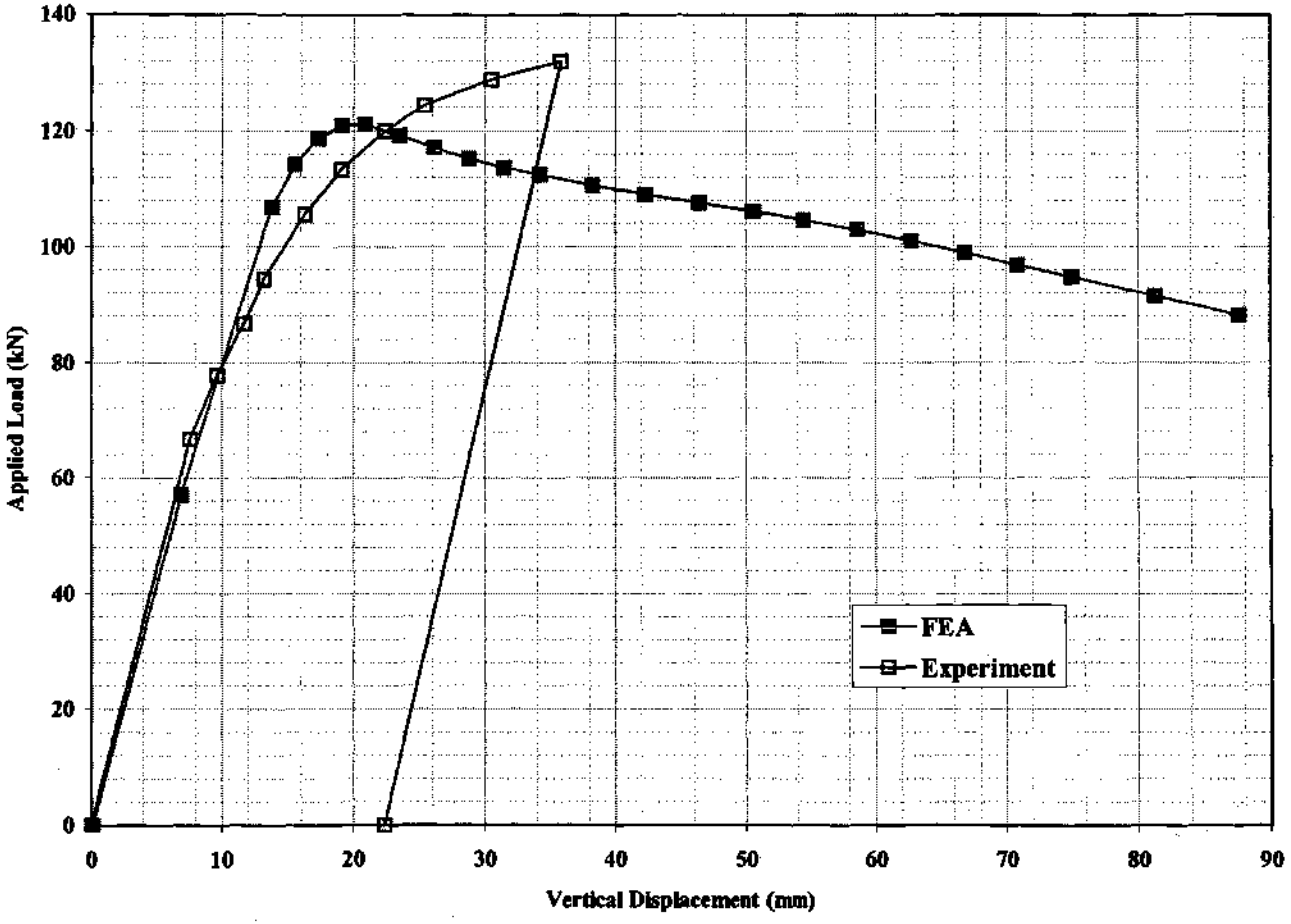

Figure 4.7.2. Applied load versus mid-span vertical displacement of Specimen L2-A.

4.7.2 Single-Girder Shear Tests

Figures 4.7.3 through 4.7.6 show the web shear versus vertical deflection results of the single-girder shear tests S1-0.10 and S1S-0.10 (Zureick et al. 2001) (see Figs. 4.1.5 and 4.1.6, and Tables 4.2.1, 4.2.2, 4.3.1, and 4.4.4). In Figs 4.7.3 through 4.7.6, the experimental results are compared to the finite element predictions with and without residual stresses and geometric imperfections. Figures 4.7.3 and 4.7.4 show the results for the "unstiffened" specimen ($d_o/D = 3$) and Figs. 4.7.5 and 4.7.6 show the results for the "stiffened" specimen ($d_o/D = 1.5$). The first of the plots in these two groups of figures gives the shear force versus the vertical displacement at the interior load location, location 2 in Fig. 4.1.7, whereas the second gives the shear force versus the vertical displacement at the exterior load location, location 4 in Fig. 4.1.7.

It can be seen that finite element models predict the behavior of these test specimens quite well. The only significant difference between the experimental results and the finite element predictions is in the elastic load-deflection response based on the vertical displacement at location 2 in the test of S1S-0.10 (see Fig. 4.7.5). As previously indicated in Table 4.4.4, the maximum shear capacity is predicted accurately by either of the finite element representations (with or without initial geometric imperfections and residual stresses). That is the shear strength of these tests appears to be insensitive to residual stresses and potential geometric imperfections relative to the perfect horizontally curved geometry. The horizontal curvature of the web panel is effectively an imperfection in itself.

It is interesting to note that the out-of-flatness of the web panel due to the horizontal curvature, measured with respect to a 1219 mm (48 in) long straight edge, is 5.08 mm (0.2 in) within these girders, whereas the AWS (1996) tolerances on the web out-of-flatness relative to the perfect geometry are $D/67 = 18.2$ mm (0.716 in) for panels of interior girders with one-sided stiffeners and $D/150 = 8.1$ mm (0.32 in) for unstiffened girders. The measured out-of-flatness relative to the perfect horizontally curved geometry in these tests (relative to a 1219 mm long straight edge) is 9.4 mm (0.369 in) for both tests. For straight girders, Aydemir (2000) observes a significant reduction in the shear capacity when a small fraction of the AWS (1996) tolerance is imposed for the web out-of-flatness, but that the sensitivity of the shear strengths to geometric imperfections is rather mild for further increases in the imperfection magnitude.

It should be noted that the loss in the shear capacity within the post-peak region of the response is very gradual in both the experiments as well as the finite element predictions.

Lastly, one can observe that there is no noticeable change in rate of increase of the vertical deflections in Figs. 4.7.3 through 4.7.6 as the shear buckling load obtained by the approximate equations and rigorous finite element eigenvalue solutions is exceeded.

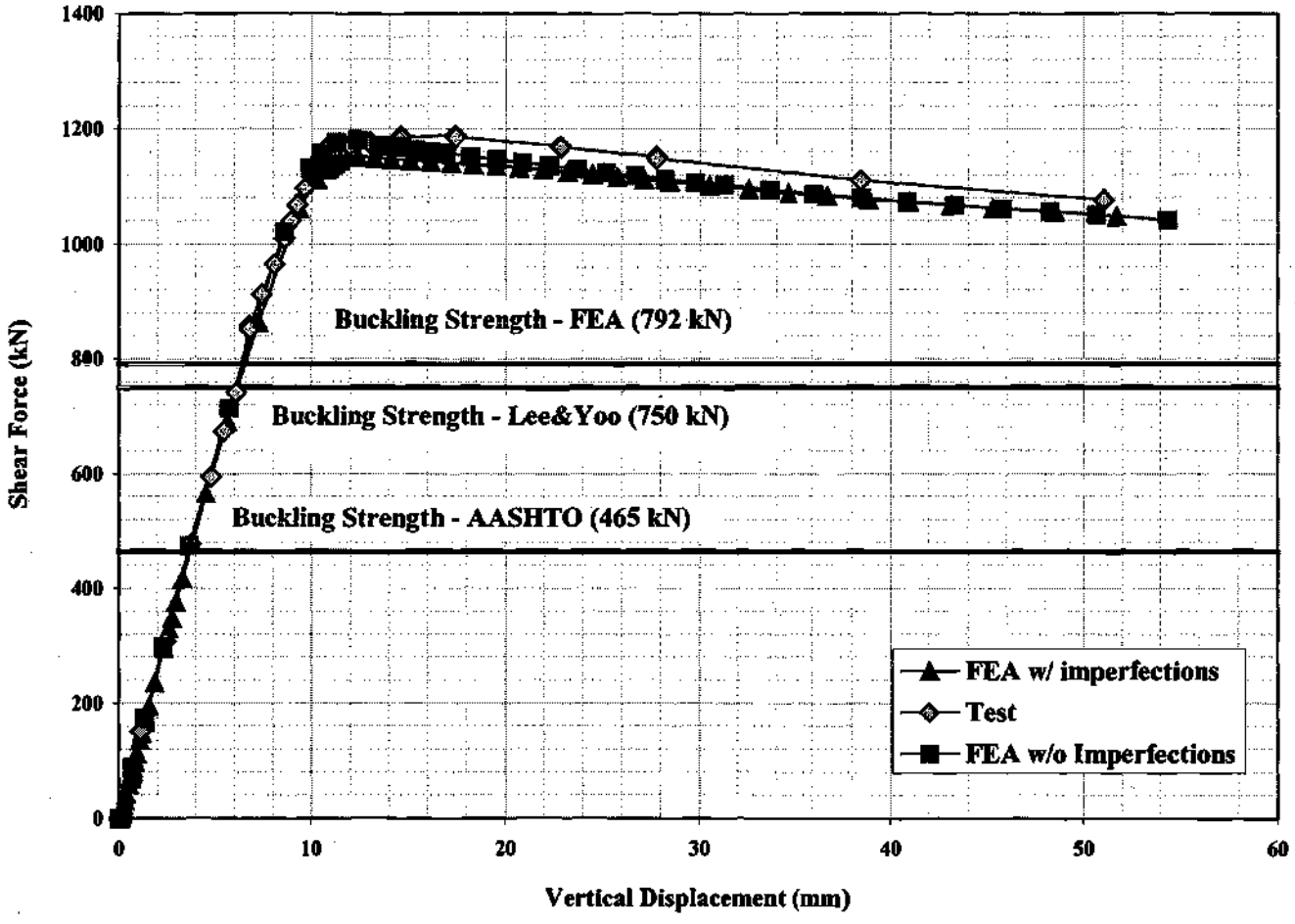

Figure 4.7.3. Shear force in the test panel versus bottom flange vertical displacement at location 2 of Specimen S1-0.10.

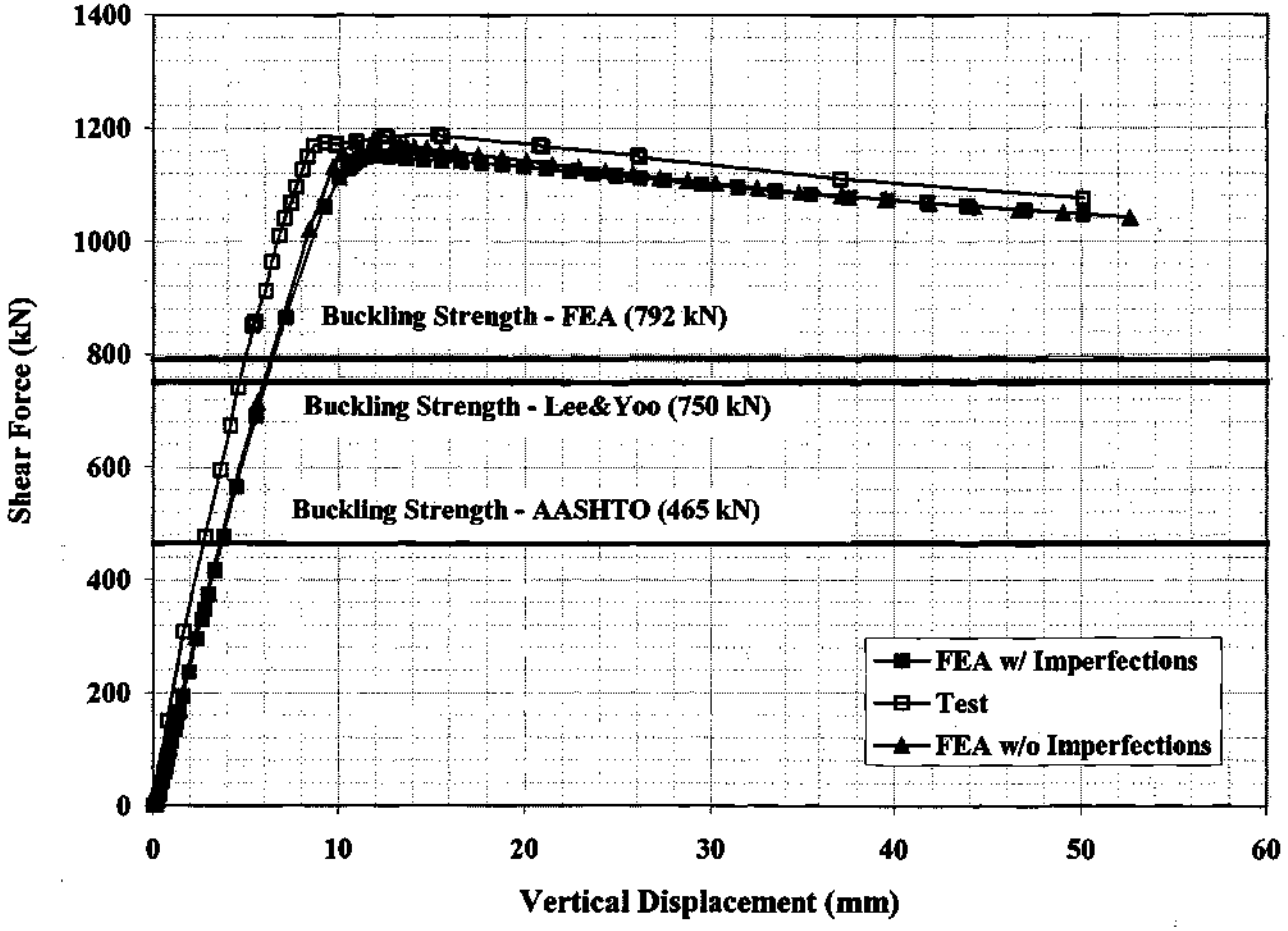

Figure 4.7.4. Shear force in the test panel versus bottom flange vertical displacement at location 4 of Specimen S1-0.10.

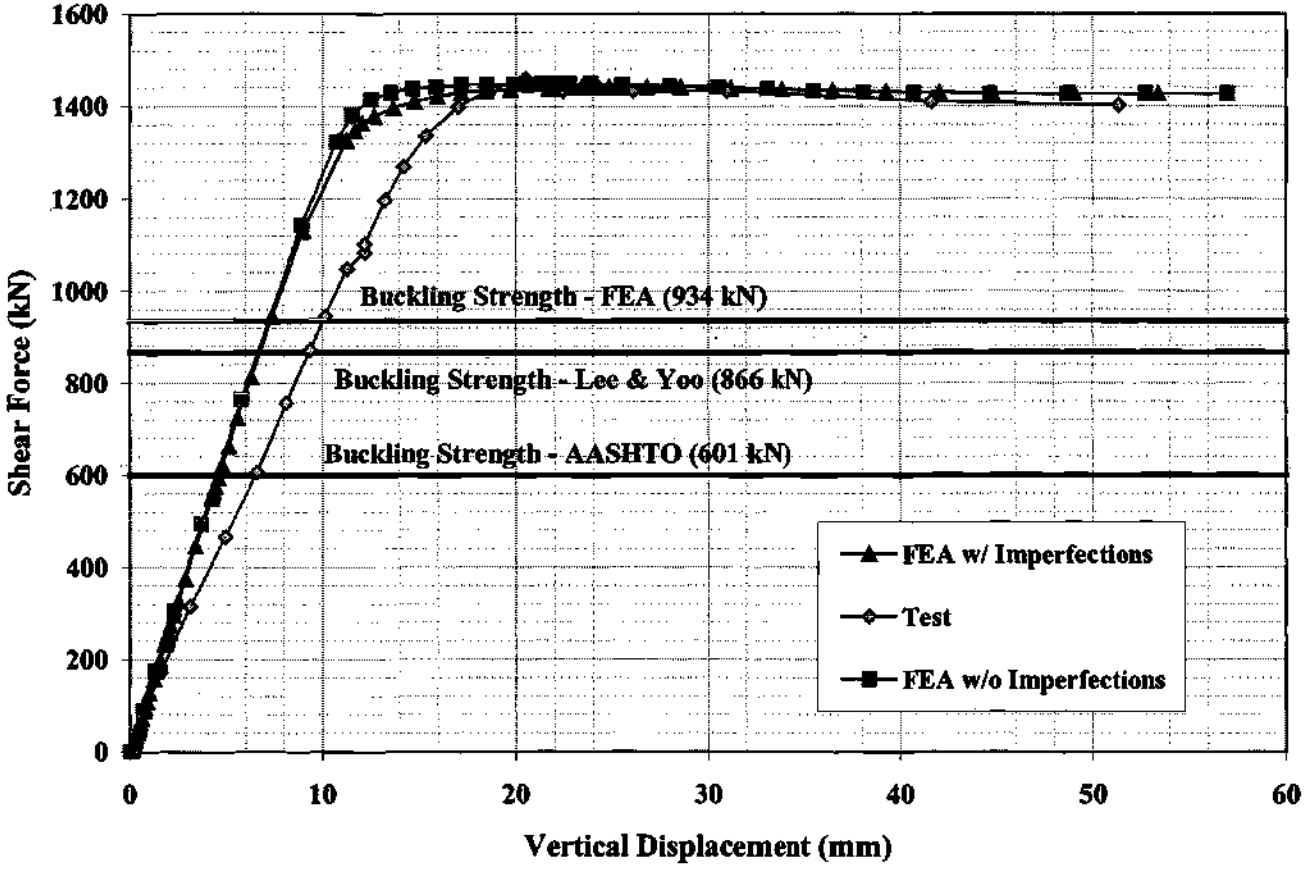

Figure 4.7.5. Shear force in the test panel versus bottom flange vertical displacement at location 2 of Specimen S1S-0.10.

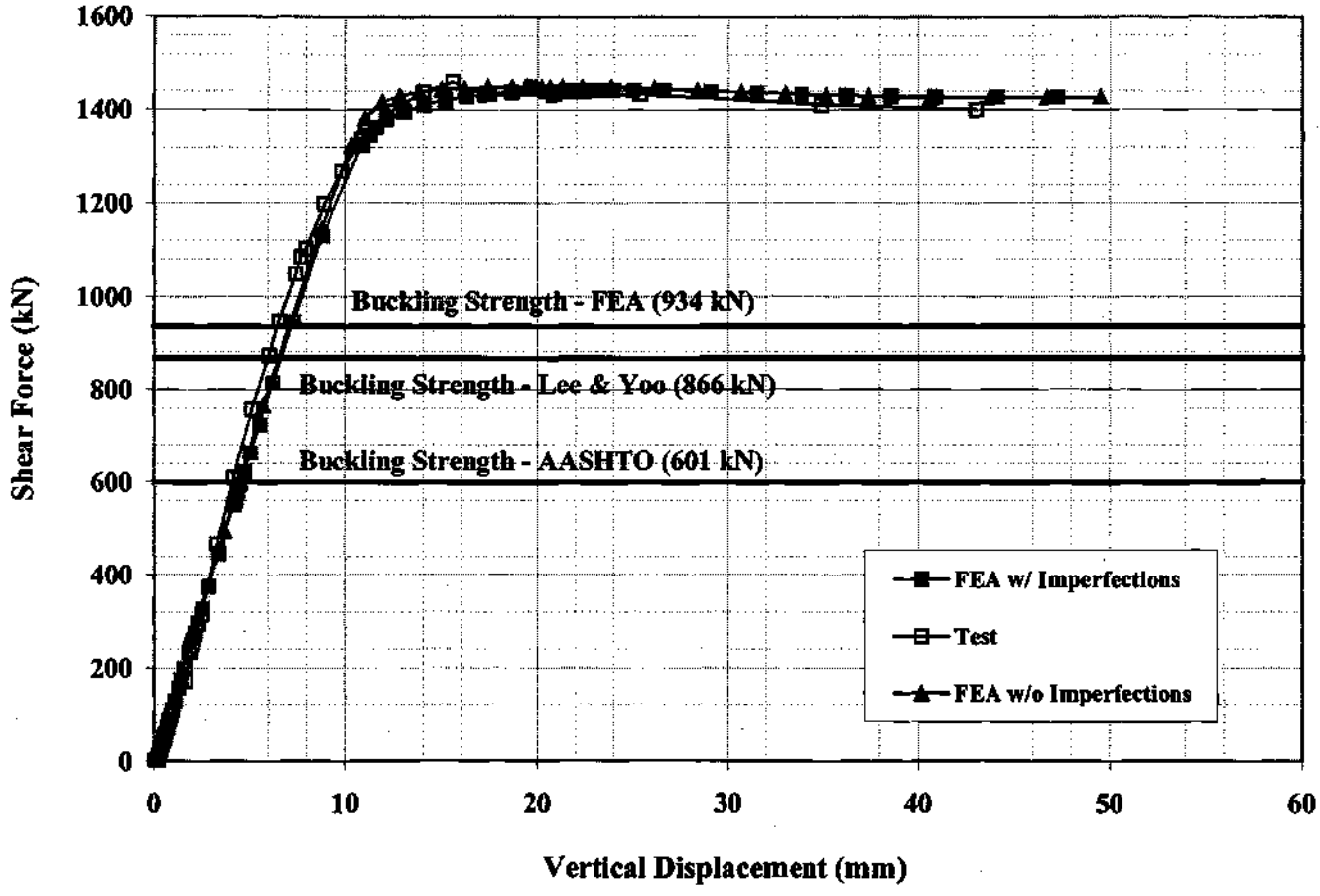

Figure 4.7.6. Shear force in the test panel versus bottom flange vertical displacement at location 4 of Specimen S1S-0.10.

4.7.3 Three-Girder System Bending Tests

Figures 4.7.7 to 4.7.13 show plots of the total applied load versus the vertical displacement at the mid-span of the component specimens for the three-girder system tests B1 through B7 (Zureick and Kim 2000; Hartmann 2000) (see Figs. 4.1.11 and 4.1.12, and Tables 4.2.5 through 4.2.7, 4.3.3, and 4.4.8 through 4.4.12). The finite element predictions are plotted for the analyses with and without geometric imperfections and residual stresses and are compared to the experimental load-deflection results (see Table 4.4.12 for a summary of the maximum strengths corresponding to these curves).

The initial slope of the load-deflection curves predicted by the finite element models is somewhat smaller than the measured response for tests B1, B2 and B4. Tests B1 and B4 have the largest difference in this slope; the measured initial slopes in these tests are more than 20 percent greater than the corresponding predicted initial slopes. However, this value is predicted quite accurately for the other bending tests. It is interesting to note that the amount of pre-peak nonlinearity is also somewhat greater in tests B1 and B4. Tests B1, B2 and B4 all have close stiffener spacing ($d_o/D = 1$) and noncompact flanges ($b_{fc}/t_{fc} \cong 23$), but otherwise there appear to be no particular characteristics that distinguish these tests from the other four tests. In each of these tests, the experimental load-deflection curve crosses the numerical ones just prior to the maximum applied load level in the physical tests. The experimental curve for test B3 also exhibits a slightly larger amount of pre-peak nonlinearity than the corresponding finite element models (see Fig. 4.7.9).

With one exception, the finite element models indicate a local limit load, followed by a minor amount of unloading (i.e., load shedding) over a small range of vertical displacements, prior to finally continuing with a stable load-deflection response at a small positive slope over a large range of vertical displacement. The unloading after the local limit load is more abrupt for the girders that have noncompact flanges ($b_{fc}/t_{fc} \cong 23$), and is more gradual for girder B5, which has a $b_{fc}/t_{fc} = 16.9$. The one exception to this response is for girder B6, which has a $b_{fc}/t_{fc} = 13.3$. For girder B6, the load-deflection response predicted by the finite element model with geometric imperfections and residual stresses included reaches a limit shortly after the onset of significant nonlinearity in the load-deflection curve, and then unloads very gradually (see Fig. 4.7.12). This model essentially holds at a constant maximum load while the vertical deflections increase after the limit load is reached. The model for test B6 that does not include geometric imperfections and residual stresses still exhibits a local limit load, followed by minor unloading and a final stable inelastic loading branch. However, the unloading in this model is significantly smaller than that observed in the models of the other girders. The finite element strength predictions reported in Tables 4.4.8 through 4.4.10 and 4.4.12 are all based on the load at the first limit point achieved in the analysis.

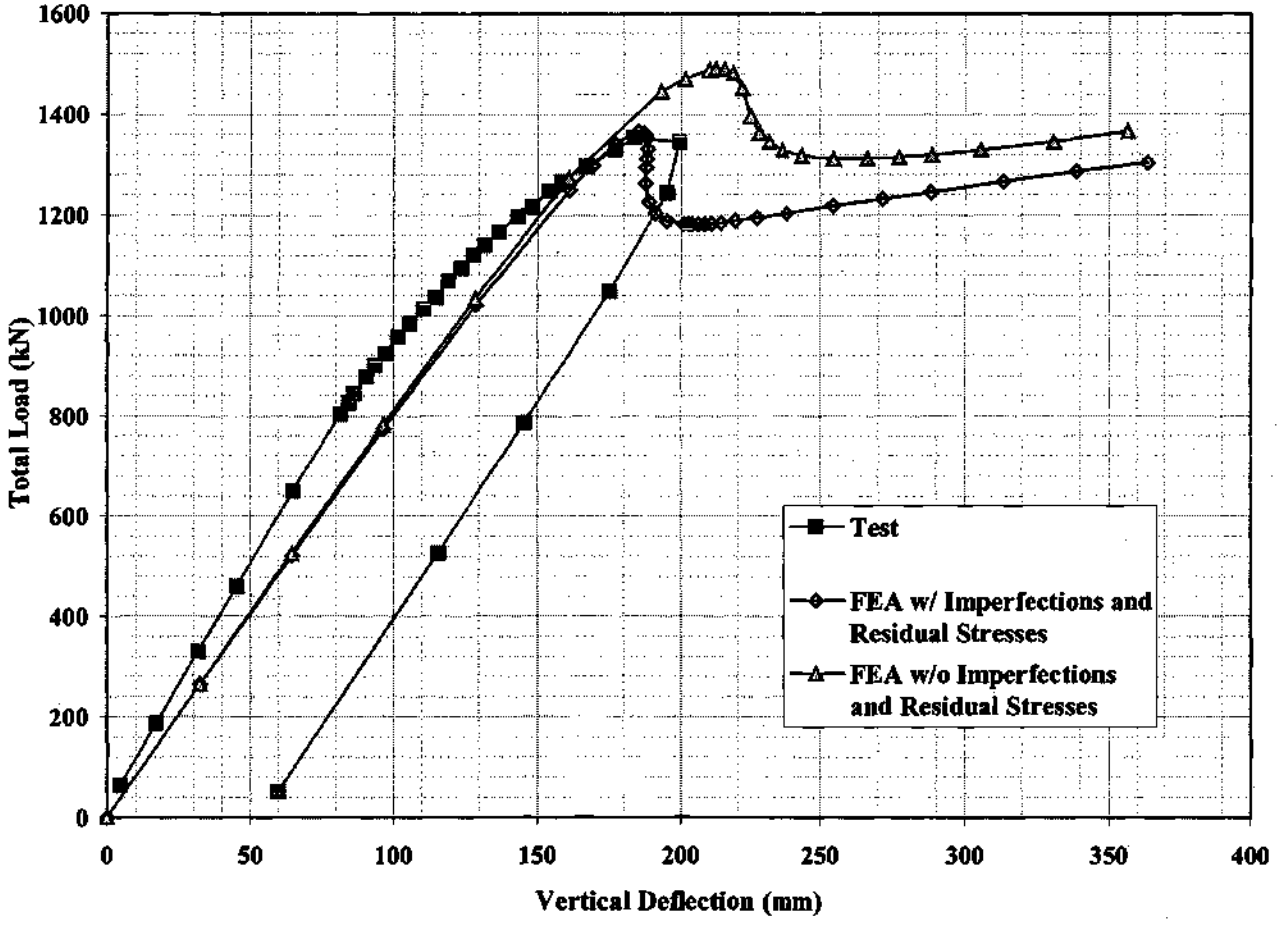

Figure 4.7.7. Test B1 load-vertical deflection at component mid-span (L_b/b_{fc} = 10.3, b_{fc}/t_{fc} = 22.8, D/t_w = 149).

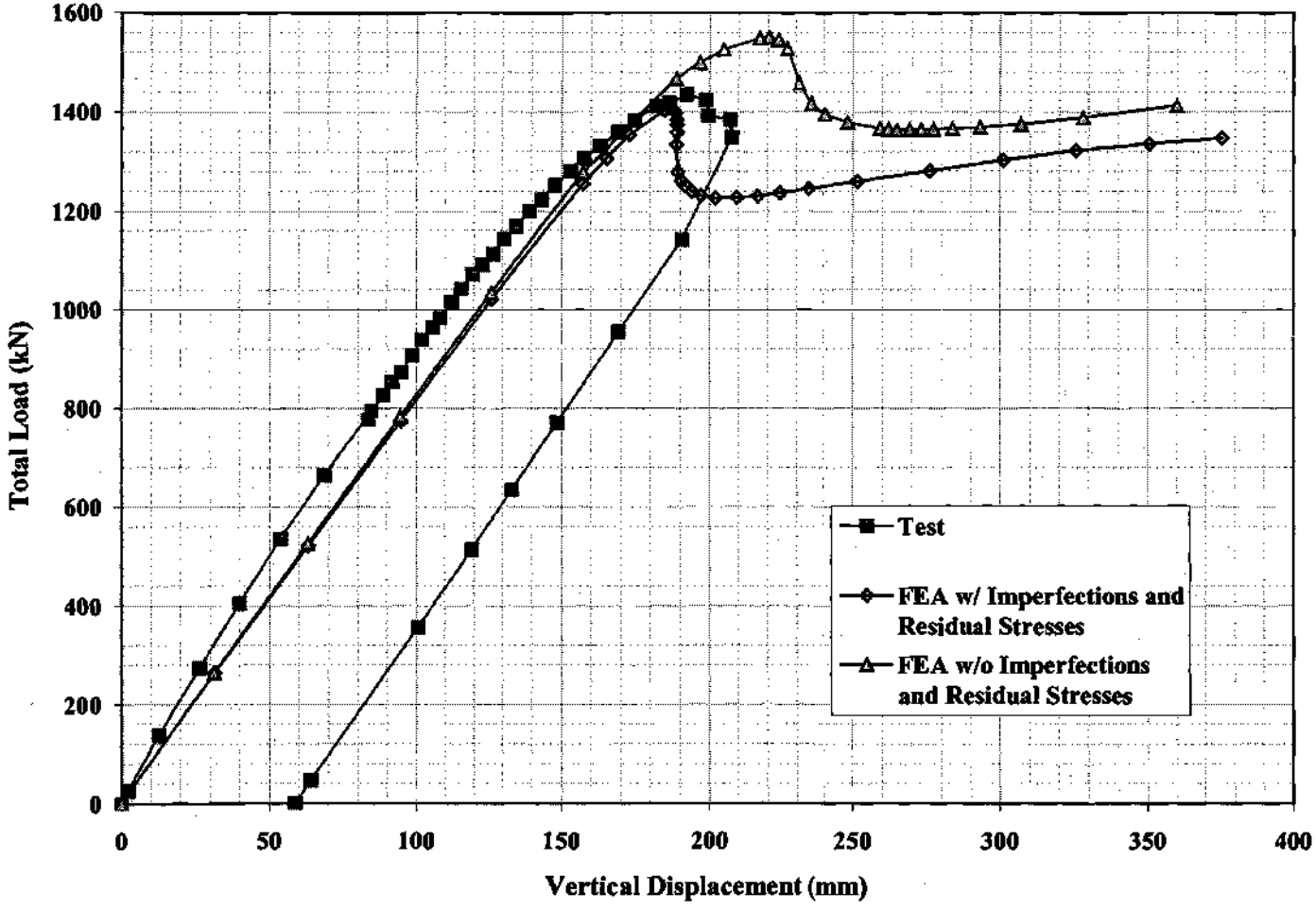

Figure 4.7.8. Test B2 load-vertical deflection at component mid-span (L_b/b_{fc} = 10.3, b_{fc}/t_{fc} = 22.9, D/t_w = 121, d_0/D = 1).

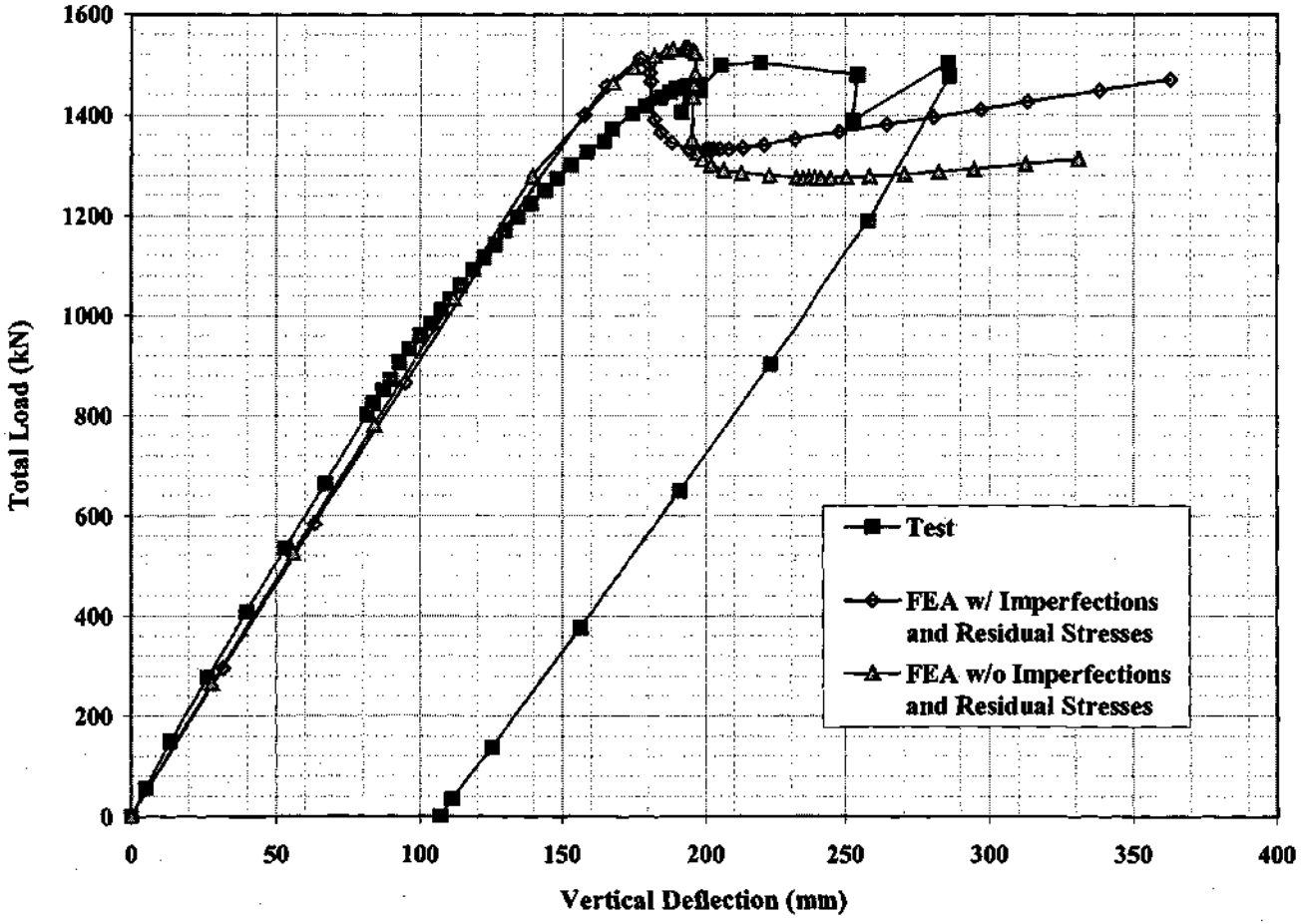

Figure 4.7.9. Test B3 load-vertical deflection at component mid-span (L_b/b_{fc} = 10.3, b_{fc}/t_{fc} = 22.8, D/t_w = 120, d_0/D = 3).

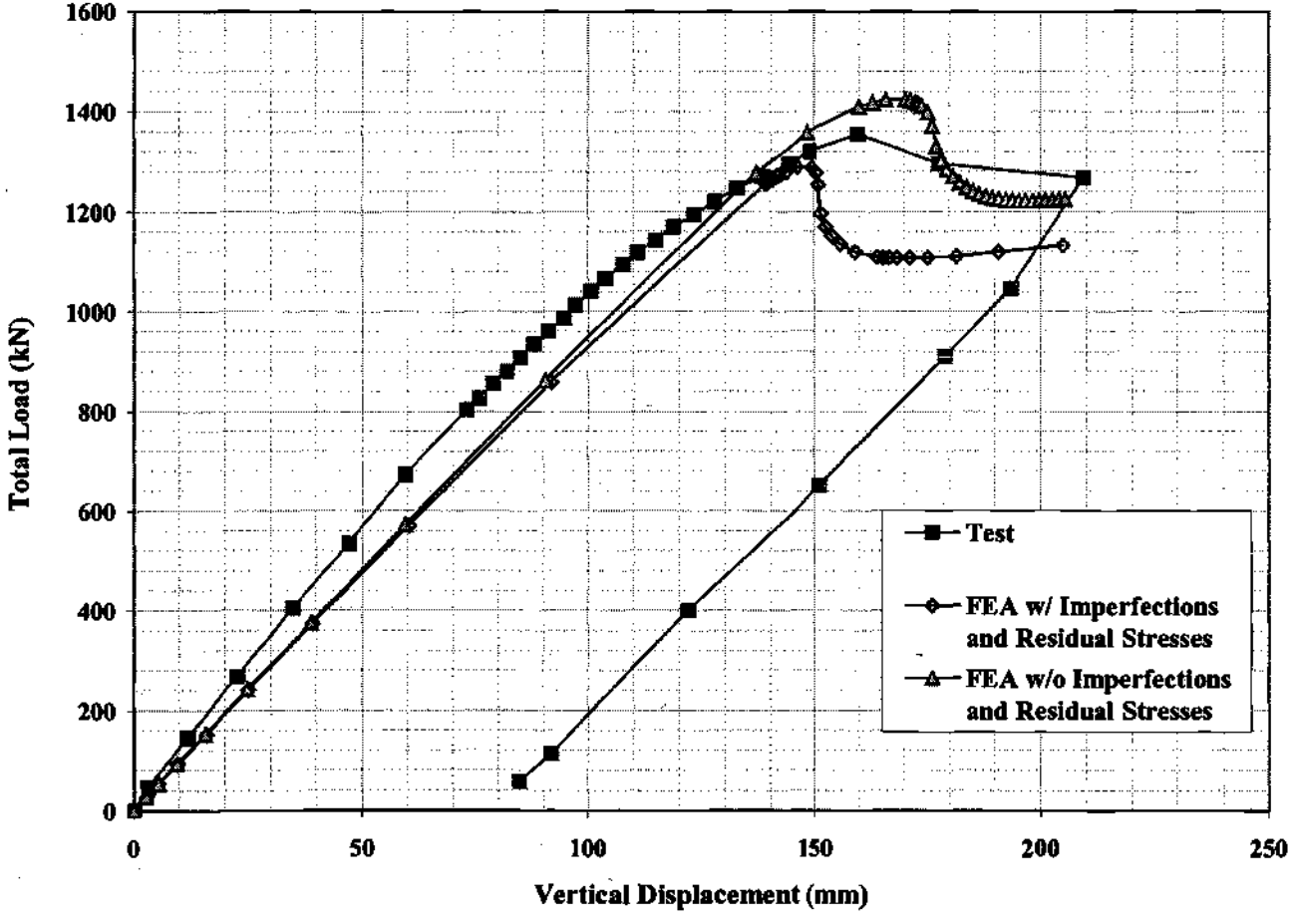

Figure 4.7.10. Test B4 load-vertical deflection at component mid-span (L_b/b_{fc} = 10.3, b_{fc}/t_{fc} = 22.8, $2D_c/t_w$ = 188, d_0/D = 0.98).

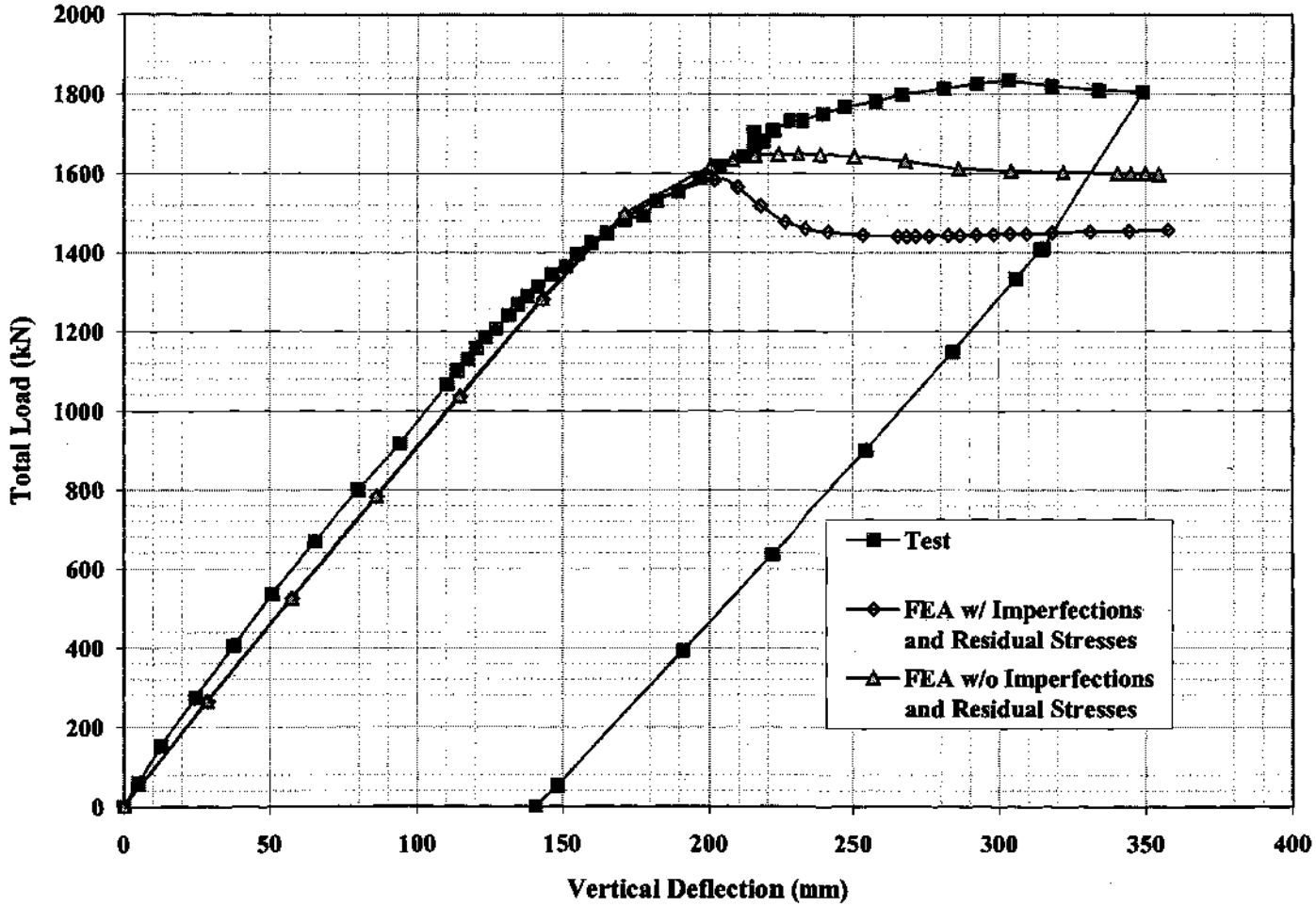

Figure 4.7.11. Test B5 load-vertical deflection at component mid-span (L_b/b_{fc} = 11.0, b_{fc}/t_{fc} = 16.9, D/t_w = 144).

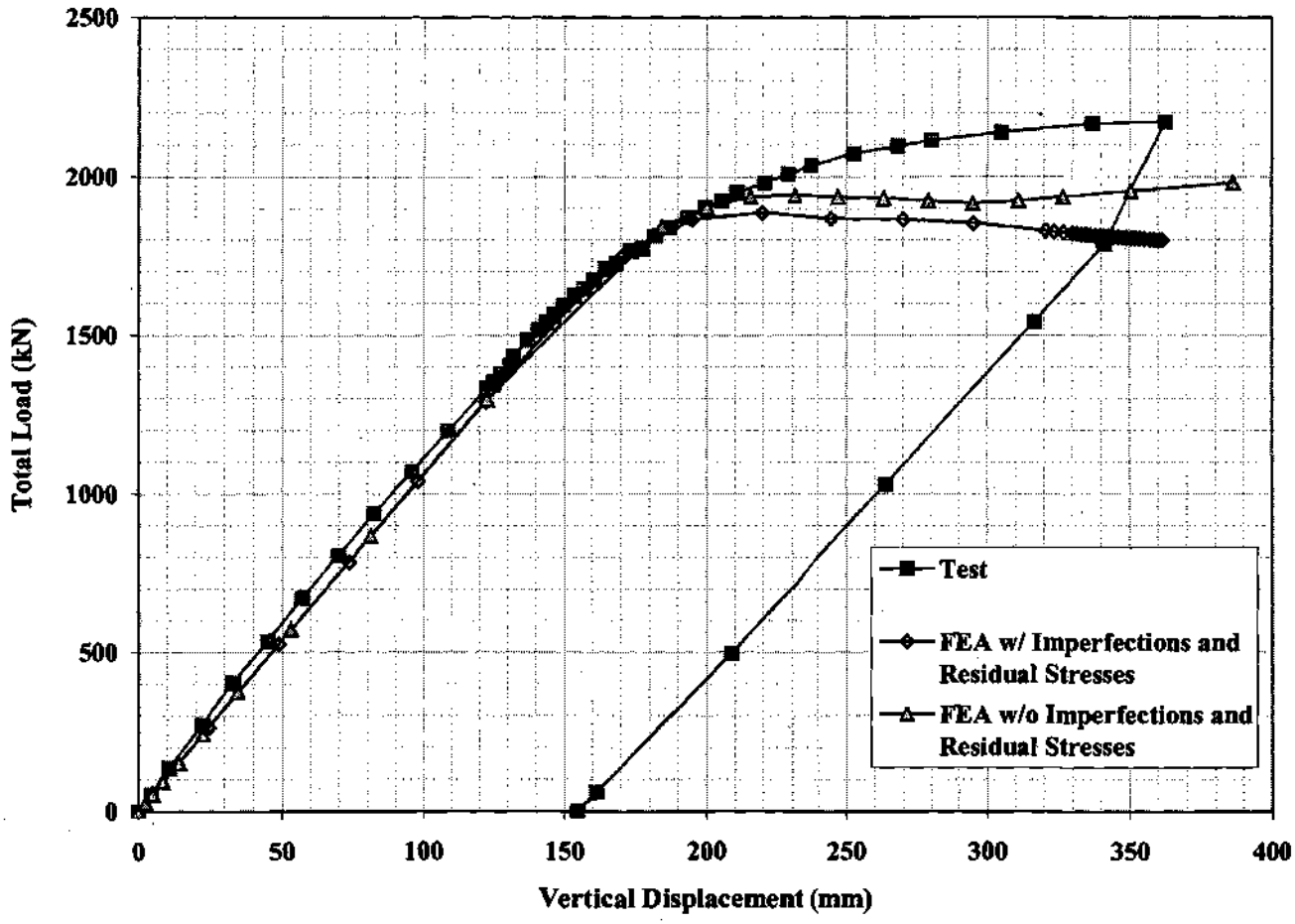

Figure 4.7.12. Test B6 load-vertical deflection at component mid-span (L_b/b_{fc} = 11.2, b_{fc}/t_{fc} = 13.3, D/t_w = 143).

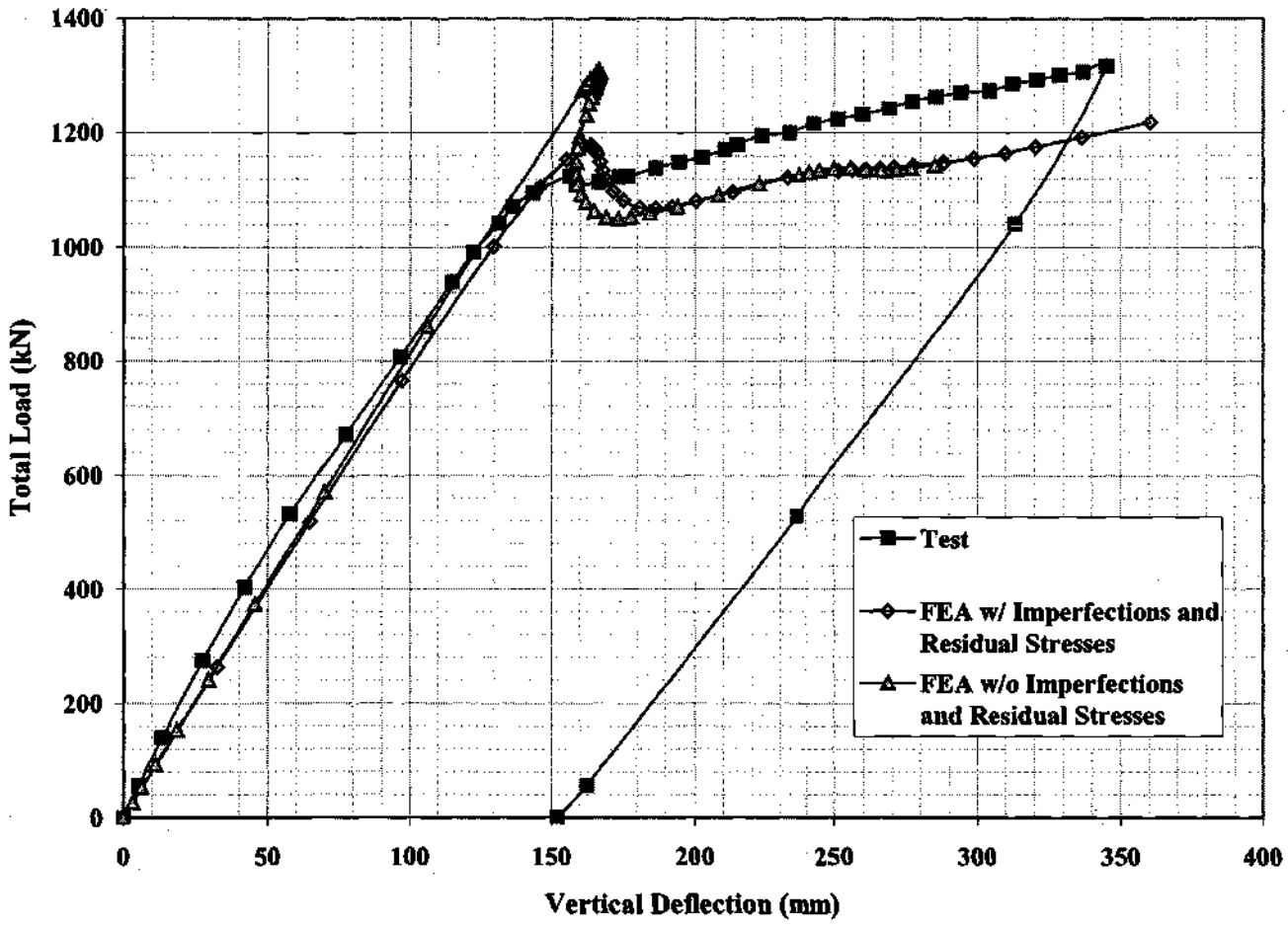

Figure 4.7.13. Test B7 load-vertical deflection at component mid-span (L_b/b_{fc} = 8.6, b_{fc}/t_{fc} = 32.5, D/t_w = 149).

A local limit followed by unloading and then reloading is evident in the experimental load-deflection response of test B7. Also, there is some indication of this type of response in test B3, although the drop in load after the initial peak in this test may be due to other factors than an unstable response of the specimen. Specimens B1, B2, and B4 were not loaded far enough into their post-peak range to discern whether this type of response occurred in the physical tests. They all showed a minor drop in load capacity after reaching a peak load at only a small amount of inelastic vertical displacement. The test results for B4 show that if an unloading-reloading type of response is occurring within this test, it is more gradual than that predicted by the finite element models.

The finite element and experimental load-deflection curves match closely for the compact-flange girders B5 and B6 up to the level at which the finite element models reach their maximum load capacity (see Figs. 4.7.11 and 4.7.12). After this point, the experimental curves continue at a small positive slope, while the finite element models predict increasing vertical deflection at nearly constant total applied load. For test B5 (Fig. 4.7.11), the finite element model predicts only a minor unloading-reloading behavior when residual stresses and geometric imperfections are included.

It is important to note that for tests B5 and B6, the maximum loads predicted by the full nonlinear finite element models are only slightly less than that associated with an elastic analysis of the bridge structure with a capacity limit based on the compression flange plastic strength $f_b = F_{yc} - f_r/3$. Conversely, the experimental tests show a maximum load capacity that is significantly in excess of this load level. This trend is also observed for tests L1-A and L2-A, as discussed at the beginning of this section. Nevertheless, the strain measurements from test B5 and B6 indicate that the tangential normal strains were generally smaller than the strain-hardening strain in uniaxial tension; maximum flange tangential normal strains of approximately 0.017 and 0.016 are reported for B5 and B6 respectively (Zureick and Kim 2000).

Many factors may have contributed to the additional load capacities in the experimental tests, compared to the finite element predictions, for girders B5 and B6. Without a thorough study of the reduced test data, and inspection of and correlation with corresponding finite element predictions, any explanation of these differences would only be conjecture.

In test B7, the local limit load is more pronounced within the finite element models than in the experiment. However, the prediction of the finite element model with residual stresses and geometric imperfections included is quite close to the load-deflection response measured within the physical test.

The unloading and reloading responses predicted in all of the finite element models, with the exception of the model of B6 that includes initial geometric imperfections and residual stresses, appears to be due to the interaction of the specimen with the three-girder bridge system. This observation is based on the fact that none of the other bending tests considered in this chapter, and none of the parametric study girders considered in Chapters VI and VII exhibit any unloading-reloading response.

Overall, it is believed that the finite element models discussed above provide a reasonably accurate and reliable prediction of the experimental behavior. However, particularly in the system tests, there are numerous factors that can influence the correlation between the experimental and numerical results. These include:

- Initial stresses that are "locked into" the component specimens due to the assembly of the redundant test system. As noted in Section 3.3, dead weight is included within the finite element models of the multiple-girder systems. However, the erection sequence and any effects that it has on the internal stresses within the system are not considered. The system dead weight is simply "turned on" during the first step in the full nonlinear finite element analysis.

- Additional incidental restraint provided by the splice connections between the bridge test frame and the component specimens. As noted in Section 3.3, these splice connections were not explicitly modeled in this research. Based on preliminary studies, the effect of this approximation is believed to be small; there is negligible change in the load-deflection behavior if the plate thicknesses within the length of the splice connections are artificially increased.

- Additional incidental restraint provided by the gusset plate connections within the cross-frames. Section 3.3 explains that rotational continuity was assumed at the joints of the cross-frame members, but that the joint size was assumed to be infinitesimal, and the connection plates were not explicitly modeled (except for the connection plate on the girder web). Based on preliminary studies, the effect of this approximation is believed to be small; there is negligible change in the load-deflection behavior if the moment of inertia of the cross-frame members is doubled in value.

- Additional incidental restraint provided by the loading system. Some inclination of the dywidag bars of the loading assemblies was evident at the end of the tests. However, it is believed that the effect of this inclination is small.

It is emphasized that an extensive interpretation of the experimental data from prior tests, and correlation of this data with the results from refined finite element analyses, is beyond the scope of this research. Results from the three-girder system tests (Zureick and Kim 2000; Hartmann and Wright 2001) are expected within the near future. The purpose of the studies conducted within this chapter is to provide some validation of the accuracy of the finite element models utilized in this research, as well as experimental confirmation of the characteristics of key design predictor equations. Chapter VI provides a more detailed assessment of curved I girder load-displacement behavior within the context of the finite element parametric studies conducted in this research.

4.8 SPECIMEN DISTORTIONS

It is important to consider the distorted geometry at and subsequent to reaching the maximum load in the tests for several reasons. First, the finite element predictions and the experimental observations can be compared to ascertain whether the numerical simulations capture the physical failure mode realistically. Secondly, if the magnitudes of the cross-section distortions at maximum load are excessive, it may prudent to consider limiting the maximum strength based on a more restrictive local deformation or distortion limit.

In this section, tests S1-0.10 and S1S-0.10 (Zureick et al. 2001) are evaluated as representative girders subjected to a shear failure, and tests B1 (Zureick and Kim 2000) and B7 (Hartmann 2000) are evaluated as representative girders subjected to a uniform vertical bending failure.

4.8.1 Shear Tests

The distortions of specimens S1-0.10 and S1S-0.10 observed in the physical tests as well as predicted by finite element models are illustrated in Figs. 4.8.1 through 4.8.7. It can be seen that, for specimen S1-0.10, which has a panel aspect ratio $d_o/D = 3$, there is an evident tension band that has formed within the girder web at the maximum load level (see Figs. 4.8.1 and 4.8.2). The flaking of the paint evident this band is due largely to the compression associated with the local plate bending transverse to the direction of the diagonal tension. The web panel is essentially being straightened out along the center of this diagonal tension band. These pictures imply that the primary diagonal tension band starts at the top of the bearing stiffener at location 3, and intersects the bottom flange of the girder at approximately 2/3 of the panel length. That is, the implied angle of the tension band with the horizontal direction is $\tan^{-1}(1/2) = 26.6^{\circ}$, which might be compared to $\theta = 0.5 \tan^{-1}(1/3) = 9.2^{\circ}$ based on Basler's Eq. (2-98b).

The maximum measured out-of-plane displacement of the web panel at the maximum load level is slightly larger than 33.3 mm (1.31 in), measured at D/4 from the bottom of the web and at the mid-length of the panel[5]. The corresponding maximum predicted radial displacement at the peak load is 74.2 and 51.3 mm (2.92 and 2.02 in) when initial geometric imperfections and residual stresses are included or neglected respectively. A small amount of vertical distortion of the flanges is evident at this load level (see Fig. 4.8.1). As the specimen is pushed beyond its peak load, which occurs at approximately 12.7 mm (0.5 in) vertical displacement at location 2, to a 50.8 mm (2.0 in) vertical displacement at this location at the end of the test, the web plate continues to fold in the direction transverse to the diagonal tension line, apparently due in part to diagonal compression in this direction. Figure 4.8.3 shows the web panel distortion at the end of the test. The corresponding distortions predicted by the full nonlinear finite element model (with residual stresses and initial geometric imperfections included) are shown in

[5] The maximum displacement within the potentiometer at this location was reached at 98 percent of the maximum applied load; the last recorded displacement is 33.3 mm (1.31 in)

Fig. 4.8.4. The distortions for the model with residual stresses and initial geometric imperfections not included are essentially the same.

Figure 4.8.5 shows the girder deformed geometry at the maximum load level in test S1S-0.10, which is identical to S1-0.10 except that an intermediate transverse stiffener is placed at the middle of the critical test length such that $d_o/D = 1.5$. The maximum measured web out-of-plane displacement in the web panel at the state shown in this figure is 32.8 mm (1.29 in) at the mid-depth of the web, which is slightly less than two times the AWS (1996) tolerance on the web out-of-flatness for an interior transversely-stiffened girder (D/67). The corresponding maximum predicted radial displacement in the two critical web panels is 68.6 and 40.6 mm (2.70 and 1.60 in) at the maximum load, with and without initial geometric imperfections and residual stresses respectively. The displacements in the adjacent critical web panel are very similar at this stage of the test, based on a visual inspection. Figure 4.8.5 illustrates that the girder distortions at the maximum load are minor.

As this specimen is pushed beyond its peak load to a vertical displacement of approximately 43.2 mm (1.7 in) at the end of the test, the primary tension-field failure manifests itself within the adjacent, non-instrumented web panel. Figure 4.8.6 shows this panel at the end of the test. It is apparent that the dominant tension band in this case runs from the top of the intermediate stiffener at the middle of the critical unsupported length, to the bottom of the bearing stiffener at location 2. Figure 4.8.7 shows the corresponding finite element prediction. The flange distortions are still relatively small at this advanced stage of the post-peak response.

The reader is referred to (Zureick et al. 2001) for a comprehensive presentation and discussion of the results of these experimental tests.

4.8.2 Bending Tests

The distortions in specimens B1 and B7 observed in the physical tests as well as predicted by the finite element models are illustrated in Figs. 4.8.8 to 4.8.11. It should be noted that test B1 has a b_f/t_f of 22.8 whereas test B7 has compression flange slenderness of 32.5. Figure 4.8.8 shows specimen B1 at the maximum load in the physical test. It can be seen that some minor flange local buckling distortions are visible. Figure 4.8.9 shows the corresponding prediction from the full nonlinear finite element model (with initial geometric imperfections and residual stresses included), magnified by a factor of two. The flange distortions in the finite element model are very similar to the distortions observed at the maximum load level in the physical test. The maximum predicted vertical displacement at the compression flange tip relative to the web-flange juncture is approximately 8.6 mm (0.34 in) at the maximum load level. This information is not available from the experimental test at this time (May 2001).

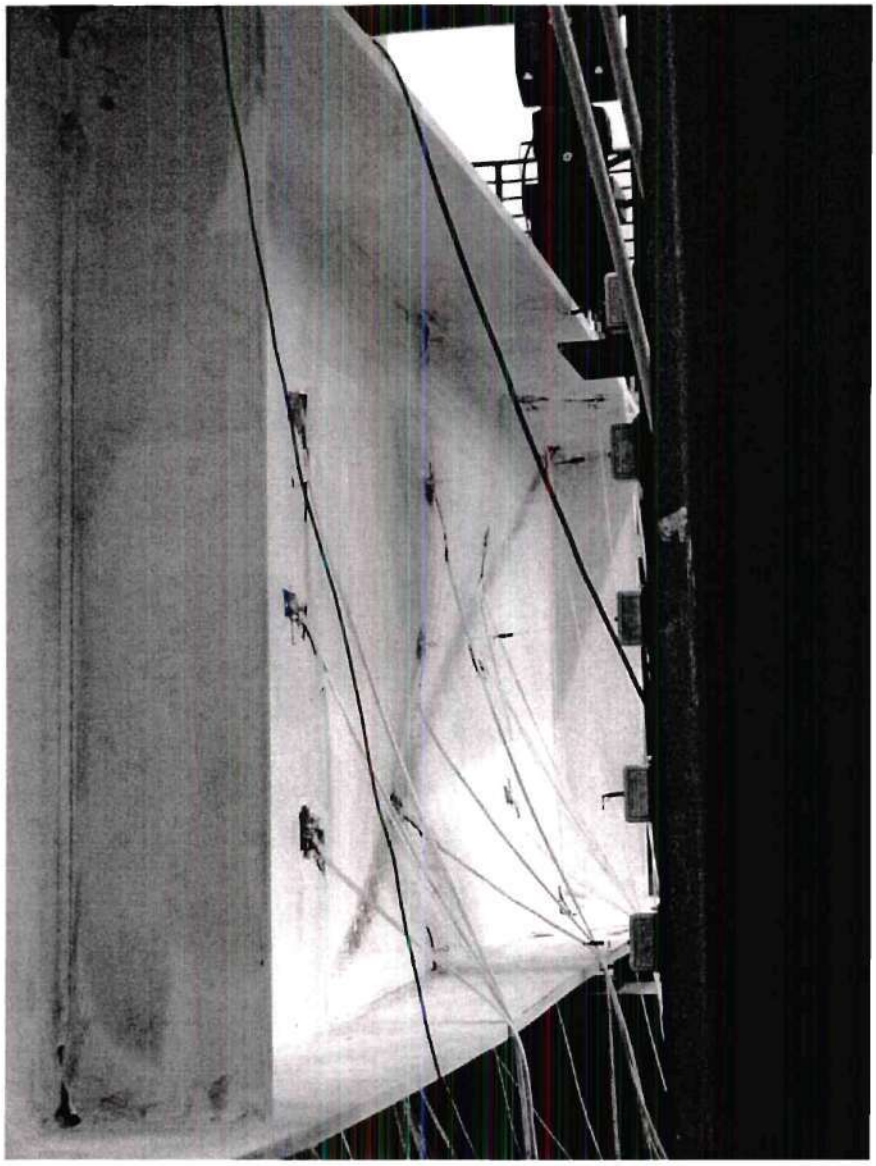

Figure 4.8.1. Web of specimen S1-0.10 at maximum load (view from convex side of location 1).

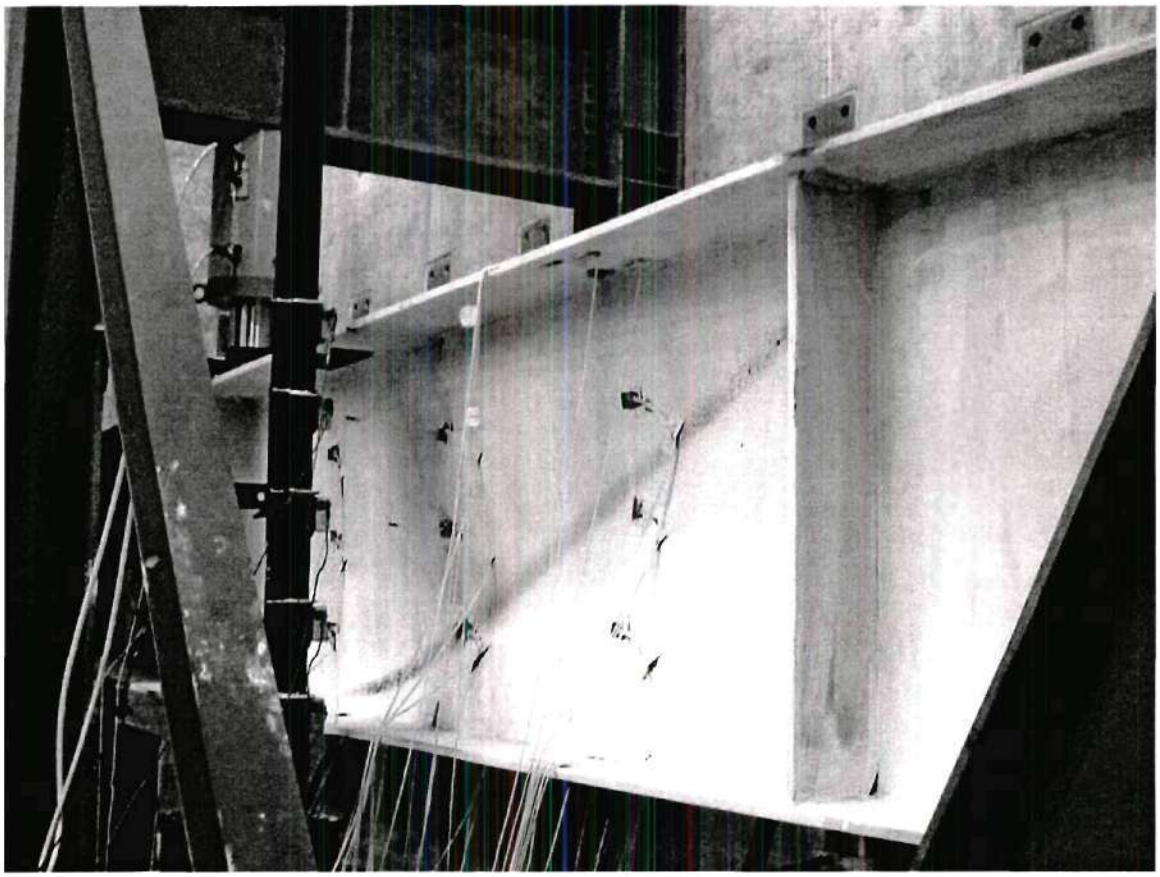

Figure 4.8.2. Specimen S1-0.10 at maximum load (view from convex side of location 4).

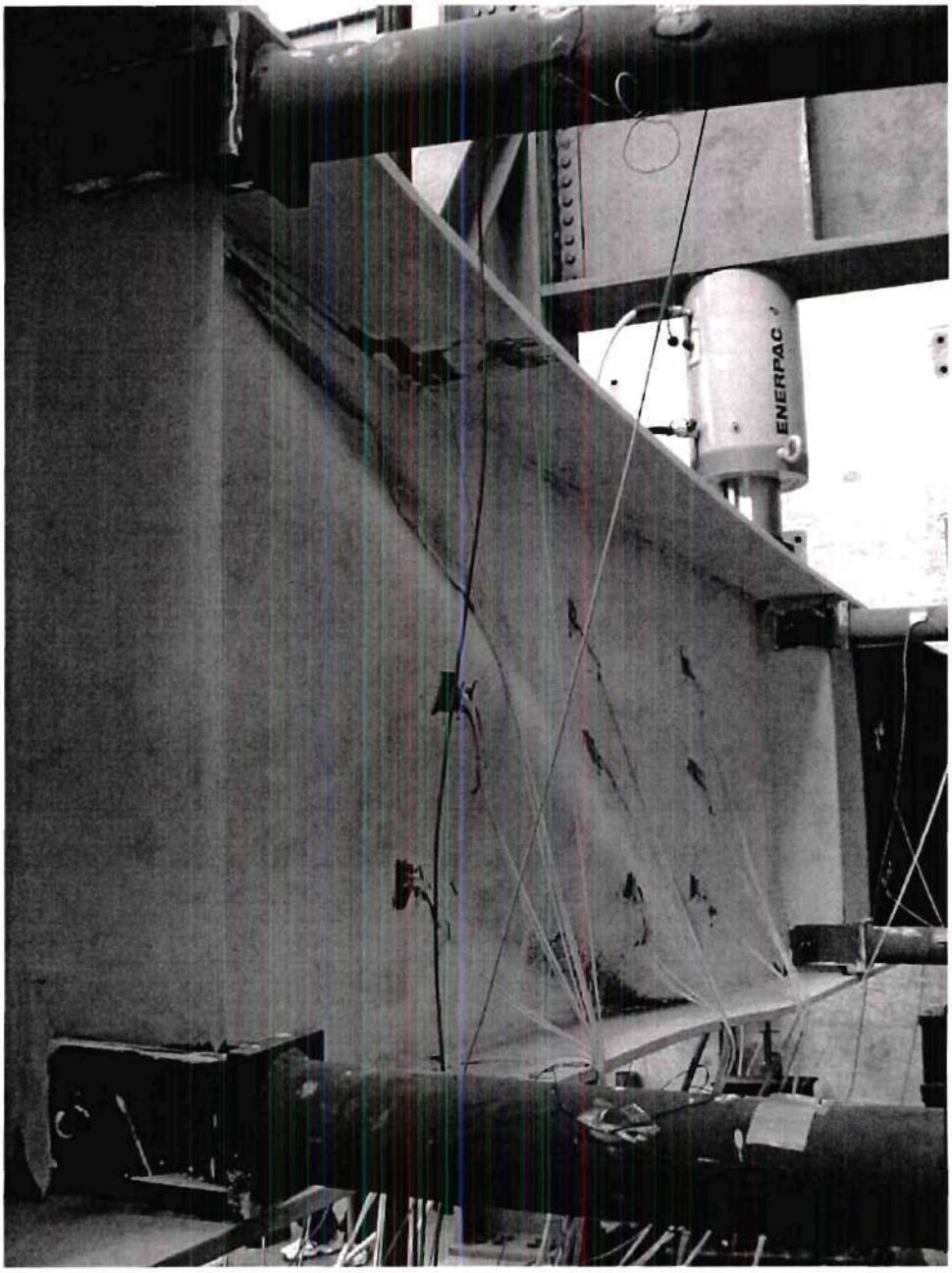

Figure 4.8.3. Specimen S1-0.10 at the end of the test (view from concave side of location 4).

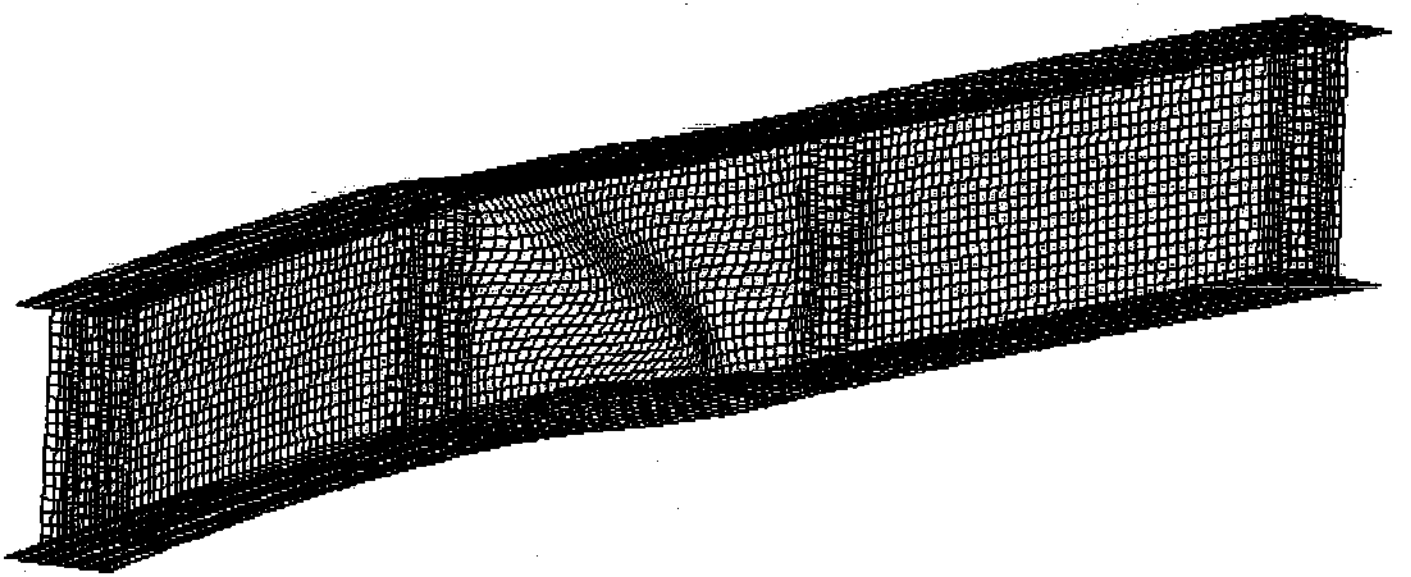

Figure 4.8.4. FEA prediction of specimen S1-0.10 at the end of the test (displacement magnification factor = 6).

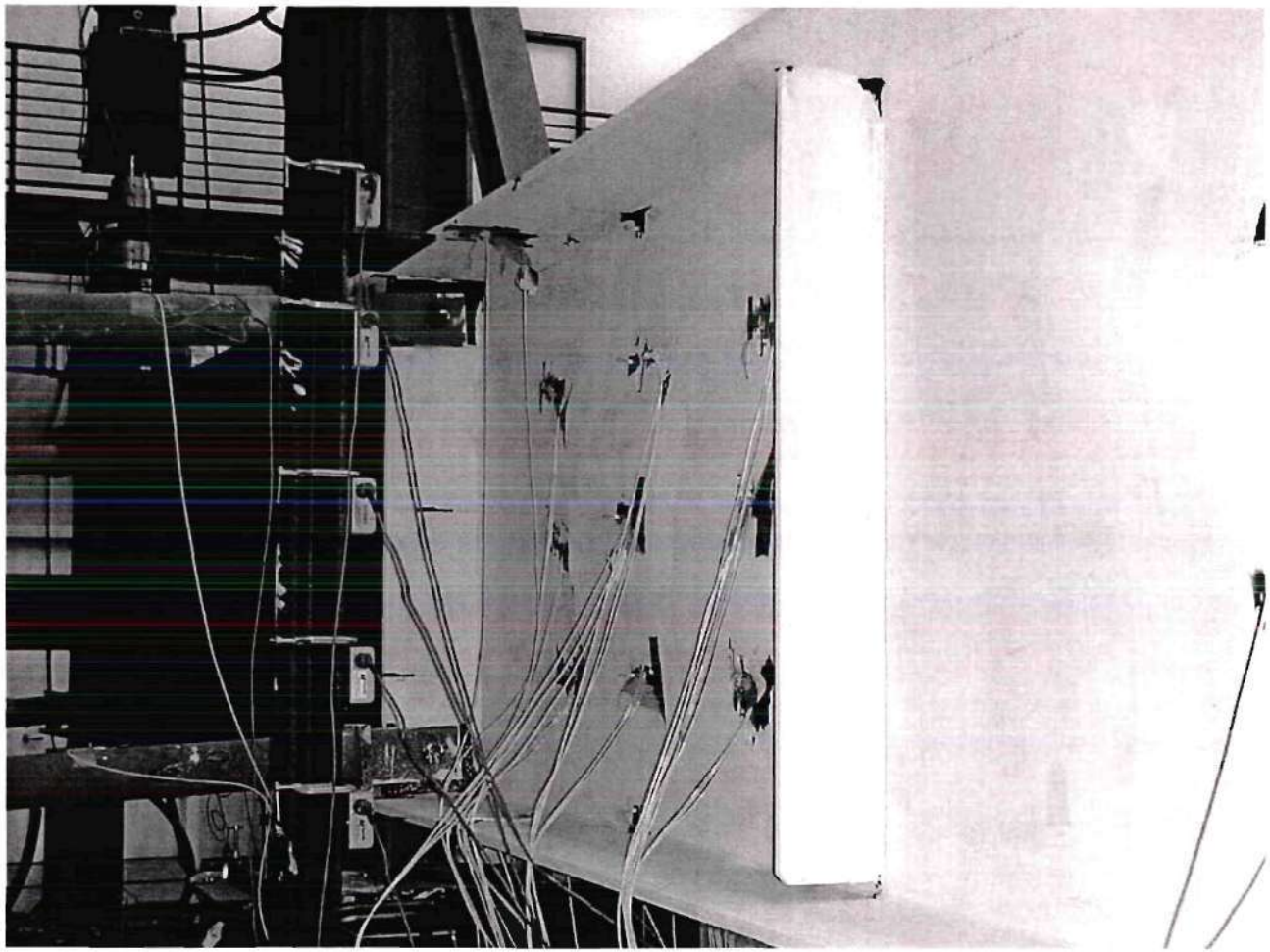

Figure 4.8.5. Specimen S1S-0.10 at maximum load (view from concave side of location 2).

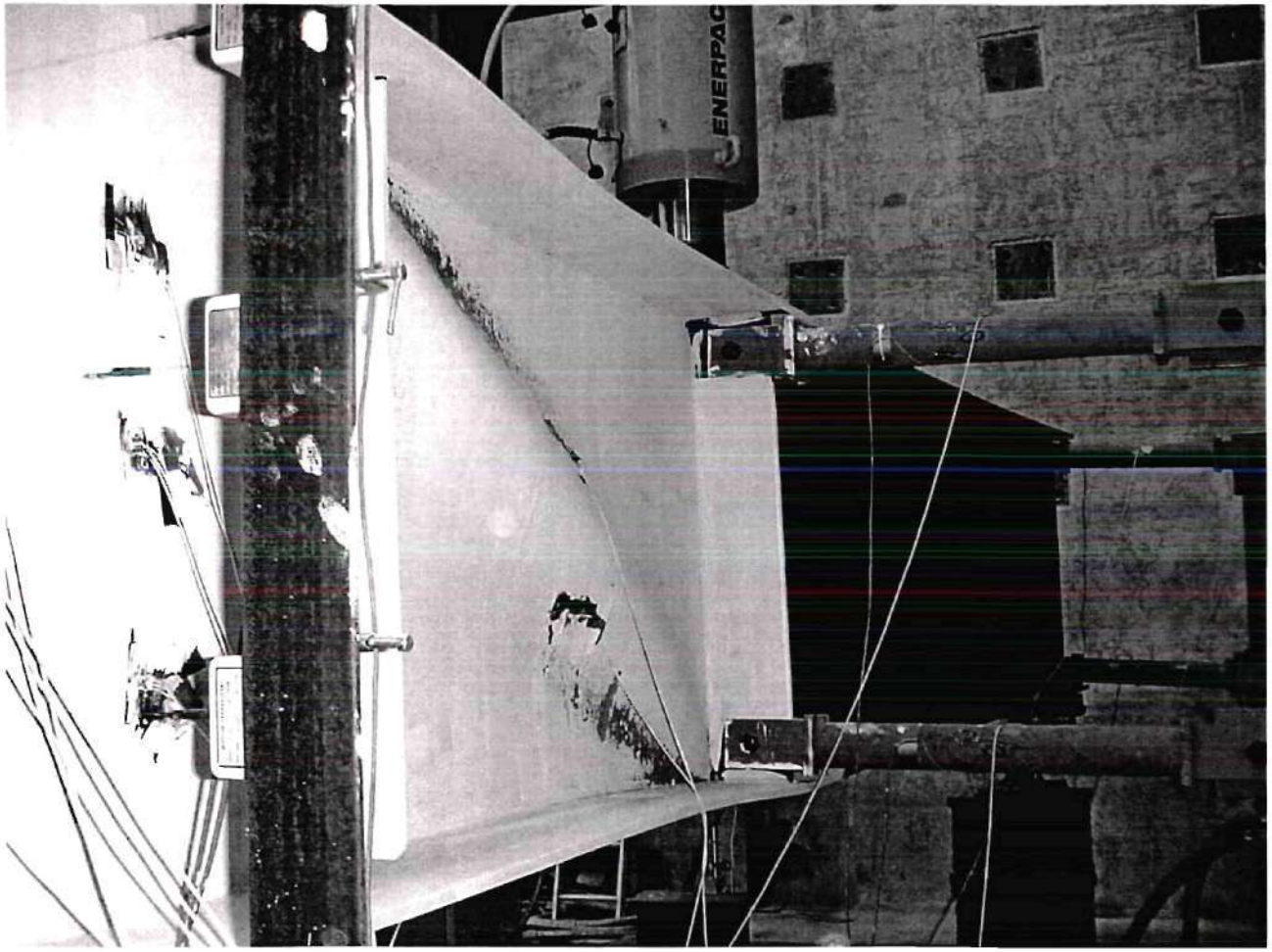

Figure 4.8.6. Specimen S1S-0.10 at the end of the test (view from concave side of location 3).

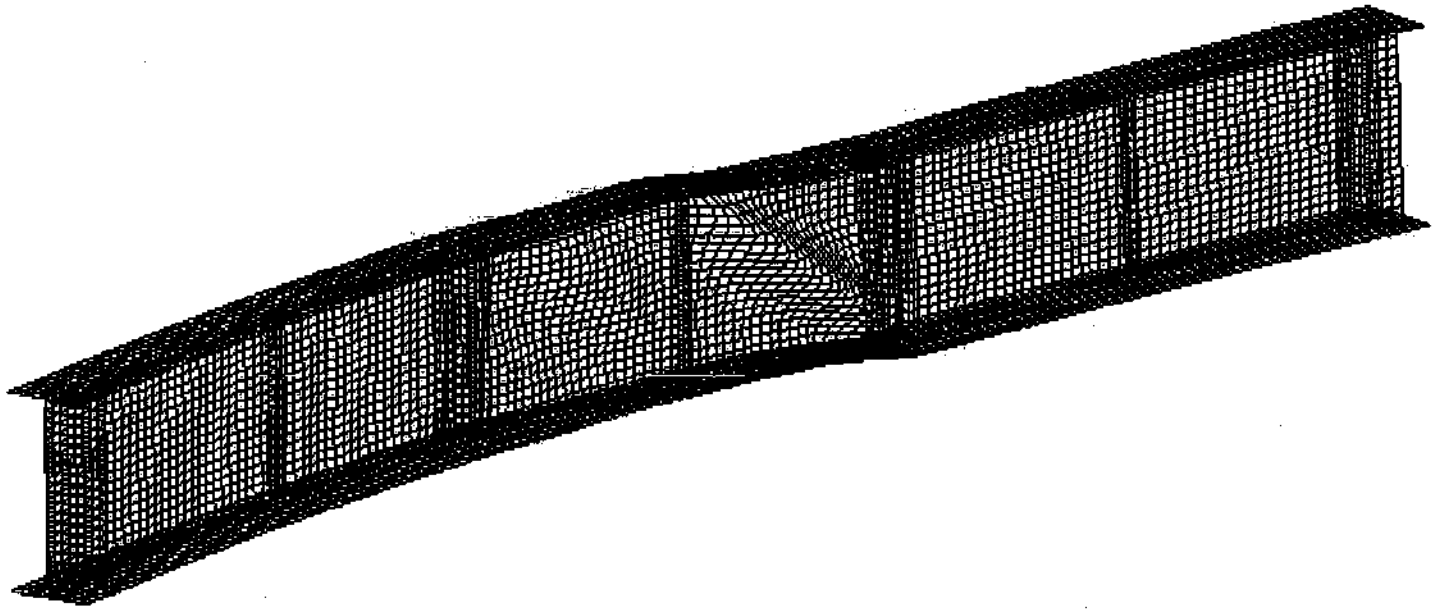

Figure 4.8.7. FEA prediction of specimen S1S-0.10 at the end of the test (displacement magnification factor = 5).

Figure 4.8.10 shows the compression flange of specimen B7 at the maximum load level in this test. As would be expected, since this flange is near the b_f/t_f limit at which the limit state is associated with elastic local flange buckling (based on the idealization of a negative restraint along the web-flange juncture), the flange local buckling distortions are more significant at the maximum load level in this test. However, it appears that the web local buckling distortions are very minor, which indicates that the web is probably not destabilizing the flange at this loading stage, and therefore, the boundary condition assumptions invoked in the development of the flange local buckling design equations are likely to be conservative here (see Section 2.1.1.2). This attribute of the behavior is also evident in the conservative predictions of the one-third rule equations for this problem (see Table 4.4.8). Figure 4.8.9 shows the predicted distortions at the maximum load level in the finite element analysis (with initial geometric imperfections and residual stresses included). Again, the flange local buckling failure mode is evident within the numerical simulation. The maximum predicted vertical displacement at the compression flange tip relative to the web-flange juncture is approximately 8.1 mm (0.32 in) at the maximum load level.

The reader is referred to (Zureick and Kim 2000) and (Hartmann and Wright 2001) for an extensive presentation and discussion of the results of these experimental tests.

4.8.3 Summary

It can be concluded that the failure modes are predicted well by the full nonlinear finite element models in the four examples considered within this section. Furthermore, these examples indicate that the cross-section distortions at maximum load are reasonably small. The web distortions at maximum load are higher in the shear test with $d_o/D = 3$ than in the one with $d_o/D = 1.5$, and the flange distortions are larger in the bending test with $b_f/t_f = 32.5$ versus the test with a flange slenderness of 22.8. However, the flange in test B7 is well beyond the limit of $b_f/t_f = 24$ permitted by the current AASHTO LRFD (2001) straight-girder specification.

The cross-section distortions at the maximum load levels are believed to be similar in magnitude to those commonly observed in tests of straight plate girders. Therefore, the authors do not believe that it is necessary to restrict the maximum load level to reduce the extent of these distortions. The pre-peak nonlinearity associated with these distortions and the development of yielding is minor in both the experimental tests as well as in the finite element predictions. The specimens do not require any large inelastic deformations to develop their vertical bending and shear capacities. At pre-peak loadings only slightly smaller than the maximum load level, the cross-section distortions are much smaller than those observed at peak load capacity. It is believed that the girder distortions under service load conditions can be controlled based on other criteria, for example the implicit restrictions on web distortions via the Daniels et al. (1980) equation (Eq. 2-51) or by limiting the service web stresses to those associated with buckling.

The load-shedding characteristics associated with the post-peak behavior deserve closer scrutiny. This issue is addressed further in Chapter VI.

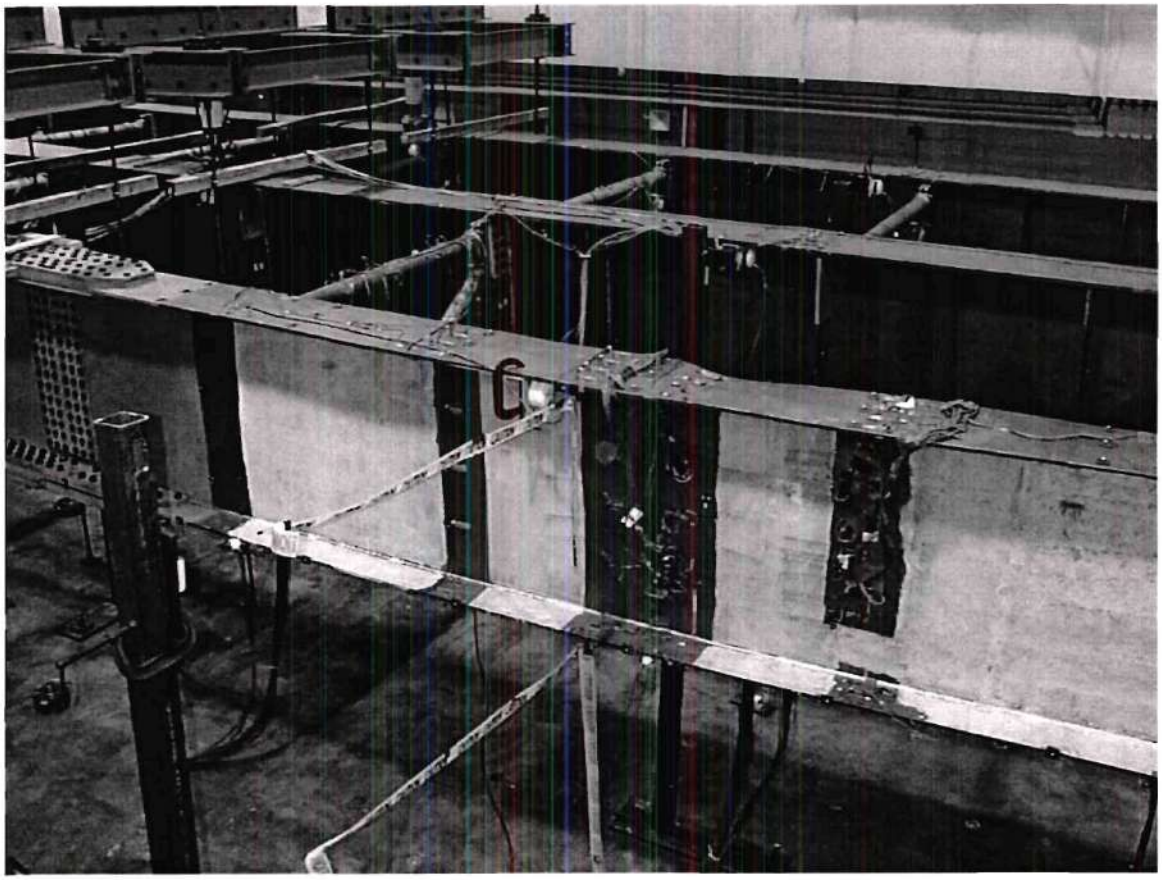

Figure 4.8.8. Test B1 component deformations at maximum load.

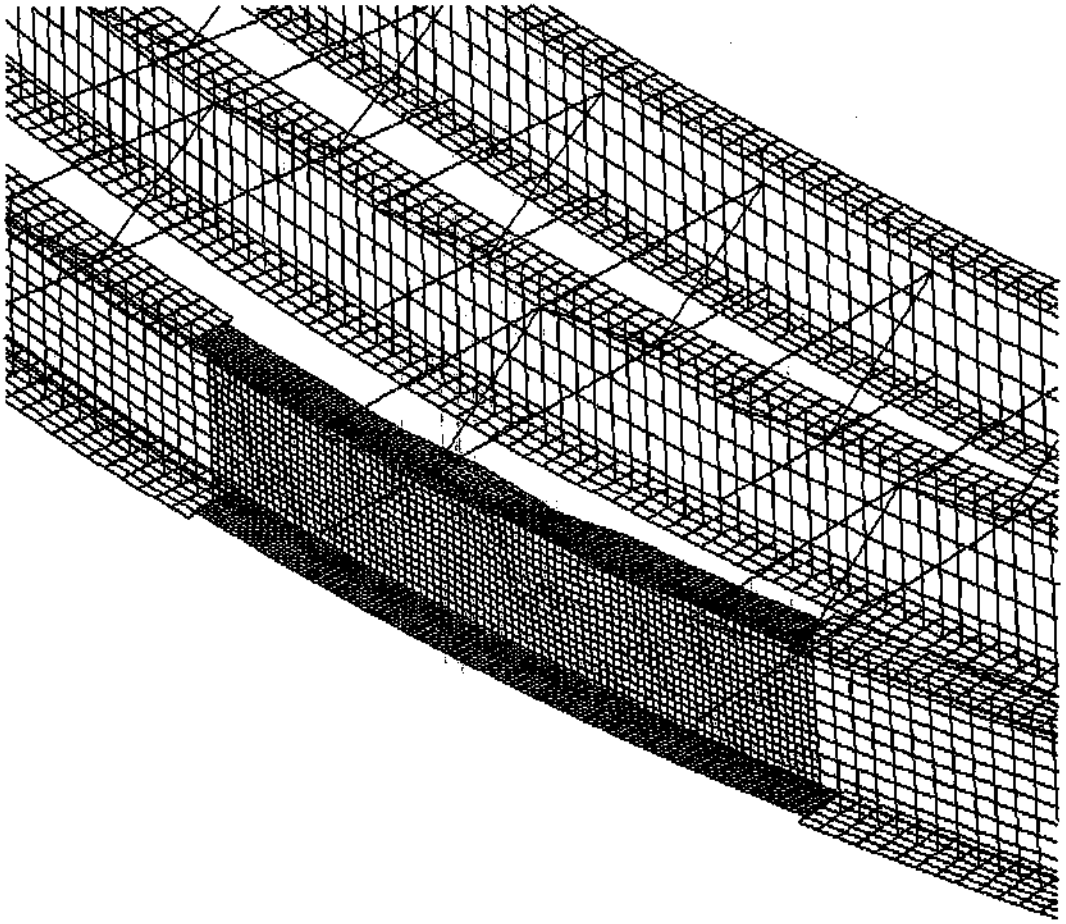

Figure 4.8.9. Test B1 predicted component deformations at maximum load (displacement magnification factor = 2, stiffeners not shown).

Figure 4.8.10. Test B7 component deformations at maximum load.

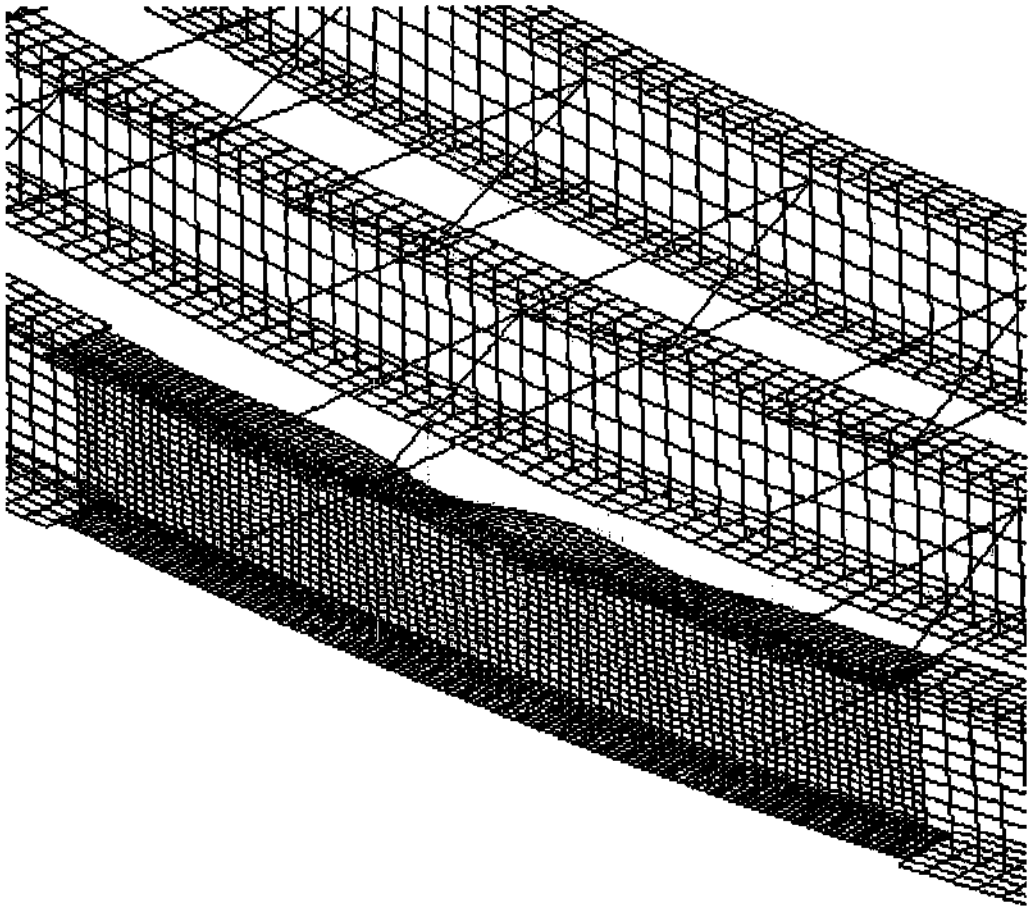

Figure 4.8.11. Test B7 predicted component deformations at maximum load (displacement magnification factor = 2, stiffeners not shown).

Page intentionally left blank

CHAPTER V

DESIGN OF PARAMETRIC STUDIES

5.1 OVERVIEW

This chapter describes the background and basis for the design of the parametric studies conducted in this research. The parametric study specimens are intended to represent a wide range of practical girder geometries and potential boundary conditions.

Unless noted otherwise, all of the parametric study test specimens are single girders with three unbraced segments. The critical test segment is always the one in the middle. The outside segments are designed to ensure that the failure occurs within the middle unsupported length.

Primary Test Suite

The parametric studies are subdivided into several "suites" or "sets." The first set of studies is referred to as the primary suite. These studies are designed to evaluate the behavior of curved steel I girders under uniform vertical bending, maximum V/M, and high shear-high moment, and serve as a base for the subsequent additional parametric study suites. The uniform vertical bending tests of course provide the base for evaluation of the curved girder flexural capacities. These are four-point bending tests in which the loads are applied at one-third and two-thirds of the total length of the girder, and vertical supports are provided at both ends.

The maximum V/M tests are designed to evaluate the shear strength of the curved I girders. In these tests, the vertical supports are located at one end and at two-thirds of the total length from this point, and concentrated loads are applied at the other end and at the other one-third position such that an inflection point occurs at the center of the critical middle unsupported segment. This minimizes the bending moment within the critical unsupported length. This is the loading and support configuration utilized in the physical tests S1-0.10 and S1-S0.10 discussed in Chapter IV.

The high moment-high shear tests are designed to evaluate potential moment-shear interaction. The locations of the vertical supports and the loadings are the same for these tests as in the maximum V/M tests, but the ratio of the two concentrated loads is changed to produce a high moment-to-shear ratio in the critical middle unsupported segment. In these tests, the maximum vertical and lateral flange bending moments occur at one end of the middle unsupported length.

In all of the studies within the primary suite, rigid radial supports are provided such that the web is held in a vertical position at each of the loading and vertical support locations. These boundary conditions are varied in some of the subsequent parametric study suites.

Modified Uniform Vertical Bending Suite

Prior experimental and numerical studies have shown that for curved I girders subjected to uniform vertical bending, the final failure mode evident within the post-peak response is typically a three-hinge mechanism in lateral flange bending. As shown in Fig. 1.1, a common idealized behavior for curved I girders subjected to near uniform vertical bending involves large lateral flange bending moments (M_ℓ) at the cross-frame locations, and M_ℓ values of approximately one-half of these end moments at the middle of the unsupported segment. This is the behavior associated with the V-load equation, Eq. (1-6), and it is a reasonable approximation of the first-order elastic flange lateral bending moments in the above "primary" uniform vertical bending tests (the first-order elastic M_ℓ values at the ends of the critical unbraced segment, calculated by refined finite element analysis, actually tend to be slightly overestimated by the V-load equation in these tests).

Due to potential relative torsional rotations at the cross-frame locations of an actual bridge, the M_ℓ values at the middle of a critical unsupported length can be increased and the moments from the lateral bending restraint at the ends of the segment can be reduced. In this research, it is hypothesized that the vertical bending capacity of a critical unbraced length is reduced the most if the boundary conditions at the ends of this length are such that the second-order elastic M_ℓ values at the cross-frames and at the middle of the segment are approximately equal. The rationale behind this hypothesis is that such a distribution of lateral flange moments eliminates the inelastic redistribution that can occur in lateral bending prior to the development of the final three-hinge failure mechanism in the compression flange.

Based on the above reasoning, a second suite of parametric studies is analyzed and referred to here as the "modified uniform vertical bending" suite. This set of parametric studies involves the same loading and boundary conditions as explained above for the uniform vertical bending tests of the primary suite, except that an outward radial displacement of the top compression flange is specified at the two interior bracing-applied load locations. These outward radial displacements are specified such that the second-order elastic M_ℓ values in the compression flange at incipient first yield are approximately equal at the brace locations and at the center of the critical middle unbraced segment.

Internal Loading Suite

It is possible that internal loadings on the top flange of a critical unbraced segment subjected to near uniform vertical bending may reduce the flexural capacity of the girder due to a load height or tipping effect. Therefore, a third parametric study suite is analyzed in which the same boundary conditions as in the uniform vertical bending tests

of the primary suite are employed, but the girder is loaded by a distributed vertical load over a small length (calculated such that local web yielding or web crippling will not control the strength) at the center of the middle critical unsupported length. This set of studies is referred to as the "internal loading" suite. It is interesting that the flange lateral bending moments (M_ℓ) associated with this loading are approximately the same at the ends and at the middle of the test segment. For larger unsupported lengths, the second-order elastic M_ℓ values at the middle of the test segment tend to be larger than the associated values at the brace points.

Free-End Suite

All of the above parametric study suites consider the strength of an interior unbraced segment within a curved bridge I girder. In a fourth set of studies, referred to as the "free-end" suite, the behavior for an idealized unsupported segment at the simply supported end of a bridge is studied. These are three-point bending tests with rigid radial supports at the ends and at the mid-length of the girder. The nominal (design) strengths of the unsupported lengths on each side of the load point are equally critical.

Laterally Unsupported Straight Girder Suite

The above four sets of parametric studies consider the behavior of curved I girders. To evaluate the behavior of straight girders subjected to both gravity and lateral loads, a fifth suite, referred to as the "laterally unsupported straight girder" suite, is analyzed. In this suite, the test specimens are modeled as straight girders with various lateral-torsional slenderness ratios ($\lambda = L_b/r_t$). The λ values considered correspond to $(\lambda-\lambda_p) / (\lambda_r-\lambda_p) = 0$, 0.25, 0.5, 0.75, and 1.0. That is, the slenderness values span the entire range of L_b/r_t from the compact bracing limit to the brace spacing corresponding to the transition from inelastic to elastic lateral-torsional buckling. The configuration of the loadings and supports for these tests is the same as that of the uniform vertical bending tests of the primary test suite, except that both the top and bottom flanges are subjected to equal specified radial displacements at the internal loading locations.

Unsymmetric Girder Suite

All of the suites of parametric studies described above address only doubly symmetric girders. In the last suite of studies, several singly symmetric I girders are subjected to all of the above test suite loading and displacement boundary conditions. The cross-sections considered are representative of the positive moment region of composite girders prior to the placement of the deck, in which the top compression flange is often smaller than the bottom tension flange.

Chapter Organization

Complete details of the parametric study designs are explained in the following sections. Section 5.2 describes key constant parameters that apply to all of the parametric

studies while Section 5.3 explains details regarding the loading and boundary conditions of the primary test suite. Section 5.4 then discusses the selection of the cross-sections and web panel aspect ratios of the doubly symmetric specimens studied in the primary suite. The same set of cross-sections and panel aspect ratios is employed in all of the first five parametric study sets. Next, Section 5.5 describes the design of the length-related parameters for the primary test suite. These lengths are utilized in each of the first three parametric study sets. In Section 5.6, the design of the end segments of the primary test suite is discussed. The same end segment designs are utilized in all of the studies of the first three test suites. This is followed by Section 5.7, which explains the design of the transverse stiffeners within all of the tests. The specimen geometries of the primary study suite are summarized in Section 5.8. Subsequently, the boundary conditions and loading configurations of the other test suites are described in Sections 5.9 to 5.13. Sections 5.9 and 5.10 explain the modified vertical bending and the internal loading suites, respectively. Then Sections 5.11 and 5.12 describe the free-end and the laterally unsupported straight girder tests. The design of the unsymmetrical girders is presented in Section 5.13.

5.2 CONSTANT PARAMETERS

Key constant parameters specified in this research are as follows:

- All the studies are conducted based on an assumed A572 Grade 50 steel material. The idealized uniaxial stress-strain curve of this material is detailed in Section 3.2.

- A depth of the web of D = 1219 mm (48 in) is selected to establish the cross-section size. This is the same depth as all of the bending specimens tested at the FHWA Turner-Fairbank Laboratory (Zureick et al. 2000; Grubb and Hall 2001).

- One-sided intermediate transverse stiffeners with a width, $b = 0.3b_f$, where b_f is the flange width, are placed on the concave side of the girder. The thickness of the transverse stiffeners is calculated based on the minimum requirements specified in the straight girder AASHTO LRFD Specifications (2001). In some cases, this thickness is increased based on the more restrictive requirements on the stiffness of the transverse stiffeners stated in the Recommended Specifications (Hall and Yoo 1998), to prevent failure of the transverse stiffeners. In all cases, the transverse stiffeners are assumed to be attached to the compression flange and cut short of the tension flange. The design of the transverse stiffeners is explained in more detail in Section 5.7.

- Double-sided bearing stiffeners with $b = 0.4b_f$ on each side of the web are used for all of the girders. The thickness of these stiffeners is calculated as per the minimum requirements specified in the AASHTO LRFD Specifications (2001) for each girder based on the maximum applied load from either the high shear-high moment or maximum V/M loading cases of the primary test suite, whichever controls.

5.3 PRIMARY TEST SUITE

The generic layout and arrangement of the loads and supports for the primary test suite is shown in Fig. 5.3.1. The girder is subdivided into three equal unsupported lengths in this test configuration, with the interior segment (2-3) serving as the test segment. The cross-section of the test segment is extended beyond locations 2 and 3 and into the outside lengths (1-2) and (3-4) by a distance of D/2, where D is the depth of the web. The plates of the cross-section in the outside segments (segments 1-2 and 3-4) are thickened over a portion of the length, and web transverse stiffeners are added to prevent premature failure prior to reaching the maximum strength of the test segment for all of the loading cases considered. The design of the end unsupported lengths (segments 1-2 and 3-4) is described in detail in Section 5.6.

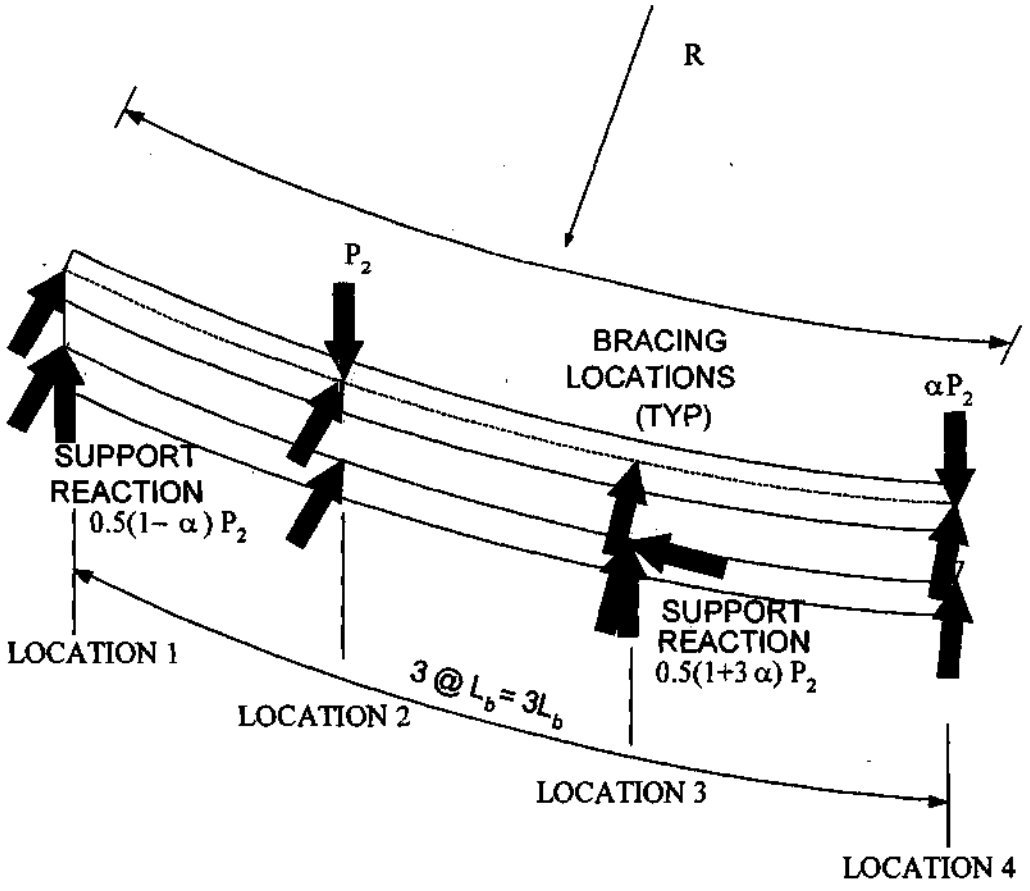

Figure 5.3.1. Configuration for the primary test suite girders.

In all of the studies of the primary test suite, rigid radial braces are provided at the web-flange juncture of both the top and bottom flanges at each loading and support location. This bracing configuration holds the girder web in a vertical position at these locations throughout the test.

The test configuration shown in Fig. 5.3.1 is believed to provide a good base representation of the limit states behavior of a critical unsupported segment of a curved girder, including the restraint provided by the other portions of the bridge. Potential torsional rotations at the cross-frame locations, and other potential boundary conditions on the critical unsupported length are addressed in the subsequent sections of this chapter.

For the maximum V/M and high-shear high-moment tests of the primary suite, vertical loads of P_2 and $P_4 = \alpha P_2$ are applied at locations 2 and 4, and vertical supports are positioned at locations 1 and 3. The shear and bending moment diagrams for the equivalent straight girder, which are for all practical purposes equal to those of the curved girders for the L_b/R values studied (≤ 0.1), are sketched as a function of α in Fig. 5.3.2. By varying the load ratio, $\alpha = P_4/P_2$, a complete range of maximum moment to shear ratios (M_{max}/V) can be developed within the test segment. This is illustrated in Fig. 5.3.3. The parameter α is set to -1 for the pure vertical bending tests, and in this case, the vertical support at location 3 is actually moved to location 4, and the loads are applied at the top of the girder at locations 2 and 3. If the loads are always proportioned such that the maximum moment is located at position 2, then the applicable equation for M_{max}/VL_b (see Fig. 5.3.3) can be rewritten as

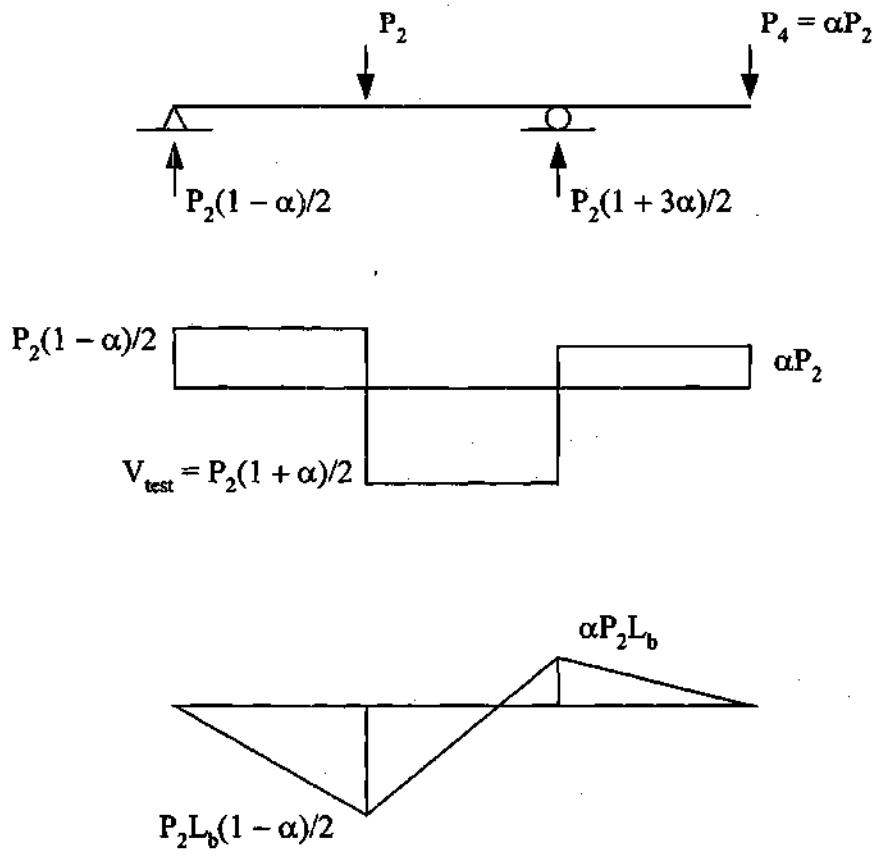

Figure 5.3.2. Shear and moment diagrams for primary test configuration.

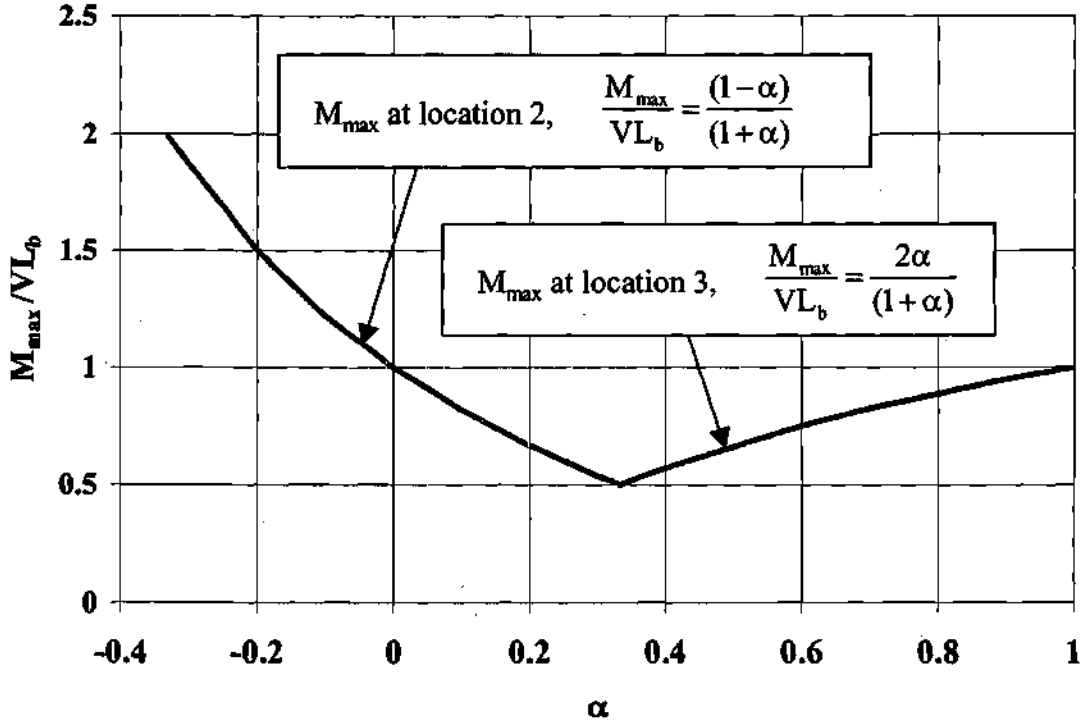

Figure 5.3.3. M/V in the critical middle unsupported segment as a function of α.

$$\alpha = \frac{1 - \frac{M_{max}}{VL_b}}{1 + \frac{M_{max}}{VL_b}} \qquad (5\text{-}1)$$

It should be noted that the ratio M_{max}/VL_b in this equation is the fraction of the unsupported length from the maximum moment location to the inflection point within the test segment, assuming that $M_{max}/VL_b \leq 1.0$. When M_{max}/VL_b is greater than one, all the moments within the test segment are of the same sign, i.e., there is no moment reversal within the critical unsupported length.

The loading cases considered within the primary test suite are:

- Pure vertical bending ($\alpha = -1$), for determination of the vertical bending capacity, $M_{n(FEA)}$.
- Maximum V/M ($\alpha = 1/3$), for determination of shear capacity, $V_{n(FEA)}$.
- High shear-high moment ($M_{max}/VL_b = M_{n(FEA)}/0.8V_{n(FEA)}L_b$), for determination of potential moment-shear interaction where $M_{n(FEA)}$ is the vertical bending capacity

predicted by the full nonlinear finite element analysis for $\alpha = -1$, and $V_{n(FEA)}$ is the shear capacity predicted for $\alpha = 1/3$.

The loading ratio of $\alpha = 1/3$ creates the lowest possible value of M_{max}/V within the test segment (segment 2-3) (see Fig. 5.3.2). The case of $\alpha = -1$ is a four-point bending test that produces constant vertical bending moment and zero shear within the test panel.

The loading case that produces $M_{max}/VL_b = M_{n(FEA)}/0.8V_{n(FEA)}L_b$ is used to examine the potential moment-shear interaction at combined high moment-high shear levels. There are two important reasons behind the selection of $M/V = M_{n(FEA)}/0.8V_{n(FEA)}$. First, preliminary analyses conducted in this research showed that at the ratio of $M_{max}/V = M_{n(FEA)}/V_{n(FEA)}$, the test specimens often exhibit negligible moment-shear interaction and predominantly fail by web shear buckling. Second, the ratio $M/V = M_{n(FEA)}/0.8V_{n(FEA)}$ gives more emphasis to flexure and accounts for the fact that, in many cases, the moment capacity is significantly increased by moment gradient effects. Also, it accounts for the fact that in many cases, the design shear capacity estimated by the current AASHTO LRFD (2001) equations underestimates the actual girder shear capacity (see Section 9.1 and Fig. 9.1.13). The position of the radial loading path given by $M_{n(FEA)}/0.8V_{n(FEA)}$ is shown relative to the current AASHTO LRFD (2001) moment-shear interaction curve with M_n taken as $M_{n(FEA)}$ and V_n as $V_{n(FEA)}$ in Fig. 5.3.4. The reader is referred to Section 2.3 for a summary of the background to the AASHTO moment-shear interaction curve, and for the recommendations from this research regarding moment-shear interaction design checks. In addition to satisfying the constraint $M_{max}/V = M_{n(FEA)}/0.8V_{n(FEA)}$, the value of α in the high-shear high-moment tests is set by the use of Eq. (5-1) such that the largest end moment always occurs at location 2 (see Figs. 5.3.1 and 5.3.2). This equation generally gives an α less than 1/3 (see Fig. 5.3.3).

Analysis results for the primary test suite are summarized in Section 7.1 for the pure vertical bending case, in Chapter VIII for the maximum V/M case, and in Chapter IX for the high moment-high shear case.

5.4 CROSS-SECTION AND PANEL ASPECT RATIO PARAMETERS

A flowchart of the doubly symmetric cross-section and panel aspect ratio parameters considered in this study is shown in Fig. 5.4.1. The key cross-section based design parameters include the web slenderness ($2D_c/t_w = D/t_w$), the flange slenderness (b_f/t_f), and the ratio of the area of the web to the area of the compression flange (A_w/A_f). The ratio of the depth of the web in compression to the total depth of the web (D_c/D), i.e., the test suite of unsymmetric girders, is considered in Section 5.13.

Three values of D/b_f are selected for the study: $D/b_f = 2.25$, 2.75 and 3.25. Three of the six bending specimens tested at the FHWA Turner-Fairbank Laboratory have a ratio of $D/b_f = 2.75$; therefore, this value of D/b_f is selected for most of the studies. Three values of b_f/t_f are studied at this D/b_f ratio: $b_f/t_f = 15$, 20, and 25. Only the value of $b_f/t_f = 25$ is studied for the D/b_f ratios of 2.25 and 3.25. The flange slenderness $b_f/t_f = 25$ is selected in order to test at a slightly more severe flange local buckling condition than

permitted by the existing AASHTO LRFD Specifications (AASHTO 2001). For each of the cases with $D/b_f = 2.25$ and 2.75, three values $2D_c/t_w$ are proposed for study: $2D_c/t_w$ = 100, 130 and 160. However, for a $D/b_f = 3.25$, only $2D_c/t_w = 160$ is considered. This is because typical plate girders with high values of D/b_f tend to have slender webs.

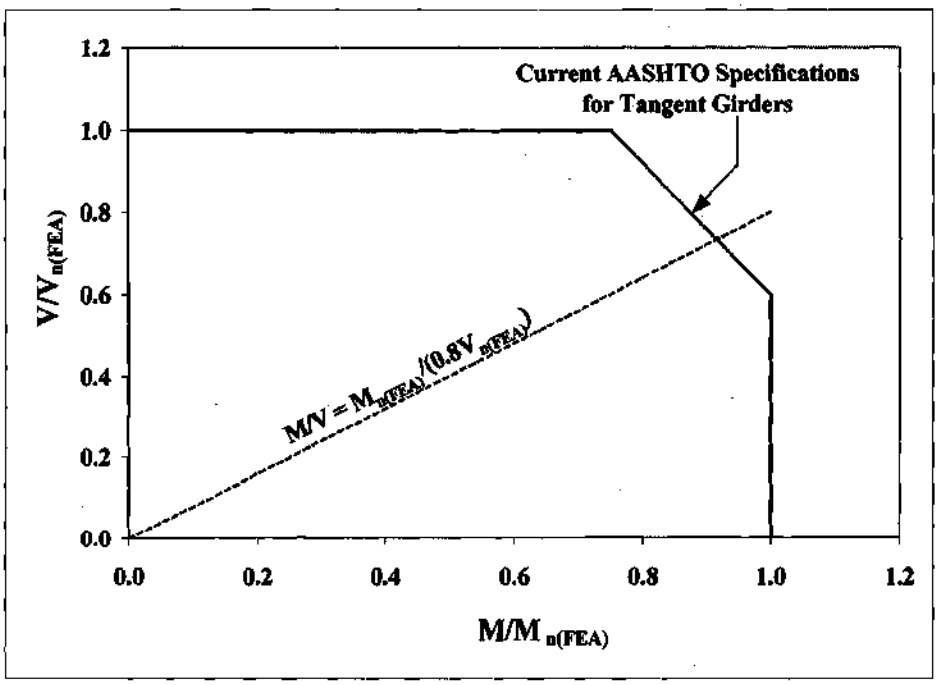

Figure 5.3.4. AASHTO LRFD (2001) moment-shear interaction curve with $M_n = M_{n(FEA)}$ and $V_n = V_{n(FEA)}$ and loading path for $M/V = M_{n(FEA)}/0.8V_{n(FEA)}$.

Although not a cross-section parameter, one additional design variable, the web panel aspect ratio (d_o/D) is also addressed in Fig. 5.4.1. Values of $d_o/D = 1$, 2 and 3 are studied for girders with $2D_c/t_w = 160$, but for girders with $2D_c/t_w = 100$ and 130, only $d_o/D = 3$ is considered (based on the rationale that girders with stockier webs would tend to be designed with wide stiffener spacing, if not as unstiffened). In some cases, the unsupported length needs to be limited to less than that necessary to allow the higher d_o/D values. In these situations, the maximum d_o/D that fits the unsupported length is utilized. Also, when the unsupported length L_b is not a multiple of d_o, the transverse stiffeners are spaced at the specified d_o/D with the exception of the panel adjacent to location 3 (the location of the smaller end moment in the high-shear high-moment tests).

5.5 LENGTH RELATED PARAMETERS

Figure 5.5.1 shows the variation of the two key length-related parameters that are considered in the primary parametric studies for each of the 23 girders specified in Fig.5.4.1. These parameters are the subtended angle between the cross-frame or diaphragm locations (L_b/R), and the target maximum elastic lateral to vertical bending

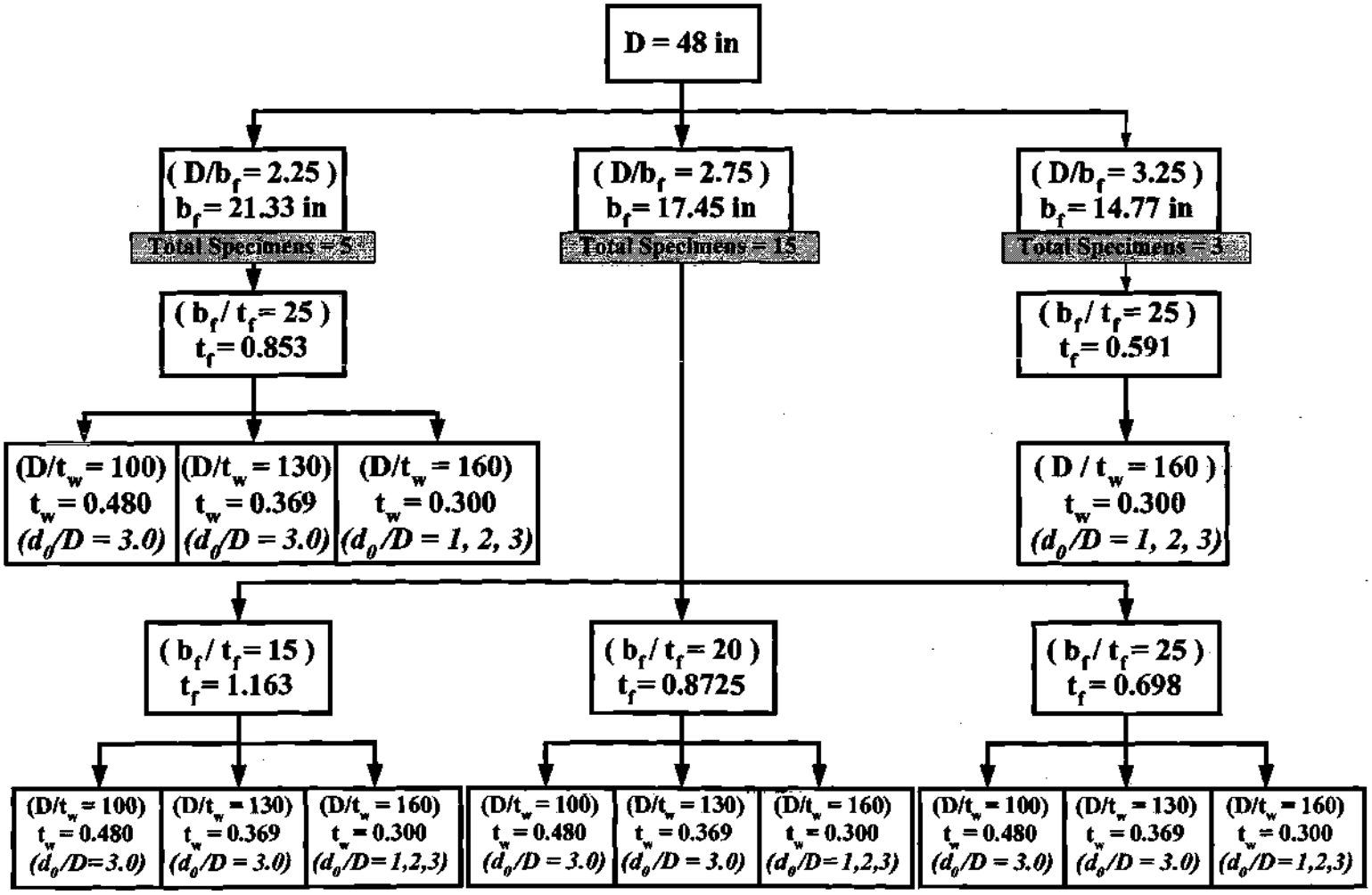

Figure 5.4.1. Cross-section and panel aspect ratio parameters.

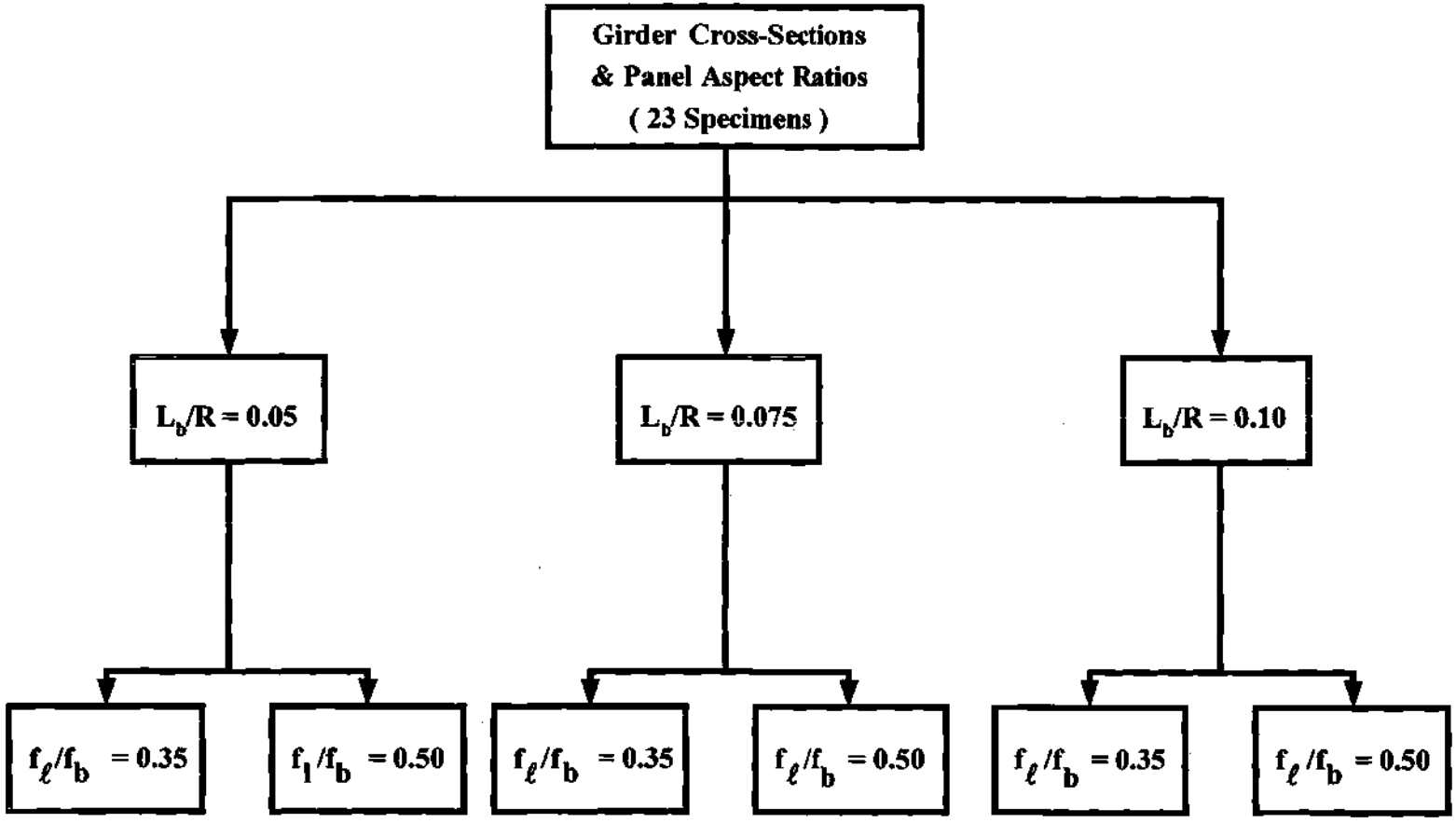

Figure 5.5.1. Length related parameters.

stress ratio (f_ℓ/f_b) in the uniform vertical bending load case of the primary test suite. The uniform vertical bending load case tends to produce the largest f_ℓ/f_b of the three load cases considered in the primary test suite. A total of six sets of girders from Fig. 5.4.1 are generated based on target f_ℓ/f_b values of 0.35 and 0.50 and L_b/R values of 0.05, 0.075 and 0.10. The unsupported length, L_b, is specified for a given L_b/R ratio to achieve approximately the desired f_ℓ/f_b value. The combination of the parameter variations shown in Figs. 5.4.1 and 5.5.1 gives a total of 133 different symmetric I girders to be studied in this research (the total number is less than 23*6=138 because in five of the cases with $D/t_w = 160$, L_b is less than $3d_o$).

The Recommended Specifications (Hall and Yoo 1998) provide the following simple formula, which can be derived using Eqs. (1-2) and (1-5), but with a coefficient of 10 within the denominator rather than 12 in Eq. (1-5), as a guide for preliminary framing:

$$L_b = \sqrt{\frac{5}{36}\left|\frac{f_\ell}{f_b}\right| R b_f} \tag{5-2}$$

where L_b and R are expressed in units of ft and b_f is expressed in units of in. The change from 12 to 10 in the denominator of Eq. (1-6) gives a larger estimate of f_ℓ/f_b, and thus makes the value of L_b associated with a given target f_ℓ/f_b, R and b_f smaller. Equation (5-2) can be written in an alternate form, in terms of the subtended angle between the cross-frames (L_b/R), and assuming consistent units for L_b and b_f, as

$$L_b = \frac{\frac{10}{6}\left|\frac{f_\ell}{f_b}\right| b_f}{L_b/R} \tag{5-3}$$

This equation is used in the design process described above to estimate the required length L_b for a given cross-section determined per Fig. 5.4.1, and a given L_b/R and f_ℓ/f_b specified per Fig. 5.5.1. In most of the designs, the unsupported lengths are selected as a multiple of the girder web depth, 1219 mm (4 ft), close to the value determined by Eq. (5-3). In two girders, L_b is selected as the closest multiple of 610 mm (2 ft).

For a given L_b/b_f and L_b/R, the estimated magnitude of f_ℓ/f_b can be expressed in consistent units using the above equation as

$$\left|\frac{f_\ell}{f_b}\right| = 0.6\frac{L_b}{R}\frac{L_b}{b_f} \tag{5-4}$$

Alternatively, the ratio of the maximum unsupported length to the bridge span length at a particular location of an I girder within a horizontally-curved bridge may be written as

$$\frac{L_b}{L} = \frac{\frac{10}{6}\left|\frac{f_\ell}{f_b}\right|}{\frac{L_b}{R}\frac{L}{D}\frac{D}{b_f}} \tag{5-5}$$

where f_ℓ/f_b is the targeted maximum ratio of the flange lateral bending to vertical bending stress, L is the span length along the girder being considered, and L/D is the span-to-depth ratio. From this equation, it can be observed that in general, the required cross-frame spacing in a horizontally-curved bridge is approximately proportional to the maximum allowed f_ℓ/f_b, and it is an inverse function of the subtended angle between the cross-frames L_b/R, the span-to-depth ratio L/D, and the aspect ratio of the cross-section profile D/b_f. This equation illustrates that there is significant design economy in making the flanges of a horizontally curved I girder as wide as possible for a given girder depth.

Given the value of L_b selected for the uniform vertical bending case ($\alpha = -1$) of the primary test suite (see Fig. 5.3.1), the maximum V/M and high shear-high moment tests of this suite are configured simply by changing the ratio α. In some of the girder designs, i.e., some of the girders with larger L_b, the moments at the ends of the critical segment in the maximum V/M tests are still significant compared to the flexural capacity of the girder. In several of these cases, $M_{n(FEA)}/0.8V_{n(FEA)}L_b$ is smaller than 0.5. That is, the desired length from the maximum moment location to the inflection point in the high shear high-moment test (see the discussion after Eq. (5-1)) is less than $L_b/2$. Of course, this is not physically possible. Therefore, only the uniform vertical bending and maximum V/M tests are analyzed for these girders. Also, if $M_{n(FEA)}/0.8V_{n(FEA)}L_b$ is less than 0.55, there are only minor differences in the loading for the high shear-high moment and maximum V/M load cases. Therefore, the high shear-high moment load case is not considered in general whenever $M_{n(FEA)}/0.8V_{n(FEA)}L_b < 0.55$.

As explained subsequently in the discussion of the parametric study results, of the 133 maximum V/M tests, only eleven fail in a mode that is clearly different than a shear strength limit state (see Chapter VIII). The high shear-high moment loading is also not considered in these eleven girders, since they already are failing in a flexural mode under the maximum V/M load case. Some of the girders tested develop moments well in excess of the yield moment M_y at the ends of the test segment when they fail by shear in the maximum V/M tests. The ranges of unsupported lengths and M_{max}/VL_b ratios considered within the maximum V/M and high shear-high moment tests provide a reasonably comprehensive evaluation of potential moment-shear interaction within horizontally-curved I girders. After the cases with $M_{n(FEA)}/0.8V_{n(FEA)}L_b < 0.55$ and flexural failure in the maximum V/M loading case are eliminated, a total of 101 high-shear high-moment tests remain to be analyzed.

5.6 DESIGN OF END SEGMENTS

Generally, the girders are designed not to fail prematurely outside of the middle test segment. In order to achieve $M_{max}/V = M_{n(FEA)}/0.8V_{n(FEA)}$ for the high moment-high

shear loading case, the load ratio α for some of test specimens must be negative, i.e., an upward force must be applied at location 4. As a result, the maximum moment is produced at location 2 and the magnitude of the shear in the outside unsupported length (1-2) is larger than the shear in the test segment. Therefore, in order to prevent a failure outside of the test segment, the outside panels are strengthened (see Fig. 5.6.1). This is achieved by:

- Increasing the thickness of the web to a value t_{wo} such that $D/t_{wo} = 100$ within a length (L_2) of the outside unsupported segments, as shown by the shaded areas in Fig 5.6.1.

- Increasing the flange thickness within the length L_2 to the value t_{fo} such that the flange slenderness becomes $b_f/t_f = 15$ (for the girders that already have $b_f/t_f = 15$, it is found that the flange sizes do not need to be increased any further).

- Placing transverse stiffeners at a spacing of $d_o = D$ within the outside unsupported segments, such that the shear capacity of the outside web panels is greater than the shear force developed from the applied load.

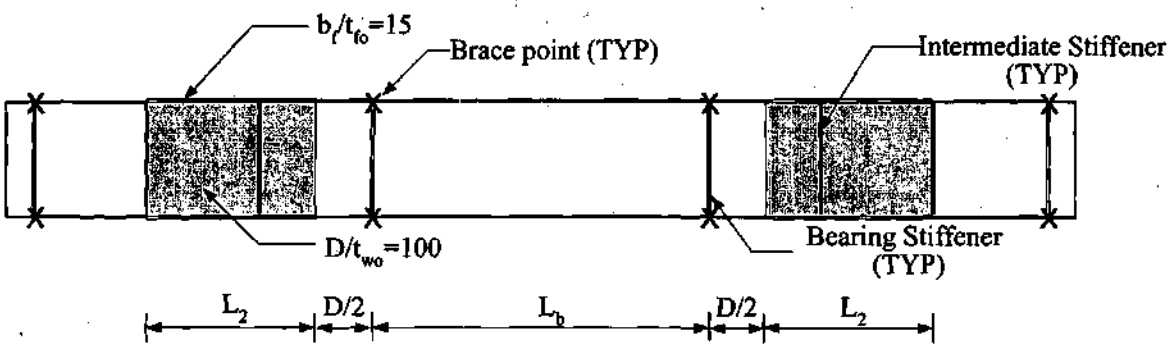

Figure 5.6.1. Strengthening of the outside unsupported segments.

As noted previously, the length L_2 is started at a distance D/2 from the interior bracing locations. In most cases, it is stopped at the stiffener location closest to where the moment is 75 percent of the bending capacity of the prismatic unreinforced outside segment, based on the one-third rule, when the capacity of the test segment is reached in the high-shear high-moment test.

The girder resulting from the above design is utilized also for the uniform vertical bending and for the high-shear low-moment tests. As noted at the end of Section 5.1, this design is also utilized for the modified uniform vertical bending and internal loading test suites. Details of the cross-section plate lengths and thicknesses for the primary parametric study girders are summarized in Appendix F.

5.7 DESIGN OF TRANSVERSE STIFFENERS

The transverse stiffeners must be designed to be sufficiently rigid such that their out-of-plane deformations due to web bending associated with the horizontal curvature and due to any web stability behavior are negligible. Also, they must be designed for their role as anchors in the development of diagonal tension within the web. In this work, the AASHTO LRFD (2001) provisions are used initially to size the transverse stiffeners. Given the constant stiffener widths of $0.3b_f$ as specified in Section 5.2 (which satisfy the AASHTO requirements), the minimum stiffener thickness that satisfies the AASHTO LRFD strength and stiffness requirements is calculated.

In some of the test specimens, the transverse stiffeners designed on this basis fail before the test specimen reaches its peak load. That is, the failure mode includes significant bending of the transverse stiffeners. The transverse stiffeners in these girders are redesigned based on the more restrictive stiffness requirements for curved web panels given in the Recommended Specifications (Hall and Yoo 1998), which are based on the research by Mariani et al. (1973). The Recommended Specification requirements account for bending of the transverse stiffeners due to the radial loading associated with the tendency of the curved web to bow away from its center of curvature. The transverse stiffener dimensions for all the parametric study girders are summarized in Appendix G. The cases that are not adequate based on the AASHTO LRFD straight-girder criteria are indicated there. It can be observed that the transverse stiffeners sized based on the AASHTO (2001) criteria are adequate in all of the girders with $L_b/R = 0.05$ and 0.075.

5.8 GIRDER DESIGN SUMMARY

Figure 5.8.1 shows an example of one of the parametric test specimens with a "long" unsupported length. This specimen is designed with a cross-section aspect ratio $D/b_f = 2.75$, a flange slenderness ratio $b_f/t_f = 25$, a panel aspect ratio $d_o/D = 3$, a subtended angle between the cross-frame locations $L_b/R = 0.05$, and a target $f_\ell/f_b = 0.50$. The web plate of the test panel for this specimen is 7.62 mm (0.3 in) thick while the flange plates are 17.7 mm (0.698 in) thick and 443.2 mm (17.45 in) wide for both the top and bottom flanges. The combination of $L_b/R = 0.05$ and $f_\ell/f_b = 0.50$ results in the longest unsupported length L_b for a given cross-section. This girder has an unsupported length of 7.315 m (24 ft). The test cross-section is extended beyond the two middle bearing stiffeners by a distance of D/2, where D is the depth of the web. The outside segments are reinforced by increasing the web and flange thickness over a length of 4.267 m (14 ft) on each side of the test section. This length is shaded within the figure and is labeled as region B. Within region A of the outside unsupported lengths, the girder has the same cross-section as the critical middle unsupported test segment. The label 2.75-25-25-160-3-0.05-0.50 is utilized to refer to this girder; the numerical values in the label correspond to D/b_f-b_f/t_f-D/t_w-d_o/D-L_b/R-f_ℓ/f_b. This format is employed for identifying the different primary study girders throughout the discussion of the parametric studies.

Figure 5.8.2 shows another example test specimen with a "short" unsupported length. This specimen is designed for a cross-section aspect ratio $D/b_f = 3.25$, a flange

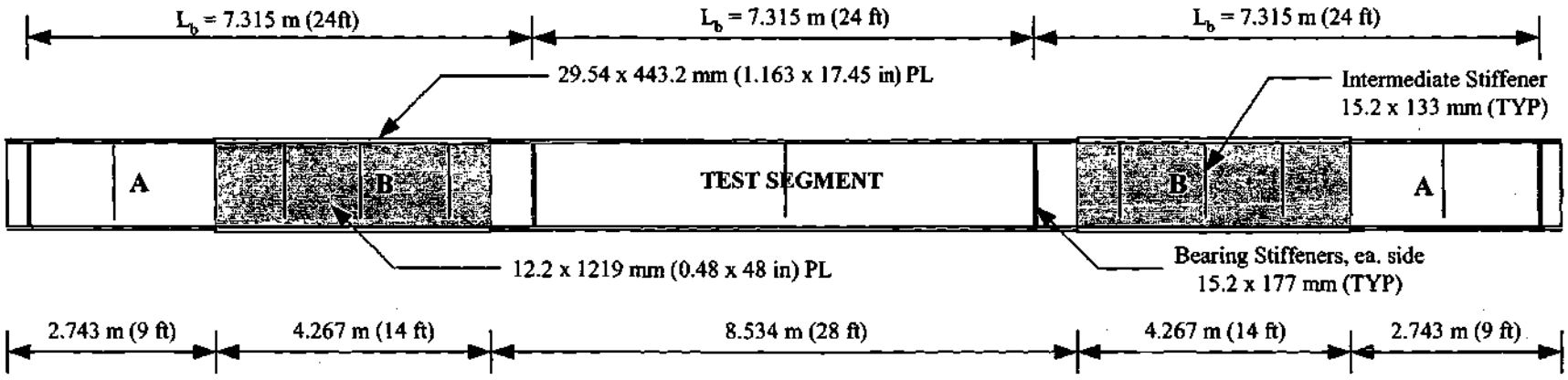

TEST SEGMENT

17.7 x 443.2 mm (0.698 x 17.45 in) Flanges ($b_f/t_f = 25$)

7.62 x 1219 mm (0.3 x 48 in) Web ($D/t_w = 160$)

Figure 5.8.1. Specimen 2.75-25-160-3-0.05-0.50.

slenderness ratio $b_f/t_f = 25$, a panel aspect ratio $d_o/D = 2$, a subtended angle between the cross-frame locations $L_b/R = 0.10$, and a target $f_\ell/f_b = 0.35$. The web plate of the test panel for this specimen is 7.62 mm (0.3 in) thick while the flange plates are 15.0 mm (0.591 in) thick and 375 mm (14.77 in) wide for both the top and bottom flanges. The combination of $L_b/R = 0.10$ and $f_\ell/f_b = 0.35$, along with a $D/b_f = 3.25$ results in the shortest unsupported length of all the specimens considered in this research. This girder has an unsupported length of 2.438 m (8 ft). The outside segments in this girder are reinforced by increasing the web and flange thickness over a length of $L_2 = 1.219$ m (4 ft) on each side of the test section. One additional transverse stiffener is placed at the center of the outside unsupported lengths, and the length L_2 is stopped at the middle of the outermost web panel in this case.

The designs of the critical middle test segment for all the primary parametric study girders are summarized in Tables 5.8.1 to 5.8.5. The additional details regarding the cross-section plate lengths and thicknesses for the reinforced outside segments of these girders are tabulated in Appendix F.

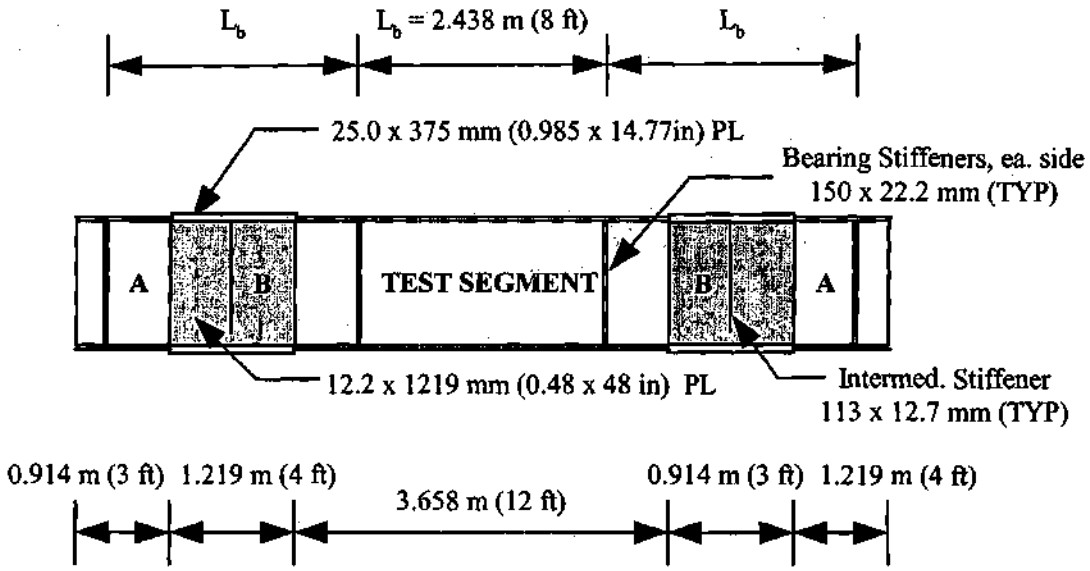

TEST SEGMENT

15.0 x 375 mm (0.591 x 14.77 in) Flanges ($b_f/t_f = 25$)

7.62 x 1219 mm (0.3 x 48 in) Web ($D/t_w = 160$)

Figure 5.8.2. Specimen 3.25-25-160-2-0.10-0.35.

Table 5.8.1. Design summary for girders with $D/b_f = 2.25$ and $b_f/t_f = 25$.

D/t_w	t_w	t_f/t_w	d_o/D	$(2D_ct_w)/(b_ft_f)$	D = 1219 mm (48 in), b_f = 541.8 mm (21.33 in), t_f = 21.7 mm (0.853 in)					
					$L_b/R = 0.05$		$L_b/R = 0.075$		$L_b/R = 0.10$	
					target f_t/f_b		target f_t/f_b		target f_t/f_b	
					0.35	0.50	0.35	0.50	0.35	0.50
100	12.2 mm (0.48 in)	1.78	3	1.27	L_b=6.1 m (20 ft)	L_b=9.8 m (32 ft)	L_b=4.9 m (16 ft)	L_b=6.1 m (20 ft)	L_b=3.7 m (12 ft)	L_b=4.9 m (16 ft)
130	9.38 mm (0.369 in)	2.31	3	0.97	R=122 m (400 ft)	R=195 m (640 ft)	R=64.9 m (213 ft)	R=81.4 m (267 ft)	R=36.6 m (120 ft)	R=48.8 m (160 ft)
160	7.62 mm (0.3 in)	2.84	1	0.79	L_b/b_f =11.3	L_b/b_f =18.0	L_b/b_f = 9.0	L_b/b_f =11.3	L_b/b_f =6.75	L_b/b_f =9.0
			2							
			3							

Table 5.8.2. Design summary for girders with $D/b_f = 2.75$ and $b_f/t_f = 15$.

D/t_w	t_w	t_f/t_w	d_o/D	$(2D_ct_w)/(b_ft_f)$	D = 1219 mm.(48 in), b_f = 443.2 mm (17.45 in), t_f = 29.54 mm (1.163 in)					
					$L_b/R = 0.05$		$L_b/R = 0.075$		$L_b/R = 0.10$	
					target f_ℓ/f_b		target f_ℓ/f_b		target f_ℓ/f_b	
					0.35	0.50	0.35	0.50	0.35	0.50
100	12.2 mm (0.48 in)	2.42	3[1]	1.13	L_b=4.9 m (16 ft)	L_b=7.3 m (24 ft)	L_b=3.7 m (12 ft)	L_b=4.9 m (16 ft)	L_b=2.4 m (8 ft)	L_b=3.7 m (12 ft)
130	9.38 mm (0.369 in)	3.15	3[1]	0.87	R=97.6 m (320 ft)	R=146 m (480 ft)	R=49 m (160 ft)	R=65 m (213 ft)	R=24 m (80 ft)	R=37 m (120 ft)
160	7.62 mm (0.3 in)	3.88	1	0.71	L_b/b_f =11.0	L_b/b_f =16.5	L_b/b_f = 8.3	L_b/b_f =11.0	L_b/b_f =5.5	L_b/b_f =8.3
			2							
			3[2]							

[1] $d_o/D = 2$ for $L_b/R = 0.10$ and target $f_\ell/f_b = 0.35$, since $L_b/D = 2$.

[2] NA for $L_b/R = 0.10$ and target $f_\ell/f_b = 0.35$, since $L_b/D = 2$.

Table 5.8.3. Design summary for girders with $D/b_f = 2.75$ and $b_f/t_f = 20$.

D/t_w	t_w	t_f/t_w	d_o/D	$(2D_ct_w)/(b_ft_f)$	D = 1219 mm (48 in), b_f = 443.2 mm (17.45 in), t_f = 22.2 mm (0.8725 in)					
					$L_b/R = 0.05$		$L_b/R = 0.075$		$L_b/R = 0.10$	
					target f_ℓ/f_b		target f_ℓ/f_b		target f_ℓ/f_b	
					0.35	0.50	0.35	0.50	0.35	0.50
100	12.2 mm (0.48 in)	1.82	3[1]	1.51	L_b=4.9 m (16 ft)	L_b=7.3 m (24 ft)	L_b=3.7 m (12 ft)	L_b=4.9 m (16 ft)	L_b=2.4 m (8 ft)	L_b=3.7 m (12 ft)
130	9.38 mm (0.369 in)	2.36	3[1]	1.16	R=97.5 m (320 ft)	R=146 m (480 ft)	R=48.8 m (160 ft)	R=64.9 m (213 ft)	R=24.4 m (80 ft)	R=36.6 m (120 ft)
160	7.62 mm (0.3 in)	2.91	1	0.95	L_b/b_f =11.0	L_b/b_f =16.5	L_b/b_f = 8.3	L_b/b_f =11.0	L_b/b_f =5.5	L_b/b_f =8.3
			2							
			3[2]							

[1] $d_o/D = 2$ for $L_b/R = 0.10$ and target $f_\ell/f_b = 0.35$, since $L_b/D = 2$.

[2] NA for $L_b/R = 0.10$ and target $f_\ell/f_b = 0.35$, since $L_b/D = 2$.

Table 5.8.4. Design summary for girders with $D/b_f = 2.75$ and $b_f/t_f = 25$.

D/t_w	t_w	t_f/t_w	d_o/D	$(2D_ct_w)/(b_ft_f)$	D = 1219 mm (48 in), b_f = 443.2 mm (17.45 in), t_f = 17.7 mm (0.698 in)					
					$L_b/R = 0.05$		$L_b/R = 0.075$		$L_b/R = 0.10$	
					target f_ℓ/f_b		target f_ℓ/f_b		target f_ℓ/f_b	
					0.35	0.50	0.35	0.50	0.35	0.50
100	12.2 mm (0.48 in)	1.45	3[1]	1.89	L_b=4.9 m (16 ft)	L_b=7.3 m (24 ft)	L_b=3.7 m (12 ft)	L_b=4.9 m (16 ft)	L_b=2.4 m (8 ft)	L_b=3.7 m (12 ft)
130	9.38 mm (0.369 in)	1.89	3[1]	1.45	R=98 m (320 ft)	R=146 m (480 ft)	R=49 m (160 ft)	R=65 m (213 ft)	R=24 m (80 ft)	R=37 m (120 ft)
160	7.62 mm (0.3 in)	2.33	1	1.18	L_b/b_f =11.0	L_b/b_f =16.5	L_b/b_f = 8.3	L_b/b_f =11.0	L_b/b_f =5.5	L_b/b_f =8.3
			2							
			3[2]							

(1) $d_o/D = 2$ for $L_b/R = 0.10$ and target $f_\ell/f_b = 0.35$, since $L_b/D = 2$.

(2) NA for $L_b/R = 0.10$ and target $f_\ell/f_b = 0.35$, since $L_b/D = 2$

Table 5.8.5. Design summary for girders with $D/b_f = 3.25$ and $b_f/t_f = 25$.

D/t_w	t_w (mm.)	t_f/t_w	d_o/D	$(2D_ct_w)/(b_ft_f)$	D = 1219 mm (48 in), b_f = 375.2 mm (14.77 in), t_f = 15.0 mm (0.591 in)					
					$L_b/R = 0.05$		$L_b/R = 0.075$		$L_b/R = 0.10$	
					target f_t/f_b		target f_t/f_b		target f_t/f_b	
					0.35	0.50	0.35	0.50	0.35	0.50
160	7.62 mm (0.3 in)	1.97	1	1.65	L_b=3.7 m (12 ft)	L_b=6.1 m (20 ft)	L_b=3.0 m (10 ft)	L_b=3.7 m (12 ft)	L_b=2.4 m (8 ft)	L_b=3.7 m (12 ft)
			2		R=73.2 m (240 ft)	R=122 m (400 ft)	R=40.5 m (133 ft)	R=48.8 m (160 ft)	R=24.4 m (80 ft)	R=36.6 m (120 ft)
			3[2]		L_b/b_f =9.7	L_b/b_f =16.2	L_b/b_f = 8.1	L_b/b_f =9.7	L_b/b_f =6.5	L_b/b_f =9.7

[2] NA for $L_b/R = 0.075$ and 0.10 with target $f_t/f_b = 0.35$, since $L_b/D = 2.5$ and 2.

5.9 MODIFIED UNIFORM VERTICAL BENDING SUITE

The modified uniform vertical bending suite is designed to consider the potential relative torsional movement between cross-frames within a bridge. This can be achieved by subjecting the compression flange to a specified lateral displacement in addition to the vertical loads at the middle cross-frame locations 2 and 3, as shown in Fig. 5.9.1. Results from the uniform vertical bending case of the primary test suite show that lateral bending stresses in the compression flanges at the cross-frame locations are higher than those at the middle of the test segment. However, at a certain magnitude of the specified lateral displacements in the modified vertical bending test concept, the maximum elastic lateral flange bending moment and f_b+f_ℓ occurs at the middle of the test segment. This is because the specified radial movements at locations 2 and 3 introduce approximately uniform lateral flange bending into the compression flange of the test segment. These moments increase the total lateral flange bending stresses at the middle of the test segment (see Fig 5.9.2). In contrast, they reduce the total lateral flange bending stresses at the cross-frame locations

Two representative sets of test specimens are considered in the modified uniform vertical bending suite: $L_b/R = 0.05$ and 0.10, both with L_b based on a target $f_\ell/f_b = 0.50$ in the uniform vertical bending load case of the primary test suite. An outward radial displacement of the top compression flange is specified at the two interior bracing-applied loading locations. The magnitude of this displacement is set such that the second-order elastic M_ℓ values in the compression flange (and the corresponding maximum elastic stresses $f_b + f_\ell$) are approximately equal at the brace locations and at the center of the critical middle unbraced segment at incipient first yielding. Table 5.9.1 summarizes the specified radial displacements applied to the compression flange at locations 2 and 3.

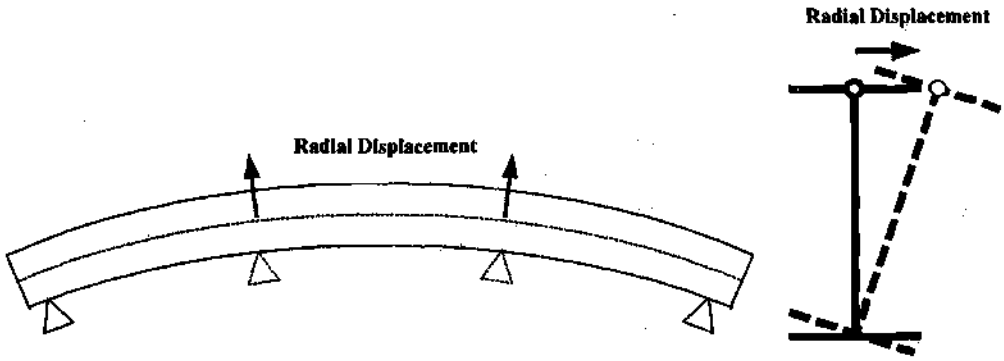

Figure 5.9.1. Application of radial displacements in the modified uniform vertical bending tests.

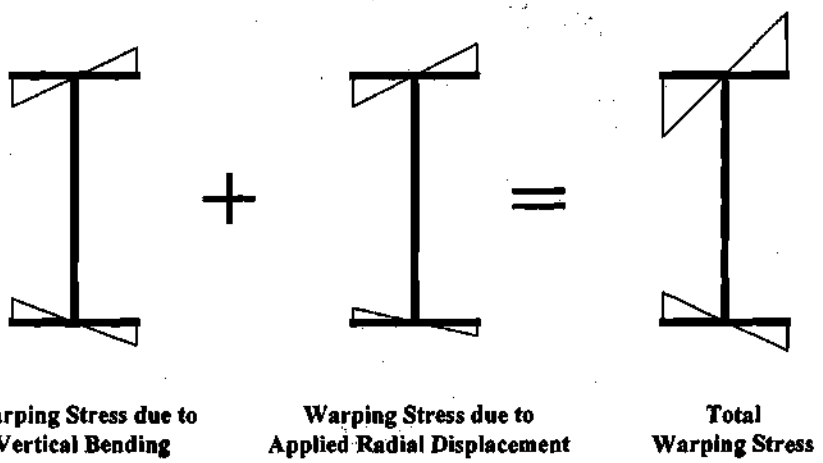

Figure 5.9.2. Effect of radial displacements on flange lateral bending stresses at the middle of the test segment.

The above radial displacements are imposed within the finite element model during the first step of the analysis. The vertical loadings are subsequently applied while the radial displacements at locations 2 and 3 are held constant at their specified values. The rationale for this loading protocol is as follows. Typically, if a critical outside curved girder unsupported segment fails, the entire bridge cross-section would tend to rotate due to this failure. This of course will tend to reduce the amount of restraint provided by the cross-frames at the ends of the critical unsupported length. However, in the vicinity of the maximum load level, the deformations within the critical segment will tend to grow at a faster rate than the overall bridge deformations. As a result, significant end restraint will still be provided to the critical segment. This restraint is of course less than if the girder web were held vertical at the cross-frame locations.

It is believed that these boundary conditions within a hypothetical bridge are represented sufficiently (in the modified uniform vertical bending model) by imposing the radial flange displacement first, followed by application of the vertical loads. As noted above, this displacement is specified such that, at incipient yielding, the lateral bending moments M_ℓ (and the maximum second-order elastic stresses $f_b + f_\ell$) are approximately equal at the cross-frames and at the mid-length of the critical unsupported segment. This tends to produce a "near worst-case" prediction of the load capacity and the load-displacement response, since it eliminates any inelastic redistribution in the top compression flange prior to formation of a three-hinge mechanism in flange lateral bending.

Table 5.9.1. Specified radial displacement of compression flange at locations 2 and 3, modified uniform vertical bending tests.

D/b_f	b_f/t_f	D/t_w	d_o/D	$L_b/R=0.05$			$L_b/R=0.10$		
				u_R (mm)	u_R/L_b	u_R/D	u_R (mm)	u_R/L_b	u_R/D
2.25	25	100	3	69.1	0.007	0.057	19.6	0.004	0.016
		130	3	75.2	0.008	0.062	22.1	0.005	0.018
		160	1	58.4	0.006	0.048	22.9	0.005	0.019
			2	73.7	0.008	0.060	27.4	0.006	0.023
			3	79.2	0.008	0.065	29.7	0.006	0.024
2.75	15	100	3	49.5	0.007	0.041	16.5	0.005	0.014
		130	3	52.3	0.007	0.043	17.0	0.005	0.014
		160	1	46.2	0.006	0.038	11.4	0.003	0.009
			2	48.8	0.007	0.040	14.7	0.004	0.012
			3	53.3	0.007	0.044	17.5	0.005	0.014
	20	100	3	54.9	0.008	0.045	19.3	0.005	0.016
		130	3	61.0	0.008	0.050	19.3	0.005	0.016
		160	1	47.8	0.007	0.039	16.0	0.004	0.013
			2	49.8	0.007	0.041	16.5	0.005	0.014
			3	65.3	0.009	0.054	19.8	0.005	0.016
	25	100	3	57.7	0.008	0.047	19.3	0.005	0.016
		130	3	65.8	0.009	0.054	20.3	0.006	0.017
		160	1	57.9	0.008	0.048	11.4	0.003	0.009
			2	65.0	0.009	0.053	17.0	0.005	0.014
			3	74.7	0.010	0.061	20.6	0.006	0.017
3.25	25	160	1	23.4	0.004	0.019	6.6	0.002	0.005
			2	26.9	0.004	0.022	8.1	0.002	0.007
			3	31.8	0.005	0.026	11.7	0.003	0.010

5.10 INTERNAL LOADING SUITE

The internal loading suite is designed to verify the applicability of design equations when:

- the maximum lateral flange bending moment occurs at the middle of the critical unsupported segment instead of at the cross-frame locations.
- the critical curved girder segment is subjected to internal loadings on its top flange, resulting in a load height or tipping effect.
- the critical unsupported length is subjected to a moment gradient

The configuration for the internal loading tests is illustrated in Fig 5.10.1. A concentrated load is applied at the middle of the test section (segment 2-3). This load is distributed along a short length of the girder calculated to prevent local web yielding and web crippling. The resulting maximum lateral flange bending moment (and $f_b + f_l$) occurs at the middle of the test segment (although these values are approximately the same at the cross-frame locations).

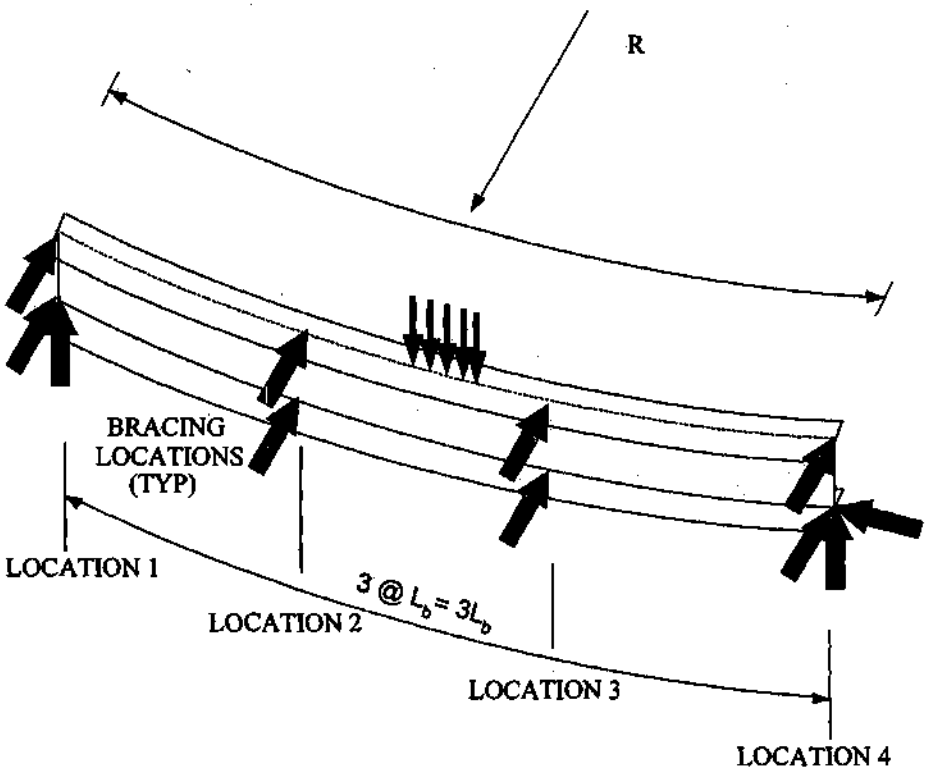

Figure 5.10.1. Internal loading test configuration.

Only girders with $d_o/D = 3$ are considered within this test suite. Two representative sets of length-related parameters are studied: $L_b/R = 0.05$ and 0.10, both with L_b established such that $f_\ell/f_b \cong 0.50$ in the uniform vertical bending case of the primary test suite. The significance of these two sets is as follows. For the set with $L_b/R = 0.05$ and target $f_\ell/f_b = 0.50$, all of the specimens have lateral-torsional buckling slenderness ratios $\lambda = L_b/r_t$ larger than the corresponding λ_p (see Eq. (2-14)). The girders in the second set have the largest $\lambda = L_b/r_t$ ratios of the girders in the primary suite with $L_b/R = 0.10$. Therefore, the tipping effect of the internal loading is "maximized," and the application of the moment gradient magnifier C_b can be verified. It should be noted that the refined formula developed by Kirby and Nethercot (1979) and provided in the commentary of the AASHTO LRFD (2001) Specifications is employed to determine C_b for this loading case.

5.11 FREE-END SUITE

The main purpose of the free-end test suite is to study the behavior and strength of the end unsupported lengths of bridge girders, where there is no flange lateral bending restraint at one end of the segment. This suite also provides an important verification of the maximum strength behavior of unbraced segments that have a significant moment gradient. Figure 5.11.1 shows the configuration of the loadings and supports for these tests. This is a three-point bending test in which the applied load is placed at the middle of the girder. Rigid radial supports are located at the load and end vertical support locations.

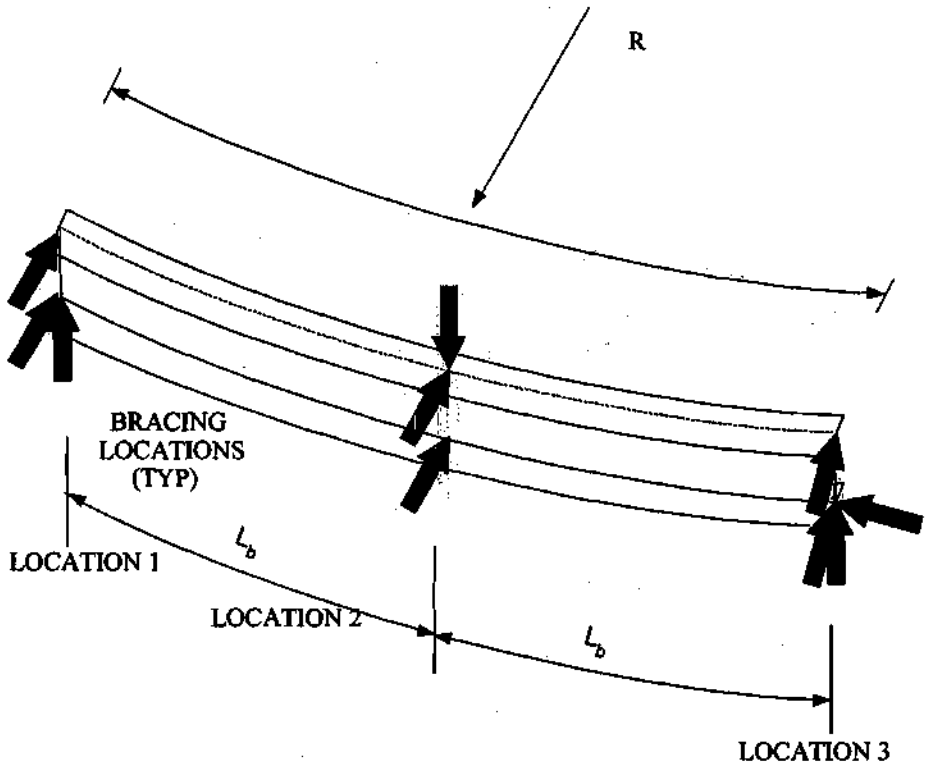

Figure 5.11.1. Free-end test configuration (three-point bending test).

Cross-sections with $D/t_w = 160$ and $d_o/D = 3$ are studied in this test suite. Values of L_b/R equal to 0.05 and 0.10 are considered along with a target second-order elastic f_ℓ/f_b of 0.60 (at the maximum load capacity of the member), based on shell finite element analysis. That is, the unsupported length L_b is selected such that $f_\ell/f_b \cong 0.60$ at the middle of the test specimens. This is accomplished by starting with an initial estimated L_b based on this requirement, conducting a full nonlinear analysis of the resulting girder to determine the maximum load capacity, performing a second-order elastic (geometric nonlinear) analysis of the girder at this load level, selecting a new L_b based on judgment, and iterating until the ratio of the second-order elastic stresses is within $\pm$ 0.05 of the desired value. Table 5.11.1 summarizes the designs of the girders considered in this suite.

Table 5.11.1. Design summary for girders considered in the free-end test configuration ($D/t_w = 160$, $d_o/D = 3$ and target second-order $f_\ell/f_b = 0.60$).

D/b_f	b_f/t_f	t_f/t_w	$2D_c t_w/b_f t_f$	$L_b/R = 0.05$	$L_b/R = 0.10$
2.25	25	2.84	0.79	L_b = 13.4 m (44 ft) R = 268 m (880 ft) L_b/b_f = 24.8	L_b = 7.92 m (26 ft) R = 79.2 m (260 ft) L_b/b_f = 14.6
2.75	15	3.88	0.71	L_b = 11.0 m (36 ft) R = 219 m (720 ft) L_b/b_f = 24.8	L_b = 6.71 m (22 ft) R = 67.1 m (220 ft) L_b/b_f =15.1
	20	2.91	0.945	L_b = 11.0 m (36 ft) R = 219 m (720 ft) L_b/b_f = 24.8	L_b = 6.41 m (21 ft) R = 65.0 m (210 ft) L_b/b_f =14.4
	25	2.33	1.18	L_b = 11.0 m (36 ft) R = 219 m (720 ft) L_b/b_f = 24.8	L_b = 6.41 m (21 ft) R = 64.0 m (210 ft) L_b/b_f =14.4
3.25	25	1.97	1.65	L_b = 8.53 m (28 ft) R = 171 m (560 ft) L_b/b_f = 22.7	L_b = 5.18 m (17 ft) R = 51.8 m (170 ft) L_b/b_f =13.8

It should be noted that all the specimens with $L_b/R = 0.05$ and target second-order $f_\ell/f_b = 0.60$ are actually configured such that the lateral-torsional buckling slenderness

ratio is equal to λ_r. Furthermore, the specimens with $L_b/R = 0.10$ and target $f_\ell / f_b = 0.60$ all have a lateral-torsional buckling slenderness ratio, $(\lambda - \lambda_p)/(\lambda_r - \lambda_p)$ equal to 0.25.

5.12 LATERALLY UNSUPPORTED STRAIGHT GIRDER SUITE

The laterally unsupported straight girder suite represents the case of straight girders with large unsupported length, subjected to combined vertical and lateral loads. In this suite, several straight girders are modeled with unbraced lengths such that the ratio $(\lambda - \lambda_p) / (\lambda_r - \lambda_p)$ associated with the lateral-torsional buckling checks within the modified AASHTO LRFD (2001) equations (see Eq. (2-2)) is equal to 0, 0.25, 0.5, 0.75, and 1.0. The corresponding values of $\lambda = L_b/r_t$ span the entire range associated with inelastic lateral-torsional buckling. Test specimens with $D/t_w = 160$ and $d_o/D = 3$ are considered within this test suite. Table 5.12.1 summarizes the unbraced lengths for these girders. A total of 25 specimens is evaluated.

Table 5.12.1. Design summary, laterally unsupported straight girders, $D/t_w = 160$, $d_o/D = 3$.

D/b_f	b_f/t_f	r_t	Unbraced Length L_b for target $(\lambda - \lambda_p) / (\lambda_r - \lambda_p)$				
			0.0	0.25	0.50	0.75	1.00
2.25	25	147 mm (5.8 in)	6.10 m (20 ft)	7.92 m (26 ft)	10.1 m (33 ft)	11.6 m (38 ft)	13.4 m (44 ft)
2.75	15	122 mm (4.8 in)	5.0 m (16.3 ft)	6.49 m (21.3 ft)	8.23 m (27 ft)	9.75 m (32 ft)	11.0 m (36 ft)
2.75	20	119 mm (4.7 in)	4.97 m (16.3 ft)	6.49 m (21.3 ft)	7.92 m (26 ft)	9.45 m (31 ft)	11.0 m (36 ft)
2.75	25	117 mm (4.6 in)	4.97 m (16.3 ft)	6.49 m (21.3 ft)	7.92 m (26 ft)	9.45 m (31 ft)	11.0 m (36 ft)
3.25	25	97 mm (3.8 in)	3.96 m (13 ft)	5.18 m (17 ft)	6.40 m (21 ft)	7.62 m (25 ft)	8.84 m (29 ft)

These girders are subjected to specified radial displacements at the middle cross-frame locations (locations 2 and 3, see Fig. 5.12.1). The loading protocol is the same as in the modified vertical bending suite, except that the radial displacements are applied at both the top and bottom flanges. These displacements are specified such that, at the maximum load capacity of the member, the value of f_ℓ/f_b in the second-order elastic design analysis is approximately 0.6. A procedure similar to that described for the free-end suite is employed to determine the appropriate L_b. Table 5.12.2 summarizes the resulting radial displacement at locations 2 and 3. In this test scheme, the critical

unsupported segment is subjected to uniform primary bending moment about both its strong and weak axes.

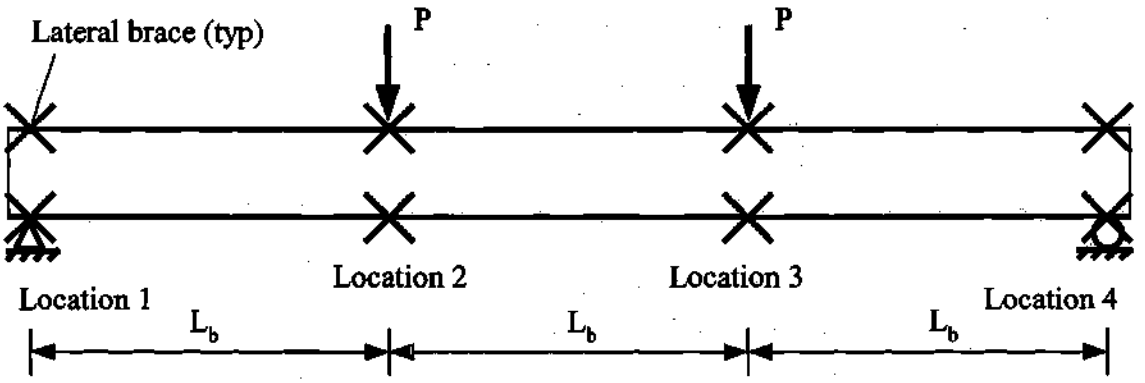

Figure 5.12.1. Configuration of laterally unsupported straight girders.

5.13 UNSYMMETRICAL GIRDERS

Based on the results of the parametric studies with doubly symmetric cross-sections, two sets of girders are designed to investigate the effect of depth of the web in compression as well as to verify the applicability of the key design equations for unsymmetrical girders. The ratio of $D_c/D = 0.65$ is selected as a representative extreme case for all the unsymmetrical girders. It should be noted that this is approximately the maximum D_c/D ratio for which the AASHTO LRFD (2001) requirement of $0.1 \le I_{yc}/I_y \le 0.9$ is satisfied. The design of the first set of unsymmetric girders starts with the doubly symmetric cross-section based on $D/b_f = 2.75$, $b_f/t_f = 25$, $D/t_w = 130$ and $d_o/D = 3$. This cross-section is then made unsymmetric by increasing the tension flange size while maintaining $b_{ft}/t_{ft} = 25$. The resulting section profile, which has an $I_{yc}/I_y = 0.14$ and $2D_c/t_w = 169$, is shown in Fig. 5.13.1.

The second set of unsymmetric girders starts with the doubly symmetric cross-section based on $D/b_f = 2.75$, $b_f/t_f = 20$, $D/t_w = 160$ and $d_o/D = 3$. This cross-section is made unsymmetric by reducing the size of the compression flange while maintaining $b_{fc}/t_{fc} = 20$. This girder, which has an $I_{yc}/I_y = 0.10$, a $D/b_{fc} = 4.77$, and a $2D_c/t_w = 208$ is shown in Fig. 5.13.2. This girder is believed to be representative of extreme conditions involving a composite girder with a small top compression flange prior to placement of the deck. The Recommended Specifications state that D/b_{fc} should be preferably less than five, but never less than 6.67. Based on the designs detailed in the previous sections of this chapter, it can be seen that even $D/b_{fc} = 3.25$ can lead to quite restrictive lateral brace spacing in order to limit f_ℓ/f_b to desired target values. Few girders with highly slender

Table 5.12.2. Specified radial displacement of tension and compression flanges at locations 2 and 3, laterally unsupported straight-girder suite, $D/t_w = 160$, $d_o/D = 3$.

D/b_f	b_f/t_f	$(\lambda-\lambda_p)/(\lambda_r-\lambda_p)$									
		0		0.25		0.5		0.75		1.0	
		u_R	u_R/L_b	u_R	u_R/L_b	u_R	u_R/L_b	u_R	u_R/L_b	u_R	u_R/L_b
2.25	25	73.74 mm (2.903 in)	0.012	130.8 mm (5.150 in)	0.017	175.8 mm (6.923 in)	0.017	204.9 mm (8.068 in)	0.018	261.9 mm (10.31 in)	0.020
2.75	15	73.94 mm (2.911 in)	0.015	113.0 mm (4.450 in)	0.017	144.6 mm (5.694 in)	0.018	171 mm (6.732 in)	0.018	197.3 mm (7.769 in)	0.018
	20	67.11 mm (2.642 in)	0.014	109.2 mm (4.300 in)	0.017	116.4 mm (4.584 in)	0.015	142.3 mm (5.601 in)	0.015	168.1 mm (6.617 in)	0.015
	25	60.12 mm (2.367 in)	0.012	104.1 mm (4.100 in)	0.016	137.7 mm (5.421 in)	0.017	162.1 mm (6.383 in)	0.017	186.6 mm (7.345 in)	0.017
3.25	25	43.38 mm (1.708 in)	0.011	72.39 mm (2.850 in)	0.014	93.57 mm (3.684 in)	0.015	124.1 mm (4.885 in)	0.016	153.8 mm (6.057 in)	0.017

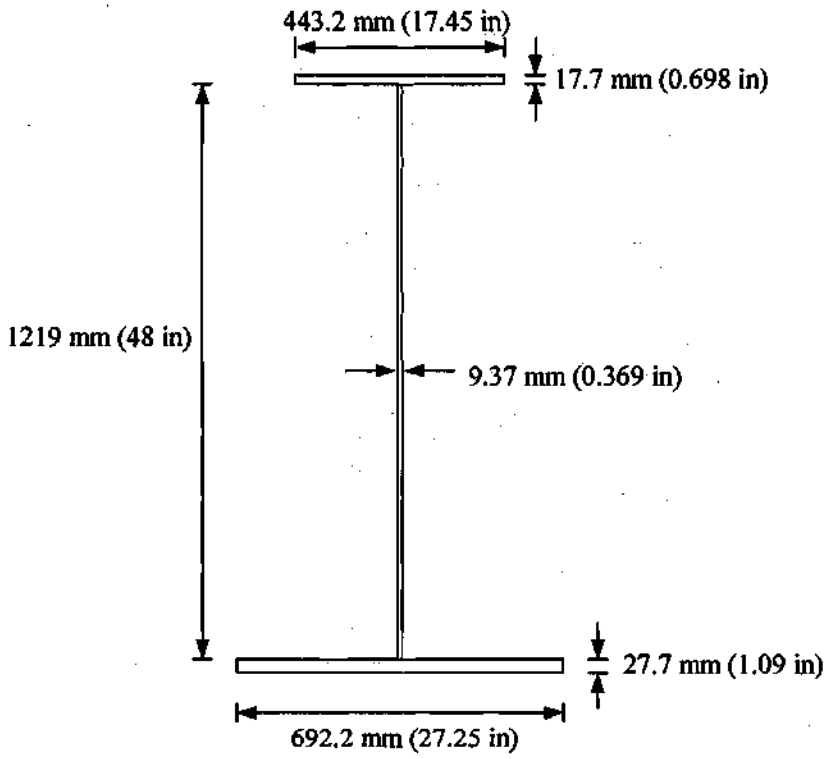

Figure 5.13.1. Unsymmetric cross-section 2.75-25-169 (area of tension flange increased, holding b_f/t_f constant, such that $D_c/D = 0.65$ and $I_{yc}/I_y = 0.14$).

aspect ratios D/b_{fc} have been tested experimentally, and these types of girders tend to be very flexible laterally. Therefore, it would appear that $D/b_{fc} = 5$ might be considered as an upper limit, and that a smaller value of D/b_{fc} should be recommended for practical design (at least in unsupported segments in which the design is controlled by flexure).

A complete set of unsymmetric girder tests is obtained by utilizing the boundary and loading conditions of:

1. The primary and the modified uniform vertical bending suites with both of the above cross-sections, for all combinations of $L_b/R = 0.05$ and 0.10 along with target first-order elastic f_t/f_b values of 0.35 and 0.50 within the compression flange in the uniform vertical bending load case of the primary suite (based on shell finite element analysis).

2. The internal loading suite for the cross-section 2.75-25-169 (area of tension flange increased) with $L_b/R = 0.05$ and 0.10 and the unsupported lengths determined in the above solutions. The internal loading cannot be applied with the cross-section 4.77-20-208, since the length of the loading required to prevent web crippling is greater than the L_b determined above in (1).

3. The free-end suite for cross-section 4.77-20-208 (area of compression flange reduced) with $L_b/R = 0.05$ and 0.10 and a target second-order elastic f_ℓ/f_b of 0.60 at the maximum load level.

That is, a total of 22 tests are considered. It should be noted that the lengths of these girders are different than the lengths of the corresponding symmetric designs in order to satisfy the f_ℓ/f_b targets.

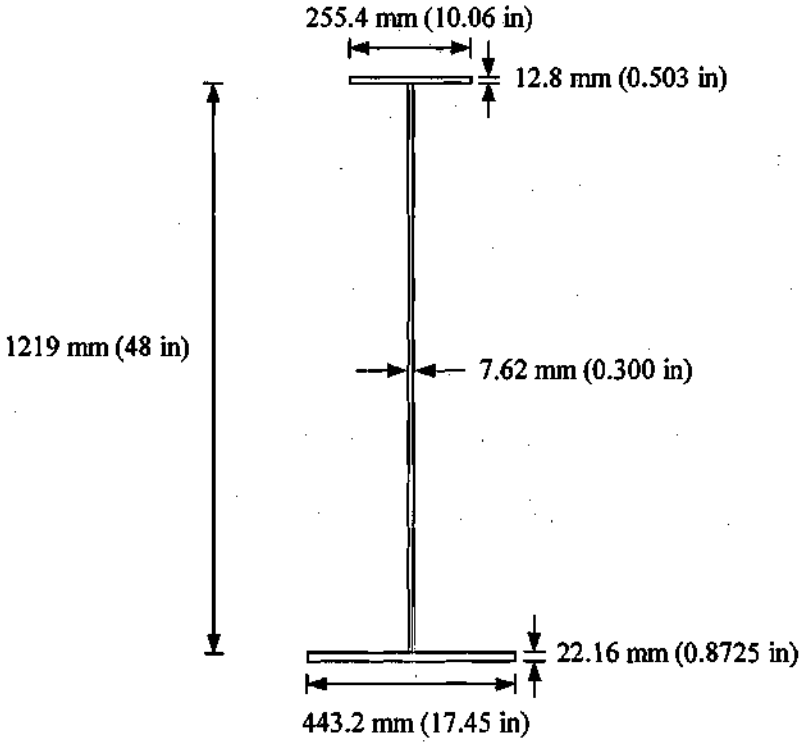

Figure 5.13.2. Unsymmetric cross-section 4.77-20-208 (area of compression flange reduced, holding b_f/t_f constant, such that $D_c/D = 0.65$ and $I_{yc}/I_y = 0.10$).

Table 5.13.1 gives the length parameters for each of the unsymmetric girder tests. It should be noted that Eqs. (5-2) through (5-5) are also applicable to monosymmetric girders, and are used to estimate the required unsupported lengths for the primary suite cases, and thus also for the cases that are extensions of the primary suite studies. With the exception of the design for $L_b/R = 0.10$ and $f_\ell/f_b = 0.5$, in which L_b is selected as a multiple of 610 mm (2 ft), L_b is selected as the closest multiple of the web depth D = 1219 mm (4 ft). The specified radial displacements for the modified uniform vertical bending tests of the unsymmetric girders are given in Table 5.13.2.

Table 5.13.1. Design summary for unsymmetric girder tests.

Test Suite	$L_b/R = 0.05$ $f_\ell/f_b = 0.35$	$L_b/R = 0.05$ $f_\ell/f_b = 0.50$ or 0.60	$L_b/R = 0.10$ $f_\ell/f_b = 0.35$	$L_b/R = 0.10$ $f_\ell/f_b = 0.50$ or 0.60
$D/b_{fc} = 2.75$, $b_{fc}/t_{fc} = 25$, $2D_c/t_w = 169$, $d_o/D = 3$				
Primary Modified Uniform Vertical Bending Internal Loading	$L_b = 4.88$ m (16 ft) R = 97.5 m (320 ft) $L_b/b_{fc} = 11.0$	$L_b = 7.31$ m (24 ft) R = 146 m (480 ft) $L_b/b_{fc} = 16.5$	$L_b = 2.43$ m (8 ft) R = 24.4 m (80 ft) $L_b/b_{fc} = 5.5$	$L_b = 3.66$ m (12 ft) R = 36.6 m (120 ft) $L_b/b_{fc} = 8.4$
$D/b_{fc} = 4.77$, $b_{fc}/t_{fc} = 20$, $2D_c/t_w = 208$, $d_o/D = 3$				
Primary Modified Uniform Vertical Bending	$L_b = 2.44$ m (8 ft) R = 48.8 m (160 ft) $L_b/b_{fc} = 9.6$	$L_b = 3.66$ m (12 ft) R = 73.2 m (240 ft) $L_b/b_{fc} = 14.3$	$L_b = 1.22$ m (4 ft) R = 12.19 m (40 ft) $L_b/b_{fc} = 4.8$	$L_b = 1.83$ m (6 ft) R = 60 (18.3 m) $L_b/b_{fc} = 7.2$
Free End		$L_b = 4.57$ m (15 ft) R = 91.4 m (300 ft) $L_b/b_{fc} = 17.9$		$L_b = 2.44$ m (8 ft) R = 24.4 m (80 ft) $L_b/b_{fc} = 9.5$

Table 5.13.2. Specified radial displacement of compression flange at locations 2 and 3, modified uniform vertical bending, unsymmetric girders.

D/b_f	b_ℓ/t_f	D/t_w	L/R	f_ℓ/f_b	u_R	u_R/L_b	u_R/D
4.77	20	208	0.05	0.35	5.72 mm (0.225 in)	0.002	0.005
				0.50	13.7 mm (0.540 in)	0.004	0.011
			0.10	0.35	1.52 mm (0.060 in)	0.001	0.001
				0.50	5.59 mm (0.220 in)	0.003	0.005
2.75	25	169	0.05	0.35	10.8 mm (0.426 in)	0.002	0.009
				0.50	42.3 mm (1.667 in)	0.006	0.035
			0.10	0.35	4.57 mm (0.180 in)	0.002	0.004
				0.50	12.8 mm (0.505 in)	0.0004	0.011

CHAPTER VI

DETAILED ANALYSIS RESULTS FOR REPRESENTATIVE PARAMETRIC SPECIMENS

This chapter presents detailed finite element analysis results for several representative parametric specimens considered in this research. The responses addressed include the load versus the vertical and radial deflections, and the deformed geometry at the maximum load level. The following girders are studied:

- Girder 3.25-25-160-1-0.10-0.35[1]. This specimen has a relatively small $L_b/b_f = 6.5$ (see Table 5.8.5), but a relatively large $D/b_f = 3.25$, $b_{fc}/t_{fc} = 25$, and $2D_c/t_w = 160$. Therefore, its design strength with respect to the one-third rule equations (see Sections 2.1.1 and 2.1.9.2) is controlled by inelastic flange local buckling, whereas it is compact with respect to lateral-torsional buckling.

- Girder 2.75-25-160-1-0.05-0.50. This specimen has a relatively large $L_b/b_f = 16.5$ (see Table 5.8.4), such the lateral-torsional check by the one-third rule is based on inelastic buckling. The lateral-torsional and local buckling checks for this girder are nearly equal. However, due to its large $b_{fc}/t_{fc} = 25$, inelastic flange local buckling controls its design strength. Nevertheless, significant lateral-torsional buckling deformations are expected at the flexural strength limit state.

- Girder 2.75-15-100-3-0.05-0.50. This specimen has a relatively large $L_b/b_f = 16.5$ (see Table 5.8.2), combined with a compact flange ($b_f/t_f = 15$) and a lightly stiffened nonslender web ($2D_c/t_w = 100$ and $d_o/D = 3$). Inelastic lateral-torsional buckling controls its flexural strength.

- Girder 2.75-15-100-3-0.10-0.50. This specimen has a relatively small $L_b/b_f = 8.3$ (see Table 5.8.2), combined with a compact flange ($b_f/t_f = 15$) and a lightly stiffened nonslender web ($2D_c/t_w = 100$ and $d_o/D = 3$). By the one-third rule equations, its flexural design strength is based on general yielding. That is, local flange and lateral-torsional buckling are assumed to have a negligible influence on the design flexural strength of this specimen.

[1] As noted in Section 5.8, the parametric study specimens are designated by specifying the numeric values for the normalized design parameters in the following order: D/b_f-b_f/t_f-D/t_w-d_o/D-L_b/R-f/f_b. Therefore, girder 3.25-25-160-1-0.10-0.35 has $D/b_f = 3.25$, $b_{fc}/t_{fc} = 25$, $2D_c/t_w = 160$, $d_o/D = 1$, $L_b/R = 0.10$ and a target $f/f_b = 0.35$.

The results for each of the above girders are presented in Sections 6.1 through 6.4 respectively. The uniform vertical bending, maximum V/M and high-shear high-moment loading tests of the primary suite are considered for both of the first two girders. For the second girder, the results for the modified vertical bending as well as the internal loading tests are also presented. Finally, for the third and fourth girders, the uniform vertical bending results from the primary test suite are provided. After the discussion of the basic load-deflection and deformed geometry results in Sections 6.1 through 6.4, Section 6.5 considers the relative flexural ductility of these specimens along with the predicted flexural ductility of the experimental tests for which the load-deflection results were previously presented in Section 4.7.

6.1 SPECIMEN 3.25-25-160-1-0.10-0.35 ($b_f/t_f = 25$, $L_b/b_f = 6.5$)

Figures 6.1.1 and 6.1.2 are plots of the load ($P_2 = P_3$) versus the vertical and radial displacements at the middle of the critical unsupported length for the primary uniform vertical bending test of specimen 3.25-25-160-1-0.10-0.35. Figure 6.1.3 shows the magnified deformed geometry at the peak load in this test. The mode of failure in this test is clearly flange local buckling.

Figure 6.1.4 is a plot of the load at location 2 versus the vertical displacement at this location in the maximum V/M test of this specimen. Figure 6.1.5 shows the magnified deformed geometry at the peak load in this test. The development of a diagonal tension field in each of the critical web panels is apparent, with the larger distortions occurring within the right-most panel in the figure.

Figure 6.1.6 is a plot of the load P_2 versus the vertical displacement at this location in the high-shear high-moment test of specimen 3.25-25-160-1-0.10-0.35, whereas Fig. 6.1.7 shows the magnified deformed shape at the peak load in this test. The load parameter α is equal to 0.06. It is apparent that the failure mode in this test involves both predominant web buckling and development of tension-field action in the left-most web panel of the middle unsupported length (adjacent to the maximum moment location), as well as local buckling within the compression flange in this panel.

All of the above load-deflection curves corresponding to high-moment exhibit mild load shedding as the specimen is displaced beyond its maximum load capacity. The shear test specimen exhibits a significant plateau in its load versus vertical displacement response when its shear capacity is reached.

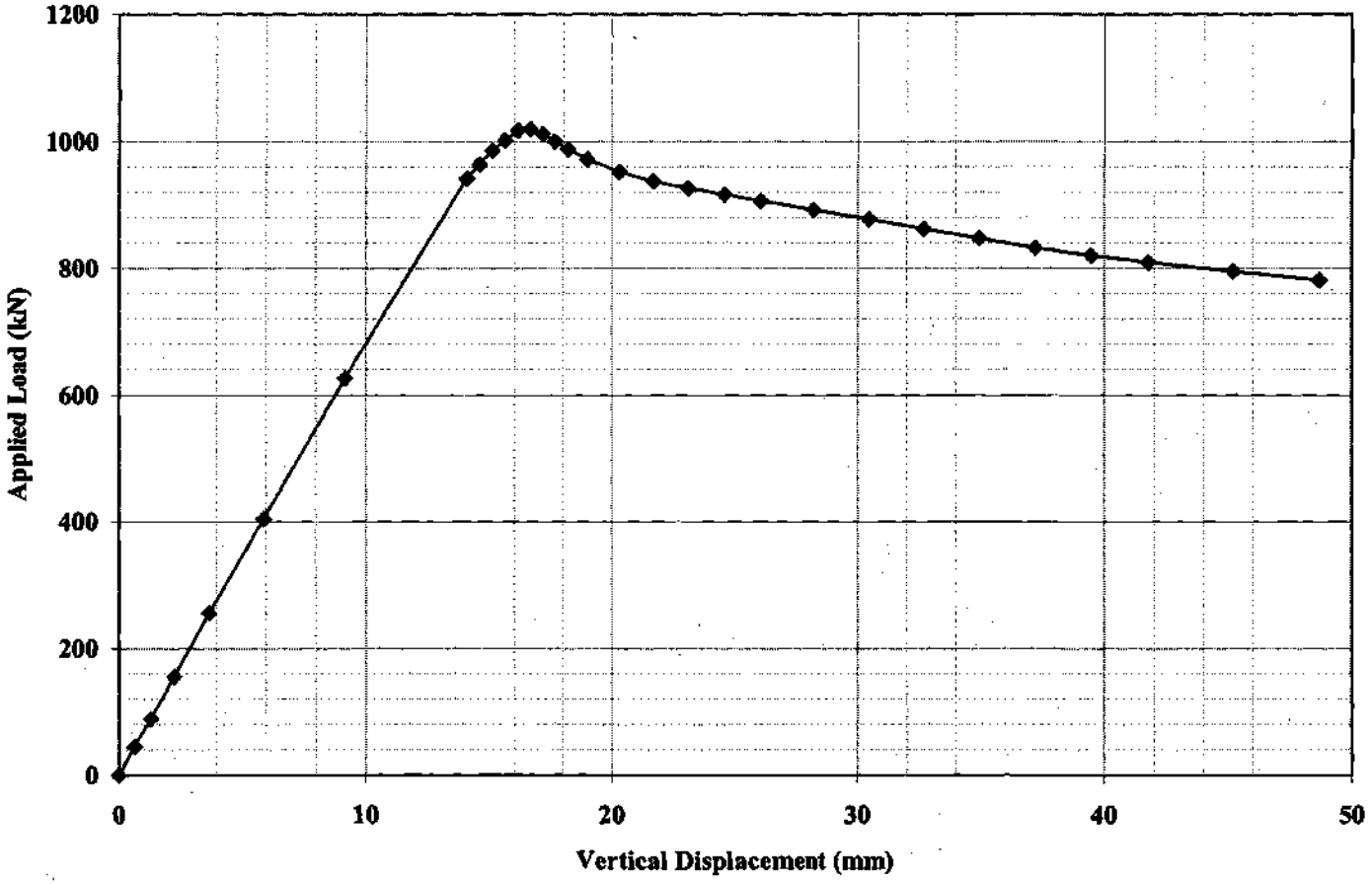

Figure 6.1.1. Load P_2 versus vertical displacement at mid-span of critical segment, uniform vertical bending, Specimen 3.25-25-160-1-0.10-0.35.

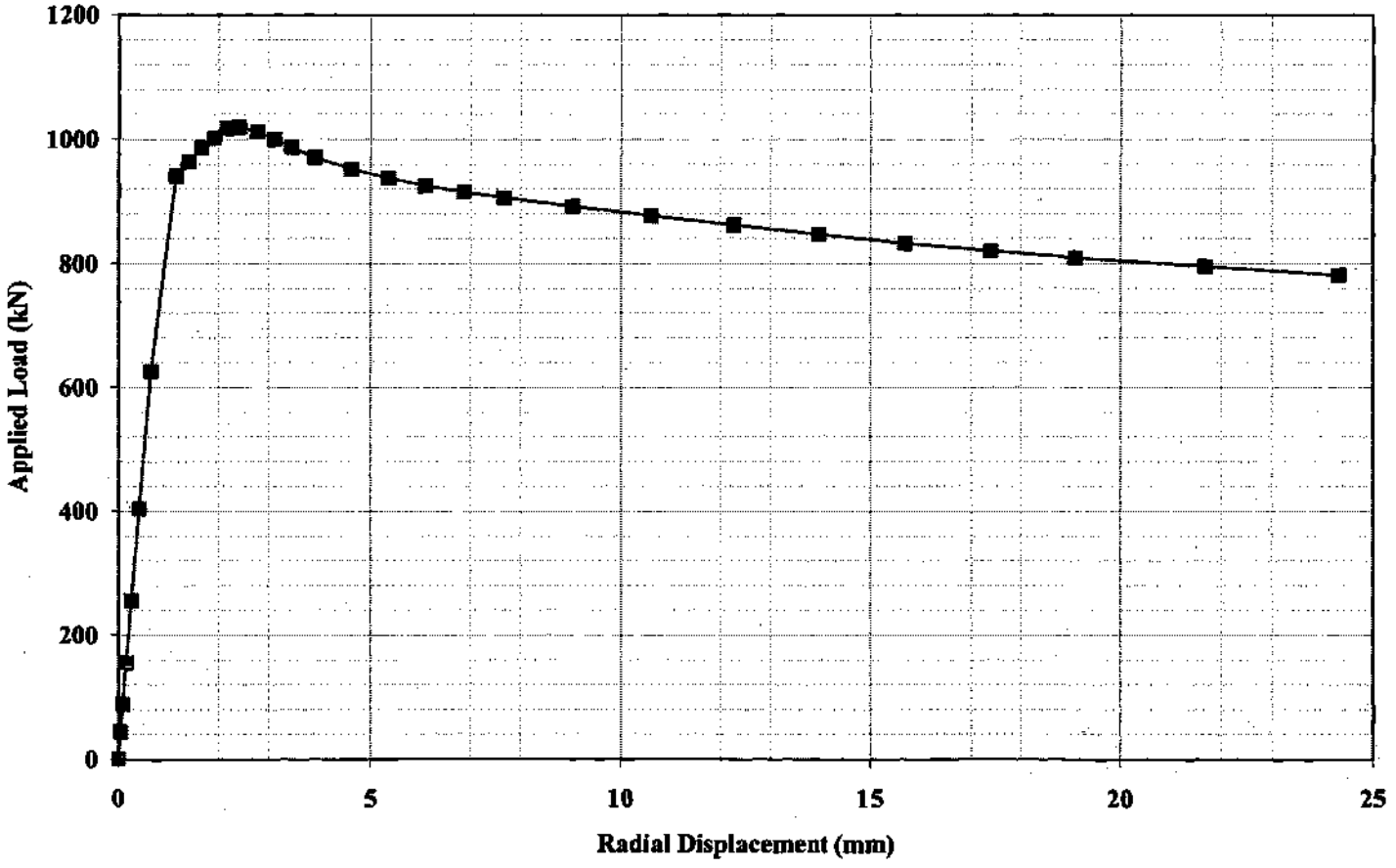

Figure 6.1.2. Load P_2 versus radial displacement of top flange at mid-span of critical segment, uniform vertical bending, Specimen 3.25-25-160-1-0.10-0.35.

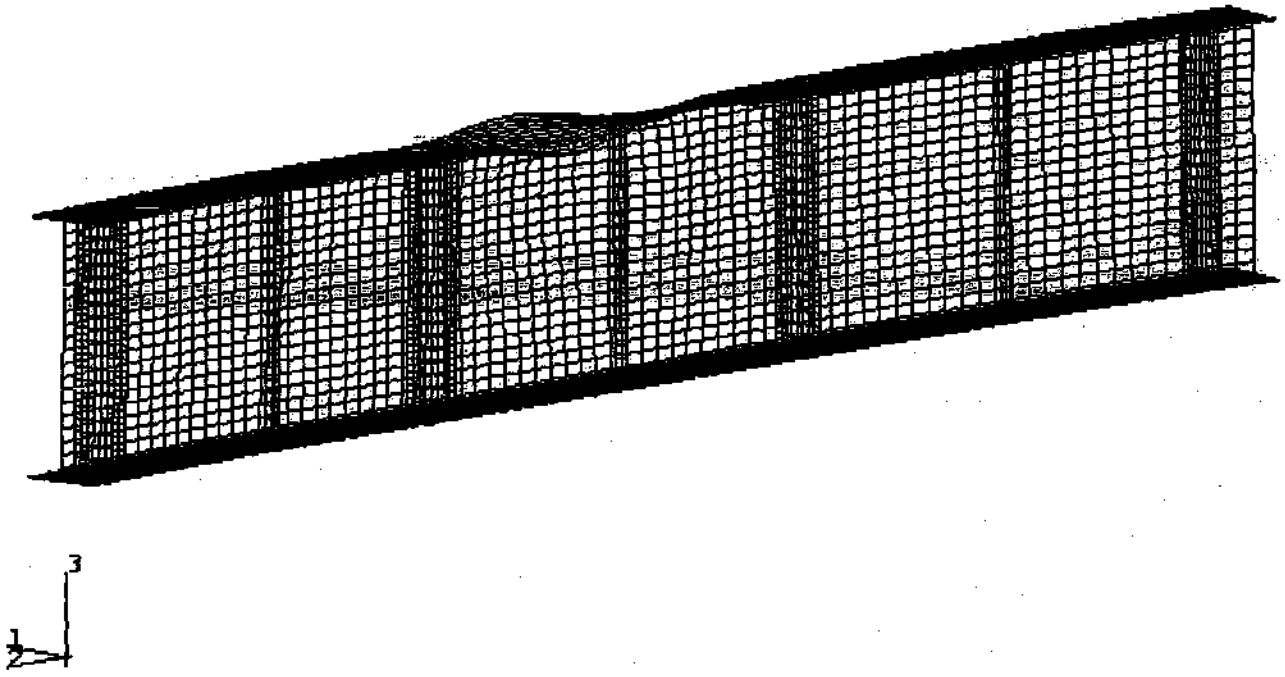

Figure 6.1.3. Deformed mesh at peak load, uniform vertical bending, Specimen 3.25-25-160-1-0.10-0.35 (displacement magnification factor = 4.0).

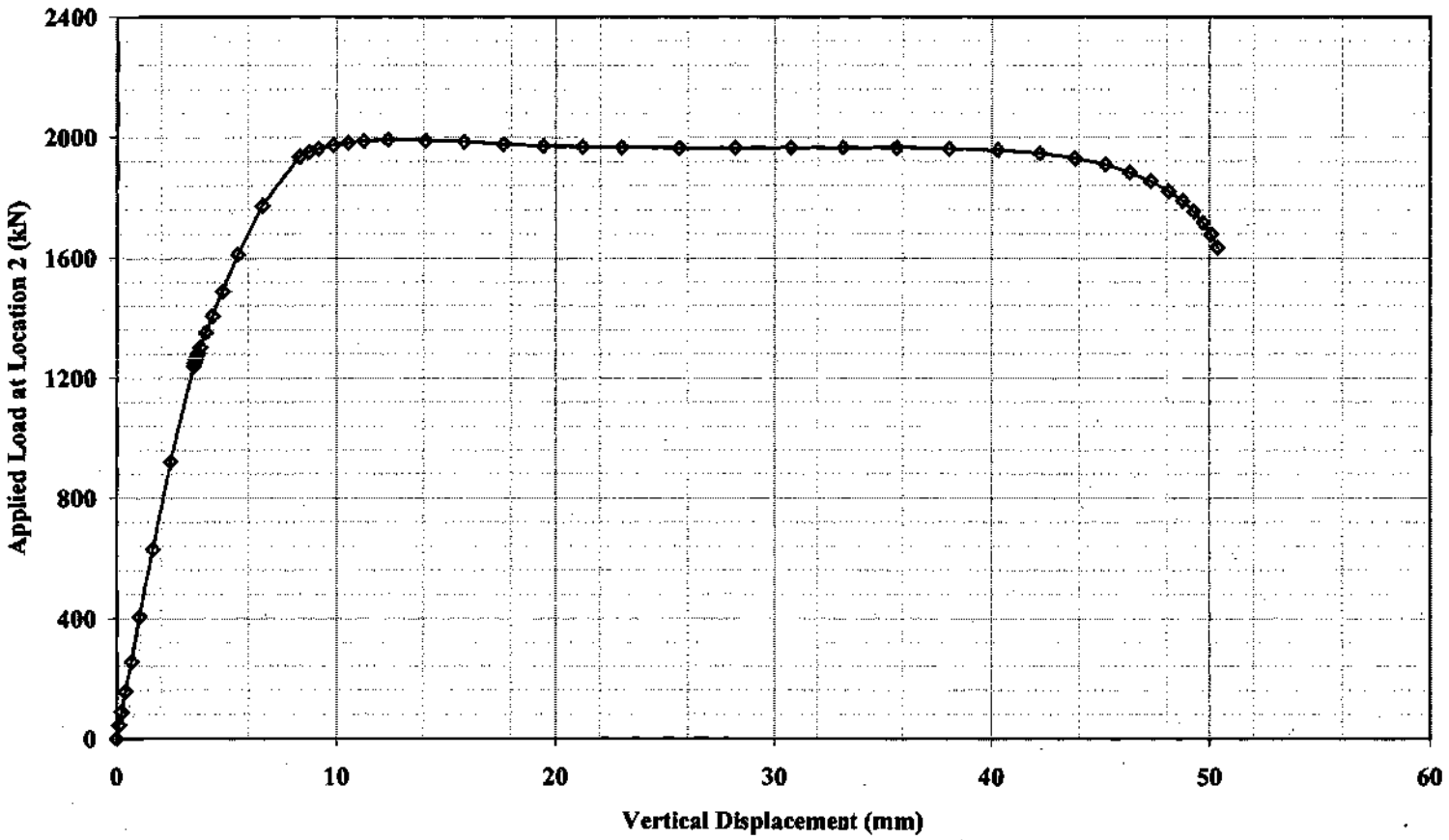

Figure 6.1.4. Load P_2 versus vertical displacement at location 2, maximum V/M, Specimen 3.25-25-160-1-0.10-0.35.

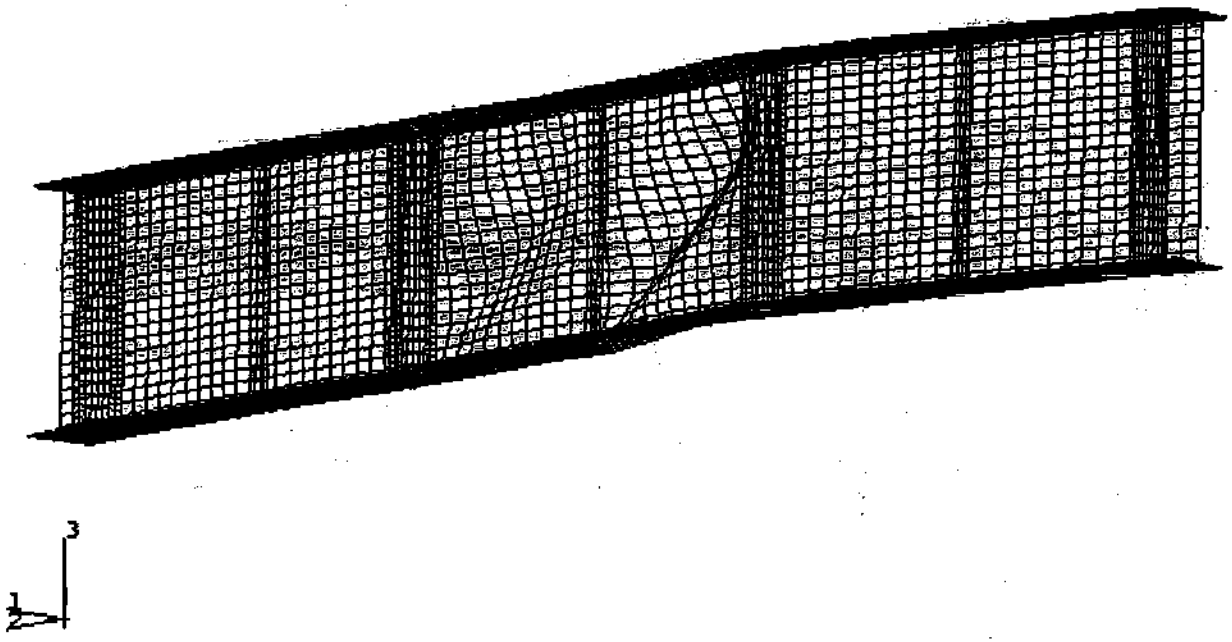

Figure 6.1.5. Deformed mesh at peak load, maximum V/M, Specimen 3.25-25-160-1-0.10-0.35 (displacement magnification factor = 10.0).

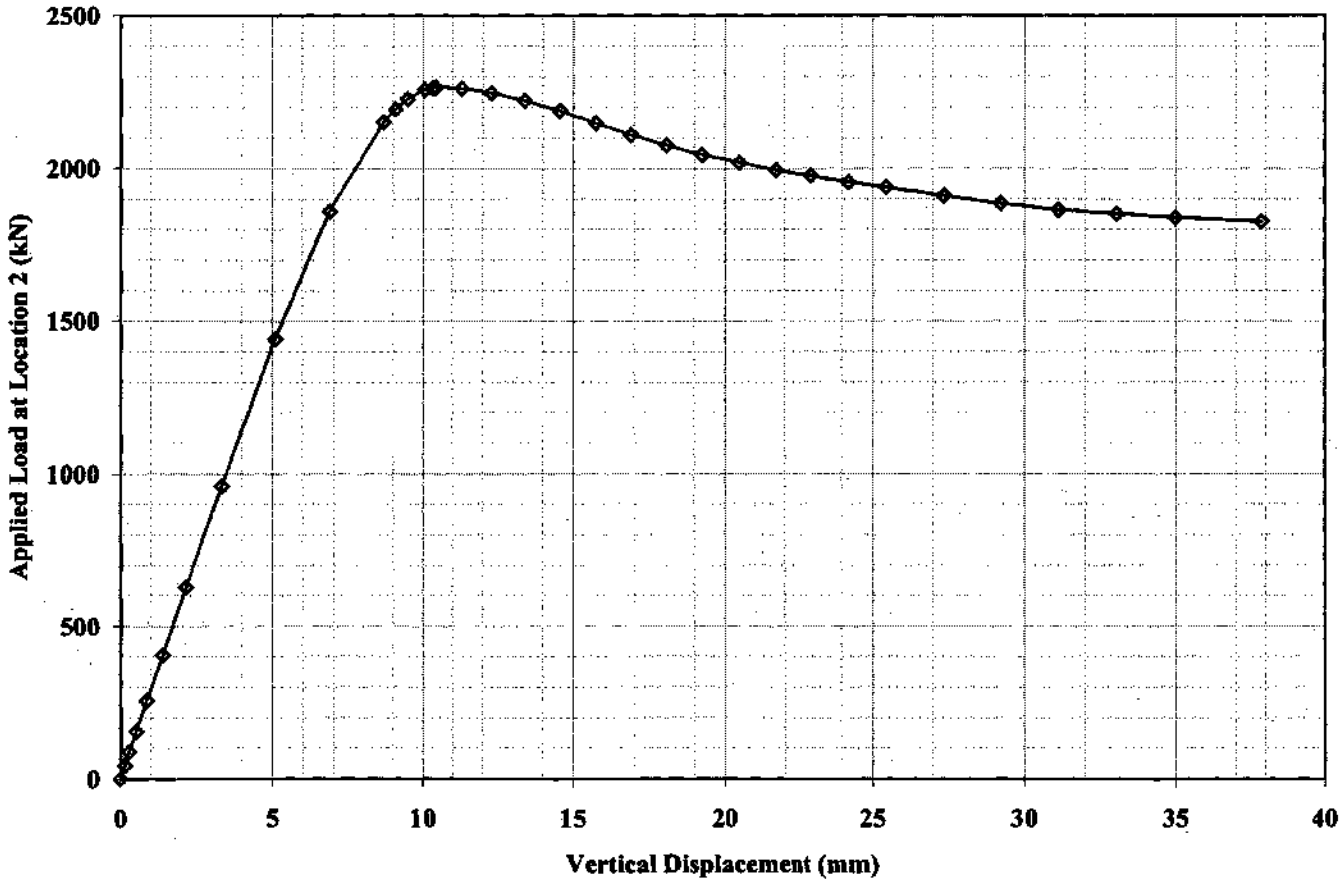

Figure 6.1.6. Load P_2 versus vertical displacement at location 2, high-shear high-moment ($\alpha = 0.06$), Specimen 3.25-25-160-1-0.10-0.35.

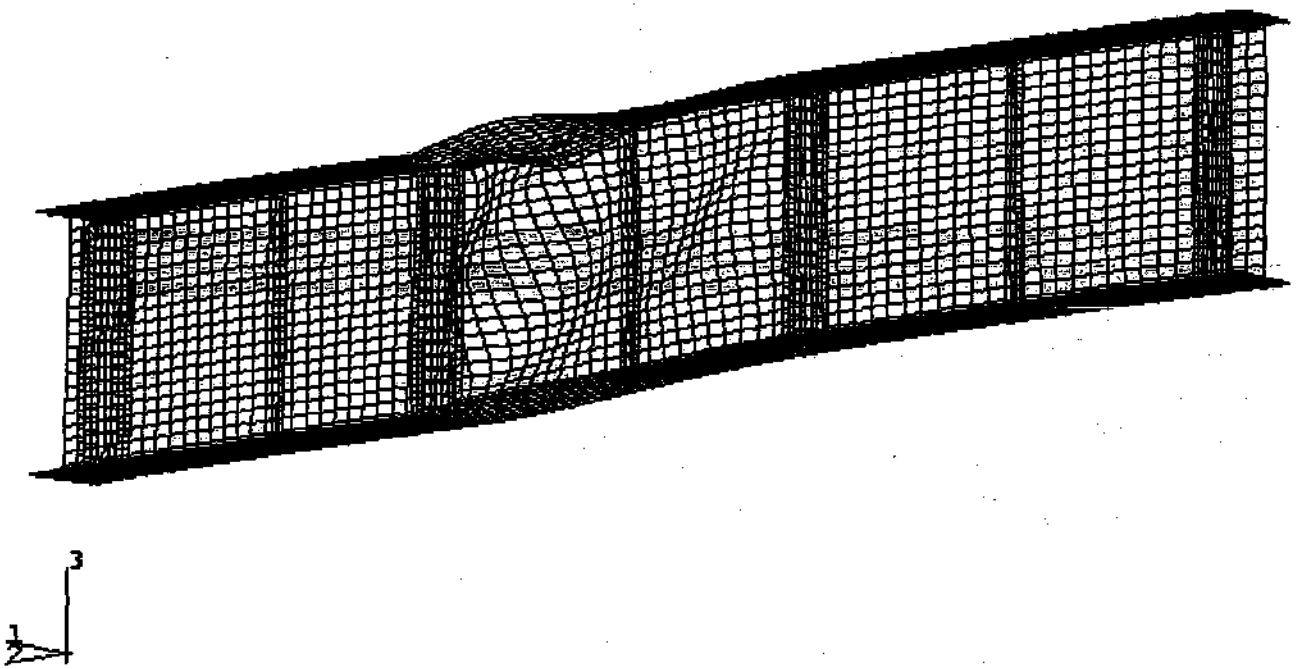

Figure 6.1.7. Deformed mesh at peak load, high-shear high-moment (α = 0.06), Specimen 3.25-25-160-1-0.10-0.35 (displacement magnification factor = 8.0).

6.2 SPECIMEN 2.75-25-160-3-0.05-0.50 (b_f/t_f = 25, L_b/b_f =16.5)

Figures 6.2.1 and 6.2.2 present the load ($P_2 = P_3$) versus the vertical and radial displacements for the primary uniform vertical bending test of specimen 2.75-25-160-3-0.05-0.50. Figure 6.2.3 shows the magnified deformed geometry at the peak load in this test. The failure mode is still dominated by flange local buckling. However, some torsional rotation at the middle of the critical unsupported length is evident.

Figure 6.2.4 is a plot of the load at location 2 versus the vertical displacement at this location in the maximum V/M test of this specimen. Apparently due to its longer unsupported length, this girder does not maintain a long plateau in the load-deflection response after the peak load in this shear test (as was the case with specimen 3.25-25-160-1-0.10-0.35). Rather, a gradual unloading similar to the behavior for the previously considered uniform vertical bending and high-shear high-moment response for specimen 3.25-25-160-1-0.10-0.35 is exhibited. Due to its longer unsupported length, the vertical bending moment at the ends of the critical unsupported segment is equal to 0.89 of the yield moment $M_y = F_{yc} S_{xc}$ when specimen 2.75-25-16-3-0.05-0.50 reaches its capacity under the maximum V/M loading. Figure 6.2.5 shows the magnified deformed geometry at the peak load in this test. Similar to the shear test discussed in Section 6.1, the magnified deformed shape at the maximum load level indicates the development of tension-field action within both web panels of the critical unsupported length. Significant flange torsional rotations are apparent within Fig. 6.2.5.

The high-shear high-moment load-deflection curve at location 2 for specimen 2.75-25-160-3-0.05-0.50 is shown in Fig. 6.2.6. This is actually one of the tests within the primary suite in which $M_{n(FEA)}/0.8V_{n(FEA)}$ is less than 0.55 (see the discussion in Section 5.5). The computed value of $M_{n(FEA)}/0.8V_{n(FEA)}$ for this test is 0.53. Therefore, this girder satisfies the criterion defined in Section 5.5 for excluding the high-shear high-moment loading case. Nevertheless, the high-shear high-moment results are analyzed and shown here. Based on $M_{n(FEA)}/0.8V_{n(FEA)} = 0.53$ and Eq. (5-1), an α of 0.32 is employed for the high-shear high-moment loading. Figure 6.2.7 shows the deformed geometry at the maximum load in this test. Significant web distortion, associated with the development of tension-field action, and significant local buckling distortion of the top flange at the left-hand end and of the bottom flange at the right-hand end of the critical unsupported length are evident. As would be expected, the deformed shape at the maximum load and the overall load-deflection results for this high-shear high-moment case are only slightly different than those shown for the maximum V/M case in Figs. 6.2.3 and 6.2.4. The influence of high bending moment on the flange and web distortions at location 2 is slightly more apparent in Fig. 6.2.7 than in Fig. 6.2.6.

The shapes of the load-deflection curves for specimen 2.75-25-160-3-0.05-0.50 are generally less ductile than those of the shorter specimen presented in Section 6.1. This difference is most dramatic for the shear tests (compare Fig. 6.2.4 to 6.1.4).

The load-deflection results for the modified uniform vertical bending test of specimen 2.75-25-160-3-0.05-0.50 are shown in Fig. 6.2.8 and 6.2.9, and the deformed geometry at the maximum load capacity is presented in Fig. 6.2.10. The vertical load-displacement

response in Fig. 6.2.8 is changed only slightly relative to the corresponding primary uniform vertical bending curve in Fig. 6.2.1. The elastic deflections are slightly larger in Fig. 6.2.8 and the maximum load is slightly reduced. The last point in both of these load-deflection curves corresponds to approximately the same load and deflection values. However, the radial displacements are significantly larger in the modified uniform vertical bending test (compare Fig. 6.2.9 to Fig. 6.2.2). The twisting of the specimen at the middle of the critical unsupported length is more significant in Fig. 6.2.10 than in Fig. 6.2.3.

Figures 6.2.11 and 6.2.12 are plots of the load versus the vertical and radial displacements of specimen 2.75-25-160-3-0.05-0.50 for the internal loading test, and Fig. 6.2.13 shows the deformed geometry at the maximum load in this test. The overall shapes of the load-displacement curves for this test are very similar to those of Figs. 6.2.1 and 6.2.2. Some web bend buckling is apparent in Fig. 6.2.13, but the clear mode of failure in this figure is flange local buckling on the right-hand side of the mid-girder maximum moment location.

6.3 SPECIMEN 2.75-15-100-3-0.05-0.50 ($b_f/t_f = 15$, $L_b/b_f = 16.5$)

Figures 6.3.1 and 6.3.2 show the load ($P_2 = P_3$) versus the vertical and radial displacements for the primary uniform vertical bending test of specimen 2.75-15-100-3-0.05-0.50. Figure 6.3.3 shows the magnified deformed geometry at the peak load for this test. Lateral buckling of the compression flange and twisting of the cross-section are apparent in this figure. Local buckling distortions of the compression flange are also visible in Fig. 6.3.3. This is to be expected, even though inelastic lateral-torsional buckling controls the design strength. It is well known that local and lateral-torsional buckling distortions generally occur together (Lukey and Adams 1969, ASCE-WRC 1971), although the design idealizations by AASHTO (2001), AISC (1999) and the one-third rule accurately capture the response without the need to consider any interaction between the lateral-torsional and local buckling limit states. The load-vertical displacement curve in Fig. 6.3.1 is slightly more rounded at its peak than the corresponding curves for the noncompact flange cases in Figs. 6.1.1 and 6.2.1. However, the overall unloading characteristics of this compact-flange specimen are not significantly different than those of the noncompact flange cases after the specimens shed about 10 percent of their maximum load. The load-radial displacement curve in Fig. 6.3.2 is also slightly more rounded at its peak than the corresponding curves in Figs. 6.1.2 and 6.2.2.

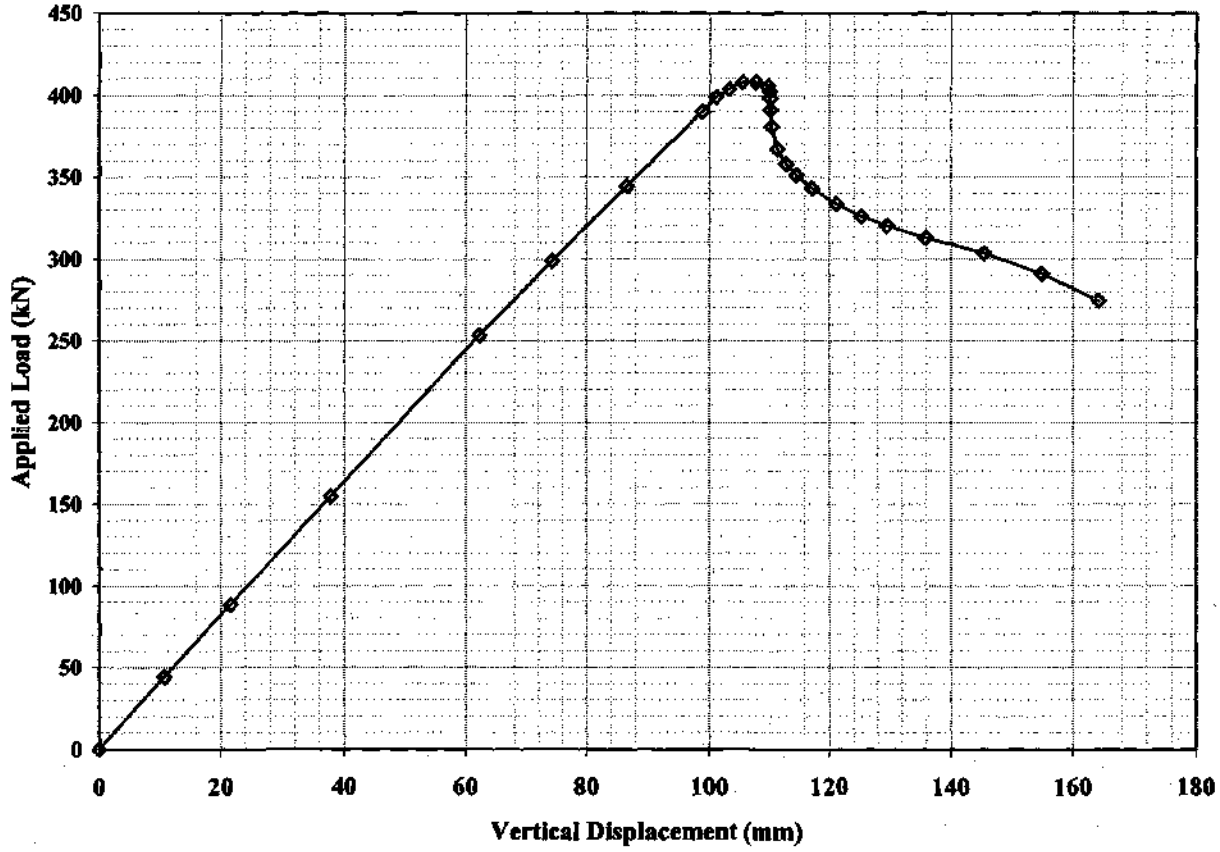

Figure 6.2.1. Load P_2 versus vertical displacement at mid-span of critical segment, uniform vertical bending, Specimen 2.75-25-160-3-0.05-0.50.

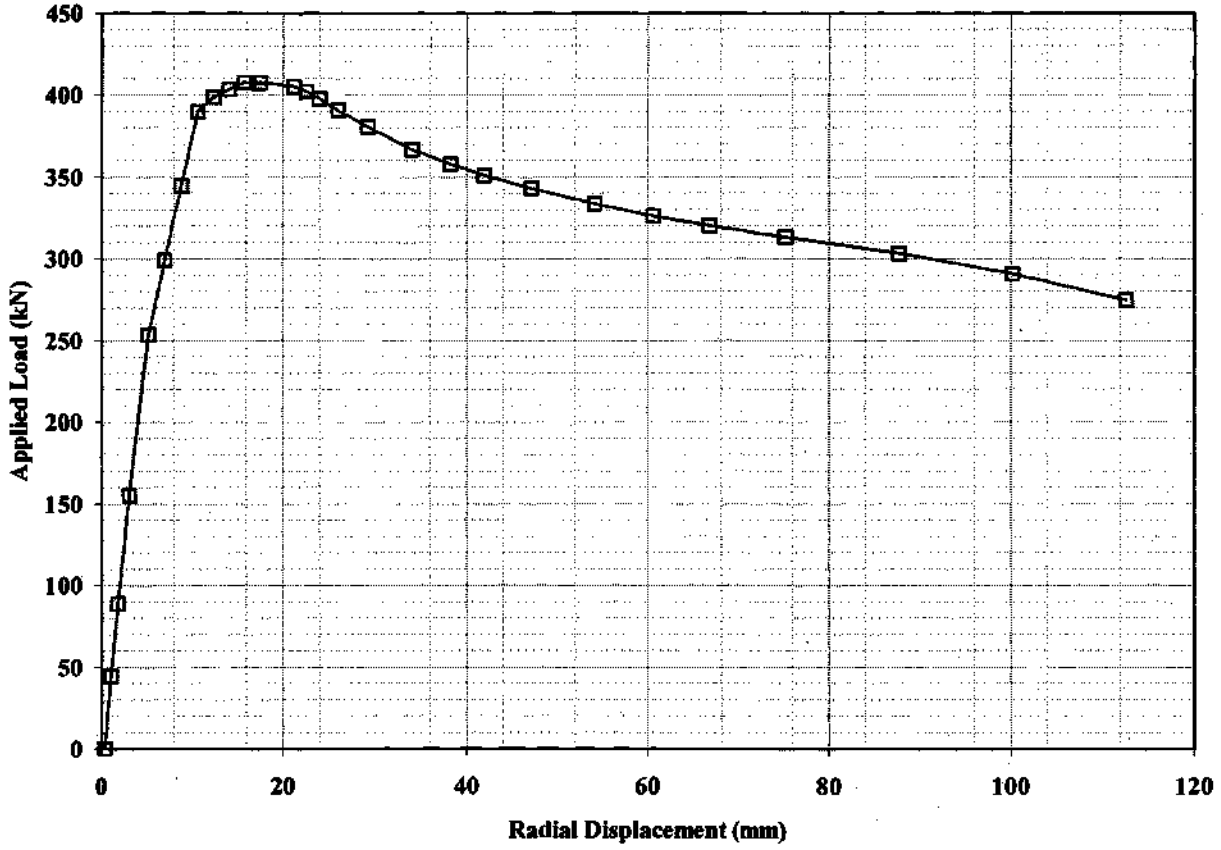

Figure 6.2.2. Load P_2 versus radial displacement of top flange at mid-span of critical segment, uniform vertical bending, Specimen 2.75-25-160-3-0.05-0.50.

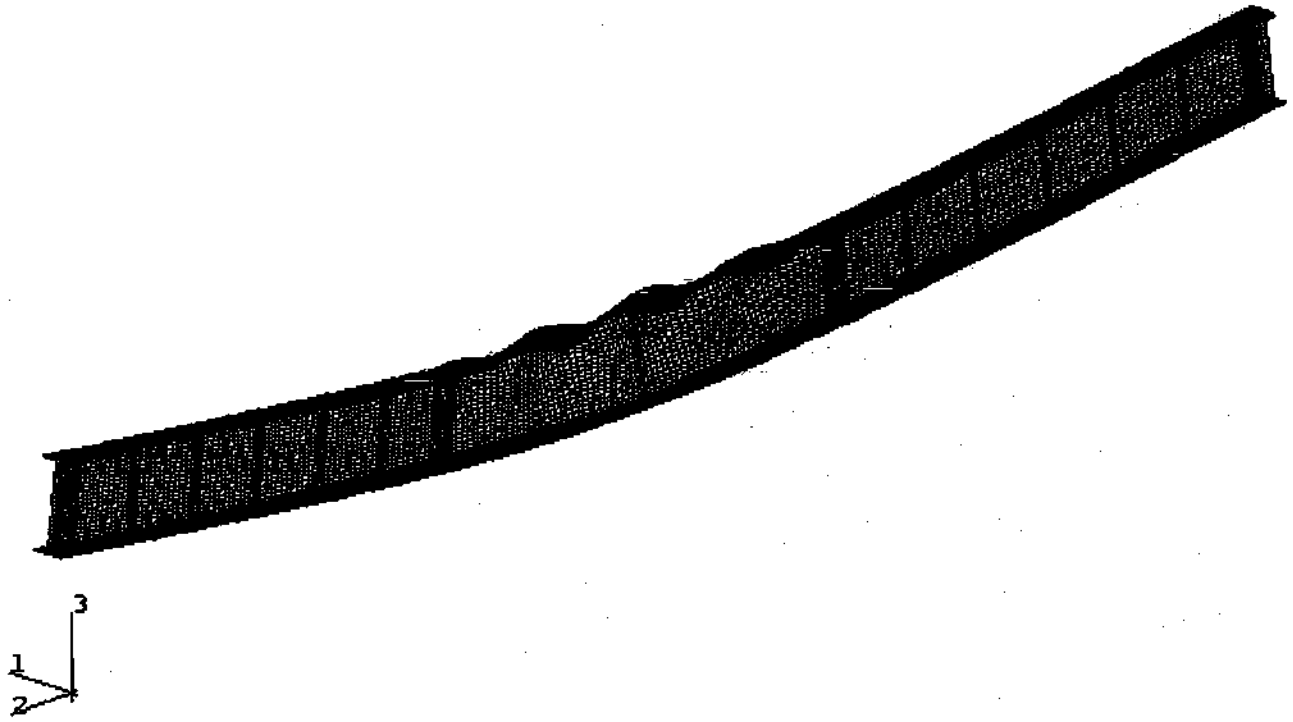

Figure 6.2.3. Deformed mesh at peak load, uniform vertical bending, Specimen 2.75-25-160-3-0.05-0.50 (displacement magnification factor = 10.0).

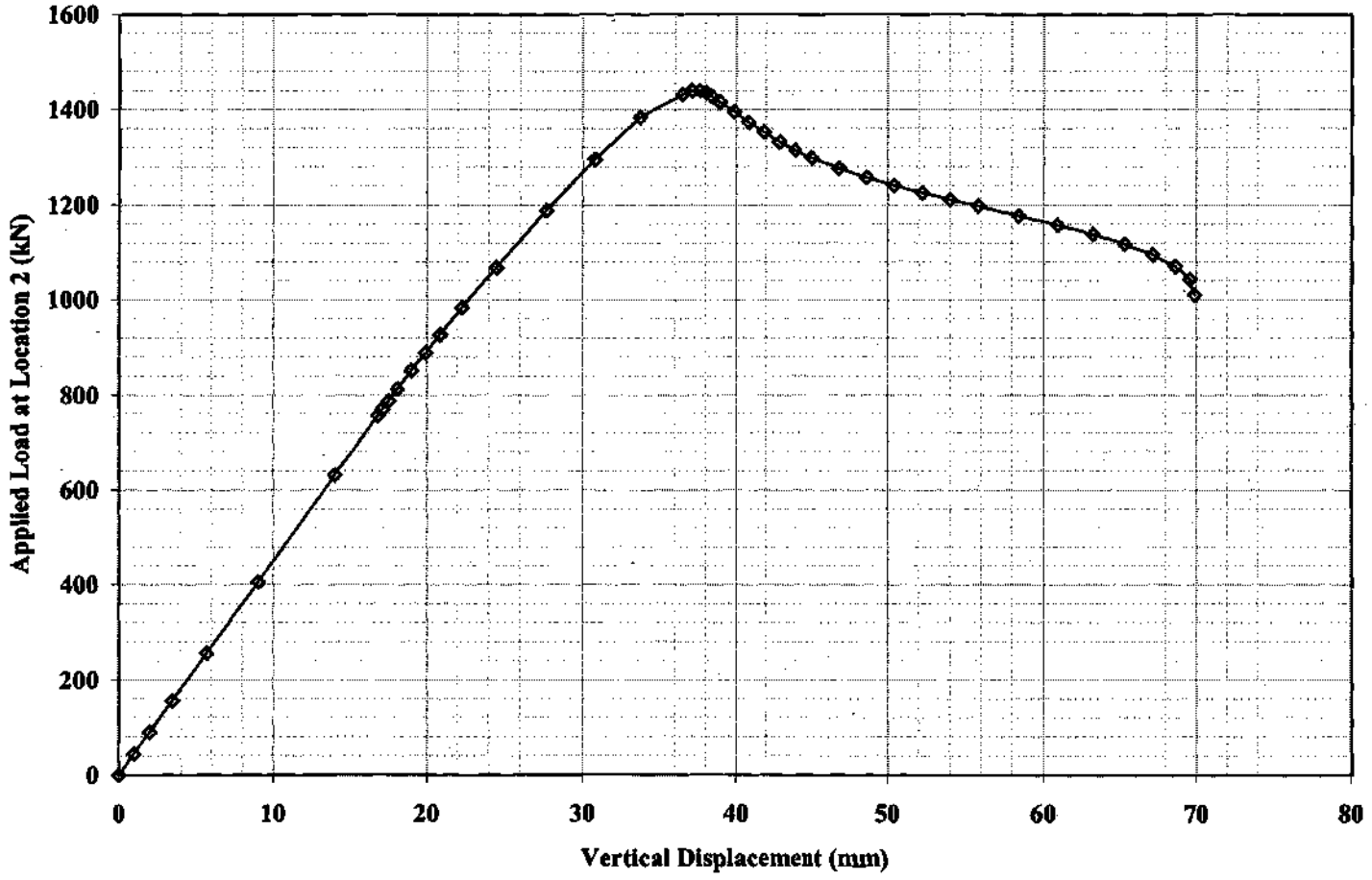

Figure 6.2.4. Load P_2 versus vertical displacement at location 2, maximum V/M, Specimen 2.75-25-160-3-0.05-0.50.

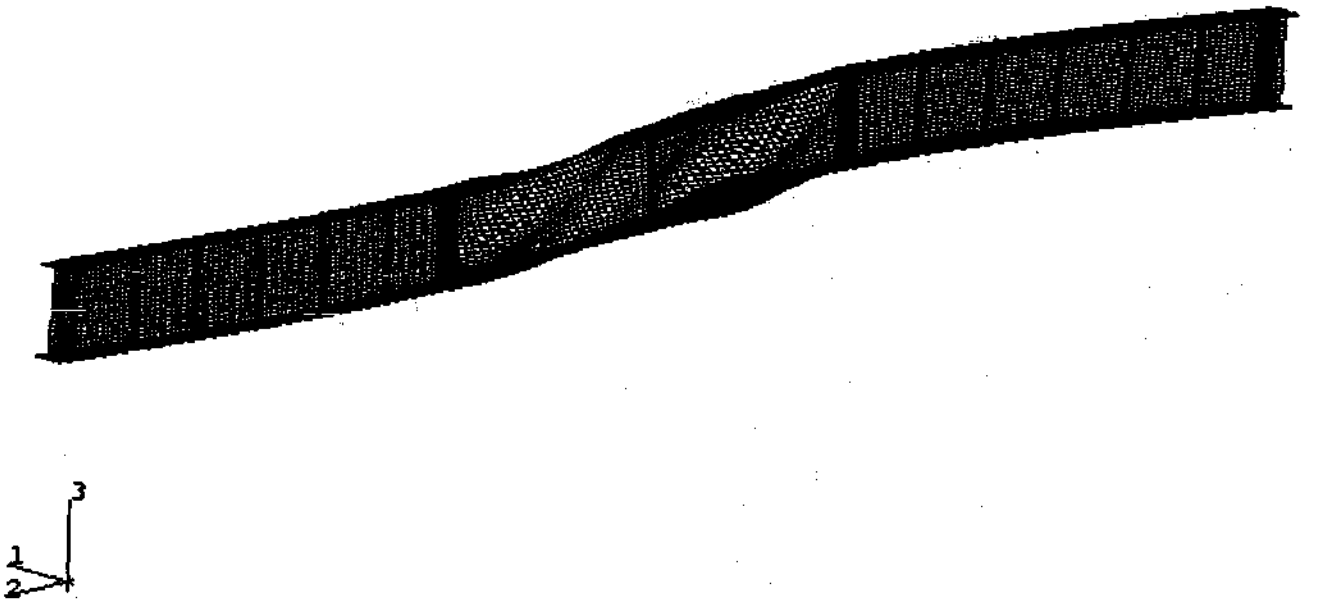

Figure 6.2.5. Deformed mesh at peak load, maximum V/M, Specimen 2.75-25-160-3-0.05-0.50 (displacement magnification factor = 10.0)

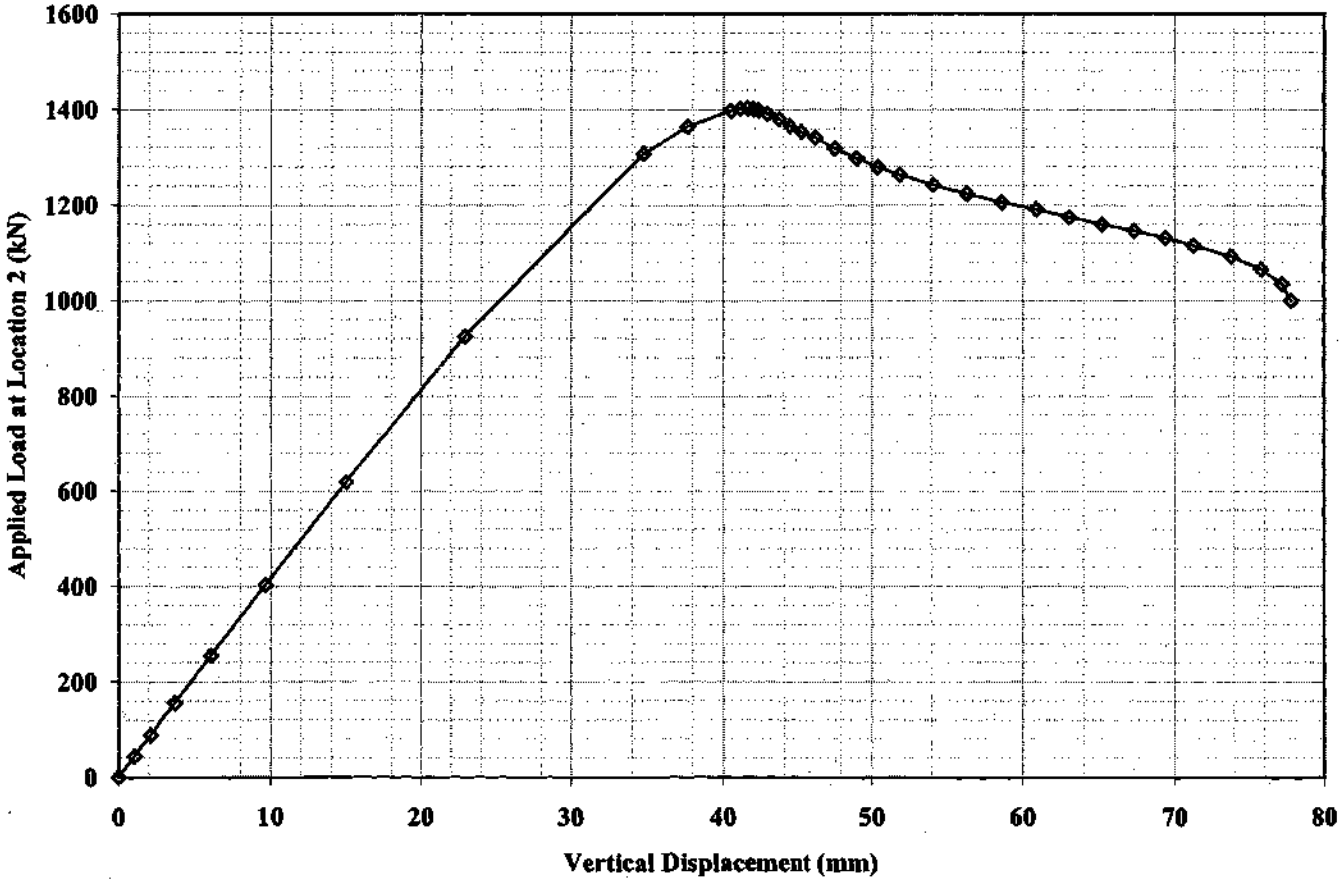

Figure 6.2.6. Load P_2 versus vertical displacement at location 2, high-shear high-moment, Specimen 2.75-25-160-3-0.05-0.50.

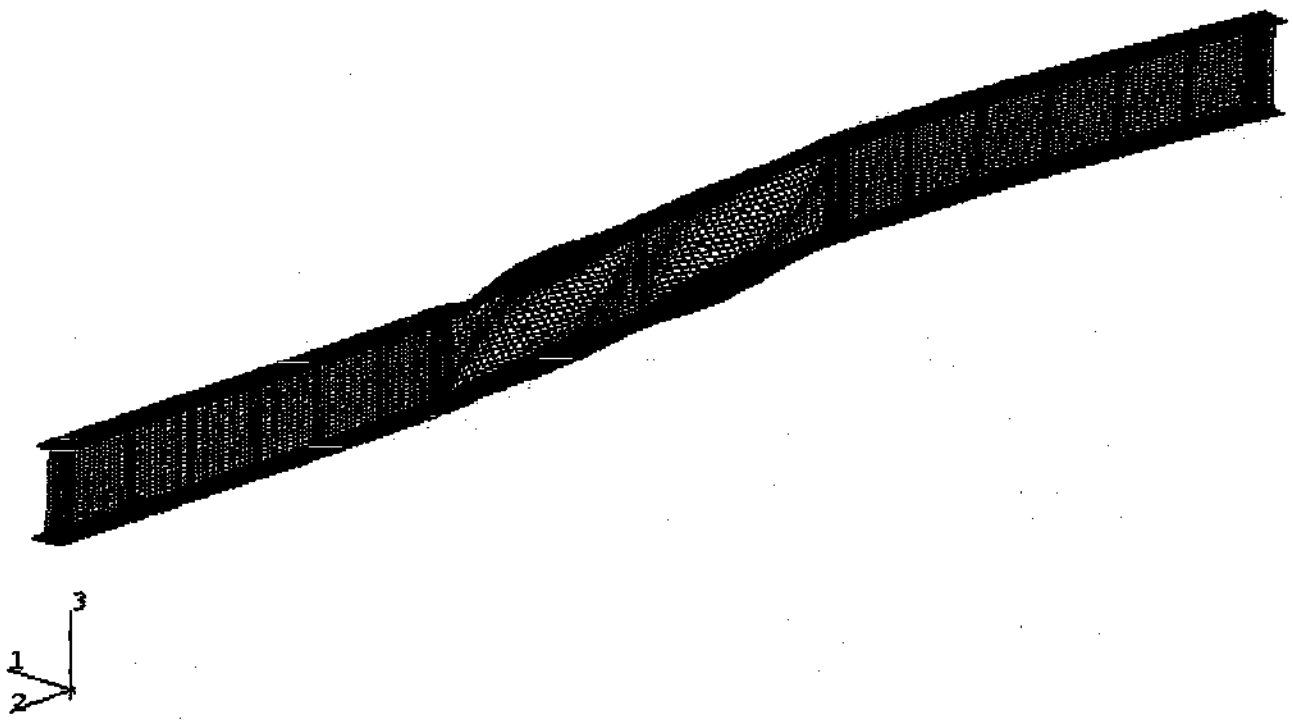

Figure 6.2.7. Deformed mesh at peak load, high-shear high-moment, Specimen 2.75-25-160-3-0.05-0.50 (displacement magnification factor = 8.0).

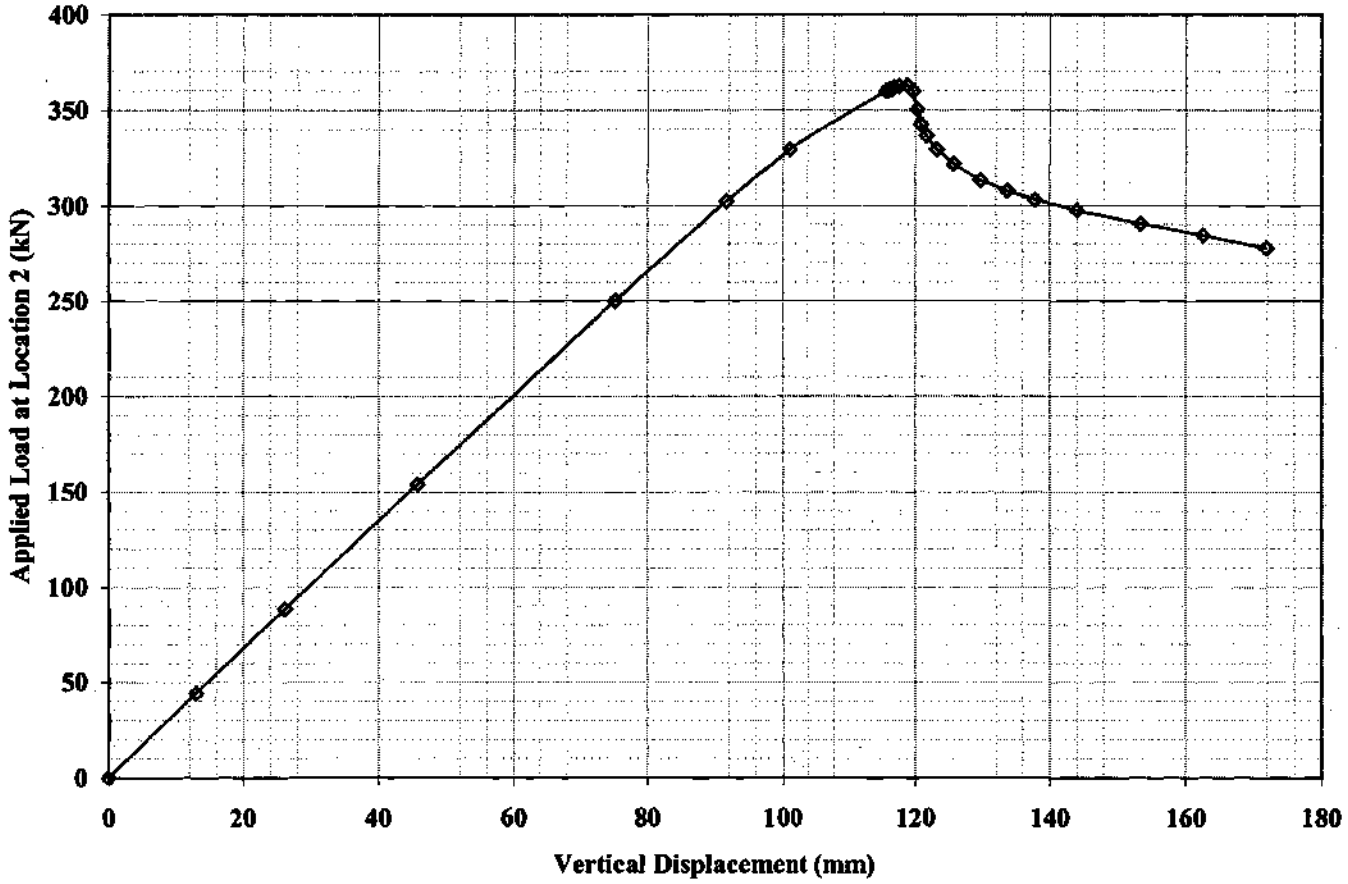

Figure 6.2.8. Load P_2 versus vertical displacement at mid-span of critical segment, modified uniform vertical bending, Specimen 2.75-25-160-3-0.05-0.50.

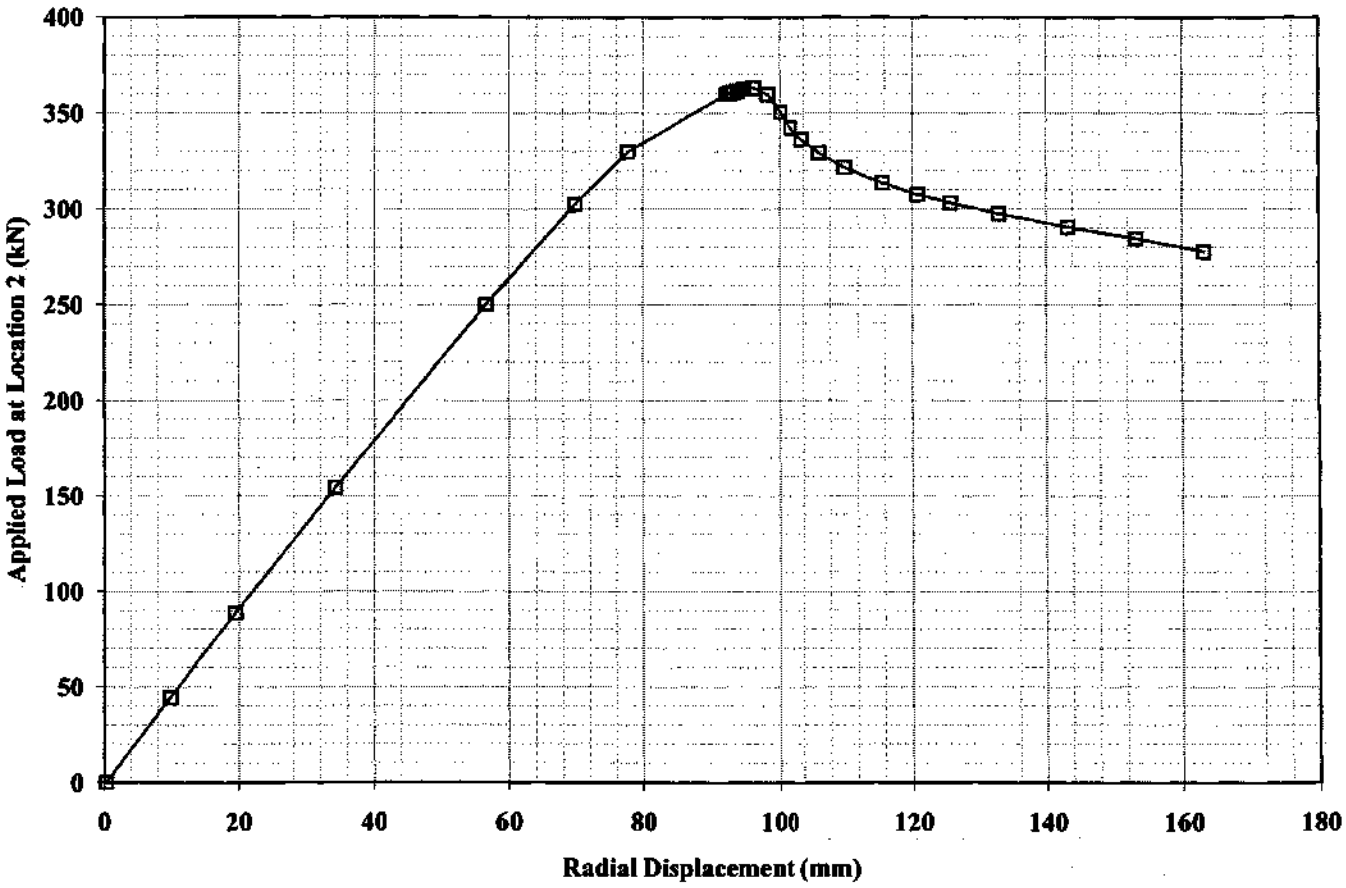

Figure 6.2.9. Load P_2 versus radial displacement at mid-span of critical segment, modified uniform vertical bending, Specimen 2.75-25-160-3-0.05-0.50.

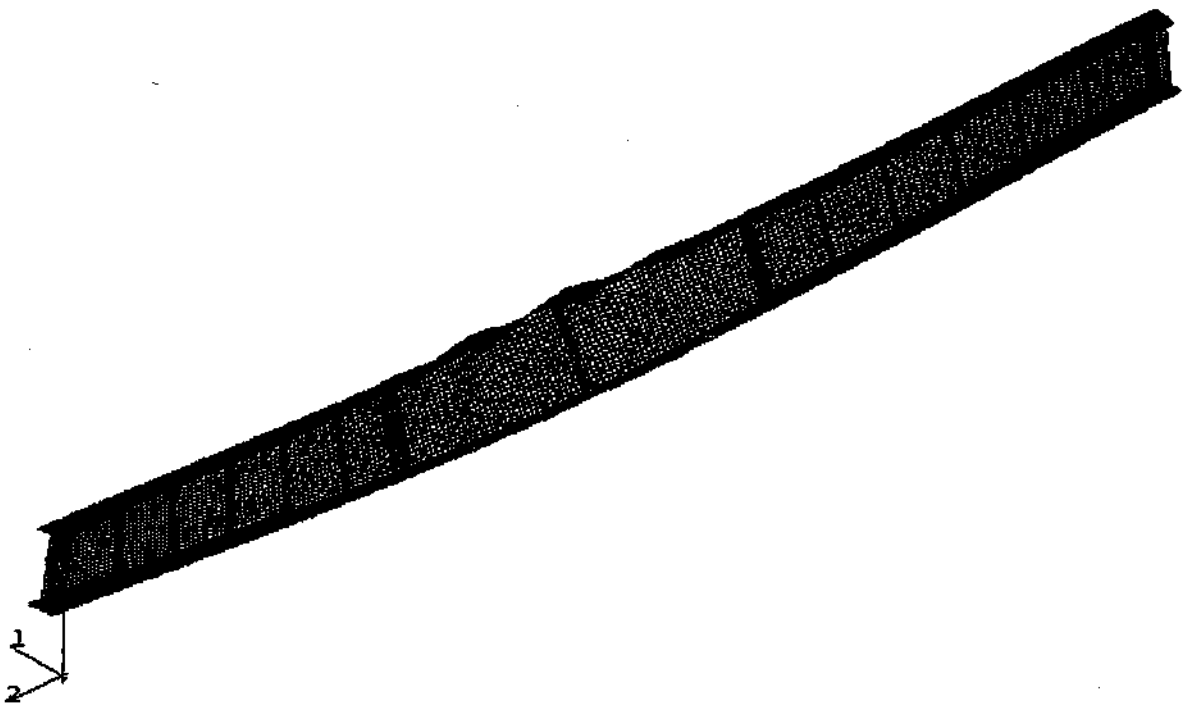

Figure 6.2.10. Deformed mesh at peak load, modified uniform vertical bending, Specimen 2.75-25-160-3-0.05-0.50 (displacement magnification factor = 8.0).

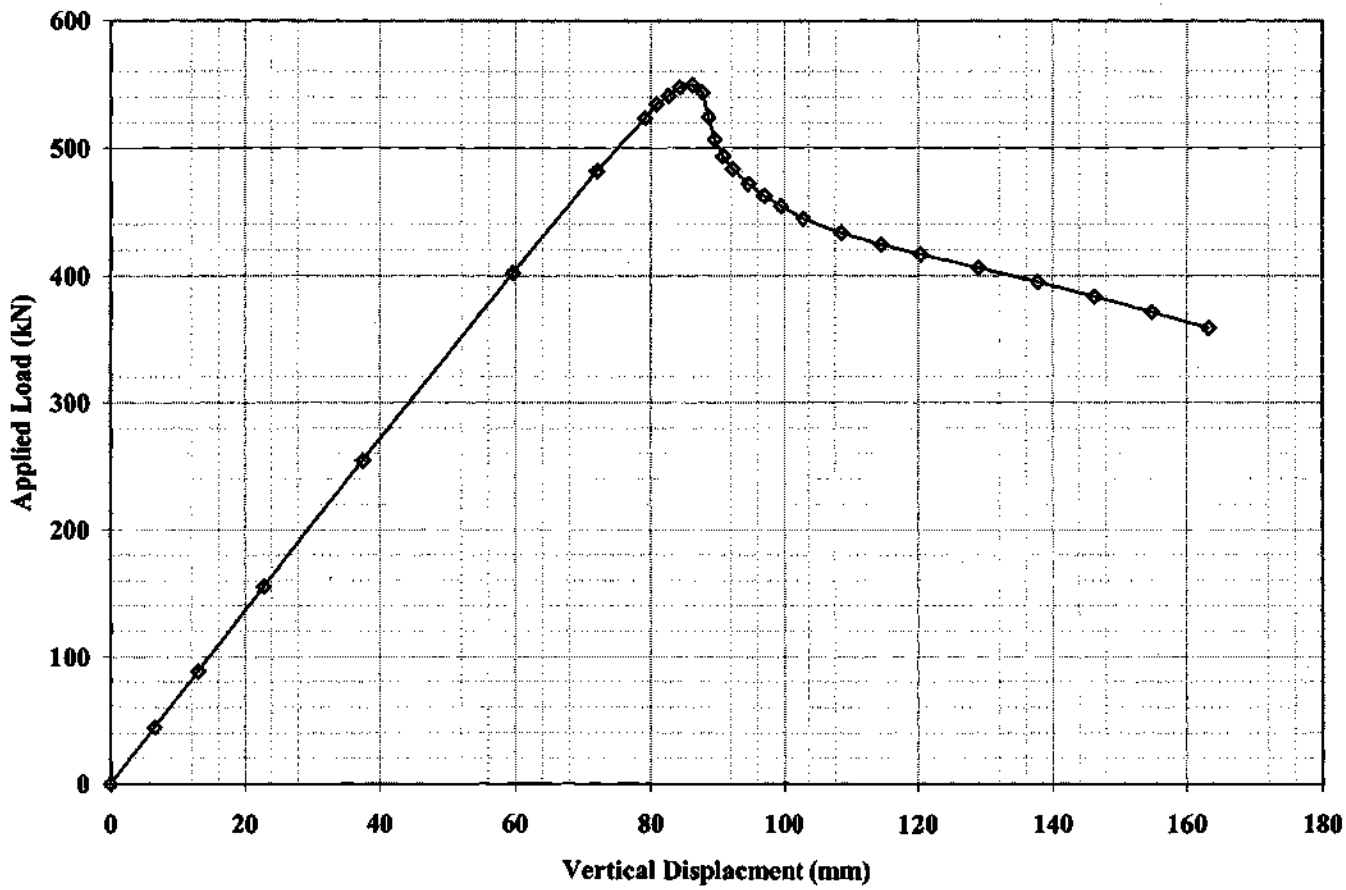

Figure 6.2.11. Load P versus vertical displacement at mid-span of critical segment, internal loading, Specimen 2.75-25-160-3-0.05-0.50.

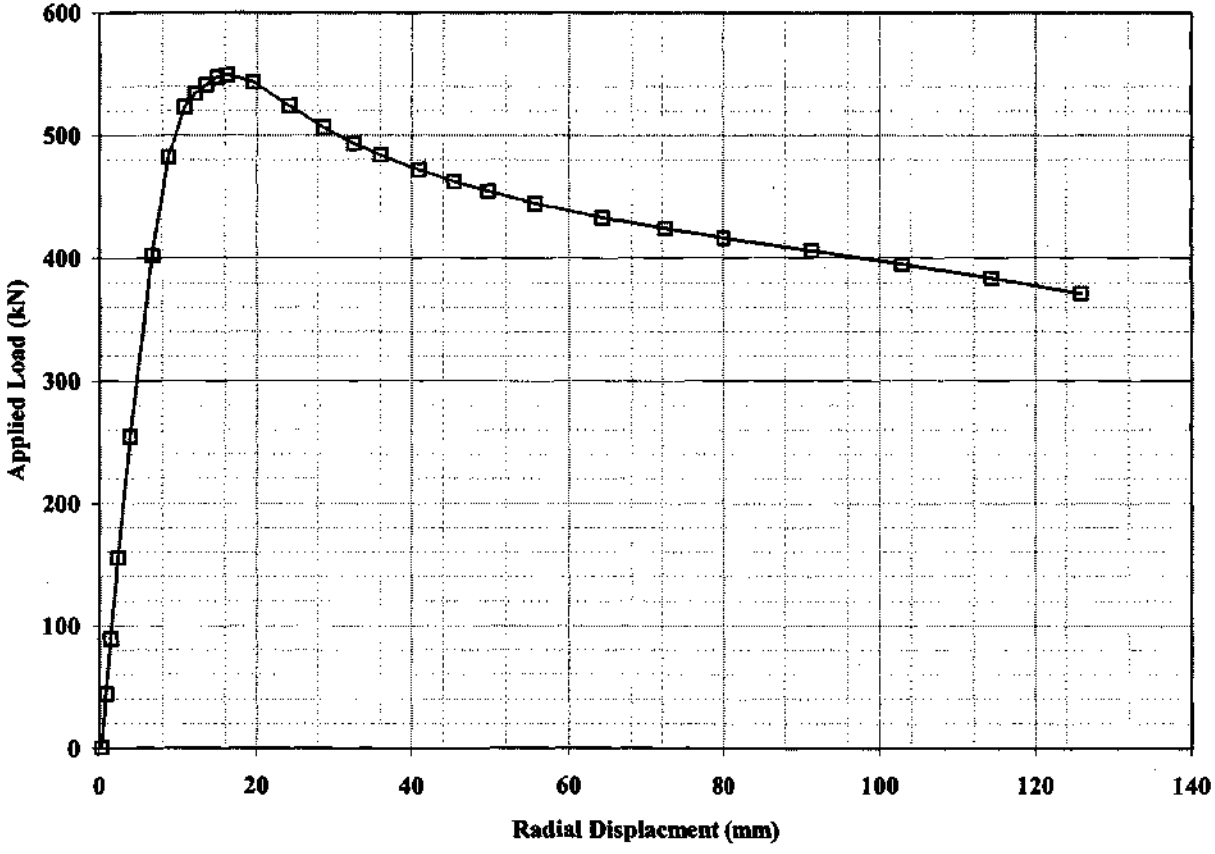

Figure 6.2.12. Load P versus radial displacement at top flange at mid-span of critical segment, internal loading, Specimen 2.75-25-160-3-0.05-0.50.

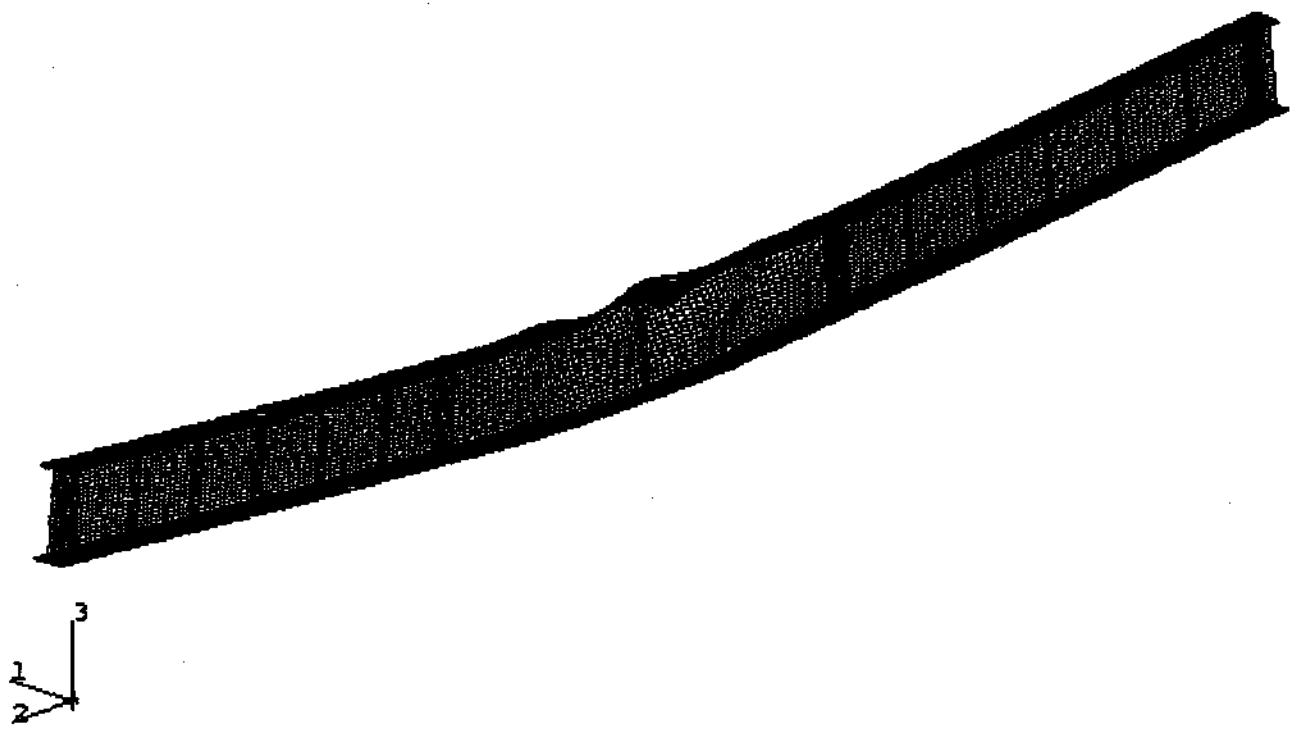

Figure 6.2.13. Deformed mesh at peak load, internal loading, Specimen 2.75-25-160-3-0.05-0.50 (displacement magnification factor = 10).

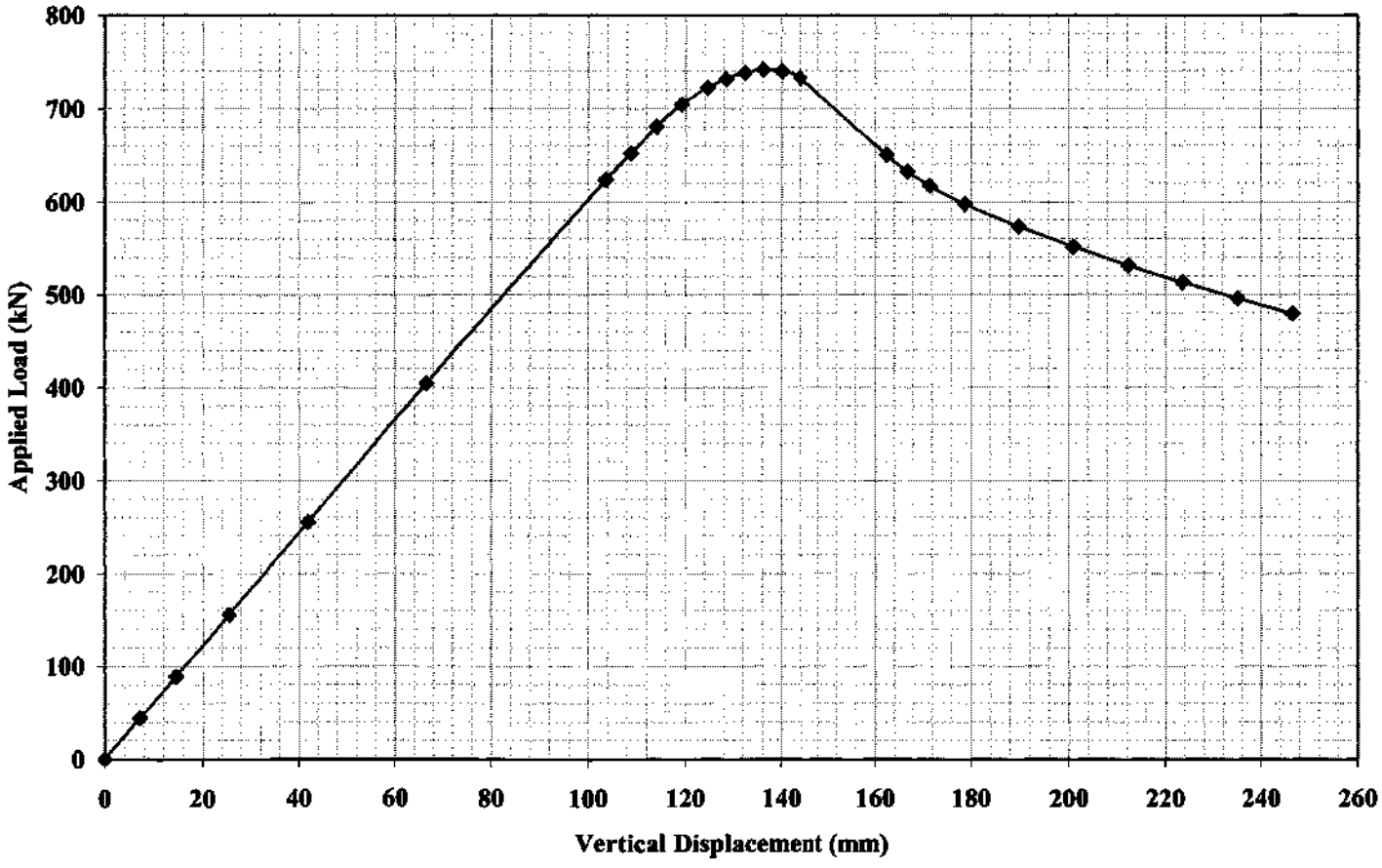

Figure 6.3.1. Load P_2 versus vertical displacement at mid-span of critical segment, uniform vertical bending, Specimen 2.75-15-100-3-0.05-0.50.

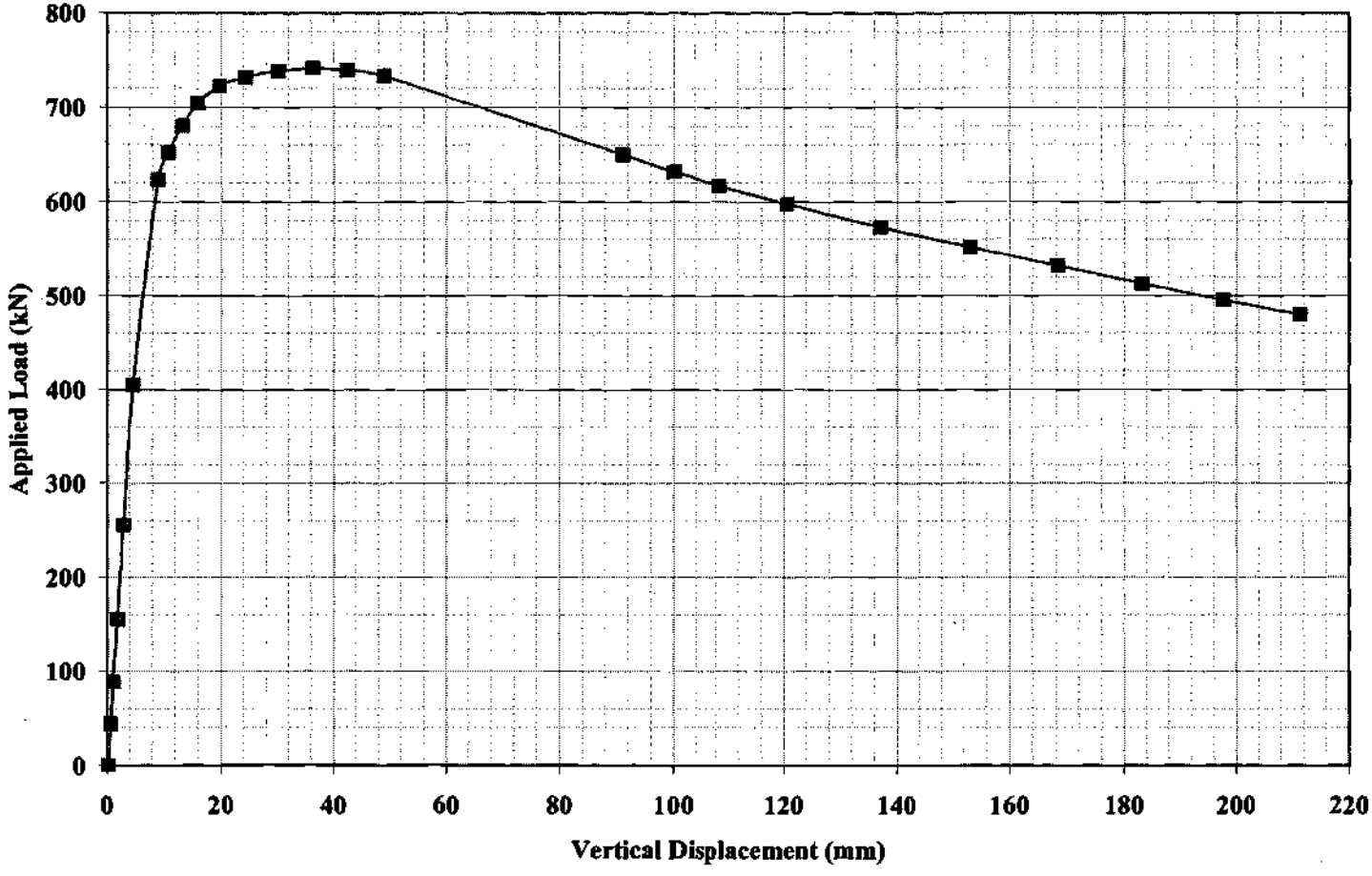

Figure 6.3.2. Load P_2 versus radial displacement at mid-span of critical segment, uniform vertical bending, Specimen 2.75-15-100-3-0.05-0.50.

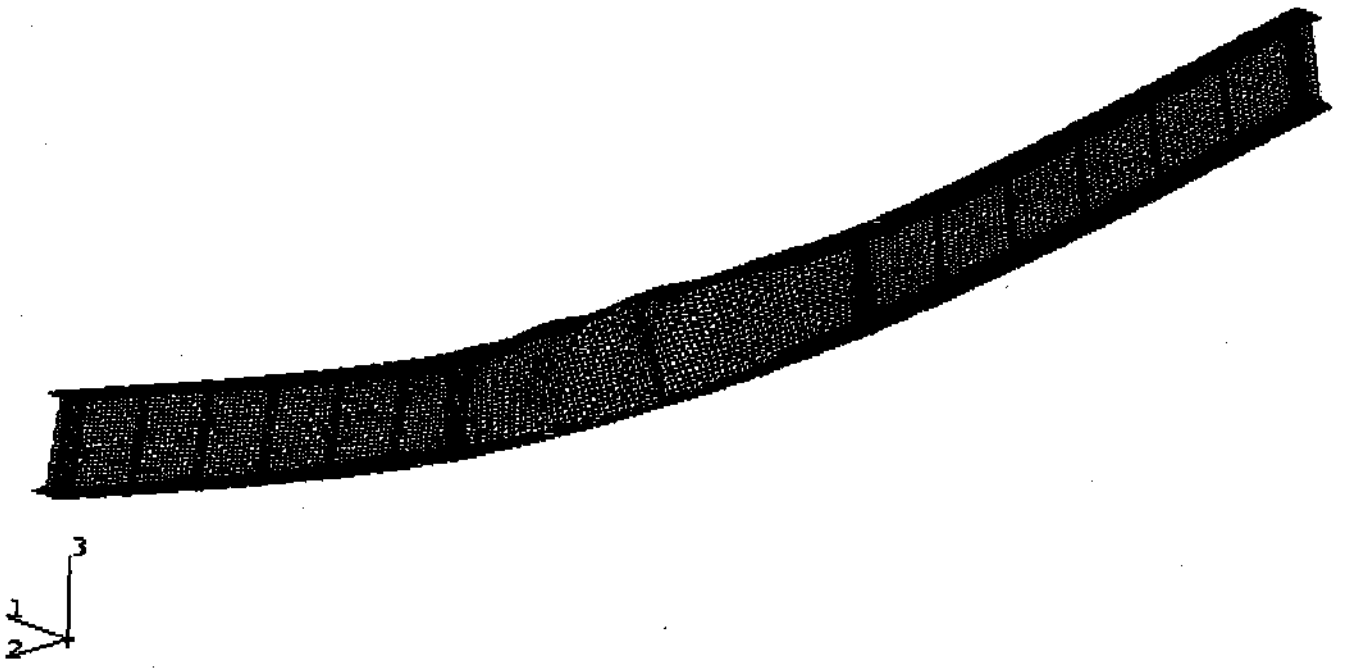

Figure 6.3.3. Deformed mesh at peak load, uniform vertical bending, Specimen 2.75-15-100-3-0.05-0.50 (displacement magnification factor = 10.0).

6.4 SPECIMEN 2.75-15-100-3-0.10-0.50 ($b_f/t_f = 15$, $L_b/b_f = 8.3$)

The load ($P_2 = P_3$) versus the vertical and radial displacement curves at the middle of the critical unsupported segment for the primary uniform vertical bending test of specimen 2.75-15-100-3-0.05-0.50 are shown in Figures 6.4.1 and 6.4.2. Figure 6.4.3 is a plot of the deformed geometry at the maximum load in this test. The load-deflection curves in Figs 6.4.1 and 6.4.2 are somewhat more ductile than all of the previous comparable curves (see Figs 6.1.1, 6.2.1 and 6.3.1 for the load-vertical displacement and Figs. 6.1.2, 6.2.2 and 6.3.2 for the load-radial displacement). However, these curves still exhibit a mild load-shedding response. In spite of the facts that this specimen has a flange that nearly meets the traditional plastic design compactness requirements and the compression flange bracing satisfies the AASHTO (2001) and AISC (1999) compactness requirements, it is not able to sustain an extended plateau in the load-vertical displacement response, as is typical of straight girders that meet these limits.

The reason for this behavior is somewhat simple. P-delta lateral bending moments are generated in the compression flange due to the radial displacements induced by the initial horizontal curvature. Sidesway beam-column members subjected to significant axial compression exhibit similar characteristic load-deflection curves. It appears that it is not practical in general to limit the lateral brace spacing and the compression flange slenderness to smaller values in an attempt to further alleviate this mild load shedding response. Fig. 6.4.3 shows that the mode of failure (i.e., the response associated with the maximum capacity limit) in specimen 2.75-15-100-3-0.05-0.50 is predominantly local flange buckling

6.5. EVALUATION OF GIRDER FLEXURAL DUCTILITY

The load versus displacement plots reviewed in the previous four sections and in Section 4.7 provide useful information about the ductility of horizontally-curved I girders, i.e., the ability of these types of girders to sustain vertical loadings after their maximum load capacities are exceeded. This characteristic is important in that it provides an indication of how rapidly a failed curved-girder segment will shed its load to other portions of the bridge system. If the adjacent components of a bridge are not sufficiently designed to sustain the extra loads that are shed from a failed girder segment, or if the equilibrium of the bridge system does not allow for significant shedding of load from the failed component, then a catastrophic failure of the full bridge system becomes more likely when the load-shedding response of the critical curved segment is more severe. This is likely to be an issue in the outside girder of a curved bridge that has only a few main girders; the three-girder system utilized in the FHWA-CSBRP tests at the Turner-Fairbank laboratory is an example of this, with the exception that its cross-frames and interior girders are designed to sustain the loads that are shed from the test components.

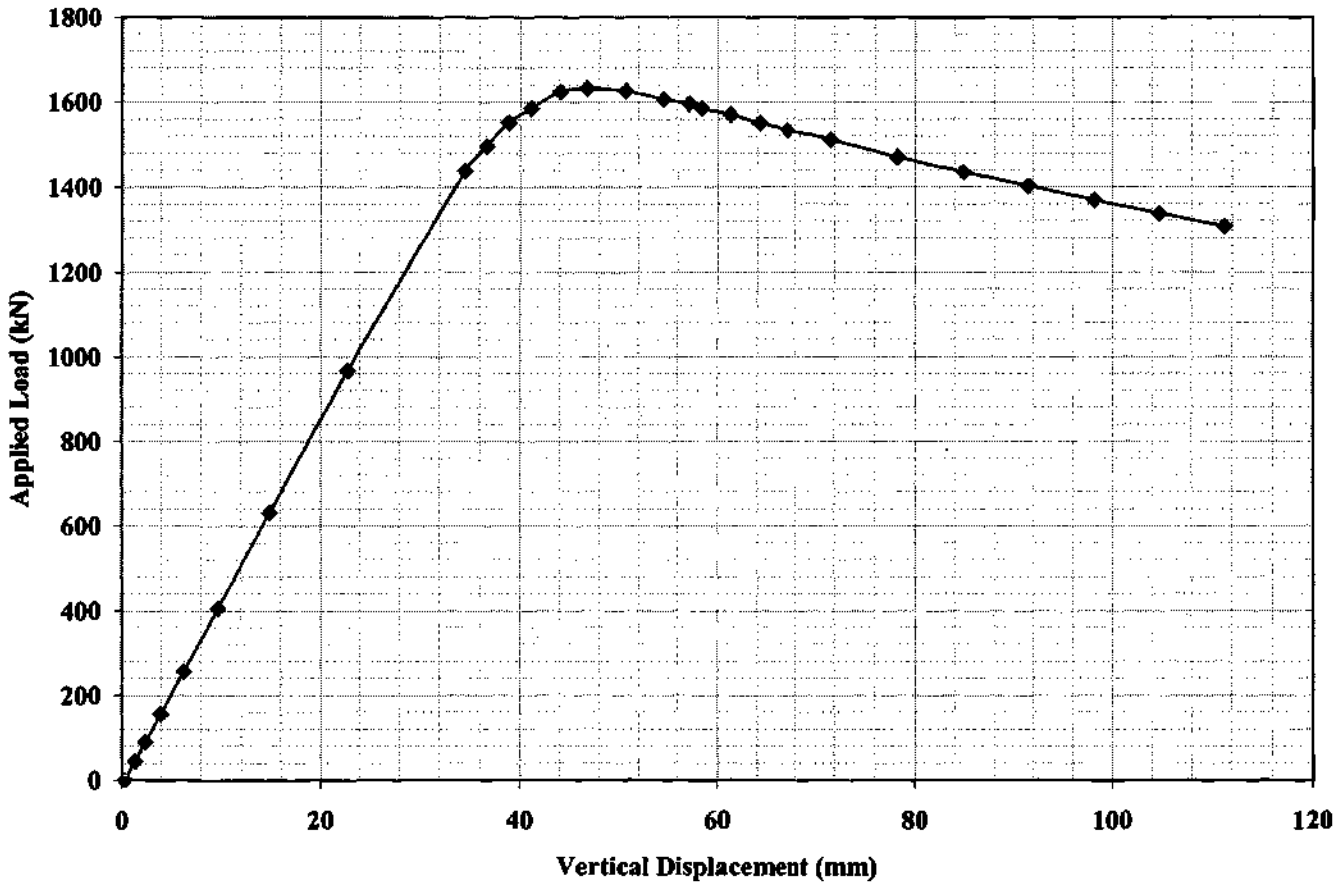

Figure 6.4.1. Load P_2 versus vertical displacement at mid-span of critical segment, uniform vertical bending, Specimen 2.75-15-100-3-0.10-0.50.

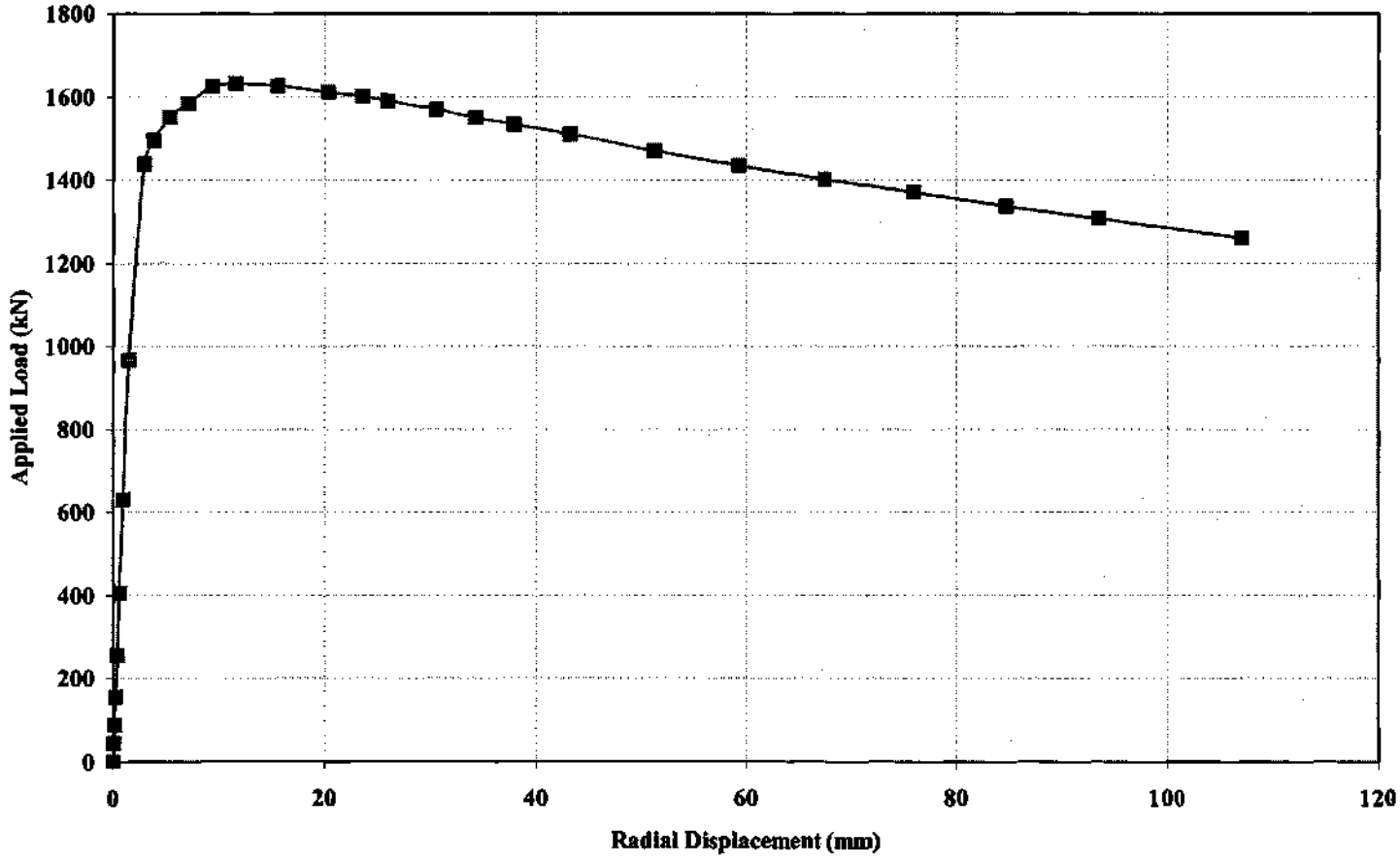

Figure 6.4.2. Load P_2 versus radial displacement at mid-span of critical segment, uniform vertical bending, Specimen 2.75-15-100-3-0.10-0.50.

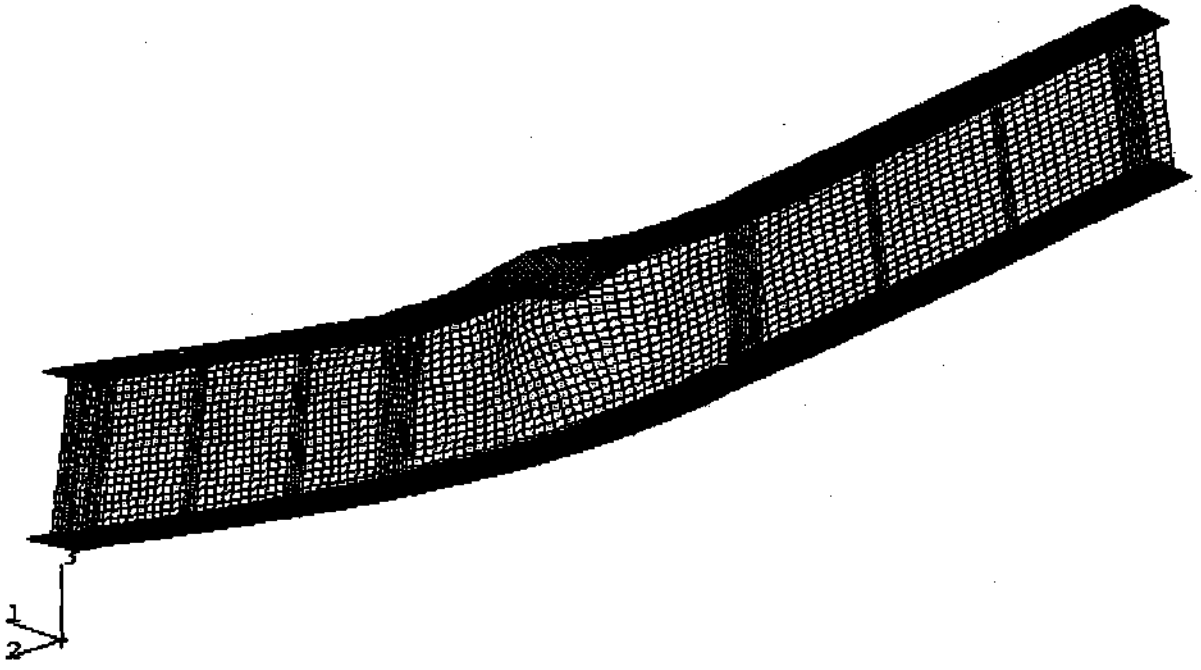

Figure 6.4.3. Deformed mesh at peak load, uniform vertical bending, Specimen 2.75-15-100-3-0.10-0.50 (displacement magnification factor = 15.0).

It can be argued that load-inelastic deflection curves provide a better indication of the member ductility than load-total deflection curves, since inelastic deflections are the primary source of load shedding or redistribution within the structural system. Therefore, the previous load-total displacement curves from the uniform vertical bending, modified uniform vertical bending, and internal load studies are converted to load-inelastic displacement curves in this section. These curves are compared directly, and also they are compared after normalization, by dividing the load by its corresponding maximum value and dividing the displacement by the unsupported length L_b. The corresponding curves for the load versus the vertical displacement at the girder mid-length are shown for all the parametric study specimens considered in the previous sections in Figs. 6.5.1 and 6.5.2. Similar curves for the load versus radial displacement at the girder mid-length are presented in Figs. 6.5.3 and 6.5.4. It should be noted that the plastic displacements are obtained simply by determining the initial elastic slope of the curves (K), and then subtracting the applied load divided by K from the displacement at each of the data points.

It can be observed that all the specimens tend to reach a peak load at relatively small plastic displacements, and subsequently exhibit a gradual shedding of their load. The specimens with compact flanges ($b_{fc}/t_{fc} = 15$) do not shed their load as rapidly while the normalized plastic displacements (vertical and radial) are less than about 0.006. However, for normalized plastic displacements larger than this magnitude, the load-shedding rate is approximately the same in all of the specimens.

Figures 6.5.5 and 6.5.6 show comparable results for the load-vertical displacement obtained from the analysis results for girders L1-A and L2-A (see Fig. 4.1.2, Tables 4.2.1 and 4.2.2, and Figs. 4.7.1 and 4.7.2). These curves are very similar in their characteristics to the curves for the compact flange girders in Fig. 6.5.1, although the curves are not quite as rounded within the vicinity of the peak load. The total loads versus the plastic vertical displacements are shown for tests B1 through B7 in Figs. 6.5.7 and 6.5.8 (see Figs. 4.1.11 and 4.1.12, Tables 4.2.5 through 4.2.7, and Figs. 4.7.7 through 4.7.13). Again, the girders with the more slender flanges appear to shed their loads more rapidly at small plastic displacements than the girders with compact flanges. However, in these tests, it is apparent that some system effects are influencing the total load on the bridge such that the girders with more slender flanges exhibit a stable reloading response after a significant fraction (approximately 10 percent) of the total load is shed.

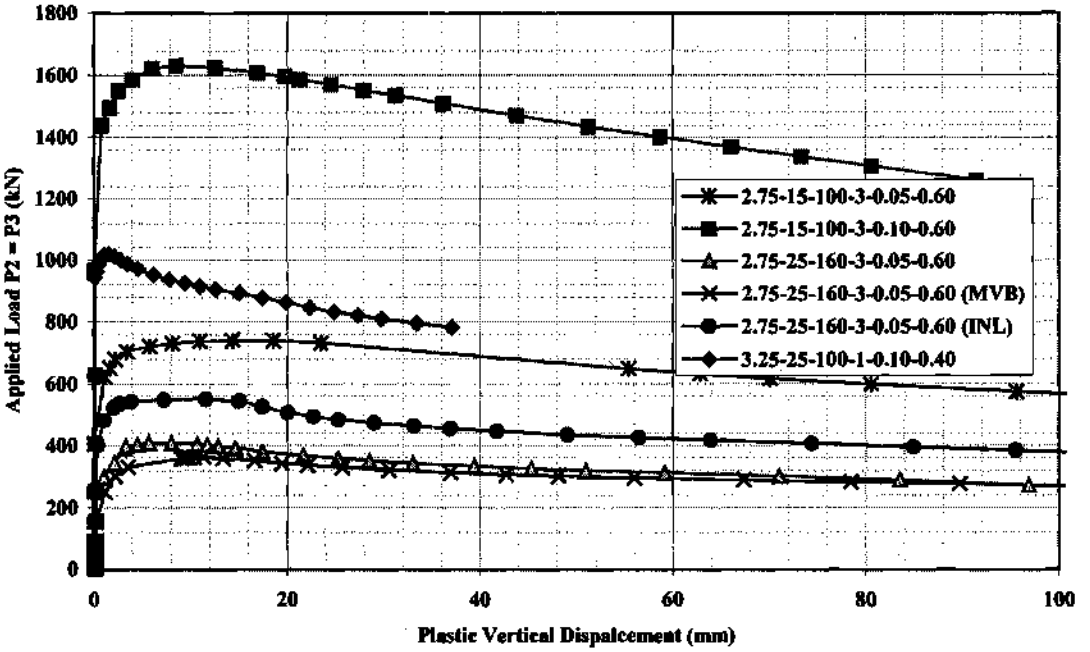

Figure 6.5.1. Load P2 versus plastic vertical displacement at the mid-length of the parametric study specimens, uniform vertical bending and internal load cases.

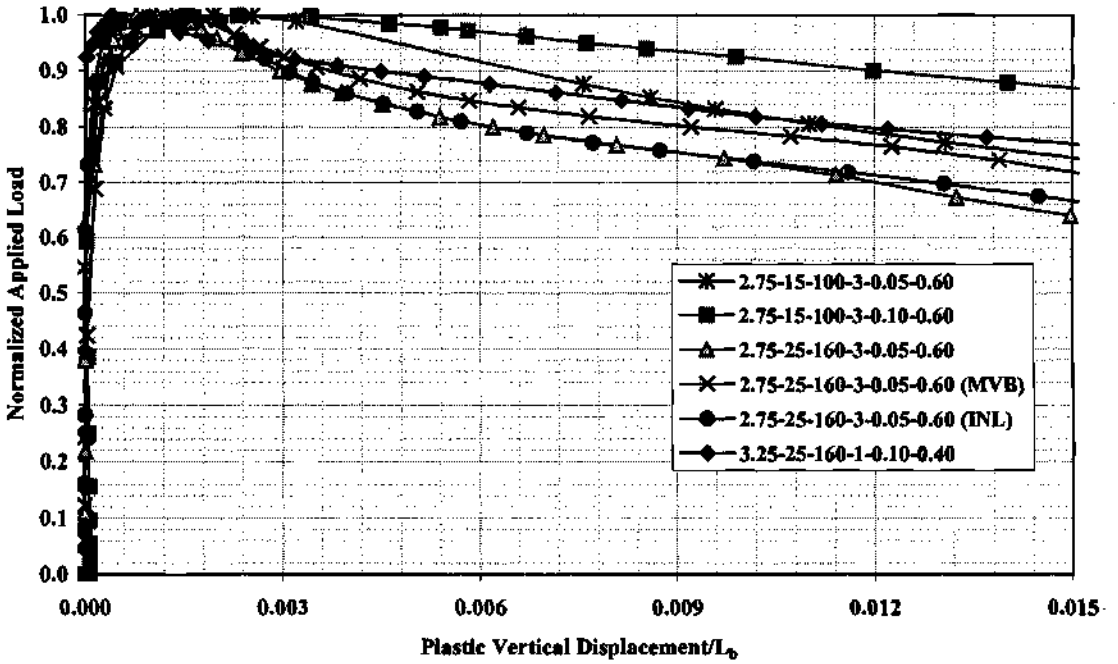

Figure 6.5.2. Normalized applied load versus plastic vertical displacement/L_b for parametric study specimens, uniform vertical bending and internal load cases.

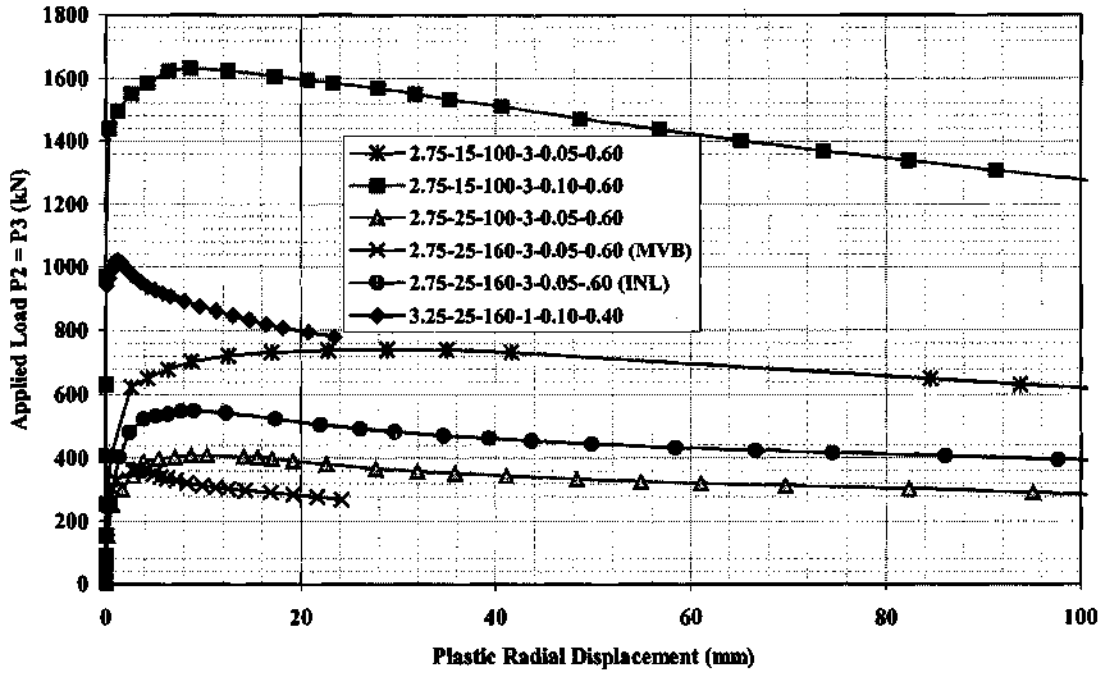

Figure 6.5.3. Load P2 versus plastic radial displacement of parametric study specimens, uniform vertical bending and internal load cases.

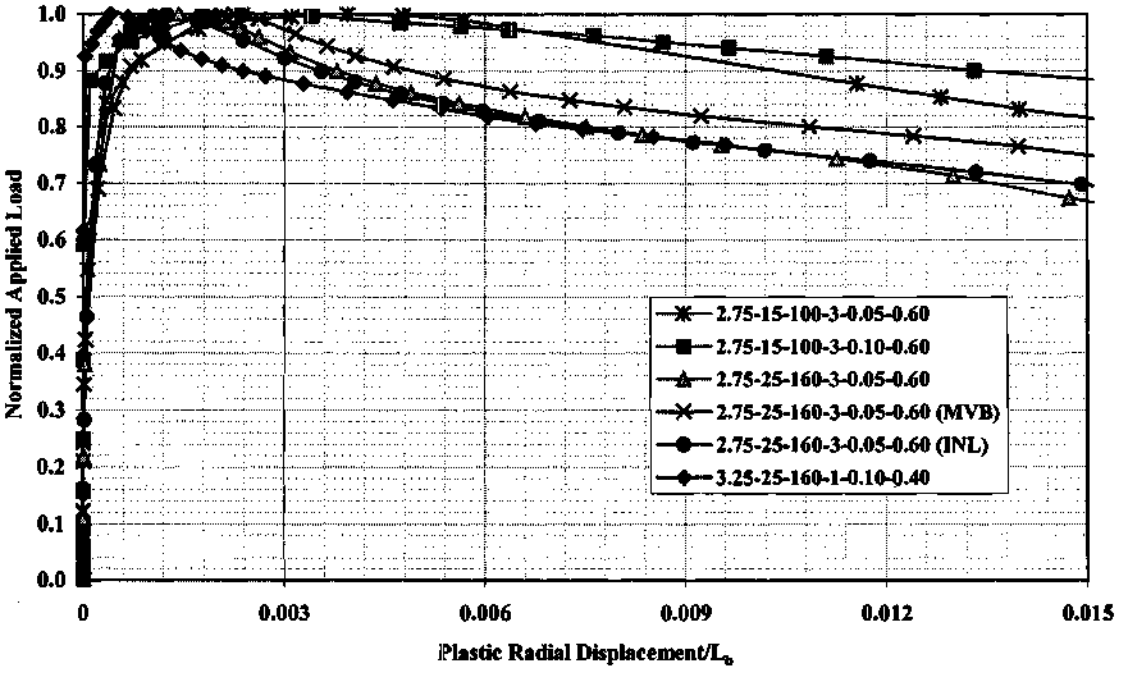

Figure 6.5.4. Normalized applied load versus plastic radial displacement/L_b of parametric study specimens, uniform vertical bending and internal load cases.

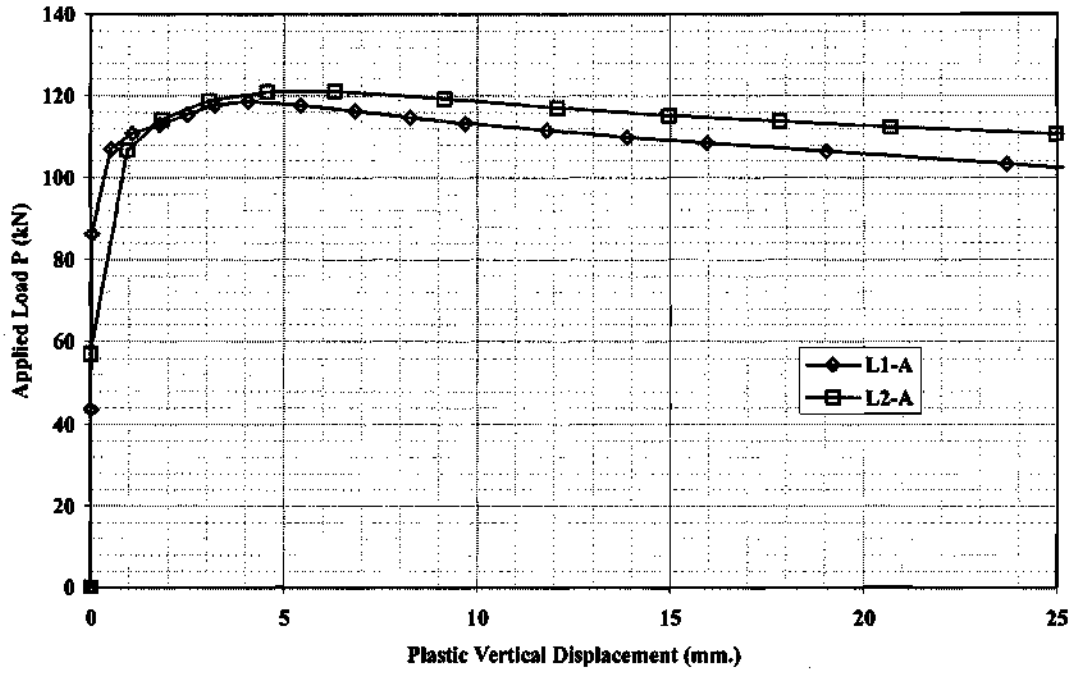

Figure 6.5.5. Applied load versus plastic vertical displacement of specimens L1-A and L2-A.

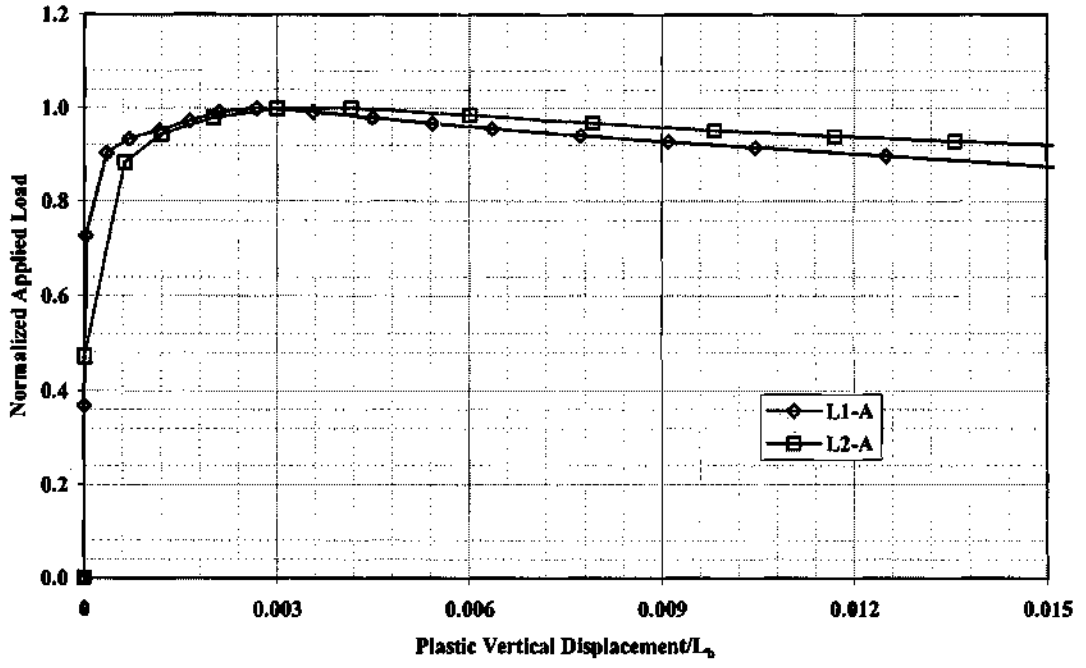

Figure 6.5.6. Normalized applied load versus plastic vertical displacement/L_b of specimens L1-A and L2-A.

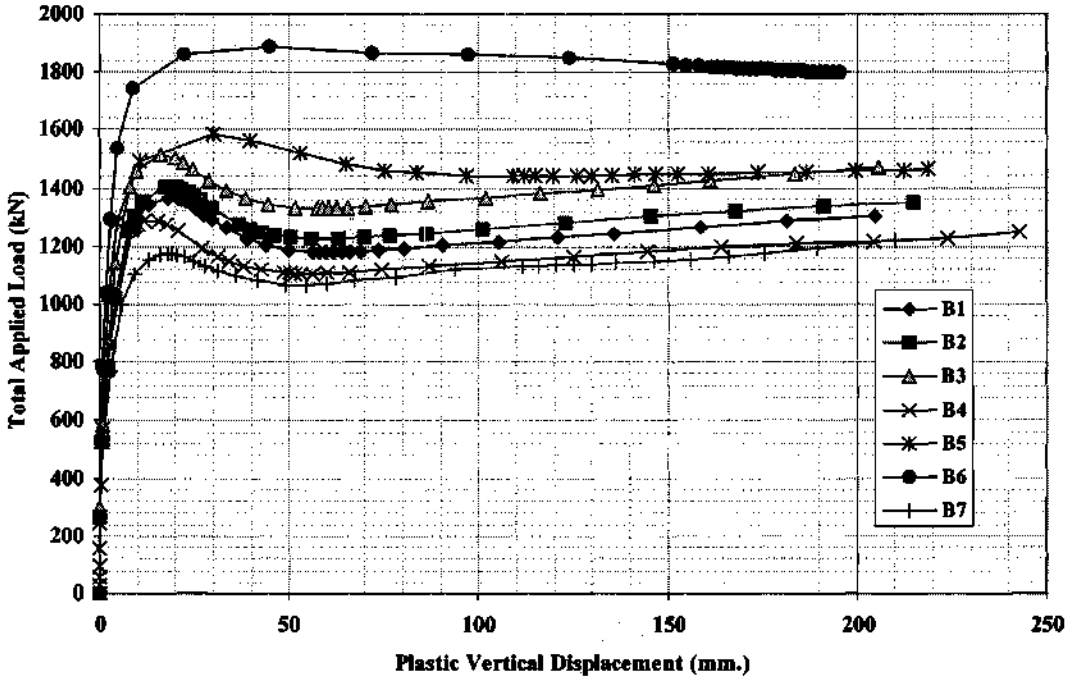

Figure 6.5.7. Total applied load versus plastic vertical displacement of specimens B1-B7.

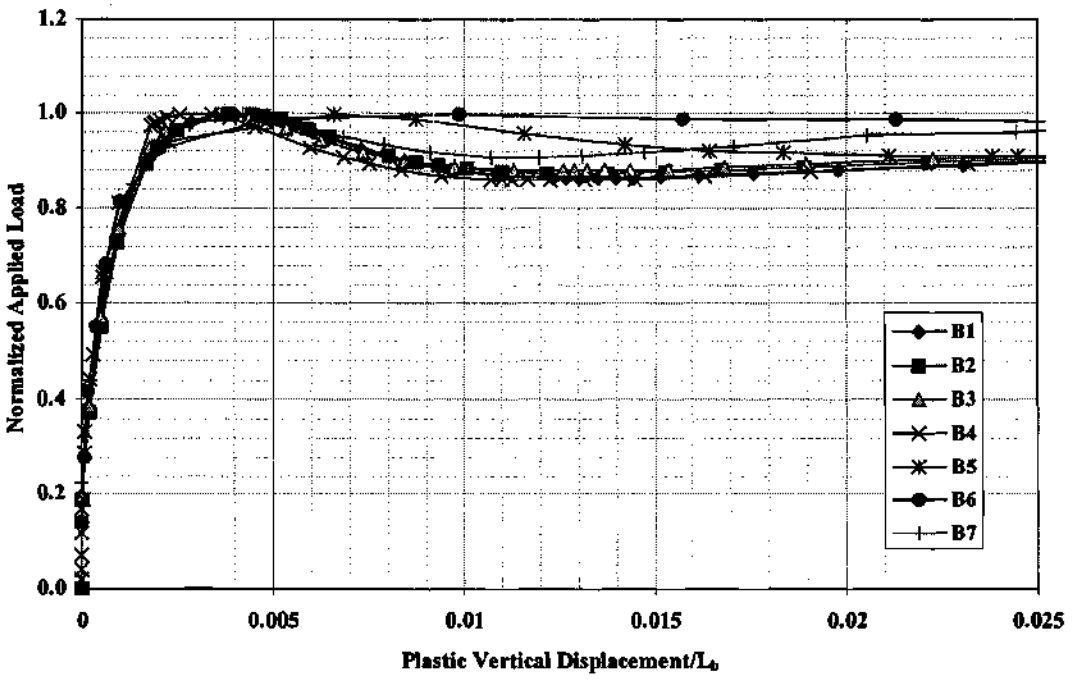

Figure 6.5.8. Total normalized applied load versus plastic vertical displacement/L_b of specimens B1-B7.

CHAPTER VII

PARAMETRIC STUDY RESULTS – VERTICAL BENDING STRENGTH

This chapter compares the flexural strengths predicted by four of the design equations discussed in Chapter II to the corresponding strengths determined within the finite element parametric study. The flexural strength equations evaluated are:

1. The design strength formulas within the Recommended Specifications (Hall and Yoo 1998), which are based on the stresses obtained from a first-order elastic analysis (see Section 2.1.2),

2. The flexural strength interaction equations of the Hanshin Guidelines (Hanshin 1988) (see Section 2.1.6),

3. Yoo's (1996) cross-section yield interaction equations, with the maximum internal flange lateral bending moment M_ℓ computed based on the V-load method, Eq. (1-6)[1] (see Section 2.1.8.2),

4. Yoo's (1996) cross-section yield interaction equations, with the flange lateral bending stresses determined from direct elastic analysis, and

5. The proposed one-third rule equations for flexural strength (see Section 2.1.9).

With the exception of the Recommended Specification equations and the combination of Yoo's cross-section yield interaction equations with the V-load solution, the design strength calculations are performed both with first and second-order elastic stresses. In all the studies within this chapter, these elastic stresses are calculated using the same shell finite element models employed in full nonlinear analyses to determine girder capacities, but with no geometric imperfections or residual stresses included and with an assumed linear elastic material response (see Section 3.6). As noted in Section 2.1.2, the Recommended Specification equations estimate the second-order elastic amplification implicitly within their strength reduction factors. Example calculations for the first, fourth and fifth methods in the above list are provided in Section 4.5.1.

The chapter is organized as follows. Sections 7.1, 7.2 and 7.3 present the overall results for the uniform vertical bending case of the primary test suite (Section 5.3), the

[1] Yoo (2000) recommends that the coefficient of "12" should be utilized in the denominator of Eq. (1-6) for the calculation of M_ℓ rather than the values "10" or "14" discussed in Section 2.1.8. Equation (1-6) is applied directly, with the coefficient of 12, in this chapter.

modified uniform vertical bending suite (Section 5.9), and the internal loading suite (Section 5.10). These are followed by several sections that evaluate the quality of the different strength predictor equations for specific girder classifications culled out of the complete results from Sections 7.1 through 7.3. Section 7.4 evaluates the predictions for cases in which the strength is controlled by flange local buckling within the proposed one-third rule checks. Section 7.5 then evaluates the predictor equations for the cases that are controlled by lateral-torsional buckling within the one-third rule equations. Section 7.6 presents the results for cases in which the girder compression flange slenderness as well as the cross-frame spacing satisfy the compactness requirements of the one-third rule provisions, i.e., cases in which the capacity is based on flange plastic strength. Sections 7.7 and 7.8 then evaluate the characteristics of the design equation predictions for nonslender and slender-web girders respectively. Lastly, Section 7.9 evaluates the influence of transverse stiffener spacing on the vertical bending strength.

The above sections focus on the vertical bending strength of internal unsupported segments within a horizontally curved bridge. Section 7.10 presents the results for the tests that target the behavior of end unsupported lengths of horizontally-curved girders, where there is no flange lateral bending restraint at one end of the segment (see Section 5.11 for the design of these tests). The strength predictor equations are evaluated for straight-girders subjected to combined vertical and lateral bending, and with relatively long unsupported lengths in Section 7.11 (the design of these tests is described in Section 5.12). Section 7.12 considers the accuracy of the design predictor equations for the unsymmetric girder suite (see Section 5.13). Then, Section 7.13 provides a discussion of effect of the idealized residual stresses from heat curving versus cut curving on vertical bending strengths. Section 7.14 presents a final summary of the flexural strength predictions by each of the methods evaluated in this chapter for the combined set of all the flexural strength tests.

The last section of the chapter, 7.15, focuses on the amplification of the compression flange lateral bending stresses obtained by the second-order elastic design analyses conducted within the parametric studies, and evaluates several simple amplification factor equations based on these results. Also, the results for the second-order elastic f_ℓ/f_b values are compared to the predictions by the simple V-load equation for several groupings of the test data.

The reader is referred to Chapter 3 for a complete description of the finite element models utilized for full nonlinear analysis to determine the flexural strengths as well as the elastic design analysis stresses. The full nonlinear analyses include the effects of nominal residual stresses and geometric imperfections. The first- and second-order elastic design analyses do not include these attributes.

In the calculation of the flexural strengths as per the Recommended Specification equations, the provisions of these Specifications are employed to define whether the section is compact or noncompact (see Section 2.1.2.8). However, the maximum limit on the flange slenderness from these Specifications (Eq. 2-47a) is not enforced. Also, the limit of $b_{fc}/t_{fc} \leq 24$ specified for the one-third rule equations (which is a practical

fabrication limit on the flange slenderness of bridge I girders adopted from AASHTO LRFD (2001)), as well as the maximum b_{fc}/t_{fc} limit specified by the Hanshin Guidelines, are not enforced here. That is, the noncompact section strength equations are applied up to the maximum $b_{fc}/t_{fc} = 25$ considered in the parametric studies. As noted in Section 5.4, the value $b_{fc}/t_{fc} = 25$ is selected for the parametric studies in order to test at a slightly more severe flange local buckling condition than permitted by the existing specifications.

Both interpretations of the flange applied lateral bending stress at the cross-frame locations (referred to as $\bar{f}_w$ in Section 2.1.2) – McManus's (1971) original interpretation and the interpretation by Hall et al. (1999) – are considered for the primary test suite in Section 7.1. However, only McManus's interpretation is considered within the subsequent studies. The reader is referred to Sections 2.1.2.6 and 2.1.2.7 for a detailed discussion of each of these interpretations.

In this chapter, the web stress limits discussed in Section 2.1.2.9 are not applied in the calculation of the design strengths per the Recommended Specifications.

Finally, in the calculation of the flexural strengths per Yoo's (1996) noncomposite compact-flange section and noncompact section yield interaction equations, the compact flange slenderness limit of the one-third rule equations (Eq. 2-5) is employed to define the transition between these two sets of equations.

This chapter focuses on the overall statistical trends in the flexural strength data from the parametric study tests. The reader is referred to Appendix A for a detailed summary of the strength data for all of the individual cases.

7.1 PRIMARY TEST SUITE

Table 7.1.1 gives statistics for the complete set of doubly symmetric specimens tested in uniform vertical bending within the primary parametric study suite. The data in this table, as well as in the subsequent tables of this chapter, are presented in the following format. The tables focus predominantly on the ratios of the strengths predicted by the different design equations to the full nonlinear finite element analysis based strengths. The arithmetic mean and the standard deviation by the nonbiased or "n-1" method for a population sample

$$\text{std. dev.} = \sqrt{\frac{n\sum x^2 - \left(\sum x\right)^2}{n(n-1)}} \tag{7-1}$$

where n is the number of tests within the sample and x is the parameter that the standard deviation is being taken of, are provided along with the maximum and minimum values for the set. The tables are subdivided into two main sections. The first section presents the data based on second-order elastic design analysis stresses and the second section gives the results based on first-order elastic design analysis stresses.

Table 7.1.1. Summary of primary test suite, vertical bending strength (133 specimens).

	FEA / M_y	FEA / M_p	Mod. LRFD / FEA	Rec Specs / FEA	Hanshin / FEA	Yoo w/ Approx M_ℓ / FEA	Yoo w/ Calc M_ℓ / FEA	1/3 Rule / FEA
Second-Order Elastic Analysis								
Avg.			1.06		0.84		0.88	0.93
Std. dev.			0.05		0.05		0.06	0.04
High	0.96	0.87	1.16		0.98		1.02	1.04
Low	0.71	0.65	0.93		0.73		0.75	0.84
First-Order Elastic Analysis								
Avg.			1.06	0.74	0.86	0.87	0.91	0.94
Std. dev.			0.05	0.15	0.05	0.06	0.06	0.04
High	0.96	0.87	1.16	1.06	0.98	1.00	1.02	1.05
Low	0.71	0.65	0.93	0.57	0.76	0.73	0.78	0.85

The second column in the tables gives the range of all the finite element based flexural strengths relative to the cross-section yield moment, neglecting lateral flange bending and residual stress effects (M_y), while the third column gives the range of all the finite element based flexural strengths (from full nonlinear analysis) to the section plastic moment capacity, neglecting flange lateral bending effects (M_p). The average and standard deviation of these strength ratios are not provided, since this information is not relevant to the discussions. The parametric study is designed to test girders with a wide range of M_n/M_y and M_n/M_p values, where M_n is the vertical bending moment capacity.

The fourth column in the tables gives the statistics for the ratio of the design strength predicted by the proposed modified AASHTO LRFD (2001) straight-girder equations (see Section 2.1.1) to the finite element based strengths. This ratio is expected to be often greater than one, since these equations do not account for the flange lateral bending effects. These results are presented to indicate the magnitude of the reduction in the vertical bending strengths relative to accurate straight girder strength estimates.

The fifth through the ninth columns of the tables present the statistics for each of the strength predictor approaches listed at the beginning of this chapter, expressed in terms of the ratio of the design strengths to the finite element based strengths. The "best" (i.e., most accurate) value or values for each of the statistical quantities is shaded within the corresponding cell(s) of the table. It should be noted that the statistics for the Recommended Specification equations and for the combination of Yoo's (1996) cross-

section yield interaction equations with the V-load formula (labeled as "Yoo w/ Approx. M_t") are not reported within the second-order elastic analysis based section of the tables. This is because the V-load solution is simply an approximate first-order elastic analysis, and also, the Recommended Specification formulas are based on a first-order elastic analysis of the bridge superstructure. Nevertheless, the Recommended Specification equations do incorporate an approximate second-order elastic amplification within their strength reduction terms. As a result, their strength ratios are based on estimated second-order elastic stresses. The Recommended Specification equation results are reported only within the first-order elastic analysis section of the table to avoid confusion about the design analysis method. When the statistical quantities for this method are the most accurate of the second-order elastic analysis-based results, the corresponding values are shown within the appropriate shaded cell in the first section of the table.

7.1.1 Differences Between First- and Second-Order Elastic Based Design Checks

The differences between the strength ratios based on first- and second-order elastic design analysis based strength ratios shown in Table 7.1.1 are typical of many of the cases studied. Section 7.15 addresses the specific amplification of the compression flange lateral bending stresses obtained in the primary test suite. The second-order elastic amplification of these stresses ranges from 1.01 to 1.39 within these tests, although 107 of the 133 girders have an amplification between five and 20 percent. This amplification is larger for some of the other test suites considered subsequently.

The one-third rule equations (Eqs. 2-90) are relatively insensitive to these small changes in the estimates of the maximum flange lateral bending stresses, compared to the other equations, due to the small slope of the resulting vertical-lateral bending interaction curves (see Figs. 2.1.21 and 2.1.22). If the lateral bending stress is equal to $0.5F_y$ (the maximum allowed value of the lateral bending stress within the one-third rule approach), and if the error in the estimate of this stress is 15 percent, the resulting error in the strength reduction due to lateral bending is only $(0.5F_y)(0.15)(1/3) = 0.025F_y$. The Hanshin equations, Yoo's (1996) noncompact section yield-interaction equations and the Recommended Specification noncompact section equations are more sensitive to errors in the estimate of the flange lateral bending stresses. Yoo's and the Recommended Specification noncompact equations are based directly on first-yield, and as noted in Section 2.1.6, the Hanshin equation reduces to a first-yield limit as R becomes large. The first-yield condition is more sensitive to the value for the flange lateral bending stress than other strength checks.

As shown in Table 7.1.1, the largest difference in the average of the strength ratios (i.e., the design equation strength divided by the finite element based strength) associated with the calculation of second-order elastic versus first-order elastic stresses is only 0.03 (0.88 versus 0.91 for Yoo's cross-section yield interaction equation). Therefore, the first-order elastic analysis based results are not discussed further within this section, except for the results of the equations that are based directly on first-order elastic analysis. The discussions focus on the second-order elastic analysis based results, since these provide the most precise evaluation of the accuracy of the design resistance

formulas. Also, the subsequent discussions in Sections 7.2 through 7.14 focus on the strength ratios based on second-order elastic analysis stresses, with the exception of the Recommended Specification and "Yoo w/ Approx. M_t" values. Estimation of the second-order elastic stresses via first-order elastic analysis and amplification factors is addressed in Section 7.15.

7.1.2 Evaluation of Strength Ratio Statistics

One can observe from Table 7.1.1 that the one-third rule equations provide the most accurate prediction on average of the finite element based strengths (0.93) along with the smallest standard deviation (0.04) and the most accurate minimum value (0.84). Their maximum strength ratio obtained in these tests (1.04) is slightly larger than the corresponding maximum values obtained with Yoo's equations (1.02) and with the Hanshin equations (0.98). The average strength ratios for the other second-order elastic stress based predictions are all significantly smaller than those of the proposed equations (0.74, 0.84 and 0.88 for the Recommended Specification, Hanshin and Yoo equations respectively). These smaller estimates are due largely to the first-yield nature of the Recommended Specification and Yoo (1996) design strength estimates when the girder compression flange is noncompact, and due to the similar form of the Hanshin equations for both compact and noncompact section girders. It should be noted that McManus's (1971) interpretation of $\bar{f}_w$ is employed for calculation of the Recommended Specification values in Table 7.1.1.

Yoo's (1996) equations combined with the V-load estimate of the flange lateral bending moment give a strength ratio of 0.87 on average. The V-load equation tends to slightly overestimate the maximum flange lateral bending moment in these tests (see Section 7.15.3), thus producing a less accurate overall prediction of the vertical bending strength. The overestimate by the V-load equation is largely due to the fact that flange warping or lateral bending rotations are not fully restrained at the ends of the critical test segment in the primary test suite. The V-load solution of Eq. (1-6) is based on the assumption of symmetry (fully-fixed) boundary conditions with respect to flange warping at the cross-frames.

The Recommended Specification equations have a significantly higher standard deviation than the other equations (0.15). This is largely due to dramatic reduction in the accuracy of the predictions by McManus's (1971) first-yield based noncompact section equations versus the predictions by his compact section equations. These differences are highlighted by the statistics for the separate girder classifications in Sections 7.4 and 7.6.

Table 7.1.2 summarizes the Recommended Specification results if the interpretation of the flange lateral bending stresses proposed by Hall et al. (1999) is employed rather than McManus's original interpretation. These results are consistent with the results from analyses of the experimental tests reported in Table 4.6.1. On average, for the girders in the primary test suite, the interpretation adopted in the Recommended Specifications (Hall and Yoo 1998) makes the predictions slightly more conservative. The average strength ratios predicted based on the Hall and Yoo (1998) interpretation is

0.68 in Table 4.6.1, with a standard deviation of 0.15 (neglecting the results for the experimental tests that have an $L_b/R > 0.10$), versus 0.72 with a standard deviation of 0.12 in Table 7.1.2. Conversely, the statistics in Table 4.6.1 are 0.72 with a standard deviation of 0.16 with McManus's (1971) original interpretation versus 0.74 with a standard deviation of 0.15 in Table 7.1.2. The maximum unconservative ratio in Table 7.1.2 is reduced from 1.06 with McManus's interpretation to a conservative ratio of 0.99 when the interpretation of the Recommended Specifications is employed.

Table 7.1.2. Effect of interpretation of McManus's equations on Recommended Specification predictions, primary test suite.

	$\frac{\text{Rec Specs}}{\text{FEA}}$ $(\bar{f}_w = f_m = 0)$ Hall and Yoo (1998)	$\frac{\text{Rec Specs}}{\text{FEA}}$ $(\bar{f}_w = f_\ell)$ McManus (1971)
Avg.	0.72	0.74
Std. dev.	0.12	0.15
High	0.99	1.06
Low	0.55	0.57

It should be noted that a slightly different interpretation of Hall and Yoo's (1998) definition of f_m is employed here, compared to the interpretation employed in Chapter IV. In performing the calculations reported in Table 7.1.2, it is recognized that since the girder web is held vertical at the cross-frame locations in the primary test suite, and since the vertical loads are applied to the specimens only at these positions, the flange lateral bending is solely due to the horizontal curvature. Therefore, if the definition that f_m is the "flange bending stress at [the] critical brace point due to effects other than curvature" is interpreted literally, f_m is equal to zero for all of these tests. The interpretation explained in Hall et al. (1999), and summarized in Section 2.1.2.7, in which the stress at the critical cross-frame based on the V-load equation is subtracted from the total computed elastic design analysis stress at this location to obtain f_m, is employed in Chapter IV. In most of the cases in Chapter IV, there are clear loading effects that are causing lateral bending in addition to the effects of horizontal curvature.

7.2 MODIFIED UNIFORM VERTICAL BENDING SUITE

Table 7.2.1 presents the overall strength ratio statistics for the modified uniform vertical bending test suite. There is a significant decrease in the finite element based capacities in these tests relative to the corresponding specimens in the primary test suite, as evidenced by the reduced "FEA/M_y" and "FEA/M_p" ratios and the larger "Mod. LRFD/FEA" ratios in this table compared to Table 7.1.1. The strength ratios for the

Hanshin and the Yoo equations based on directly computed second-order elastic stresses are decreased slightly from their corresponding values in Table 7.1.1, and the strength ratios for the one-third rule equations are slightly increased on average. The Hanshin and Yoo equations are slightly less accurate for the tests considered in Table 7.2.1 than in the earlier table, whereas the one-third rule equations are slightly more accurate. The total number of specimens studied within the modified uniform vertical bending suite (46) is different than the total number considered in the primary suite (133) (only girders with target $f_\ell/f_b = 0.50$ are considered and girders with $L_b/R = 0.075$ are excluded in the modified vertical bending suite). The reader is cautioned that the larger number of specimens included in Table 7.1.1 has a small effect on relative results between Tables 7.2.1 and 7.1.1. However, the trends discussed here are the same if only the corresponding 46 tests from Table 7.1.1 are considered.

Table 7.2.1. Summary of modified vertical bending results (46 specimens).

	$\frac{FEA}{M_y}$	$\frac{FEA}{M_p}$	$\frac{Mod.\ LRFD}{FEA}$	$\frac{Rec\ Specs}{FEA}$	$\frac{Hanshin}{FEA}$	$\frac{Yoo\ w/\ Approx\ M_\ell}{FEA}$	$\frac{Yoo\ w/\ Calc\ M_\ell}{FEA}$	$\frac{1/3\ Rule}{FEA}$
Second-Order Elastic Analysis								
Avg.			1.17		0.82		0.87	0.97
Std. dev.			0.05		0.04		0.08	0.04
High	0.86	0.80	1.27		0.90		1.07	1.04
Low	0.66	0.60	1.07		0.74		0.77	0.88
First-Order Elastic Analysis								
Avg.			1.17	0.73	0.85	0.94	0.91	0.99
Std. dev.			0.05	0.19	0.05	0.07	0.07	0.04
High	0.86	0.80	1.27	1.17	0.96	1.12	1.09	1.06
Low	0.66	0.60	1.07	0.58	0.76	0.82	0.80	0.91

The one-third rule equations provide the best overall predictions for this test suite, with an average strength ratio of 0.97, a standard deviation of 0.04, and maximum and minimum ratios of 1.04 and 0.88 for the solutions based on second-order elastic stresses. The M_ℓ values determined by the V-load equation tend to underestimate the lateral bending moments from the direct analysis in these tests. This results in a significant increase in the "Yoo w/ Approx. M_ℓ" ratios reported in Table 7.2.1 versus 7.1.1 (e.g., 0.94 for the average value in Table 7.2.1 versus 0.87 in Table 7.1.1). The dispersion in the predictions by the Recommended Specification equations is larger for the modified uniform vertical bending suite than for the primary test suite. The standard deviation of

the strength ratios from the Recommended Specification equations is 0.19. Furthermore, although their mean (0.73) and minimum (0.58) strength ratios are the lowest of all the predictor equations, they predict a maximum unconservative value of 1.17. This value corresponds to a girder with a compact flange ($b_{fc}/t_{fc} = 15$) but with a relatively large unsupported length such that the inelastic stability effects are significant. The standard deviation of Yoo's (1996) equations with M_ℓ calculated by direct second-order analysis is high in both Tables 7.2.1 and 7.1.1 (0.06 and 0.08), relative to the other design equations except for the Recommended Specifications. This is due to differences in the accuracy of the compact-flange versus the noncompact section yield interaction equations, as demonstrated subsequently in Sections 7.4 and 7.6.

7.3 INTERNAL LOADING SUITE

Table 7.3.1 summarizes the results for the internal loading suite. Similar to the modified uniform vertical bending suite, there is a significant increase in the average strength ratios for a number of the design equations in this set of tests, relative to the primary studies. The strength ratios for the one-third rule equations, for Yoo's cross-section yield interaction equations with directly calculated M_ℓ values, and for the Hanshin equations are noticeably increased relative to Table 7.1.1. However, the strength ratios for the Recommended Specification equations and for Yoo's equations with M_ℓ determined by the V-load method are not significantly affected relative to the primary test suite.

Table 7.3.1. Summary of internal loading results (26 specimens).

	FEA / M_y	FEA / M_p	Mod. LRFD / FEA	Rec Specs / FEA	Hanshin / FEA	Yoo w/ Approx M_ℓ / FEA	Yoo w/ Calc M_ℓ / FEA	1/3 Rule / FEA
Second-Order Elastic Analysis								
Avg.			1.15		0.86		0.91	1.00
Std. dev.			0.05		0.03		0.06	0.04
High	0.86	0.78	1.25		0.91		1.04	1.08
Low	0.68	0.62	1.06		0.79		0.80	0.93
First-Order Elastic Analysis								
Avg.			1.15	0.73	0.88	0.89	0.93	1.01
Std. dev.			0.05	0.17	0.03	0.06	0.05	0.04
High	0.86	0.78	1.25	1.06	0.93	1.00	1.04	1.09
Low	0.68	0.62	1.06	0.58	0.83	0.79	0.85	0.94

Again, the one-third rule equations produce the best overall results, with a mean of 1.00, a standard deviation of 0.04 and a low value of 0.93 based on second-order elastic analysis. However, these equations have a maximum strength ratio of 1.08 for the internal load tests. Yoo's equations give a more accurate maximum value (1.04), but have a wider dispersion in their strength predictions. The Recommended Specification equations also give a smaller maximum strength ratio for these tests (1.06), but similar to the previously discussed test suites, the standard deviation of their strength ratio is very large (0.17), and their mean and minimum values (0.73 and 0.59) are quite small. The Hanshin equations are also significantly conservative, although they have the smallest standard deviation of the strength ratios for these tests.

7.4 RESULTS FOR CASES CONTROLLED BY FLANGE LOCAL BUCKLING

In this section, the statistics for the combined primary, modified vertical bending, and internal loading suites are presented for all the girders in which the strength is controlled by inelastic flange local buckling within the one-third rule provisions. This includes all the girders that have a flange slenderness $b_{fc}/2t_{fc} > (\lambda_p = 0.382\sqrt{E/F_{yc}} = 9.2)$ for F_{yc} = 345 MPa (50 ksi), and in which the flange local buckling strength check is more critical than the lateral-torsional buckling strength check in Eqs. (2-90). The results for all the specimens that fit this definition are listed in Table 7.4.1. Tables 7.4.2 and 7.4.3 then present the results from Table 7.4.1 separately for the two flange b_f/t_f values considered in the parametric study that exceed the above compact slenderness limit, b_f/t_f = 20 and 25.

Table 7.4.1. Summary of primary, modified vertical bending and internal loading suites, vertical bending strength for cases controlled by flange local buckling (141 specimens).

	$\frac{FEA}{M_y}$	$\frac{FEA}{M_p}$	$\frac{Mod.\ LRFD}{FEA}$	$\frac{Rec\ Specs}{FEA}$	$\frac{Hanshin}{FEA}$	$\frac{Yoo\ w/\ Approx\ M_\ell}{FEA}$	$\frac{Yoo\ w/\ Calc\ M_\ell}{FEA}$	$\frac{1/3\ Rule}{FEA}$
Second-Order Elastic Analysis								
Avg.			1.08		0.84		0.86	0.94
Std. dev.			0.08	0.04	0.05		0.05	0.05
High	0.93	0.84	1.27		0.98		1.00	1.07
Low	0.66	0.61	0.93		0.74		0.75	0.84
First-Order Elastic Analysis								
Avg.			1.08	0.66	0.87	0.87	0.89	0.95
Std. dev.			0.08	0.04	0.05	0.06	0.05	0.05
High	0.93	0.84	1.27	0.78	0.98	1.01	1.00	1.08
Low	0.66	0.61	0.93	0.57	0.76	0.73	0.78	0.85

Table 7.4.2. Vertical bending strength for cases controlled by flange local buckling, $b_f/t_f = 20$, primary, modified vertical bending and internal loading sets (32 tests).

	FEA / M_y	FEA / M_p	Mod. LRFD / FEA	Rec Specs / FEA	Hanshin / FEA	Yoo w/ Approx M_ℓ / FEA	Yoo w/ Calc M_ℓ / FEA	1/3 Rule / FEA
Second-Order Elastic Analysis								
Avg.			1.11		0.80		0.81	0.97
Std. dev.			0.07	0.04	0.04		0.04	0.04
High	0.93	0.84	1.27		0.87		0.89	1.07
Low	0.76	0.69	1.04		0.74		0.75	0.93
First-Order Elastic Analysis								
Avg.			1.11	0.64	0.82	0.83	0.84	0.98
Std. dev.			0.07	0.04	0.04	0.05	0.04	0.04
High	0.93	0.84	1.27	0.71	0.90	0.90	0.92	1.08
Low	0.76	0.69	1.04	0.57	0.76	0.73	0.78	0.94

Table 7.4.3. Vertical bending strength for cases controlled by flange local buckling, $b_f/t_f = 25$, primary, modified vertical bending and internal loading sets (109 tests).

	FEA / M_y	FEA / M_p	Mod. LRFD / FEA	Rec Specs / FEA	Hanshin / FEA	Yoo w/ Approx M_ℓ / FEA	Yoo w/ Calc M_ℓ / FEA	1/3 Rule / FEA
Second-Order Elastic Analysis								
Avg.			1.07		0.86		0.87	0.92
Std. dev.			0.08	0.04	0.04		0.04	0.04
High	0.90	0.82	1.25		0.98		1.00	1.03
Low	0.66	0.61	0.93		0.77		0.78	0.84
First-Order Elastic Analysis								
Avg.			1.07	0.66	0.88	0.88	0.90	0.94
Std. dev.			0.08	0.04	0.04	0.05	0.04	0.05
High	0.90	0.82	1.25	0.78	0.98	1.01	1.00	1.06
Low	0.66	0.61	0.93	0.58	0.79	0.78	0.80	0.85

The one-third rule equations again give the best overall predictions of the finite element based strengths. These equations are slightly more accurate for the girders with $b_f/t_f = 20$ versus the ones with $b_f/t_f = 25$. The largest unconservative strength ratio for these equations is 1.07 (based on second-order elastic stresses). The maximum unconservative predictions are obtained for a specimen with $D/b_f = 2.75$, $D/t_w = 130$ and $b_f/t_f = 20$ from the internal loading suite (see Table A.3.4). The maximum conservative prediction (0.84) is obtained for a specimen with $D/b_f = 2.75$, $b_f/t_f = 25$ and $D/t_w = 160$ in the primary test suite (see Table A.1.14)

Yoo's (1996) cross-section yield interaction equations predict conservative strengths for these noncompact girders with both methods of calculating M_ℓ. The smallest strength ratio predicted by these equations, based on direct second-order elastic analysis, is 0.75 for a specimen with $D/b_f = 2.75$, $D/t_w = 100$ and $b_f/t_f = 20$ in the primary suite (see Table A.1.13). Yoo's equations are on average less accurate for the girders with the stockier flanges, $b_f/t_f = 20$ (compare Tables 7.4.2 and 7.4.3). These results clearly show the conservatism of limiting $f_b \le F_y - f_\ell$ according to the cross-section yield interaction equations.

The Hanshin equations have about the same accuracy as Yoo's equations for the noncompact girder sections. The mean value of the strength ratios based on the Hanshin equations is 0.84 in Table 7.4.1 with a standard deviation of 0.05. The Hanshin equations also perform slightly better for girders with $b_f/t_f = 25$ (see Tables 7.4.2 and 7.4.3) compared to the cases with $b_f/t_f = 20$. Their most conservative prediction (0.74) is obtained for specimens with $D/b_f = 2.75$, $b_f/t_f = 20$ and $D/t_w = 100$ and 130 in the primary test suite (see Table A.1.13).

As discussed earlier, the Recommended Specification equations significantly underestimate vertical bending strength of girders with noncompact flanges. The predictions are equally poor for both of the cases $b_f/t_f = 20$ and 25. The mean value of the strength ratios is 0.66 in Table 7.4.1. However, the standard deviation in this table (0.04) is much smaller than that reported in the earlier Tables in Sections 7.1 through 7.3. As noted earlier, this is due to the fact that McManus's compact section equations exhibit much better accuracy relative to the finite element based solutions. The fact that the Recommended Specification equations for noncompact girders are based on first yield, combined with an over conservative amplification of the lateral bending stresses in McManus's (1971) approximate second-order elastic analysis, leads to the significant conservatism of these equations as shown in the tables of this section. The most conservative predictions (0.57) are obtained from the primary suite for two specimens with $D/b_f = 2.75$, $D/t_w = 100$ and $b_f/t_f = 20$ (see Table A.1.13).

7.5 RESULTS FOR CASES CONTROLLED BY LATERAL-TORSIONAL BUCKLING

Table 7.5.1 shows the results for the combined primary, modified vertical bending and internal loading suites for all the girders in which the strength is controlled by

inelastic lateral-torsional buckling within the one-third rule equations. Based on the parametric study design, this entails a subset of the girders with $L_b/R = 0.05$ and target $f_\ell/f_b = 0.50$ (some of the girders with these length-based design parameters and $b_f/t_f = 25$ are controlled by local flange buckling).

Table 7.5.1. Summary of primary, modified vertical bending and internal loading suites, vertical bending strength, cases controlled by lateral-torsional buckling (32 specimens).

	FEA / M_y	FEA / M_p	Mod. LRFD / FEA	Rec Specs / FEA	Hanshin / FEA	Yoo w/ Approx M_ℓ / FEA	Yoo w/ Calc M_ℓ / FEA	1/3 Rule / FEA
Second-Order Elastic Analysis								
Avg.			1.13		0.84		0.92	0.96
Std. dev.			0.06		0.03		0.09	0.04
High	0.86	0.78	1.27		0.92		1.07	1.03
Low	0.66	0.60	1.02		0.79		0.80	0.89
First-Order Elastic Analysis								
Avg.			1.13	0.79	0.86	0.94	0.94	0.98
Std. dev.			0.06	0.24	0.04	0.09	0.08	0.04
High	0.86	0.78	1.27	1.17	0.96	1.12	1.09	1.06
Low	0.66	0.60	1.02	0.56	0.80	0.79	0.82	0.89

It is expected that these tests would exhibit the largest difference between the results predicted based on direct second-order versus first-order analysis of the suites from Sections 7.1 through 7.3. However, the effect of the second-order amplification of the compression flange lateral bending stresses is still minor in Table 7.5.1. It appears that the warping restraint at the ends of the critical unbraced length, due to the continuity with the adjacent unsupported segments, leads to a substantial increase in the elastic lateral-torsional buckling capacity relative to the elastic stress levels at the design load limits. Consequently, this leads to a reasonably small amplification of the compression flange lateral bending stresses in the elastic design analysis. Also, in order to restrict f_ℓ/f_b to 0.50 within the design of these tests, the lateral-torsional buckling slenderness $\lambda = L_b/r_t$ for all these girders falls within the range $0.38 \leq (\lambda - \lambda_p)/(\lambda_r - \lambda_p) \leq 0.52$ based on the unsupported length L_b. As shown subsequently in Sections 7.10 and 7.11, the second-order amplification effects are more significant in the free-end and laterally unsupported straight girder tests.

The mean value of the strength ratio produced by the one-third rule equations is 0.96, with a standard deviation of only 0.04, a maximum value of 1.03 and a minimum of 0.89 (based on second-order elastic stresses). The maximum conservative prediction (0.89) is obtained from the primary test suite for a specimen with D/b_f =2.75, D/t_w = 100 and b_f/t_f = 15 (see Table A.1.12). The maximum unconservative prediction (1.03) is obtained from the modified uniform vertical bending suite for a specimen with D/b_f =2.25, D/t_w = 130 and b_f/t_f = 25 (see Table A.2.3).

The average for Yoo's equations is somewhat lower (0.94), their standard deviation is more than double (0.09), their maximum strength ratio is slightly higher (1.07) and their low value is significantly smaller (0.80) compared to the results for the one-third rule equations. Their maximum unconservative prediction (1.07) is obtained from the modified vertical bending suite for a specimen with D/b_f = 2.75, D/t_w = 160 and b_f/t_f = 15 (see Table A.2.3), and their maximum conservative prediction (0.80) is obtained from the internal loading suite for a girder with D/b_f = 2.75, D/t_w = 100 and b_f/t_f = 20 (see Table A.2.3). It is interesting that the results for Yoo's equations combined with the V-load solution are nearly the same as those based on direct first-order elastic analysis. The V-load estimate is reasonably accurate for the girders in this set.

The Hanshin equations have the smallest standard deviation in the ratio of the predicted to the finite element based strengths (0.03 based on the second-order stresses). However, the mean value of their strength ratio is only 0.84. Their maximum ratio (0.92) is obtained from the primary suite for specimens with D/b_f =2.25, D/t_w = 130 and 160 and b_f/t_f = 25 (see Table A.2.3), and their minimum ratio (0.79) is obtained from the modified uniform vertical bending suite for a specimen with D/b_f =2.75, D/t_w = 100 and b_f/t_f = 20 (see Table A.2.3).

On average, the Recommended Specification equations give the most conservative prediction of all the design formulas for the girders controlled by lateral-torsional buckling, although they are also significantly unconservative for certain tests. The mean value of the strength ratios based on these formulas is 0.79, and their standard deviation for these girders (0.24) is the highest standard deviation of all the groups of tests considered in this chapter. The girders controlled by lateral-torsional buckling include specimens with b_f/t_f = 15, which are considered to be compact by the Recommended Specifications, as well as specimens with b_f/t_f = 20 and 25 which are considered to be noncompact within the Recommended Specification provisions. The Recommended Specification equations yield significantly conservative strength predictions for noncompact sections (0.56 for a specimen with D/b_f =2.75, D/t_w = 100 and b_f/t_f = 20, see Table A.1.18). In contrast, they yield significantly unconservative predictions in some of the tests of the compact flange sections (1.17 for the modified uniform vertical bending suite and a specimen with D/b_f = 2.75, D/t_w = 160 and b_f/t_f = 15, see Table A.2.3).

7.6 RESULTS FOR CASES CONTROLLED BY FLANGE PLASTIC STRENGTH

Table 7.6.1 presents the combined results of the primary, modified vertical bending and internal loading suites for all the girders whose strengths are controlled by the flange

plastic capacity in the one-third rule equations, i.e., for all the girders which have compact flanges and compact lateral brace spacing. Tables 7.6.2 through 7.6.4 then show the separate statistics for these girders for the different values of D/t_w considered in the parametric study (i.e., $D/t_w = 100$, 130 and 160). These tables provide an important indication of the potential conservatism of the design equations for compact-flange, compactly braced girders as the web slenderness approaches its compact limit.

From Table 7.6.1, one can observe that for these girders, all of the predictor equations perform well with the exception of the Hanshin equations. The one-third rule equations give an average strength ratio of 1.00 for these tests, based on second-order elastic stresses, but have a slightly larger maximum value than Yoo's and the Recommended Specification's formulas (1.08 versus 1.03 and 1.06). The Recommended Specification equations give the most accurate minimum value (0.95), versus 0.89 and 0.94 for Yoo's compact-section yield interaction equation and for the one-third rule equations.

When these tests are grouped based on the web slenderness, the Recommended Specification equations show the best performance for $D/t_w = 100$ (see Table 7.6.2), the Recommended Specification formulas and the one-third rule equations are the best predictors and essentially perform equally well for $D/t_w = 130$ (see Table 7.6.3), and the one-third rule equations show the best performance for $D/t_w = 160$ (see Table 7.6.4).

From Tables 7.6.1 through 7.6.4, it is apparent that Eq. (1-6) gives a reasonably good estimate of the first- and second-order flange moments and stresses for these problems. The predictions by Yoo's equations are only slightly improved by direct calculation of the flange lateral bending stresses.

The Hanshin equations yield the most conservative predictions for these tests. The mean strength ratio for these equations is 0.81 with a standard deviation of 0.04 for the full set of these girders (see Table 7.6.1), due to the first-yield nature of these equations.

It is important to note that the Recommended Specification and the one-third rule equations are both somewhat more conservative for the girders with the stockiest webs ($D/t_w = 100$). For both of these sets of equations, the mean ratios are a factor of 0.04 smaller for the $D/t_w = 100$ cases compared to the $D/t_w = 160$ cases. However, the predictions for $D/t_w = 130$ and 160 are essentially equally accurate for both approaches. The slight conservatism in the predictions for $D/t_w = 100$, combined with the fact that the finite element based strengths tend to underestimate the flexural capacities obtained in experimental tests of sections with stocky flanges (see Sections 4.4 and 4.7), indicates that some additional benefit may be gained for these types of sections and for sections with stockier webs by basing the underlying straight-girder strengths on equations that give capacities larger than M_y. However, based on the finite element analysis data summarized here, the stockier webs ($D/t_w = 100$) appear to provide only a minimal benefit with respect to the flexural strength. With even stockier webs, typical of rolled I sections, the benefits may be more significant. This issue is discussed further in the recommendations for further research in Chapter X.

Table 7.6.1. Summary of primary, modified vertical bending and internal loading suites, vertical bending strength, cases controlled by flange plastic strength (32 specimens).

	$\frac{\text{FEA}}{M_y}$	$\frac{\text{FEA}}{M_p}$	$\frac{\text{Mod. LRFD}}{\text{FEA}}$	$\frac{\text{Rec Specs}}{\text{FEA}}$	$\frac{\text{Hanshin}}{\text{FEA}}$	$\frac{\text{Yoo w/ Approx } M_\ell}{\text{FEA}}$	$\frac{\text{Yoo w/ Calc } M_\ell}{\text{FEA}}$	$\frac{\text{1/3 Rule}}{\text{FEA}}$
Second-Order Elastic Analysis								
Avg.			1.13		0.81		0.96	1.00
Std. dev.			0.05	0.03	0.04		0.03	0.03
High	0.96	0.87	1.22		0.89		1.03	1.08
Low	0.81	0.75	1.04	0.95	0.73		0.89	0.94
First-Order Elastic Analysis								
Avg.			1.13	1.01	0.83	0.95	0.97	1.01
Std. dev.			0.05	0.03	0.04	0.03	0.03	0.03
High	0.96	0.87	1.22	1.06	0.91	1.01	1.04	1.09
Low	0.81	0.75	1.04	0.95	0.76	0.88	0.91	0.95

Table 7.6.2. Summary of primary, modified vertical bending and internal loading suites, vertical bending strength, cases controlled by flange plastic strength and $D/t_w = 100$ (7 specimens).

	$\frac{\text{FEA}}{M_y}$	$\frac{\text{FEA}}{M_p}$	$\frac{\text{Mod. LRFD}}{\text{FEA}}$	$\frac{\text{Rec Specs}}{\text{FEA}}$	$\frac{\text{Hanshin}}{\text{FEA}}$	$\frac{\text{Yoo w/ Approx } M_\ell}{\text{FEA}}$	$\frac{\text{Yoo w/ Calc } M_\ell}{\text{FEA}}$	$\frac{\text{1/3 Rule}}{\text{FEA}}$
Second-Order Elastic Analysis								
Avg.			1.10	0.98	0.77		0.92	0.97
Std. dev.			0.06	0.03	0.03		0.03	0.03
High	0.96	0.87	1.19	1.03	0.80		0.97	1.03
Low	0.84	0.76	1.04	0.95	0.73		0.89	0.94
First-Order Elastic Analysis								
Avg.			1.10	0.98	0.79	0.91	0.93	0.98
Std. dev.			0.06	0.03	0.03	0.03	0.03	0.03
High	0.96	0.87	1.19	1.03	0.83	0.96	0.99	1.04
Low	0.84	0.76	1.04	0.95	0.76	0.88	0.91	0.95

Table 7.6.3. Summary of primary, modified vertical bending and internal loading suites, vertical bending strength, cases controlled by flange plastic strength and $D/t_w = 130$ (7 specimens).

	FEA / M_y	FEA / M_p	Mod. LRFD / FEA	Rec Specs / FEA	Hanshin / FEA	Yoo w/ Approx M_ℓ / FEA	Yoo w/ Calc M_ℓ / FEA	1/3 Rule / FEA
Second-Order Elastic Analysis								
Avg.			1.13	1.01	0.80		0.95	1.01
Std. dev.			0.06	0.03	0.04		0.04	0.04
High	0.92	0.84	1.22		0.86		1.03	1.08
Low	0.82	0.75	1.09		0.76		0.92	0.98
First-Order Elastic Analysis								
Avg.			1.13	1.01	0.82	0.95	0.97	1.02
Std. dev.			0.06	0.03	0.04	0.03	0.04	0.04
High	0.92	0.84	1.22	1.06	0.88	0.99	1.04	1.09
Low	0.82	0.75	1.09	0.97	0.78	0.91	0.93	0.99

Table 7.6.4. Summary of primary, modified vertical bending and internal loading suites, vertical bending strength, cases controlled by flange plastic strength and $D/t_w = 160$ (18 specimens).

	FEA / M_y	FEA / M_p	Mod. LRFD / FEA	Rec Specs / FEA	Hanshin / FEA	Yoo w/ Approx M_ℓ / FEA	Yoo w/ Calc M_ℓ / FEA	1/3 Rule / FEA
Second-Order Elastic Analysis								
Avg.			1.13		0.82		0.97	1.01
Std. dev.			0.04		0.04		0.03	0.02
High	0.93	0.86	1.22		0.89		1.02	1.06
Low	0.81	0.75	1.06		0.74		0.92	0.97
First-Order Elastic Analysis								
Avg.			1.13	1.02	0.84	0.96	0.98	1.02
Std. dev.			0.04	0.03	0.04	0.03	0.02	0.03
High	0.93	0.86	1.22	1.06	0.91	1.01	1.03	1.07
Low	0.81	0.75	1.06	0.95	0.79	0.90	0.95	0.98

7.7 RESULTS FOR NONSLENDER-WEB GIRDERS

Table 7.7.1 presents the results for the combined primary, modified vertical bending and internal loading suites for all the girders that have nonslender webs, i.e., $R_b = 1$ at $f_b = F_{yc}$. This includes all of the girders in these sets with $D/t_w = 100$ and 130, regardless of the flange or the lateral-torsional buckling slenderness. Tables 7.7.2 and 7.7.3 give the statistics for these tests for the separate D/t_w values of 100 and 130.

One can observe that the average, maximum and minimum strength ratios for all of the predictor equations are slightly higher for $D/t_w = 130$ compared to $D/t_w = 100$. As shown in several of the previous tables, the Recommended Specification predictions are hampered here by the poor quality of McManus's (1971) noncompact section equations. Also, if these tables are compared to the tables in Section 7.6, it can be seen that the one-third rule and Yoo's equations are slightly more accurate, and the Hanshin equations are slightly less accurate for this group of tests. Aside from these differences, Tables 7.7.1 through 7.7.3 are fairly redundant with the previous tables.

Table 7.7.1. Summary of primary, modified vertical bending and internal loading suites, vertical bending strength, specimens with a nonslender web (80 specimens).

	$\frac{FEA}{M_y}$	$\frac{FEA}{M_p}$	$\frac{\text{Mod. LRFD}}{FEA}$	$\frac{\text{Rec Specs}}{FEA}$	$\frac{\text{Hanshin}}{FEA}$	$\frac{\text{Yoo w/ Approx } M_\ell}{FEA}$	$\frac{\text{Yoo w/ Calc } M_\ell}{FEA}$	$\frac{\text{1/3 Rule}}{FEA}$
Second-Order Elastic Analysis								
Avg.			1.10		0.82		0.87	0.96
Std. dev.			0.08		0.04		0.07	0.05
High	0.96	0.87	1.27		0.92		1.06	1.08
Low	0.66	0.60	0.97		0.73		0.75	0.86
First-Order Elastic Analysis								
Avg.			1.10	0.73	0.84	0.88	0.89	0.97
Std. dev.			0.08	0.17	0.04	0.07	0.06	0.05
High	0.96	0.87	1.27	1.15	0.96	1.10	1.07	1.09
Low	0.66	0.60	0.97	0.57	0.76	0.73	0.78	0.87

Table 7.7.2. Summary of primary, internal and modified vertical bending tests, vertical bending strength, specimens with $D/t_w = 100$ (40 specimens).

	$\frac{FEA}{M_y}$	$\frac{FEA}{M_p}$	$\frac{Mod.\ LRFD}{FEA}$	$\frac{Rec\ Specs}{FEA}$	$\frac{Hanshin}{FEA}$	$\frac{Yoo\ w/\ Approx\ M_\ell}{FEA}$	$\frac{Yoo\ w/\ Calc\ M_\ell}{FEA}$	$\frac{1/3\ Rule}{FEA}$
Second-Order Elastic Analysis								
Avg.			1.09		0.80		0.86	0.95
Std. dev.			0.07		0.04		0.07	0.04
High	0.96	0.87	1.24		0.89		1.05	1.04
Low	0.68	0.61	0.97		0.73		0.75	0.86
First-Order Elastic Analysis								
Avg.			1.09	0.72	0.83	0.86	0.88	0.96
Std. dev.			0.07	0.17	0.04	0.07	0.06	0.05
High	0.96	0.87	1.24	1.13	0.93	1.08	1.05	1.06
Low	0.68	0.61	0.97	0.57	0.76	0.73	0.78	0.87

Table 7.7.3. Summary of primary, internal and modified vertical bending tests, vertical bending strength, specimens with $D/t_w = 130$ (40 specimens).

	$\frac{FEA}{M_y}$	$\frac{FEA}{M_p}$	$\frac{Mod.\ LRFD}{FEA}$	$\frac{Rec\ Specs}{FEA}$	$\frac{Hanshin}{FEA}$	$\frac{Yoo\ w/\ Approx\ M_\ell}{FEA}$	$\frac{Yoo\ w/\ Calc\ M_\ell}{FEA}$	$\frac{1/3\ Rule}{FEA}$
Second-Order Elastic Analysis								
Avg.			1.11		0.83		0.88	0.97
Std. dev.			0.08		0.04		0.07	0.05
High	0.92	0.84	1.27		0.92		1.06	1.08
Low	0.66	0.60	0.97		0.74		0.76	0.88
First-Order Elastic Analysis								
Avg.			1.11	0.74	0.85	0.89	0.91	0.98
Std. dev.			0.08	0.17	0.04	0.07	0.06	0.05
High	0.92	0.84	1.27	1.15	0.96	1.10	1.07	1.09
Low	0.66	0.60	0.97	0.58	0.77	0.76	0.79	0.89

7.8 RESULTS FOR SLENDER-WEB GIRDERS

The results for all of the slender-web ($D/t_w = 160$) girders studied in the primary, modified vertical bending and internal loading suites are shown in Table 7.8.1. The one-third rule equations give the best overall accuracy for this set, with an average strength ratio of 0.95, a standard deviation of 0.05, a maximum value of 1.06, and a minimum value of 0.84 (based on second-order elastic stresses). These are followed in accuracy by Yoo's equations, then the Hanshin equations and the Recommended Specification formulas.

Similar to the previous results reported in this chapter, the Recommended Specifications give the most conservative prediction on average (0.74) for these tests as well as the largest dispersion of the strength predictions, as indicated by the standard deviation of 0.16, the maximum ratio of 1.17 and the minimum value of 0.59 in Table 7.8.1. As noted previously in Section 7.5, the maximum unconservative prediction with these equations (1.17) is from the modified vertical bending suite for a specimen with $D/b_f = 2.75$, $D/t_w = 160$ and $b_f/t_f = 15$ (see Table A.2.3). The maximum conservative prediction (0.59) is from the primary test suite for a specimen with $D/b_f = 2.75$, $D/t_w = 160$ and $b_f/t_f = 20$ (see Table A.1.18).

Table 7.8.1. Summary of primary, modified vertical bending and internal loading suites, vertical bending strength, specimens with a slender web (125 specimens).

	$\frac{FEA}{M_y}$	$\frac{FEA}{M_p}$	$\frac{Mod.\ LRFD}{FEA}$	$\frac{Rec\ Specs}{FEA}$	$\frac{Hanshin}{FEA}$	$\frac{Yoo\ w/\ Approx\ M_\ell}{FEA}$	$\frac{Yoo\ w/\ Calc\ M_\ell}{FEA}$	$\frac{1/3\ Rule}{FEA}$
Second-Order Elastic Analysis								
Avg.			1.09		0.85		0.89	0.95
Std. dev.			0.07		0.05		0.06	0.05
High	0.93	0.86	1.25		0.98		1.07	1.06
Low	0.66	0.61	0.93		0.74		0.77	0.84
First-Order Elastic Analysis								
Avg.			1.09	0.74	0.87	0.90	0.92	0.96
Std. dev.			0.07	0.16	0.04	0.07	0.06	0.05
High	0.93	0.86	1.25	1.17	0.98	1.12	1.09	1.07
Low	0.66	0.61	0.93	0.59	0.78	0.77	0.80	0.85

7.9 EFFECT OF TRANSVERSE STIFFENERS ON VERTICAL BENDING STRENGTH

In previous research (Mozer 1970, 1971 and 1973; Davidson 1996), the panel aspect ratio is considered to be one of the factors that can influence the bending strength of curved steel I girders. The above researchers observed that the transverse stiffeners tend to enhance the bending resistance by restraining the distortion of the web. Therefore, it is useful to consider the magnitude of these effects as detected by full nonlinear analysis of the parametric specimens considered in this research.

Figure 7.9.1 summarizes the results obtained from the primary test suite. As the panel aspect ratio is increased, the vertical bending capacity of the test specimens tends to decrease only very slightly. Therefore, it can be concluded that, within the range of parameters studied here, the spacing of the transverse stiffeners does not have any significant effect on the vertical bending strength of the specimens. It should be noted that the present parametric studies consider only $d_o/D = 3$ for webs with D/t_w less than 160. Furthermore, stiffener spacing d_o at less than the web depth D is not considered in the current research. Also, the transverse stiffeners are cut short of the tension flange in the girders considered in this work. It is possible that for girders with stockier webs, smaller stiffener spacing and/or transverse stiffeners attached to both flanges, the restraint offered to the web and to the flanges by the transverse stiffeners may have a larger influence on the flexural strength. It is conservative to neglect this potential benefit.

The uniform vertical bending tests in the three-girder system at the FHWA Turner Fairbank laboratories provide some confirmation of the above results (see Sections 4.4.3 and 4.7). In these tests, specimens B2 and B3 have the same geometric proportions, except B2 has a $d_o/D = 1$ whereas B3 has a web panel aspect ratio of 3.9. As shown in Table 4.4.8, specimen B3 exhibits a higher flexural capacity both within the experimental test as well as within the corresponding full nonlinear finite element analysis. In addition, the preliminary data reduction conducted by Zureick and Kim (2000) shows that the maximum internal moment in B3 (including dead load effects) is eight percent higher than that in specimen B2. It is three percent higher if dead load effects are not included.

7.10 FREE-END SUITE

As discussed in Section 5.11, the free-end suite is designed to evaluate the accuracy of the different flexural strength predictor equations for unsupported segments at the end of a horizontally curved I girder bridge. These three-point bending studies (see Fig. 5.11.1) test the influence of free warping conditions at the end of a bridge girder along with the influence of a significant moment gradient, which is likely to occur for these types of unsupported segments.

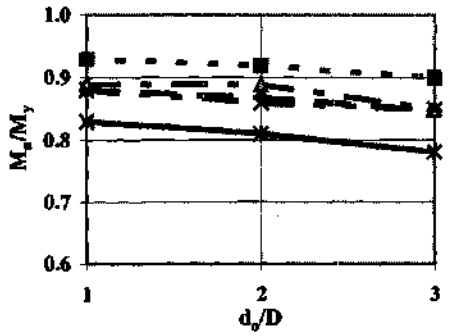

(a) $L_b/R = 0.05$ and $f_t/f_b = 0.35$

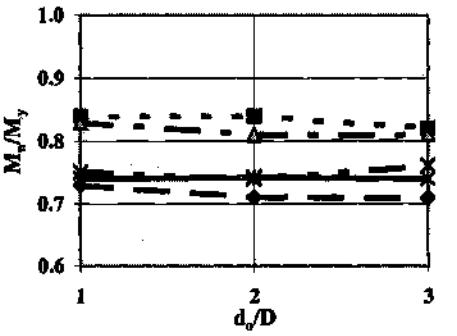

(d) $L_b/R = 0.05$ and $f_t/f_b = 0.50$

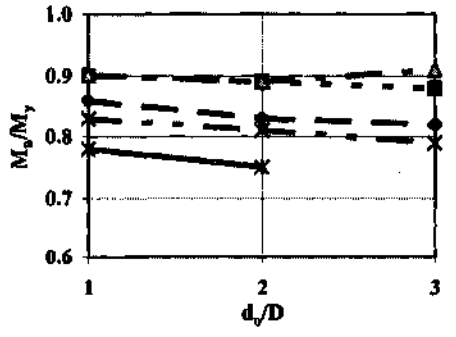

(b) $L_b/R = 0.075$ and $f_t/f_b = 0.35$

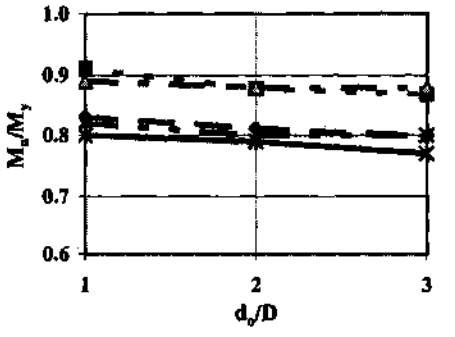

(e) $L_b/R = 0.075$ and $f_t/f_b = 0.50$

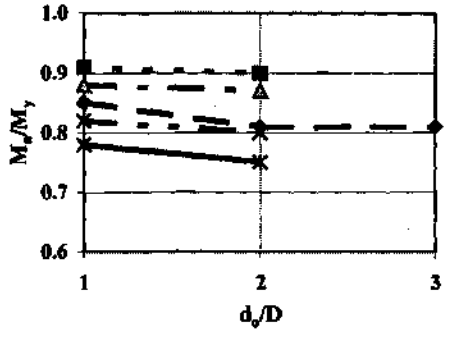

(c) $L_b/R = 0.10$ and $f_t/f_b = 0.35$

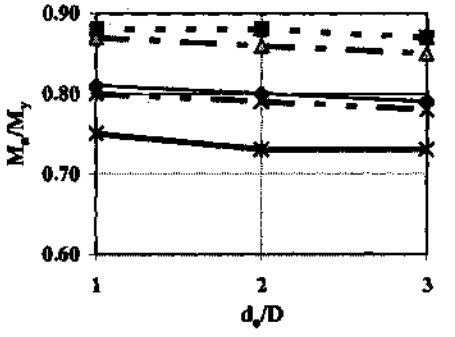

(f) $L_b/R = 0.10$ and $f_t/f_b = 0.50$

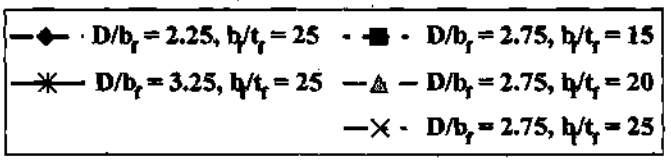

Figure 7.9.1. Vertical bending strength as a function of panel aspect ratio for all the specimens of the primary test suite with $D/t_w = 160$.

Table 7.10.1 summarizes the results of the free-end tests. The second-order amplification of the compression flange lateral bending stresses is slightly larger in this test suite than in the primary, modified vertical bending, and internal loading test suites (see Tables 7.1.1, 7.2.1 and 7.3.1). This is expected due to the free warping condition at one end of the unbraced lengths, and due to the fact that one sub-set of these girders has a lateral-torsional buckling slenderness $\lambda = L_b/r_t$ equal to the noncompact bracing limit λ_r (the other sub-set of these girders is designed at $(\lambda - \lambda_p) / (\lambda - \lambda_r) = 0.25$, see Section 5.11). Nevertheless, the difference between the second-order amplification effects in Table 7.10.1 versus Table 7.1.1 is very small.

Table 7.10.1. Summary of vertical bending strength, free-end tests (10 specimens).

	$\frac{FEA}{M_y}$	$\frac{FEA}{M_p}$	$\frac{Mod.\ LRFD}{FEA}$	$\frac{Rec\ Specs}{FEA}$	$\frac{Hanshin}{FEA}$	$\frac{Yoo\ w/\ Approx\ M_\ell}{FEA}$	$\frac{Yoo\ w/\ Calc\ M_\ell}{FEA}$	$\frac{1/3\ Rule}{FEA}$
Second-Order Elastic Analysis								
Avg.			1.11		0.77		0.82	0.92
Std. dev.			0.05		0.04		0.05	0.05
High	0.86	0.80	1.20		0.81		0.91	0.99
Low	0.73	0.65	1.02		0.71		0.76	0.85
First-Order Elastic Analysis								
Avg.			1.11	0.53	0.81	0.75	0.86	0.94
Std. dev.			0.05	0.13	0.04	0.06	0.05	0.05
High	0.86	0.80	1.20	0.79	0.86	0.87	0.96	1.01
Low	0.73	0.65	1.02	0.41	0.73	0.70	0.80	0.88

One can observe that the one-third rule equations again give the best prediction for these tests, with a mean strength ratio of 0.92, a standard deviation of 0.05, a high value of 0.99 and a low value of 0.85 based on direct second-order analysis. The minimum ratio (0.85) is obtained for a specimen with $D/b_f = 2.75$, $D/t_w = 160$ and $b_f/t_f = 25$ (see Table A.4.3) and the maximum ratio (0.99) is obtained for a specimen with $D/b_f = 2.75$, $D/t_w = 160$ and $b_f/t_f = 20$ (see Table A.4.4).

The cross-section yield interaction equations (Yoo 1996) give significantly conservative predictions both with M_ℓ calculated based on the V-load equation and based on direct analysis. In these tests, the V-load equation overestimates the maximum lateral bending moment within the unsupported length, and therefore increases the conservatism of the yield interaction equation checks.

The Hanshin equations also yield conservative predictions for these tests that are somewhat smaller on average than those of Yoo's equations (0.77 versus 0.82 when based on the second-order stresses); however the Hanshin equations have the smallest standard deviation for these girders (0.04).

The Recommended Specification equations give the most conservative predictions of the design equations considered for the free end tests, with a mean strength ratio of only 0.53. The standard deviation of the Recommended Specification predictions is also high (0.13). These tests include all three values of flange slenderness considered within the full parametric studies, $b_f/t_f = 15$, 20 and 25, but only two of the 10 tests have a compact flange by the definition of the Recommended Specifications.

The free-end test suite highlights a major advantage of the one-third rule over all of the other strength predictor equations. The one-third rule is the only one of these approaches that accounts for moment gradient (C_b) effects on the vertical bending strengths. These tests illustrate that: (1) the idealization of the compression flange as an equivalent beam-column, subjected to a variable axial compression along its length as well as to lateral bending, and (2) the representation of the effect of the variation in the axial force along the length of this component through the standard C_b moment gradient modifier, provide a highly accurate and understandable design approximation.

7.11 LATERALLY UNSUPPORTED STRAIGHT GIRDER SUITE

The laterally unsupported straight girder test suite is designed to evaluate the accuracy of the different design equations for straight I girders with large unsupported lengths, subjected to both vertical and lateral flange bending (see Section 5.12). Table 7.11.1 summarizes the results for these tests.

This test suite exhibits the most significant second-order elastic amplification effects of all of the parametric study suites. A primary reason for this behavior is that, for the horizontally-curved girder suites, the magnitude of the unsupported length generally has to be restricted in order to meet the targeted f_f/f_b restrictions. However, for a straight girder, significantly larger unsupported lengths can be designed without exceeding these targets. As noted in Section 5.12, the laterally unsupported straight girder tests are designed to span the entire range of $(\lambda - \lambda_p) / (\lambda - \lambda_r)$ values with respect to inelastic lateral-torsional buckling.

The Yoo (1996) and Hanshin equations are very sensitive to the changes in the magnitude of the flange lateral bending stresses due to second-order effects, compared to the one-third rule equations. The average strength ratio of Yoo's equations changes from 0.97 when based on the second-order elastic stresses to 1.11 when based on a first-order analysis, while the average value of the Hanshin equations changes from 0.93 to 1.08. Conversely, the average strength ratio produced by the one-third rule changes only from 0.97 to 1.03 when the stress calculations are changed from second-order to first-order. As noted previously in Section 7.1, this is due to the small slope of the resulting vertical-lateral bending interaction curves, as shown in Figs. 2.1.21 and 2.1.22. It can be seen that

the results with Yoo's formulas and with the Hanshin equations can be significantly unconservative (maximum strength ratios of 1.51) if based on first-order stresses.

Table 7.11.1. Summary of vertical bending strength, laterally unsupported straight girders (25 specimens).

	$\frac{FEA}{M_y}$	$\frac{FEA}{M_p}$	$\frac{Mod.\ LRFD}{FEA}$	$\frac{Rec\ Specs}{FEA}$	$\frac{Hanshin}{FEA}$	$\frac{Yoo\ w/\ Calc\ M_\ell}{FEA}$	$\frac{1/3\ Rule}{FEA}$
Second-Order Elastic Analysis							
Avg.			1.17		0.93	0.97	0.97
Std. dev.			0.07		0.09	0.11	0.06
High	0.76	0.69	1.32		1.12	1.19	1.10
Low	0.56	0.50	1.04		0.80	0.80	0.86
First-Order Elastic Analysis							
Avg.			1.17	1.06	1.08	1.11	1.03
Std. dev.			0.07	0.12	0.18	0.18	0.05
High	0.76	0.69	1.32	1.33	1.51	1.51	1.16
Low	0.56	0.50	1.04	0.85	0.85	0.85	0.94

Although the one-third rule equations give a maximum strength ratio of 1.10 and a minimum of 0.86 for these tests, they are the most accurate of the design predictor equations. The mean strength ratio predicted by the one-third rule is 0.97 with a standard deviation of 0.06 (see Table 7.11.1). The maximum strength ratio (1.10) is obtained for a girder with $D/b_f = 2.75$, $b_f/t_f = 15$, and $(\lambda - \lambda_p) / (\lambda - \lambda_r) = 0.0$ (see Table A.5.4) while the minimum strength ratio (0.86) is obtained for a girder with $D/b_f = 2.75$, $b_f/t_f = 15$ and $(\lambda - \lambda_p) / (\lambda - \lambda_r) = 1.0$ (see Table A.5.8). All of the specimens in the laterally unsupported straight girder suite have a $D/t_w = 160$.

Yoo's (1996) cross-section yield interaction equations are evaluated only with the use of direct analysis in Table 7.11.1, since the V-load equation is particularly not applicable for this test suite. Yoo's equations predict the finite element based strengths reasonably well on average, with a mean strength ratio of 0.97 when based on second-order elastic stresses. However, these equations have a large standard deviation (0.11), a large maximum value (1.19) and a small minimum value (0.80). Their minimum strength ratio (0.80) is obtained for a specimen with $D/b_f = 2.75$, $b_f/t_f = 20$ and $(\lambda - \lambda_p) / (\lambda - \lambda_r) = 0.0$ (see Table A.5.4), whereas their maximum strength ratio (1.19) is obtained for a specimen with $D/b_f = 2.75$, $b_f/t_f = 15$ and $(\lambda - \lambda_p) / (\lambda - \lambda_r) = 1.0$ (see Table A.5.8). It is

apparent that the cross-section yield interaction strengths tend to be unconservative for girders in which the strength is dominated by significant inelastic stability effects. This is because the yield interaction equations do not consider the effects of residual stresses and the resulting reductions in stiffness due to distributed yielding along the length of the compression flange.

The Hanshin equations provide a slightly better estimate of the strengths than Yoo's cross-section yield interaction equations for these tests, with a mean of 0.93, a standard deviation of 0.09, a maximum value of 1.12 and a minimum value of 0.80. This is because Eq. (2-73) simplifies to $F_{bc} = F_y$ for these straight girders, and therefore, the Hanshin equations reduce to first-yield strength equations for this group of tests. Conversely, Yoo's compact-flange section equations are applied to evaluate the strengths of the girders with $b_f/t_f = 15$. These equations provide a more liberal estimate of the vertical bending strength, and hence produce more highly unconservative predictions relative to the finite element based strengths (i.e., a change from 1.12 to 1.19 for the maximum strength ratio). The equations actually exhibit an opposite trend in their accuracy compared to the trends of the one-third rule equations and Yoo's (1996) equations discussed above. Their maximum strength ratio (1.12) corresponds to a girder with $D/b_f = 3.25$, $b_f/t_f = 25$ and $(\lambda - \lambda_p) / (\lambda - \lambda_r) = 1.0$ (see Table A.5.8) while their minimum strength ratio (0.80) is for a girder with $D/b_f = 2.75$, $b_f/t_f = 20$ and $(\lambda - \lambda_p) / (\lambda - \lambda_r) = 0$ (see Table A.5.4).

The Recommended Specifications give similar predictions to Yoo's equations for the laterally unsupported straight girders, with a mean strength ratio of 1.06, a standard deviation of 0.12, a maximum value of 1.33, and a minimum value of 0.85. It should be noted that $L_b/R = 0.01$ is assumed in the application of Eq. (2-33) for this problem, to avoid the anomaly associated with this formula as L_b/R approaches zero. The maximum strength ratio of the Recommended Specification equations (1.33) corresponds to a girder with $D/b_f = 3.25$, $b_f/t_f = 25$ and $(\lambda - \lambda_p) / (\lambda - \lambda_r) = 1.0$ (see Table A.5.8), whereas the minimum value (0.85) is for a girder with $D/b_f = 2.75$, $b_f/t_f = 20$ and $(\lambda - \lambda_p) / (\lambda - \lambda_r) = 0$ (see Table A.5.4). It appears that although McManus's (1971) noncompact section equations are significantly conservative in all the groups of horizontally-curved girders evaluated in the previous sections, they are significantly unconservative when applied within the context of a straight girder subjected to combined vertical and lateral bending when the laterally unsupported length is large.

7.12 UNSYMMETRICAL GIRDER SUITE

Table 7.12.1 presents a summary of the results for the unsymmetrical girders studied in this research. As discussed in Section 5.13, these girders are tested using the boundary and loading conditions of the primary and modified uniform vertical bending suites, the internal loading suite, and the free-end suite.

The second-order amplification effects on the strength predictions are again relatively minor for these tests, with an average change in the strength ratio by the one-third rule of

only 0.90 to 0.91 when the analysis is changed from second-order to first-order. Yoo's equations show a slightly larger corresponding change from 0.88 to 0.91.

Table 7.12.1. Summary results for unsymmetrical girders, vertical bending strength (22 specimens).

	$\frac{FEA}{M_y}$	$\frac{FEA}{M_p}$	$\frac{Mod.\ LRFD}{FEA}$	$\frac{Rec\ Specs}{FEA}$	$\frac{Hanshin}{FEA}$	$\frac{Yoo\ w/\ Approx\ M_\ell}{FEA}$	$\frac{Yoo\ w/\ Calc\ M_\ell}{FEA}$	$\frac{1/3\ Rule}{FEA}$
Second-Order Elastic Analysis								
Avg.			1.03		0.87		0.88	0.90
Std. dev.			0.09	0.08	0.08		0.08	0.08
High	0.90	0.69	1.20		1.04		1.06	1.04
Low	0.66	0.47	0.86		0.73		0.75	0.76
First-Order Elastic Analysis								
Avg.			1.03	0.68	0.89	0.88	0.91	0.91
Std. dev.			0.09	0.08	0.07	0.08	0.07	0.08
High	0.90	0.69	1.20	0.85	1.04	1.00	1.06	1.05
Low	0.66	0.47	0.86	0.53	0.76	0.69	0.77	0.78

The proposed one-third rule again provides the best prediction of the finite element based strengths, with an average ratio of 0.90, a standard deviation of 0.08, a maximum value of 1.04 and a minimum value of 0.76, based on second-order elastic stresses. The maximum unconservative value of 1.04 is obtained from the modified vertical bending case of specimen with $D/b_{fc} = 4.77$, $2D_c/t_w = 208$, $b_{fc}/t_{fc} = 20$, $L_b/R = 0.10$ and target $f_\ell/f_b = 0.50$ (see Table A.6.9). The minimum strength ratio (0.90) corresponds to the internal loading case with $D/b_{fc} = 2.75$, $2D_c/t_w = 169$, $b_{fc}/t_{fc} = 25$, $L_b/R = 0.05$ and target $f_\ell/f_b = 0.35$. The results for these tests are also reported in Table A.6.9. It should be noted that the equation for R_b specified by AASHTO LRFD (2001) is utilized for the monosymmetric girders, with the exception that f_{bc} is conservatively assumed equal to F_{yc}. For girders in which D_c/D is greater than 0.5, AASHTO LRFD uses Eq. (4-1), except that the coefficient 5.76 is reduced to 4.64. The value 4.64 is based on simply supported boundary conditions for the web at the web-flange juncture. This reduces the value of R_b from 0.889 to 0.846 for the unsymmetric girders with $2D_c/t_w = 208$, and it reduces R_b from 0.967 to 0.938 for the monosymmetric girders with $2D_c/t_w = 169$.

The Hanshin equations and Yoo's equations give essentially the same results. They are both slightly more conservative than the one-third rule equations on average, with

mean strength ratios of 0.87 and 0.88, they have the same standard deviation as the one-third rule equations (0.08), and they produce similar maximum values (1.04 and 1.06 versus 1.04) and minimum values (0.73 and 0.75 versus 0.76) compared to the one-third rule equations. The results for Yoo's equations combined with the V-load solution for the flange lateral bending moment are slightly more conservative than those based on the directly computed second-order elastic stresses.

The Recommended Specification equations once again perform poorly for this test suite, with an average strength ratio of only 0.68, a standard deviation of 0.08, a maximum value of 0.85 and a minimum value of 0.53. Their most conservative prediction (0.53) is obtained from the free-end case of the specimen with $D/b_f = 4.77$, $2D_c/t_w = 208$, $b_{fc}/t_{fc} = 20$, $L_b/R = 0.05$ and target second-order $f_\ell/f_b = 0.6$, and their maximum strength ratio (0.85) is obtained for the modified uniform vertical bending case with this same girder but with $L_b/R = 0.05$ and target first-order $f_\ell/f_b = 0.35$ (see Table A.6.9). The reason for these significantly conservative predictions is due in part to the simple use of 0.9 of the compression flange width when evaluating Eq. (2-32) for unsymmetrical sections (see Section 2.1.2.4).

Overall, all of the design predictor equations are somewhat more conservative for the unsymmetrical girder suite compared to the results from the other parametric study suites. This is due to the fact that none of these equations account for any ability of the cross-section to develop bending moments larger than the yield moment M_y. However, the shape factor of the unsymmetric girder cross-section with $D/b_f = 4.77$ is 1.4, and the shape factor for the unsymmetric cross-section with $D/b_f = 2.75$ is 1.3. Tables 7.12.2 and 7.12.3 present the separate results for the tests under each of these groups. It can be seen that although the web of the specimen with $D/b_f = 4.77$ has a slenderness of $2D_c/t_w = 208$, the proposed one-third rule equations are still reasonably accurate. However, for the specimen with $D/b_f = 2.75$ and $2D_c/t_w = 169$, it is apparent that the web is providing a significant contribution to the flexural strength such that the one-third rule equations tend to be significantly conservative, although they provide slightly better accuracy than Yoo's equations and the Hanshin equations when based on the second-order elastic flange stresses. It may be possible to quantify this reserve strength by the use of flexural strength equations that are anchored by straight-girder capacities which are greater than M_y. This issue is discussed further in the recommendations for further research in Chapter X.

7.13 EFFECT OF IDEALIZED STRESSES FROM HEAT CURVING VERSUS CUT CURVING ON VERTICAL BENDING STRENGTHS

As noted previously, all the full nonlinear finite element models utilized to establish the benchmark solutions within this chapter include both initial geometric imperfections and residual stresses defined as per the procedures outlined in Chapter III. All of the studies presented in Sections 7.1 through 7.2 are based on the ECCS (1976) model for residual stresses caused by welding and flame cutting (see Section 3.5.1). The residual stresses due to the combination of flame cutting, welding and heat curving can be somewhat more detrimental to the maximum flexural strength (Culver and Nasir 1971).

Table 7.12.2. Results for unsymmetrical girders with $D/b_f = 4.77$, $2D_c/t_w = 208$, $b_{fc}/t_{fc} = 20$, $D_c/D = 0.65$ and $M_p/M_y = 1.4$ ($I_{yc}/I_y = 0.1$) , vertical bending strength (10 specimens).

	FEA / M_y	FEA / M_p	Mod. LRFD / FEA	Rec Specs / FEA	Hanshin / FEA	Yoo w/ Approx M_ℓ / FEA	Yoo w/ Calc M_ℓ / FEA	1/3 Rule / FEA
Second-Order Elastic Analysis								
Avg.			1.07		0.90		0.92	0.95
Std. dev.			0.07		0.08		0.08	0.06
High	0.81	0.57	1.20		1.04		1.06	1.04
Low	0.67	0.47	0.98		0.79		0.80	0.87
First-Order Elastic Analysis								
Avg.			1.07	0.72	0.92	0.88	0.94	0.95
Std. dev.			0.07	0.09	0.07	0.09	0.08	0.06
High	0.81	0.57	1.20	0.85	1.04	0.99	1.06	1.05
Low	0.67	0.47	0.98	0.53	0.80	0.69	0.82	0.88

Table 7.12.3. Results for unsymmetrical girders with $D/b_f = 2.75$, $2D_c/t_w = 169$, $b_{fc}/t_{fc} = 25$, $D_c/D = 0.66$ and $M_p/M_y = 1.3$ ($I_{yc}/I_y = 0.14$), vertical bending strength (12 specimens).

	FEA / M_y	FEA / M_p	Mod. LRFD / FEA	Rec Specs / FEA	Hanshin / FEA	Yoo w/ Approx M_ℓ / FEA	Yoo w/ Calc M_ℓ / FEA	1/3 Rule / FEA
Second-Order Elastic Analysis								
Avg.			1.00		0.85		0.86	0.86
Std. dev.			0.10		0.05		0.05	0.07
High	0.90	0.69	1.18		0.92		0.94	0.98
Low	0.66	0.51	0.86		0.73		0.75	0.76
First-Order Elastic Analysis								
Avg.			1.00	0.66	0.86	0.88	0.88	0.87
Std. dev.			0.10	0.06	0.05	0.07	0.05	0.07
High	0.90	0.69	1.18	0.77	0.93	1.00	0.96	0.99
Low	0.66	0.51	0.86	0.57	0.76	0.75	0.77	0.78

Table 7.13.1 compares the results for two specimens with $D/b_f = 3.25$, $b_f/t_f = 25$, $D/t_w = 160$, and target $f_t/f_b = 0.50$ from the primary test suite based on three idealizations of the residual stresses:

- zero residual stress,
- the idealized ECCS (1976) residual stress model (see Fig. E.4.13), and
- the Culver-Nasir (1971) residual stress pattern (see Fig. 3.5.5).

These specimens are selected because the effects of the different residual stress models should tend to be the largest for their combinations of the design parameters. The results indicate that the predicted strengths obtained with the two residual stress models are approximately the same. However, the reduction in strength relative to the model with zero residual stresses is nine to 10 percent for the specimen with $L_b/R = 0.05$, and 14 to 15 percent for the specimen with $L_b/R = 0.10$.

Table 7.13.1. Ultimate bending strength of test specimens with D/bf = 3.25, $b_f/t_f = 25$, $D/t_w = 160$, $d_o/D = 3$ and target $f_t/f_b = 0.50$.

L_b/R	$M_{n(FEA)}/M_y$ w/o Residual Stresses (1)	$M_{n(FEA)}/M_y$ w/ ECCS (1976) Residual Stresses (2)	(2)/(1)	$M_{n(FEA)}/M_y$ Culver-Nasir (1969) Residual Stresses (3)	(3)/(1)
0.05	0.810	0.740	0.914	0.730	0.901
0.10	0.843	0.730	0.866	0.719	0.852

7.14 SUMMARY

Table 7.14.1 gives a summary of the strength ratio statistics for all of the vertical bending strength tests considered in the parametric study (not including the results based on the Culver and Nasir (1971) residual stress assumptions discussed in the previous section). All of the statistical quantities in this table are most accurate for the one-third rule. The average ratio between the predicted design strength and the fully nonlinear finite element analysis based strength is 0.95 for the proposed method, when based on second-order elastic stresses, with a standard deviation of only 0.06. The maximum unconservative strength ratio is 1.10, and the most conservative prediction of all the cases studied is 0.76.

Figures 7.14.1 through 7.14.5 provide histogram plots of the strength ratios for each of the predictor equations evaluated in this chapter. The one-third rule has the highest

number of tests with strength ratios between 0.90 and 1.00 (see Fig. 7.14.1). Only five of the 262 tests considered have strength ratios larger than 1.05 with this method. These tests and their strength ratios are listed in Table 7.14.2.

Six of the 262 tests have strength ratios less than 0.85 with the one-third rule. These tests and their strength ratios are listed in Table 7.14.3. It can be seen that all of these girders have b_f/t_f values of 25, and that the five of these girders with the lowest strength ratios are unsymmetric specimens

Yoo's yield interaction equations produce strength ratios predominantly in the range of 0.80 to 0.95 when utilized with the V-load equation (see Fig. 7.14.2). Five of these tests have strength ratios larger than 1.05 with this approach, and 10 of the tests have strength ratios less than 0.75. It should be noted that only 237 tests are considered with the combination of Yoo's cross-section yield interaction equations and the V-load method, since the V-load solution is not valid for the straight-girder studies.

When utilized with directly computed second-order elastic flange moments, Yoo's equations still give strength ratios predominantly between the 0.80 and 0.95 limits, but produce values greater than 1.05 in nine of the girders studied and strength ratios less than 0.75 in two tests (see Fig. 7.14.3). Tables 7.14.4 and 7.14.5 list these tests.

Table 7.14.1. Summary of all analysis results, vertical bending strength (262 specimens).

	$\frac{FEA}{M_y}$	$\frac{FEA}{M_p}$	$\frac{Mod.\ LRFD}{FEA}$	$\frac{Rec\ Specs}{FEA}$	$\frac{Hanshin}{FEA}$	$\frac{Yoo\ w/\ Approx\ M_\ell}{FEA}$	$\frac{Yoo\ w/\ Calc\ M_\ell}{FEA}$	$\frac{1/3\ Rule}{FEA}$
Second-Order Elastic Analysis								
Avg.			1.10		0.84		0.89	0.95
Std. dev.			0.08		0.06		0.08	0.06
High	0.96	0.87	1.32		1.12		1.19	1.10
Low	0.56	0.47	0.86		0.71		0.75	0.76
First-Order Elastic Analysis								
Avg.			1.10	0.75	0.88	0.89	0.93	0.96
Std. dev.			0.08	0.19	0.10	0.07	0.10	0.06
High	0.96	0.87	1.32	1.33	1.51	1.12	1.51	1.16
Low	0.56	0.47	0.86	0.41	0.73	0.69	0.77	0.78

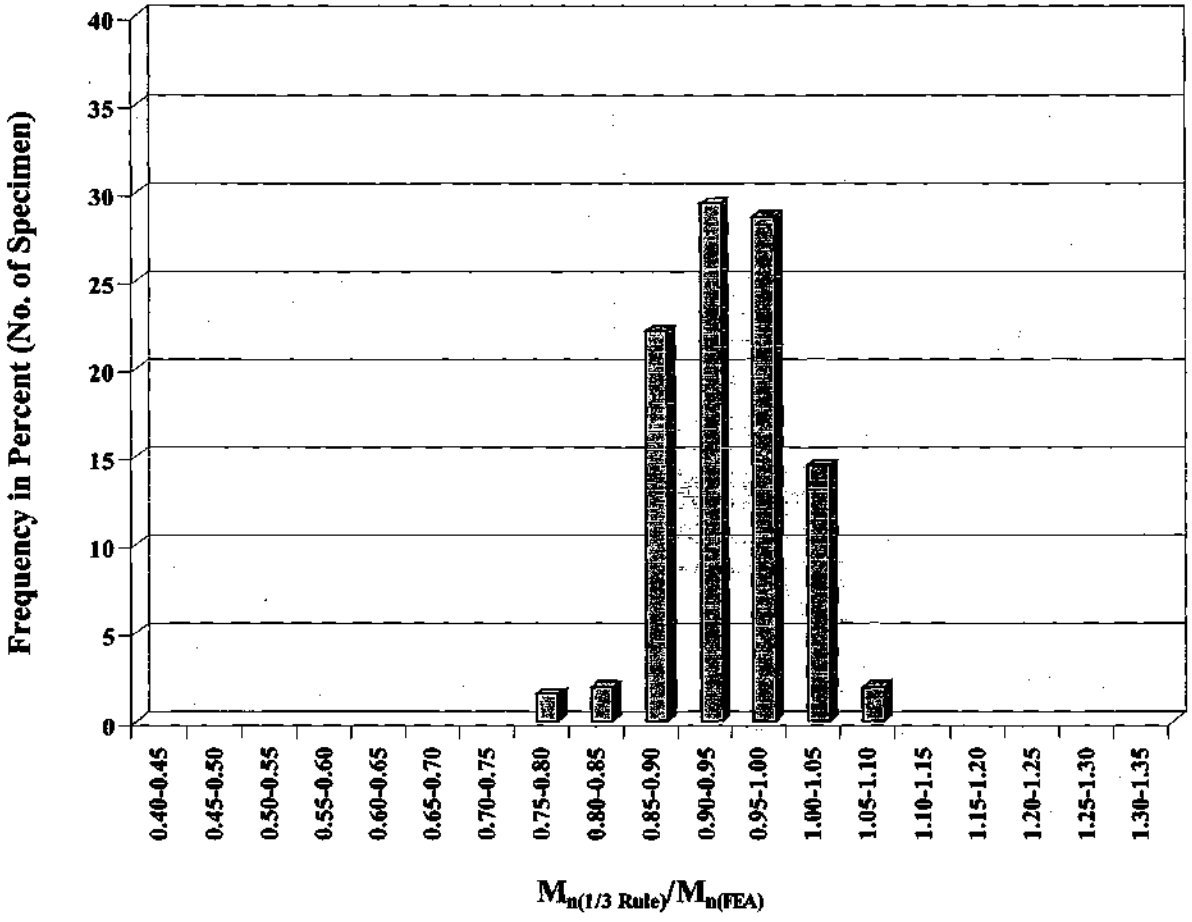

Figure 7.14.1. Strength ratio histogram for all of the parametric vertical bending tests, one-third rule based on second-order elastic flange lateral bending stresses (262 specimens).

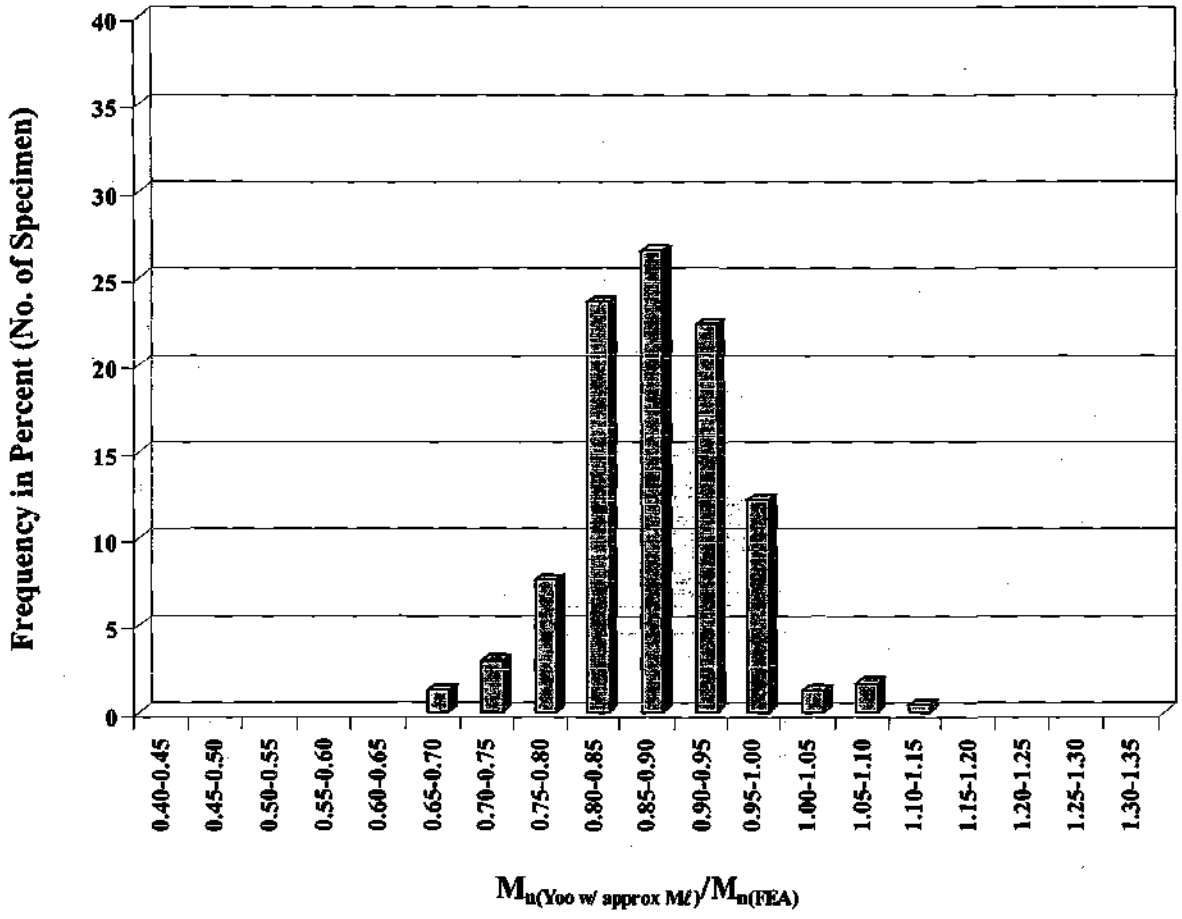

Figure 7.14.2. Strength ratio histogram for all of the parametric vertical bending tests, Yoo's (1996) cross-section yield interaction equations with the flange lateral bending moment computed by the V-load method (237 specimens).

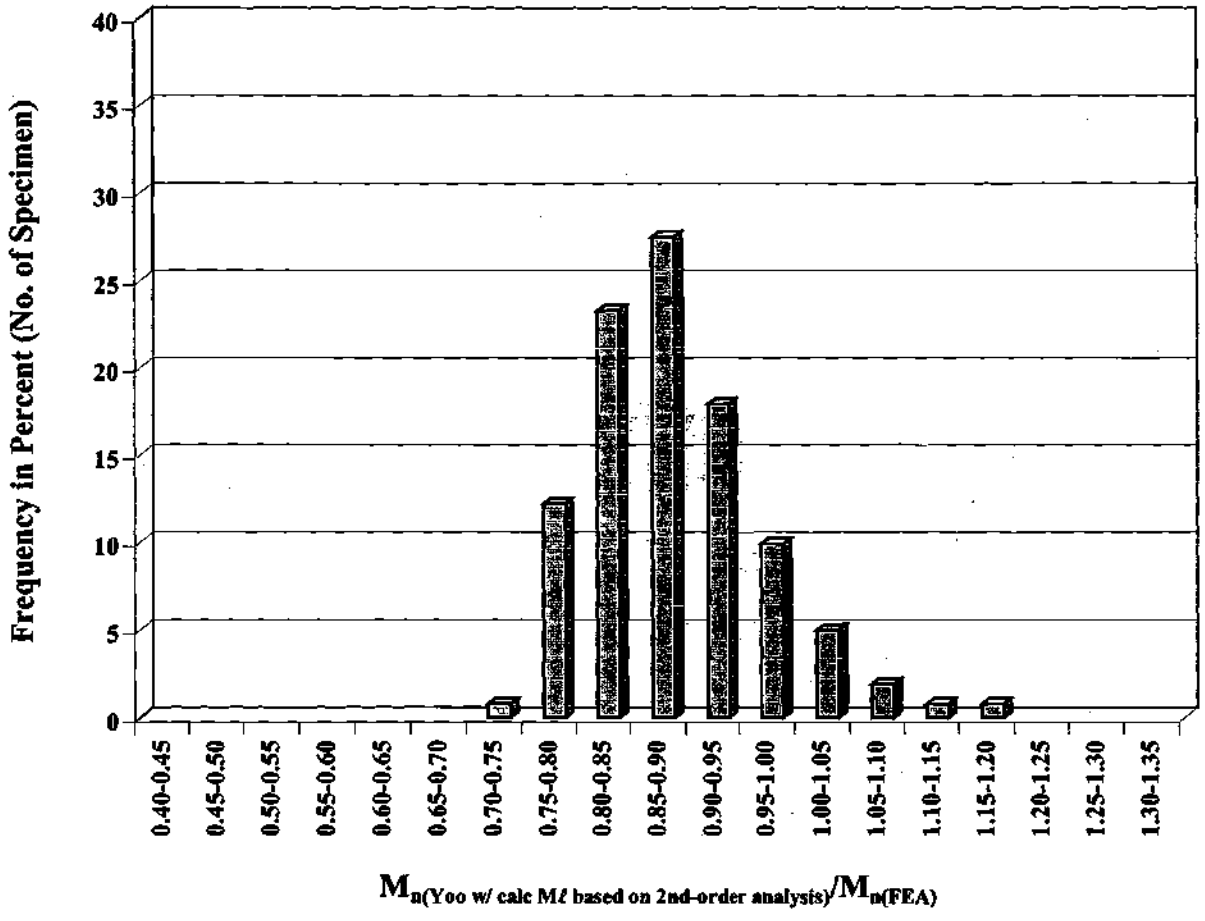

Figure 7.14.3. Strength ratio histogram for all of the parametric vertical bending tests, Yoo's (1996) cross-section yield interaction equations with the flange lateral bending moment computed by direct second-order analysis (262 specimens).

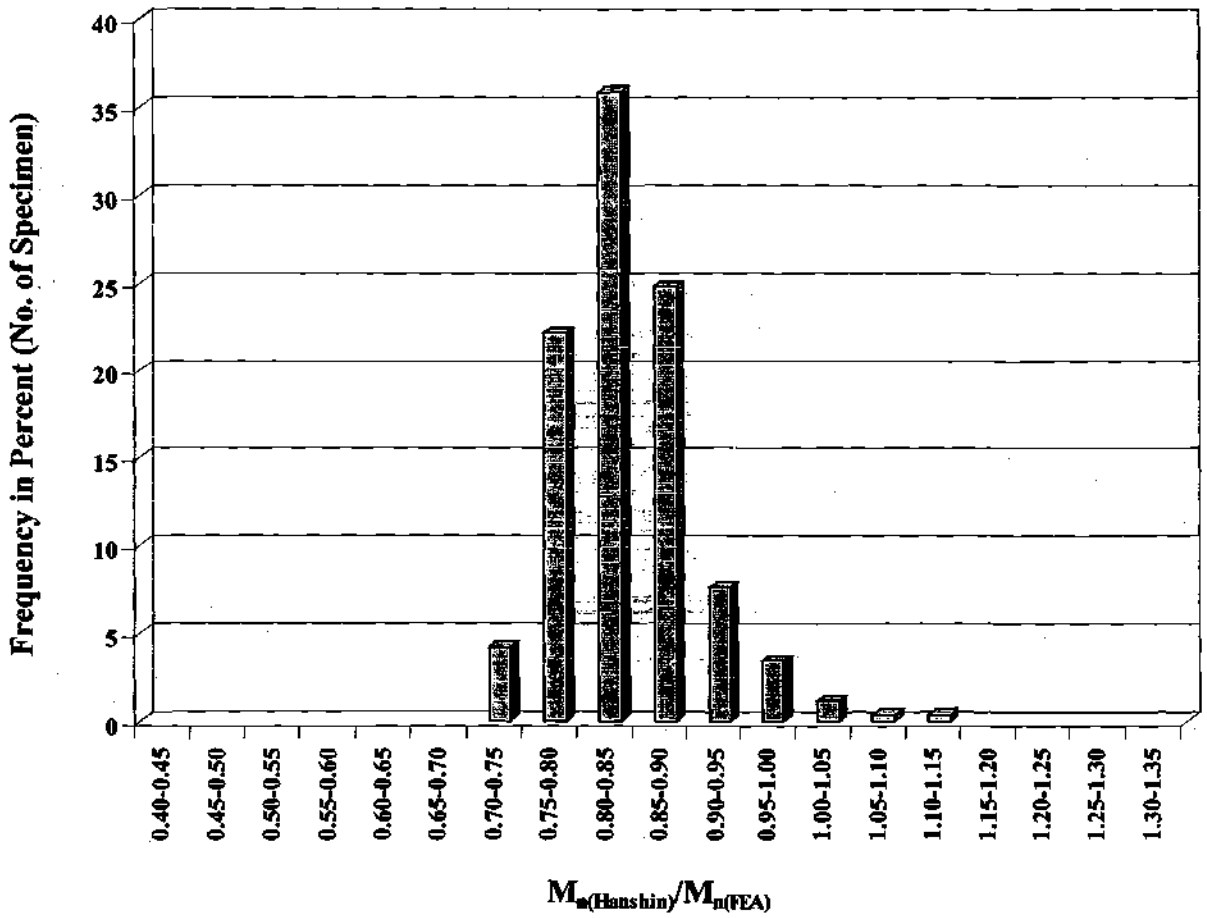

Figure 7.14.4. Strength ratio histogram for all of the parametric vertical bending tests, Hanshin equations based on second-order elastic flange lateral bending stresses (262 specimens).

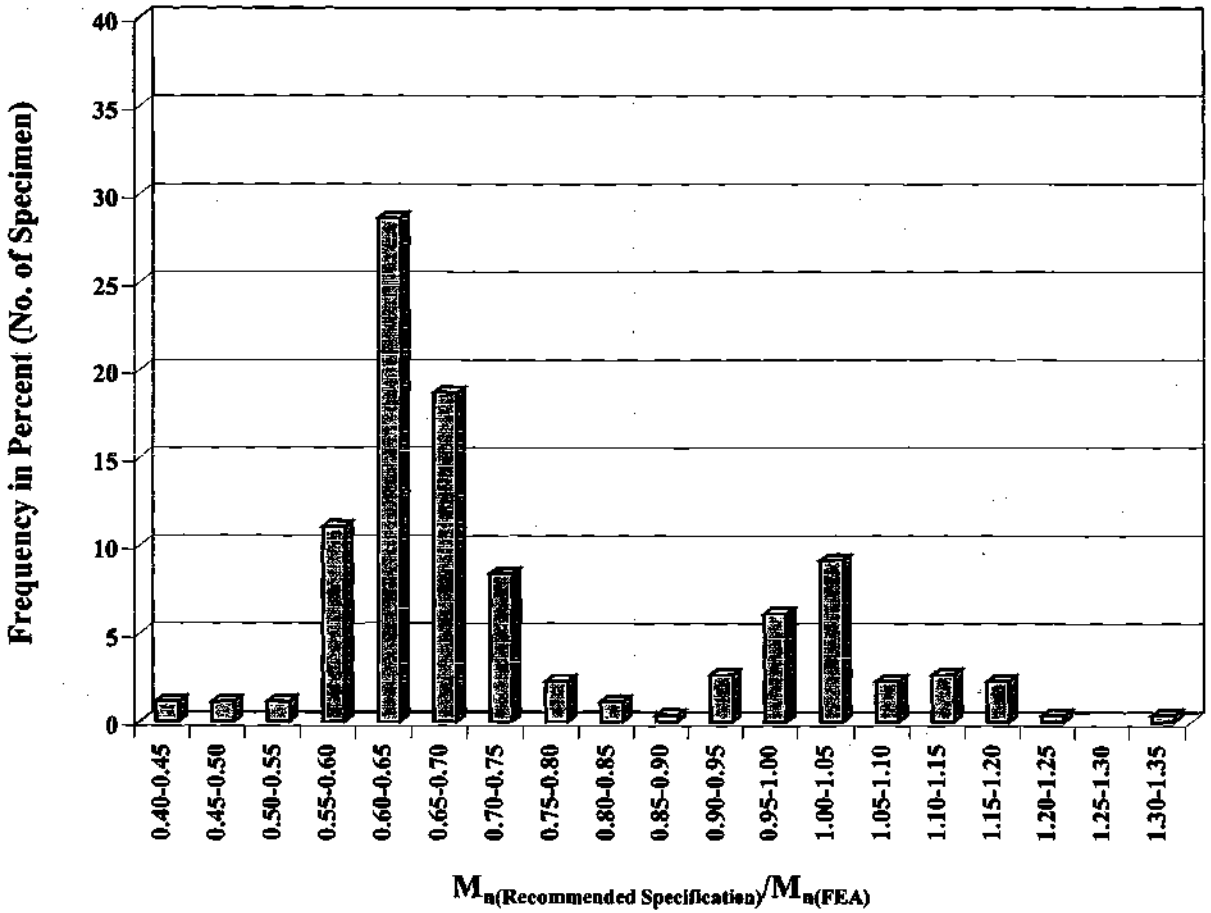

Figure 7.14.5. Strength ratio histogram for all of the parametric vertical bending tests, Recommended Specification equations (262 specimens).

Table 7.14.2. Parametric study tests for which the strength ratio of the one-third rule is greater than 1.05.

Test Suite	D/b_{fc}	b_{fc}/t_{fc}	$2D_c/t_w$	d_o/D	L_b/R	Target f_ℓ/f_b	$\frac{\lambda-\lambda_p}{\lambda_r-\lambda_p}$ LTB	Strength Ratio
Internal Loading	2.75	15	130	3	0.1	0.50	–0.24	1.08
	2.75	15	160	3	0.1	0.50	–0.24	1.06
	2.75	20	130	3	0.1	0.50	–0.22	1.07
Laterally Unsupported Straight	2.75	15	160	3	NA	0.6	0.0	1.10
	3.25	25	160	3	NA	0.6	0.5	1.09

Table 7.14.3. Parametric study tests for which the strength ratio of the one-third rule is less than 0.85.

Test Suite	D/b_{fc}	b_{fc}/t_{fc}	$2D_c/t_w$	d_o/D	L_b/R	Target f_ℓ/f_b	$\frac{\lambda-\lambda_p}{\lambda_r-\lambda_p}$ LTB	Str. Ratio
Primary	2.75	25	160	1	0.05	0.35	–0.01	0.84
Unsymmetric Primary	2.75	25	169	3	0.05	0.35	0.03	0.80
Unsymmetric Modified Vert. Bending	2.75	25	169	3	0.05	0.35	0.03	0.83
Unsymmetric Internal Loading	2.75	25	169	3	0.05	0.35	0.03	0.76
	2.75	25	169	3	0.10	0.50	–0.19	0.77
	2.75	25	169	2	0.10	0.35	–0.41	0.80

Table 7.14.4. Parametric study tests for which the strength ratio of Yoo's (1996) yield interaction equations is greater than 1.05.

Test Suite	D/b_{fc}	b_{fc}/t_{fc}	$2D_c/t_w$	d_o/D	L_b/R	Target f_ℓ/f_b	$\frac{\lambda-\lambda_p}{\lambda_r-\lambda_p}$ LTB	Str. Ratio
Modified Vertical Bending	2.75	15	130	3	0.05	0.50	0.38	1.06
	2.75	25	160	1	0.05	0.50	0.40	1.07
	2.75	15	160	3	0.05	0.50	0.36	1.06
Laterally Unsupported Straight	2.75	15	160	3	NA	0.60	0.5	1.11
	2.75	15	160	3	NA	0.60	0.75	1.17
	2.75	15	160	3	NA	0.60	1.0	1.19
	2.75	25	160	3	NA	0.60	1.0	1.08
	3.25	25	160	3	NA	0.60	1.0	1.12
Unsymmetric Modified Vert. Bending	4.77	20	208	3	0.05	0.35	0.0	1.06

Table 7.14.5. Parametric study tests for which the strength ratio of Yoo's (1996) yield interaction equations is less than or equal to 0.75.

Test Suite	D/b_{fc}	b_{fc}/t_{fc}	$2D_c/t_w$	d_o/D	L_b/R	Target f_ℓ/f_b	$\frac{\lambda-\lambda_p}{\lambda_r-\lambda_p}$ LTB	Str. Ratio
Primary	2.75	20	100	3	0.10	0.50	-0.21	0.75
Unsymmetric Internal Loading	2.75	25	160	3	0.10	0.50	-0.19	0.75

The Hanshin equations produce strength ratios predominantly between 0.75 and 0.90, and are generally more conservative than Yoo's cross-section yield interaction equations (see Fig. 7.14.4). Only two of the tests have strength ratios greater than 1.05 with these equations; both of these are straight girders with $b_f/t_f = 25$, $D/t_w = 160$, and $(\lambda - \lambda_p) / (\lambda_r - \lambda_p) = 1.0$. However, the strength ratios are less than or equal to 0.75 in eleven of the 262 tests with these equations, without any consistent trend with respect to the design parameters.

Finally, the Recommended Specification equations are essentially bi-polar, with the noncompact section equations producing strength ratios predominantly between 0.60 and 0.70, and the compact section equations giving strength ratios predominantly between 0.95 and 1.05. However, these equations produce values greater than 1.05 in twenty cases, and they produce values smaller than 0.55 in nine cases. Tables 7.14.6 and 7.14.7 list these tests. It is apparent that both the Recommended Specifications and Yoo's cross-section yield interaction equations have difficulty in representing the strength of girders with unsupported lengths larger than the compact bracing limit, particularly when the lateral bending is due to sources other than horizontal curvature. Also, these formulas do not account for the beneficial effects of moment gradient in these types of problems.

It is important to realize that the statistical results reported here are of course influenced by the design of the parametric study. Specifically, 148 of the 262 girders tested have a flange slenderness of $b_{fc}/t_{fc} = 25$. Also, 168 of the girders have a $D/b_{fc} = 2.75$, and 160 of the girders have a $D/t_w = 160$. Nevertheless, the parametric study evaluates the girder response for a reasonably comprehensive range of all the girder parameters. An ideal set of design equations would give a strength ratio equal to one for all of the tests, regardless of the distribution of the design parameters. Of the predictor equations studied, the one-third rule comes closest to this ideal.

7.15 ESTIMATION OF FLANGE SECOND-ORDER ELASTIC LATERAL BENDING STRESSES

7.15.1 Flange Elastic Lateral Bending Stress Amplification Factor for Horizontally-Curved I Girders

The amplification of f_ℓ due to second-order effects is illustrated for the primary suite, uniform vertical bending case of several specimens with $L_b/R = 0.05$, 0.075, and 0.10 and target $f_\ell/f_b = 0.50$ in Figs 7.15.1 to 7.15.3. Girders with the largest web slenderness $D/t_w = 160$ and with the largest panel aspect ratio used with these transversely stiffened girders, $d_o/D = 3$, are selected for this study. Also, similar plots for the specimens with $D/t_w = 160$, $d_o/D = 3$, $L_b/R = 0.05$ and target second-order $f_\ell/f_b = 0.60$ from the free-end test suite are shown in Fig. 7.15.4. In these figures, the normalized elastic flange vertical bending stress (f_b/F_y) is plotted versus the normalized elastic flange lateral bending stress (f_ℓ/F_y) at five load levels: 0.2, 0.4, 0.6, 0.8, and 1.0 of the maximum load attained based on the one-third rule predictor equations. It should be noted that the specimens with

Table 7.14.6. Parametric study tests for which the strength ratio of the Recommended Specification equations is greater than 1.05.

Test Suite	D/b_{fc}	b_{fc}/t_{fc}	$2D_c/t_w$	d_o/D	L_b/R	Target f_c/f_b	$\frac{\lambda-\lambda_p}{\lambda_r-\lambda_p}$ LTB	Str. Ratio
Primary	2.75	15	160	2	0.10	0.35	-0.44	1.06
Modified Vertical Bending	2.75	15	100	3	0.05	0.50	0.40	1.13
	2.75	15	130	3	0.05	0.50	0.38	1.15
	2.75	15	160	1	0.05	0.50	0.36	1.14
	2.75	15	160	2	0.05	0.50	0.36	1.12
	2.75	15	160	3	0.05	0.50	0.36	1.17
	2.75	15	160	3	0.10	0.50	0.36	1.06
Internal Loading	2.75	15	130	3	0.10	0.50	-0.24	1.06
Laterally-Unsupported Straight	2.75	15	160	3	NA	0.60	0.0	1.12
	2.75	15	160	3	NA	0.60	0.25	1.15
	2.75	15	160	3	NA	0.60	0.50	1.19
	3.25	25	160	3	NA	0.60	0.50	1.16
	2.25	25	160	3	NA	0.60	0.75	1.07
	2.75	15	160	3	NA	0.60	0.75	1.09
	2.75	20	160	3	NA	0.60	0.75	1.14
	2.75	25	160	3	NA	0.60	0.75	1.16
	3.25	25	160	3	NA	0.60	0.75	1.22
	2.25	25	160	3	NA	0.60	1.0	1.09
	2.75	20	160	3	NA	0.60	1.0	1.16
	2.75	25	160	3	NA	0.60	1.0	1.20
	3.25	25	160	3	NA	0.60	1.0	1.33

Table 7.14.7. Parametric study tests for which the strength ratio of the Recommended Specification equations is less than 0.55.

Test Suite	D/b_{fc}	b_{fc}/t_{fc}	$2D_c/t_w$	d_o/D	L_b/R	Target f_ℓ/f_b	$\frac{\lambda-\lambda_p}{\lambda_r-\lambda_p}$ LTB	Str. Ratio
Free-End	2.25	25	160	3	0.05	0.60	1.04	0.44
	2.75	20	160	3	0.05	0.60	1.07	0.41
	2.75	25	160	3	0.05	0.60	1.12	0.42
	3.25	25	160	3	0.05	0.60	0.93	0.48
	2.25	25	160	3	0.10	0.60	0.27	0.51
	2.75	25	160	3	0.10	0.60	0.30	0.50
	3.25	25	160	3	0.10	0.60	0.23	0.53
Unsymmetric Free-End	4.77	20	208	3	0.05	0.60	0.73	0.53

$L_b/R = 0.05$ and target $f_\ell/f_b = 0.50$ of the primary test suite, as well as the selected free-end test specimens, all have lateral-torsional buckling slenderness values $\lambda = L_b/r_t$ greater than λ_p. Therefore, the stress amplification is more pronounced in these specimens than in most of the other tests of the parametric study. The slenderness $\lambda = L_b/r_t$ is equal to λ_r for the selected free-end test specimens.

The maximum amplification of the flange lateral bending stresses in Figs. 7.15.1 through 7.15.4 is approximately 20 percent at the maximum load level. This value of the second-order amplification occurs for the free-end test specimen with $D/b_f = 3.25$ and $b_f/t_f = 25$ (see Fig. 7.15.4e). At the peak load (based on the one-third rule), the maximum first-order elastic f_ℓ/F_y for this specimen is 0.352 and the maximum second-order elastic f_ℓ/F_y is 0.423. Based on Eq. (2-90b), considering both the flange local bucking and lateral-torsional buckling limit states, and accounting for the moment gradient effect in the lateral-torsional buckling check through the parameter C_b, the local buckling limit state controls. The resulting nominal bending strength predicted by the one-third rule is $0.70F_y$ if based on the first-order elastic lateral bending stress, and $0.68F_y$ if based on the second-order elastic lateral bending stress. That is, the 20 percent amplification of the lateral bending stresses at the peak load level reduces the nominal vertical bending strength by only $0.02F_y$. This indicates that a simple approximate estimate of the second-order elastic amplification effects should be sufficient with the proposed one-third rule.

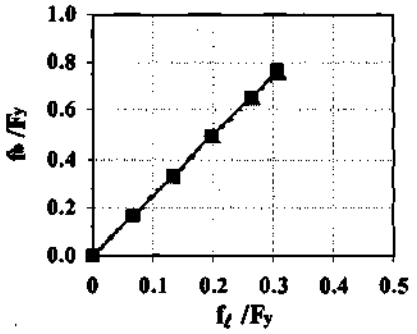

(a) $D/b_f = 2.75$ and $b_f/t_f = 15$

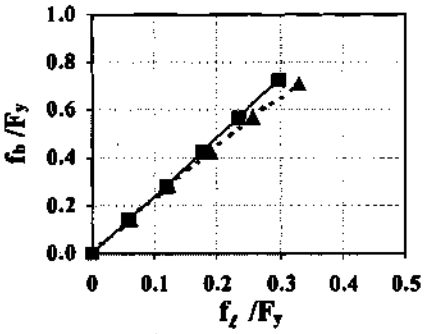

(d) $D/b_f = 2.25$ and $b_f/t_f = 25$

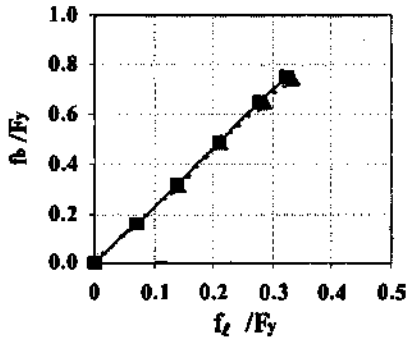

(b) $D/b_f = 2.75$ and $b_f/t_f = 20$

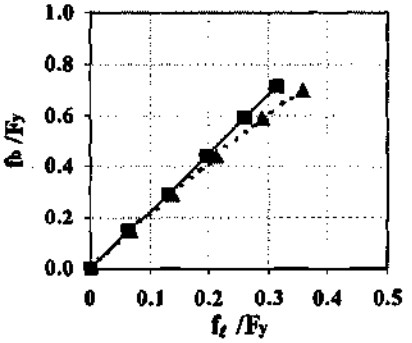

(e) $D/b_f = 3.25$ and $b_f/t_f = 25$

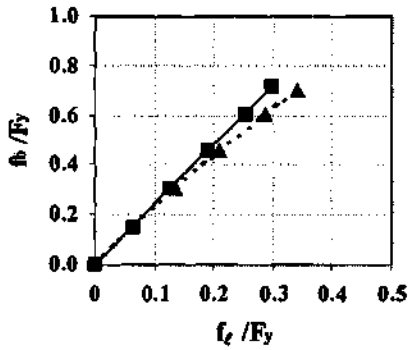

(c) $D/b_f = 2.75$ and $b_f/t_f = 25$

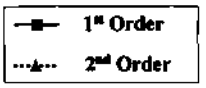

Figure 7.15.1. Elastic stresses from first- and second-order analyses for specimens with $D/t_w = 160$, $d_o/D = 3$, $L_b/R = 0.05$ and target $f_\ell/f_b = 0.50$ (uniform vertical bending, primary test suite).

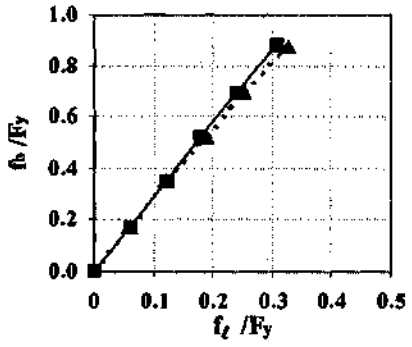

(a) $D/b_f = 2.75$ and $b_f/t_f = 15$

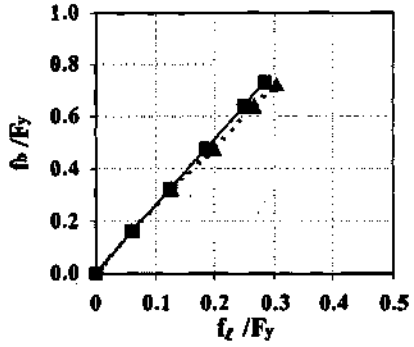

(d) $D/b_f = 2.25$ and $b_f/t_f = 25$

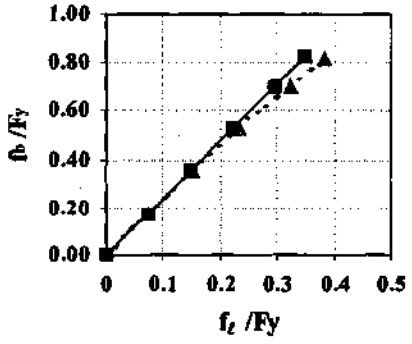

(b) $D/b_f = 2.75$ and $b_f/t_f = 20$

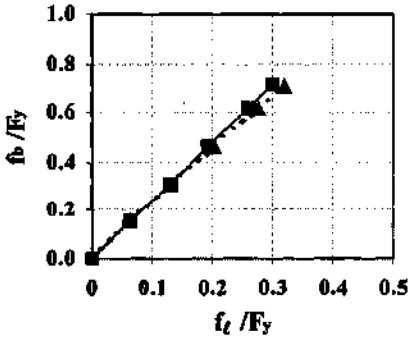

(e) $D/b_f = 3.25$ and $b_f/t_f = 25$

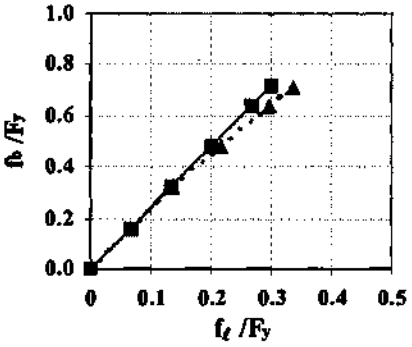

(c) $D/b_f = 2.75$ and $b_f/t_f = 25$

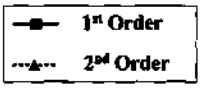

Figure 7.15.2. Elastic stresses from first and second-order analyses for specimens with $D/t_w = 160$, $d_o/D = 3$, $L_b/R = 0.075$ and target $f_\ell/f_b = 0.50$ (uniform vertical bending, primary test suite).

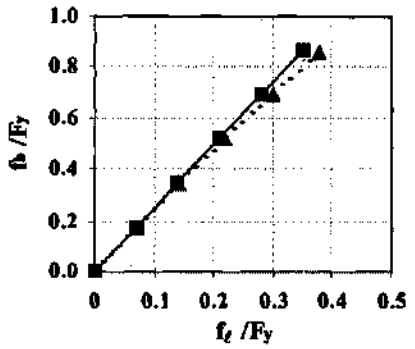

(a) $D/b_f = 2.75$ and $b_f/t_f = 15$

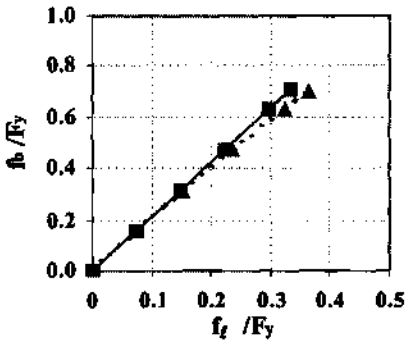

(d) $D/b_f = 2.25$ and $b_f/t_f = 25$

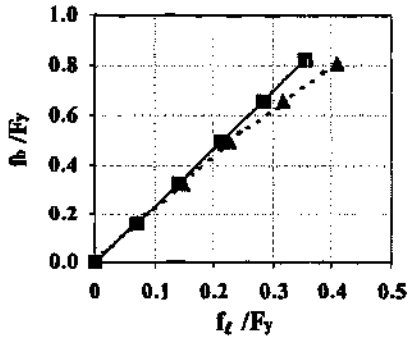

(b) $D/b_f = 2.75$ and $b_f/t_f = 20$

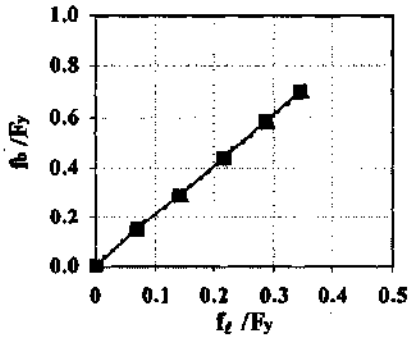

(e) $D/b_f = 3.25$ and $b_f/t_f = 25$

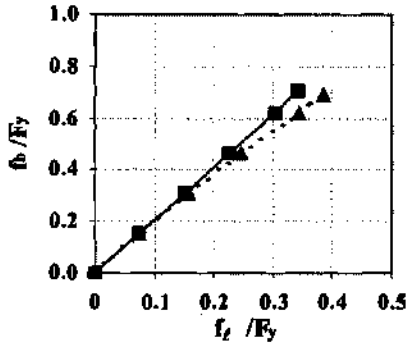

(c) $D/b_f = 2.75$ and $b_f/t_f = 25$

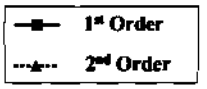

Figure 7.15.3. Elastic stresses from first and second-order analyses for specimens with $D/t_w = 160$, $d_o/D = 3$, $L_b/R = 0.10$ and target $f/f_b = 0.50$ (uniform vertical bending, primary test suite)

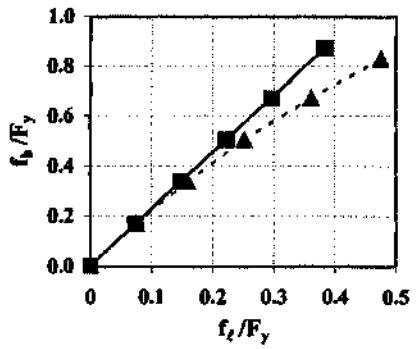

(a) $D/b_f = 2.75$ and $b_f/t_f = 15$

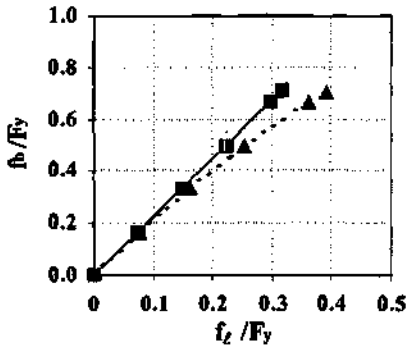

(d) $D/b_f = 2.25$ and $b_f/t_f = 25$

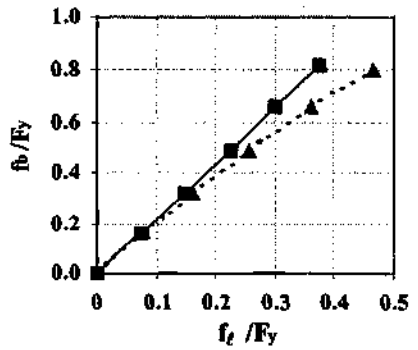

(b) $D/b_f = 2.75$ and $b_f/t_f = 20$

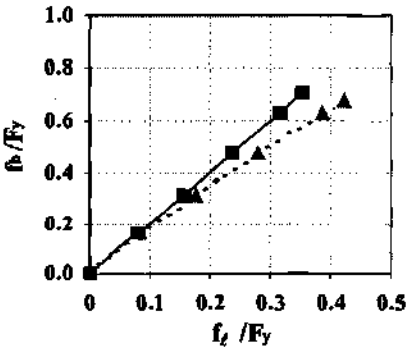

(e) $D/b_f = 3.25$ and $b_f/t_f = 25$

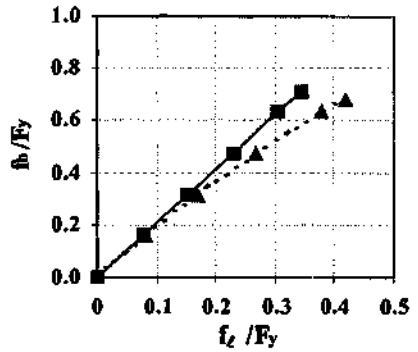

(c) $D/b_f = 2.75$ and $b_f/t_f = 25$

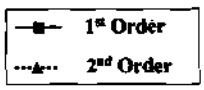

Figure 7.15.4. Elastic stresses from first- and second-order analyses for specimens with $D/t_w = 160$, $d_o/D = 3$, $L_b/R = 0.05$ and target second-order $f_\ell/f_b = 0.60$ (free-end test suite).

It is interesting to consider the applicability of the most basic form for the second-order elastic amplification factor:

$$AF = \frac{1}{1 - \frac{f_b}{F_e}} \tag{7-2}$$

where f_b and F_e are the first-order elastic flange vertical bending stress and the elastic lateral-torsional buckling stress respectively, and F_e is evaluated from Eq. (2-23) but potentially with a lateral-torsional buckling effective length rather than the actual unsupported length. Substantial flange warping restraint typically exists with respect to lateral-torsional stability within the interior unsupported lengths of a horizontally-curved bridge I girder due to: (1) continuity with the adjacent unsupported lengths, and (2) the fact that the horizontal curvature tends to induce a lateral bending outward from the center of curvature within each of the unsupported segments. Therefore, it is suggested that an effective length with respect to lateral-torsional buckling of $0.5L_b$ may be sufficient for practical purposes in computing the term F_e in Eq. (7-2) for interior unsupported lengths of horizontally-curved I girders. This suggestion is based on the assumption that the horizontal curvature of the girder is large enough such that the compression flange will not unwind into a buckling mode in which the adjacent unsupported lengths buckle in opposite directions with an inflection point close to or at the cross-frame locations.

Within the free-end tests, the warping of the compression flange is unrestrained at one end and fixed at the other with respect to lateral-torsional buckling, assuming that the horizontal curvature is large enough such that the flange does not unwind into an S shape with an inflection point at the braced loading location. In this case, the theoretical effective length for lateral-torsional buckling (for the case of uniform vertical bending) is $0.7L_b$. However, the flange vertical bending stress varies linearly from zero at the free end to its maximum value at the braced loading location, and thus the equivalent lateral distributed loading on the compression flange (acting as an equivalent beam-column) also varies linearly between these two points (see the discussion regarding the equivalent beam-column idealization in Section 1.4.2). If we derive the theoretical amplification factor for the moments within a pinned-fixed beam-column subjected to a constant distributed axial load along its length (producing a linear variation in the axial force along the length) plus a triangular distributed lateral load, we find that Eq. (7-2) with F_e based on an effective length of $0.7L_b$ and $C_b = 1.75$ is conservative. After some trial experimentation with the free-end tests, the authors find that the use of $KL_b = 0.5L_b$ and $C_b = 1$ in Eqs. (2-23) and (7-2) also gives a reasonable approximation for these tests.

Hall et al. (1999) suggest Eq. (7-2) as an amplification factor, but with F_e given by

$$F_e = \frac{EI_{yc}}{A_f R^2}\left(\frac{4\pi^2 R^2}{\ell_e^{\,2}} - 1\right) \tag{7-3}$$

with a value of ℓ_e of $0.6L_b$. Equation (7-3) is based on the buckling of a uniformly loaded circular arch. For bridge I girders with $L_b/R \leq 0.10$, this equation is for all practical purposes equal to

$$F_e = \frac{4\pi^2 EI_{yc}}{A_f \ell_e^{\,2}} \tag{7-4}$$

Therefore, if ℓ_e is taken as $0.6L_b$, we obtain a buckling stress larger than physically possible in the limit that R becomes large (i.e., the "effective" length based on Eq. (2-23) is essentially $0.3L_b$). The authors are hesitant to use a more liberal estimate of F_e than that obtained from Eq. (2-23) with an effective length of $0.5L_b$; furthermore, for small L_b/R, the engineer should exercise his or her judgment in that it may be appropriate to use a value larger than $0.5L_b$ to estimate the second-order elastic amplification effect.

In Figs. 7.15.5 and 7.15.6, normalized f_b versus f_ℓ curves obtained using Eq. (7-2) with:

- F_e based on Eq. (2-23) and an effective length of $0.5L_b$ and
- F_e based on Eq. (7-3) with $\ell_e = 0.6L_b$

are compared to the finite element based curves shown earlier in Figs. 7.15.1 and 7.15.4. These figures correspond to the cases with the largest second-order elastic amplification within the parametric studies (with the exception of some of the girders in the laterally unsupported straight girder suite). It can be observed that the recommended amplification factor approximates the finite element based solution very well in Fig. 7.15.5, but it over predicts the second-order finite element based amplification by four to 13 percent in Fig. 7.15.6. Conversely, the equation suggested by Hall et al. (1999) significantly under predicts the second-order amplification of the lateral bending stresses in all but two of the plots in the combined Figs. 7.15.5 and 7.15.6. If $0.7L_b$ is utilized for the effective length with Eq. (2-23), and if the corresponding F_e (including $C_b = 1.75$) is substituted into Eq. (7-2), the second-order amplification is over predicted by nine to 22 percent.

Table 7.15.1 presents statistical data for the performance of the suggested simple amplification factor (Eq. (7-2) with F_e determined using Eq. (2-23) with $C_b = 1$ and an effective length of $0.5L_b$). This table summarizes the statistics for the ratio of the first-order elastic design stresses, amplified by Eq. (7-2), to the "exact" lateral bending stresses obtained from direct second-order elastic shell finite element analysis at the load level corresponding to satisfaction of the one-third rule equations. The data is presented for each of the major groups of tests considered previously in Sections 7.1 through 7.14,

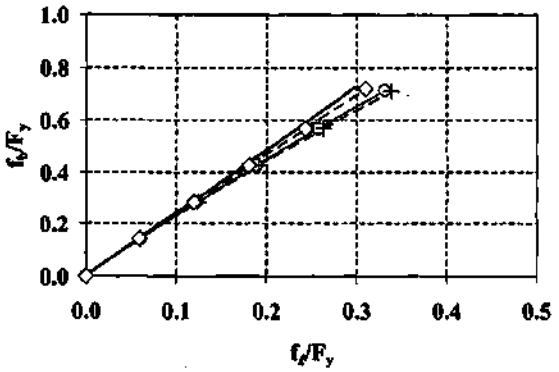

(a) $D/b_f = 2.25$ and $b_f/t_f = 25$

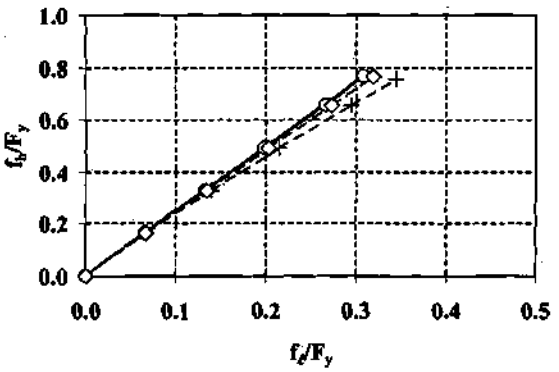

(b) $D/b_f = 2.75$ and $b_f/t_f = 15$

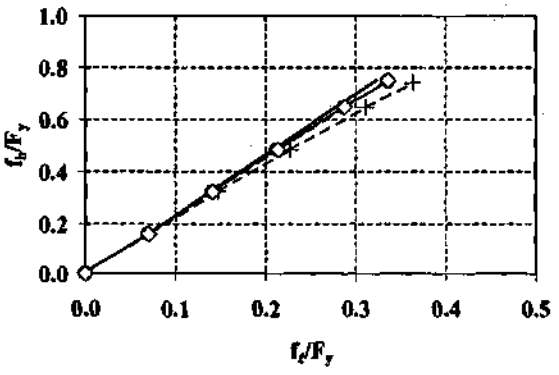

(c) $D/b_f = 2.75$ and $b_f/t_f = 20$

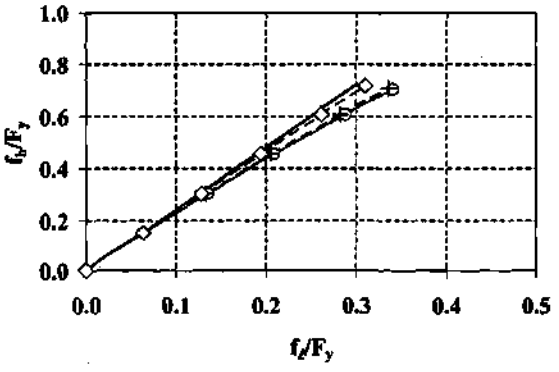

(d) $D/b_f = 2.75$ and $b_f/t_f = 25$

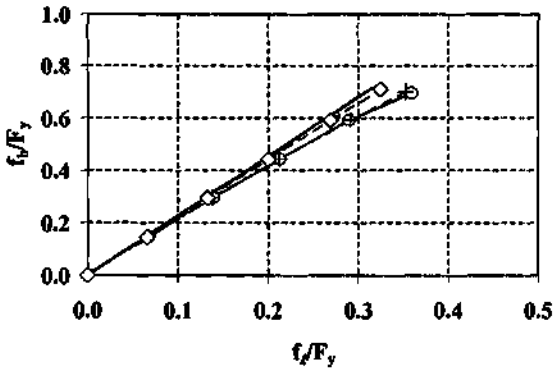

(e) $D/b_f = 3.25$ and $b_f/t_f = 25$

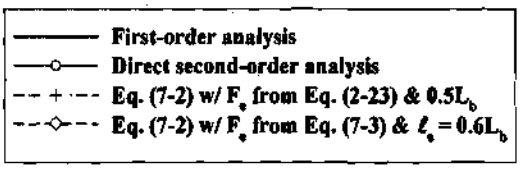

Figure 7.15.5. Comparison of elastic f_a and f_b values obtained by direct analysis and by amplification of first-order stresses by Eq. (7-2) for specimens with $D/t_w = 160$, $d_o/D = 3$, $L_b/R = 0.05$ and target $f_a/f_b = 0.50$ (uniform vertical bending, primary test suite).

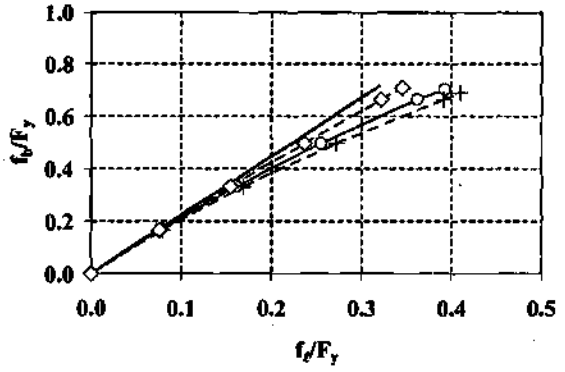

(a) $D/b_f = 2.25$ and $b_f/t_f = 25$

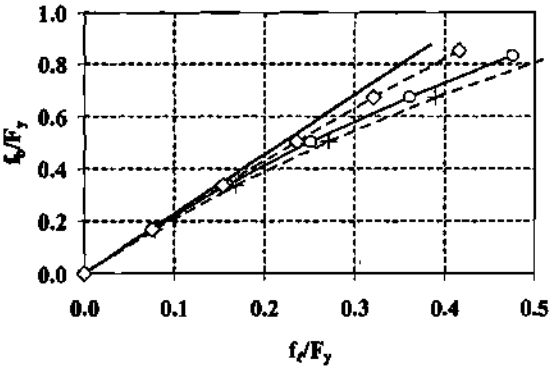

(d) $D/b_f = 2.75$ and $b_f/t_f = 15$

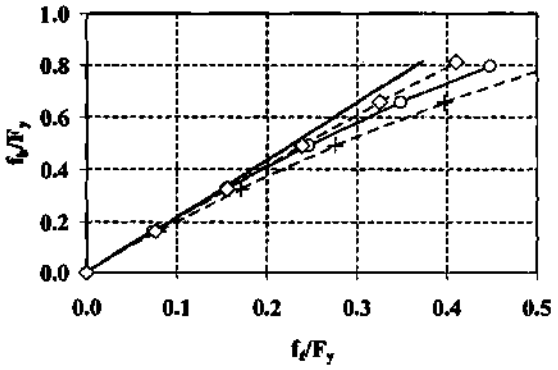

(b) $D/b_f = 2.75$ and $b_f/t_f = 20$

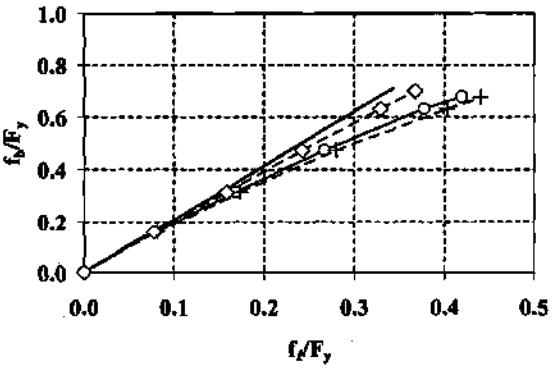

(e) $D/b_f = 2.75$ and $b_f/t_f = 25$

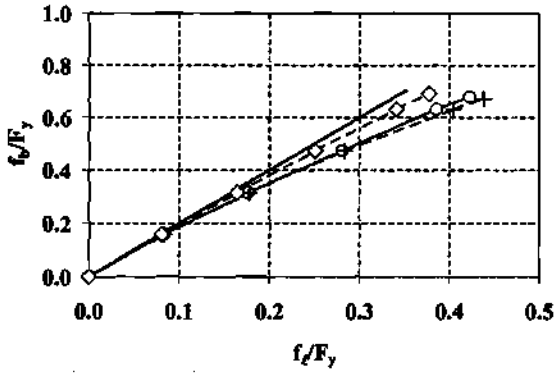

(c) $D/b_f = 3.25$ and $b_f/t_f = 25$

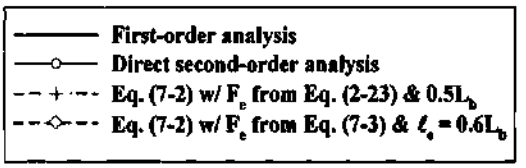

Figure 7.15.6. Comparison of elastic f_t and f_b values obtained by direct analysis and by amplification of first-order stresses by Eq. (7-2) for specimens with $D/t_w = 160$, $d_o/D = 3$, $L_b/R = 0.05$ and target second-order $f/f_b = 0.60$ (free-end suite).

with the exception of the laterally unsupported girder suite which is considered subsequently. For the vast majority of the girders studied, the suggested approach estimates the finite element based second-order elastic stress within $\pm$ 10 percent. However, if we take the primary suite as an example, there are six girders in which the second-order elastic stress computed within the finite element analysis is very small such that it is overestimated by more than 10 percent by the suggested equation. Furthermore, there are 10 of the 133 girders considered in the primary suite for which the finite element analysis gives a high second-order elastic amplification such that the simple amplification factor equation under predicts the second-order stresses by more than 10 percent. In the worst case, which corresponds to the specimen with $D/b_f = 2.75$, $b_f/t_f = 20$, $D/t_w = 130$, $d_o/D = 3$, $L_b/R = 0.075$ and target $f_f/f_b = 0.35$, an AF of 1.34 is calculated by finite element analysis whereas the simple equation gives an AF of only 1.04 (giving the reported minimum value of 0.78 in the table). The same girder, but with $D/t_w = 160$, has an amplification factor of 1.32 by finite element analysis but only 1.04 from the simple equation. The next smallest ratio of the estimated to the finite element based amplification in the primary suite is 0.87. There is no clear trend in the data as to the source of the discrepancies between the simple amplification factor estimates and the finite element based solutions in the cases where the discrepancies are large. If it is assumed that the finite element solutions are "exact", then in the worst case, the flexural capacity predicted by the one-third rule equation could be $(0.5F_y)(0.26)/3 = 0.04F_y$ in error (unconservative) relative to the correct solution due to the use of the suggested simple amplification factor equation (Eq. 7-2).

Table 7.15.1. Ratio of estimated second-order elastic flange lateral bending stress based on Eqs. (7-2) and (2-23) with $KL_b = 0.5L_b$ to the stress based on direct second-order elastic analysis. In each of the two solutions, the stress is calculated at the load level corresponding to satisfaction of the one-third rule equations.

	Average	Standard Deviation	Max.	Min.
Primary suite	0.97	0.06	1.14	0.78
Modified vertical bending suite	0.96	0.09	1.12	0.75
Internal loading suite	1.00	0.06	1.10	0.91
Cases controlled by flange local buckling	0.96	0.06	1.08	0.75
Cases controlled by lateral-torsional buckling	1.06	0.06	1.14	0.93
Cases controlled by flange plastic strength	0.95	0.04	1.01	0.85
Nonslender-web girders	0.98	0.06	1.14	0.78
Slender-web girders	0.96	0.07	1.13	0.75
Free-end suite	1.07	0.04	1.16	1.03
Unsymmetric girders	0.97	0.08	1.11	0.74

It should be noted that, based on the approximate equivalence of the compression flange in the primary loading suite to an end-restrained beam-column subjected to uniform axial compression and a uniformly distributed lateral loading, one might consider the use of the factor $C_m = (1 - 0.4\, f_b/F_e)$ within the numerator of Eq. (7-2) as discussed in the commentary to Chapter C of the AISC LRFD Specification (1999). It can be argued that this term, combined with the calculation of F_e based on an effective length larger than $0.5L_b$, might provide a better estimate of the second-order amplification. The authors do not find this to be the case.

7.15.2 Flange Elastic Lateral Bending Stress Amplification for Straight I Girders

The results for the amplification of the lateral bending stresses in the laterally unsupported straight-girder suite require special consideration. For these girders, the authors find that the use of Eq. (7-2) along with Eq. (2-23) and an effective length of $0.5L_b$ grossly underestimates the computed second-order elastic amplification. A reasonably good approximation of the second-order amplification is obtained for most of these girders with $KL_b = 0.8L_b$ (see Table 7.15.2). It is interesting to note that Lay and Galambos (1965) state that $K = 0.8$ is representative of worst case restraint conditions in laboratory uniform bending tests of straight compact rolled beams. Nevertheless, it is expected that the use of the actual unsupported length would be preferred within a design context. The results for the laterally unsupported straight girders with the use of Eqs. (7-2) and (2-23) along with the actual unsupported length are shown in Table 7.15.3.

It can be observed from Tables 7.15.2 and 7.15.3 that at least in the case in which an internal unsupported segment of a straight I-girder is subjected to uniform primary lateral and vertical bending, the influence of end restraint (due to continuity with the adjacent unsupported lengths) is likely to be small with respect to the amplification of the flange lateral bending stresses. The use of the actual unsupported length in the calculation of the stress amplification per Eqs. (7-2) and (2-23) is conservative for all the cases analyzed. Conversely, it should be noted that the lateral bending stresses in the girder with $D/b_f = 3.25$, $b_f/t_f = 25$, $D/t_w = 160$, $d_o/D = 3$, and $(\lambda - \lambda_p) / (\lambda_r - \lambda_p) = 1.0$ are underestimated significantly with $KL_b = 0.8L_b$ (see Table 7.15.2).

Based on the amplification results reported here, it is recommended that for girders with $L_b/R < 0.05$, the actual unsupported length should be utilized in calculating the flange lateral bending stress amplification per Eq. (7-2). For I girders with $L_b/R \geq 0.05$, it appears that the use of $KL_b = 0.5L_b$ is appropriate.

7.15.3 Estimation of Flange Lateral Bending Stresses by the V-Load Equation

As stated in Section 1.2, evaluation of the accuracy of various methods for estimating the elastic design analysis stresses in curved I-girder bridge superstructures is beyond the scope of this research. In order to determine the stresses due to vertical and lateral bending with high accuracy, including both second-order effects as well as the potential influence of web distortion, the shell finite element models utilized in the full nonlinear analyses to determine the girder capacities are also used – with zero geometric

Table 7.15.2. Summary of analysis results, stress amplification from Eq. (7-2) compared to direct second-order elastic analysis for laterally unsupported straight girder suite based on $KL_b = 0.80L_b$.

D/b_{fc}	b_{fc}/t_{fc}	$2D_c/t_w$	d_o/D	$\frac{\lambda - \lambda_p}{\lambda_r - \lambda_p}$ LTB	Ratio 2nd to 1st order elastic f_ℓ/F_y	AF estimated by Eq. (7-2)	Ratio Approx. to Exact f_ℓ/F_y
2.25	25	160	3	0	1.15	1.15	1.00
				0.25	1.28	1.29	1.01
				0.5	1.49	1.55	1.04
				0.75	1.60	1.77	1.11
				1.0	2.41	2.09	0.87
2.75	15	160	3	0	1.09	1.18	1.08
				0.25	1.26	1.32	1.05
				0.5	1.51	1.54	1.03
				0.75	1.83	1.83	1.00
				1.0	2.48	2.07	0.83
2.75	20	160	3	0	1.16	1.18	1.01
				0.25	1.25	1.34	1.07
				0.5	1.41	1.53	1.08
				0.75	1.75	1.79	1.02
				1.0	2.27	2.11	0.93
2.75	25	160	3	0	1.13	1.16	1.03
				0.25	1.31	1.31	1.00
				0.5	1.38	1.55	1.12
				0.75	1.88	1.81	0.97
				1.0	2.51	2.15	0.85
3.25	25	160	3	0	1.18	1.15	0.97
				0.25	1.35	1.28	0.95
				0.5	1.55	1.52	0.98
				0.75	2.05	1.77	0.86
				1.0	3.27	2.10	0.64
Average							0.98
Standard Deviation							0.11
Max.					3.27	2.15	1.12
Min.					1.09	1.15	0.64

Table 7.15.3. Summary of analysis results, stress amplification from Eq. (7-2) compared to direct second-order elastic analysis for laterally unsupported straight girder suite based on $KL_b = L_b$.

D/b_{fc}	b_{fc}/t_{fc}	$2D_c/t_w$	d_o/D	$\frac{\lambda-\lambda_p}{\lambda_r-\lambda_p}$ LTB	Ratio 2nd to 1st order elastic f_ℓ/F_y	AF estimated by Eq. (7-2)	Ratio Approx. to Exact f_ℓ/F_y
2.25	25	160	3	0	1.15	1.26	1.10
				0.25	1.28	1.53	1.20
				0.5	1.49	2.25	1.51
				0.75	1.60	3.12	1.95
				1.0	2.41	5.37	2.23
2.75	15	160	3	0	1.09	1.32	1.21
				0.25	1.26	1.61	1.28
				0.5	1.50	2.22	1.48
				0.75	1.83	3.44	1.88
				1.0	2.48	5.20	2.10
2.75	20	160	3	0	1.16	1.31	1.13
				0.25	1.25	1.65	1.32
				0.5	1.41	2.16	1.54
				0.75	1.75	3.24	1.85
				1.0	2.28	5.66	2.49
2.75	25	160	3	0	1.13	1.27	1.13
				0.25	1.31	1.58	1.21
				0.5	1.38	2.24	1.62
				0.75	1.88	3.35	1.78
				1.0	2.52	6.04	2.40
3.25	25	160	3	0	1.18	1.25	1.06
				0.25	1.35	1.53	1.14
				0.5	1.55	2.15	1.39
				0.75	2.05	3.12	1.52
				1.0	3.27	5.47	1.67
Average							1.57
Standard Deviation							0.42
Max.					3.27	6.04	2.49
Min.					1.09	1.25	1.06

imperfections and residual stresses – for the elastic design analysis calculations. However, it is useful to compare the magnitude of these stresses to the simple beam-theory solutions, to build confidence in the correctness of the elastic finite element solutions, to gain some feel for the nature and extent of the simple beam-theory approximations, and to develop some understanding of the relationship of the different parametric study suites to expected bridge I girder responses. The V-load solution (Eq. 1-6) is possibly the simplest of the beam-theory based approximations, and is considered in this section.

As noted in Section 5.8, the V-load equation (Eq. 1-6) can be reduced to a rather simple and elegant form for estimation of the lateral to vertical bending stress ratio, given by Eq. (5-4). This formula is a reasonably good approximation of the equation

$$\left|\frac{f_\ell}{f_b}\right| = \frac{S_{xc} L_b^{\,2}}{12\,R\,h\,S_{yc}} \tag{7-5}$$

obtained by direct substitution for M_ℓ and M in Eq. (1-6), but with a coefficient of 10 rather than 12 in the denominator. Equation (7-5) is utilized directly for the calculations presented here.

Table 7.15.4 gives the statistics for the ratio of f_ℓ/f_b based on Eq. (7-5) to the first-order elastic f_ℓ/f_b values obtained by direct finite element analysis. As noted previously, the V-load equation tends to overestimate the flange maximum lateral bending moment or stress in the primary suite. However it does not overestimate the lateral bending in all of the tests. Figure 7.15.7 shows a histogram of this ratio for the primary test suite. The above ratio is less than one in thirty-five of the 133 specimens, and it is less than 0.90 in 12 of the tests. It is greater than 1.30 in 13 of the studies, and it is greater than 1.40 in one study. No clear trend is evident pertaining to causes for the magnitude of these ratios.

Table 7.15.4. Ratio of f_ℓ/f_b based on the V-load equation (Eq. 7-5) to the finite element based first-order elastic f_ℓ/f_b.

	Average	Standard Deviation	Max.	Min.
Primary Suite (133 tests)	1.16	0.12	1.56	0.86
Modified Vert. Bending (46 tests)	0.90	0.10	1.18	0.74
Internal Loading (26 tests)	1.18	0.14	1.35	0.87
Free-End (10 tests)	1.45	0.08	1.53	1.32
Unsymmetric Girders (22 tests)	1.12	0.19	1.54	0.81

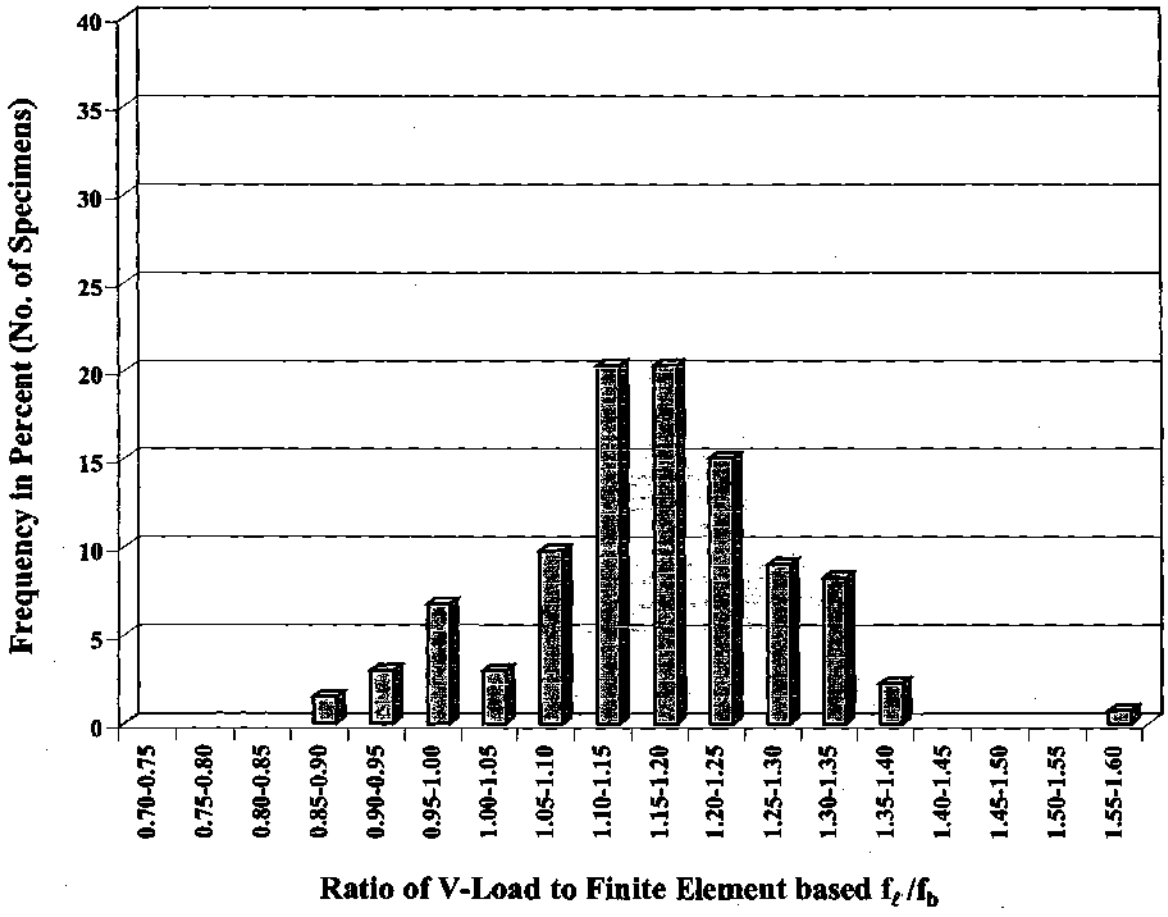

Figure 7.15.7. Histogram of the ratio of the V-Load (Eq. 7-5) to finite element based first-order f_t/f_b values for the primary test suite (133 tests).

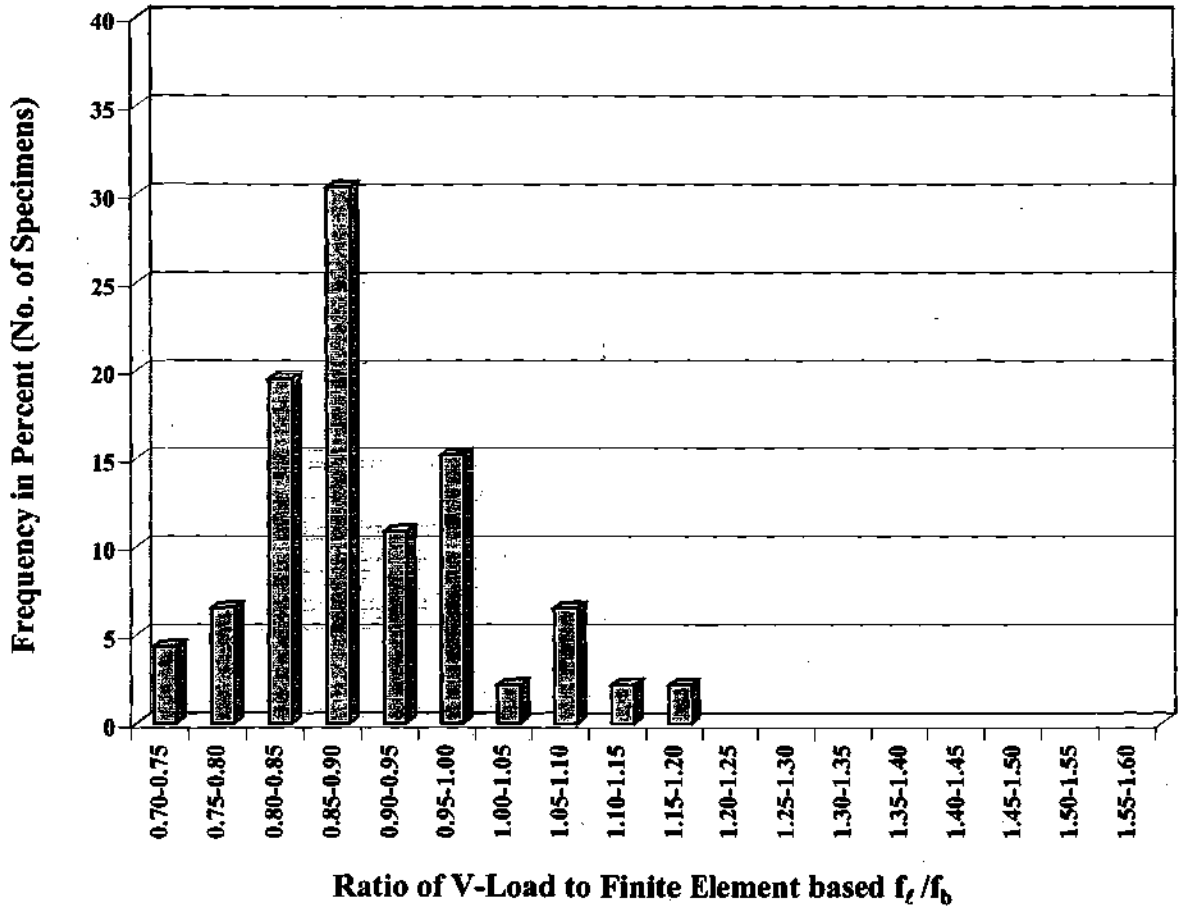

Figure 7.15.8. Histogram of the ratio of the V-load (Eq. 7-5) to finite element based first-order f_t/f_b values for the modified uniform vertical bending suite (46 tests).

Also as noted previously, the V-load equation tends to underestimate the first-order flange maximum lateral bending stress in the modified uniform vertical bending suite. Figure 7.15.8 shows a histogram of the ratio of the V-load and finite element based f_ℓ/f_b values for this suite. It can be seen that the V-load predictions fall predominantly between 0.85 and 0.95 of the finite element based solutions.

The V-load equation tends to overestimate the first-order stresses in both the internal loading and the free end suites. The histograms for these predictions are provided in Figs. 7.15.9 and 7.15.10. Finally, the values obtained for the above ratio do not appear to be significantly affected by girder nonsymmetry for the different types of boundary conditions. The overall statistics for all the test cases of the unsymmetric girders are provided in Table 7.15.4.

Tables 7.15.5 and 7.15.6 parallel Table 7.15.4. However, Table 7.15.5 presents the statistics for the ratio of the first-order V-load predictions for f_ℓ/f_b to the second-order finite element based f_ℓ/f_b values at the load level for which the one-third rule is satisfied based on the second-order elastic stresses. The first-order f_ℓ/f_b values are of course independent of the load level. Table 7.15.6 presents the statistics for the ratio of the amplified V-load based f_ℓ/f_b values (determined by multiplying the values computed from Eq. (7-5) by the amplification factor obtained from Eqs. (7-2) and (2-23) with $KL_b = 0.5L_b$, based on the load level at which the one-third rule is satisfied) versus the corresponding finite element based second-order f_ℓ/f_b values.

It can be observed that with the exception of the modified uniform vertical bending suite, the V-load equation tends to overestimate the flange lateral bending stresses, particularly if combined with the approximate amplification factor of Eq. (7-2). The use of the V-load equation to determine the lateral bending stress thus will produce a conservative estimate of the vertical bending capacity in a majority of the specimens considered. There are a significant number of cases in which the stresses are underestimated by the V-load equation, but the largest unconservative estimate in Table 7.15.5 is 26 percent low, with the exception of the modified vertical bending suite. If we assume an upper bound of $f_b = F_y$, and if we assume that the predicted f_ℓ is at the maximum limit permitted by the one-third rule (i.e., $f_\ell = 0.5F_y$), then we obtain an upper-bound estimate for the unconservative effect on the vertical bending capacity in the one-third rule equations of $(0.5F_y)(0.26)/3 = 0.04F_y$.

In closing, it should be emphasized that in general, flange lateral bending stresses can be generated due to numerous sources. This section has concentrated only on the stresses due to horizontal curvature. It is important to separate the calculation of the girder elastic stresses from the design resistance equations, both for reasons of clarity and generality.

Table 7.15.5. Ratio of f_t/f_b based on the V-load equation (Eq. 7-5) to the finite element based second-order f_t/f_b values at the load level for which the one-third rule is satisfied based on the second-order elastic stresses.

	Average	Standard Deviation	Max.	Min.
Primary Suite (133 tests)	1.06	0.12	1.52	0.76
Modified Vert. Bending (46 tests)	0.79	0.07	0.92	0.67
Internal Loading (26 tests)	1.07	0.11	1.24	0.84
Free-End (10 tests)	1.26	0.07	1.35	1.14
Unsymmetric Girders (22 tests)	1.02	0.19	1.39	0.74

Table 7.15.6. Ratio of f_t/f_b based on the V-load equation (Eq. 7-5), amplified by Eqs. (7-2) and (2-23) with $KL_b = 0.5L_b$ to the corresponding finite element based second-order f_t/f_b. In each of the two solutions, the stress is calculated at the load level corresponding to satisfaction of the one-third rule equations.

	Average	Standard Deviation	Max.	Min.
Primary Suite (133 tests)	1.12	0.14	1.59	0.77
Modified Vert. Bending (46 tests)	0.86	0.08	1.02	0.69
Internal Loading (26 tests)	1.17	0.17	1.42	0.86
Free-End (10 tests)	1.53	0.10	1.72	1.40
Unsymmetric Girders (22 tests)	1.09	0.23	1.58	0.75

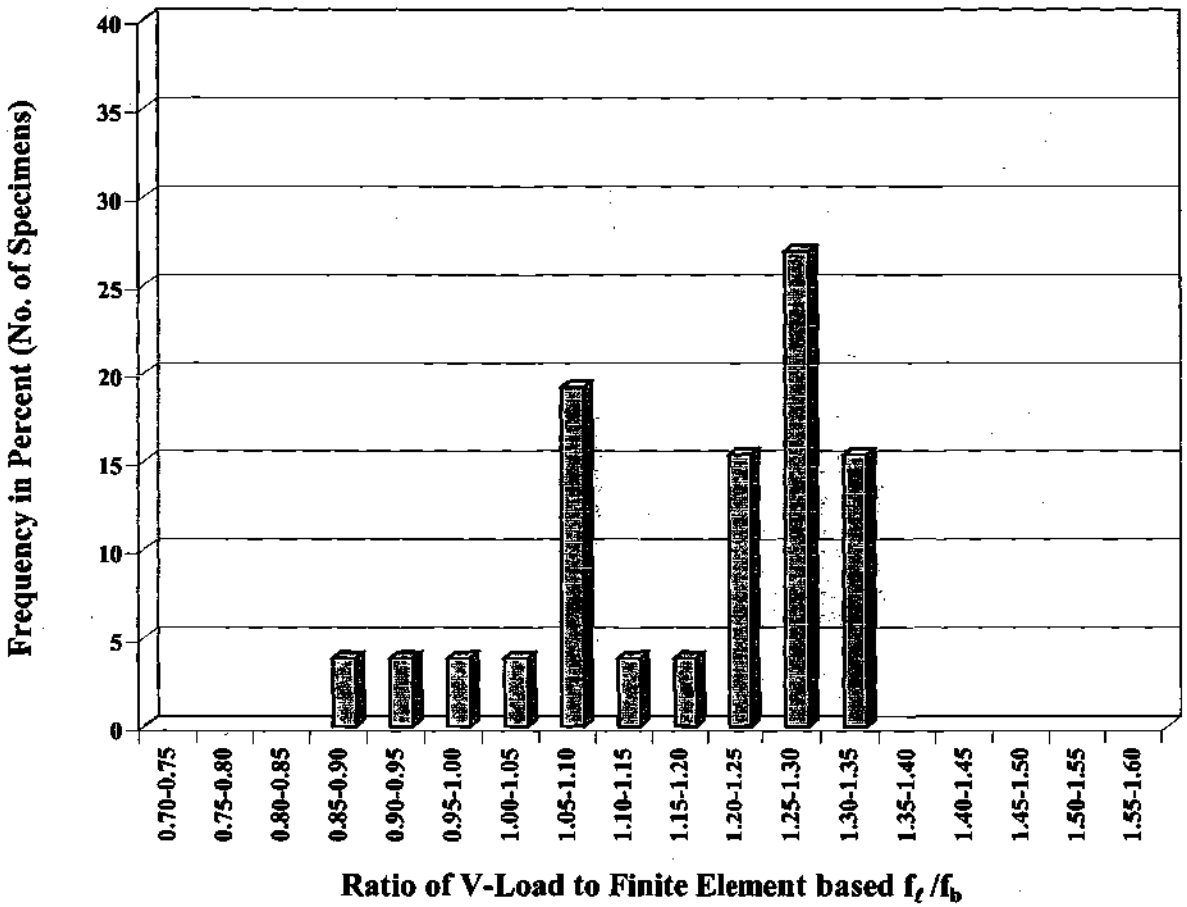

Figure 7.15.9. Histogram of the ratio of the V-load to finite element based first-order f_ℓ/f_b values for the internal loading suite (26 tests).

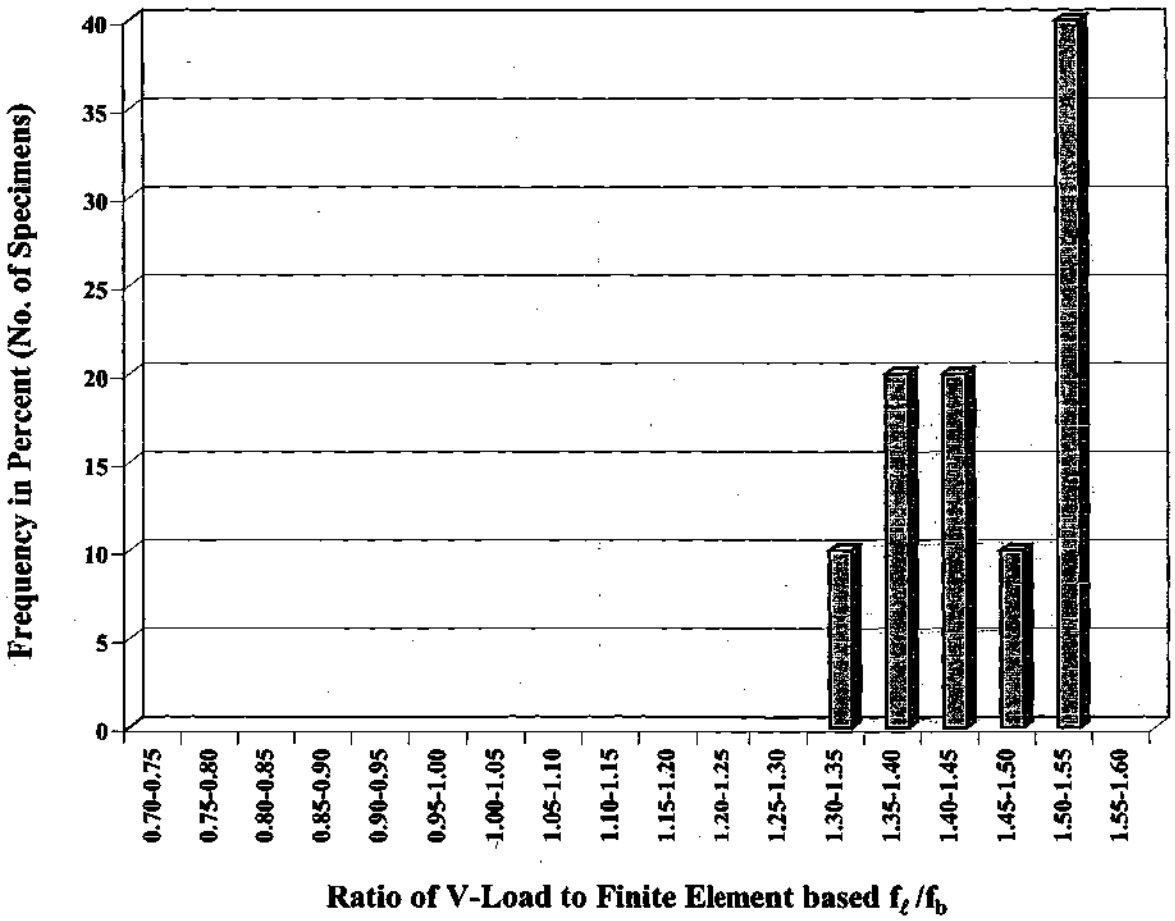

Figure 7.15.10. Histogram of the ratio of the V-load and finite element based first-order f_t/f_b values for the free-end suite (10 tests).

CHAPTER VIII

PARAMETRIC STUDY RESULTS – SHEAR STRENGTH

In this chapter, the shear strengths predicted by the design equations reviewed in Section 2.2 are compared to the corresponding strengths determined within the finite element parametric study. These equations are:

- The current AASHTO LRFD (2001) formulas, which are based on Basler's (1961b) research (see Sections 2.2.1 and 2.2.2),
- The equations recommended by Lee and Yoo (1998) (see Section 2.2.3), and
- A modified form of the AASHTO LRFD (2001) formulas in which the shear buckling coefficients proposed by Lee et al. (1996) are utilized in the calculation of the web shear buckling load (see Section 2.2.4).

All of these predictors include a contribution from the web postbuckling strength. The current and modified AASHTO LRFD (2001) formulas are based on the tension-field model forwarded by Basler (1961b), whereas Lee and Yoo (1998) propose an alternative simplified description of the postbuckling shear strength. The shear buckling load in the current AASHTO LRFD equations is based on the assumption of simply-supported boundary conditions at the flanges, whereas the shear buckling coefficients proposed by Lee et al. (1996), and utilized by Lee and Yoo (1998) and in the modified AASHTO LRFD equations, account for the buckling restraint offered by the flanges at the top and bottom of the web. All of these strength predictors utilize the fundamental web shear buckling equations proposed by Basler (1961b), albeit with different shear buckling coefficients. Lee and Yoo (1998) include an additional reduction factor that accounts directly for the influence of nominal geometric imperfections and plate bending within the web on the maximum strength.

It should be noted that in these studies, the postbuckling contribution to the shear strength is included in the calculations for all values of d_o/D, i.e., the $d_o/D \leq 1$ limit specified by Hall and Yoo (1998) is not enforced.

Section 8.1 addresses the calculation of ultimate shear strength. This is followed by Section 8.2, which addresses the accuracy of elastic shear buckling estimates from the AASHTO LRFD (2001) and Lee et al. (1996) formulas. Section 8.3 then focuses on the accuracy of the web postbuckling shear strength estimates from Lee and Yoo's (1998) equations as well as from the current and modified AASHTO LRFD (2001) formulas. Finally, Section 8.4 provides an overall assessment of the results of this study.

Similar to Chapter VII, this chapter focuses primarily on the overall statistical trends in the data from the parametric study tests. The reader is referred to Appendix B for a detailed summary of the strength data for the individual specimens.

8.1 ULTIMATE SHEAR STRENGTH

Table 8.1.1 gives statistics for the complete set of doubly symmetric shear tests considered within the parametric study. The data in this table as well as in the subsequent tables of this chapter are presented in a similar format to that adopted in Chapter VII. The arithmetic mean and standard deviation are provided along with the maximum and minimum values for the set. The second column of the table gives the range of the finite element based shear strengths relative to the web plastic shear capacity V_p. The average and standard deviation of these strength ratios are not provided, since this data is not relevant to the discussions. The parametric study is designed to test girders with a wide range of $V_{n(FEA)}/V_p$. The third through the fifth columns of the table provide the statistics for the three key design predictor equations evaluated in this research, expressed in terms of the ratio of the design strengths to the finite element based strengths. As in Chapter VII, the "best" value for each of the statistical quantities is shaded within the tables.

Table 8.1.1. Summary of ultimate shear strengths, primary test suite, doubly symmetric specimens (122 girders).

	$V_{n(FEA)}/V_p$	Current AASHTO / FEA	Lee and Yoo / FEA	Modified AASHTO / FEA
Avg.		0.88	1.01	1.02
Std. Dev.		0.09	0.12	0.06
High	0.84	1.09	1.27	1.16
Low	0.46	0.74	0.73	0.88

8.1.1 Overall Assessment of Ultimate Strength Predictions for Doubly-Symmetric Girders

From Table 8.1.1, it can be observed that the equations proposed by Lee and Yoo (1998) give the most accurate prediction of the finite element based strengths on average (1.01). However, the modified AASHTO LRFD equations have essentially the same accuracy (1.02) along with the smallest standard deviation (0.06) and the most accurate minimum value (0.88) in the design to finite element strength ratio. The modified AASHTO equations are somewhat more liberal than the current AASHTO equations for the worst overestimate of the finite element predictions (1.16 versus 1.09). The overall improved accuracy in the modified AASHTO equations is entirely due to the more accurate prediction of the shear buckling strength based on the buckling coefficients

proposed by Lee et al. (1996). The relative accuracy of the current AASHTO (2001) and Lee et al. (1996) shear buckling coefficients is addressed subsequently in Section 8.2.

Although the Lee and Yoo (1998) equations give an accurate prediction of the finite element based strengths on average (1.01), their predictions have a wide dispersion relative to the finite element based strengths as evidenced by the standard deviation of 0.12, the minimum of 0.73 and the maximum of 1.27 in Table 8.1.1. This is due to the simplified expression for the postbuckling strength in (Lee and Yoo 1998), which leads to anomalous postbuckling strength predictions as discussed in Section 2.2.3. That is, the Lee and Yoo (1998) equations predict that the web shear postbuckling strength increases with increasing panel aspect ratio d_o/D, which is counter intuitive and does not follow the trends in established experimental data. The accuracy of the postbuckling strength predictions from each of the design equations is addressed in Section 8.3.

It should be noted that a total of 133 high-shear low-moment tests are executed within this finite element parametric study. However, 11 of the specimens for $L_b/R = 0.05$ and target $f/f_b = 0.50$ fail in a lateral bending mode rather than a shear mode[1]. Overall, the specimens with these design parameters have the largest unsupported lengths L_b of all the tests (see Tables 5.8.1 through 5.8.5), and the girders that fail in lateral bending provide an important verification of the accuracy of the design predictor equations for cases in which the flanges are not able to hold a node line to support the development of the web shear strength. However, the strengths in the cases that are governed by a lateral bending failure are captured by the flexural strength predictor equations; the load capacities based on the flexural strength check are smaller than that those based on the web ultimate shear strength. Therefore, the 11 specimens that fail by lateral bending are not included within the ultimate shear strength statistics presented here. Rather, they are considered directly as part of the evaluation of moment-shear strength interaction in Chapter IX. These tests are distinguished from the other high-shear low-moment tests by the use of *italics* for the associated data values reported within Table B.1.2.

8.1.2 Ultimate Strength Predictions as a Function of the Panel Aspect Ratio d_o/D

Tables 8.1.2 through 8.1.4 focus on the results of the design predictor equations for the specific cases out of the full study involving a relatively slender web ($D/t_w = 160$) and different web aspect ratios d_o/D. Table 8.1.2 gives these results for $d_o/D = 1$, Table 8.1.3 focuses on the results for $d_o/D = 2$, and Table 8.1.4 addresses the results for $d_o/D = 3$. Five of the girders with $D/t_w = 160$ and $d_o/D = 1$ failed by lateral bending rather than by shear. These girders are not included within Table 8.1.2. All of the girders studied with $D/t_w = 160$ and $d_o/D = 2$ or 3 failed by shear. Table 8.1.4 is based on five fewer tests than Table 8.1.3 due to the fact that the unsupported length L_b is equal to $2d_o$ in five of the tests.

[1] Note that f/f_b is set approximately to the target values only in the uniform vertical bending studies of the primary test suite. The values of f/f_b are generally somewhat smaller in the maximum V/M tests.

Table 8.1.2. Summary of ultimate shear strengths, primary test suite, doubly symmetric specimens with $D/t_w = 160$ and $d_o/D = 1$, excluding cases that fail by lateral bending (25 girders).

	$V_{n(FEA)}/V_p$	Current AASHTO FEA	Lee and Yoo FEA	Modified AASHTO FEA
Avg.		0.98	0.81	1.02
Std. Dev.		0.05	0.04	0.05
High	0.84	1.09	0.90	1.12
Low	0.69	0.89	0.73	0.92

Table 8.1.3. Summary of ultimate shear strengths, primary test suite, doubly symmetric specimens with $D/t_w = 160$ and $d_o/D = 2$ (30 girders).

	$V_{n(FEA)}/V_p$	Current AASHTO FEA	Lee and Yoo FEA	Modified AASHTO FEA
Avg.		0.93	1.06	1.04
Std. Dev.		0.05	0.06	0.06
High	0.62	1.04	1.18	1.16
Low	0.50	0.84	0.95	0.95

Table 8.1.4. Summary of ultimate shear strengths, primary test suite, doubly symmetric specimens with $D/t_w = 160$ and $d_o/D = 3$ (25 girders).

	$V_{n(FEA)}/V_p$	Current AASHTO FEA	Lee and Yoo FEA	Modified AASHTO FEA
Avg.		0.79	1.12	0.95
Std. Dev.		0.04	0.05	0.05
High	0.56	0.90	1.27	1.07
Low	0.46	0.74	1.04	0.88

Table 8.1.2 shows that the current and modified AASHTO shear strength equations have equal accuracy on average for problems involving a slender web and $d_o/D = 1$. The current AASHTO equations are slightly conservative (0.98) and the modified AASHTO equations are slightly liberal on average (1.02). Both sets of equations have the same standard deviation (0.05) in the ratio of their predictions to the finite element based strengths. The largest overestimate of the finite element based strengths is slightly higher

with the modified AASHTO equations compared to the current AASHTO equations for this case (1.12 versus 1.09), and the largest underestimate is slightly more accurate for the modified AASHTO equations (0.92 versus 0.89). The Lee and Yoo (1998) equations significantly underestimate the finite element based strengths for this case, although the dispersion of the Lee and Yoo predictions is smaller than that for the other equations.

For $D/t_w = 160$ and $d_o/D = 2$ (Table 8.1.3), the predictions by the modified AASHTO equations are slightly more liberal than for the case in Table 8.1.2, overestimating the finite element based strengths by four percent on average, with the largest overestimate being 16 percent unconservative. Conversely, the current AASHTO equations are more conservative for this case than for $D/t_w = 160$ and $d_o/D = 1$. The Lee and Yoo (1998) equations over predict the finite element based strengths for 24 of the 30 girders in this set, with the largest overestimate being 18 percent unconservative.

Finally, for the case of $D/t_w = 160$ and $d_o/D = 3$ (Table 8.1.4), the modified AASHTO equations become slightly conservative on average, with a largest overestimate of only seven percent, the current AASHTO equations become highly conservative with an average ratio of the design prediction to the finite element based strength of only 0.79, and the Lee and Yoo (1998) equations exhibit a high degree of unconservatism on average (12 percent), with their largest over prediction of the finite element based strength being 27 percent.

8.1.3 Ultimate Strength Predictions as a Function of the Web Slenderness D/t_w

The previous section focuses on the behavior of the different prediction equations for a web slenderness $D/t_w = 160$, which is essentially the maximum limit allowed by AAHSTO LRFD (2001) for a transversely stiffened girder with $F_y = 345$ MPa (50 ksi). It is important also to consider the behavior of the prediction equations for transversely stiffened girders having stockier webs. Tables 8.1.5 and 8.1.6 show the results from the parametric study for transversely stiffened girders with $d_o/D = 3$ and $D/t_w = 130$ and 100 respectively. These tables may be studied along with Table 8.1.4 to ascertain the accuracy of the predictions as a function of D/t_w for cases with wide stiffener spacing.

It can be observed that the current AASHTO equations become more accurate and the dispersion of their predictions relative to the finite element based strengths is reduced as D/t_w is decreased. However, these changes are rather small. The predictions by Lee and Yoo's (1998) equations are significantly improved with smaller D/t_w. As noted in the previous section, for $D/t_w = 160$ and $d_o/D = 3$, the Lee and Yoo equations exhibit large unconservative errors and significant dispersion. However, for $D/t_w = 130$, these equations exhibit the same standard deviation as the other two predictors (0.03), and the best low value (1.02) (along with the modified AASHTO equations (0.98)) relative to the finite element based strengths. For $D/t_w = 100$, the Lee and Yoo equations give the best overall prediction of the girder strengths, with an average strength ratio of 0.97, a standard deviation of 0.02, a maximum value of 1.01 and a minimum of 0.94. Nevertheless, the modified AASHTO equations give the best overall predictions for $D/t_w = 160$ and 130, and their statistics for $D/t_w = 100$ are liberal but generally more

accurate than those pertaining to the full set of girders studied (compare Tables 8.1.6 and 8.1.1). For $D/t_w = 100$, the modified AASHTO equations have equal accuracy to the Lee and Yoo equations for the minimum strength ratio, and the same standard deviation as the Lee and Yoo equations.

Table 8.1.5. Summary of ultimate shear strengths, primary test suite, doubly symmetric specimens with $D/t_w = 130$ and $d_o/D = 3$ (19 girders).

	$V_{n(FEA)}/V_p$	Current AASHTO FEA	Lee and Yoo FEA	Modified AASHTO FEA
Avg.		0.82	1.06	1.02
Std. Dev.		0.03	0.03	0.03
High	0.63	0.86	1.12	1.07
Low	0.56	0.77	1.02	0.98

Table 8.1.6. Summary of ultimate shear strengths, primary test suite, doubly symmetric specimens with $D/t_w = 100$ and $d_o/D = 3$ (17 girders).

	$V_{n(FEA)}/V_p$	Current AASHTO FEA	Lee and Yoo FEA	Modified AASHTO FEA
Avg.		0.84	0.97	1.07
Std. Dev.		0.03	0.02	0.02
High	0.79	0.88	1.01	1.12
Low	0.71	0.80	0.94	1.06

Unfortunately, only a few girders with $D/t_w < 160$ and $d_o/D < 3$ are considered within the current parametric study. As explained in Section 5.4, this restriction is based on the rational that girders with stockier webs would tend to be designed with wide stiffener spacing, if not as unstiffened. The only girders considered with $D/t_w < 160$ and $d_o/D < 3$ are six tests with $D/b_f = 2.75$, $L_b/R = 0.1$ and a target $f_\ell/f_b = 0.35$, which leads to $L_b = 2d_o$ in the design of the girders. The results from these tests are shown in Table 8.1.7. One can observe that the current AASHTO equations give very accurate predictions for these cases, whereas the predictions by Lee and Yoo's equations are reasonably accurate (with strength ratios ranging from 0.94 to 1.09). The modified AASHTO equations have a narrow dispersion in their strength ratios for these girders, but with values ranging from 1.11 to 1.16. However, maximum strength ratio of 1.16 is obtained with these equations for one of the girders with $D/t_w = 160$ and $d_o/D = 2$ as well (a girder with $L_b/R = 0.10$, target $f_\ell/f_b = 0.50$, $D/b_f = 3.25$ and $b_f/t_f = 25$). It is apparent that the horizontal curvature has some effect on reducing the finite element based

strength and thus increasing the strength ratio in all of the above tests. In fact, the maximum strength ratios of all of the prediction equations for $D/t_w = 160$, for all the values of d_o/D studied, occur for the girder with $L_b/R = 0.10$, target $f_t/f_b = 0.50$, $D/b_f = 3.25$ and $b_f/t_f = 25$. Therefore, the predictions of the modified AASHTO equations shown in Table 8.1.7 are considered to be acceptable, although the strength ratios are somewhat large. The influence of horizontal curvature on the shear capacity is addressed subsequently in Section 8.1.5.

Table 8.1.7. Ultimate shear strengths, primary test suite, doubly-symmetric specimens with $L_b/R = 0.1$, target $f_t/f_b = 0.35$, $D/t_w < 160$ and $d_o/D = 2$.

b_f/t_f	D/t_w	$V_{n(FEA)} / V_p$	Current AASHTO FEA	Lee and Yoo FEA	Modified AASHTO FEA
15	130	0.62	0.95	1.03	1.11
20	130	0.60	0.98	1.06	1.14
25	130	0.59	1.00	1.09	1.16
15	100	0.80	0.91	0.94	1.11
20	100	0.76	0.95	0.99	1.15
25	100	0.73	1.00	1.00	1.15

8.1.4 Assessment of Ultimate Strength Predictions for Singly-Symmetric Girders

Table 8.1.8 summarizes the ultimate strength predictions for the unsymmetrical specimens considered in this research. The overall statistics for these girders are similar to those for the doubly symmetric girder tests (Table 8.1.1). Lee and Yoo's equations provide the best overall predictions on average (1.07), but they have the widest dispersion relative to the finite element based strengths, with a standard deviation of 0.12, the largest under prediction of 0.82 and the largest over prediction of 1.18. The current and modified AASHTO equations are equally accurate in their average results, with the current equations erring on the conservative side (0.92) and the modified equations providing a liberal average strength ratio (1.08). However, the modified AASHTO equations have the smallest standard deviation (0.06) and best minimum strength ratio (0.99) of the three prediction equations. The largest over prediction by the modified AASHTO equations (1.15) is smaller than the corresponding ratio within the full set of doubly symmetric girders studied (see Table 8.1.1). It should be noted that the average of the flange thicknesses is used with equations for the shear buckling coefficient in Lee and Yoo's and the modified AASHTO procedures (Eqs. (2-104) and (2-105)) for the monosymmetric girders.

Table 8.1.8. Summary of ultimate shear strengths, singly symmetric specimens (8 girders).

	$V_{n(FEA)}/V_p$	Current AASHTO FEA	Lee and Yoo FEA	Modified AASHTO FEA
Avg.		0.92	1.07	1.08
Std. Dev.		0.09	0.12	0.06
High	0.75	1.05	1.18	1.15
Low	0.50	0.82	0.82	0.99

8.1.5 Summary

Overall, the modified AASHTO equations provide the best predictions of the finite element based strengths within all of the Tables 8.1.1 through 8.1.8. Their average strength ratios are either the best, or do not differ significantly from the best values, in all of the above tables. Also, they provide the smallest standard deviation in the ratio of the predicted to finite element based strengths for the complete sets of doubly- and singly-symmetric girders (see Tables 8.1.1 and 8.1.8), and their standard deviation is small across all of the above tables. However, they show a maximum unconservative error of 16 percent, whereas the maximum unconservative error in the current AASHTO equations is only nine percent. For $D/t_w = 160$, the Lee and Yoo (1998) equations show a clear trend of being significantly conservative for small d_o/D ratios, with a smallest under prediction of 0.69, to significantly unconservative for $d_o/D = 3$, with a largest over prediction of 1.27.

Figures 8.1.1 through 8.1.3 show histograms of the shear strength ratios (design to finite element based strengths) for each of the above predictor equations. Both the doubly- and singly-symmetric girders considered in Tables 8.1.1 through 8.1.4 are included in the histogram plots. The modified AASHTO shear strengths clearly exhibit the best distribution, followed by the current AASHTO shear strength equations and Lee and Yoo's equations. The significant conservatism of the current AASHTO shear strength equations for the majority of the test cases is evident in Fig. 8.1.2, whereas the wide scatter in the Lee and Yoo shear strength predictions is apparent in Fig. 8.1.3.

8.1.6 Influence of Horizontal Curvature on Ultimate Shear Strength

Table 8.1.9 presents the results of the finite element strength predictions as a function of horizontal curvature, as represented by the parameter L_b/R. Only girders with $D/t_w = 160$ and $d_o/D = 2$ are included within this table. The reason for this specific focus is, as noted previously, five of the girders with $D/t_w = 160$ and $d_o/D = 1$ failed by lateral bending. Furthermore, the unbraced length L_b is not sufficient to allow $d_o/D = 3$ in a number of cases. Therefore, if the cases with $d_o/D = 1$ and $d_o/D = 3$ are included, the statistical results for different L_b/R ratios are falsely skewed by the fact that a different

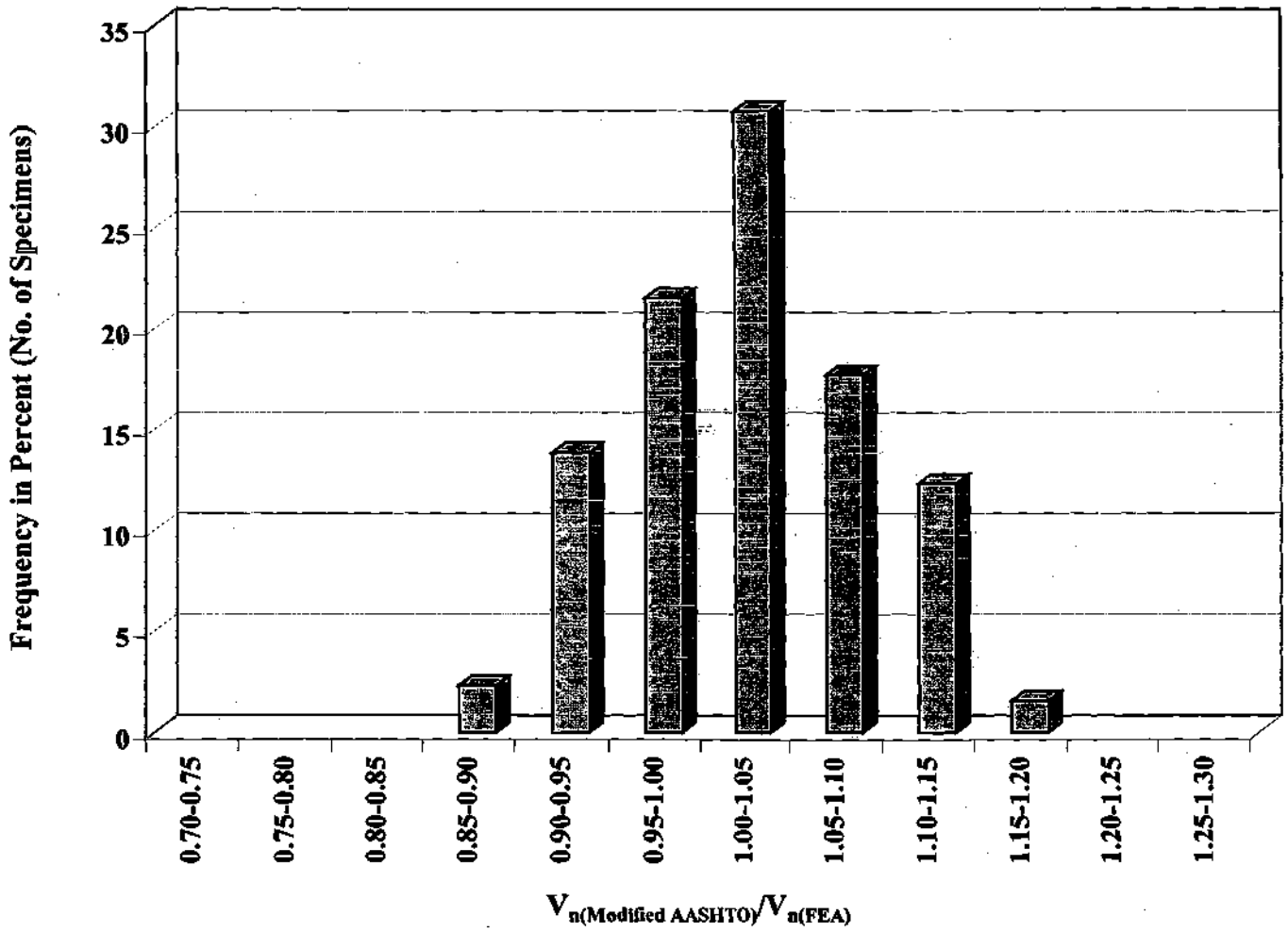

Figure 8.1.1. Distribution of the predicted to finite element shear strengths based on the modified AASHTO LRFD equations (130 girders).

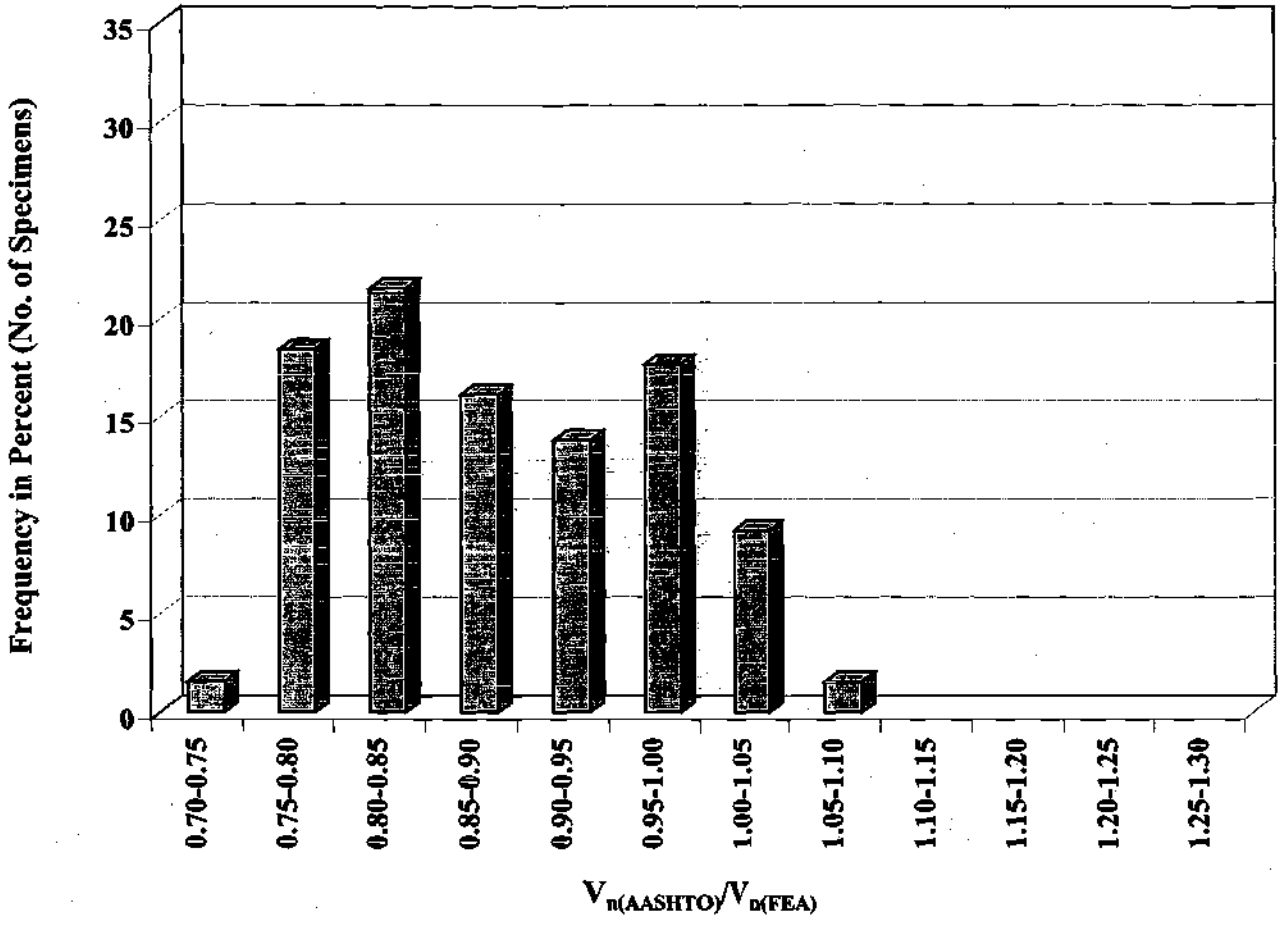

Figure 8.1.2. Distribution of the predicted to the finite element shear strengths based on the current AASHTO LRFD (2001) (130 girders).

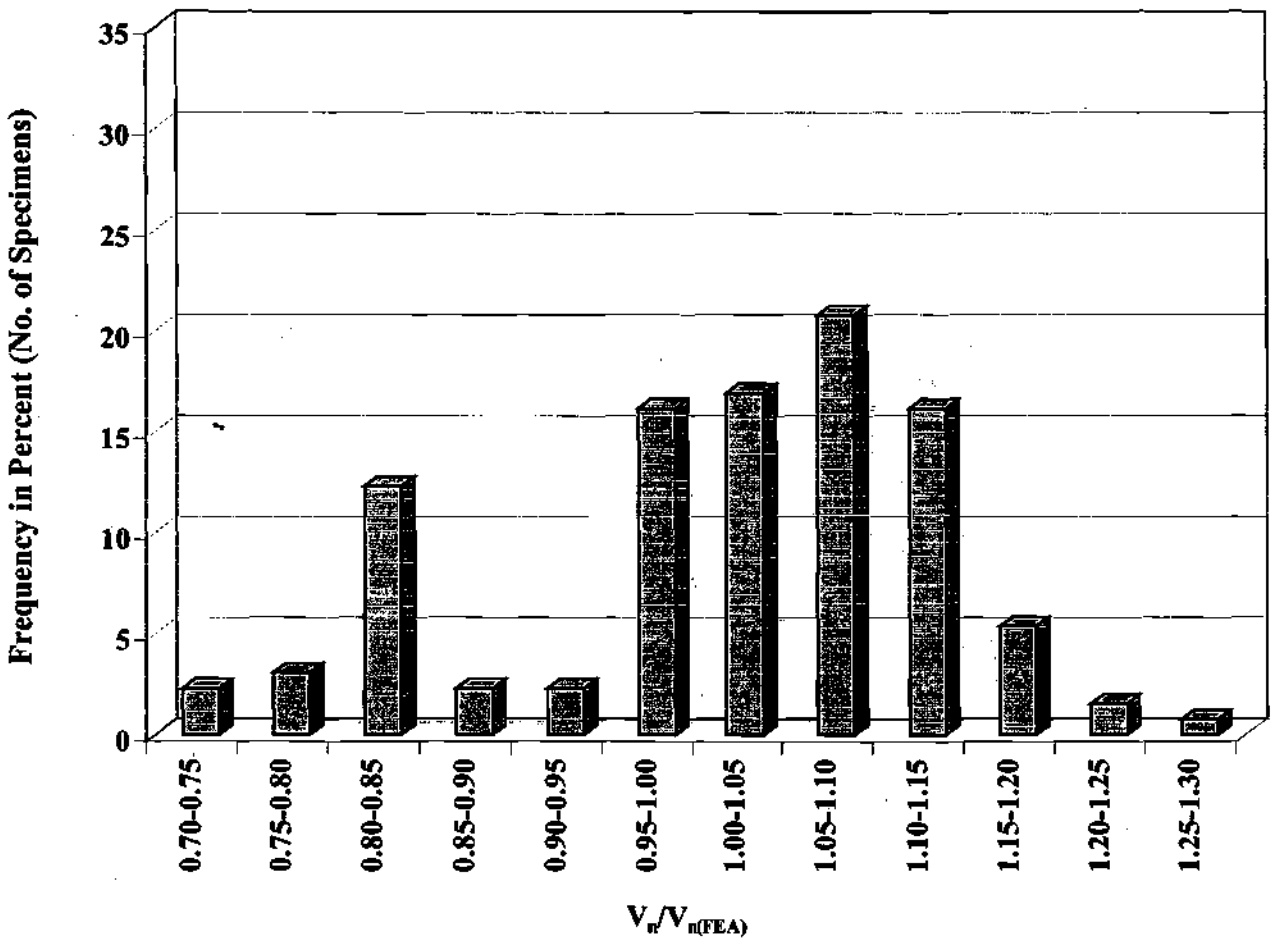

Figure 8.1.3. Distribution of the predicted to the finite element shear strengths based on Lee and Yoo's (1998) equations (130 girders)

number and set of girders is considered for each L_b/R. Table 8.1.9 illustrates the well-known result (Mozer et al. 1970, 1971 and 1975; Lee and Yoo (1999); Zureick et al. 2001) that there is typically a small reduction in the maximum shear strength due to horizontal curvature. The reduction in the shear strength due to horizontal curvature evidenced within this table is approximately 0.02 to 0.03 V_p (or four to six percent of the shear capacity) as L_b/R is increased from 0.05 to 0.10. This reduction is smaller than the typical errors in the strength predictions due to the approximate nature of the different shear strength equations. For girders that satisfy the design limit of $L_b/R \leq 0.10$, one can conclude that this strength reduction may be neglected.

Table 8.1.9. Influence of L_b/R on ultimate shear strengths predicted by finite element analysis, primary test suite, specimens with $D/t_w = 160$ and $d_o/D = 2$.

	$V_{n(FEA)}/V_p$ ($L_b/R = 0.05$) (10 girders)	$V_{n(FEA)}/V_p$ ($L_b/R = 0.075$) (10 girders)	$V_{n(FEA)}/V_p$ ($L_b/R = 0.1$) (10 girders)
Avg.	0.57	0.56	0.55
Std. Dev.	0.03	0.03	0.03
High	0.62	0.61	0.61
Low	0.53	0.52	0.50

8.2 ELASTIC BUCKLING STRENGTHS

The ratios of the two elastic buckling predictors evaluated in this research to the web buckling strengths $V_{cr(FEA)}$ obtained from elastic linear buckling finite element analysis are summarized in Table 8.2.1. These predictors are the AASHTO LRFD (2001) formulas, which are based on the assumption of simply-supported boundary conditions at the flanges, and the formulas proposed by Lee et al. (1996) and Lee and Yoo (1998), which account for the buckling restraint offered by the flanges. Both predictors are based on Timoshenko's (1910) elastic buckling strength equation (Eq. (2-95c) for the AASHTO LRFD calculations and Eq. (4-2) for Lee and Yoo's calculations). In the application of the AASHTO LRFD (2001) equations, the shear buckling coefficient is calculated as per Eq. (2-96b) (webs with $d_o/D > 3$ are not considered in these studies). The formulas for the shear buckling coefficient proposed by Lee et al. (1996) are summarized in Eqs. (2-104) through (2-106). The range of the finite element based buckling strengths relative to the web plastic shear capacity $V_{cr(FEA)}/V_p$ for the girders considered in this study is shown in the second column of the table.

From Table 8.2.1, it can be observed that the shear buckling coefficients proposed by Lee et al. (1996) provide a significantly better prediction of the elastic buckling strengths than the current AASHTO LRFD (2001) equations on average (0.98 versus 0.66), with a lower standard deviation (0.05 versus 0.06) and a significantly more accurate low value

for the ratio between the predicted and the directly computed buckling strengths (0.84 versus 0.58). This is consistent with the research results reported by Bradford (1996), which also indicate that the web shear-buckling boundary conditions at the flanges in practical plate girders are generally intermediate between simple and fixed, and that they are generally close to fixed for $t_f/t_w \geq 2$. The worst-case overestimate of the finite element based buckling strengths by the Lee et al. equations is 1.14, whereas the strength ratio for the current AASHTO LRFD (2001) equations never exceeds 0.83. Generally, the predictions by the Lee et al. equations tend to be slightly more liberal for the specimens with stockier webs (i.e., $D/t_w = 100$ and 130).

Table 8.2.1. Ratios of elastic shear buckling strengths obtained by the design predictor equations to the corresponding values from elastic linear buckling analysis, doubly-symmetric specimens (122 girders).

	$V_{cr(FEA)}/V_p$	Current AASHTO / FEA	Lee et al. / FEA
Avg.		0.66	0.98
Std. Dev.		0.06	0.05
High	0.82	0.83	1.14
Low	0.28	0.58	0.84

It should be noted that in 11 of the girders that have an L_b/R of 0.05 and a target f_f/f_b of 0.50, the elastic buckling mode shape differs significantly from that associated with web shear buckling. Therefore, these specimens are not included within the elastic buckling strength statistics shown in Table 8.2.1. These are the same 11 girders that are excluded from the statistics reported in Table 8.1.1. However, the elastic buckling mode shapes of these girders are significantly different than the inelastic stability failure mode associated with their maximum strengths. As noted previously, the ultimate strength of these girders is dominated by flange lateral bending. Figures 8.2.1 and 8.2.2 illustrate the elastic buckling mode shapes for two of these 11 girders. The mode in Fig. 8.2.1 shows significant participation of web bend and flange local buckling along with an influence of web shear, whereas the mode in Fig. 8.2.2 indicates significant web bend buckling in one critical panel, combined with associated flange local buckling (torsional) rotations.

Figures 8.2.3 and 8.2.4 show histograms of the predicted elastic buckling strengths versus the computed finite element values for the Lee et al. (1996) and the current AASHTO equations respectively. There is only one girder for which the unconservative error in the prediction by the Lee et al. equations is greater than 10 percent. This girder belongs to the above set of girders with $L_b/R = 0.05$ and $f_f/f_b = 0.50$, from which 11 specimens are excluded from consideration as shear tests. It is suspected that there may be some minor interaction between the shear and flexural strengths in this test as well.

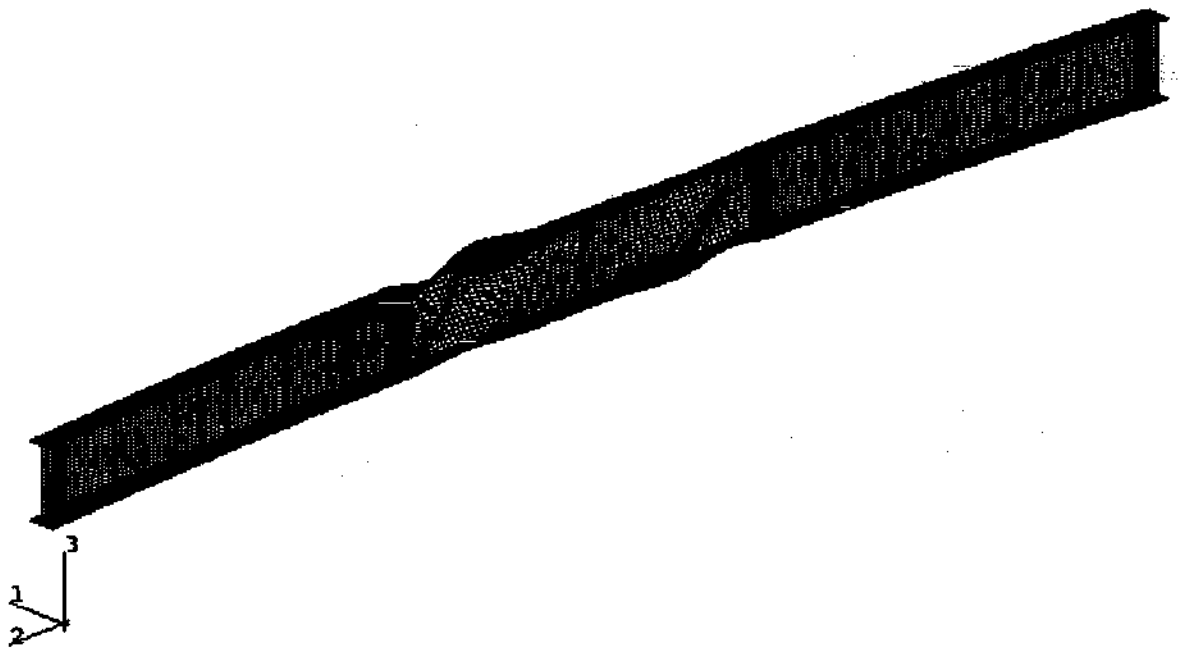

Figure 8.2.1. Buckling mode shape of specimen with $D/b_f = 2.75$, $b_f/t_f = 25$, $D/t_w = 100$, $d_o/D = 3$, $L_b/R = 0.05$, and target $f/f_b = 0.50$ under maximum V/M loading.

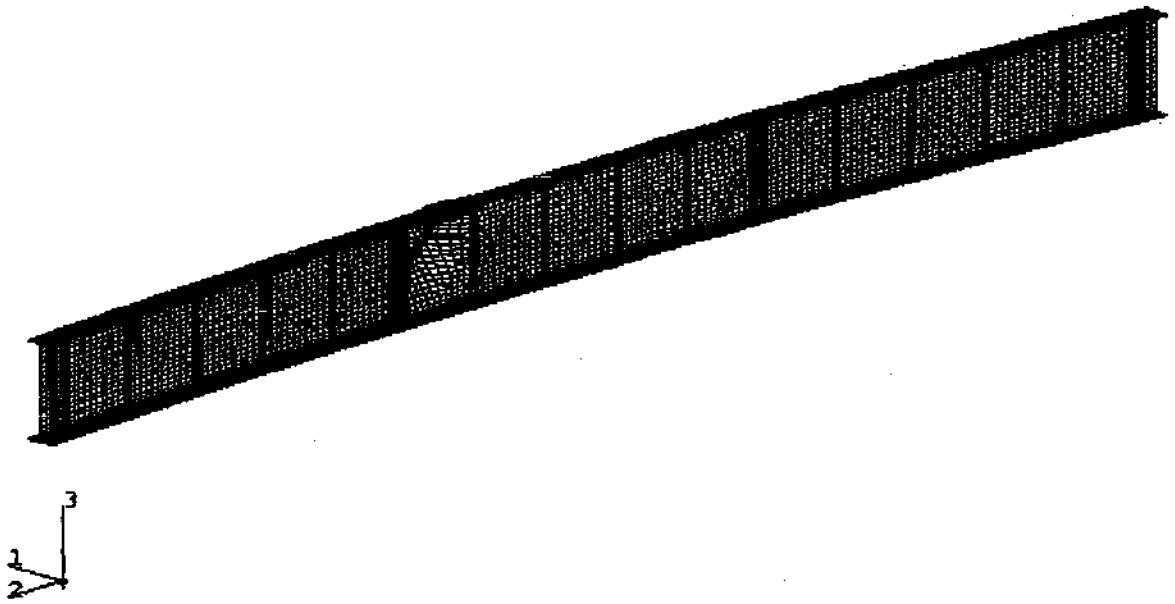

Figure 8.2.2. Buckling mode shape of specimen with $D/b_f = 3.25$, $b_f/t_f = 25$, $D/t_w = 160$, $d_o/D = 1$, $L_b/R = 0.05$, and target $f/f_b = 0.50$, maximum V/M loading.

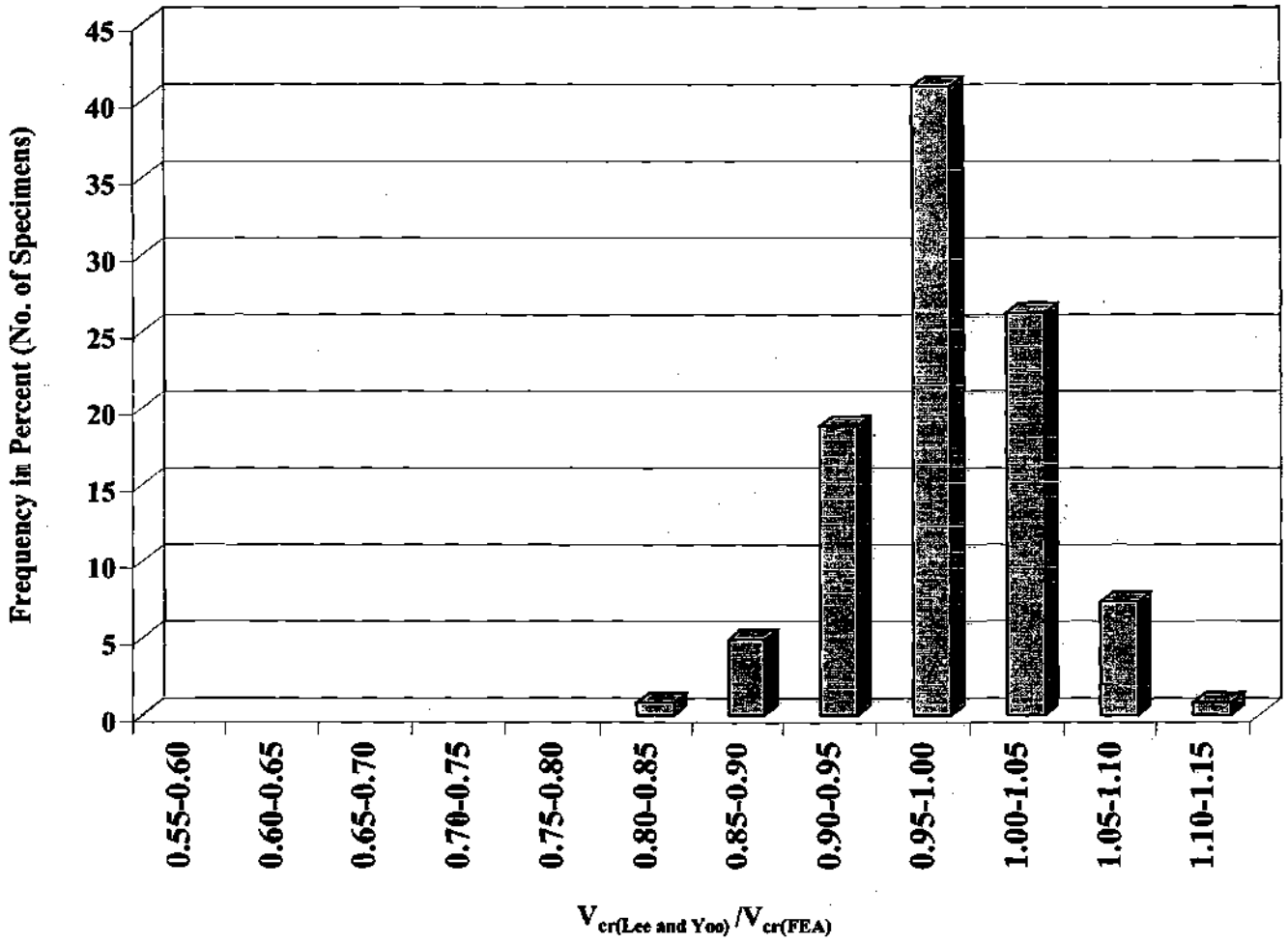

Figure 8.2.3. Distribution of the predicted to the finite element elastic shear buckling strengths based on Lee and Yoo's (1998) equations (122 doubly-symmetric girders)

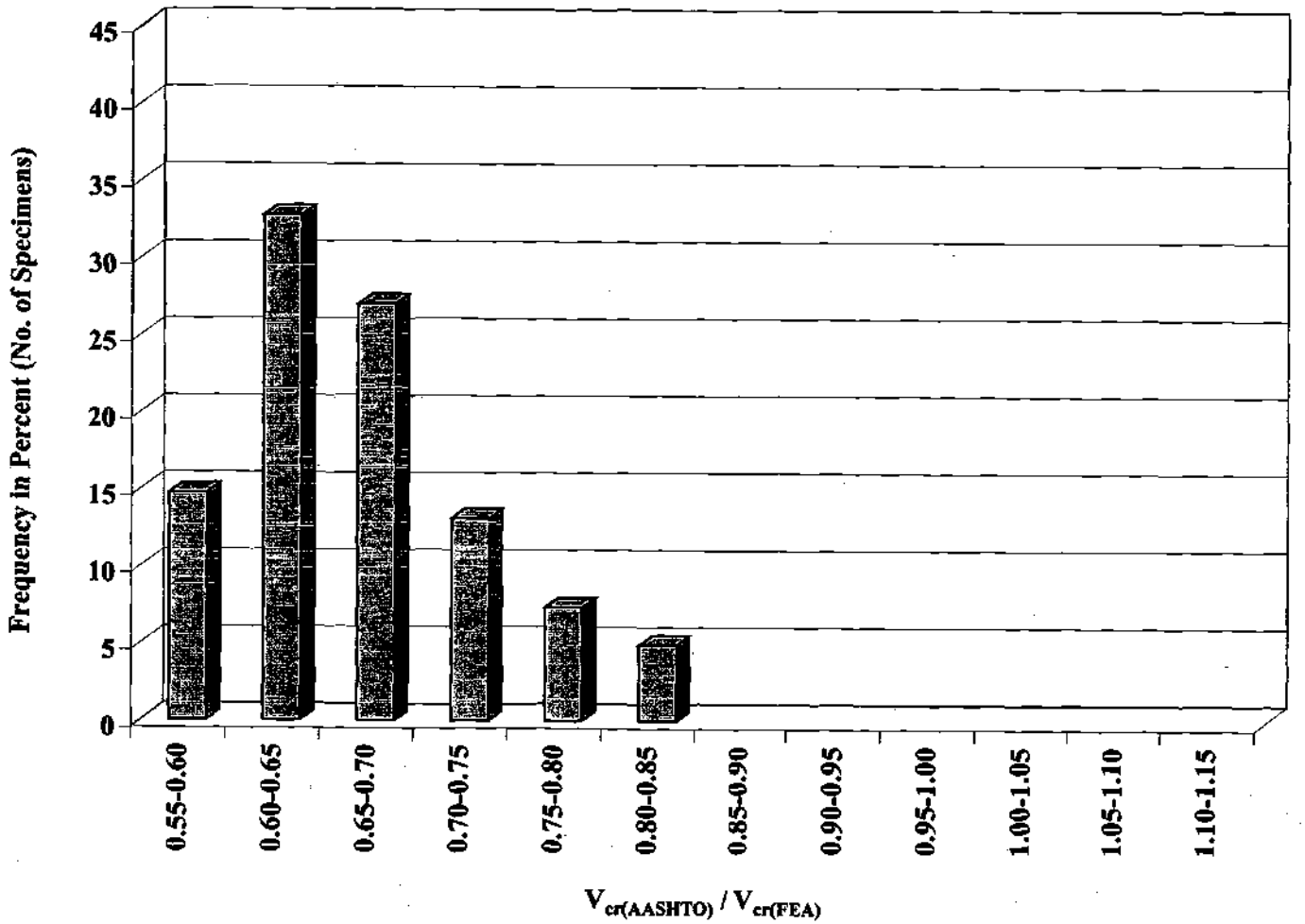

Figure 8.2.4. Distribution of the predicted to the finite element elastic shear buckling strengths based on the current AASHTO LRFD (2001) equations (122 doubly-symmetric girders).

Figure 8.2.5 plots the ratios of the elastic buckling strengths obtained from finite element analysis and from the two design predictor equations to the web plastic shear capacities ($C = V_{cr}/V_p$) versus the web panel aspect ratio d_o/D for the girders with $D/t_w = 160$ and $D/b_f = 2.75$. It can be observed that there is a clear reduction in the elastic buckling strengths as d_o/D increases. The Lee et al. (1996) shear buckling coefficient gives a reasonably accurate estimate of the finite element elastic buckling shear strengths in all of the cases shown in the figure – its most conservative predictions are obtained for the girders with $L_b/R = 0.10$ and target $f_f/f_b = 0.35$, which have the smallest R values. Conversely, the buckling strength based on the current AASHTO LRFD (2001) shear buckling coefficient is significantly smaller than the finite element based strengths in all of the cases.

Table 8.2.2 summarizes the elastic buckling predictions for the unsymmetrical girders considered in this research. The trends in the data for these girders are very similar to those for the doubly-symmetric specimens reported in Table 8.2.1

Table 8.2.2. Summary of elastic shear buckling strengths, singly-symmetric specimens (8 girders).

	$V_{cr(FEA)}/V_p$	Current AASHTO FEA	Lee et al. FEA
Avg.		0.66	1.00
Std. Dev.		0.04	0.11
High	0.51	0.70	1.13
Low	0.27	0.61	0.82

Finally, Table 8.2.3 illustrates the influence of horizontal curvature on the web elastic buckling strengths for the doubly-symmetric girders tested. It can be observed that as the subtended angle L_b/R increases, there is a small but nonnegligible increase in the elastic shear buckling strengths. This attribute of the behavior of curved I girders has been well established in prior research (Abdel-Sayed 1973; Mozer et al. 1970, 1971 and 1973; Yoo 1996; Lee and Yoo 1999b). However, the increase in the web elastic shear buckling capacity due to horizontal curvature is similar in magnitude to the range of the error in the accurate Lee et al. (1996) elastic shear buckling equation. Also, as discussed in the next section, the web postbuckling strength is generally decreased due to the horizontal curvature such that the ultimate shear strength of curved girder web panels is actually smaller for larger L_b/R. If the increase in the web buckling strength due to horizontal curvature were considered within design predictor equations, the corresponding decrease in the postbuckling strength would have to be directly addressed. Therefore, in the view of the authors, it is not worthwhile to consider the effect of the horizontal curvature within the design predictor equations. The fact that the web buckling strength is

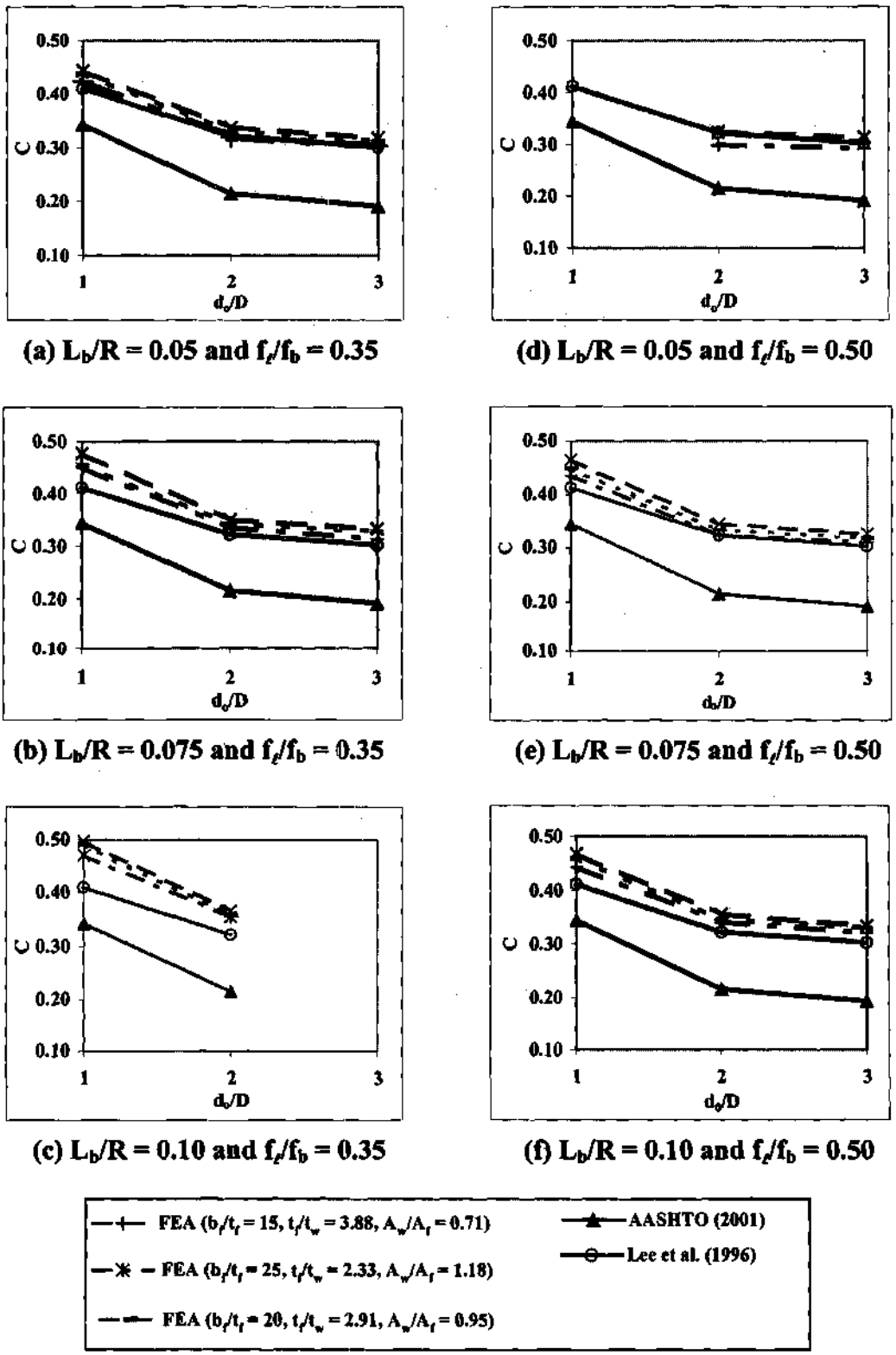

Figure 8.2.5. $C = V_{cr}/V_p$ versus d_o/D for doubly-symmetric specimens with constant $D/b_f = 2.75$ and $D/t_w = 160$ and different t_f/t_w and b_f/t_f.

increased somewhat due to horizontal curvature might be considered as providing an additional margin of safety against any limit states that are closely related to web buckling, e.g., possibly the fatigue strength of curved girder web panels.

Table 8.2.3. Influence of L_b/R on elastic shear buckling strengths, doubly-symmetric specimens.

	$V_{cr(FEA)}/V_p$ ($L_b/R = 0.05$) (35 girders)	$V_{cr(FEA)}/V_p$ ($L_b/R = 0.075$) (45 girders)	$V_{cr(FEA)}/V_p$ ($L_b/R = 0.1$) (42 girders)
Avg.	0.40	0.45	0.48
Std. Dev.	0.13	0.15	0.15
High	0.76	0.78	0.82
Low	0.28	0.28	0.31

8.3 POSTBUCKLING STRENGTH

For the girders in which the web buckles elastically, i.e., for $V_{cr} < 0.8V_p$, an accurate estimate of the web postbuckling strength may be calculated as the difference between the ultimate shear capacity, determined from full nonlinear finite element analysis $V_{n(FEA)}$, and the elastic buckling strengths obtained from the finite element elastic linear buckling (eigenvalue) analysis $V_{cr(FEA)}$. That is,

$$V_{PB(FEA)} = V_{n(FEA)} - V_{cr(FEA)} \tag{8-1}$$

In Figure 8.3.1, these strengths are normalized by the theoretical upper bound of the postbuckling strength ($V_p - V_{cr(FEA)}$) and plotted as a function of d_o/D for the girders considered in this study with $D/b_f = 2.75$ and $D/t_w = 160$. This figure also compares these normalized "exact" postbuckling strengths to similar normalized postbuckling strengths obtained from the AASHTO (2001), modified AASHTO and Lee and Yoo (1998) predictor equations. The finite element based postbuckling strengths are connected by the dashed lines in the figure, while the normalized postbuckling strengths obtained from the design predictor equations are connected by the solid lines.

In the current and modified AASHTO equations, the postbuckling strength may be written as

$$V_{PB} = V_p \frac{0.87(1-C)}{\sqrt{1+\left(\frac{d_o}{D}\right)^2}} \tag{8-2}$$

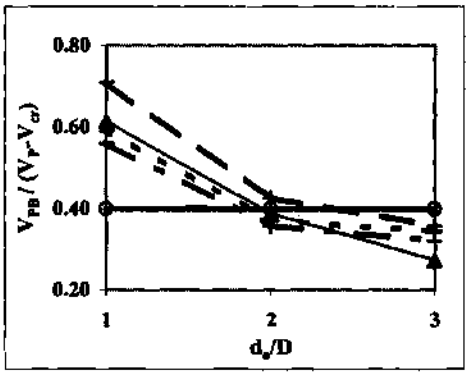

(a) $L_b/R = 0.05$ and $f_f/f_b = 0.35$

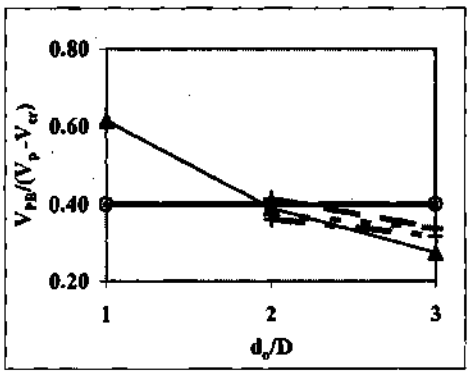

(d) $L_b/R = 0.05$ and $f_f/f_b = 0.50$

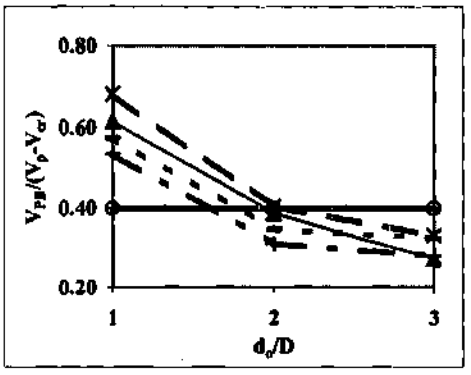

(b) $L_b/R = 0.075$ and $f_f/f_b = 0.35$

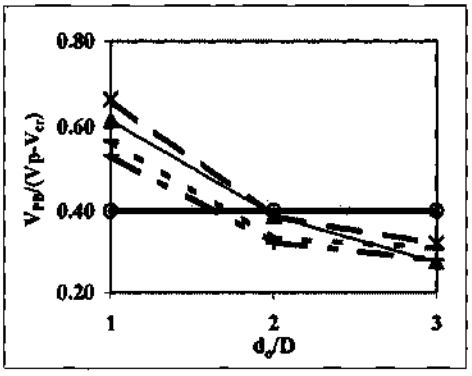

(e) $L_b/R = 0.075$ and $f_f/f_b = 0.50$

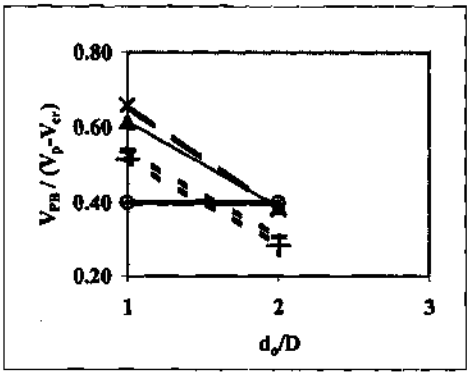

(c) $L_b/R = 0.10$ and $f_f/f_b = 0.35$

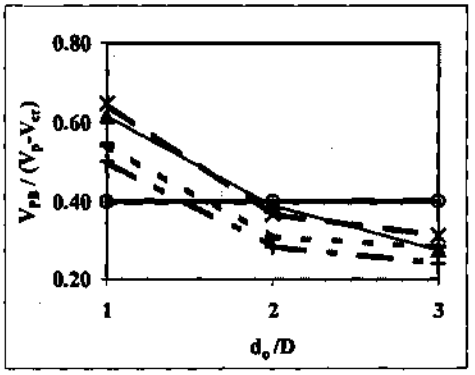

(f) $L_b/R = 0.10$ and $f_f/f_b = 0.50$

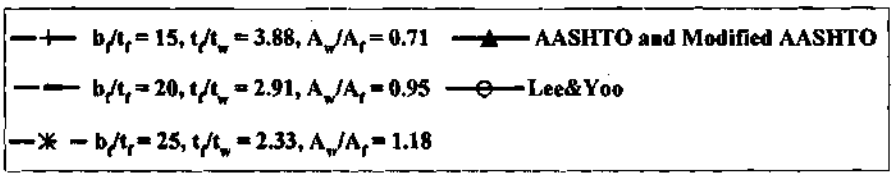

Figure 8.3.1. $V_{PB}/(V_p - V_{cr})$ based on finite element analysis and design predictor equations versus d_o/D – doubly-symmetric specimens with constant $D/b_f = 2.75$ and $D/t_w = 160$ and different t_f/t_w and b_f/t_f.

based on Basler's (1961b) tension-field theory, where $C = V_{cr}/V_p$ and V_{cr} is the web shear buckling strength obtained using the respective AASHTO (2001) and Lee et al. (1996) shear buckling coefficients. Therefore, when normalized in the above fashion, this postbuckling strength becomes

$$\frac{V_{PB}}{(V_p - V_{cr})} = \frac{0.87}{\sqrt{1+\left(\frac{d_o}{D}\right)^2}} \tag{8-3}$$

The normalized postbuckling strength assumed within the Lee and Yoo (1998) equations (see Section 2.2.3 and Eq. (2-107)) may be written as

$$\frac{V_{PB}}{(V_p - V_{cr})} = 0.4 \tag{8-4a}$$

prior to adjustment by the reduction coefficient R, which accounts for geometric imperfection and web plate bending effects. Since R is applied to both the buckling and postbuckling contributions to the strength in Eq. (2-110), the normalized *reduced* postbuckling strength by Lee and Yoo's equations may be written as

$$\frac{RV_{PB}}{(V_p - RV_{cr})} \tag{8-4b}$$

which varies as a function of D/t_w, d_o/D and t_f/t_w. Generally, R is smaller for smaller values of d_o/D, and therefore Eq. (8-4b) tends to give a ratio that increases as d_o/D increases. Therefore, only Eq. (8-4a) is considered in the figure.

It can be observed from Fig. 8.3.1 that the above "exact" normalized postbuckling strengths decrease significantly as d_o/D increases. This decrease is most pronounced when d_o/D is changed from one to two, but the decrease in strength from $d_o/D = 2$ to $d_o/D = 3$ is nonnegligible. This trend is expected since, by increasing the stiffener spacing, the tension field becomes less and less effective and approaches zero as the panel length becomes large according to Basler's (1961b) theory. Also, this trend is clearly evident within the data from various experimental studies, e.g., (Basler 1961b; Lee and Yoo 1999a; Porter et al. 1975).

The normalized current and modified AASHTO postbuckling strengths as shown in Fig. 8.3.1 are reasonably good predictions of the corresponding finite element based values. However, the Lee and Yoo (1998) assumption of constant normalized postbuckling shear strength (Eq. 8-4a) (or a postbuckling strength that decreases with increasing d_o/D if Eq. (8-4b) is utilized) is clearly flawed. This flaw is the primary cause of the inaccuracies in Lee and Yoo's ultimate shear strength predictions reported in Section 8.1.

It can be argued that the results in Fig. 8.3.1 are somewhat skewed by the fact that different values of V_{cr} are utilized in normalizing the finite element based curves, the current AASHTO LRFD (2001) based curves, and the modified AASHTO and Lee and Yoo (1998) based curves. Therefore, Fig. 8.3.2 is provided, in which all the above calculated postbuckling shear strengths are normalized by the same parameter V_p. The average strengths for the three girder cross-sections considered in Figs. 8.3.1 and 8.3.2 are plotted in Fig. 8.3.2 for the Lee and Yoo and modified AASHTO equations; the differences in the design postbuckling strengths obtained for these different cross-section geometries is less than 0.01 V_p. The unreduced postbuckling strength from Eq. (2-107), i.e., $V_{PB} = 0.4(V_p - V_{cr})$, is plotted for Lee and Yoo's equations; the increase in the predicted strength with increasing d_o/D is even larger if the postbuckling strength by Lee and Yoo's equations is taken as $(V_n - V_{cr})$. The finite element and modified AASHTO postbuckling strengths are taken as $V_{PB} = (V_n - V_{cr})$.

As in Fig. 8.3.1, dashed lines connect the finite element based results while solid lines connect the design predictor equation results in Fig. 8.3.2. One can observe from this figure that Lee and Yoo's equations predict an increase in the web postbuckling strength as d_o/D is increased. Conversely, the finite element based solutions all show a decrease in this strength as a function of increasing panel aspect ratio, although the change from $d_o/D = 2$ to $d_o/D = 3$ is relatively small.

Lee and Yoo's postbuckling strength equation tends to underestimate the finite element based strength for small d_o/D, it provides a reasonably good prediction of these "exact" strengths for $d_o/D = 2$, and it tends to overestimate the finite element solutions for $d_o/D = 3$. The modified AASHTO calculations provide the best estimate of the shear postbuckling strength, although they are slightly high compared to many of the values determined directly from the finite element solutions. The postbuckling strengths estimated by the current AASHTO formulas are slightly higher than the modified AASHTO strengths. This is due to the fact that the AASHTO shear buckling formulas tend to significantly underestimate the web shear buckling capacity.

One can observe from Fig. 8.3.2 that at $d_o/D = 3$, the finite element based postbuckling strengths range from 0.16 to 0.24V_p for the girders studied here. That is, there is still significant postbuckling strength exhibited by the curved web panels even at this upper limit on d_o/D beyond which the straight-girder specification (AASHTO 2001) does not allow the calculation of a postbuckling contribution to the resistance. The $V_{PB(FEA)}/V_p$ values for $d_o/D = 2$ are somewhat larger, but are more dispersed (0.18 to 0.28), whereas the $V_{PB(FEA)}/V_p$ values for $d_o/D = 1$ have the widest range (0.27 to 0.40). The dispersion in the $V_{PB(FEA)}/V_p$ values for $d_o/D = 1$ and 2 is due in large part to the horizontal curvature. There is a reduction in most of the $V_{PB(FEA)}/V_p$ values with increasing L_b/R in the figure (compare Figs. 8.3.2(c) and (f) to Figs. 8.3.2(b) and (e) and to Figs. 8.3.2(a) and (d)).

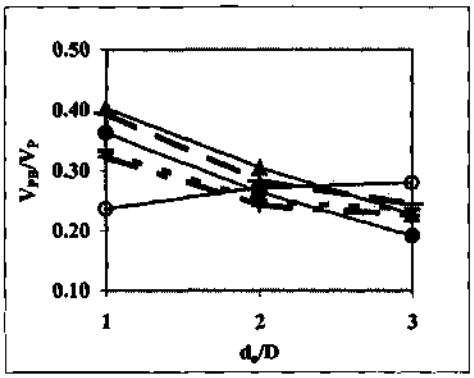

(a) $L_b/R = 0.05$ and $f_f/f_b = 0.35$

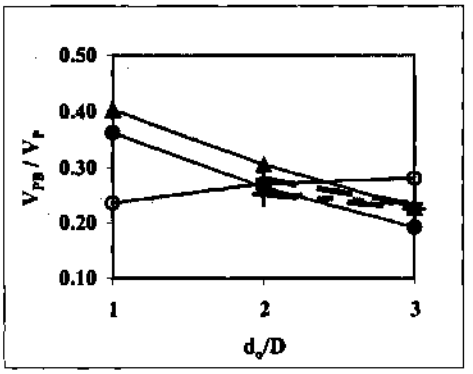

(d) $L_b/R = 0.05$ and $f_f/f_b = 0.50$

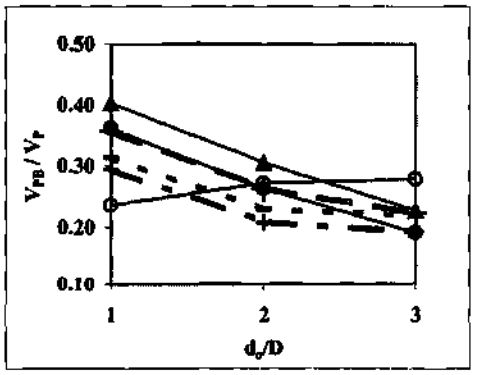

(b) $L_b/R = 0.075$ and $f_f/f_b = 0.35$

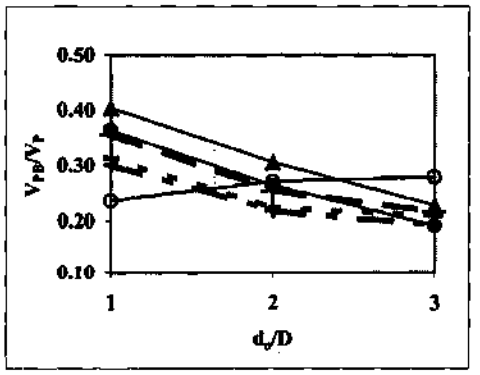

(e) $L_b/R = 0.075$ and $f_f/f_b = 0.50$

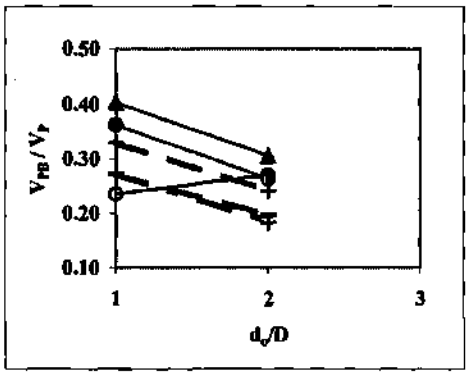

(c) $L_b/R = 0.10$ and $f_f/f_b = 0.35$

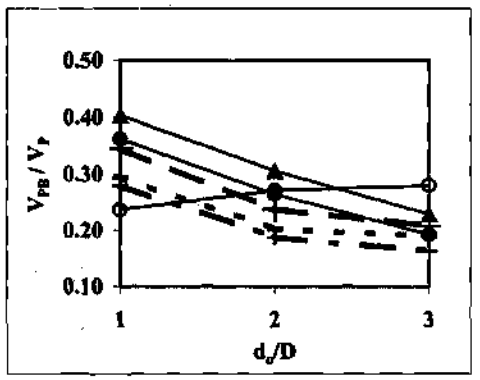

(f) $L_b/R = 0.10$ and $f_f/f_b = 0.50$

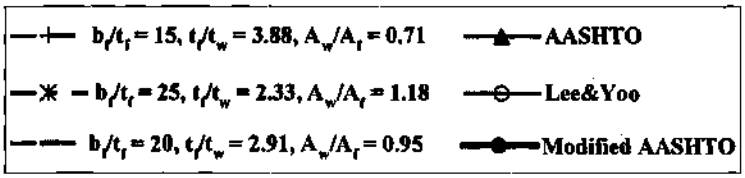

Figure 8.3.2. V_{PB}/V_p based on finite element analysis and average results from design predictor equations versus d_o/D – doubly-symmetric specimens with constant $D/b_f = 2.75$ and $D/t_w = 160$ and different t_f/t_w and b_f/t_f.

8.4 ASSESSMENT OF SHEAR STRENGTH EQUATIONS

Based on the data presented in Section 8.1 through 8.3, the modified AASHTO shear strength equations, which are based on Basler's (1961b) tension-field theory combined with the web shear-buckling coefficients developed by Lee et al. (1996), clearly provide the most accurate characterization of the web shear capacity of the three design strength predictors that have been studied. Aydemir (2000) also reaches this conclusion in his studies of straight hybrid I girders. The largest unconservative error in the modified AASHTO shear strength predictions in the current study is 16 percent (see Tables 8.1.1 and 8.1.3), whereas the current AASHTO LRFD (2001) shear strength equations exhibit a maximum unconservative error of nine percent for the girders studied here. Aydemir (2000) obtains a maximum unconservative error in the modified AASHTO shear strength predictions of 11 percent, while he obtains a maximum unconservative error of seven percent with the current AAHSTO LRFD (2001) equations. The larger percentage errors obtained in the current study are believed to be due largely to the effects of horizontal curvature and lateral flange bending.

Based on the accurate predictions of the finite element based shear strengths provided by the modified AASHTO formulas, as well as accurate predictions of experimental shear strengths from various studies, one can conclude that the modified AASHTO equations would be preferred over the current AASHTO LRFD (2001) equations. The distribution in the predicted shear capacities relative to the finite element based strengths and/or experimentally determined shear strengths, and the unconservative nature of the predictions by these equations for certain cases, can be addressed in the development of design load and resistance factors (as is the case in the development of the resistance factor of $\phi = 1.0$ with the current AASHTO LRFD (2001) shear strengths). Based on a preliminary assessment of the overall shear strength statistics for the modified AASHTO equations versus the finite element based shear strengths, Nowak (2000) obtains a ϕ of 0.95.

As noted in Section 2.2.4, the increase in the predicted shear capacity associated with the use of the Lee et al. (1996) shear buckling coefficients is a maximum of only six percent for $d_o/D = 1$ and D/t_w from 100 to 160. However, the increase in the nominal maximum shear strengths ranges from 33 percent for $D/t_w = 100$ to 19 percent for $D/t_w = 160$ when d_o/D is equal to three. Therefore, the modified AASHTO shear strength equations, with the shear buckling coefficients developed by Lee et al. (1996), provide substantial additional design capacity for large panel aspect ratios. It should be noted that the largest errors in the modified AASHTO equations occur for girders with low to intermediate values of D/t_w (100 and 130), and with low to intermediate values of d_o/D (one and two).

It is apparent from the present parametric studies and from the results of experimental tests (Zureick et al. 2001) that the straight-girder based AASHTO and/or modified AASHTO shear strength equations are adequate for webs of curved I girders with $L_b/R \leq 0.10$ for d_o/D values up three. Therefore, it is recommended that the AASHTO LRFD

(2001) limit of $d_o/D \leq 3$ can be extended to curved I girders within the limits of $L_b/R \leq 0.10$ for characterization of the maximum strength.

Although the modified AASHTO equations provide improved accuracy relative to the current AASHTO LRFD (2001) formulas, there is one issue that still needs to be addressed before these equations can be recommended for universal application within the AASHTO Specifications. As noted in Section 2.2.5, the current AASHTO LRFD (2001) straight-girder Specifications prevent web buckling under fatigue loading conditions in order to avoid fatigue issues. These provisions are based on the current AASHTO shear buckling coefficients, which are in turn based on the assumption of simply-supported boundary conditions at the flanges. Therefore, the impact of the more accurate but more liberal calculation of the web buckling loads on the fatigue performance of I girder webs would need to be investigated before the more accurate shear buckling coefficients could be introduced in this part of the specifications.

Also, it might be questioned whether the additional accuracy obtained for high d_o/D values is sufficient to merit the longer more involved combination of equations required for evaluation of the shear buckling coefficient in the approach recommended by Lee et al. (1996) (compare Eqs. (2-103) through (2-106) to Eqs. (2-96a and b)). In the view of the authors, the more accurate shear buckling coefficient equations are merited. Design strength checks are often automated within software at the present time, and the simpler but more approximate current formulas for the shear buckling coefficient can still be retained for manual calculation. The simpler equations might be moved to the commentary of the specifications.

CHAPTER IX

PARAMETRIC STUDY RESULTS – HIGH-MOMENT HIGH-SHEAR

This chapter presents the parametric study results for the high-shear high-moment tests of the primary (Section 5.3) and unsymmetrical (Section 5.13) girder suites. The data from these tests, as well as that from the uniform vertical bending ($\alpha = -1$) and maximum V/M ($\alpha = 1/3$) studies of Chapters VII and VIII, are presented within normalized moment-shear (M/M_n versus V/V_n) strength interaction plots. The moments M and shears V in these ratios are the values associated with the maximum strength predicted by full nonlinear finite element analysis. The value M is the maximum moment within the critical panel of the test unsupported length. The importance of calculating the moment in this manner is discussed in Sections 1.1 and 2.3.2. The value V is the constant shear within the test length. Two different calculations are utilized for the flexural capacity M_n in plotting normalized M/M_n values in this chapter:

- The uniform vertical bending capacity obtained from full nonlinear finite element analysis, $M_{n(FEA)}$, and

- The flexural capacity determined based on the proposed one-third rule, $M_{n(1/3\ rule)}$ (see Section 2.1.9).

Three different calculations are utilized for the shear strength V_n in plotting normalized V/V_n values:

- The shear capacity obtained from full nonlinear finite element analysis of the maximum V/M tests, $V_{n(FEA)}$,

- The AASHTO LRFD (2001) shear strength equations, including tension field action, $V_{n(AASHTO)}$ (see Section 2.2.2), and

- The modified AASHTO shear strength formulas obtained by use of the equations proposed by Lee et al. (1996) for the shear buckling coefficient (see Section 2.2.4).

As noted in Section 2.3.3, the flexural capacity within the one-third rule, $M_{n(1/3\ rule)}$, depends on the flange elastic lateral bending stress f_ℓ. Also as noted previously, although f_ℓ is calculated using geometric nonlinear shell finite element models in the previous chapters, it is calculated in this chapter by use of a first-order, open-walled section curved beam finite element. This beam model is utilized to determine the maximum ratio of f_ℓ/f_b within the test segment, which is a constant for all load levels in each test (since the

analysis is first order). This ratio is then substituted into Eqs. (2-90), and these equations are solved for the single unknown f_b corresponding to the nominal vertical bending strength. The nominal moment capacity $M_{n(1/3\ rule)}$ is then obtained by multiplying this f_b by the elastic section modulus. Example flexural capacity calculations are provided in Section 4.5.1. Details regarding the beam finite element analysis calculations are discussed in Sections 3.1 and 3.6.

By use of a first-order open-walled section beam analysis for calculation of f_ℓ/f_b, the implications of neglecting second-order amplification and web distortion effects in the context of the proposed one-third rule are highlighted. The elastic lateral bending stresses based on first-order beam theory tend to be somewhat smaller than those associated with the second-order shell finite element solutions, and therefore the capacities predicted by the recommended resistance equations are somewhat larger and the corresponding ratios $M/M_{n(1/3\ rule)}$ are somewhat smaller.

Section 9.1 focuses on the results for the doubly symmetric girders, with M_n and V_n taken as either $M_{n(FEA)}$ and $V_{n(FEA)}$ or $M_{n(1/3\ rule)}$ and $V_{n(AASHTO)}$. Section 9.2 then presents the results for the unsymmetrical girder suite within this same context. Subsequently, Section 9.3 addresses the implications of using $V_{n(modified\ AASHTO)}$ on the normalized moment-shear strength interaction behavior. Section 9.4 summarizes the results and poses recommendations. The reader is referred to Appendix C for a complete listing of data values.

9.1 DOUBLY SYMMETRIC SPECIMENS

Two normalized moment-shear interaction plots are presented for each combination of L_b/R and target f_ℓ/f_b in Figs. 9.1.1 through 9.1.12. One plot presents the data normalized by the finite element based uniform vertical bending and maximum V/M test capacities $M_{n(FEA)}$ and $V_{n(FEA)}$, and the other plot gives the data normalized by the one-third rule and current AASHTO LRFD (2001) moment and shear strengths, $M_{n(1/3\ rule)}$ and $V_{n(AASHTO)}$. The border of the safe design region, assuming negligible moment-shear strength interaction, is indicated by a thick solid line in the plots.

As noted above, the moments M and the shears V within all the strength ratios considered here are the values associated with the maximum strength predicted by full nonlinear finite element analysis. Therefore, in the $M/M_{n(FEA)}$ versus $V/V_{n(FEA)}$ plots, $M/M_{n(FEA)}$ is equal to one for all the data points corresponding to uniform vertical bending, and $V/V_{n(FEA)} = 1$ for all the data points corresponding to the maximum V/M tests (see Figs. 9.1.1, 9.1.3, 9.1.5, 9.1.7, 9.1.9 and 9.1.11). The abscissa for the maximum V/M test data points in these plots tends to be smaller than one for most of the girders, since with the maximum V/M loading ($\alpha = 1/3$), an inflection point exists at the middle of the test length and the girders tend to fail in shear (see Figs. 5.3.1 through 5.3.3). It can be observed that the value of $M/M_{n(FEA)}$ for these points ranges from 0.46 to 1.38 in Fig. 9.1.1 ($L_b/R = 0.05$), 0.35 to 1.07 in Fig. 9.1.3 ($L_b/R = 0.075$) and 0.26 to 0.81 in Fig. 9.1.5 ($L_b/R = 0.10$), corresponding to girders with target $f_\ell/f_b = 0.35$ in the uniform vertical bending load case. It ranges from 0.74 to 1.51 in Fig. 9.1.7 ($L_b/R = 0.05$), 0.46 to

1.43 in Fig. 9.1.9 ($L_b/R = 0.075$) and 0.34 to 1.10 in Fig. 9.1.11 ($L_b/R = 0.10$), corresponding to girders with target $f_\ell/f_b = 0.50$ in the uniform vertical bending load case. That is, $M/M_{n(FEA)}$ for the maximum V/M test data points tends to be greater for smaller L_b/R and larger target f_ℓ/f_b. This is mainly due to the fact that the girders with smaller L_b/R and larger target f_ℓ/f_b have longer unsupported lengths L_b. One can observe that in several of the plots, the $M/M_{n(FEA)}$ values for a number of the maximum V/M tests are larger than the corresponding values for the high-shear high-moment tests (see Figs 9.1.1 and 9.1.7). In Fig. 9.1.7, it can be seen that eleven of the maximum V/M tests with large $M/M_{n(FEA)}$ actually fail by lateral bending. These eleven shear tests have been discussed previously in Sections 8.1.1 and 8.2.

The data points ($M/M_{n(FEA)}$, $V/V_{n(FEA)}$) for the high-shear high-moment loading case all fall approximately along the radial line $(M/M_{n(FEA)}) / (V/V_{n(FEA)}) = 0.8$ as per the design of these studies (see Section 5.3). Some of these points deviate slightly from the above radial line due to rounding of the load parameter α to two significant digits. A few data points that are labeled as high-shear high-moment deviate significantly from this radial line (see Fig. 9.1.1 and 9.1.11). These cases correspond to data errors in setting the value of α for the high-moment high-shear case, and are retained in the plots as extra data points.

Figures 9.1.1, 9.1.3, 9.1.5, 9.1.7, 9.1.9 and 9.1.11 show that in all of the cases involving high-shear high-moment loading or in which the maximum V/M tests fail by lateral bending, the moments developed at the ends of the critical test segment are larger than the corresponding moment capacities in uniform vertical bending $M_{n(FEA)}$. The ability of the girders to develop larger vertical bending moments in these cases is due to:

- The occurrence of the maximum vertical and flange lateral bending moments at one or both brace locations, where the girder is restrained from radial displacements,

- Smaller flange maximum lateral bending moments and f_ℓ/f_b values than in the uniform vertical bending load cases, and

- Rapid decrease in the vertical bending moment as we move away from the braced maximum moment location(s).

The above-mentioned figures give a picture of the "true" moment-shear-lateral bending interaction. However, it is important to recognize that the one-third rule is designed to account for the effect of lateral bending on the vertical bending strength. Also, all the different design strength predictors for M_n and V_n have inaccuracies associated with their idealizations of the true strength behavior. Therefore, for practical design purposes, it is more useful to consider plots of $M/M_{n(1/3\ rule)}$ versus $V/V_{n(AASHTO)}$. These are shown in Figs. 9.1.2, 9.1.4, 9.1.6, 9.1.8, 9.1.10 and 9.1.12. It should be noted that the $V/V_{n(AASHTO)}$ values in the plots are the inverse of the AASHTO (2001) shear strength ratios evaluated in Chapter IX. Also, the $M/M_{n(1/3\ rule)}$ values here are similar in

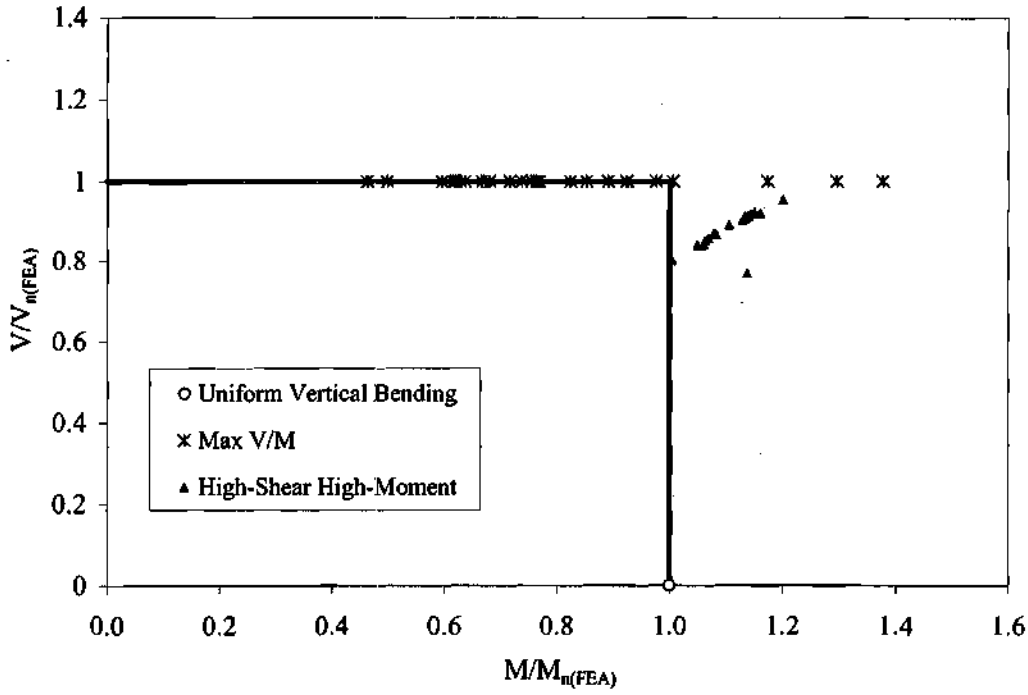

Figure 9.1.1. Moment-shear interaction, normalized by $M_{n(FEA)}$ and $V_{n(FEA)}$, for specimens with $L_b/R = 0.05$ and target $f_\ell/f_b = 0.35$.

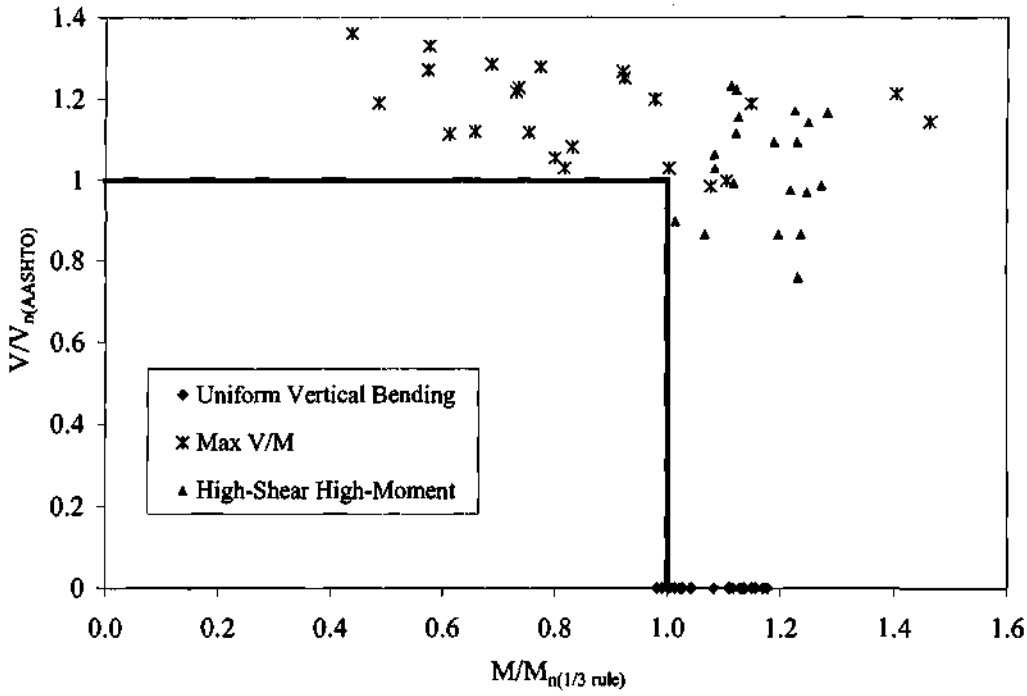

Figure 9.1.2. Moment-shear interaction, normalized by $M_{n(1/3\ rule)}$ and $V_{n(AASHTO)}$, for specimens with $L_b/R = 0.05$ and target $f_\ell/f_b = 0.35$.

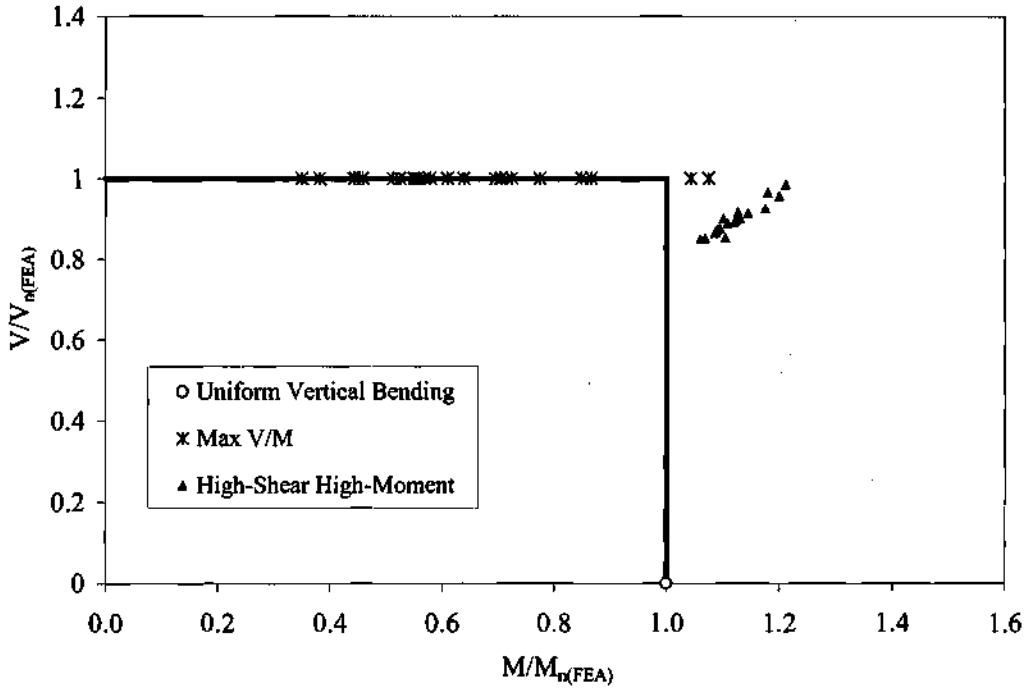

Figure 9.1.3. Moment-shear interaction, normalized by $M_{n(FEA)}$ and $V_{n(FEA)}$, for specimens with $L_b/R = 0.075$ and target $f_t/f_b = 0.35$.

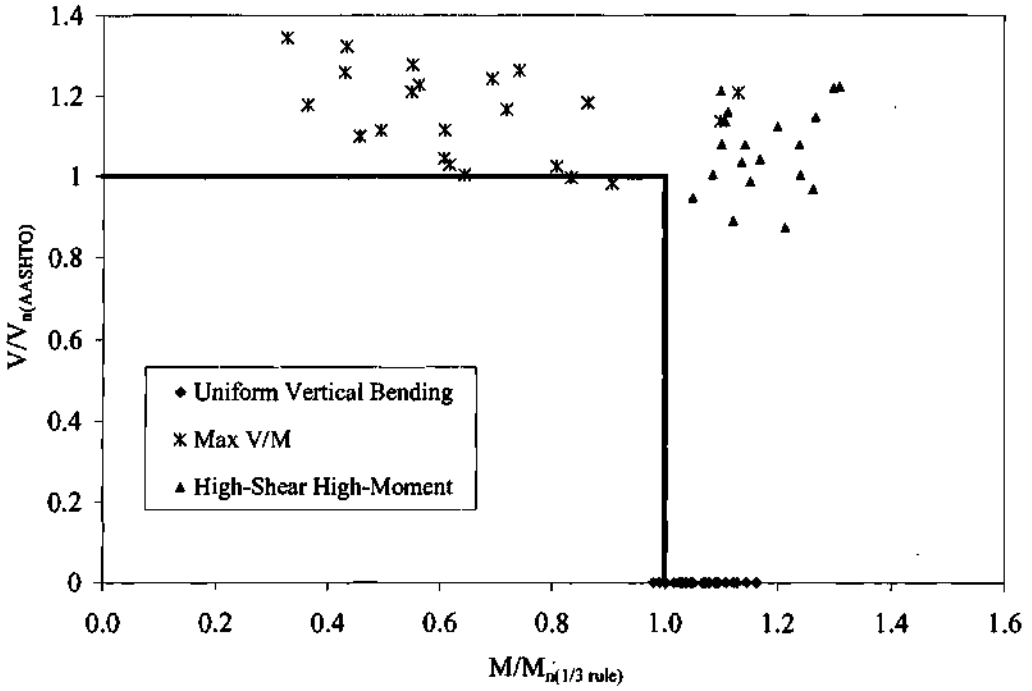

Figure 9.1.4. Moment-shear interaction, normalized by $M_{n(1/3\ rule)}$ and $V_{n(AASHTO)}$, for specimens with $L_b/R = 0.075$ and target $f_t/f_b = 0.35$.

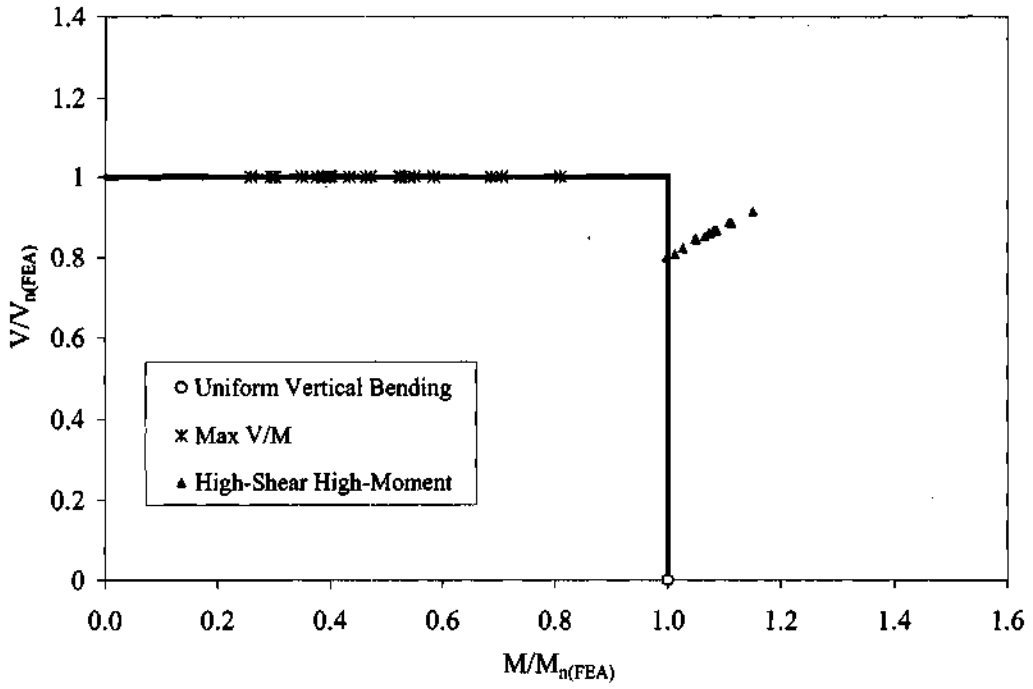

Figure 9.1.5. Moment-shear interaction, normalized by $M_{n(FEA)}$ and $V_{n(FEA)}$, for specimens with $L_b/R = 0.1$ and target $f_t/f_b = 0.35$.

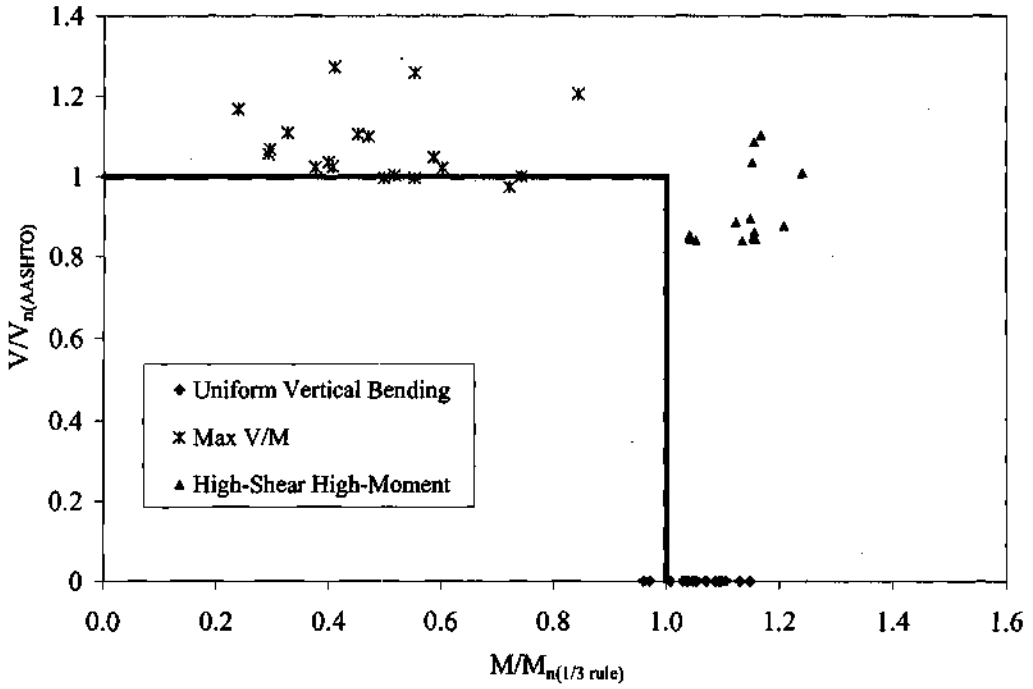

Figure 9.1.6. Moment-shear interaction, normalized by $M_{n(1/3\ rule)}$ and $V_{n(AASHTO)}$, for specimens with $L_b/R = 0.1$ and target $f_t/f_b = 0.35$.

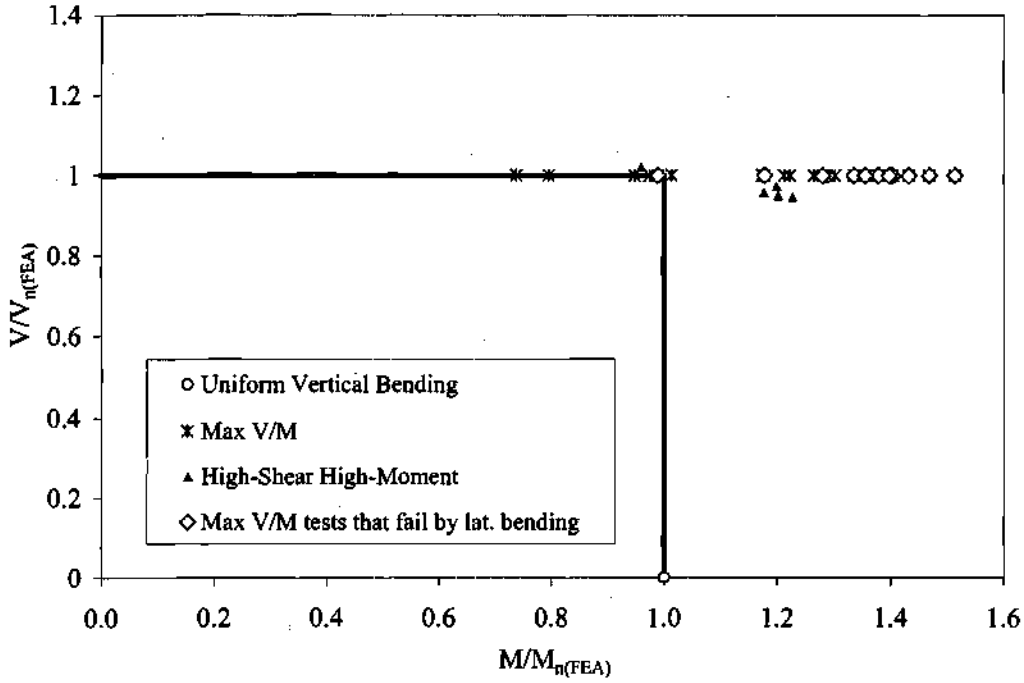

Figure 9.1.7. Moment-shear interaction, normalized by $M_{n(FEA)}$ and $V_{n(FEA)}$, for specimens with $L_b/R = 0.05$ and target $f_t/f_b = 0.50$.

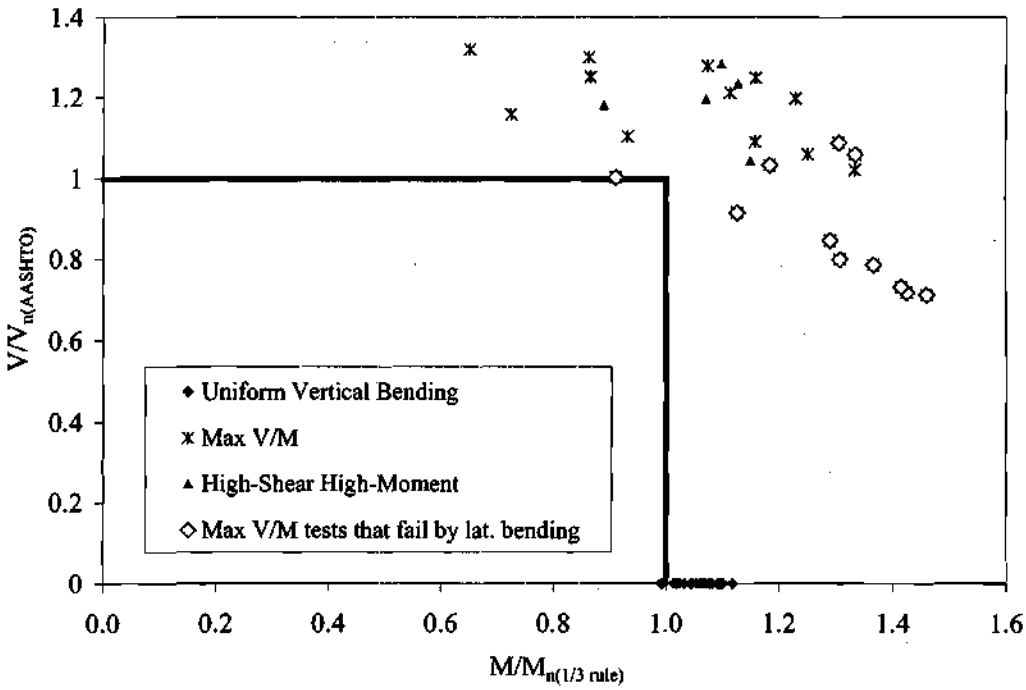

Figure 9.1.8. Moment-shear interaction, normalized by $M_{n(1/3\ rule)}$ and $V_{n(AASHTO)}$, for specimens with $L_b/R = 0.05$ and target $f_t/f_b = 0.50$.

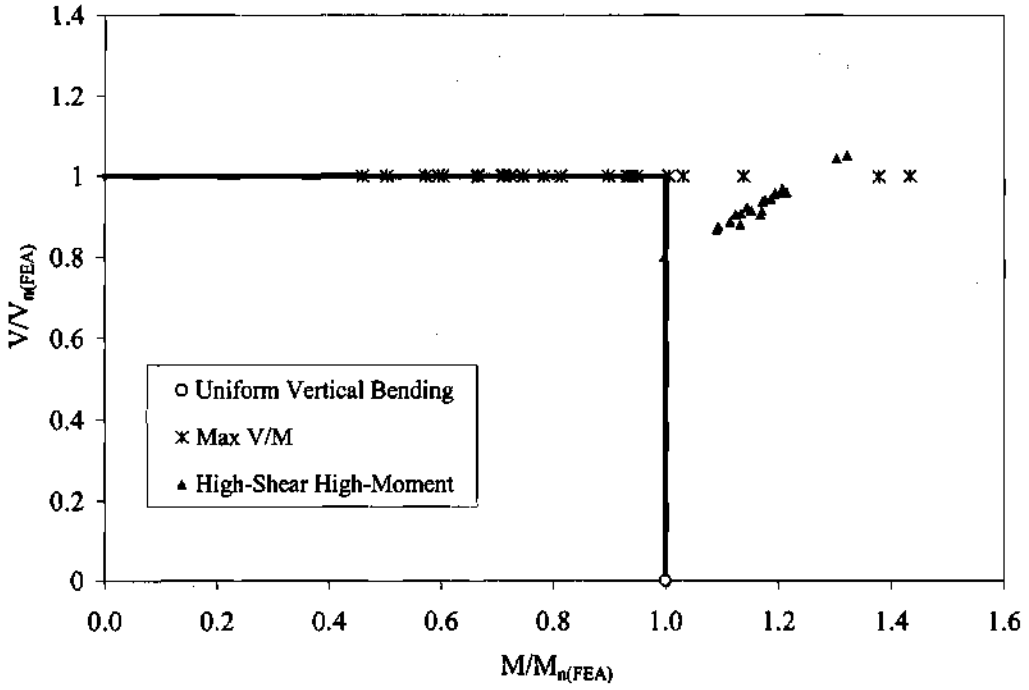

Figure 9.1.9. Moment-shear interaction, normalized by $M_{n(FEA)}$ and $V_{n(FEA)}$, for specimens with $L_b/R = 0.075$ and target $f_e/f_b = 0.50$.

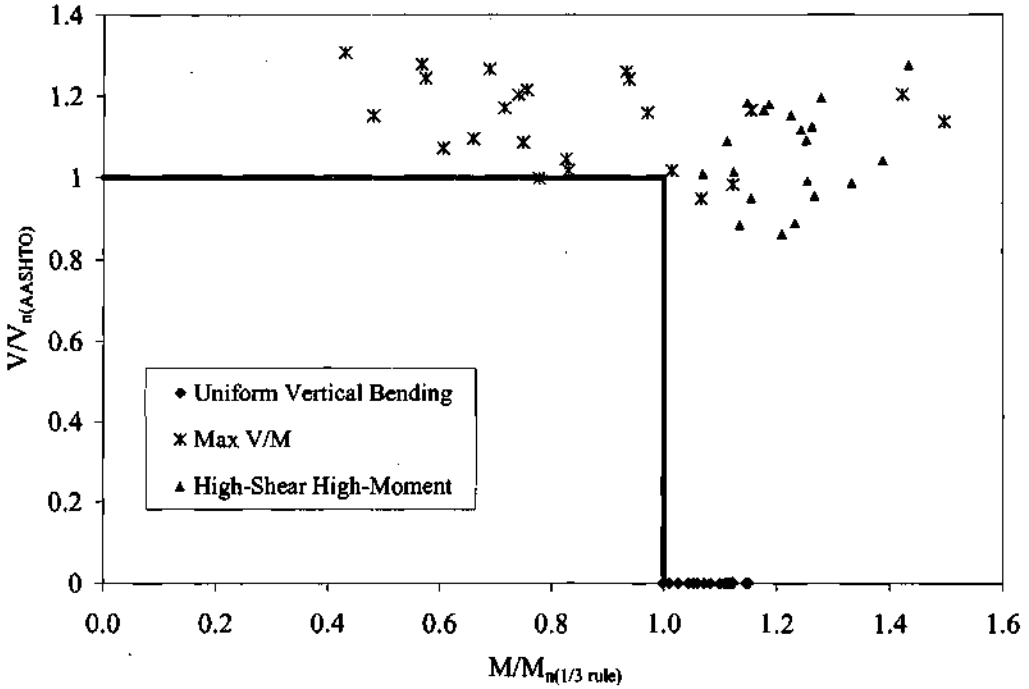

Figure 9.1.10. Moment-shear interaction, normalized by $M_{n(1/3\ rule)}$ and $V_{n(AASHTO)}$, for specimens with $L_b/R = 0.075$ and target $f_e/f_b = 0.50$.

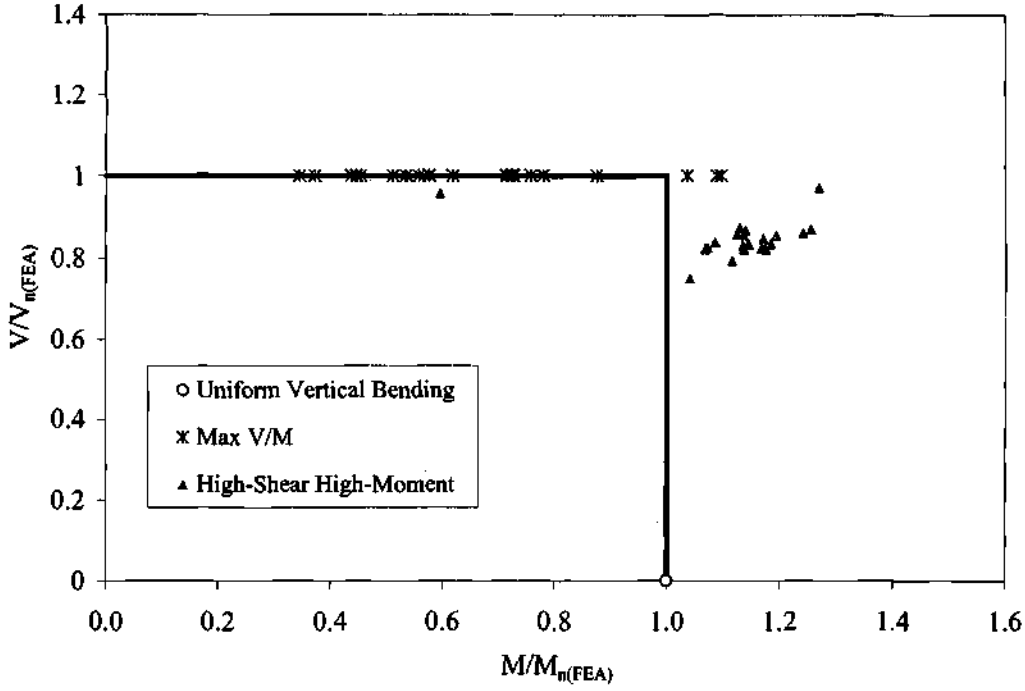

Figure 9.1.11. Moment-shear interaction, normalized by $M_{n(FEA)}$ and $V_{n(FEA)}$, for specimens with $L_b/R = 0.1$ and target $f_\ell/f_b = 0.50$.

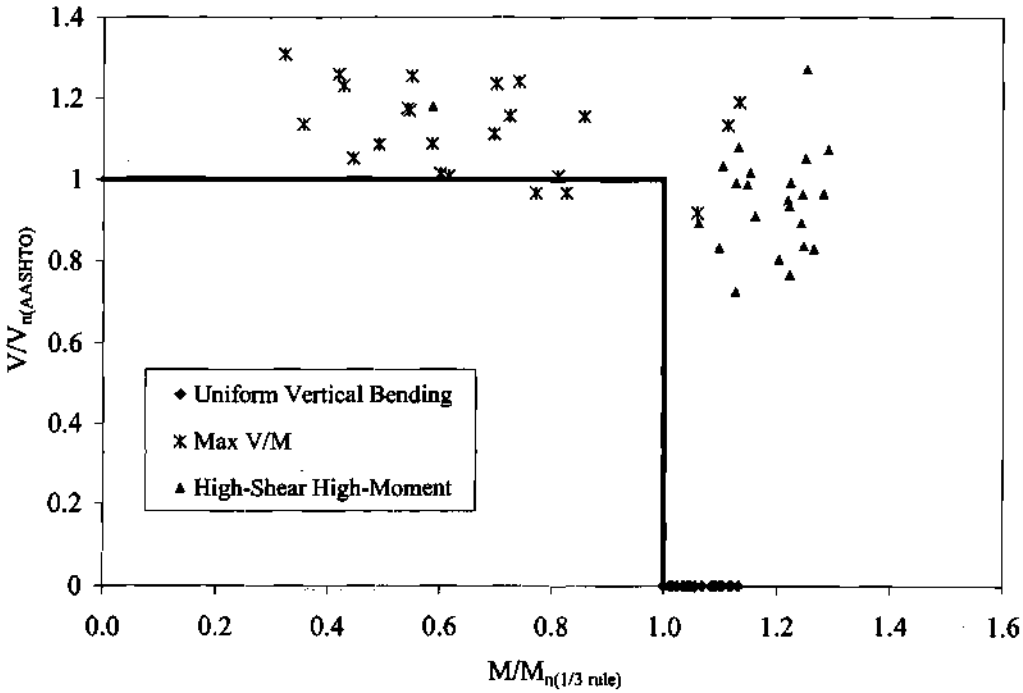

Figure 9.1.12. Moment-shear interaction, normalized by $M_{n(1/3\ rule)}$ and $V_{n(AASHTO)}$, for specimens with $L_b/R = 0.1$ and target $f_\ell/f_b = 0.50$.

magnitude but typically slightly smaller than the inverse of the one-third rule capacity ratios evaluated in Chapter VIII. Example calculations of $M_{n(1/3\ rule)}$ are provided in Section 4.5.1. An example calculation of $V_{n(AASHTO)}$ is provided in Section 4.5.2.

Figure 9.1.13 shows a summary plot of all the data from Figs. 9.1.2, 9.1.4, 9.1.6, 9.1.8, 9.1.10 and 9.1.12. It can be seen that there is no evidence of any significant moment-shear interaction in any of these plots. All the data points for the high-shear high-moment tests fall outside of the dark lines, indicating a safe or conservative prediction of the strength. A few of the maximum V/M test data points fall slightly inside of the dark lines, but the unconservative errors for these data points are generally smaller than the largest unconservative errors in the AASHTO (2001) equations based on the shear capacity tests from Basler's (1961b) research and from Aydemir's (2000) studies.

Figure 9.1.14 shows the data points from Fig. 9.1.13, but with the data normalized by the plastic vertical bending capacity M_p and the web plastic shear capacity V_p (Eq. 2-95d). The shear strengths in this plot fall predominantly in two clusters. The girders with $D/t_w = 100$ and with $D/t_w = 160$ but with $d_o/D = 1$ have finite element based shear strengths in the vicinity of 80 percent of V_p, and the other girders have shear strengths in the vicinity of 60 percent of V_p. The uniform vertical bending capacities are all significantly smaller than M_p, due to the nature of the cross-section geometries and due to flange lateral bending. As in the previous plots, the larger moments at the maximum load level in the high-shear high-moment tests, and in the maximum V/M tests with large unsupported lengths, is apparent. The reader is referred to Appendix C for a tabular presentation of the data and discussion of additional details of the moment-shear interaction parametric studies. Moment-shear interaction plots in which the data is grouped by the cross-section profile are also presented in Appendix C.

It is evident that the beneficial M-V strength interaction for the girders studied in this research is more related to the interaction between the vertical and lateral bending strength of the compression flange, along with the boundary conditions at the location of the failure and the rapid decrease in the magnitude of the vertical and flange lateral moments as we move away from the critical section, than interaction between the girder vertical bending and web shear strengths. Obviously, the same cannot be said for a straight I-girder. The reader is referred to Aydemir (2000) for parametric study results pertaining to M-V interaction in straight hybrid and homogeneous I girders.

Aydemir (2000) studies a number of straight girders with slender webs, values of $2A_w/(A_{fc}+A_{ft})$ up to 2.4 and b_f/t_f values up to 8.75. As discussed in Sections 1.1 and 2.3.2, based on Aydemir's data, one can conclude that M-V interaction can also be neglected in straight homogeneous and hybrid I girders up to $2A_w/(A_{fc} + A_{ft}) = 2.4$. However, as noted in Section 2.3.2, Aydemir (2000) considered residual stress effects in only a few of his analyses pertaining to M-V interaction. Further finite element studies are needed to consider the effect of residual stresses on the M-V interaction behavior of straight girders for a wide range of girder geometries, and further experimental tests are needed to confirm the finite element predictions. As noted in Section 1.1, a number of

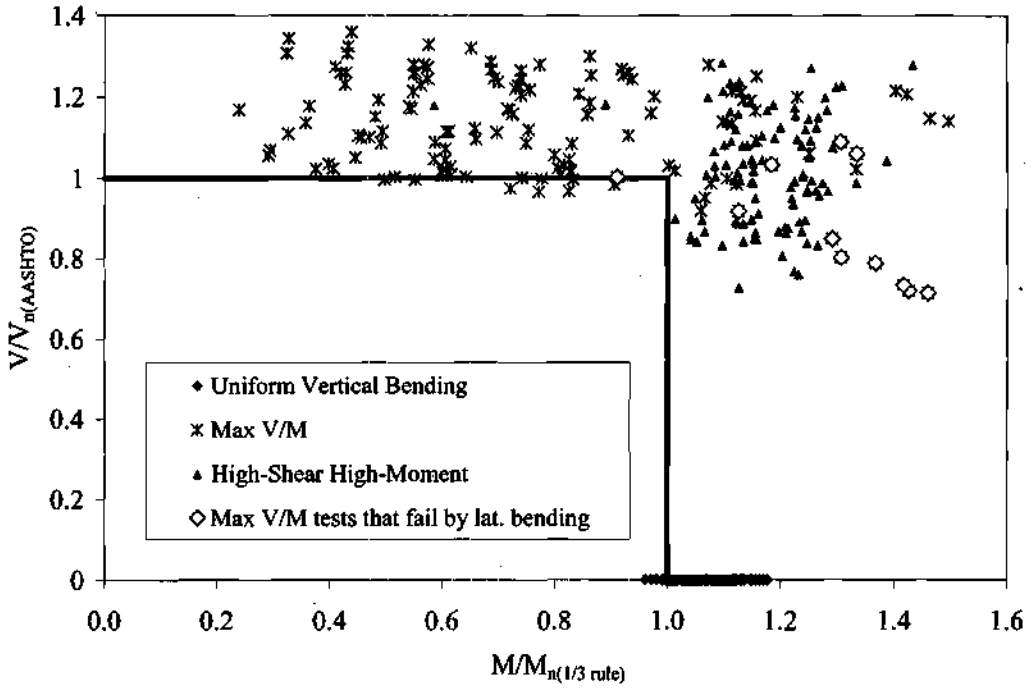

Figure 9.1.13. Summary of moment-shear strength interaction results, normalized by $M_{n(1/3\ rule)}$ and $V_{n(AASHTO)}$, for all the primary test suite parametric studies.

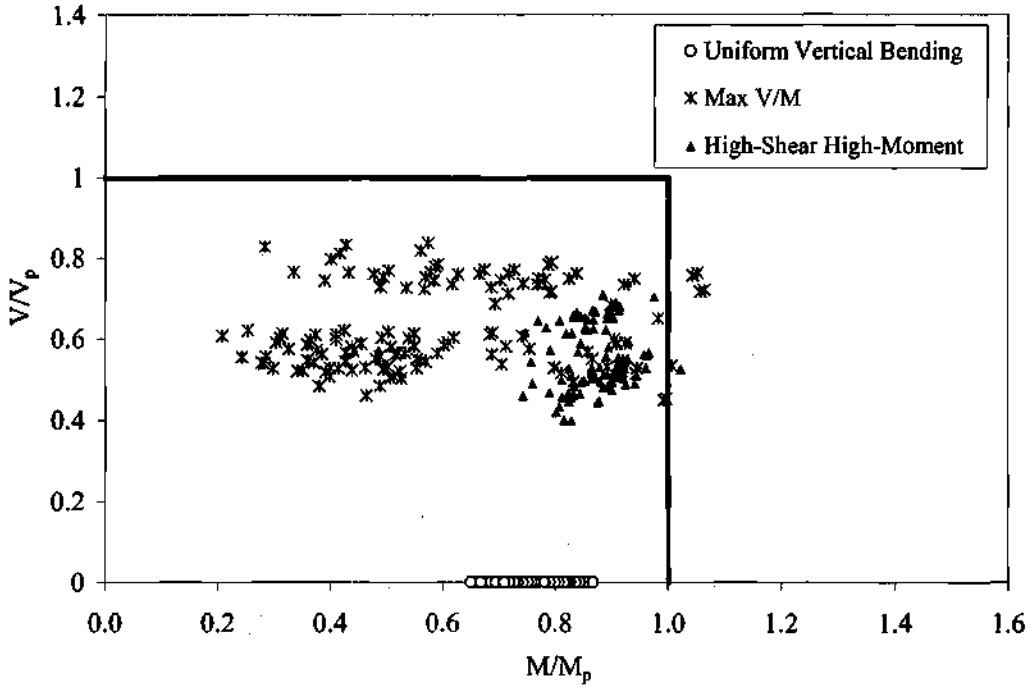

Figure 9.1.14. Summary of moment-shear strength interaction results, normalized by M_p and V_p, for all the primary test suite parametric studies.

experimental tests of this type are underway at the University of Nebraska, Lincoln and at the University of Missouri at Columbia. Experimental tests are underway at the FHWA Turner-Fairbank laboratory pertaining to the strength of curved I girders subjected to high moment and high shear.

9.2 UNSYMMETRIC SPECIMENS

Figures 9.2.1 through 9.2.4 present the moment-shear strength interaction results for the singly symmetric girders studied in this research (see Table 5.13.1). Figures 9.2.1 and 9.2.2 give the results for the cross-section with $D/b_{fc} = 2.75$, $b_f/t_f = 25$ and $2D_c/t_w = 169$ (see Fig. 5.13.1), and Figs. 9.2.3 and 9.2.4 show the data for the case with $D/b_{fc} = 4.77$, $b_f/t_f = 20$ and $2D_c/t_w = 208$ (see Fig. 5.13.2). The first of the two figures in each of these sets shows the data as normalized by $M_{n(FEA)}$ and $V_{n(FEA)}$ while the second presents the data as normalized by $M_{n(1/3\ rule)}$ and $V_{n(AASHTO)}$. That is, the organization of these plots is the same as that employed for the doubly symmetric girders in Section 9.1.

It can be observed from the plots normalized by $M_{n(FEA)}$ and $V_{n(FEA)}$ that the bending capacity is increased due to high shear in all of these girders. Furthermore, the plots normalized by $M_{n(1/3\ rule)}$ and $V_{n(AASHTO)}$ indicate that these design strength predictors are conservative relative to the finite element based strengths for the specimens with $D/b_{fc} = 2.75$ and $2D_c/t_w = 169$. The moment strength prediction is slightly unconservative for one of the tests of the girders with $D/b_{fc} = 4.77$ and $2D_c/t_w = 208$ (see Fig. 9.2.4), but is well within the range of the $M/M_{n(1/3\ rule)}$ predictions for the doubly symmetric girders. Figure 9.2.4 shows that the shear strength predictions by the AASHTO (2001) LRFD equations are highly accurate to slightly unconservative for three of the maximum V/M tests in this group.

It is interesting that although L_b/b_{fc} is equal to 14.3 within the unsymmetrical girder corresponding to $D/b_{fc} = 4.77$ with $L_b/R = 0.05$ and target $f_c/f_b = 0.50$ (i.e., although the lateral-torsional buckling slenderness for this girder is significantly larger than the compact bracing limit, and although it has a very small flange compared to the size of the web), this specimen does not fail by lateral bending of the compression flange prior to the failure of the web in shear in the maximum V/M test. It is believed that this is partly due to the fact that the larger tension flange provides some additional restraint against lateral-torsional buckling than is counted upon within the design equations (see Figs. 2.1.4 through 2.1.9). The girder with $D/b_{fc} = 2.75$, $b_f/t_f = 25$ and $2D_c/t_w = 169$ is not tested in high-moment and high-shear since it has a value of $M_{n(FEA)}/0.8V_{n(FEA)} < 0.55$ (see Appendix C).

9.3 IMPLICATIONS OF THE MODIFIED AASHTO SHEAR STRENGTH EQUATIONS ON CHECKING OF MOMENT-SHEAR INTERACTION

Figures 9.3.1 through 9.3.6 are a repeat of Figs. 9.1.2, 9.1.4, 9.1.6, 9.1.8, 9.1.10 and 9.1.12, but with the shear strengths normalized by the modified AASHTO value for the shear capacity $V_{n(modified\ AASHTO)}$. The values of the abscissa are calculated in the same way as in the previous plots. However, as noted in Chapter VIII, the accuracy of the

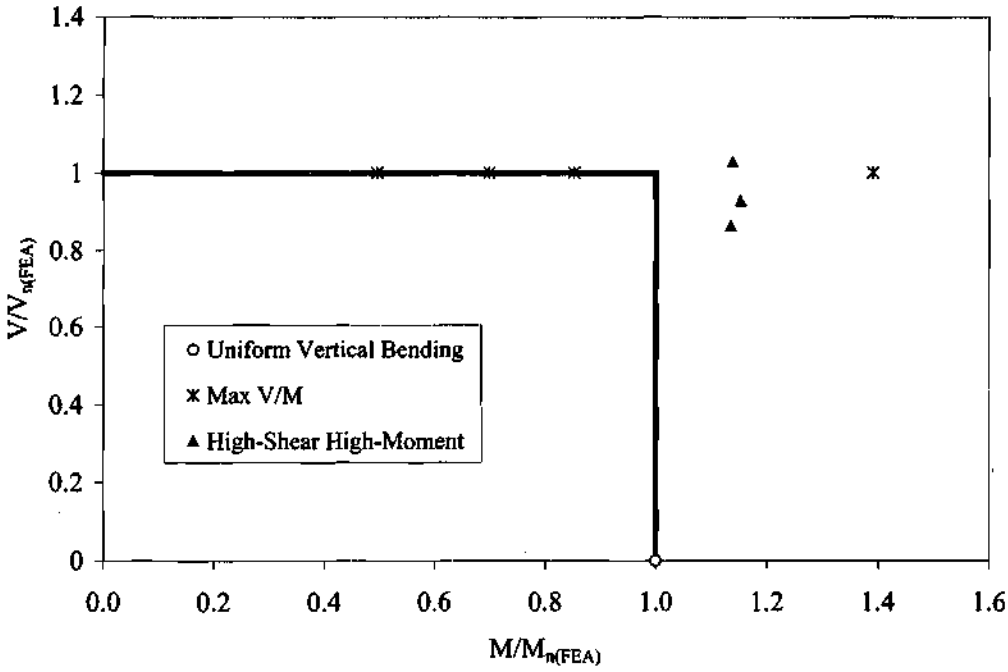

Figure 9.2.1. Moment-shear interaction, normalized by $M_{n(FEA)}$ and $V_{n(FEA)}$, for the singly symmetric girders with $D/b_{fc} = 2.75$, $b_f/t_f = 25$, and $2D_c/t_w = 169$.

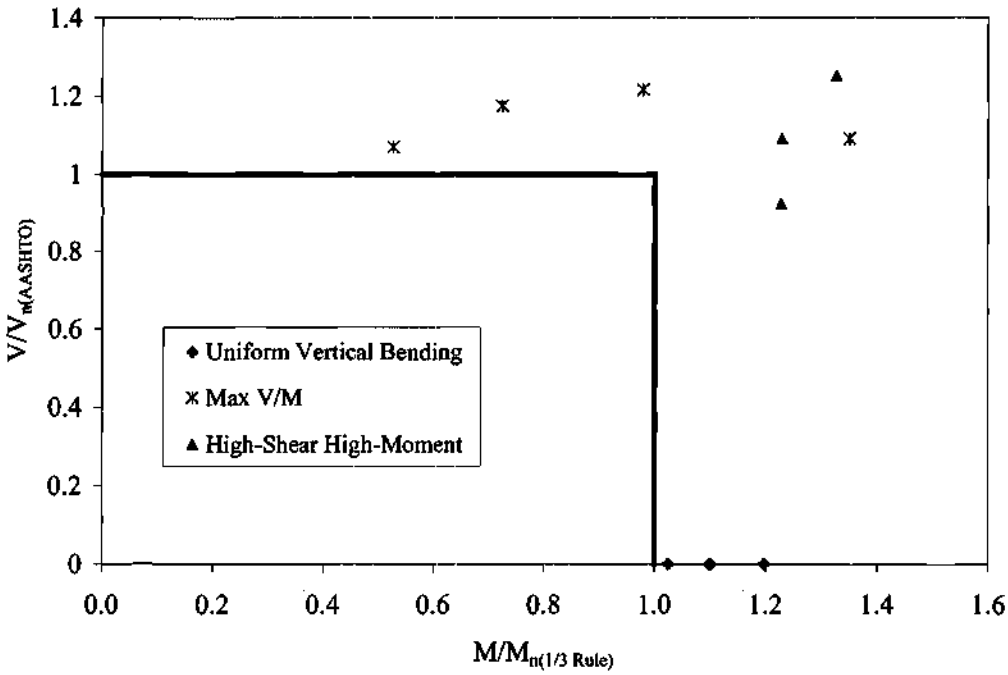

Figure 9.2.2. Moment-shear interaction, normalized by $M_{n(1/3\ rule)}$ and $V_{n(AASHTO)}$, for the singly symmetric girders with $D/b_{fc} = 2.75$, $b_f/t_f = 25$ and $2D_c/t_w = 169$.

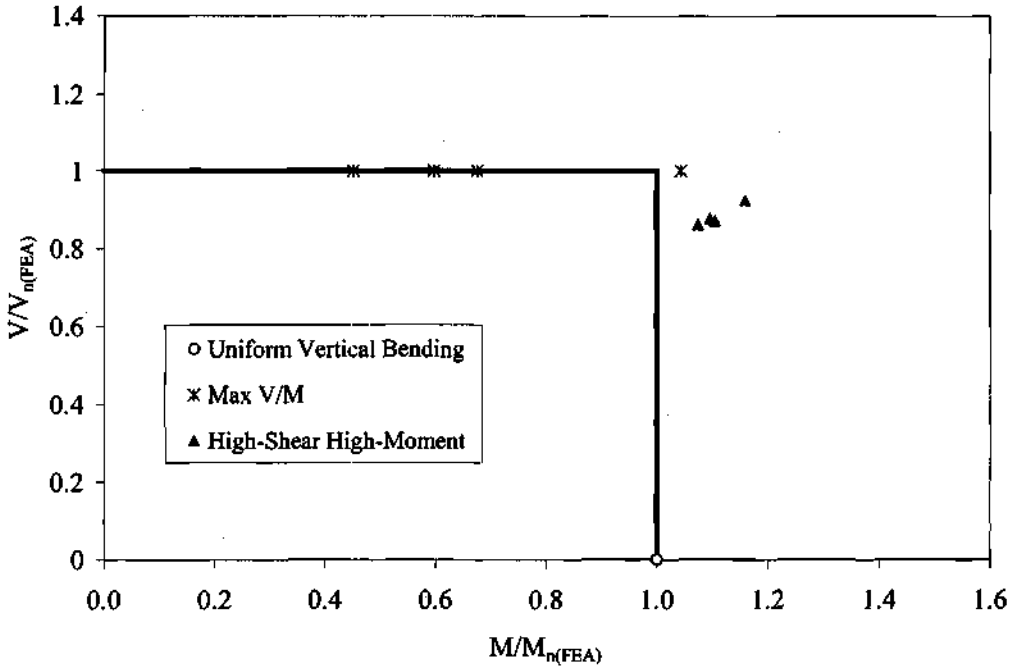

Figure 9.2.3. Moment-shear interaction, normalized by $M_{n(FEA)}$ and $V_{n(FEA)}$, for the singly symmetric girders with $D/b_{fc} = 4.77$, $b_f/t_f = 20$ and $2D_c/t_w = 208$.

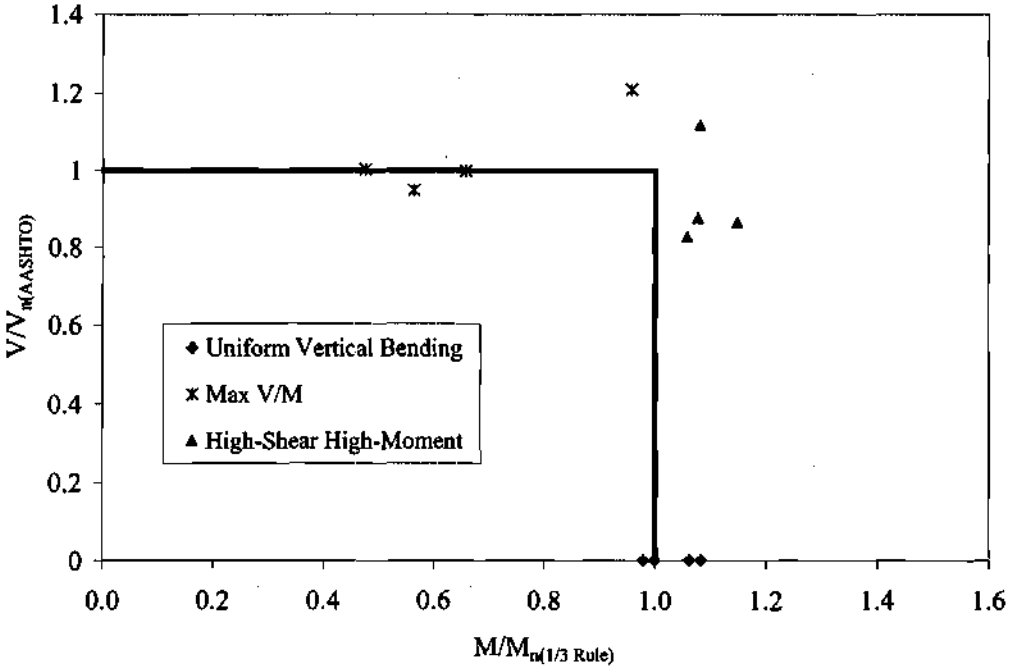

Figure 9.2.4. Moment-shear interaction, normalized by $M_{n(1/3\ rule)}$ and $V_{n(AASHTO)}$, for the singly symmetric girders with $D/b_{fc} = 4.77$, $b_f/t_f = 20$ and $2D_c/t_w = 208$.

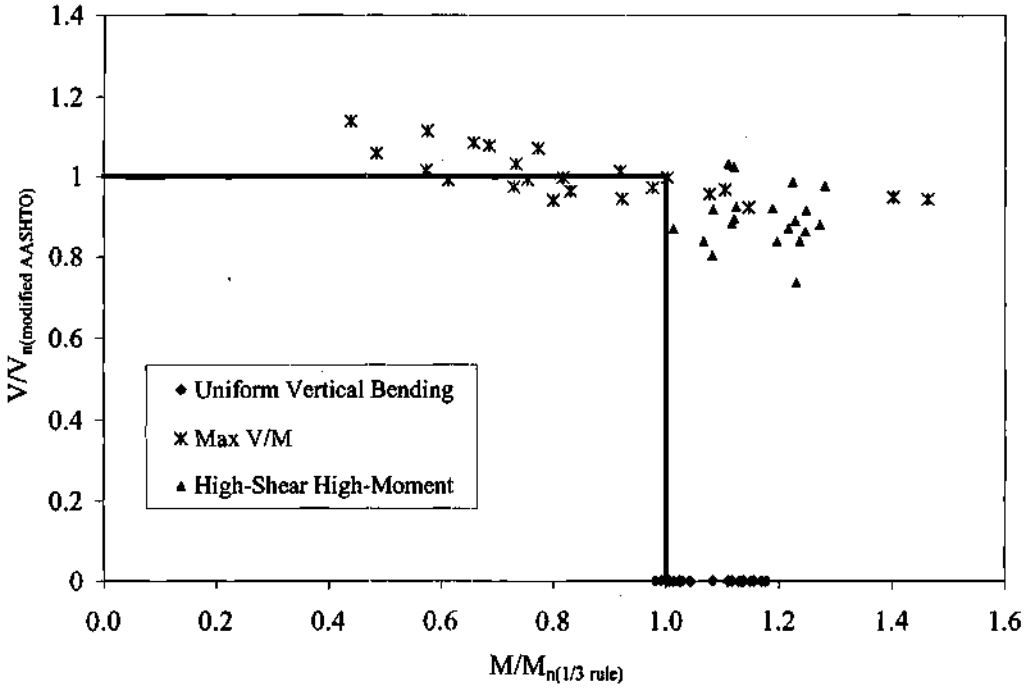

Figure 9.3.1. Moment-shear interaction, normalized by $M_{n(1/3\ rule)}$ and $V_{n(modified\ AASHTO)}$, for specimens with $L_b/R = 0.05$ and target $f_t/f_b = 0.35$.

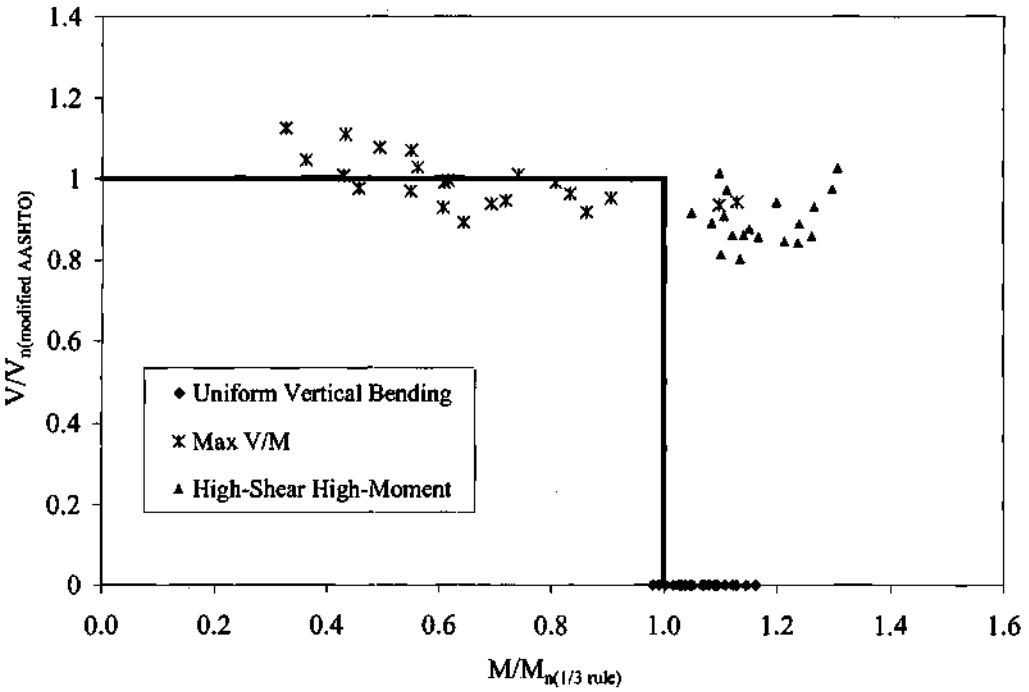

Figure 9.3.2. Moment-shear interaction, normalized by $M_{n(1/3\ rule)}$ and $V_{n(modified\ AASHTO)}$, for specimens with $L_b/R = 0.075$ and target $f_t/f_b = 0.35$.

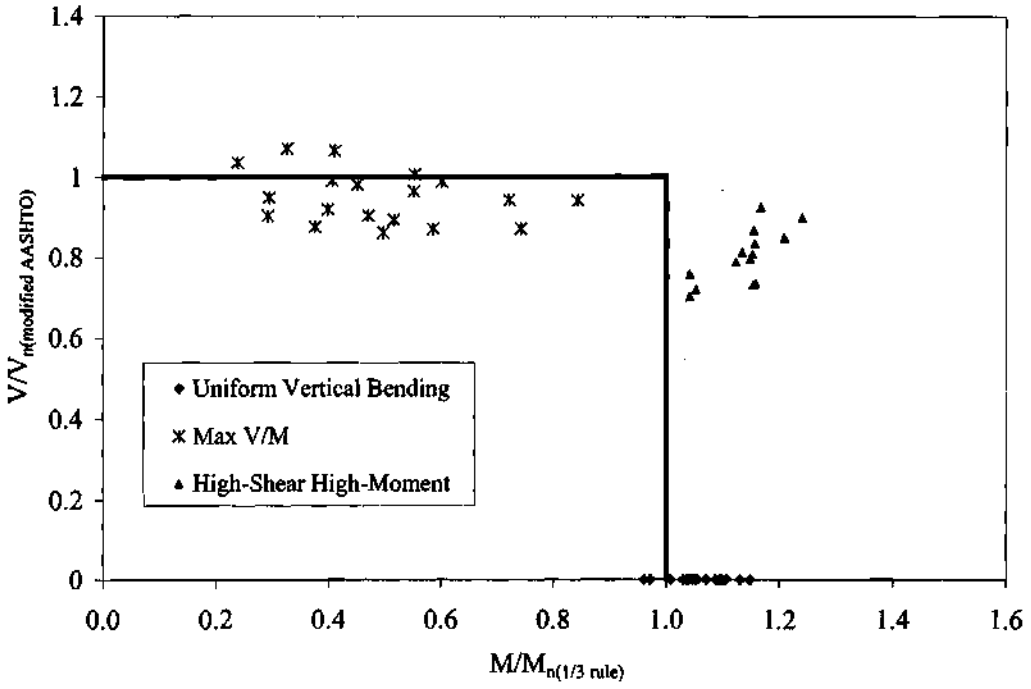

Figure 9.3.3. Moment-shear interaction, normalized by $M_{n(1/3\ rule)}$ and $V_{n(modified\ AASHTO)}$, for specimens with $L_b/R = 0.1$ and target $f_t/f_b = 0.35$.

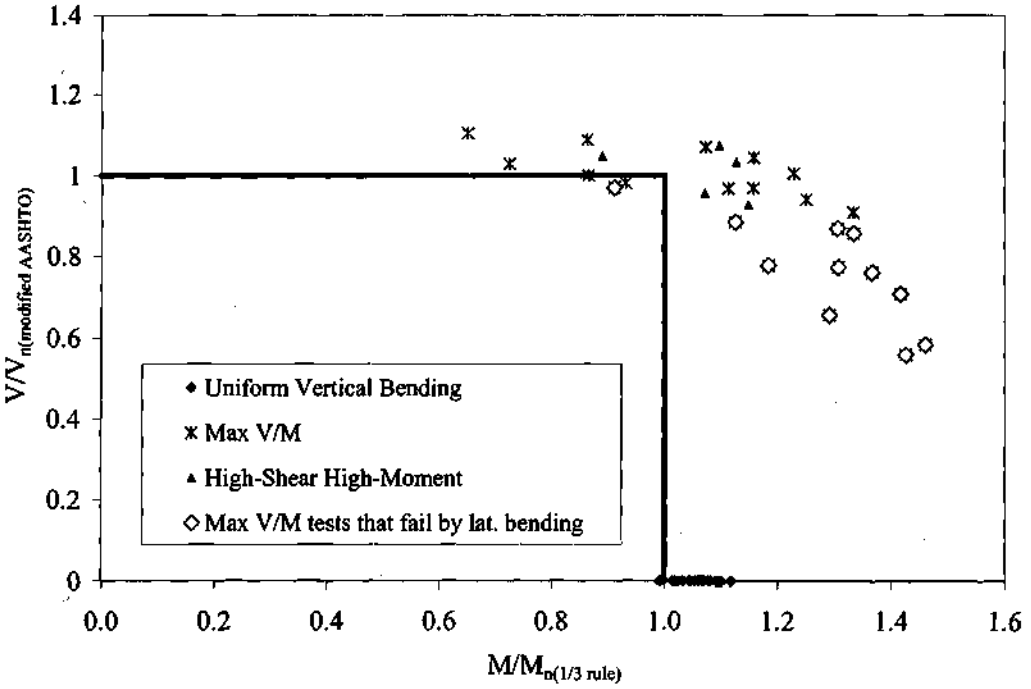

Figure 9.3.4. Moment-shear interaction, normalized by $M_{n(1/3\ rule)}$ and $V_{n(modified\ AASHTO)}$, for specimens with $L_b/R = 0.05$ and target $f_t/f_b = 0.50$.

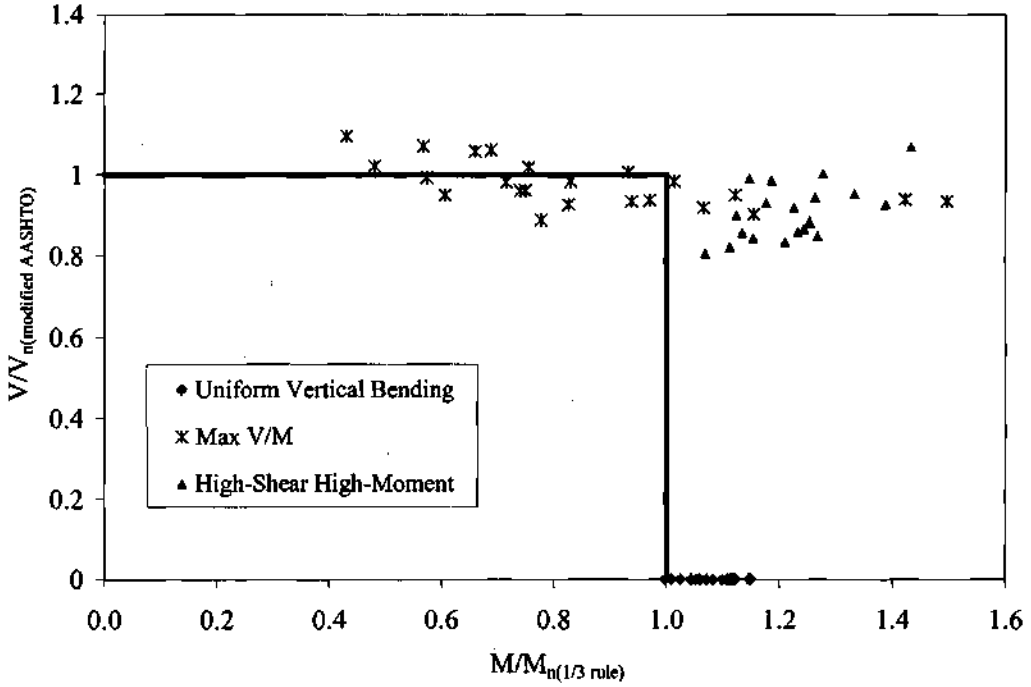

Figure 9.3.5. Moment-shear interaction, normalized by $M_{n(1/3\ rule)}$ and $V_{n(modified\ AASHTO)}$, for specimens with $L_b/R = 0.075$ and target $f_t/f_b = 0.50$.

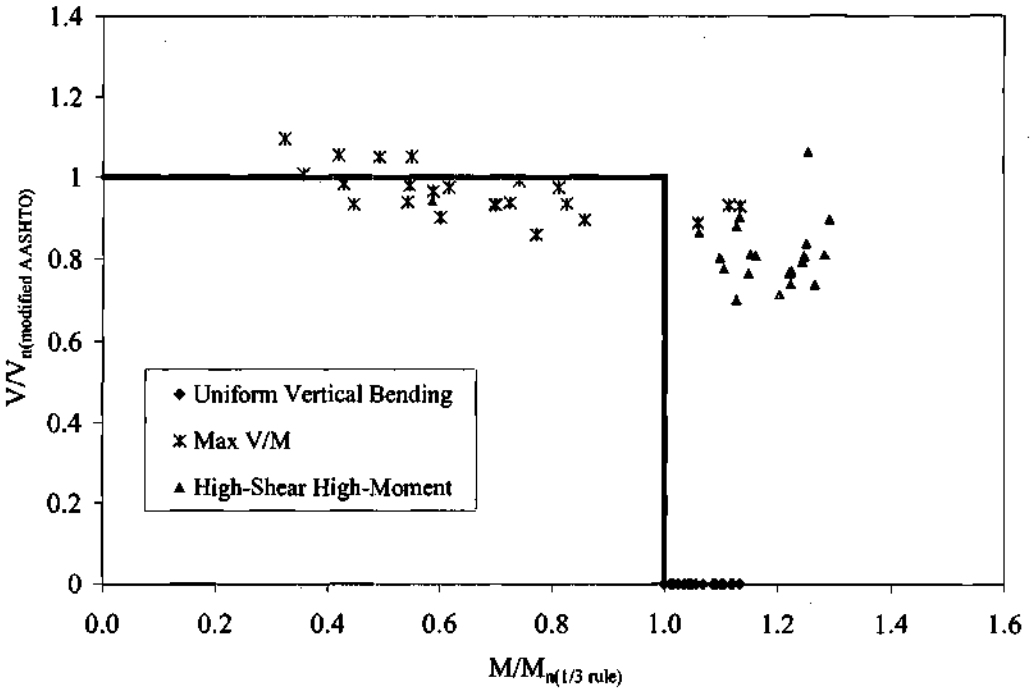

Figure 9.3.6. Moment-shear interaction, normalized by $M_{n(1/3\ rule)}$ and $V_{n(modified\ AASHTO)}$, for specimens with $L_b/R = 0.10$ and target $f_t/f_b = 0.50$.

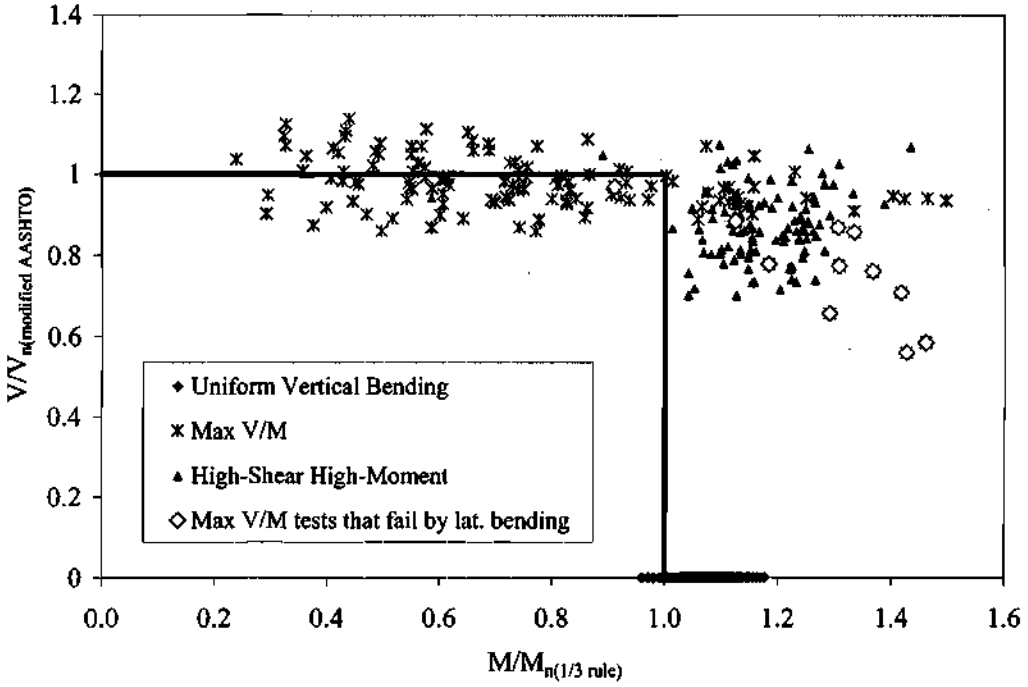

Figure 9.3.7. Summary of moment-shear strength interaction results, normalized by $M_{n(1/3\ rule)}$ and $V_{n(modified\ AASHTO)}$, for all the primary test suite parametric studies.

modified AASHTO shear strength equations is somewhat better than that of the current AASHTO LRFD (2001) shear strength formulas. The average of the $V/V_{n(modified\ AASHTO)}$ values is closer to one and the dispersion of these values is smaller than that for the corresponding values in Figs. 9.1.2, 9.1.4, 9.1.6, 9.1.8, 9.1.10 and 9.1.12.

Figure 9.3.7 plots all of the data from the above six figures together, and parallels Fig. 9.1.13[1]. Although the finite element based strengths are overestimated in nearly one-half of the maximum V/M tests, the modified AASHTO equations give improved predictions in terms of the arithmetic mean and standard deviation relative to the finite element based shear strengths (see Section 8.1). Several of these plots show some reduction in the shear strength with increasing values of $M/M_{n(1/3\ rule)}$, but this reduction is small. As in the previous plots presented in Sections 9.1 and 9.2, the flexural capacity predicted by the one-third rule equations tends to be particularly conservative for the high-shear high-moment tests, and for the maximum V/M tests that fail by lateral bending.

9.4 SUMMARY ASSESSMENT OF MOMENT-SHEAR INTERACTION

The results presented in this chapter indicate that if the design shear strengths are calculated based on either the current AASHTO LRFD (2001) or the modified AASHTO equations, and if the flexural strengths are quantified by the proposed one-third rule,

[1] This plot is shown previously as Fig. 2.3.4.

moment-shear interaction does not need to be considered in cases of combined high moment and high shear.

Further studies are needed to fully evaluate the implications of the use of the modified AASHTO shear strength equations on the moment-shear interaction predictions for straight I girders. The parametric studies conducted by Aydemir (2000) indicate that it may be possible to neglect moment-shear interaction effects also in straight homogeneous and hybrid I girders.

Page intentionally left blank

CHAPTER X

CONCLUSIONS

10.1 SUMMARY

This research addresses the maximum strength of curved and straight I girders subjected to a reasonably comprehensive range of loading and boundary conditions. The loading conditions considered include uniform vertical bending, high shear with low vertical bending moment, and high shear with high vertical bending moment, combined with lateral bending within the flanges due to torsion and lateral loading. The behavior of both internal unsupported lengths as well as unbraced lengths with torsionally simple boundary conditions at one end is studied. The effects of potential relative torsional rotations between cross-frame locations as well as of concentrated internal loadings within the critical unsupported length are addressed. A wide range of unsupported lengths is studied, including girders with compact lateral brace spacing, cases involving inelastic lateral-torsional stability failure, as well as specimens that fail essentially by elastic lateral-torsional buckling. The primary focus of this research is on horizontally curved I girders with a subtended angle between the cross-frame locations, L_b/R, ranging from 0.05 to 0.10; however, straight girders subjected to combined vertical and lateral bending are also studied. Cross-sections with slender and non-slender noncompact webs, and flange slenderness ranging from values close to traditional plastic design limits up to values that slightly exceed the current b_f/t_f fabrication limit within the AASHTO LRFD (2001) straight-girder specifications are evaluated. The cross-sections include D/b_{fc} values ranging from 2.25 to 4.77 and $2D_ct_w/b_{fc}t_{fc}$ values ranging from 0.79 to 3.70. Both doubly- and singly-symmetric cross-sections are considered.

10.1.1 Evaluation of Maximum Strength and Pre- and Post-Peak Load-Deflection Characteristics

This research is based predominantly on the development and execution of refined full nonlinear shell finite element models of various physical I girder configurations. The primary focus is on the maximum strength as well as the overall load-deformation response, including the post-peak or load-shedding behavior. Chapter IV details a number of prior experimental test specimens that are evaluated in this research, and Chapter V outlines the overall design of a parametric study involving the above ranges of design parameters. Nominal residual stresses due to cut curving and welding as well as flame cutting, welding and heat curving are addressed, although the study focuses predominantly on girders with nominal residual stresses due to cut curving and welding. Nominal geometric imperfections, i.e., web out-of-flatness, compression flange tilt, and compression flange sweep are modeled based on the buckling mode shapes from finite element linear buckling analysis solutions, with peak imperfection amplitudes set at

AASHTO-AWS (1996) fabrication tolerances. The studies show that girder maximum strengths in flexure and in flexure with high-shear can be significantly affected by the combined nominal residual stresses and geometric imperfections, but that the maximum shear strengths of horizontally curved I girders are not greatly affected by these attributes. The details of the full nonlinear shell finite element models are described in Chapter III.

Reasonably extensive comparisons are made between finite element solutions based on the adopted modeling approach and the results of prior and on-going experimental tests. Chapter IV focuses on these comparisons. These studies indicate that the full nonlinear shell finite element models give an accurate to conservative representation of the experimental responses. The pre-peak nonlinearity in many of the experimental tests is somewhat greater than that predicted based on the nominal residual stresses and geometric imperfections. However, the pre-peak nonlinearity in the experimental tests is mild. In girders with stocky flanges close to or smaller than traditional plastic design limits, the maximum vertical displacement at the peak load within the tests considered is roughly on the order of about two times the elastic deflection at this load level. For girders with more slender flanges, the inelastic vertical deflections at peak load tend to be smaller.

The full nonlinear finite element models tend to underestimate the maximum flexural strength of compact-flange girders to some extent, but typically provide highly accurate predictions of the maximum strength for girders with non-compact flanges. The under prediction of the experimental strengths for cases with stocky flanges may be attributable in part to strain-hardening response within the experiments, since the maximum strengths attained in the full-nonlinear finite element models of the stocky-flange sections correlate well with strength estimates based on full plastification of the compression flange, not including strain hardening. No evidence of large longitudinal normal strains at peak load is evident in the available experimental test data; however, it is possible that strain-hardening characteristics may be exhibited in the experimental tests due to strain gradients within the specimens.

The experimental test data on post-peak load-deformation response is limited. The full nonlinear finite element models indicate that the specimens with stocky flanges do not shed their load as rapidly for normalized plastic vertical displacements (maximum displacement divided by the unsupported length in uniform vertical bending tests, approximately equal to a plastic end rotation within the critical unsupported length in the case of the parametric study specimens) less than about 0.006. However, for normalized plastic displacements larger than this magnitude, the load-shedding rate is approximately the same both for the stocky flange and for the non-compact flange sections. The full nonlinear shell finite element models appear to provide a highly accurate characterization of experimental shear capacity tests of horizontally curved I girders.

10.1.2 Development of Design Recommendations

An effort is made to thoroughly evaluate the characteristics of various predictor equations from existing design specifications and from prior research for characterization

of vertical bending and shear strengths, as well as vertical bending moment-shear strength interaction for high-moment and high-shear. These equations are evaluated theoretically and conceptually in Chapter II, and the predictions from several of the most promising and/or well known equations are compared to experimental as well as finite element parametric study results in Chapters IV, VI, VII, VIII and IX.

Specific maximum strength predictor equations are recommended which allow for a unified approach to the design of all types of I girders, both straight and horizontally curved, including the effects of lateral flange bending from any potential source. The specific proposed equations for nominal flexural design strength are presented in Section 2.1.9, detailed suggestions for evaluation of shear strength are discussed in Section 2.2.5, and specific findings pertaining to moment-shear strength interaction are outlined in Section 2.3.3. The studies providing the background to these recommendations are addressed in Chapters III through IX. The recommended design equations are close in format to current AASHTO LRFD (2001) equations for straight I girders.

10.1.2.1 Vertical Bending Strength

One of the most important findings of this research is that the current AASHTO LRFD (2001) straight I girder flexural strength equations need to be modified slightly to make them simpler, more consistent in their application for composite and non-composite design, more rational with respect to the characterization of local and lateral-torsional buckling limit states, and more accurate with respect to available experimental and refined finite element test data. Specific improvements for straight girders, detailed in Section 2.1.1 include:

- Significantly improved, simple equations for characterization of flange local buckling resistance (see Section 2.1.1.2 and Figs. 2.1.1 and 2.1.2),

- Simple and consistent unified equations for characterization of the lateral-torsional buckling strength of symmetric and unsymmetric non-composite I girders, and composite I girders subjected to negative bending (see Sections 2.1.1.3 through 2.1.1.7, and Figs. 2.1.10 and 2.1.11), and

- Clarification of the conservative and practical AASHTO LRFD (2001) provisions for calculation of the moment-gradient magnifier C_b based on "worst-case" moment envelope values (see Section 2.1.1.8).

This research finds that, within the design limits of $b_f/t_f \leq 24$, $f_\ell/F_y \leq 0.5$, $L_b/R \leq 0.10$ and $L_b/r_t \leq \lambda_r$, the effect of flange lateral bending due to horizontal curvature, bridge geometry, and/or applied loadings is significant, but it is reasonably small. A simple extension of the proposed modified AASHTO LRFD (2001) straight-girder equations is developed based on the analogy of the flanges as equivalent steel beam-columns. The basic concepts behind this idealization are explained in Sections 1.4 and 2.1.9.1. It is found that by simply subtracting $f_\ell/3$ from the modified AASHTO LRFD (2001) straight-

girder vertical bending capacity equations, where f_ℓ is in general the maximum estimated second-order elastic flange lateral bending stress within the subject unsupported length, the effect of flange lateral bending from any source is accurately characterized. The resulting equations, based on an extension of recommendations by (Hall and Yoo 1998) for checking of horizontally curved compact-flange I girders to general I girder cross-sections, is referred to in this research as the one-third rule.

A simple equation for estimation of the second-order lateral bending stress amplification is suggested in Sections 7.15.1 and 7.15.2; however, the evaluation of appropriate methods for calculation of flange lateral bending stresses in general bridge superstructures is beyond the scope of this work. Fortunately, the vertical bending strength predicted by the one-third rule is fairly insensitive to approximations in the calculation of the elastic flange lateral bending stresses.

10.1.2.2 Shear Strength

This research supports the conclusions made in prior research that the nominal maximum shear resistance of horizontally curved I girders can be based adequately on shear strength equations developed for straight I girders, including tension field action, within the limit of $L_b/R \leq 0.10$. The typical increases in the elastic shear web buckling and decreases in the ultimate shear capacities due to horizontal curvature are small compared to the effects of various other factors that lead to variability in the design shear strength predictions relative to shear strengths obtained from experimental tests and refined finite element models. Based on the current study, prior research, and on preliminary results from recent experimental studies, it appears that based solely on maximum strength considerations, the maximum limit on transverse stiffener spacing of $d_o/D = 3$ in the AASHTO LRFD (2001) straight girder specifications is also sufficient for horizontally curved I girders with $L_b/R \leq 0.10$.

It is found that the current AASHTO LRFD (2001) shear strength equations provide a reasonably good characterization of the maximum shear strength, even though as noted within the literature, these equations are based on Basler's tension-field model, which serendipitously is based on the post-buckling strength associated with a complete uniform tension field throughout the web panel with an orientation of $\theta = \tan^{-1}(D/d_o)/2$ relative to the horizontal (see Section 2.2.2). Also, this research demonstrates that the accuracy of the AASHTO LRFD (2001) shear strength equations can be improved by basing the web shear buckling coefficient on equations developed by Lee and Yoo (1996).

As noted below, further research is recommended to evaluate the implications of web panel aspect ratios d_o/D greater than one on the fatigue performance of transversely stiffened horizontally curved I girders.

10.1.2.3 Moment-Shear Strength Interaction

Based on the large number of finite element parametric studies considered, this research finds that the above mentioned flexure and shear strength equations adequately capture the maximum strength of all horizontally curved I girders within the stated design limits, without the need for consideration of interaction between the vertical bending and shear strengths under combined high moment and high shear. The parametric shear strength studies include cases in which the flanges are not able to hold a node line for development of the I girder shear strengths. That is, some of the high-shear high-moment studies involve a failure of the compression flange in lateral bending. It is shown that the proposed one-third rule adequately accounts for a physical reduction in the vertical bending strengths due to lateral flange bending combined with high-vertical bending moment and high-shear. Other recent research is cited that indicates the potential for eliminating moment-shear interaction checks also for hybrid and homogenous straight transversely stiffened I girders.

Particularly when one considers that: (1) bridge I girders are typically designed based on maximum shear and moment envelope values, without account for the fact that these maximum values do not occur at the same time, (2) composite I girders typically have some incidental additional shear capacity relative to the strength of the steel girder alone, and (3) the overall statistics for the predictions in the strengths for high-shear and high-vertical bending, without any consideration of moment-shear interaction, appear to be more conservative than the overall statistics for prediction in the shear strength combined with low-vertical bending moment, it would appear that the complexities of checking M-V interaction in design are unmerited. It is emphasized that if one considers certain individual straight girder geometries under high-shear low moment, high-shear high-moment and high-moment low-shear, some interaction between the moment and shear strengths is evident. However, when the whole of the refined finite element and available experimental data is compared to the proposed nominal flexural and shear resistances, one can conclude that moment-shear interaction effects can be considered within the development of resistance ϕ factors without incurring any substantial penalty on the design vertical bending and shear strengths. The results of the analyses conducted in this research indicate that moment-shear interaction is less of an issue, and indeed appears to be essentially nonexistent in horizontally curved I girders with L_b/R between 0.05 and 0.10.

The experimental test data on moment-shear strength interaction in straight and horizontally curved transversely stiffened I girders is sparse. Therefore, it is suggested that the above conclusions should be checked by further experimental studies prior to implementation.

10.2 RECOMMENDATIONS FOR FURTHER RESEARCH

The present research has involved a reasonably comprehensive assessment of the strength and load-deformation behavior of horizontally curved and straight steel I-girders under a wide range of loading conditions, with a primary focus on lateral-flange bending

effects. However, there are still important needs for further research to provide a more complete understanding of the behavior of curved and straight I girders and I girder bridges. Some of the most promising potential areas for further study are as follows:

- The implications of D/b_f ratios larger than 3.25 on the maximum strength and design economy of horizontally curved I girder bridges should be studied more carefully. It can be shown based on simple V-load type calculations (see Eq. (5-3)), that if $L_b/R = 0.10$ and $D/b_f = 3.25$, L_b/D must be less than 2.56 to restrict f_f/f_b to 0.5[1]. If $D/b_f = 5$ is employed, L_b/D must be less than 1.67. If f_f/f_b is restricted to a smaller value, the corresponding restrictions on L_b/D become more severe, or practically speaking, D/b_f must be limited. Guidance on the most economical spacing of cross-frames within typical horizontally curved I girder bridges would be useful.

- The current parametric study might be extended by including additional loadings and boundary conditions. For instance, the internal loading suite might be modified to include a directly applied eccentric and/or torsional loading, to more explicitly model the strength of a girder subjected to loadings from overhang brackets, deck forms, screed rails, etc. The laterally unsupported straight-girder suite might be extended to include loadings other than uniform lateral bending. Nevertheless, the view of the authors, the current studies are sufficient to establish the validity of the proposed design equations.

- The design checks in Chapter IV for a limited number of girders with L_b/R significantly larger than 0.10 indicate that the one-third rule may be applicable for larger values of the subtended angle between the cross-frame locations. Studies should be conducted with larger L_b/R values to ascertain the limits at which the proposed design rules are no longer valid.

- Unstiffened girders, with $d_o/D > 3$ based on $d_o = L_b$ (the distance between the connection plates for the cross-frames) have not been considered in this work. The maximum strength of these types of horizontally curved girders should be studied. It is expected that the current formulas for the shear strength of unstiffened girders provided within the Recommended Specifications should be sufficient for these cases, but that it may be possible to liberalize the Recommended Specification limits on the web slenderness D/t_w for unstiffened webs.

- Studies should be conducted to extend the design rules proposed within this research to include the use of Grade 70W high-performance steels (HPS), for both homogenous and hybrid (Grade 50 or HPS 50W web) I girder design. The high-performance steels offer significant potential advantages in strength, toughness and weldability. Industry marketing of high-performance steel emphasizes the potential for at least a 10 percent cost reduction (AISI 2000). Studies have indicated that significant design economy is obtained by use of a Grade 50 or HPS 50W web with

[1] This result can be obtained by dividing both sides of Eq. (5-3) by D, and substituting $L_b/R = 0.10$, $D/b_f = 3.25$ and $f_f/f_b = 0.5$.

HPS 70W flanges for straight bridge I girders. Additional advantages should be possible in horizontally curved I girders, if design rules such as in the current AASHTO (2001) straight-girder Specifications are utilized which allow the hybrid web to yield in flexure under the maximum strength design conditions. Although several of the experimental tests considered in Chapter IV were effectively hybrid girders, further studies are needed to better understand the influence of a hybrid web on the behavior of horizontally curved I girders, particularly at the higher strength levels associated with HPS 70W material.

- Experimental tests are needed to verify the findings of this research regarding moment-shear strength interaction. Specifically, a number of these experimental tests should include configurations in which the flanges are not sufficient to hold a node line under high-shear low-moment conditions. Eleven of the girders with $L_b/R = 0.05$ and target $f_f/f_b = 0.5$ failed in this fashion in the maximum V/M parametric tests (see Section 8.1.1).

- Most of the experimental tests considered in Chapter IV have L_b/b_f ratios less than the compact bracing limit. Additional experimental tests of horizontally curved I girders with larger lateral-torsional buckling slenderness values would be useful.

- At the present time, the AASHTO LRFD (2001) Specifications provide a separate equation that predicts flexural strengths larger than M_y for girders that are braced at close intervals. This equation is commonly referred to as the Q formula. There is excellent potential for extension of the proposed modified AASHTO straight-girder flexural strength equations to unify the "standard" and "Q formula" equations into one set of flexural-strength predictor equations. Based on the experimental test results discussed in Chapter IV, it appears that there is also potential for design economy in extending these unified equations to include the effects of torsion and lateral flange bending. Unfortunately, the finite element studies detailed in Chapters IV and VII of this report do not indicate significant gains by liberalizing the current proposed one-third rule equations. However, the finite element solutions produced in this research tend to be somewhat conservative relative to the experimental strengths for girders with stocky flanges. It should be noted that the magnitude of the inelastic deformations required to reach the maximum strengths should be given careful consideration. The implications of inelastic girder deformations on cross-frame forces and the response of bridge structural systems should be studied, particularly for horizontally curved bridge I girders.

- The one-third rule flexural strength equations recommended in this research are in certain cases expected to give somewhat conservative solutions for unsymmetric I girders and for composite I girders in positive bending (see Section 7.12). This is due to the fact that they are based on the strength of the flanges as equivalent beam-columns, and as such, they limit the flexural strength of the member to an upper bound of M_y. They do not consider directly the substantial reserve flexural strength that can be achieved by yielding of the web in these types of cross-sections, in which

the shape factor M_p/M_y can be substantially larger than one. The composite section yield interaction equations discussed by Yoo (1996) and Yoo and Davidson (1997) (see Section 2.1.8.1) are a useful and elegant means of extending the current AASHTO LRFD (2001) formulas for the strength of composite I girders in positive bending to include the effects of lateral bending within the bottom flange. These formulas should be given careful consideration for characterization of the behavior and strength of composite horizontally curved bridge I girders and systems. The issues discussed in the previous item pertaining to the effects of inelastic girder deformations on cross-frame forces and bridge system response should also be addressed with respect to the use of the composite section yield interaction equations.

- The fatigue behavior of horizontally curved I girder webs needs to be better understood. As noted in Section 2.1.2.9, the Recommended Specifications (Hall and Yoo 1998) restrict the web stresses to the elastic buckling stress under all loading conditions. For transversely stiffened girders with $d_o/D \leq 1$, the Recommended Specification restrictions are typically more restrictive than the Daniels et al. (1980) equation (Eq. 2-51). However, for girders with larger stiffener spacing, the Daniels et al. equation can be more restrictive than the Recommended Specification limits on D/t_w. Either of these rules would disallow the use of slender webs with large d_o/D, which may indeed be appropriate. Conversely, it may be possible to justify more liberal restrictions based on prevention of web buckling only under fatigue loading conditions, at least up to certain curvature limits.

  Daniels et al. (1980) arrived at their proposed equation for a maximum limit on D/t_w (Eq. 2-51) by observing that the radial deflections at the web-to-flange boundaries in curved I girders tend to reduce the relative web deflections and the subsequent plate bending stresses from that in straight I girders. As a result, they concluded that previous D/t_w restrictions, developed by Culver et al. (1972c and 1973) and CURT (1975), were too severe. The Culver et al. (1972c and 1973) and CURT (1975) recommendations were based on restricting estimated web plate bending stresses in curved I girder webs to estimated values associated with web plate bending in straight girder webs, assuming a maximum AWS (1996) out-of-flatness. The girders tested by Daniels and Herbein (1980) exceeded the CURT-proposed limits in all cases, but no fatigue crack developed along the web boundaries. The web slenderness D/t_w ranged from 139 to 192 and the panel aspect ratio d_o/D ranged from to 2.03 to 2.36 in these girders. However, in the development of their design recommendations Daniels et al. (1980) state, "To estimate the lateral deflections of the web boundaries would be mathematically highly involved, if not impossible. Thus, a rigorous reexamination of the web boundary bending stresses is not warranted for the sake of establishing web slenderness ratios. A relatively simple although empirical way to liberate the slenderness reduction factor is to reduce the (CURT) adopted initial out-of-straightness." Daniels et al. (1980) developed Eq. (2-51) simply by assuming an initial web out-of-straightness of one-half that assumed by Culver et al. (1972c and 1973).

- Studies are needed to further quantify the qualities and limitations of different elastic design analysis methods for calculation of flange lateral bending stresses due to horizontal curvature, different bridge geometries including skew, and various practical loading conditions.

- Finally, the overall behavior of horizontally curved I girder bridge systems designed by the proposed equations needs to be studied extensively, both under erection and final composite conditions. Some of the issues that should be given particular attention in this regard include the influence of incidental stresses induced within the girders during the erection processes, the influence of girder inelastic deformations on the system response, and the potential in some bridge geometries for collapse of the bridge system due to failure of the girder that is farthest from the center of curvature (as well as the implications of this type of behavior). The reserve strength and potential inelastic redistribution within the final composite bridge superstructure should be given particular attention with respect to this last issue.

Page intentionally left blank

APPENDIX A

BENDING STRENGTH DATA

This appendix provides data from all of the individual analyses pertaining to the flexural strength parametric studies conducted in this research. This data is useful for engineers and researchers to verify the results presented in Chapter VII. In addition, it can be used to evaluate other potential design predictor equations.

The organization of the appendix is as follows:

- Section A.1 – primary test suite.
- Section A.2 – modified uniform vertical bending suite.
- Section A.3 – internal loading suite.
- Section A.4 – free-end suite.
- Section A.5 – laterally unsupported straight girder suite.
- Section A.6 – unsymmetric girder suite.

Each of sections A.1 through A.6 is divided into four subsections, which provide:

1. The computed *second-order* elastic lateral and vertical bending stresses normalized by the yield stress F_y = 345 MPa (50 ksi), f_ℓ/F_y and f_b/F_y, which satisfy the one-third rule design equations for each test.
2. The *ratio* of the *first-order* elastic lateral and vertical bending stresses, f_ℓ/f_b, for each test.
3. The vertical bending strengths obtained from full nonlinear finite element analysis, normalized by the yield and plastic moment capacities of the cross-section, and the ratios of the strengths predicted by the various design equations to the finite element based strengths, based on the second-order elastic stresses provided in the first subsection.
4. The same information as in the third subsection, but with the strengths predicted by the design equations based on the first-order elastic f_ℓ/f_b values reported in the second subsection.

Section A.6 is divided into five subsections. The first four of these sections correspond to each of the test suites studied for the unsymmetric girders: primary, modified uniform vertical bending, internal loading, and free end. The last subsection presents the vertical bending strengths of the unsymmetric sections based on second- and first-order elastic analysis stresses.

All of the elastic analysis stresses reported in this appendix are based on the same shell finite element models employed for calculation of the girder capacities, but with zero geometric imperfections and residual stresses, and with the assumption of linear elastic material response. In the first of the above subsections, the second-order elastic stresses corresponding to satisfaction of the strength checks are provided only for the one-third rule equations. However, since the ratio of the lateral to the vertical bending stress, f_ℓ/f_b is independent of the load level in the first-order analyses, the first-order elastic stress information provided in the second group of tables is sufficient to verify all of the first-order elastic based design strength results.

The average, standard deviation, maximum and minimum values for strength ratios are presented at the end of the tables containing this data. As in Chapter VII, the best statistical values are shaded.

Strength ratios calculated per the Recommended Specifications (Hall and Yoo 1998) are presented in both the tables based on second-order and first-order elastic analysis, to facilitate comparison of results, although as discussed in Section 2.1.2, the Recommended Specification equations are always utilized with first-order elastic stresses from the design analysis (these equations estimate the second-order elastic amplification implicitly within their strength reduction factors).

The reader is referred to Chapter III for discussion of the finite element analysis models, illustrative example design flexural strength calculations are presented in Section 4.5.1, and Chapter V discusses the overall design of the parametric studies. Other details regarding the application of the different design equations are discussed at the beginning of Chapter VII.

A.1 PRIMARY TEST SUITE

A.1.1 Second-Order Elastic f/F_y and f_b/F_y Values at the One-Third Rule Strength Limit

Table A.1.1. Second-order elastic f_ℓ/F_y and f_b/F_y values at the one-third rule strength limit, primary test suite, uniform vertical bending, specimens with $D/b_f = 2.25$ and $b_f/t_f = 25$.

D/t_w	d_o/D		$L_b/R = 0.05$		$L_b/R = 0.075$		$L_b/R = 0.10$	
			target $f_\ell/f_b = 0.35$	target $f_\ell/f_b = 0.50$	target $f_\ell/f_b = 0.35$	target $f_\ell/f_b = 0.50$	target $f_\ell/f_b = 0.35$	target $f_\ell/f_b = 0.50$
100	3	f_ℓ/F_y	0.240	0.352	0.254	0.321	0.320	0.386
		f_b/F_y	0.788	0.707	0.784	0.761	0.765	0.740
130	3	f_ℓ/F_y	0.228	0.343	0.239	0.304	0.311	0.379
		f_b/F_y	0.773	0.719	0.769	0.748	0.748	0.723
160	1	f_ℓ/F_y	0.218	0.329	0.224	0.289	0.264	0.322
		f_b/F_y	0.748	0.711	0.746	0.725	0.736	0.714
	2	f_ℓ/F_y	0.219	0.330	0.240	0.290	0.286	0.347
		f_b/F_y	0.747	0.711	0.740	0.724	0.729	0.706
	3	f_ℓ/F_y	0.228	0.331	0.261	0.304	0.296	0.364
		f_b/F_y	0.745	0.711	0.734	0.720	0.725	0.700

Table A.1.2. Second-order elastic f_ℓ/F_y and f_b/F_y values at the one-third rule strength limit, primary test suite, uniform vertical bending, specimens with $D/b_f = 2.75$ and $b_f/t_f = 15$.

D/t_w	d_o/D		$L_b/R = 0.05$		$L_b/R = 0.075$		$L_b/R = 0.10$	
			target $f_\ell/f_b = 0.35$	target $f_\ell/f_b = 0.50$	target $f_\ell/f_b = 0.35$	target $f_\ell/f_b = 0.50$	target $f_\ell/f_b = 0.35$	target $f_\ell/f_b = 0.50$
100	3[1]	f_ℓ/F_y	0.268	0.327	0.301	0.337	0.289	0.400
		f_b/F_y	0.907	0.760	0.896	0.884	0.900	0.863
130	3[1]	f_ℓ/F_y	0.263	0.317	0.296	0.335	0.274	0.392
		f_b/F_y	0.909	0.768	0.898	0.885	0.905	0.866
160	1	f_ℓ/F_y	0.237	0.300	0.246	0.314	0.230	0.337
		f_b/F_y	0.907	0.767	0.904	0.882	0.909	0.874
	2	f_ℓ/F_y	0.248	0.306	0.253	0.316	0.257	0.360
		f_b/F_y	0.903	0.766	0.902	0.881	0.900	0.867
	3	f_ℓ/F_y	0.254	0.308	0.284	0.328	NA[2]	0.377
		f_b/F_y	0.901	0.758	0.891	0.877		0.861

[1] $d_o/D = 2$ for $L_b/R = 0.10$ and target $f_\ell/f_b = 0.35$, since $L_b/D = 2$

[2] NA for $L_b/R = 0.10$ and target $f_\ell/f_b = 0.35$, since $L_b/D = 2$

Table A.1.3. Second-order elastic f_ℓ/F_y and f_b/F_y values at the one-third rule strength limit, primary test suite, uniform vertical bending, specimens with $D/b_f = 2.75$ and $b_f/t_f = 20$.

D/t_w	d_o/D		$L_b/R = 0.05$		$L_b/R = 0.075$		$L_b/R = 0.10$	
			target $f_\ell/f_b = 0.35$	target $f_\ell/f_b = 0.50$	target $f_\ell/f_b = 0.35$	target $f_\ell/f_b = 0.50$	target $f_\ell/f_b = 0.35$	target $f_\ell/f_b = 0.50$
100	3[1]	f_ℓ/F_y	0.283	0.345	0.318	0.357	0.324	0.423
		f_b/F_y	0.871	0.743	0.859	0.846	0.857	0.824
130	3[1]	f_ℓ/F_y	0.280	0.343	0.320	0.355	0.318	0.422
		f_b/F_y	0.867	0.750	0.854	0.849	0.854	0.820
160	1	f_ℓ/F_y	0.251	0.324	0.249	0.333	0.284	0.362
		f_b/F_y	0.859	0.752	0.860	0.832	0.850	0.823
	2	f_ℓ/F_y	0.263	0.328	0.269	0.336	0.301	0.391
		f_b/F_y	0.856	0.750	0.854	0.826	0.843	0.814
	3	f_ℓ/F_y	0.274	0.335	0.313	0.382	NA[2]	0.410
		f_b/F_y	0.852	0.748	0.839	0.816		0.808

[1] $d_o/D = 2$ for $L_b/R = 0.10$ and target $f_\ell/f_b = 0.35$, since $L_b/D = 2$

[2] NA for $L_b/R = 0.10$ and target $f_\ell/f_b = 0.35$, since $L_b/D = 2$

Table A.1.4. Second-order elastic f_ℓ/F_y and f_b/F_y values at the one-third rule strength limit, primary test suite, uniform vertical bending, specimens with $D/b_f = 2.75$ and $b_f/t_f = 25$.

D/t_w	d_o/D		$L_b/R = 0.05$		$L_b/R = 0.075$		$L_b/R = 0.10$	
			target $f_\ell/f_b = 0.35$	target $f_\ell/f_b = 0.50$	target $f_\ell/f_b = 0.35$	target $f_\ell/f_b = 0.50$	target $f_\ell/f_b = 0.35$	target $f_\ell/f_b = 0.50$
100	3[1]	f_ℓ/F_y	0.269	0.367	0.287	0.333	0.316	0.401
		f_b/F_y	0.779	0.722	0.773	0.758	0.763	0.735
130	3[1]	f_ℓ/F_y	0.264	0.358	0.283	0.310	0.318	0.398
		f_b/F_y	0.761	0.730	0.755	0.746	0.743	0.716
160	1	f_ℓ/F_y	0.239	0.329	0.216	0.289	0.285	0.341
		f_b/F_y	0.737	0.708	0.745	0.721	0.722	0.704
	2	f_ℓ/F_y	0.255	0.336	0.248	0.314	0.305	0.376
		f_b/F_y	0.732	0.706	0.742	0.713	0.716	0.693
	3	f_ℓ/F_y	0.260	0.341	0.271	0.335	NA[2]	0.387
		f_b/F_y	0.730	0.704	0.727	0.706		0.689

[1] $d_o/D = 2$ for $L_b/R = 0.10$ and target $f_\ell/f_b = 0.35$, since $L_b/D = 2$

[2] NA for $L_b/R = 0.10$ and target $f_\ell/f_b = 0.35$, since $L_b/D = 2$

Table A.1.5. Second-order elastic f_ℓ/F_y and f_b/F_y values at the one-third rule strength limit, primary test suite, uniform vertical bending, specimens with $D/b_f = 3.25$ and $b_f/t_f = 25$.

D/t_w	d_o/D		$L_b/R = 0.05$		$L_b/R = 0.075$		$L_b/R = 0.10$	
			target $f_\ell/f_b = 0.35$	target $f_\ell/f_b = 0.50$	target $f_\ell/f_b = 0.35$	target $f_\ell/f_b = 0.50$	target $f_\ell/f_b = 0.35$	target $f_\ell/f_b = 0.50$
160	1	f_ℓ/F_y	0.252	0.351	0.215	0.275	0.294	0.288
		f_b/F_y	0.730	0.698	0.749	0.722	0.720	0.718
	2	f_ℓ/F_y	0.265	0.353	0.224	0.318	0.305	0.312
		f_b/F_y	0.725	0.697	0.746	0.708	0.716	0.710
	3	f_ℓ/F_y	0.269	0.360	NA[1]	0.318	NA[2]	0.349
		f_b/F_y	0.724	0.695		0.708		0.705

[1] NA for $L_b/R = 0.075$ and target $f_\ell/f_b = 0.35$, since $L_b/D = 2.5$

[2] NA for $L_b/R = 0.10$ and target $f_\ell/f_b = 0.35$, since $L_b/D = 2$

A.1.2 First-Order Elastic f/f_b Values

Table A.1.6. First-order elastic f_ℓ/f_b values, primary test suite, uniform vertical bending, specimens with $D/b_f = 2.25$ and $b_f/t_f = 25$.

D/t_w	d_o/D	$L_b/R = 0.05$		$L_b/R = 0.075$		$L_b/R = 0.10$	
		target $f_\ell/f_b = 0.35$	target $f_\ell/f_b = 0.50$	target $f_\ell/f_b = 0.35$	target $f_\ell/f_b = 0.50$	target $f_\ell/f_b = 0.35$	target $f_\ell/f_b = 0.50$
100	3	0.289	0.436	0.310	0.407	0.405	0.481
130	3	0.283	0.422	0.298	0.397	0.390	0.473
160	1	0.265	0.407	0.282	0.350	0.324	0.403
	2	0.268	0.408	0.296	0.376	0.357	0.466
	3	0.276	0.412	0.313	0.388	0.388	0.472

Table A.1.7. First-order elastic f_ℓ/f_b values, primary test suite, uniform vertical bending, specimens with $D/b_f = 2.75$ and $b_f/t_f = 15$.

D/t_w	d_o/D	$L_b/R = 0.05$		$L_b/R = 0.075$		$L_b/R = 0.10$	
		target $f_\ell/f_b = 0.35$	target $f_\ell/f_b = 0.50$	target $f_\ell/f_b = 0.35$	target $f_\ell/f_b = 0.50$	target $f_\ell/f_b = 0.35$	target $f_\ell/f_b = 0.50$
100	3[1]	0.272	0.425	0.306	0.358	0.285	0.414
130	3[1]	0.264	0.412	0.295	0.345	0.267	0.418
160	1	0.240	0.383	0.253	0.329	0.227	0.364
	2	0.247	0.398	0.258	0.332	0.250	0.385
	3	0.257	0.402	0.284	0.346	NA[2]	0.402

[1] $d_o/D = 2$ for $L_b/R = 0.10$ and target $f_\ell/f_b = 0.35$, since $L_b/D = 2$

[2] NA for $L_b/R = 0.10$ and target $f_\ell/f_b = 0.35$, since $L_b/D = 2$

Table A.1.8. First-order elastic f_t/f_b values, primary test suite, uniform vertical bending, specimens with $D/b_f = 2.75$ and $b_f/t_f = 20$.

D/t_w	d_o/D	$L_b/R = 0.05$		$L_b/R = 0.075$		$L_b/R = 0.10$	
		target $f_t/f_b = 0.35$	target $f_t/f_b = 0.50$	target $f_t/f_b = 0.35$	target $f_t/f_b = 0.50$	target $f_t/f_b = 0.35$	target $f_t/f_b = 0.50$
100	3[1]	0.293	0.446	0.322	0.411	0.352	0.465
130	3[1]	0.286	0.369	0.280	0.405	0.331	0.456
160	1	0.257	0.391	0.272	0.358	0.304	0.412
	2	0.268	0.422	0.277	0.378	0.324	0.410
	3	0.280	0.430	0.282	0.419	NA[2]	0.432

[1] $d_o/D = 2$ for $L_b/R = 0.10$ and target $f_t/f_b = 0.35$, since $L_b/D = 2$

[2] NA for $L_b/R = 0.10$ and target $f_t/f_b = 0.35$, since $L_b/D = 2$

Table A.1.9. First-order elastic f_t/f_b values, primary test suite, uniform vertical bending, specimens with $D/b_f = 2.75$ and $b_f/t_f = 25$.

D/t_w	d_o/D	$L_b/R = 0.05$		$L_b/R = 0.075$		$L_b/R = 0.10$	
		target $f_t/f_b = 0.35$	target $f_t/f_b = 0.50$	target $f_t/f_b = 0.35$	target $f_t/f_b = 0.50$	target $f_t/f_b = 0.35$	target $f_t/f_b = 0.50$
100	3[1]	0.310	0.443	0.350	0.411	0.381	0.500
130	3[1]	0.304	0.427	0.357	0.391	0.387	0.495
160	1	0.275	0.402	0.288	0.361	0.354	0.428
	2	0.285	0.410	0.330	0.395	0.378	0.467
	3	0.299	0.416	0.344	0.416	NA[2]	0.486

[1] $d_o/D = 2$ for $L_b/R = 0.10$ and target $f_t/f_b = 0.35$, since $L_b/D = 2$

[2] NA for $L_b/R = 0.10$ and target $f_t/f_b = 0.35$, since $L_b/D = 2$

Table A.1.10. First-order elastic f_t/f_b values, primary test suite, uniform vertical bending, specimens with $D/b_f = 3.25$ and $b_f/t_f = 25$.

D/t_w	d_o/D	$L_b/R = 0.05$		$L_b/R = 0.075$		$L_b/R = 0.10$	
		target $f_t/f_b = 0.35$	target $f_t/f_b = 0.50$	target $f_t/f_b = 0.35$	target $f_t/f_b = 0.50$	target $f_t/f_b = 0.35$	target $f_t/f_b = 0.50$
160	1	0.315	0.425	0.285	0.357	0.366	0.392
	2	0.331	0.437	0.295	0.398	0.419	0.437
	3	0.339	0.441	NA[1]	0.420	NA[2]	0.491

[1] NA for $L_b/R = 0.075$ and target $f_t/f_b = 0.35$, since $L_b/D = 2.5$

[2] NA for $L_b/R = 0.10$ and target $f_t/f_b = 0.35$, since $L_b/D = 2$

A.1.3 Vertical Bending Strengths from Full Nonlinear Analysis and Ratios of Design Strengths Based on Second-Order Elastic Stresses to these Capacities

Table A.1.11. Vertical bending strengths, primary test suite, full-nonlinear analysis and second-order elastic analysis with design checks, specimens with $D/b_f = 2.25$ and $b_f/t_f = 25$.

L_b/R	Target f_ℓ/f_b	D/t_w	d_o/D	FEA / M_y	FEA / M_p	Mod. LRFD / FEA	Rec.[1] Specs / FEA	Hanshin / FEA	Yoo w/ Approx M_ℓ / FEA	Yoo w/ Calc M_ℓ / FEA	1/3 Rule / FEA
0.05	0.35	100	3	0.90	0.81	0.97	0.66	0.83	0.83	0.84	0.88
		130	3	0.88	0.80	0.97	0.69	0.85	0.87	0.87	0.88
		160	1	0.88	0.82	0.94	0.69	0.86	0.87	0.88	0.85
			2	0.87	0.81	0.95	0.70	0.87	0.88	0.89	0.86
			3	0.85	0.79	0.97	0.71	0.88	0.90	0.90	0.88
	0.50	100	3	0.73	0.66	1.13	0.62	0.89	0.89	0.91	0.97
		130	3	0.72	0.66	1.16	0.64	0.92	0.92	0.94	1.00
		160	1	0.73	0.68	1.13	0.63	0.92	0.91	0.94	0.98
			2	0.71	0.66	1.16	0.65	0.94	0.94	0.96	1.01
			3	0.71	0.66	1.16	0.65	0.94	0.94	0.96	1.01
0.075	0.35	100	3	0.89	0.80	0.98	0.65	0.83	0.80	0.85	0.88
		130	3	0.86	0.79	0.99	0.68	0.87	0.84	0.89	0.90
		160	1	0.86	0.80	0.96	0.69	0.87	0.85	0.89	0.87
			2	0.83	0.77	0.99	0.71	0.89	0.88	0.91	0.90
			3	0.82	0.76	1.00	0.71	0.88	0.89	0.90	0.90
	0.50	100	3	0.84	0.76	1.04	0.62	0.80	0.79	0.82	0.90
		130	3	0.83	0.76	1.03	0.63	0.82	0.82	0.84	0.90
		160	1	0.83	0.77	0.99	0.64	0.84	0.82	0.86	0.88
			2	0.81	0.75	1.02	0.65	0.86	0.84	0.88	0.90
			3	0.80	0.74	1.03	0.65	0.85	0.85	0.87	0.90
0.10	0.35	100	3	0.86	0.78	1.01	0.64	0.80	0.83	0.82	0.89
		130	3	0.83	0.76	1.03	0.67	0.83	0.87	0.85	0.90
		160	1	0.85	0.79	0.97	0.67	0.85	0.86	0.87	0.87
			2	0.81	0.75	1.02	0.70	0.87	0.90	0.89	0.90
			3	0.81	0.75	1.02	0.69	0.86	0.90	0.88	0.90
	0.50	100	3	0.84	0.76	1.04	0.58	0.77	0.78	0.78	0.88
		130	3	0.81	0.74	1.05	0.61	0.79	0.82	0.81	0.90
		160	1	0.81	0.75	1.02	0.63	0.83	0.82	0.85	0.88
			2	0.80	0.74	1.03	0.62	0.82	0.83	0.84	0.89
			3	0.79	0.73	1.04	0.62	0.81	0.84	0.83	0.89
Average						1.03	0.66	0.85	0.86	0.87	0.90
Standard Deviation						0.06	0.03	0.04	0.04	0.04	0.04
High				0.91	0.82	1.16	0.71	0.94	0.94	0.96	1.01
Low				0.71	0.66	0.94	0.58	0.77	0.78	0.78	0.85

[1] Recommended Specification values are calculated based on first-order elastic stresses

Table A.1.12. Vertical bending strengths, primary test suite, full-nonlinear analysis and second-order elastic analysis with design checks, specimens with $D/b_f = 2.75$ and $b_f/t_f = 15$.

L_b/R	Target f_t/f_b	D/t_w	d_o/D	FEA / M_y	FEA / M_p	Mod. LRFD / FEA	Rec.[1] Specs / FEA	Hanshin / FEA	Yoo w/ Approx M_ℓ / FEA	Yoo w/ Calc M_ℓ / FEA	1/3 Rule / FEA
0.05	0.35	100	3	0.95	0.86	1.05	0.97	0.80	0.91	0.92	0.96
		130	3	0.92	0.84	1.09	1.00	0.83	0.94	0.95	0.99
		160	1	0.93	0.86	1.06	1.00	0.84	0.94	0.95	0.98
			2	0.92	0.85	1.08	1.00	0.84	0.95	0.96	0.99
			3	0.90	0.83	1.10	1.02	0.85	0.97	0.98	1.01
	0.50	100	3	0.85	0.74	1.02	1.01	0.80	0.95	0.97	0.89
		130	3	0.83	0.75	1.06	1.03	0.83	0.98	1.00	0.93
		160	1	0.84	0.77	1.04	1.02	0.84	0.98	1.00	0.92
			2	0.84	0.75	1.04	1.02	0.83	0.98	0.99	0.92
			3	0.82	0.75	1.06	1.05	0.85	1.00	1.02	0.94
0.075	0.35	100	3	0.93	0.84	1.08	0.98	0.79	0.91	0.92	0.97
		130	3	0.92	0.84	1.09	0.99	0.80	0.93	0.94	0.98
		160	1	0.90	0.83	1.10	1.02	0.85	0.95	0.98	1.01
			2	0.89	0.83	1.11	1.03	0.86	0.96	0.99	1.02
			3	0.88	0.82	1.12	1.04	0.84	0.97	0.98	1.02
	0.50	100	3	0.92	0.83	1.09	0.95	0.77	0.88	0.92	0.96
		130	3	0.90	0.82	1.11	0.97	0.79	0.91	0.94	0.99
		160	1	0.91	0.84	1.09	0.95	0.79	0.90	0.93	0.97
			2	0.88	0.81	1.13	0.99	0.82	0.93	0.97	1.01
			3	0.87	0.80	1.14	1.00	0.82	0.94	0.97	1.01
0.10	0.35	100	2	0.96	0.87	1.04	0.95	0.77	0.90	0.90	0.94
		130	2	0.92	0.84	1.09	1.00	0.82	0.94	0.95	0.99
		160	1	0.88	0.81	1.12	1.04	0.89	0.99	1.01	1.04
			2	0.87	0.81	1.14	1.06	0.88	1.00	1.01	1.04
	0.50	100	3	0.91	0.82	1.10	0.97	0.73	0.89	0.89	0.95
		130	3	0.89	0.82	1.12	0.99	0.76	0.92	0.92	0.98
		160	1	0.88	0.82	1.12	0.99	0.80	0.93	0.95	1.00
			2	0.88	0.82	1.12	0.99	0.79	0.93	0.94	0.99
			3	0.87	0.81	1.14	1.01	0.78	0.94	0.95	0.99
Average						1.09	1.00	0.82	0.94	0.96	0.98
Standard Deviation						0.03	0.03	0.04	0.03	0.03	0.04
High				0.96	0.87	1.14	1.06	0.89	1.00	1.02	1.04
Low				0.81	0.74	1.02	0.95	0.73	0.88	0.89	0.89

[1] Recommended Specification values are calculated based on first-order elastic stresses

Table A.1.13. Vertical bending strengths, primary test suite, full-nonlinear analysis and second-order elastic analysis with design checks, specimens with $D/b_f = 2.75$ and $b_f/t_f = 20$.

L_b/R	Target f_ℓ/f_b	D/t_w	d_o/D	$\frac{FEA}{M_y}$	$\frac{FEA}{M_p}$	$\frac{\text{Mod. LRFD}}{FEA}$	$\frac{\text{Rec}^{(1)}\ \text{Specs}}{FEA}$	$\frac{\text{Hanshin}}{FEA}$	$\frac{\text{Yoo w/ Approx } M_\ell}{FEA}$	$\frac{\text{Yoo w/ Calc } M_\ell}{FEA}$	$\frac{\text{1/3 Rule}}{FEA}$
0.05	0.35	100	3	0.90	0.80	1.08	0.67	0.82	0.83	0.84	0.97
		130	3	0.88	0.80	1.10	0.69	0.84	0.86	0.86	0.99
		160	1	0.89	0.82	1.06	0.69	0.85	0.86	0.87	0.97
			2	0.89	0.81	1.06	0.68	0.84	0.86	0.86	0.97
			3	0.85	0.78	1.11	0.71	0.87	0.90	0.89	1.01
	0.50	100	3	0.82	0.73	1.05	0.58	0.81	0.81	0.83	0.91
		130	3	0.82	0.74	1.06	0.60	0.82	0.82	0.84	0.92
		160	1	0.83	0.76	1.04	0.59	0.82	0.82	0.84	0.91
			2	0.81	0.74	1.06	0.59	0.84	0.84	0.86	0.93
			3	0.81	0.74	1.06	0.59	0.83	0.84	0.85	0.93
0.075	0.35	100	3	0.93	0.83	1.04	0.64	0.77	0.78	0.78	0.93
		130	3	0.91	0.83	1.06	0.66	0.78	0.81	0.80	0.94
		160	1	0.90	0.83	1.05	0.67	0.84	0.82	0.86	0.96
			2	0.89	0.82	1.06	0.68	0.84	0.83	0.85	0.96
			3	0.88	0.81	1.08	0.69	0.81	0.84	0.83	0.96
	0.50	100	3	0.91	0.81	1.06	0.57	0.75	0.73	0.77	0.93
		130	3	0.89	0.81	1.08	0.59	0.77	0.76	0.79	0.95
		160	1	0.89	0.82	1.06	0.60	0.78	0.77	0.80	0.94
			2	0.88	0.81	1.08	0.60	0.79	0.77	0.81	0.95
			3	0.88	0.81	1.08	0.59	0.76	0.77	0.77	0.93
0.10	0.35	100	2	0.92	0.82	1.05	0.65	0.77	0.81	0.79	0.94
		130	2	0.91	0.83	1.06	0.66	0.79	0.83	0.80	0.94
		160	1	0.91	0.84	1.04	0.67	0.81	0.84	0.82	0.94
			2	0.90	0.83	1.05	0.67	0.80	0.85	0.82	0.94
	0.50	100	3	0.88	0.78	1.10	0.57	0.74	0.76	0.75	0.94
		130	3	0.87	0.79	1.11	0.58	0.74	0.78	0.76	0.95
		160	1	0.87	0.80	1.09	0.60	0.78	0.78	0.80	0.95
			2	0.86	0.79	1.10	0.60	0.77	0.79	0.79	0.95
			3	0.85	0.78	1.11	0.60	0.76	0.80	0.78	0.95
Average						1.07	0.63	0.80	0.81	0.82	0.95
Standard Deviation						0.02	0.04	0.04	0.04	0.04	0.02
High				0.93	0.84	1.11	0.71	0.87	0.90	0.89	1.01
Low				0.82	0.75	1.04	0.56	0.74	0.73	0.75	0.91

(1) Recommended Specification values are calculated based on first-order elastic stresses

Table A.1.14. Vertical bending strengths, primary test suite, full-nonlinear analysis and second-order elastic analysis with design checks, specimens with $D/b_f = 2.75$ and $b_f/t_f = 25$.

L_b/R	Target f_ℓ/f_b	D/t_w	d_c/D	FEA / M_y	FEA / M_p	Mod. LRFD / FEA	Rec.[1] Specs / FEA	Hanshin / FEA	Yoo w/ Approx M_ℓ / FEA	Yoo w/ Calc M_ℓ / FEA	1/3 Rule / FEA
0.05	0.35	100	3	0.88	0.77	0.99	0.68	0.83	0.84	0.84	0.89
		130	3	0.86	0.77	0.99	0.70	0.85	0.87	0.86	0.89
		160	1	0.88	0.80	0.93	0.69	0.84	0.86	0.86	0.84
			2	0.86	0.78	0.95	0.70	0.85	0.88	0.86	0.85
			3	0.85	0.77	0.96	0.71	0.85	0.89	0.87	0.86
	0.50	100	3	0.77	0.68	1.10	0.62	0.84	0.85	0.86	0.94
		130	3	0.75	0.67	1.14	0.64	0.88	0.89	0.89	0.98
		160	1	0.75	0.68	1.09	0.65	0.89	0.90	0.91	0.95
			2	0.74	0.67	1.11	0.65	0.90	0.91	0.92	0.96
			3	0.76	0.69	1.08	0.63	0.87	0.89	0.89	0.93
0.075	0.35	100	3	0.84	0.74	1.04	0.70	0.85	0.85	0.87	0.92
		130	3	0.82	0.74	1.04	0.71	0.87	0.89	0.89	0.92
		160	1	0.83	0.76	0.99	0.73	0.91	0.88	0.93	0.90
			2	0.81	0.74	1.01	0.73	0.91	0.91	0.93	0.91
			3	0.79	0.72	1.04	0.74	0.90	0.93	0.92	0.92
	0.50	100	3	0.84	0.74	1.04	0.62	0.81	0.78	0.83	0.90
		130	3	0.82	0.74	1.04	0.64	0.84	0.81	0.86	0.91
		160	1	0.82	0.74	1.00	0.65	0.85	0.82	0.87	0.88
			2	0.80	0.73	1.02	0.66	0.85	0.84	0.87	0.89
			3	0.80	0.73	1.02	0.65	0.83	0.84	0.85	0.89
0.10	0.35	100	2	0.89	0.78	0.98	0.66	0.78	0.83	0.79	0.86
		130	2	0.85	0.76	1.00	0.69	0.81	0.88	0.82	0.88
		160	1	0.82	0.75	1.00	0.72	0.86	0.92	0.87	0.88
			2	0.80	0.73	1.02	0.73	0.86	0.94	0.88	0.90
	0.50	100	3	0.82	0.72	1.06	0.61	0.77	0.80	0.79	0.90
		130	3	0.79	0.71	1.08	0.63	0.80	0.84	0.81	0.91
		160	1	0.80	0.73	1.02	0.64	0.82	0.84	0.84	0.88
			2	0.79	0.72	1.04	0.64	0.80	0.85	0.82	0.88
			3	0.78	0.71	1.05	0.64	0.80	0.86	0.82	0.89
Average						1.03	0.67	0.85	0.87	0.86	0.90
Standard Deviation						0.05	0.04	0.04	0.04	0.04	0.03
High				0.89	0.80	1.14	0.74	0.91	0.94	0.93	0.98
Low				0.74	0.67	0.93	0.61	0.77	0.78	0.79	0.84

[1] Recommended Specification values are calculated based on first-order elastic stresses

Table A.1.15. Vertical bending strengths, primary test suite, full-nonlinear analysis and second-order elastic analysis with design checks, specimens with $D/b_f = 3.25$ and $b_f/t_f = 25$.

L_b/R	Target f_ℓ/f_b	D/t_w	d_o/D	$\frac{FEA}{M_y}$	$\frac{FEA}{M_p}$	$\frac{Mod.\ LRFD}{FEA}$	$\frac{Rec.^{(1)}\ Specs}{FEA}$	$\frac{Hanshin}{FEA}$	$\frac{Yoo\ w/\ Approx\ M_\ell}{FEA}$	$\frac{Yoo\ w/\ Calc\ M_\ell}{FEA}$	$\frac{1/3\ Rule}{FEA}$
0.05	0.35	160	1	0.83	0.74	0.98	0.74	0.88	0.92	0.90	0.88
			2	0.81	0.72	1.01	0.75	0.89	0.95	0.90	0.90
			3	0.78	0.70	1.05	0.78	0.92	0.98	0.93	0.93
	0.50	160	1	0.74	0.66	1.10	0.65	0.88	0.90	0.90	0.95
			2	0.74	0.66	1.10	0.65	0.88	0.89	0.89	0.94
			3	0.74	0.66	1.10	0.65	0.87	0.90	0.89	0.94
0.075	0.35	160	1	0.80	0.71	1.02	0.76	0.95	0.90	0.97	0.93
			2	0.77	0.69	1.06	0.78	0.98	0.94	1.00	0.96
	0.50	160	1	0.80	0.71	1.02	0.69	0.88	0.86	0.90	0.91
			2	0.79	0.70	1.03	0.69	0.85	0.87	0.87	0.90
			3	0.77	0.69	1.06	0.70	0.88	0.89	0.90	0.92
0.10	0.35	160	1	0.78	0.69	1.05	0.73	0.89	0.91	0.91	0.92
			2	0.75	0.67	1.09	0.74	0.92	0.95	0.94	0.95
	0.50	160	1	0.75	0.67	1.09	0.66	0.93	0.83	0.95	0.96
			2	0.73	0.65	1.12	0.67	0.93	0.85	0.95	0.98
			3	0.73	0.65	1.12	0.65	0.89	0.85	0.92	0.96
Average						1.06	0.71	0.90	0.90	0.92	0.93
Standard Deviation						0.04	0.05	0.03	0.04	0.03	0.03
High				0.83	0.74	1.12	0.80	0.98	0.98	1.00	0.98
Low				0.73	0.65	0.98	0.65	0.85	0.83	0.87	0.88

(1) Recommended Specification values are calculated based on first-order elastic stresses

A.1.4 Vertical Bending Strengths from Full Nonlinear Analysis and Ratios of Design Strengths Based on the First-Order Elastic f_ℓ / f_b to these Capacities

Table A.1.16. Vertical bending strengths, primary test suite, full-nonlinear analysis and first-order elastic analysis with design checks, specimens with $D/b_f = 2.25$ and $b_f/t_f = 25$.

L_b/R	Target f_ℓ/f_b	D/t_w	d_o/D	FEA / M_y	FEA / M_p	Mod. LRFD / FEA	Rec. Specs / FEA	Hanshin / FEA	Yoo w/ Approx M_ℓ / FEA	Yoo w/ Calc M_ℓ / FEA	1/3 Rule / FEA
0.05	0.35	100	3	0.90	0.81	0.97	0.66	0.84	0.83	0.86	0.88
		130	3	0.88	0.80	0.97	0.69	0.87	0.87	0.89	0.89
		160	1	0.88	0.82	0.94	0.69	0.88	0.87	0.90	0.86
			2	0.87	0.81	0.95	0.70	0.89	0.88	0.91	0.87
			3	0.85	0.79	0.97	0.71	0.91	0.90	0.93	0.89
	0.50	100	3	0.73	0.66	1.13	0.62	0.93	0.89	0.95	0.99
		130	3	0.72	0.66	1.16	0.64	0.96	0.92	0.98	1.02
		160	1	0.73	0.68	1.13	0.63	0.95	0.91	0.97	0.99
			2	0.71	0.66	1.16	0.65	0.98	0.94	1.00	1.02
			3	0.71	0.66	1.16	0.65	0.98	0.94	1.00	1.02
0.075	0.35	100	3	0.89	0.80	0.98	0.65	0.84	0.80	0.86	0.89
		130	3	0.86	0.79	0.99	0.68	0.88	0.84	0.90	0.90
		160	1	0.86	0.80	0.96	0.69	0.89	0.85	0.91	0.88
			2	0.83	0.77	0.99	0.71	0.91	0.88	0.93	0.90
			3	0.82	0.76	1.00	0.71	0.91	0.89	0.93	0.91
	0.50	100	3	0.84	0.76	1.04	0.62	0.83	0.79	0.85	0.91
		130	3	0.83	0.76	1.03	0.63	0.84	0.82	0.86	0.91
		160	1	0.83	0.77	0.99	0.64	0.87	0.82	0.89	0.89
			2	0.81	0.75	1.02	0.65	0.88	0.84	0.90	0.90
			3	0.80	0.74	1.03	0.65	0.88	0.85	0.90	0.91
0.10	0.35	100	3	0.86	0.78	1.01	0.64	0.81	0.83	0.83	0.89
		130	3	0.83	0.76	1.03	0.67	0.85	0.87	0.87	0.91
		160	1	0.85	0.79	0.97	0.67	0.87	0.86	0.89	0.87
			2	0.81	0.75	1.02	0.70	0.89	0.90	0.91	0.91
			3	0.81	0.75	1.02	0.69	0.87	0.90	0.89	0.90
	0.50	100	3	0.84	0.76	1.04	0.58	0.79	0.78	0.80	0.89
		130	3	0.81	0.74	1.05	0.61	0.82	0.82	0.84	0.91
		160	1	0.81	0.75	1.02	0.63	0.86	0.82	0.88	0.90
			2	0.80	0.74	1.03	0.62	0.83	0.83	0.85	0.89
			3	0.79	0.73	1.04	0.62	0.84	0.84	0.86	0.90
Average						1.03	0.66	0.88	0.86	0.90	0.91
Standard Deviation						0.06	0.03	0.05	0.04	0.05	0.05
High				0.91	0.82	1.16	0.71	0.98	0.94	1.00	1.02
Low				0.71	0.66	0.94	0.58	0.79	0.78	0.80	0.86

Table A.1.17. Vertical bending strengths, primary test suite, full-nonlinear analysis and first-order elastic analysis with design checks, specimens with $D/b_f = 2.75$ and $b_f/t_f = 15$.

L_b/R	Target f_ℓ/f_b	D/t_w	d_o/D	$\frac{FEA}{M_y}$	$\frac{FEA}{M_p}$	$\frac{\text{Mod. LRFD}}{FEA}$	$\frac{\text{Rec. Specs}}{FEA}$	$\frac{\text{Hanshin}}{FEA}$	$\frac{\text{Yoo w/ Approx } M_\ell}{FEA}$	$\frac{\text{Yoo w/ Calc } M_\ell}{FEA}$	$\frac{\text{1/3 Rule}}{FEA}$
0.05	0.35	100	3	0.95	0.86	1.05	0.97	0.81	0.91	0.93	0.97
		130	3	0.92	0.84	1.09	1.00	0.84	0.94	0.96	1.00
		160	1	0.93	0.86	1.06	1.00	0.85	0.94	0.96	0.99
			2	0.92	0.85	1.08	1.00	0.85	0.95	0.97	0.99
			3	0.90	0.83	1.10	1.02	0.87	0.97	0.99	1.01
	0.50	100	3	0.85	0.74	1.02	1.01	0.81	0.95	0.97	0.89
		130	3	0.83	0.75	1.06	1.03	0.83	0.98	1.00	0.93
		160	1	0.84	0.77	1.04	1.02	0.84	0.98	1.00	0.92
			2	0.84	0.75	1.04	1.02	0.83	0.98	1.00	0.92
			3	0.82	0.75	1.06	1.05	0.85	1.00	1.02	0.94
0.075	0.35	100	3	0.93	0.84	1.08	0.98	0.81	0.91	0.93	0.98
		130	3	0.92	0.84	1.09	0.99	0.82	0.93	0.95	0.99
		160	1	0.90	0.83	1.10	1.02	0.87	0.95	0.99	1.01
			2	0.89	0.83	1.11	1.03	0.87	0.96	1.00	1.02
			3	0.88	0.82	1.12	1.04	0.86	0.97	1.00	1.03
	0.50	100	3	0.92	0.83	1.09	0.95	0.78	0.88	0.92	0.97
		130	3	0.90	0.82	1.11	0.97	0.81	0.91	0.95	1.00
		160	1	0.91	0.84	1.09	0.95	0.81	0.90	0.95	0.98
			2	0.88	0.81	1.13	0.99	0.83	0.93	0.98	1.02
			3	0.87	0.80	1.14	1.00	0.83	0.94	0.98	1.02
0.10	0.35	100	2	0.96	0.87	1.04	0.95	0.79	0.90	0.91	0.95
		130	2	0.92	0.84	1.09	1.00	0.84	0.94	0.96	1.00
		160	1	0.88	0.81	1.12	1.04	0.91	0.99	1.02	1.05
			2	0.87	0.81	1.14	1.06	0.90	1.00	1.02	1.05
	0.50	100	3	0.91	0.82	1.10	0.97	0.76	0.89	0.91	0.97
		130	3	0.89	0.82	1.12	0.99	0.78	0.92	0.93	0.99
		160	1	0.88	0.82	1.12	0.99	0.81	0.93	0.96	1.00
			2	0.88	0.82	1.12	0.99	0.80	0.93	0.96	1.00
			3	0.87	0.81	1.14	1.01	0.80	0.94	0.96	1.00
Average						1.09	1.00	0.83	0.94	0.97	0.99
Standard Deviation						0.03	0.03	0.04	0.03	0.03	0.04
High				0.96	0.87	1.14	1.06	0.91	1.00	1.02	1.05
Low				0.81	0.74	1.02	0.95	0.76	0.88	0.91	0.89

Table A.1.18. Vertical bending strengths, primary test suite, full-nonlinear analysis and first-order elastic analysis with design checks, specimens with $D/b_f = 2.75$ and $b_f/t_f = 20$.

L_b/R	Target f_t/f_b	D/t_w	d_o/D	$\frac{FEA}{M_y}$	$\frac{FEA}{M_p}$	$\frac{Mod.\ LRFD}{FEA}$	$\frac{Rec.\ Specs}{FEA}$	$\frac{Hanshin}{FEA}$	$\frac{Yoo\ w/\ Approx\ M_\ell}{FEA}$	$\frac{Yoo\ w/\ Calc\ M_\ell}{FEA}$	$\frac{1/3\ Rule}{FEA}$
0.05	0.35	100	3	0.90	0.80	1.08	0.67	0.84	0.83	0.86	0.98
		130	3	0.88	0.80	1.10	0.69	0.87	0.86	0.88	1.00
		160	1	0.89	0.82	1.06	0.69	0.88	0.86	0.89	0.98
			2	0.89	0.81	1.06	0.68	0.87	0.86	0.89	0.98
			3	0.85	0.78	1.11	0.71	0.90	0.90	0.92	1.02
	0.50	100	3	0.82	0.73	1.05	0.56	0.82	0.81	0.84	0.91
		130	3	0.82	0.74	1.06	0.60	0.87	0.82	0.89	0.94
		160	1	0.83	0.76	1.04	0.59	0.85	0.82	0.87	0.92
			2	0.81	0.74	1.06	0.59	0.85	0.84	0.87	0.93
			3	0.81	0.74	1.06	0.59	0.84	0.84	0.86	0.93
0.075	0.35	100	3	0.93	0.83	1.04	0.64	0.80	0.78	0.81	0.94
		130	3	0.91	0.83	1.06	0.66	0.84	0.81	0.86	0.97
		160	1	0.90	0.83	1.05	0.67	0.85	0.82	0.87	0.96
			2	0.89	0.82	1.06	0.68	0.86	0.83	0.88	0.97
			3	0.88	0.81	1.08	0.69	0.87	0.84	0.89	0.98
	0.50	100	3	0.91	0.81	1.06	0.57	0.76	0.73	0.78	0.94
		130	3	0.89	0.81	1.08	0.59	0.78	0.76	0.80	0.95
		160	1	0.89	0.82	1.06	0.60	0.81	0.77	0.83	0.95
			2	0.88	0.81	1.08	0.60	0.80	0.77	0.82	0.96
			3	0.88	0.81	1.08	0.59	0.78	0.77	0.80	0.94
0.10	0.35	100	2	0.92	0.82	1.05	0.65	0.79	0.81	0.80	0.94
		130	2	0.91	0.83	1.06	0.66	0.81	0.83	0.83	0.95
		160	1	0.91	0.84	1.04	0.67	0.83	0.84	0.84	0.95
			2	0.90	0.83	1.05	0.67	0.82	0.85	0.84	0.95
	0.50	100	3	0.88	0.78	1.10	0.57	0.76	0.76	0.78	0.95
		130	3	0.87	0.79	1.11	0.58	0.77	0.78	0.79	0.96
		160	1	0.87	0.80	1.09	0.60	0.80	0.78	0.81	0.96
			2	0.86	0.79	1.10	0.60	0.81	0.79	0.82	0.97
			3	0.85	0.78	1.11	0.60	0.80	0.80	0.82	0.97
Average						1.07	0.63	0.82	0.81	0.84	0.96
Standard Deviation						0.02	0.04	0.04	0.04	0.04	0.02
High				0.93	0.84	1.11	0.71	0.90	0.90	0.92	1.02
Low				0.82	0.75	1.04	0.56	0.76	0.73	0.78	0.91

Table A.1.19. Vertical bending strengths, primary test suite, full-nonlinear analysis and first-order elastic analysis with design checks, specimens with $D/b_f = 2.75$ and $b_f/t_f = 25$.

L_b/R	Target f_ℓ/f_b	D/t_w	d_o/D	FEA / M_y	FEA / M_p	Mod. LRFD / FEA	Rec. Specs / FEA	Hanshin / FEA	Yoo w/ Approx M_ℓ / FEA	Yoo w/ Calc M_ℓ / FEA	1/3 Rule / FEA
0.05	0.35	100	3	0.88	0.77	0.99	0.68	0.85	0.84	0.87	0.90
		130	3	0.86	0.77	0.99	0.70	0.87	0.87	0.89	0.90
		160	1	0.88	0.80	0.93	0.69	0.87	0.86	0.89	0.85
			2	0.86	0.78	0.95	0.70	0.89	0.88	0.90	0.87
			3	0.85	0.77	0.96	0.71	0.89	0.89	0.91	0.88
	0.50	100	3	0.77	0.68	1.10	0.62	0.88	0.85	0.90	0.96
		130	3	0.75	0.67	1.14	0.64	0.91	0.89	0.93	0.99
		160	1	0.75	0.68	1.09	0.65	0.93	0.90	0.95	0.97
			2	0.74	0.67	1.11	0.65	0.94	0.91	0.96	0.98
			3	0.76	0.69	1.08	0.63	0.91	0.89	0.93	0.95
0.075	0.35	100	3	0.84	0.74	1.04	0.70	0.86	0.85	0.88	0.93
		130	3	0.82	0.74	1.04	0.71	0.88	0.89	0.90	0.93
		160	1	0.83	0.76	0.99	0.73	0.91	0.88	0.94	0.90
			2	0.81	0.74	1.01	0.73	0.91	0.91	0.93	0.91
			3	0.79	0.72	1.04	0.74	0.92	0.93	0.94	0.93
	0.50	100	3	0.84	0.74	1.04	0.62	0.82	0.78	0.84	0.91
		130	3	0.82	0.74	1.04	0.64	0.86	0.81	0.88	0.92
		160	1	0.82	0.74	1.00	0.65	0.87	0.82	0.90	0.89
			2	0.80	0.73	1.02	0.66	0.87	0.84	0.90	0.91
			3	0.80	0.73	1.02	0.65	0.86	0.84	0.88	0.90
0.10	0.35	100	2	0.89	0.78	0.98	0.66	0.80	0.83	0.81	0.87
		130	2	0.85	0.76	1.00	0.69	0.83	0.88	0.85	0.89
		160	1	0.82	0.75	1.00	0.72	0.88	0.92	0.90	0.90
			2	0.80	0.73	1.02	0.73	0.89	0.94	0.91	0.91
	0.50	100	3	0.82	0.72	1.06	0.61	0.80	0.80	0.81	0.91
		130	3	0.79	0.71	1.08	0.63	0.83	0.84	0.85	0.93
		160	1	0.80	0.73	1.02	0.64	0.86	0.84	0.88	0.90
			2	0.79	0.72	1.04	0.64	0.84	0.85	0.86	0.90
			3	0.78	0.71	1.05	0.64	0.84	0.86	0.86	0.91
Average						1.03	0.67	0.87	0.87	0.89	0.91
Standard Deviation						0.05	0.04	0.04	0.04	0.04	0.03
High				0.89	0.80	1.14	0.74	0.94	0.94	0.96	0.99
Low				0.74	0.67	0.93	0.61	0.80	0.78	0.81	0.85

Table A.1.20. Vertical bending strengths, primary test suite, full-nonlinear analysis and first-order elastic analysis with design checks, specimens with $D/b_f = 3.25$ and $b_f/t_f = 25$.

L_b/R	Target f_t/f_b	D/t_w	d_o/D	FEA / M_y	FEA / M_p	Mod. LRFD / FEA	Rec. Specs / FEA	Hanshin / FEA	Yoo w/ Approx M_ℓ / FEA	Yoo w/ Calc M_ℓ / FEA	1/3 Rule / FEA
0.05	0.35	160	1	0.83	0.74	0.98	0.74	0.90	0.92	0.92	0.89
			2	0.81	0.72	1.01	0.75	0.91	0.95	0.93	0.91
			3	0.78	0.70	1.05	0.78	0.94	0.98	0.96	0.94
	0.50	160	1	0.74	0.66	1.10	0.65	0.93	0.90	0.95	0.97
			2	0.74	0.66	1.10	0.65	0.92	0.89	0.94	0.96
			3	0.74	0.66	1.10	0.65	0.92	0.90	0.94	0.96
0.075	0.35	160	1	0.80	0.71	1.02	0.76	0.95	0.90	0.97	0.93
			2	0.77	0.69	1.06	0.78	0.98	0.94	1.00	0.97
	0.50	160	1	0.80	0.71	1.02	0.69	0.90	0.86	0.92	0.91
			2	0.79	0.70	1.03	0.69	0.88	0.87	0.91	0.91
			3	0.77	0.69	1.06	0.70	0.89	0.89	0.91	0.93
0.10	0.35	160	1	0.78	0.69	1.05	0.73	0.92	0.91	0.94	0.93
			2	0.75	0.67	1.09	0.74	0.92	0.95	0.94	0.96
	0.50	160	1	0.75	0.67	1.09	0.66	0.93	0.83	0.96	0.96
			2	0.73	0.65	1.12	0.67	0.93	0.85	0.95	0.98
			3	0.73	0.65	1.12	0.65	0.90	0.85	0.92	0.96
Average						1.06	0.71	0.92	0.90	0.94	0.94
Standard Deviation						0.04	0.05	0.03	0.03	0.02	0.03
High				0.83	0.74	1.12	0.78	0.98	0.98	1.00	0.98
Low				0.73	0.65	0.98	0.65	0.88	0.83	0.91	0.89

A.2 MODIFIED UNIFORM VERTICAL BENDING SUITE

A.2.1 Second-Order Elastic f/F_y and f_b/F_y Values at the One-Third Rule Strength Limit

Table A.2.1. Second-order elastic f_ℓ/F_y and f_b/F_y values at the one-third rule strength limit, modified uniform vertical bending suite, specimens with target $f_\ell/f_b = 0.50$.

D/b_f	b_f/t_f	D/t_w	d_o/D		$L_b/R = 0.05$	$L_b/R = 0.10$
2.25	25	100	3	f_ℓ/F_y f_b/F_y	0.435 0.687	0.429 0.730
		130	3	f_ℓ/F_y f_b/F_y	0.468 0.685	0.416 0.715
		160	1	f_ℓ/F_y f_b/F_y	0.415 0.686	0.373 0.692
			2	f_ℓ/F_y f_b/F_y	0.437 0.680	0.382 0.698
			3	f_ℓ/F_y f_b/F_y	0.461 0.671	0.396 0.692
2.75	15	100	3	f_ℓ/F_y f_b/F_y	0.409 0.734	0.483 0.843
		130	3	f_ℓ/F_y f_b/F_y	0.414 0.738	0.476 0.841
		160	1	f_ℓ/F_y f_b/F_y	0.375 0.747	0.454 0.841
			2	f_ℓ/F_y f_b/F_y	0.420 0.736	0.462 0.838
			3	f_ℓ/F_y f_b/F_y	0.427 0.728	0.472 0.835
	20	100	3	f_ℓ/F_y f_b/F_y	0.456 0.706	0.523 0.796
		130	3	f_ℓ/F_y f_b/F_y	0.468 0.712	0.518 0.793
		160	1	f_ℓ/F_y f_b/F_y	0.424 0.722	0.478 0.790
			2	f_ℓ/F_y f_b/F_y	0.439 0.717	0.481 0.789
			3	f_ℓ/F_y f_b/F_y	0.475 0.701	0.512 0.779
	25	100	3	f_ℓ/F_y f_b/F_y	0.457 0.696	0.499 0.707
		130	3	f_ℓ/F_y f_b/F_y	0.451 0.698	0.495 0.688
		160	1	f_ℓ/F_y f_b/F_y	0.435 0.668	0.449 0.673
			2	f_ℓ/F_y f_b/F_y	0.453 0.675	0.455 0.673
			3	f_ℓ/F_y f_b/F_y	0.457 0.669	0.480 0.663

Table A.2.1. Second-order elastic f_t/F_y and f_b/F_y values at the one-third rule strength limit, modified uniform vertical bending suite, specimens with target $f_t/f_b = 0.50$ (continued).

D/b_f	b_f/t_f	D/t_w	d_o/D		$L_b/R = 0.05$	$L_b/R = 0.10$
3.25	25	160	1	f_t/F_y	0.424	0.449
				f_b/F_y	0.678	0.670
			2	f_t/F_y	0.445	0.452
				f_b/F_y	0.673	0.669
			3	f_t/F_y	0.450	0.455
				f_b/F_y	0.672	0.668

A.2.2 First-Order Elastic f/f_b Values

Table A.2.2. First-order elastic f_t/f_b values, modified uniform vertical bending suite, specimens with target $f_t/f_b = 0.50$.

D/b_f	b_f/t_f	D/t_w	d_o/D	$L_b/R = 0.05$	$L_b/R = 0.10$
2.25	25	100	3	0.559	0.546
		130	3	0.601	0.530
		160	1	0.532	0.449
			2	0.565	0.522
			3	0.554	0.531
2.75	15	100	3	0.522	0.540
		130	3	0.537	0.524
		160	1	0.468	0.442
			2	0.517	0.484
			3	0.521	0.509
	20	100	3	0.633	0.598
		130	3	0.537	0.582
		160	1	0.548	0.520
			2	0.557	0.538
			3	0.634	0.576
	25	100	3	0.624	0.651
		130	3	0.610	0.645
		160	1	0.555	0.562
			2	0.601	0.588
			3	0.654	0.633
3.25	25	160	1	0.530	0.554
			2	0.559	0.564
			3	0.581	0.568

A.2.3 Vertical Bending Strengths from Full Nonlinear Analysis and Ratios of Design Strengths Based on Second-Order Elastic Stresses to these Capacities

Table A.2.3. Vertical bending strengths, modified uniform vertical bending suite, full-nonlinear analysis and second-order elastic analysis with design checks, specimens with target $f_\ell/f_b = 0.50$ and $L_b/R = 0.05$.

D/b_f	b_f/t_f	D/t_w	d_o/D	$\frac{FEA}{M_y}$	$\frac{FEA}{M_p}$	$\frac{Mod.\ LRFD}{FEA}$	$\frac{Rec.^{(1)}\ Specs}{FEA}$	$\frac{Hanshin}{FEA}$	$\frac{Yoo\ w/\ Approx\ M_\ell}{FEA}$	$\frac{Yoo\ w/\ Calc\ M_\ell}{FEA}$	$\frac{1/3\ Rule}{FEA}$
2.25	25	100	3	0.68	0.61	1.23	0.63	0.89	0.97	0.91	1.01
		130	3	0.66	0.60	1.27	0.64	0.88	1.00	0.90	1.03
		160	1	0.68	0.64	1.21	0.64	0.90	0.98	0.92	1.01
			2	0.67	0.62	1.23	0.64	0.89	1.00	0.91	1.01
			3	0.66	0.61	1.25	0.65	0.88	1.01	0.90	1.02
2.75	15	100	3	0.75	0.68	1.16	1.13	0.84	1.08	1.05	0.98
		130	3	0.74	0.68	1.18	1.15	0.85	1.10	1.06	1.00
		160	1	0.75	0.70	1.16	1.14	0.87	1.09	1.07	1.00
			2	0.76	0.70	1.15	1.12	0.82	1.08	1.03	0.96
			3	0.73	0.68	1.19	1.17	0.85	1.12	1.06	1.00
	20	100	3	0.75	0.67	1.14	0.58	0.79	0.89	0.81	0.94
		130	3	0.73	0.66	1.19	0.62	0.81	0.92	0.83	0.97
		160	1	0.75	0.69	1.15	0.60	0.82	0.91	0.84	0.96
			2	0.74	0.68	1.16	0.61	0.82	0.92	0.84	0.97
			3	0.72	0.66	1.20	0.60	0.81	0.95	0.83	0.98
	25	100	3	0.72	0.63	1.18	0.61	0.82	0.91	0.84	0.97
		130	3	0.68	0.61	1.25	0.65	0.88	0.98	0.89	1.03
		160	1	0.70	0.64	1.17	0.64	0.85	0.96	0.86	0.96
			2	0.68	0.62	1.20	0.65	0.86	0.99	0.88	0.99
			3	0.67	0.61	1.22	0.64	0.87	1.01	0.89	1.00
3.25	25	160	1	0.71	0.63	1.15	0.65	0.85	0.93	0.87	0.95
			2	0.73	0.65	1.12	0.62	0.81	0.91	0.83	0.92
			3	0.71	0.63	1.16	0.64	0.84	0.94	0.85	0.95
Average						1.19	0.74	0.85	0.98	0.91	0.98
Standard Deviation						0.04	0.22	0.03	0.07	0.08	0.03
High				0.76	0.71	1.27	1.17	0.90	1.12	1.07	1.03
Low				0.67	0.61	1.12	0.58	0.79	0.89	0.81	0.92

(1) Recommended Specification values are calculated based on first-order elastic stresses

Table A.2.4. Vertical bending strengths, modified uniform vertical bending suite, full-nonlinear analysis and second-order elastic analysis with design checks, specimens with target $f_\ell/f_b = 0.50$ and $L_b/R = 0.10$.

D/b_f	b_f/t_f	D/t_w	d_o/D	FEA / M_y	FEA / M_p	Mod. LRFD / FEA	Rec.[1] Specs / FEA	Hanshin / FEA	Yoo w/ Approx M_ℓ / FEA	Yoo w/ Calc M_ℓ / FEA	1/3 Rule / FEA
2.25	25	100	3	0.76	0.69	1.15	0.62	0.81	0.86	0.83	0.96
		130	3	0.76	0.70	1.12	0.63	0.81	0.87	0.83	0.94
		160	1	0.77	0.71	1.07	0.64	0.83	0.87	0.84	0.91
			2	0.75	0.70	1.10	0.64	0.84	0.89	0.86	0.93
			3	0.74	0.69	1.11	0.65	0.84	0.90	0.86	0.94
2.75	15	100	3	0.84	0.76	1.19	1.01	0.74	0.96	0.93	1.00
		130	3	0.82	0.75	1.22	1.04	0.76	0.99	0.95	1.03
		160	1	0.86	0.80	1.15	1.01	0.74	0.95	0.92	0.98
			2	0.82	0.76	1.21	1.05	0.77	1.00	0.96	1.02
			3	0.81	0.75	1.22	1.06	0.77	1.01	0.97	1.03
	20	100	3	0.78	0.70	1.24	0.61	0.76	0.85	0.77	1.02
		130	3	0.76	0.69	1.27	0.63	0.78	0.89	0.80	1.04
		160	1	0.79	0.73	1.20	0.62	0.77	0.86	0.79	1.00
			2	0.77	0.71	1.23	0.64	0.79	0.89	0.81	1.02
			3	0.77	0.71	1.23	0.62	0.77	0.89	0.78	1.01
	25	100	3	0.73	0.64	1.19	0.64	0.79	0.89	0.80	0.97
		130	3	0.73	0.66	1.17	0.64	0.78	0.91	0.80	0.94
		160	1	0.72	0.66	1.14	0.67	0.82	0.94	0.83	0.93
			2	0.71	0.65	1.15	0.67	0.82	0.95	0.84	0.94
			3	0.69	0.63	1.19	0.68	0.83	0.98	0.84	0.96
3.25	25	160	1	0.76	0.68	1.07	0.61	0.77	0.82	0.79	0.88
			2	0.76	0.68	1.07	0.60	0.77	0.82	0.79	0.88
			3	0.76	0.68	1.07	0.60	0.77	0.82	0.78	0.88
Average						1.17	0.72	0.79	0.90	0.84	0.97
Standard Deviation						0.06	0.17	0.03	0.06	0.07	0.05
High				0.86	0.79	1.27	1.06	0.84	1.01	0.97	1.04
Low				0.69	0.62	1.07	0.60	0.74	0.82	0.77	0.88

[1] Recommended Specification values are calculated based on first-order elastic stresses

A.2.4 Vertical Bending Strengths from Full Nonlinear Analysis and Ratios of Design Strengths Based on the First-Order Elastic f_ℓ/f_b to these Capacities

Table A.2.5. Vertical bending strengths, modified uniform vertical bending suite, full-nonlinear analysis and first-order elastic analysis with design checks, specimens with target $f_\ell/f_b = 0.50$ and $L_b/R = 0.05$.

D/b_f	b_f/t_f	D/t_w	d_o/D	$\frac{FEA}{M_y}$	$\frac{FEA}{M_p}$	$\frac{Mod.\ LRFD}{FEA}$	$\frac{Rec.\ Specs}{FEA}$	$\frac{Hanshin}{FEA}$	$\frac{Yoo\ w/\ Approx\ M_\ell}{FEA}$	$\frac{Yoo\ w/\ Calc\ M_\ell}{FEA}$	$\frac{1/3\ Rule}{FEA}$
2.25	25	100	3	0.68	0.61	1.23	0.63	0.93	0.97	0.95	1.03
		130	3	0.66	0.60	1.27	0.64	0.93	1.00	0.95	1.06
		160	1	0.68	0.64	1.21	0.64	0.94	0.98	0.96	1.03
			2	0.67	0.62	1.23	0.64	0.93	1.00	0.95	1.04
			3	0.66	0.61	1.25	0.65	0.96	1.01	0.98	1.06
2.75	15	100	3	0.75	0.68	1.16	1.13	0.85	1.08	1.05	0.98
		130	3	0.74	0.68	1.18	1.15	0.86	1.10	1.07	1.00
		160	1	0.75	0.70	1.16	1.14	0.89	1.09	1.08	1.01
			2	0.76	0.70	1.15	1.12	0.85	1.08	1.05	0.98
			3	0.73	0.68	1.19	1.17	0.88	1.12	1.09	1.02
	20	100	3	0.75	0.67	1.14	0.58	0.80	0.89	0.82	0.94
		130	3	0.73	0.66	1.19	0.62	0.87	0.92	0.89	1.01
		160	1	0.75	0.69	1.15	0.60	0.84	0.91	0.86	0.97
			2	0.74	0.68	1.16	0.61	0.85	0.92	0.87	0.98
			3	0.72	0.66	1.20	0.60	0.83	0.95	0.85	0.99
	25	100	3	0.72	0.63	1.18	0.61	0.84	0.91	0.86	0.97
		130	3	0.68	0.61	1.25	0.65	0.90	0.98	0.91	1.04
		160	1	0.70	0.64	1.17	0.64	0.90	0.96	0.92	0.99
			2	0.68	0.62	1.20	0.65	0.90	0.99	0.92	1.01
			3	0.67	0.61	1.22	0.64	0.89	1.01	0.90	1.01
3.25	25	160	1	0.71	0.63	1.15	0.65	0.90	0.93	0.92	0.98
			2	0.73	0.65	1.12	0.62	0.86	0.91	0.88	0.95
			3	0.71	0.63	1.16	0.64	0.88	0.94	0.90	0.98
Average				0.71	0.65	1.19	0.74	0.88	0.98	0.94	1.00
Standard Deviation				0.03	0.03	0.04	0.22	0.04	0.07	0.08	0.03
High				0.76	0.71	1.27	1.17	0.96	1.12	1.09	1.06
Low				0.67	0.61	1.12	0.58	0.80	0.89	0.82	0.94

Table A.2.6. Vertical bending strengths, modified uniform vertical bending suite, full-nonlinear analysis and first-order elastic analysis with design checks, specimens with, target $f_\ell/f_b = 0.50$ and $L_b/R = 0.10$.

D/b_f	b_f/t_f	D/t_w	d_o/D	$\frac{FEA}{M_y}$	$\frac{FEA}{M_p}$	$\frac{\text{Mod. LRFD}}{FEA}$	$\frac{\text{Rec. Specs}}{FEA}$	$\frac{\text{Hanshin}}{FEA}$	$\frac{\text{Yoo w/ Approx } M_\ell}{FEA}$	$\frac{\text{Yoo w/ Calc } M_\ell}{FEA}$	$\frac{\text{1/3 Rule}}{FEA}$
2.25	25	100	3	0.76	0.69	1.15	0.62	0.83	0.86	0.85	0.97
		130	3	0.76	0.70	1.12	0.63	0.84	0.87	0.86	0.95
		160	1	0.77	0.71	1.07	0.64	0.88	0.87	0.90	0.93
			2	0.75	0.70	1.10	0.64	0.86	0.89	0.88	0.94
			3	0.74	0.69	1.11	0.65	0.86	0.90	0.88	0.95
2.75	15	100	3	0.84	0.76	1.19	1.01	0.76	0.96	0.94	1.01
		130	3	0.82	0.75	1.22	1.04	0.78	0.99	0.97	1.04
		160	1	0.86	0.80	1.15	1.01	0.79	0.95	0.96	1.00
			2	0.82	0.76	1.21	1.05	0.80	1.00	0.98	1.04
			3	0.81	0.75	1.22	1.06	0.80	1.01	0.99	1.05
	20	100	3	0.78	0.70	1.24	0.61	0.79	0.85	0.80	1.04
		130	3	0.76	0.69	1.27	0.63	0.82	0.89	0.83	1.06
		160	1	0.79	0.73	1.20	0.62	0.82	0.86	0.83	1.02
			2	0.77	0.71	1.23	0.64	0.83	0.89	0.84	1.04
			3	0.77	0.71	1.23	0.62	0.81	0.89	0.82	1.03
	25	100	3	0.73	0.64	1.19	0.64	0.81	0.89	0.83	0.98
		130	3	0.73	0.66	1.17	0.64	0.82	0.91	0.83	0.96
		160	1	0.72	0.66	1.14	0.67	0.87	0.94	0.89	0.96
			2	0.71	0.65	1.15	0.67	0.87	0.95	0.89	0.97
			3	0.69	0.63	1.19	0.68	0.87	0.98	0.89	0.98
3.25	25	160	1	0.76	0.68	1.07	0.61	0.83	0.82	0.85	0.91
			2	0.76	0.68	1.07	0.60	0.83	0.82	0.84	0.91
			3	0.76	0.68	1.07	0.60	0.82	0.82	0.84	0.91
Average						1.16	0.72	0.83	0.90	0.88	0.98
Standard Deviation						0.06	0.17	0.03	0.06	0.05	0.05
High				0.86	0.79	1.27	1.06	0.88	1.01	0.99	1.06
Low				0.69	0.62	1.07	0.60	0.76	0.82	0.80	0.91

A.3 INTERNAL LOADING SUITE

A.3.1 Second-Order Elastic f_ℓ/F_y and f_b/F_y Values at the One-Third Rule Strength Limit

Table A.3.1. Second-order elastic f_ℓ/F_y and f_b/F_y values at the one-third rule strength limit, internal loading suite, specimens with $d_o/D = 3$ and target $f_\ell/f_b = 0.50$.

D/b_f	b_f/t_f	D/t_w		$L_b/R = 0.05$	$L_b/R = 0.10$
2.25	25	100	f_ℓ/F_y	0.365	0.383
			f_b/F_y	0.750	0.749
		130	f_ℓ/F_y	0.348	0.374
			f_b/F_y	0.735	0.727
		160	f_ℓ/F_y	0.307	0.349
			f_b/F_y	0.722	0.709
2.75	15	100	f_ℓ/F_y	0.325	0.385
			f_b/F_y	0.835	0.872
		130	f_ℓ/F_y	0.318	0.338
			f_b/F_y	0.845	0.883
		160	f_ℓ/F_y	0.304	0.330
			f_b/F_y	0.841	0.872
	20	100	f_ℓ/F_y	0.388	0.439
			f_b/F_y	0.803	0.829
		130	f_ℓ/F_y	0.365	0.428
			f_b/F_y	0.821	0.823
		160	f_ℓ/F_y	0.336	0.379
			f_b/F_y	0.827	0.820
	25	100	f_ℓ/F_y	0.353	0.434
			f_b/F_y	0.754	0.727
		130	f_ℓ/F_y	0.344	0.417
			f_b/F_y	0.737	0.708
		160	f_ℓ/F_y	0.314	0.399
			f_b/F_y	0.720	0.690
3.25	25	160	f_ℓ/F_y	0.322	0.405
			f_b/F_y	0.710	0.685

A.3.2 First-Order Elastic f/f_b Values

Table A.3.2. First-order elastic f_t/f_b values, internal loading suite, specimens with $d_o/D = 3$ and target $f_t/f_b = 0.50$.

D/b_f	b_f/t_f	D/t_w	$L_b/R = 0.05$	$L_b/R = 0.10$
2.25	25	100	0.428	0.467
		130	0.416	0.477
		160	0.387	0.461
2.75	15	100	0.365	0.393
		130	0.355	0.355
		160	0.340	0.347
	20	100	0.399	0.466
		130	0.381	0.465
		160	0.379	0.436
	25	100	0.394	0.542
		130	0.395	0.555
		160	0.364	0.556
3.25	25	160	0.428	0.568

A.3.3 Vertical Bending Strengths from Full Nonlinear Analysis and Ratios of Design Strengths Based on Second-Order Elastic Stresses to these Capacities

Table A.3.3. Vertical bending strengths, internal loading suite, full-nonlinear analysis and second-order elastic analysis with design checks, specimens with $d_o/D = 3$, target $f_\ell/f_b = 0.50$ and $L_b/R = 0.05$.

D/b_f	b_f/t_f	D/t_w	FEA / M_y	FEA / M_p	Mod. LRFD / FEA	Rec. Specs / FEA	Hanshin / FEA	Yoo w/ Approx M_ℓ / FEA	Yoo w/ Calc M_ℓ / FEA	1/3 Rule / FEA
2.25	25	100	0.77	0.70	1.14	0.59	0.86	0.85	0.88	0.98
		130	0.76	0.70	1.12	0.60	0.88	0.87	0.89	0.97
		160	0.76	0.70	1.09	0.61	0.91	0.88	0.93	0.95
2.75	15	100	0.86	0.78	1.10	0.99	0.82	0.94	0.98	0.97
		130	0.84	0.77	1.13	1.02	0.85	0.97	1.00	1.01
		160	0.82	0.76	1.16	1.04	0.88	1.00	1.04	1.03
	20	100	0.84	0.75	1.11	0.58	0.79	0.79	0.80	0.96
		130	0.82	0.74	1.15	0.60	0.83	0.82	0.84	1.00
		160	0.81	0.74	1.16	0.60	0.86	0.84	0.88	1.02
	25	100	0.80	0.70	1.09	0.61	0.83	0.82	0.85	0.94
		130	0.77	0.69	1.11	0.63	0.87	0.86	0.89	0.96
		160	0.77	0.70	1.06	0.64	0.89	0.87	0.91	0.93
3.25	25	160	0.77	0.69	1.06	0.63	0.88	0.86	0.90	0.93
Average					1.11	0.70	0.86	0.88	0.91	0.97
Standard Deviation					0.03	0.18	0.03	0.06	0.07	0.03
High			0.86	0.78	1.16	1.04	0.91	1.00	1.04	1.03
Low			0.76	0.69	1.06	0.58	0.79	0.79	0.80	0.93

[1] Recommended Specification values are calculated based on first-order elastic stresses

Table A.3.4. Vertical bending strengths, internal loading suite, full-nonlinear analysis and second-order elastic analysis with design checks, specimens with $d_o/D = 3$, target $f_\ell/f_b = 0.50$ and $L_b/R = 0.10$.

D/b_f	b_f/t_f	D/t_w	$\frac{FEA}{M_y}$	$\frac{FEA}{M_p}$	$\frac{Mod.\ LRFD}{FEA}$	$\frac{Rec.\ Specs}{FEA}$	$\frac{Hanshin}{FEA}$	$\frac{Yoo\ w/\ Approx\ M_\ell}{FEA}$	$\frac{Yoo\ w/\ Calc\ M_\ell}{FEA}$	$\frac{1/3\ Rule}{FEA}$
2.25	25	100	0.75	0.68	1.16	0.66	0.86	0.87	0.88	0.99
		130	0.73	0.67	1.17	0.67	0.88	0.91	0.90	1.00
		160	0.73	0.68	1.13	0.68	0.90	0.91	0.92	0.97
2.75	15	100	0.85	0.77	1.18	1.03	0.80	0.95	0.97	1.03
		130	0.82	0.75	1.22	1.06	0.86	0.99	1.03	1.08
		160	0.83	0.77	1.19	1.04	0.85	0.99	1.02	1.06
	20	100	0.79	0.70	1.23	0.64	0.81	0.84	0.83	1.04
		130	0.77	0.70	1.25	0.66	0.84	0.88	0.85	1.07
		160	0.78	0.72	1.21	0.66	0.86	0.87	0.88	1.05
	25	100	0.74	0.65	1.18	0.66	0.83	0.88	0.85	0.98
		130	0.70	0.63	1.22	0.69	0.88	0.95	0.90	1.02
		160	0.68	0.62	1.20	0.71	0.91	0.99	0.93	1.01
3.25	25	160	0.73	0.65	1.12	0.63	0.84	0.85	0.86	0.94
Average					1.19	0.75	0.86	0.91	0.91	1.02
Standard Deviation					0.04	0.17	0.03	0.05	0.06	0.04
High			0.85	0.77	1.25	1.06	0.91	0.99	1.03	1.08
Low			0.68	0.62	1.12	0.63	0.80	0.84	0.83	0.94

(1) Recommended Specification values are calculated based on first-order elastic stresses

A.3.4 Vertical Bending Strengths from Full Nonlinear Analysis and Ratios of Design Strengths Based on the First-Order Elastic f_ℓ / f_b to these Capacities

Table A.3.5. Vertical bending strengths, internal loading suite, full-nonlinear analysis and first-order elastic analysis with design checks, specimens with $d_o/D = 3$, target $f_\ell/f_b = 0.50$ and $L_b/R = 0.05$.

D/b_f	b_f/t_f	D/t_w	$\frac{FEA}{M_y}$	$\frac{FEA}{M_p}$	$\frac{Mod.\ LRFD}{FEA}$	$\frac{Rec.\ Specs}{FEA}$	$\frac{Hanshin}{FEA}$	$\frac{Yoo\ w/\ Approx\ M_\ell}{FEA}$	$\frac{Yoo\ w/\ Calc\ M_\ell}{FEA}$	$\frac{1/3\ Rule}{FEA}$
2.25	25	100	0.77	0.70	1.14	0.59	0.89	0.85	0.91	1.00
		130	0.76	0.70	1.12	0.60	0.91	0.87	0.93	0.99
		160	0.76	0.70	1.09	0.61	0.93	0.88	0.95	0.96
2.75	15	100	0.86	0.78	1.10	0.99	0.83	0.94	0.99	0.98
		130	0.84	0.77	1.13	1.02	0.86	0.97	1.01	1.01
		160	0.82	0.76	1.16	1.04	0.89	1.00	1.04	1.04
	20	100	0.84	0.75	1.11	0.58	0.83	0.79	0.85	0.98
		130	0.82	0.74	1.15	0.60	0.86	0.82	0.88	1.02
		160	0.81	0.74	1.16	0.60	0.87	0.84	0.90	1.03
	25	100	0.80	0.70	1.09	0.61	0.88	0.82	0.90	0.96
		130	0.77	0.69	1.11	0.63	0.91	0.86	0.93	0.98
		160	0.77	0.70	1.06	0.64	0.93	0.87	0.95	0.95
3.25	25	160	0.77	0.69	1.06	0.63	0.89	0.86	0.91	0.94
Average					1.11	0.70	0.88	0.88	0.94	0.99
Standard Deviation					0.03	0.18	0.03	0.06	0.05	0.03
High			0.86	0.78	1.16	1.04	0.93	1.00	1.04	1.04
Low			0.76	0.69	1.06	0.58	0.83	0.79	0.85	0.94

Table A.3.6. Vertical bending strengths, internal loading suite, full-nonlinear analysis and first-order elastic analysis with design checks, specimens with $d_o/D = 3$, target $f_\ell/f_b = 0.50$ and $L_b/R = 0.10$.

D/b_f	b_f/t_f	D/t_w	$\frac{FEA}{M_y}$	$\frac{FEA}{M_p}$	$\frac{Mod.\ LRFD}{FEA}$	$\frac{Rec.\ Specs}{FEA}$	$\frac{Hanshin}{FEA}$	$\frac{Yoo\ w/\ Approx\ M_\ell}{FEA}$	$\frac{Yoo\ w/\ Calc\ M_\ell}{FEA}$	$\frac{1/3\ Rule}{FEA}$
2.25	25	100	0.75	0.68	1.16	0.66	0.89	0.87	0.91	1.01
		130	0.73	0.67	1.17	0.67	0.91	0.91	0.93	1.01
		160	0.73	0.68	1.13	0.68	0.92	0.91	0.94	0.98
2.75	15	100	0.85	0.77	1.18	1.03	0.83	0.95	0.99	1.04
		130	0.82	0.75	1.22	1.06	0.88	0.99	1.04	1.09
		160	0.83	0.77	1.19	1.04	0.87	0.99	1.03	1.07
	20	100	0.79	0.70	1.23	0.64	0.84	0.84	0.86	1.06
		130	0.77	0.70	1.25	0.66	0.87	0.88	0.89	1.08
		160	0.78	0.72	1.21	0.66	0.87	0.87	0.89	1.06
	25	100	0.74	0.65	1.18	0.66	0.86	0.88	0.88	1.00
		130	0.70	0.63	1.22	0.69	0.90	0.95	0.92	1.03
		160	0.68	0.62	1.20	0.71	0.93	0.99	0.94	1.02
3.25	25	160	0.73	0.65	1.12	0.63	0.86	0.85	0.87	0.94
Average					1.19	0.75	0.88	0.91	0.93	1.03
Standard Deviation					0.04	0.17	0.04	0.04	0.06	0.04
High			0.85	0.77	1.25	1.06	0.93	0.99	1.04	1.09
Low			0.68	0.62	1.12	0.63	0.83	0.84	0.86	0.94

A.4 FREE-END SUITE

A.4.1 Second-Order Elastic f/F_y and f_f/F_y Values at the One-Third Rule Strength Limit

Table A.4.1. Second-order elastic f_ℓ/F_y and f_b/F_y values at the one-third rule strength limit, free-end suite, $D/t_w = 160$, $d_o/D = 3$ and target second-order $f_\ell/f_b = 0.60$.

D/b_f	D/b_f		$L_b/R = 0.05$	$L_b/R = 0.10$
2.25	25	f_ℓ/F_y	0.394	0.435
		f_b/F_y	0.702	0.689
2.75	15	f_ℓ/F_y	0.475	0.506
		f_b/F_y	0.832	0.830
	20	f_ℓ/F_y	0.448	0.495
		f_b/F_y	0.796	0.793
	25	f_ℓ/F_y	0.420	0.434
		f_b/F_y	0.677	0.672
3.25	25	f_ℓ/F_y	0.423	0.434
		f_b/F_y	0.679	0.672

A.4.2 First-Order Elastic f/f_b Values

Table A.4.2. First-order elastic f_ℓ/f_b values, free-end suite, $D/t_w = 160$, $d_o/D = 3$ and target second-order $f_\ell/f_b = 0.60$.

D/b_f	D/b_f	$L_b/R = 0.05$	$L_b/R = 0.10$
2.25	25	0.447	0.612
2.75	15	0.440	0.567
	20	0.458	0.580
	25	0.483	0.612
3.25	25	0.500	0.634

A.4.3 Vertical Bending Strengths from Full Nonlinear Analysis and Ratios of Design Strengths Based on Second-Order Elastic Stresses to these Capacities

Table A.4.3. Vertical bending strengths, free-end suite, full-nonlinear analysis and second-order elastic analysis with design checks, L_b/R= 0.05 and target f_ℓ/f_b = 0.60.

D/b_f	b_f/t_f	D/t_w	d_o/D	FEA M_y	FEA M_p	Mod. LRFD FEA	Rec.[1] Specs. FEA	Hanshin FEA	Yoo w/ approx. M_ℓ FEA	Yoo w/ calc. M_ℓ FEA	1/3 rule FEA
2.25	25	160	3	0.78	0.72	1.06	0.44	0.80	0.76	0.82	0.89
2.75	15	160	3	0.86	0.80	1.15	0.74	0.72	0.87	0.91	0.97
	20	160	3	0.84	0.77	1.13	0.41	0.74	0.70	0.76	0.95
	25	160	3	0.80	0.73	1.02	0.42	0.75	0.72	0.77	0.85
3.25	25	160	3	0.76	0.68	1.07	0.48	0.79	0.77	0.81	0.89
Avg.						1.09	0.50	0.76	0.77	0.81	0.91
Std. Dev.						0.05	0.14	0.03	0.07	0.06	0.05
High				0.84	0.78	1.15	0.74	0.80	0.87	0.91	0.97
Low				0.79	0.71	1.02	0.41	0.72	0.70	0.76	0.85

[1] Recommended Specification values are calculated based on first-order elastic stresses

Table A.4.4. Vertical bending strengths, free-end suite, full-nonlinear analysis and second-order elastic analysis with design checks, L_b/R= 0.10 and target f_ℓ/f_b = 0.60.

D/b_f	b_f/t_f	D/t_w	d_o/D	FEA M_y	FEA M_p	Mod. LRFD FEA	Rec.[1] Specs. FEA	Hanshin FEA	Yoo w/ approx. M_ℓ FEA	Yoo w/ calc. M_ℓ FEA	1/3 rule FEA
2.25	25	160	3	0.75	0.70	1.10	0.51	0.80	0.74	0.82	0.91
2.75	15	160	3	0.85	0.79	1.16	0.79	0.71	0.84	0.90	0.97
	20	160	3	0.79	0.73	1.20	0.49	0.76	0.70	0.78	0.99
	25	160	3	0.76	0.69	1.08	0.50	0.78	0.71	0.80	0.89
3.25	25	160	3	0.73	0.65	1.12	0.53	0.81	0.73	0.83	0.92
Avg.						1.13	0.56	0.77	0.74	0.83	0.94
Std. Dev.						0.05	0.13	0.04	0.06	0.05	0.04
High				0.85	0.79	1.20	0.79	0.81	0.84	0.90	0.99
Low				0.73	0.65	1.08	0.49	0.71	0.70	0.78	0.89

[1] Recommended Specification values are calculated based on first-order elastic stresses

A.4.4 Vertical Bending Strengths from Full Nonlinear Analysis and Ratios of Design Strengths Based on the First-Order Elastic f_ℓ/f_b to these Capacities

Table A.4.5. Vertical bending strengths, free-end suite, full-nonlinear analysis and first-order elastic analysis with design checks, L_b/R= 0.05 and target f_ℓ/f_b = 0.60.

D/b_f	b_f/t_f	D/t_w	d_c/D	FEA M_y	FEA M_p	Mod. LRFD FEA	Rec. Specs. FEA	Hanshin FEA	Yoo w/ approx. M_ℓ FEA	Yoo w/ calc. M_ℓ FEA	1/3 rule FEA
2.25	25	160	3	0.78	0.72	1.06	0.44	0.86	0.76	0.89	0.92
2.75	15	160	3	0.86	0.80	1.15	0.74	0.79	0.87	0.96	1.00
	20	160	3	0.84	0.77	1.13	0.41	0.80	0.70	0.82	0.98
	25	160	3	0.80	0.73	1.02	0.42	0.82	0.72	0.84	0.88
3.25	25	160	3	0.76	0.68	1.07	0.48	0.86	0.77	0.88	0.92
Avg.						1.09	0.50	0.82	0.77	0.88	0.94
Std. Dev.						0.05	0.14	0.03	0.07	0.05	0.05
High				0.84	0.78	1.15	0.74	0.86	0.87	0.96	1.00
Low				0.79	0.71	1.02	0.41	0.79	0.70	0.82	0.88

Table A.4.6. Vertical bending strengths, free-end suite, full-nonlinear analysis and first-order elastic analysis with design checks, L_b/R= 0.10 and target f_ℓ/f_b = 0.60.

D/b_f	b_f/t_f	D/t_w	d_c/D	FEA M_y	FEA M_p	Mod. LRFD FEA	Rec. Specs. FEA	Hanshin FEA	Yoo w/ approx. M_ℓ FEA	Yoo w/ calc. M_ℓ FEA	1/3 rule FEA
2.25	25	160	3	0.75	0.70	1.10	0.51	0.81	0.74	0.83	0.91
2.75	15	160	3	0.85	0.79	1.16	0.79	0.73	0.84	0.92	0.98
	20	160	3	0.79	0.73	1.20	0.49	0.78	0.70	0.80	1.01
	25	160	3	0.76	0.69	1.08	0.50	0.79	0.71	0.82	0.90
3.25	25	160	3	0.73	0.65	1.12	0.53	0.82	0.73	0.84	0.93
Avg.						1.13	0.56	0.79	0.74	0.84	0.94
Std. Dev.						0.05	0.13	0.03	0.06	0.05	0.05
High				0.85	0.79	1.20	0.79	0.82	0.84	0.92	1.01
Low				0.73	0.65	1.08	0.49	0.73	0.70	0.80	0.90

A.5 LATERALLY UNSUPPORTED STRAIGHT GIRDER SUITE

A.5.1 Second-Order Elastic f/F_y and f_b/F_y Values at the One-Third Rule Strength Limit

Table A.5.1. Second-order elastic f_ℓ/F_y and f_b/F_y values at the one-third rule strength limit, laterally unsupported straight girder suite, $D/t_w = 160$, $d_o/D = 3$.

D/b_f	b_f/t_f		$(\lambda - \lambda_p)/(\lambda_r - \lambda_p)$				
			0.0	0.25	0.5	0.75	1.0
2.25	25	f_ℓ/F_y	0.43	0.42	0.42	0.38	0.33
		f_b/F_y	0.68	0.68	0.68	0.63	0.56
2.75	15	f_ℓ/F_y	0.51	0.49	0.43	0.35	0.34
		f_b/F_y	0.83	0.75	0.68	0.63	0.56
	20	f_ℓ/F_y	0.50	0.45	0.41	0.36	0.33
		f_b/F_y	0.78	0.76	0.69	0.63	0.55
	25	f_ℓ/F_y	0.42	0.42	0.39	0.36	0.33
		f_b/F_y	0.66	0.68	0.69	0.61	0.54
3.25	25	f_ℓ/F_y	0.42	0.42	0.39	0.38	0.33
		f_b/F_y	0.68	0.68	0.69	0.62	0.55

A.5.2 First-Order Elastic f/f_b Values

Table A.5.2. First-order elastic f_ℓ/f_b values, laterally unsupported straight girder suite, $D/t_w = 160$, $d_o/D = 3$.

D/b_f	b_f/t_f	$(\lambda - \lambda_p)/(\lambda_r - \lambda_p)$				
		0.0	0.25	0.5	0.75	1.0
2.25	25	0.551	0.487	0.416	0.378	.248
2.75	15	0.563	0.514	0.417	0.303	0.243
	20	0.554	0.481	0.419	0.326	0.261
	25	0.554	0.479	0.412	0.314	0.239
3.25	25	0.529	0.456	0.366	0.300	0.182

A.5.3 Vertical Bending Strengths from Full Nonlinear Analysis and Ratios of Design Strengths Based on Second-Order Elastic Stresses to these Capacities

Table A.5.3. Vertical bending strengths, laterally unsupported straight girder suite, full-nonlinear analysis and second-order elastic analysis with design checks, $D/t_w = 160$, $d_o/D = 3$, $(\lambda - \lambda_p)/(\lambda_r - \lambda_p) = 0.0$.

D/b_f	b_f/t_f	$\frac{FEA}{M_y}$	$\frac{FEA}{M_p}$	$\frac{Mod.\ LRFD}{FEA}$	$\frac{Rec.^{(1)}\ Specs}{FEA}$	$\frac{Hanshin}{FEA}$	$\frac{Yoo\ w/\ Calc\ M_\ell}{FEA}$	$\frac{1/3\ Rule}{FEA}$
2.25	25	0.71	0.66	1.16	0.91	0.86	0.86	0.96
2.75	15	0.75	0.69	1.32	1.12	0.83	1.02	1.10
2.75	20	0.76	0.69	1.24	0.85	0.80	0.80	1.03
2.75	25	0.74	0.67	1.11	0.87	0.83	0.83	0.92
3.25	25	0.72	0.64	1.13	0.91	0.86	0.86	0.94
Average				1.19	0.93	0.84	0.87	0.99
Standard Deviation				0.09	0.11	0.03	0.09	0.07
High		0.76	0.69	1.32	1.12	0.86	1.02	1.10
Low		0.71	0.64	1.11	0.85	0.80	0.80	0.92

(1) Recommended Specification values are calculated based on first-order elastic stresses

Table A.5.4. Vertical bending strengths, laterally unsupported straight girder suite, full-nonlinear analysis and second-order elastic analysis with design checks, $D/t_w = 160$, $d_o/D = 3$, $(\lambda - \lambda_p)/(\lambda_r - \lambda_p) = 0.25$.

D/b_f	b_f/t_f	$\frac{FEA}{M_y}$	$\frac{FEA}{M_p}$	$\frac{Mod.\ LRFD}{FEA}$	$\frac{Rec.^{(1)}\ Specs}{FEA}$	$\frac{Hanshin}{FEA}$	$\frac{Yoo\ w/\ Calc\ M_\ell}{FEA}$	$\frac{1/3\ Rule}{FEA}$
2.25	25	0.70	0.65	1.17	0.96	0.88	0.88	0.97
2.75	15	0.74	0.69	1.24	1.15	0.82	1.02	1.02
2.75	20	0.74	0.68	1.22	0.91	0.84	0.84	1.02
2.75	25	0.72	0.65	1.14	0.94	0.85	0.85	0.94
3.25	25	0.68	0.60	1.20	1.01	0.91	0.91	1.00
Average				1.19	1.00	0.86	0.90	0.99
Standard Deviation				0.04	0.10	0.04	0.07	0.03
High		0.74	0.69	1.24	1.15	0.91	1.02	1.02
Low		0.68	0.60	1.14	0.91	0.82	0.84	0.94

(1) Recommended Specification values are calculated based on first-order elastic stresses

Table A.5.5. Vertical bending strengths, laterally unsupported straight girder suite, full-nonlinear analysis and second-order elastic analysis with design checks, $D/t_w = 160$, $d_o/D = 3$, $(\lambda - \lambda_p)/(\lambda_r - \lambda_p) = 0.50$.

D/b_f	b_f/t_f	$\frac{FEA}{M_y}$	$\frac{FEA}{M_p}$	$\frac{\text{Mod. LRFD}}{FEA}$	$\frac{\text{Rec.}^{(1)}\ \text{Specs}}{FEA}$	$\frac{\text{Hanshin}}{FEA}$	$\frac{\text{Yoo w/ Calc } M_\ell}{FEA}$	$\frac{\text{1/3 Rule}}{FEA}$
2.25	25	0.70	0.65	1.17	1.01	0.88	0.88	0.97
2.75	15	0.69	0.64	1.19	1.19	0.89	1.11	0.99
2.75	20	0.68	0.62	1.22	1.04	0.92	0.92	1.02
2.75	25	0.69	0.62	1.19	1.03	0.92	0.92	1.00
3.25	25	0.63	0.56	1.29	1.16	1.01	1.01	1.09
Average				1.21	1.08	0.93	0.97	1.01
Standard Deviation				0.05	0.08	0.05	0.09	0.05
High		0.70	0.65	1.29	1.19	1.01	1.11	1.09
Low		0.63	0.56	1.17	1.01	0.88	0.88	0.97

(1) Recommended Specification values are calculated based on first-order elastic stresses

Table A.5.6. Vertical bending strengths, laterally unsupported straight girder suite, full-nonlinear analysis and second-order elastic analysis with design checks, $D/t_w = 160$, $d_o/D = 3$, $(\lambda - \lambda_p)/(\lambda_r - \lambda_p) = 0.75$.

D/b_f	b_f/t_f	$\frac{FEA}{M_y}$	$\frac{FEA}{M_p}$	$\frac{\text{Mod. LRFD}}{FEA}$	$\frac{\text{Rec.}^{(1)}\ \text{Specs}}{FEA}$	$\frac{\text{Hanshin}}{FEA}$	$\frac{\text{Yoo w/ Calc } M_\ell}{FEA}$	$\frac{\text{1/3 Rule}}{FEA}$
2.25	25	0.66	0.61	1.14	1.07	0.94	0.94	0.95
2.75	15	0.67	0.62	1.10	1.09	0.96	1.17	0.93
2.75	20	0.64	0.59	1.16	1.14	0.99	0.99	0.98
2.75	25	0.63	0.58	1.16	1.16	1.00	1.00	0.98
3.25	25	0.62	0.55	1.19	1.22	1.00	1.00	0.99
Average				1.15	1.14	0.98	1.02	0.97
Standard Deviation				0.03	0.06	0.03	0.09	0.02
High		0.67	0.62	1.19	1.22	1.00	1.17	0.99
Low		0.62	0.55	1.10	1.07	0.94	0.94	0.93

(1) Recommended Specification values are calculated based on first-order elastic stresses

Table A.5.7. Vertical bending strengths, laterally unsupported straight girder suite, full-nonlinear analysis and second-order elastic analysis with design checks, $D/t_w = 160$, $d_o/D = 3$, $(\lambda - \lambda_p)/(\lambda_r - \lambda_p) = 1.0$.

D/b_f	b_f/t_f	$\frac{FEA}{M_y}$	$\frac{FEA}{M_p}$	$\frac{Mod.\ LRFD}{FEA}$	$\frac{Rec.^{(1)}\ Specs}{FEA}$	$\frac{Hanshin}{FEA}$	$\frac{Yoo\ w/\ Calc\ M_\ell}{FEA}$	$\frac{1/3\ Rule}{FEA}$
2.25	25	0.64	0.59	1.05	1.09	0.98	0.98	0.87
2.75	15	0.65	0.61	1.04	1.04	0.96	1.19	0.86
2.75	20	0.60	0.56	1.10	1.16	1.05	1.05	0.92
2.75	25	0.58	0.53	1.12	1.20	1.08	1.08	0.94
3.25	25	0.56	0.50	1.17	1.33	1.12	1.12	0.98
Average				1.10	1.16	1.04	1.08	0.92
Standard Deviation				0.06	0.11	0.07	0.08	0.05
High		0.65	0.61	1.17	1.33	1.12	1.19	0.98
Low		0.56	0.50	1.04	1.04	0.96	0.98	0.86

(1) Recommended Specification values are calculated based on first-order elastic stresses

A.5.4 Vertical Bending Strengths from Full Nonlinear Analysis and Ratios of Design Strengths Based on the First-Order Elastic f_ℓ/f_b to these Capacities

Table A.5.8. Vertical bending strengths, laterally unsupported straight girder suite, full-nonlinear analysis and first-order elastic analysis with design checks, $D/t_w = 160$, $d_o/D = 3$, $(\lambda - \lambda_p)/(\lambda_r - \lambda_p) = 0.0$.

D/b_f	b_f/t_f	$\frac{FEA}{M_y}$	$\frac{FEA}{M_p}$	$\frac{Mod.\ LRFD}{FEA}$	$\frac{Rec.\ Specs}{FEA}$	$\frac{Hanshin}{FEA}$	$\frac{Yoo\ w/\ Calc\ M_\ell}{FEA}$	$\frac{1/3\ Rule}{FEA}$
2.25	25	0.71	0.66	1.16	0.91	0.91	0.91	0.98
2.75	15	0.75	0.69	1.32	1.12	0.85	1.04	1.11
2.75	20	0.76	0.69	1.24	0.85	0.85	0.85	1.05
2.75	25	0.74	0.67	1.11	0.87	0.87	0.87	0.94
3.25	25	0.72	0.64	1.13	0.91	0.91	0.91	0.97
Average				1.19	0.93	0.88	0.92	1.01
Standard Deviation				0.09	0.11	0.03	0.08	0.07
High		0.76	0.69	1.32	1.12	0.91	1.04	1.11
Low		0.71	0.64	1.11	0.85	0.85	0.85	0.94

Table A.5.9. Vertical bending strengths, laterally unsupported straight girder suite, full-nonlinear analysis and first-order elastic analysis with design checks, $D/t_w = 160$, $d_o/D = 3$, $(\lambda - \lambda_p)/(\lambda_r - \lambda_p) = 0.25$.

D/b_f	b_f/t_f	$\frac{FEA}{M_y}$	$\frac{FEA}{M_p}$	$\frac{\text{Mod. LRFD}}{FEA}$	$\frac{\text{Rec. Specs}}{FEA}$	$\frac{\text{Hanshin}}{FEA}$	$\frac{\text{Yoo w/ Calc } M_\ell}{FEA}$	$\frac{\text{1/3 Rule}}{FEA}$
2.25	25	0.70	0.65	1.18	0.96	0.96	0.96	1.01
2.75	15	0.74	0.69	1.24	1.15	0.89	1.08	1.06
2.75	20	0.74	0.68	1.23	0.91	0.91	0.91	1.06
2.75	25	0.72	0.65	1.14	0.94	0.94	0.94	0.98
3.25	25	0.68	0.60	1.20	1.01	1.01	1.01	1.04
Average				1.20	1.00	0.94	0.98	1.03
Standard Deviation				0.04	0.10	0.05	0.07	0.03
High		0.74	0.69	1.24	1.15	1.01	1.08	1.06
Low		0.68	0.60	1.14	0.91	0.89	0.91	0.98

Table A.5.10. Vertical bending strengths, laterally unsupported straight girder suite, full-nonlinear analysis and first-order elastic analysis with design checks, $D/t_w = 160$, $d_o/D = 3$, $(\lambda - \lambda_p)/(\lambda_r - \lambda_p) = 0.50$.

D/b_f	b_f/t_f	$\frac{FEA}{M_y}$	$\frac{FEA}{M_p}$	$\frac{\text{Mod. LRFD}}{FEA}$	$\frac{\text{Rec. Specs}}{FEA}$	$\frac{\text{Hanshin}}{FEA}$	$\frac{\text{Yoo w/ Calc } M_\ell}{FEA}$	$\frac{\text{1/3 Rule}}{FEA}$
2.25	25	0.70	0.65	1.17	1.01	1.01	1.01	1.03
2.75	15	0.69	0.64	1.19	1.19	1.02	1.20	1.05
2.75	20	0.68	0.62	1.22	1.04	1.04	1.04	1.07
2.75	25	0.69	0.62	1.19	1.03	1.03	1.03	1.05
3.25	25	0.63	0.56	1.29	1.16	1.16	1.16	1.16
Average				1.21	1.08	1.05	1.09	1.07
Standard Deviation				0.05	0.08	0.06	0.09	0.05
High		0.70	0.65	1.29	1.19	1.16	1.20	1.16
Low		0.63	0.56	1.17	1.01	1.01	1.01	1.03

Table A.5.11. Vertical bending strengths, laterally unsupported straight girder suite, full-nonlinear analysis and first-order elastic analysis with design checks, $D/t_w = 160$, $d_o/D = 3$, $(\lambda - \lambda_p)/(\lambda_r - \lambda_p) = 0.75$.

D/b_f	b_f/t_f	$\frac{FEA}{M_y}$	$\frac{FEA}{M_p}$	$\frac{\text{Mod. LRFD}}{FEA}$	$\frac{\text{Rec. Specs}}{FEA}$	$\frac{\text{Hanshin}}{FEA}$	$\frac{\text{Yoo w/ Calc } M_\ell}{FEA}$	$\frac{\text{1/3 Rule}}{FEA}$
2.25	25	0.66	0.61	1.14	1.07	1.10	1.10	1.01
2.75	15	0.67	0.62	1.10	1.09	1.15	1.30	1.00
2.75	20	0.64	0.59	1.16	1.14	1.18	1.18	1.05
2.75	25	0.63	0.58	1.17	1.16	1.21	1.21	1.06
3.25	25	0.62	0.55	1.19	1.22	1.24	1.24	1.09
Average				1.15	1.14	1.17	1.21	1.04
Standard Deviation				0.03	0.06	0.05	0.07	0.03
High		0.67	0.62	1.19	1.22	1.24	1.30	1.09
Low		0.62	0.55	1.10	1.07	1.10	1.10	1.00

Table A.5.12. Vertical bending strengths, laterally unsupported straight girder suite, full-nonlinear analysis and first-order elastic analysis with design checks, $D/t_w = 160$, $d_o/D = 3$, $(\lambda - \lambda_p)/(\lambda_r - \lambda_p) = 1.0$.

D/b_f	b_f/t_f	$\frac{FEA}{M_y}$	$\frac{FEA}{M_p}$	$\frac{\text{Mod. LRFD}}{FEA}$	$\frac{\text{Rec. Specs}}{FEA}$	$\frac{\text{Hanshin}}{FEA}$	$\frac{\text{Yoo w/ Calc } M_\ell}{FEA}$	$\frac{\text{1/3 Rule}}{FEA}$
2.25	25	0.64	0.59	1.05	1.09	1.25	1.25	0.97
2.75	15	0.65	0.61	1.04	1.04	1.24	1.37	0.96
2.75	20	0.60	0.56	1.10	1.16	1.34	1.34	1.02
2.75	25	0.58	0.53	1.12	1.20	1.39	1.39	1.04
3.25	25	0.56	0.50	1.17	1.33	1.51	1.51	1.11
Average				1.10	1.16	1.35	1.37	1.02
Standard Deviation				0.06	0.11	0.11	0.09	0.06
High		0.65	0.61	1.17	1.33	1.51	1.51	1.11
Low		0.56	0.50	1.04	1.04	1.24	1.25	0.96

A.6 UNSYMMETRIC GIRDER SUITE

A.6.1 Design Analysis Stresses

Table A.6.1. Second-order elastic f_ℓ/F_y and f_b/F_y values at the one-third rule strength limit, unsymmetric specimens.

D/b_{fc}	b_f/t_f	$2D_c/t_w$		$L_b/R = 0.05$		$L_b/R = 0.10$	
				target $f_\ell/f_b = 0.35$	target $f_\ell/f_b = 0.50$ or 0.60	target $f_\ell/f_b = 0.35$	target $f_\ell/f_b = 0.50$ or 0.60
Uniform vertical bending, primary test suite							
4.77	20	208	f_ℓ/F_y f_b/F_y	0.236 0.739	0.320 0.640	0.289 0.724	0.383 0.697
2.75	25	169	f_ℓ/F_y f_b/F_y	0.285 0.687	0.380 0.657	0.294 0.684	0.381 0.657
Modified uniform vertical bending							
4.77	20	208	f_ℓ/F_y f_b/F_y	0.240 0.738	0.314 0.642	0.288 0.724	0.376 0.699
2.75	25	169	f_ℓ/F_y f_b/F_y	0.329 0.673	0.411 0.648	0.335 0.671	0.438 0.639
Internal loading suite							
2.75	25	169	f_ℓ/F_y f_b/F_y	0.300 0.682	0.346 0.668	0.292 0.685	0.367 0.662
Free-end suite							
4.77	20	208	f_ℓ/F_y f_b/F_y	NA[1]	0.397 0.693	NA	0.400 0.693

[1] Only a target second-order $f_\ell/f_b = 0.60$ is considered with the free-end suite

Table A.6.2. First-order elastic f_ℓ/f_b values, unsymmetric specimens.

D/b_{fc}	b_f/t_f	$2D_c/t_w$	$L_b/R = 0.05$		$L_b/R = 0.10$	
			target $f_\ell/f_b = 0.35$	target $f_\ell/f_b = 0.50$	target $f_\ell/f_b = 0.35$	target $f_\ell/f_b = 0.50$
Uniform vertical bending, primary test suite						
4.77	20	208	0.315	0.487	0.389	0.532
2.75	25	169	0.350	0.485	0.361	0.535
Modified uniform vertical bending						
4.77	20	208	0.310	0.462	0.377	0.525
2.75	25	169	0.446	0.600	0.454	0.635
Internal loading suite						
2.75	25	169	0.305	0.458	0.394	0.504
Free-end suite						
4.77	20	208	NA[1]	0.515	NA	0.520

[1] Only a target second-order $f_\ell/f_b = 0.60$ is considered with the free-end suite

A.6.2 Vertical Bending Strengths from Full Nonlinear Analysis and Ratios of Design Strengths to these Capacities

Table A.6.3. Vertical bending strengths, full-nonlinear analysis and second-order elastic analysis with design checks, 22 unsymmetric specimens.

L_b/R	Target f_e/f_b	$2D_c/t_w$	d_o/D	FEA / M_y	FEA / M_p	Mod. LRFD / FEA	Rec.[1] Specs. / FEA	Hanshin / FEA	Yoo w/ approx. M_ℓ / FEA	Yoo w/ calc. M_ℓ / FEA	1/3 rule / FEA
D/b_{fc} = 4.77 and b_f/t_f = 20 (Primary Test Suite)											
0.05	0.35	208	2	0.75	0.53	1.07	0.81	0.99	0.95	1.01	0.98
	0.50	208	3	0.70	0.50	1.04	0.69	0.93	0.89	0.95	0.91
0.10	0.35	208	1	0.81	0.57	0.99	0.74	0.87	0.88	0.88	0.89
	0.50	208	1.5	0.71	0.50	1.13	0.71	0.89	0.88	0.91	0.98
D/b_{fc} = 2.75 and b_f/t_f = 25 (Primary Test Suite)											
0.05	0.35	169	3	0.86	0.66	0.90	0.67	0.81	0.85	0.82	0.80
	0.50	169	3	0.71	0.55	1.09	0.63	0.87	0.91	0.89	0.93
0.10	0.35	169	2	0.79	0.61	0.98	0.75	0.87	0.93	0.89	0.87
	0.50	169	3	0.76	0.59	1.02	0.64	0.82	0.85	0.83	0.86
D/b_{fc} = 4.77 and b_f/t_f = 20 (Modified Vertical Bending Suite)											
0.05	0.35	208	2	0.72	0.51	1.12	0.85	1.04	0.99	1.06	1.03
	0.50	208	3	0.68	0.48	1.07	0.72	0.97	0.92	0.99	0.94
0.10	0.35	208	1	0.80	0.57	1.01	0.75	0.88	0.89	0.90	0.91
	0.50	208	1.5	0.67	0.47	1.20	0.76	0.95	0.93	0.97	1.04
D/b_{fc} = 2.75 and b_f/t_f = 25 (Modified Vertical Bending Suite)											
0.05	0.35	169	3	0.81	0.62	0.96	0.68	0.81	0.90	0.83	0.83
	0.50	169	3	0.66	0.51	1.18	0.64	0.91	0.98	0.93	0.98
0.10	0.35	169	2	0.73	0.56	1.06	0.77	0.90	1.00	0.91	0.92
	0.50	169	3	0.70	0.54	1.11	0.66	0.83	0.92	0.85	0.91
D/b_{fc} = 2.75 and b_f/t_f = 25 (Internal Loading Suite)											
0.05	0.35	169	3	0.90	0.69	0.86	0.65	0.76	0.81	0.77	0.76
	0.50	169	3	0.76	0.59	1.02	0.60	0.85	0.85	0.87	0.88
0.1	0.35	169	2	0.86	0.66	0.90	0.67	0.80	0.85	0.82	0.80
	0.50	169	3	0.86	0.66	0.90	0.57	0.73	0.75	0.75	0.77
D/b_{fc} = 4.77 and b_f/t_f = 20 (Free-End Test Suite)											
0.05	0.6	208	3	0.77	0.54	1.05	0.53	0.81	0.74	0.83	0.90
0.1	0.6	208	3	0.80	0.57	1.01	0.57	0.77	0.69	0.79	0.87
Average						1.03	0.68	0.87	0.88	0.88	0.90
Standard Deviation						0.09	0.08	0.08	0.08	0.08	0.08
High				0.90	0.69	1.20	0.85	1.04	1.00	1.06	1.04
Low				0.66	0.47	0.86	0.53	0.73	0.69	0.75	0.76

[1] Recommended Specification values are calculated based on first-order elastic stresses

Table A.6.4. Vertical bending strengths, primary test suite, full-nonlinear analysis and first-order elastic analysis with design checks, 22 unsymmetric specimens.

L_b/R	Target f_f/f_b	$2D_c/t_w$	d_o/D	$\frac{FEA}{M_y}$	$\frac{FEA}{M_p}$	$\frac{Mod.\ LRFD}{FEA}$	$\frac{Rec.\ Specs.}{FEA}$	$\frac{Hanshin}{FEA}$	$\frac{Yoo\ w/\ approx.\ M_\ell}{FEA}$	$\frac{Yoo\ w/\ calc.\ M_\ell}{FEA}$	$\frac{1/3\ rule}{FEA}$
$D/b_{fc} = 4.77$ and $b_f/t_f = 20$ (Primary Test Suite)											
0.05	0.35	208	2	0.75	0.53	1.07	0.81	0.99	0.95	1.01	0.99
	0.50	208	3	0.70	0.50	1.04	0.69	0.94	0.89	0.96	0.92
0.10	0.35	208	1	0.81	0.57	0.99	0.74	0.87	0.88	0.89	0.90
	0.50	208	1.5	0.71	0.50	1.13	0.71	0.90	0.88	0.92	0.99
$D/b_{fc} = 2.75$ and $b_f/t_f = 25$ (Primary Test Suite)											
0.05	0.35	169	3	0.86	0.66	0.90	0.67	0.84	0.85	0.86	0.81
	0.50	169	3	0.71	0.55	1.09	0.63	0.93	0.91	0.95	0.95
0.10	0.35	169	2	0.79	0.61	0.98	0.75	0.91	0.93	0.93	0.88
	0.50	169	3	0.76	0.59	1.02	0.64	0.84	0.85	0.86	0.87
$D/b_{fc} = 4.77$ and $b_f/t_f = 20$ (Modified Vertical Bending Suite)											
0.05	0.35	208	2	0.72	0.51	1.12	0.85	1.04	0.99	1.06	1.03
	0.50	208	3	0.68	0.48	1.07	0.72	0.98	0.92	1.01	0.95
0.1	0.35	208	1	0.80	0.57	1.01	0.75	0.89	0.89	0.91	0.91
	0.50	208	1.5	0.67	0.47	1.20	0.76	0.96	0.93	0.98	1.05
$D/b_{fc} = 2.75$ and $b_f/t_f = 25$ (Modified Vertical Bending Suite)											
0.05	0.35	169	3	0.81	0.62	0.96	0.68	0.84	0.90	0.85	0.84
	0.50	169	3	0.66	0.51	1.18	0.64	0.93	0.98	0.95	0.99
0.1	0.35	169	2	0.73	0.56	1.06	0.77	0.93	1.00	0.94	0.93
	0.50	169	3	0.70	0.54	1.11	0.66	0.86	0.92	0.87	0.93
$D/b_{fc} = 2.75$ and $b_f/t_f = 25$ (Internal Loading Suite)											
0.05	0.35	169	3	0.90	0.69	0.86	0.64	0.80	0.81	0.82	0.78
	0.50	169	3	0.76	0.59	1.02	0.60	0.88	0.85	0.90	0.89
0.1	0.35	169	2	0.86	0.66	0.90	0.67	0.82	0.85	0.83	0.80
	0.50	169	3	0.86	0.66	0.90	0.57	0.76	0.75	0.77	0.78
$D/b_{fc} = 4.77$ and $b_f/t_f = 20$ (Free End Suite)											
0.05	0.6	208	3	0.77	0.54	1.05	0.53	0.81	0.74	0.83	0.90
0.1	0.6	208	3	0.8	0.57	1.01	0.57	0.77	0.69	0.79	0.87
Average						1.03	0.68	0.89	0.88	0.91	0.91
Standard Deviation						0.09	0.08	0.07	0.08	0.07	0.08
High				0.90	0.69	1.20	0.85	1.04	1.00	1.06	1.05
Low				0.66	0.47	0.86	0.53	0.76	0.69	0.77	0.78

APPENDIX B

SHEAR STRENGTH DATA

This appendix presents detailed data pertaining to the shear strength (i.e., maximum V/M) parametric studies. The organization of the appendix is as follows:

- Section B.1 presents the ultimate shear strength data computed by full nonlinear finite element analysis, as well as the ratios of predicted ultimate shear strengths to the finite element values.

- Section B.2 summarizes the elastic buckling strengths calculated by finite element linear buckling analysis and gives the ratios of the elastic buckling predictions by:

  1. The current AASHTO LRFD (2001) equations (Eqs. (2-95c) and (2-96)) and

  2. The equations proposed by Lee and Yoo (1998) (Eqs. (4-1) and (2-104) through (2-106b))

  to the analysis-based strengths. In the modified AASHTO shear strength equations (see Section 2.2.4), Lee and Yoo's shear buckling coefficient is utilized with Eq. (2-95c). Equation (2-95d) is utilized for the web plastic shear capacity in all the calculations. Therefore, the elastic shear buckling strength in the modified AASHTO procedure is 1.52/1.55 = 0.98 of that determined based on Lee and Yoo's equations.

- Section B.3 gives values for the normalized post-buckling strengths $V_{PB} / (V_p - V_{cr})$ obtained from the finite element values of V_n and V_{cr}, where V_{PB} is taken as $V_n - V_{cr}$. This ratio is always equal to 0.4 in the design approximation proposed by Lee and Yoo (1998), and it is given by Eq. (8-3) in the current and modified AASHTO procedures. This section also summarizes the $V_{PB}/V_p = (V_n - V_{cr})/V_p$ ratios from analysis and from the design equations.

- Each of the above sections focuses only on doubly symmetric specimens. Section B.4 presents the above data for the unsymmetric girders considered in the parametric study

As stated in Chapter VIII, some specimens with large unbraced length ($L_b > L_p$) fail by lateral bending instead of web shear buckling under the high-shear low-moment loading. The results for these specimens are displayed in italic font and are not included in the calculations of statistical values (see Tables B.1.2, B.3.1 and B.3.3).

Illustrative example design shear strength calculations are presented in Section 4.5.2.

B.1 ULTIMATE SHEAR STRENGTH

Table B.1.1. Ultimate shear strengths for specimens with $L_b/R = 0.05$ and target $f_\ell/f_b = 0.35$.

D/b_f	b_f/t_f	D/t_w	d_o/D	$V_{n(FEA)}/V_p$	Current AASHTO FEA	Lee and Yoo FEA	Modified AASHTO FEA
2.25	25	100	3	0.76	0.83	0.96	1.06
		130	3	0.62	0.79	1.03	0.99
		160	1	0.77	0.97	0.80	1.00
			2	0.58	0.89	1.03	1.01
			3	0.53	0.79	1.11	0.94
2.75	15	100	3	0.79	0.80	0.94	1.06
		130	3	0.62	0.79	1.02	0.98
		160	1	0.84	0.89	0.73	0.92
			2	0.62	0.84	0.95	0.95
			3	0.56	0.74	1.04	0.88
2.75	20	100	3	0.75	0.84	0.98	1.09
		130	3	0.59	0.82	1.07	1.03
		160	1	0.77	0.97	0.80	1.00
			2	0.58	0.90	1.02	1.01
			3	0.55	0.75	1.06	0.90
2.75	25	100	3	0.72	0.87	0.98	1.06
		130	3	0.58	0.83	1.08	1.03
		160	1	0.75	1.00	0.82	1.04
			2	0.56	0.92	1.05	1.04
			3	0.53	0.78	1.11	0.94
3.25	25	160	1	0.74	1.01	0.83	1.05
			2	0.55	0.95	1.08	1.06
			3	0.51	0.82	1.15	0.97

Table B.1.2. Ultimate shear strengths for specimens with $L_b/R = 0.05$ and target $f_\ell/f_b = 0.50$.

D/b_f	b_f/t_f	D/t_w	d_o/D	$V_{n(FEA)}/V_p$	Current AASHTO FEA	Lee and Yoo FEA	Modified AASHTO FEA
2.25	25	100	3	***0.45***[1]	***1.40***	***1.62***	***1.79***
		130	3	***0.53***	***0.92***	***1.19***	***1.15***
		160	1	***0.60***	***1.25***	***1.03***	***1.29***
			2	0.57	0.92	1.05	1.03
			3	0.52	0.79	1.11	0.94
2.75	15	100	3	***0.65***	***0.97***	***1.14***	***1.29***
		130	3	0.61	0.80	1.04	1.00
		160	1	***0.75***	***1.00***	***0.82***	***1.03***
			2	0.60	0.86	0.98	0.97
			3	0.55	0.75	1.07	0.91
2.75	20	100	3	***0.53***	***1.18***	***1.37***	***1.52***
		130	3	0.59	0.82	1.07	1.03
		160	1	***0.68***	***1.09***	***0.90***	***1.13***
			2	0.57	0.91	1.03	1.02
			3	0.54	0.77	1.09	0.92
2.75	25	100	3	***0.45***	***1.40***	***1.58***	***1.71***
		130	3	***0.51***	***0.94***	***1.22***	***1.16***
		160	1	***0.59***	***1.27***	***1.04***	***1.31***
			2	0.55	0.94	1.07	1.06
			3	0.52	0.80	1.13	0.96
3.25	25	160	1	***0.55***	***1.36***	***1.12***	***1.41***
			2	0.53	0.98	1.12	1.11
			3	0.49	0.84	1.19	1.00

[1] Values in bold italic font indicate specimens in which the failure is dominated by lateral bending.

Table B.1.3. Ultimate shear strengths for specimens with $L_b/R = 0.075$ and target $f_t/f_b = 0.35$.

D/b_f	b_f/t_f	D/t_w	d_o/D	$V_{n(FEA)}/V_p$	Current AASHTO FEA	Lee and Yoo FEA	Modified AASHTO FEA
2.25	25	100	3	0.76	0.83	0.96	1.06
		130	3	0.61	0.79	1.03	0.99
		160	1	0.77	0.98	0.80	1.01
			2	0.58	0.90	1.03	1.01
			3	0.53	0.78	1.10	0.93
2.75	15	100	3	0.78	0.80	0.95	1.07
		130	3	0.61	0.79	1.03	0.99
		160	1	0.83	0.90	0.74	0.93
			2	0.61	0.85	0.96	0.96
			3	0.56	0.75	1.05	0.89
2.75	20	100	3	0.75	0.85	0.98	1.09
		130	3	0.59	0.82	1.07	1.03
		160	1	0.77	0.97	0.80	1.01
			2	0.57	0.91	1.03	1.02
			3	0.55	0.76	1.07	0.90
2.75	25	100	3	0.72	0.88	0.99	1.07
		130	3	0.57	0.86	1.11	1.06
		160	1	0.74	1.00	0.83	1.04
			2	0.54	0.96	1.09	1.08
			3	0.51	0.82	1.15	0.97
3.25	25	160	1	0.74	1.02	0.84	1.05
			2	0.52	1.00	1.13	1.12

Table B.1.4. Ultimate shear strengths for specimens with $L_b/R = 0.075$ and target $f_t/f_b = 0.50$.

D/b_f	b_f/t_f	D/t_w	d_o/D	$V_{n(FEA)}/V_p$	Current AASHTO FEA	Lee and Yoo FEA	Modified AASHTO FEA
2.25	25	100	3	0.76	0.83	0.96	1.06
		130	3	0.61	0.79	1.03	0.99
		160	1	0.76	0.98	0.81	1.02
			2	0.57	0.92	1.06	1.04
			3	0.52	0.79	1.11	0.94
2.75	15	100	3	0.78	0.80	0.95	1.07
		130	3	0.60	0.80	1.05	1.01
		160	1	0.82	0.91	0.75	0.94
			2	0.60	0.87	0.99	0.98
			3	0.54	0.76	1.08	0.91
2.75	20	100	3	0.73	0.86	1.00	1.11
		130	3	0.58	0.83	1.08	1.04
		160	1	0.76	0.98	0.81	1.02
			2	0.56	0.93	1.06	1.05
			3	0.53	0.78	1.10	0.93
2.75	25	100	3	0.72	0.88	0.99	1.07
		130	3	0.56	0.86	1.11	1.06
		160	1	0.74	1.02	0.84	1.05
			2	0.54	0.96	1.09	1.08
			3	0.50	0.82	1.16	0.98
3.25	25	160	1	0.71	1.05	0.87	1.09
			2	0.52	1.00	1.14	1.13
			3	0.48	0.85	1.21	1.02

Table B.1.5. Ultimate shear strengths for specimens with $L_b/R = 0.1$ and target $f_t/f_b = 0.35$.

D/b_f	b_f/t_f	D/t_w	d_o/D	$V_{n(FEA)}/V_p$	Current AASHTO FEA	Lee and Yoo FEA	Modified AASHTO FEA
2.25	25	100	3	0.76	0.83	0.96	1.06
		130	3	0.61	0.79	1.03	0.99
		160	1	0.76	0.98	0.81	1.01
			2	0.57	0.91	1.04	1.02
			3	0.53	0.79	1.11	0.94
2.75	15	100	2	0.80	0.91	0.94	1.11
		130	2	0.62	0.95	1.03	1.11
		160	1	0.83	0.90	0.74	0.93
			2	0.61	0.86	0.97	0.96
2.75	20	100	2	0.76	0.95	0.99	1.15
		130	2	0.60	0.98	1.06	1.14
		160	1	0.77	0.98	0.80	1.01
			2	0.56	0.94	1.06	1.06
2.75	25	100	2	0.73	1.00	1.00	1.15
		130	2	0.59	1.00	1.09	1.16
		160	1	0.74	1.00	0.83	1.04
			2	0.54	0.97	1.11	1.09
3.25	25	160	1	0.73	1.03	0.85	1.06
			2	0.52	1.00	1.13	1.12

Table B.1.6. Ultimate shear strengths for specimens with $L_b/R = 0.1$ and target $f_t/f_b = 0.50$.

D/b_f	b_f/t_f	D/t_w	d_o/D	$V_{n(FEA)}/V_p$	Current AASHTO FEA	Lee and Yoo FEA	Modified AASHTO FEA
2.25	25	100	3	0.75	0.84	0.97	1.08
		130	3	0.60	0.81	1.05	1.01
		160	1	0.75	0.99	0.82	1.03
			2	0.57	0.92	1.06	1.04
			3	0.52	0.79	1.13	0.95
2.75	15	100	3	0.78	0.81	0.96	1.07
		130	3	0.60	0.81	1.06	1.02
		160	1	0.81	0.92	0.76	0.95
			2	0.59	0.88	1.00	0.99
			3	0.54	0.76	1.08	0.91
2.75	20	100	3	0.73	0.87	1.01	1.12
		130	3	0.57	0.85	1.11	1.06
		160	1	0.75	0.99	0.82	1.03
			2	0.55	0.95	1.08	1.07
			3	0.52	0.79	1.12	0.95
2.75	25	100	3	0.71	0.88	0.99	1.07
		130	3	0.56	0.86	1.12	1.07
		160	1	0.72	1.03	0.85	1.07
			2	0.53	0.99	1.12	1.11
			3	0.48	0.85	1.21	1.02
3.25	25	160	1	0.69	1.09	0.90	1.12
			2	0.50	1.04	1.18	1.16
			3	0.46	0.90	1.27	1.07

B.2 ELASTIC SHEAR BUCKLING STRENGTH

Table B.2.1. Elastic shear buckling strengths for specimens with $L_b/R = 0.05$ and target $f_t/f_b = 0.35$.

D/b_f	b_f/t_f	D/t_w	d_o/D	$V_{cr(FEA)}/V_p$	Current AASHTO FEA	Lee and Yoo FEA
2.25	25	100	3	0.72	0.68	1.04
		130	3	0.46	0.63	1.02
		160	1	0.43	0.80	0.97
			2	0.33	0.65	1.00
			3	0.32	0.61	0.98
2.75	15	100	3	0.76	0.64	1.04
		130	3	0.47	0.62	0.99
		160	1	0.44	0.78	0.95
			2	0.34	0.64	0.98
			3	0.32	0.60	0.97
2.75	20	100	3	0.72	0.68	1.06
		130	3	0.46	0.63	1.02
		160	1	0.44	0.79	0.96
			2	0.33	0.65	1.00
			3	0.31	0.61	0.98
2.75	25	100	3	0.66	0.74	1.05
		130	3	0.44	0.65	1.03
		160	1	0.42	0.81	0.99
			2	0.32	0.67	1.03
			3	0.30	0.63	1.02
3.25	25	160	1	0.42	0.83	1.01
			2	0.31	0.69	1.05
			3	0.29	0.66	1.05

Table B.2.2. Elastic shear buckling strengths for specimens with $L_b/R = 0.05$ and target $f_\ell/f_b = 0.50$.

D/b_f	b_f/t_f	D/t_w	d_o/D	$V_{cr(FEA)}/V_p$	Current AASHTO FEA	Lee and Yoo FEA
2.25	25	100	3	***0.70***[1]	***0.71***	***1.08***
		130	3	***0.46***	***0.63***	***1.02***
		160	1	***0.38***	***0.91***	***1.11***
			2	0.31	0.69	1.06
			3	0.30	0.64	1.03
2.75	15	100	3	***0.74***	***0.66***	***1.07***
		130	3	0.46	0.63	1.01
		160	1	***0.42***	***0.82***	***0.99***
			2	0.32	0.67	1.02
			3	0.31	0.61	0.98
2.75	20	100	3	***0.67***	***0.73***	***1.13***
		130	3	0.44	0.66	1.06
		160	1	***0.40***	***0.87***	***1.05***
			2	0.32	0.67	1.03
			3	0.30	0.63	1.02
2.75	25	100	3	***0.58***	***0.85***	***1.20***
		130	3	***0.41***	***0.71***	***1.11***
		160	1	***0.37***	***0.93***	***1.13***
			2	0.30	0.72	1.10
			3	0.29	0.66	1.06
3.25	25	160	1	***0.36***	***0.96***	***1.17***
			2	0.29	0.75	1.14
			3	0.28	0.69	1.09

[1] The values in bold italic font correspond to specimens in which the failure is dominated by lateral-torsional buckling.

Table B.2.3. Elastic shear buckling strengths for specimens with $L_b/R = 0.075$ and target $f_t/f_b = 0.35$.

D/b_f	b_f/t_f	D/t_w	d_o/D	$V_{cr(FEA)}/V_p$	Current AASHTO FEA	Lee and Yoo FEA
2.25	25	100	3	0.75	0.65	0.99
		130	3	0.48	0.61	0.98
		160	1	0.46	0.75	0.91
			2	0.35	0.62	0.95
			3	0.33	0.59	0.95
2.75	15	100	3	0.78	0.63	1.02
		130	3	0.48	0.60	0.97
		160	1	0.48	0.72	0.88
			2	0.35	0.62	0.95
			3	0.33	0.58	0.93
2.75	20	100	3	0.73	0.67	1.03
		130	3	0.47	0.62	1.00
		160	1	0.45	0.76	0.92
			2	0.34	0.63	0.97
			3	0.33	0.59	0.94
2.75	25	100	3	0.69	0.71	1.01
		130	3	0.45	0.65	1.02
		160	1	0.45	0.77	0.93
			2	0.34	0.64	0.99
			3	0.31	0.61	0.98
3.25	25	160	1	0.44	0.79	0.96
			2	0.33	0.66	1.01

Table B.2.4. Elastic shear buckling strengths for specimens with $L_b/R = 0.075$ and target $f_t/f_b = 0.50$.

D/b_f	b_f/t_f	D/t_w	d_o/D	$V_{cr(FEA)}/V_p$	Current AASHTO / FEA	Lee and Yoo / FEA
2.25	25	100	3	0.74	0.66	1.01
		130	3	0.47	0.61	0.98
		160	1	0.44	0.78	0.95
			2	0.33	0.65	0.99
			3	0.32	0.59	0.95
2.75	15	100	3	0.77	0.63	1.02
		130	3	0.48	0.61	0.98
		160	1	0.46	0.75	0.91
			2	0.34	0.63	0.96
			3	0.32	0.59	0.95
2.75	20	100	3	0.73	0.67	1.04
		130	3	0.46	0.63	1.01
		160	1	0.45	0.77	0.93
			2	0.33	0.64	0.99
			3	0.32	0.60	0.97
2.75	25	100	3	0.67	0.73	1.03
		130	3	0.44	0.66	1.03
		160	1	0.43	0.79	0.97
			2	0.32	0.66	1.02
			3	0.31	0.62	1.00
3.25	25	160	1	0.41	0.83	1.01
			2	0.33	0.66	1.01
			3	0.29	0.66	1.06

Table B.2.5. Elastic shear buckling strengths for specimens with $L_b/R = 0.1$ and target $f_l/f_b = 0.35$.

D/b_f	b_f/t_f	D/t_w	d_o/D	$V_{cr(FEA)}/V_p$	Current AASHTO FEA	Lee and Yoo FEA
2.25	25	100	3	0.75	0.65	0.99
		130	3	0.48	0.61	0.97
		160	1	0.47	0.73	0.88
			2	0.36	0.60	0.92
			3	0.33	0.58	0.93
2.75	15	100	2	0.82	0.67	1.02
		130	2	0.52	0.63	0.95
		160	1	0.50	0.69	0.84
			2	0.37	0.59	0.90
2.75	20	100	2	0.79	0.70	1.02
		130	2	0.51	0.64	0.97
		160	1	0.49	0.70	0.85
			2	0.36	0.60	0.92
2.75	25	100	2	0.76	0.73	0.98
		130	2	0.50	0.65	0.97
		160	1	0.47	0.73	0.89
			2	0.36	0.61	0.93
3.25	25	160	1	0.46	0.75	0.92
			2	0.34	0.63	0.96

Table B.2.6. Elastic shear buckling strengths for specimens with $L_b/R = 0.1$ and target $f_\ell/f_b = 0.50$.

D/b_f	b_f/t_f	D/t_w	d_o/D	$V_{cr(FEA)}/V_p$	Current AASHTO FEA	Lee and Yoo FEA
2.25	25	100	3	0.74	0.66	1.01
		130	3	0.49	0.60	0.95
		160	1	0.45	0.77	0.93
			2	0.35	0.62	0.95
			3	0.32	0.59	0.96
2.75	15	100	3	0.78	0.63	1.02
		130	3	0.48	0.60	0.97
		160	1	0.47	0.74	0.90
			2	0.35	0.61	0.93
			3	0.33	0.58	0.93
2.75	20	100	3	0.74	0.66	1.03
		130	3	0.47	0.62	0.99
		160	1	0.46	0.75	0.91
			2	0.34	0.63	0.96
			3	0.33	0.58	0.93
2.75	25	100	3	0.69	0.71	1.00
		130	3	0.45	0.64	1.00
		160	1	0.44	0.78	0.95
			2	0.34	0.63	0.97
			3	0.32	0.60	0.96
3.25	25	160	1	0.43	0.81	0.98
			2	0.33	0.66	1.00
			3	0.31	0.62	1.00

B.3 POST-BUCKLING STRENGTH

Table B.3.1. $V_{PB} / (V_p - V_{cr}) = (V_n - V_{cr}) / (V_p - V_{cr})$ from finite element analysis[1].

Specimens	D/t_w	d_o/D	Target $f_\ell/f_b = 0.35$			Target $f_\ell/f_b = 0.50$		
			L_b/R			L_b/R		
			0.05	0.075	0.10	0.05	0.075	0.10
$D/b_f = 2.25$	100	3	0.18	0.03	0.02	***-0.81***[2]	0.09	0.04
$b_f/t_f = 25$	130	3	0.29	0.26	0.25	***0.13***	0.26	0.22
	160	1	0.60	0.57	0.55	***0.36***	0.57	0.55
		2	0.38	0.35	0.34	0.37	0.35	0.34
		3	0.32	0.30	0.29	0.33	0.30	0.29
$D/b_f = 2.75$	100	2	NA[3]	NA	-0.15	NA	NA	NA
$b_f/t_f = 15$		3	0.11	0.04	NA	***-0.33***	0.04	0.00
	130	2	NA	NA	0.20	NA	NA	NA
		3	0.28	0.25	NA	0.27	0.24	0.22
	160	1	0.71	0.68	0.66	***0.57***	0.66	0.64
		2	0.43	0.40	0.38	0.41	0.39	0.37
		3	0.36	0.33	NA[4]	0.34	0.32	0.31
$D/b_f = 2.75$	100	2	NA	NA	-0.17	NA	NA	NA
$b_f/t_f = 20$		3	0.11	0.05	NA	***-0.41***	0.03	-0.04
	130	2	NA	NA	0.18	NA	NA	NA
		3	0.25	0.23	NA	0.26	0.23	0.19
	160	1	0.59	0.58	0.54	***0.48***	0.57	0.54
		2	0.37	0.35	0.31	0.37	0.34	0.31
		3	0.34	0.33	NA	0.34	0.31	0.29
$D/b_f = 2.75$	100	2	NA	NA	-0.14	NA	NA	NA
$b_f/t_f = 25$		3	0.18	0.10	NA	***-0.31***	0.15	0.08
	130	2	NA	NA	0.17	NA	NA	NA
		3	0.25	0.22	NA	***0.18***	0.22	0.20
	160	1	0.56	0.54	0.52	***0.35***	0.53	0.50
		2	0.36	0.31	0.28	0.36	0.32	0.28
		3	0.32	0.28	NA	0.32	0.28	0.24
$D/b_f = 3.25$	160	1	0.55	0.53	0.50	***0.29***	0.51	0.45
$b_f/t_f = 25$		2	0.35	0.29	0.27	0.34	0.28	0.26
		3	0.31	NA	NA	0.30	0.27	0.22

[1] Unreduced value specified by Lee and Yoo (1998) is 0.4; values predicted by AASHTO and modified AASHTO are 0.615 ($d_o/D = 1$), 0.389 ($d_o/D = 2$) and 0.275 ($d_o/D = 3$)).

[2] Values in bold italic font indicate specimens that fail by lateral bending.

[3] Only the specimens with $L_b/R = 0.10$ and target $f_\ell/f_b = 0.35$ have $d_o/D = 2$ for $D/t_w = 100$ and 130.

[4] NA for $L_b/R = 0.10$ and target $f_\ell/f_b = 0.35$, since $L_b/D < 3$.

Table B.3.2. $(V_n - V_{cr}) / V_p$ from design equations and from FEA for target $f_t/f_b = 0.35$.

Specimens	D/t_w	d_o/D	Current AASHTO	Modified AASHTO	Lee and Yoo	FEA		
						$L_b/R = 0.05$	$L_b/R = 0.075$	$L_b/R = 0.10$
$D/b_f = 2.25$	100	3	0.14	0.07	-0.02	0.05	0.01	0.01
$b_f/t_f = 25$	130	3	0.20	0.15	0.17	0.16	0.14	0.13
	160	1	0.40	0.36	0.20	0.34	0.30	0.29
		2	0.30	0.26	0.26	0.25	0.23	0.22
		3	0.22	0.19	0.28	0.22	0.20	0.20
$D/b_f = 2.75$	100	2	0.18	0.07	-0.06	NA[1]	NA	-0.03
$b_f/t_f = 15$		3	0.14	0.06	-0.04	0.03	0.01	NA
	130	2	0.26	0.20	0.14	NA	NA	0.10
		3	0.20	0.15	0.17	0.15	0.13	NA
	160	1	0.40	0.36	0.20	0.40	0.36	0.33
		2	0.30	0.26	0.26	0.28	0.26	0.24
		3	0.22	0.19	0.28	0.24	0.22	NA[2]
$D/b_f = 2.75$	100	2	0.18	0.08	-0.06	NA	NA	-0.03
$b_f/t_f = 20$		3	0.14	0.07	-0.02	0.03	0.01	NA
	130	2	0.26	0.20	0.14	NA	NA	0.09
		3	0.20	0.15	0.17	0.13	0.12	NA
	160	1	0.40	0.36	0.20	0.33	0.31	0.27
		2	0.30	0.26	0.26	0.25	0.23	0.20
		3	0.22	0.19	0.28	0.24	0.22	NA
$D/b_f = 2.75$	100	2	0.18	0.10	-0.01	NA	NA	-0.03
$b_f/t_f = 25$		3	0.14	0.09	0.02	0.06	0.03	NA
	130	2	0.26	0.20	0.15	NA	NA	0.09
		3	0.20	0.15	0.17	0.14	0.12	NA
	160	1	0.40	0.36	0.20	0.32	0.29	0.27
		2	0.30	0.26	0.26	0.24	0.21	0.18
		3	0.22	0.19	0.28	0.22	0.19	NA
$D/b_f = 3.25$	160	1	0.40	0.36	0.20	0.32	0.30	0.27
$b_f/t_f = 25$		2	0.30	0.26	0.27	0.24	0.20	0.18
		3	0.22	0.19	0.28	0.22	NA	NA

[1] Only the specimens with $L_b/R = 0.10$ and target $f_t/f_b = 0.35$ have $d_o/D = 2$ for $D/t_w = 100$ and 130.

[2] NA for $L_b/R = 0.10$ and target $f_t/f_b = 0.35$, since $L_b/D < 3$.

Table B.3.3. $(V_n - V_{cr}) / V_p$ from design equations and from FEA for target $f_t/f_b = 0.50$.

Specimens	D/t_w	d_o/D	Current AASHTO	Modified AASHTO	Lee and Yoo	FEA		
						$L_b/R = 0.05$	$L_b/R = 0.075$	$L_b/R = 0.10$
$D/b_f = 2.25$	100	3	0.14	0.07	-0.02	***-0.24***[1]	0.02	0.01
$b_f/t_f = 25$	130	3	0.20	0.15	0.17	***0.07***	0.14	0.12
	160	1	0.40	0.36	0.20	***0.22***	0.32	0.30
		2	0.30	0.26	0.26	0.26	0.23	0.22
		3	0.22	0.19	0.28	0.23	0.20	0.20
$D/b_f = 2.75$	100	3	0.14	0.06	-0.04	***-0.09***	0.01	0.00
$b_f/t_f = 15$	130	3	0.20	0.15	0.17	0.15	0.12	0.12
	160	1	0.40	0.36	0.2	***0.33***	0.36	0.35
		2	0.30	0.26	0.26	0.28	0.26	0.24
		3	0.22	0.19	0.28	0.23	0.22	0.21
$D/b_f = 2.75$	100	3	0.14	0.07	-0.02	***-0.14***	0.01	-0.01
$b_f/t_f = 20$	130	3	0.20	0.15	0.17	0.15	0.12	0.10
	160	1	0.40	0.36	0.20	***0.29***	0.31	0.29
		2	0.30	0.26	0.26	0.25	0.22	0.20
		3	0.22	0.19	0.28	0.23	0.21	0.19
$D/b_f = 2.75$	100	3	0.14	0.09	0.02	***-0.13***	0.05	0.02
$b_f/t_f = 25$	130	3	0.20	0.15	0.17	***0.11***	0.12	0.11
	160	1	0.40	0.36	0.20	***0.22***	0.30	0.28
		2	0.30	0.26	0.26	0.25	0.22	0.19
		3	0.22	0.19	0.28	0.23	0.19	0.16
$D/b_f = 3.25$	160	1	0.40	0.36	0.20	***0.19***	0.30	0.26
$b_f/t_f = 25$		2	0.30	0.26	0.27	0.24	0.19	0.18
		3	0.22	0.19	0.28	0.22	0.19	0.15

[1] Values in bold italic font indicate specimens in which the failure is dominated by lateral bending.

B.4 UNSYMMETRIC GIRDERS

Table B.4.1. Ultimate shear strengths for unsymmetric girders, $D/b_{fc} = 2.75$ and $b_f/t_f = 25$ (tension flange size is increased).

L_b/R	Target f_t/f_b	D/t_w	d_o/D	$V_{n(FEA)}/V_p$	Current AASHTO FEA	Lee and Yoo FEA	Modified AASHTO FEA
0.05	0.35	130	3	0.59	0.82	1.06	1.03
	0.50	130	3	0.53	0.92	1.18	1.15
0.10	0.35	130	2	0.63	0.93	1.02	1.09
	0.50	130	3	0.57	0.85	1.10	1.06

Table B.4.2. Ultimate shear strengths for unsymmetric girders, $D/b_{fc} = 4.77$ and $b_f/t_f = 20$ (compression flange size is decreased).

L_b/R	Target f_ℓ/f_b	D/t_w	d_o/D	$V_{u(FEA)}/V_p$	Current AASHTO FEA	Lee and Yoo FEA	Modified AASHTO FEA
0.05	0.35	160	2	0.52	1.00	1.14	1.13
	0.50	160	3	0.50	0.83	1.18	0.99
0.10	0.35	160	1	0.75	1.00	0.82	1.03
	0.50	160	1.5	0.58	1.05	1.03	1.14

Table B.4.3. Elastic shear buckling strengths for unsymmetric girders, $D/b_{fc} = 2.75$ and $b_f/t_f = 25$ (tension flange size is increased).

L_b/R	Target f_ℓ/f_b	D/t_w	d_o/D	$V_{cr(FEA)}/V_p$	Current AASHTO FEA	Lee and Yoo FEA
0.05	0.35	130	3	0.48	0.61	0.98
	0.50	130	3	0.41	0.70	1.13
0.10	0.35	130	2	0.51	0.63	0.97
	0.50	130	3	0.45	0.63	1.03

Table B.4.4. Elastic shear buckling strengths for unsymmetric girders, $D/b_{fc} = 4.77$ and $b_f/t_f = 20$ (compression flange size is decreased).

L_b/R	Target f_ℓ/f_b	D/t_w	d_o/D	$V_{cr(FEA)}/V_p$	Current AASHTO FEA	Lee and Yoo FEA
0.05	0.35	160	2	0.31	0.70	1.07
	0.50	160	3	0.27	0.70	1.13
0.10	0.35	160	1	0.51	0.67	0.82
	0.50	160	1.5	0.41	0.61	0.87

Page intentionally left blank

APPENDIX C

MOMENT-SHEAR INTERACTION DATA

This appendix presents complete listings of the data values and key background data for the moment-shear interaction parametric studies discussed in Chapter IX. As noted previously, these studies involve uniform vertical bending, maximum V/M and high-moment high-shear loadings on the primary test suite of girders (see Sections 5.1 and 5.2). Also, in these studies, the elastic design analysis flange lateral bending stresses are obtained by use of a first-order open-walled section curved beam element (see Sections 3.1 and 3.6).

Section C.1 presents the uniform vertical bending data for the doubly symmetric I girders. The ratio of the flange first-order elastic lateral and vertical bending stresses f_ℓ/f_b, obtained via the curved-beam analysis, is reported for each of the tests. Also, the ratio of this f_ℓ/f_b to the corresponding second-order elastic values, obtained from the shell finite element models and reported in Appendix A, is listed. The first-order elastic beam theory underestimates the second-order elastic shell finite element predictions by as much as 31 percent (see Table C.1.4), and as is expected, the beam theory based solutions generally tend to under predict the shell finite element based elastic stresses. However, for some of the girders analyzed, the beam finite element analysis gives f_ℓ/f_b values that are larger than obtained by the elastic second-order shell finite element solutions. In one case, the beam solution gives an f_ℓ/f_b value that is 38 percent higher than the corresponding shell solution (see Table C.1.5). Nevertheless, the maximum change in the ratio of the uniform vertical bending capacity to the strength predicted by the one-third rule equations, compared to the values calculated using second-order elastic shell finite element analysis, is $\pm$ four percent (see the last column in Tables C.1.1 through C.1.5). This is due to the insensitivity of the one-third rule equations to approximations in the flange lateral bending stresses. It is expected that the over predictions by the beam theory for some of the girders may be due to a combination of:

- The simplified procedure utilized to calculate the flange elastic lateral and vertical bending stresses from the shell finite element models (see Section 3.6), and

- As discussed in Section 3.1, the shell finite element meshes are essentially twice as dense as required for convergence of the maximum load prediction in the full nonlinear shell finite element solutions. However, convergence of the elastic stresses at the maximum moment locations was not verified. Some additional mesh refinement may be necessary for accurate prediction of the maximum elastic stresses in some of the girders.

In addition to the data values discussed above, the ratio of the uniform vertical bending capacity to the cross-section yield moment, M_{FEA}/M_y, is also presented. This information is repeated from the corresponding tables in Appendix A for convenience of reference. Finally, the ratio of the uniform vertical bending capacity (obtained from full nonlinear shell finite

element analysis) to the vertical bending strength estimate per the one-third rule equations, using the first-order f_ℓ/f_b values obtained from beam theory ($M_{FEA}/M_{(1/3\ rule)}$), are presented in the tables of Section C.1 (see the next to last column of Tables C.1.1 through C.1.5). The inverse of these values is generally a close estimate the "1/3 Rule/FEA" values reported in Section A.1.3.

Section C.2 presents the moment-shear interaction plot data from the maximum V/M tests of the symmetric I girders. Again, the first-order elastic f_ℓ/f_b values are reported. These values are utilized for calculation of $M_{n(1/3\ rule)}$ per equations (2-90), and the corresponding values of $M_{FEA}/M_{n(1/3\ rule)}$ are provided in the tables of this section, where M_{FEA} is the maximum moment within the test unsupported length at the girder capacity in the maximum V/M tests. The ratio M_{FEA}/M_y is also reported. Finally, three normalized values of the web shear force at the girder capacity in the maximum V/M tests are listed:

- V_{FEA}/V_p, where V_{FEA} is the shear at the girder capacity in the full nonlinear analysis and V_p is the web plastic strength per Eq. (2-95d),

- $V_{FEA}/V_{n(AASHTO)}$, where $V_{n(AASHTO)}$ is the AASHTO LRFD (2001) shear strength, including tension field action (see Section 2.2.4).

As noted in Sections 8.1.1 and 9.1, the failure mode is dominated by lateral bending in eleven of the maximum V/M tests. These tests are highlighted by bold italic font in the tables of Section C.2.

Section C.3 presents the high-moment high-shear data for the moment-shear interaction parametric study. The tables in this section present the same information as those in Section C.2 along with the load parameter α and the ratio of the smaller to the larger end moments within the test length M_3/M_2 (see Section 5.3 for a description of the loading arrangement and associated moment and shear diagrams in these tests). As discussed in Section 5.5, some of the primary test suite girders have unsupported lengths that are large enough such that the desired distance from the maximum moment location to the inflection point, $M_{max}/V = M_{n(FEA)}/0.8V_{n(FEA)}$ is smaller than $L_b/2$, where $M_{n(FEA)}$ is the uniform vertical bending flexural capacity and $V_{n(FEA)}$ is the maximum V/M test shear capacity in the primary test suite. Of course, this is not physically possible. Also, in some of the girders $M_{n(FEA)}/0.8V_{n(FEA)}L_b$ is smaller than 0.55, such that the desired high-moment high-shear loading is very similar to that utilized in the corresponding maximum V/M test. Therefore, as explained in Section 5.5, additional high-shear high-moment tests are not conducted for these girders.

Ten of the eleven girders that fail by dominant lateral bending in the maximum V/M tests also have $M_{n(FEA)}/0.8V_{n(FEA)} < 0.55$. The additional girder that failed in lateral bending in the maximum V/M test is indicated in Table C.3.2.

In several of the high-moment high-shear tests, significant distortion occurs within the web panel outside of the test length at the maximum moment location, and the maximum capacities are reached at load levels significantly smaller than expected based on the prediction equations. In several of these cases, the web bearing stiffener also exhibits

significant distortion at the capacity of the girder. These girders are not considered in the assessment of the moment-shear interaction strengths (see Tables C.3.2 and C.3.3). In one set of these tests, the girders with $D/b_f = 2.75$, $b_f/t_f = 15$, $L_b/R = 0.10$ and target $f_\ell/f_b = 0.35$, the length of the test segment L_b is only 2D. It is observed that the effect of transverse patch loadings on the behavior of thin webs in curved I girders deserves further study. However, this issue is outside of the scope of this research effort.

Finally, the analyses of four of the high-moment high-shear tests are inadvertently omitted within the moment-shear interaction study. Timing of the preparation of the final report was not sufficient to allow these tests to be included. The authors intend to complete these analyses at a later time. Nevertheless, the results from these analyses are not expected to influence the overall conclusions from the moment-shear interaction parametric study. Also, as noted in Chapter IX, the α values for some of the tests differ from the values associated with $M_{max}/V = M_{n(FEA)}/0.8V_{n(FEA)}$. In one of the tests, the resulting analysis is more of a high-shear low-moment test than high-shear high-moment. However, in all the other cases, the loading is still effectively high-shear high-moment. The tests that differ from the targeted α values are marked in the tables.

There is one trend in the data in Tables C.3.1 through C.3.5 that is in many cases opposite from the expected strength behavior, and opposite from the trends observed in the uniform vertical bending and maximum V/M tests. In many cases, the bending strength M_{FEA}/M_y increases with increasing panel aspect ratio d_o/D. The only logical explanation of this trend that the authors have been able to arrive at is that there may be some interaction between the anchorage of the web tension field and the compression flange lateral and local stability. Further detailed studies are needed to better understand the underlying mechanisms associated with this behavior. Nevertheless, a key characteristic of all the high-moment high-shear flexural strengths is that in all cases, they are greater than the corresponding uniform vertical bending strengths (although in a significant number of cases, the high-shear high-moment and uniform vertical bending strengths are approximately the same).

Section C.4 shows data for the unsymmetric girders. This data parallels that shown for the symmetric girders in Sections C.1 through C.3. Also, since the shape factor of the monosymmetric girders is significantly larger than that of the doubly symmetric ones, the ratio M_{FEA}/M_p is listed in the tables of this section. It can be observed from Tables C.4.3 and C.4.4 that the monosymmetric girder with $D/b_{fc} = 2.75$, $b_f/t_f = 25$ and $2D_c/t_w = 169$ has an $M_{n(FEA)}/0.8V_{n(FEA)} < 0.55$ for the case of $L_b/R = 0.05$ and target $f_\ell/f_b = 0.5$. Therefore, only seven of the eight unsymmetric girders are analyzed with the high-moment high-shear loading. Actually, from the values of $M_{FEA}/M_y = 0.99$ and $M_{FEA}/M_{n(1/3\ rule)} = 1.35$ shown for this girder in Table C.4.2, it is clear that the maximum V/M test of this girder is effectively a high-moment high-shear test. It is interesting to note that the ratio of the first-order beam theory based f_ℓ/f_b to the second-order elastic f_ℓ/f_b from the shell finite element analysis is generally rather small in the uniform vertical bending studies of these girders, with an average value of 0.70, a high value of 0.81 and a low of 0.61 (see Table C.4.1). However, the maximum effect on the ratio $M_{FEA}/M_{n(1/3\ rule)}$ is only five percent.

Section C.5 presents moment-shear interaction strength plots for the doubly symmetric girders, normalized by the nominal design strengths $M_{n(1/3\ rule)}$, $V_{n(AASHTO)}$, and $V_{n(modified\ AASHTO)}$ and in which the data is grouped by cross-section profile. Strength plots in which the data is grouped by L_b/R and target f_t/f_b are presented in Chapter IX. Comparison of the plots for the different cross-section profiles reveals some interesting trends. It can be observed that the shear strengths attained in the maximum V/M tests tend to be largest for the cross-sections with $D/b_f = 2.25$ and $b_f/t_f = 25$. These cross-sections have the smallest ratio of the area of the web to the area of the flanges A_w/A_f. The smallest shear strengths tend to be obtained for the cross-sections with $D/b_f = 3.25$ and $b_f/t_f = 25$. These cross-sections have the largest A_w/A_f of the sections considered in the parametric study for a given D/t_w. It can be observed that a significant degree of the overall scatter in the shear strength predictions by the AASHTO or modified AASHTO equations is due to the fact that neither of these formulas accounts for the different contributions to the shear strength from different size flanges. By comparing the figures in this section based on $V_{n(AASHTO)}$ to those based on $V_{n(modified\ AASHTO)}$, the reduced scatter in the shear strength predictions with the modified AASHTO equations is particularly evident.

Lastly, based on the figures in Section C.5, it can be observed that for the high-shear high-moment loading cases, the smallest ratios of $M/M_{n(1/3\ rule)}$ are obtained with the cross-sections having $D/b_{fc} = 2.75$ and $b_f/t_f = 15$ and 20 (see Figs. C.5.3 through C.5.6). Also, if one studies the plots in Figs. 9.1.2, 9.1.4, 9.1.6, 9.1.8, 9.1.10 and 9.1.12, it can be concluded that the smallest ratios of $M/M_{n(1/3\ rule)}$ occur also for the cases with the smallest target f_t/f_b values. In other words, the largest degradation in the flexural strengths due to high shear appears for the cases in which the most plasticity is required in developing the flexural strengths, and in which the flange lateral bending moments are the smallest. More slender cross-sections with larger flange lateral bending moments appear to exhibit less degradation in the strength due to high shear. Nevertheless, the beneficial effects of moment gradient, lateral restraint at the maximum moment location, and smaller flange lateral bending moments for the high-moment high-shear relative to the uniform vertical bending load cases actually causes *all* of the high-moment high-shear flexural strengths to be greater than the corresponding flexural strength in uniform vertical bending.

C.1 UNIFORM VERTICAL BENDING DATA, SYMMETRIC GIRDERS

Table C.1.1. Uniform vertical bending data, specimens with $D/b_f = 2.25$ and $b_f/t_f = 25$.

L_b/R	Target f_ℓ/f_b	D/t_w	d_o/D	$\frac{f_\ell}{f_b}$	Ratio to 2nd-order shell FEA $\frac{f_\ell}{f_b}$	$\frac{M_{FEA}}{M_y}$	$\frac{M_{FEA}}{M_{n(1/3\ rule)}}$	Ratio to $\frac{M_{FEA}}{M_{n(1/3\ rule)}}$ based on 2nd-order shell FEA
0.05	0.35	100	3	0.305	1.00	0.90	1.14	1.00
		130	3	0.293	0.99	0.88	1.13	1.00
		160	1	0.286	0.98	0.88	1.17	1.00
			2	0.286	0.97	0.87	1.16	1.00
			3	0.286	0.93	0.85	1.13	1.01
	0.50	100	3	0.483	0.97	0.73	1.03	1.00
		130	3	0.465	0.97	0.72	0.99	1.00
		160	1	0.453	0.98	0.73	1.02	1.00
			2	0.453	0.98	0.71	0.99	1.00
			3	0.453	0.97	0.71	0.99	1.00
0.075	0.35	100	3	0.367	1.13	0.89	1.15	0.99
		130	3	0.353	1.14	0.86	1.13	0.99
		160	1	0.344	1.15	0.86	1.16	0.99
			2	0.344	1.06	0.83	1.12	0.99
			3	0.344	0.97	0.82	1.11	1.00
	0.50	100	3	0.455	1.08	0.84	1.11	0.99
		130	3	0.438	1.08	0.83	1.12	0.99
		160	1	0.427	1.07	0.83	1.15	0.99
			2	0.427	1.07	0.81	1.12	0.99
			3	0.427	1.01	0.80	1.11	1.00
0.10	0.35	100	3	0.364	0.87	0.86	1.11	1.02
		130	3	0.350	0.84	0.83	1.09	1.02
		160	1	0.341	0.95	0.85	1.15	1.01
			2	0.341	0.87	0.81	1.09	1.02
			3	0.341	0.84	0.81	1.09	1.02
	0.50	100	3	0.489	0.94	0.84	1.12	1.01
		130	3	0.471	0.90	0.81	1.10	1.01
		160	1	0.459	1.02	0.81	1.13	1.00
			2	0.459	0.93	0.80	1.12	1.01
			3	0.459	0.88	0.79	1.10	1.02
Average					0.98		1.10	1.00
Standard Deviation					0.084		0.050	0.010
High				0.489	1.15	0.90	1.17	1.02
Low				0.286	0.84	0.71	0.99	0.99

Table C.1.2. Uniform vertical bending data, specimens with $D/b_f = 2.75$ and $b_f/t_f = 15$.

L_b/R	Target f_ℓ/f_b	D/t_w	d_o/D	$\frac{f_\ell}{f_b}$	Ratio to 2nd-order shell FEA $\frac{f_\ell}{f_b}$	$\frac{M_{FEA}}{M_y}$	$\frac{M_{FEA}}{M_{n(1/3\,rule)}}$	Ratio to $\frac{M_{FEA}}{M_{n(1/3\,rule)}}$ based on 2nd-order shell FEA
0.05	0.35	100	3	0.289	0.98	0.95	1.04	1.00
		130	3	0.279	0.97	0.92	1.01	1.00
		160	1	0.273	1.04	0.93	1.02	1.00
			2	0.273	0.99	0.92	1.01	1.00
			3	0.273	0.97	0.90	0.99	1.00
	0.50	100	3	0.427	0.99	0.85	1.12	1.00
		130	3	0.412	1.00	0.83	1.08	1.00
		160	1	0.403	1.03	0.84	1.09	1.00
			2	0.403	1.01	0.84	1.09	1.00
			3	0.403	0.99	0.82	1.07	1.00
0.075	0.35	100	3	0.328	0.98	0.93	1.03	1.00
		130	3	0.317	0.96	0.92	1.02	1.00
		160	1	0.310	1.14	0.90	1.00	0.99
			2	0.310	1.10	0.89	0.99	0.99
			3	0.310	0.97	0.88	0.98	1.00
	0.50	100	3	0.434	1.14	0.92	1.05	0.98
		130	3	0.419	1.11	0.90	1.03	0.99
		160	1	0.410	1.15	0.91	1.04	0.98
			2	0.410	1.14	0.88	1.01	0.98
			3	0.410	1.10	0.87	1.00	0.99
0.10	0.35	100	2	0.296	0.92	0.96	1.05	1.01
		130	2	0.286	0.95	0.92	1.01	1.00
		160	1	0.280	1.11	0.88	0.97	0.99
			2	0.280	0.98	0.87	0.96	1.00
	0.50	100	3	0.438	0.94	0.91	1.04	1.01
		130	3	0.423	0.93	0.89	1.02	1.01
		160	1	0.413	1.07	0.88	1.01	0.99
			2	0.413	1.00	0.88	1.01	1.00
			3	0.413	0.94	0.87	1.00	1.01
Average					1.02		1.03	1.00
Standard Deviation					0.072		0.038	0.007
High				0.438	1.15	0.96	1.12	1.01
Low				0.273	0.92	0.82	0.96	0.98

Table C.1.3. Uniform vertical bending data, specimens with $D/b_f = 2.75$ and $b_f/t_f = 20$.

L_b/R	Target f_ℓ/f_b	D/t_w	d_o/D	$\frac{f_\ell}{f_b}$	Ratio to 2nd-order shell FEA $\frac{f_\ell}{f_b}$	$\frac{M_{FEA}}{M_y}$	$\frac{M_{FEA}}{M_{n(1/3\,rule)}}$	Ratio to $\frac{M_{FEA}}{M_{n(1/3\,rule)}}$ based on 2nd-order shell FEA
0.05	0.35	100	3	0.305	0.94	0.90	1.02	1.01
		130	3	0.292	0.90	0.88	1.00	1.01
		160	1	0.283	0.97	0.89	1.03	1.00
			2	0.283	0.92	0.89	1.03	1.01
			3	0.283	0.88	0.85	0.98	1.01
	0.50	100	3	0.455	0.98	0.82	1.10	1.00
		130	3	0.435	0.95	0.82	1.08	1.01
		160	1	0.423	0.98	0.83	1.10	1.00
			2	0.423	0.97	0.81	1.07	1.00
			3	0.423	0.94	0.81	1.07	1.01
0.075	0.35	100	3	0.345	0.93	0.93	1.07	1.01
		130	3	0.329	0.88	0.91	1.05	1.01
		160	1	0.320	1.10	0.90	1.05	0.99
			2	0.320	1.02	0.89	1.04	1.00
			3	0.320	0.86	0.88	1.03	1.02
	0.50	100	3	0.461	1.09	0.91	1.08	0.99
		130	3	0.440	1.05	0.89	1.06	0.99
		160	1	0.428	1.07	0.89	1.07	0.99
			2	0.428	1.05	0.88	1.06	0.99
			3	0.428	0.91	0.88	1.06	1.01
0.10	0.35	100	2	0.309	0.82	0.92	1.05	1.02
		130	2	0.295	0.79	0.91	1.04	1.02
		160	1	0.287	0.86	0.91	1.05	1.01
			2	0.287	0.80	0.90	1.04	1.02
	0.50	100	3	0.460	0.90	0.88	1.05	1.01
		130	3	0.439	0.85	0.87	1.03	1.02
		160	1	0.426	0.97	0.87	1.05	1.00
			2	0.426	0.89	0.86	1.04	1.01
			3	0.426	0.84	0.85	1.02	1.02
Average					0.94		1.05	1.01
Standard Deviation					0.085		0.027	0.010
High				0.461	1.10	0.93	1.10	1.02
Low				0.283	0.79	0.81	0.98	0.99

Table C.1.4. Uniform vertical bending data, specimens with $D/b_f = 2.75$ and $b_f/t_f = 25$.

L_b/R	Target f_ℓ/f_b	D/t_w	d_o/D	$\frac{f_\ell}{f_b}$	Ratio to 2nd-order shell FEA $\frac{f_\ell}{f_b}$	$\frac{M_{FEA}}{M_y}$	$\frac{M_{FEA}}{M_{n(1/3\,rule)}}$	Ratio to $\frac{M_{FEA}}{M_{n(1/3\,rule)}}$ based on 2nd-order shell FEA
0.05	0.35	100	3	0.320	0.93	0.88	1.12	1.01
		130	3	0.303	0.87	0.86	1.11	1.01
		160	1	0.293	0.90	0.88	1.18	1.01
			2	0.293	0.84	0.86	1.15	1.02
			3	0.293	0.82	0.85	1.14	1.02
	0.50	100	3	0.481	0.95	0.77	1.05	1.01
		130	3	0.456	0.93	0.75	1.01	1.01
		160	1	0.440	0.95	0.75	1.05	1.01
			2	0.440	0.92	0.74	1.03	1.01
			3	0.440	0.91	0.76	1.06	1.01
0.075	0.35	100	3	0.361	0.97	0.84	1.08	1.00
		130	3	0.342	0.91	0.82	1.07	1.01
		160	1	0.330	1.14	0.83	1.12	0.99
			2	0.330	0.99	0.81	1.10	1.00
			3	0.330	0.88	0.79	1.07	1.01
	0.50	100	3	0.486	1.11	0.84	1.12	0.99
		130	3	0.460	1.11	0.82	1.11	0.99
		160	1	0.444	1.11	0.82	1.15	0.99
			2	0.444	1.01	0.80	1.12	1.00
			3	0.444	0.94	0.80	1.12	1.01
0.10	0.35	100	2	0.322	0.78	0.89	1.13	1.03
		130	2	0.305	0.71	0.85	1.10	1.04
		160	1	0.294	0.75	0.82	1.10	1.03
			2	0.294	0.69	0.80	1.07	1.04
	0.50	100	3	0.481	0.88	0.82	1.09	1.02
		130	3	0.456	0.82	0.79	1.07	1.03
		160	1	0.439	0.91	0.80	1.12	1.01
			2	0.439	0.81	0.79	1.10	1.03
			3	0.439	0.78	0.78	1.09	1.03
Average					0.91		1.10	1.01
Standard Deviation					0.115		0.037	0.015
High				0.486	1.14	0.89	1.18	1.04
Low				0.293	0.69	0.74	1.01	0.99

Table C.1.5. Uniform vertical bending data, specimens with $D/b_f = 3.25$ and $b_f/t_f = 25$.

L_b/R	Target f_ℓ/f_b	D/t_w	d_o/D	$\frac{f_\ell}{f_b}$	Ratio to 2nd-order shell FEA $\frac{f_\ell}{f_b}$	$\frac{M_{FEA}}{M_y}$	$\frac{M_{FEA}}{M_{n(1/3\,rule)}}$	Ratio to $\frac{M_{FEA}}{M_{n(1/3\,rule)}}$ based on 2nd-order shell FEA
0.05	0.35	160	1	0.277	0.80	0.83	1.11	1.02
			2	0.277	0.76	0.81	1.08	1.03
			3	0.277	0.75	0.78	1.04	1.03
	0.50	160	1	0.463	0.92	0.74	1.04	1.01
			2	0.463	0.91	0.74	1.04	1.01
			3	0.463	0.89	0.74	1.04	1.01
0.075	0.35	160	1	0.342	1.19	0.80	1.09	0.98
			2	0.342	1.14	0.77	1.05	0.99
	0.50	160	1	0.414	1.09	0.80	1.11	0.99
			2	0.414	0.92	0.79	1.10	1.01
			3	0.414	0.92	0.77	1.07	1.01
0.10	0.35	160	1	0.368	0.90	0.78	1.07	1.01
			2	0.368	0.86	0.75	1.03	1.02
	0.50	160	1	0.552	1.38	0.75	1.09	0.96
			2	0.552	1.26	0.73	1.06	0.97
			3	0.552	1.12	0.73	1.06	0.98
Average					0.99		1.07	1.00
Standard Deviation					0.184		0.026	0.021
High				0.552	1.38	0.83	1.11	1.03
Low				0.277	0.75	0.73	1.03	0.96

C.2 MAXIMUM V/M DATA, SYMMETRIC GIRDERS

Table C.2.1. Maximum V/M data, specimens with $D/b_f = 2.25$ and $b_f/t_f = 25$.

L_b/R	Target f_ℓ/f_b	D/t_w	d_o/D	$\frac{f_\ell}{f_b}$	$\frac{M_{FEA}}{M_y}$	$\frac{M_{FEA}}{M_{n(1/3\ rule)}}$	$\frac{V_{FEA}}{V_p}$	$\frac{V_{FEA}}{V_{n(AASHTO)}}$	$\frac{V_{FEA}}{V_{n(mod\ AASHTO)}}$
0.05	0.35	100	3	0.144	1.17	1.40	0.77	1.21	0.95
		130	3	0.133	0.75	0.92	0.62	1.27	1.01
		160	1	0.159	0.78	1.00	0.77	1.03	1.00
			2	0.147	0.59	0.75	0.58	1.12	0.99
			3	0.135	0.54	0.69	0.53	1.29	1.08
	0.50	100	3[1]	***0.374***	***1.10***	***1.43***	***0.45***	***0.72***	***0.56***
		130	3	***0.238***	***1.03***	***1.31***	***0.53***	***1.09***	***0.87***
		160	1	***0.315***	***0.97***	***1.31***	***0.60***	***0.80***	***0.77***
			2	0.094	0.92	1.16	0.57	1.09	0.97
			3	0.080	0.86	1.07	0.53	1.28	1.07
0.075	0.35	100	3	0.178	0.93	1.13	0.76	1.21	0.94
		130	3	0.164	0.60	0.74	0.61	1.26	1.01
		160	1	0.197	0.62	0.81	0.77	1.02	0.99
			2	0.181	0.47	0.61	0.58	1.11	0.99
			3	0.158	0.43	0.55	0.53	1.28	1.07
	0.50	100	3	0.215	1.16	1.42	0.76	1.20	0.94
		130	3	0.198	0.75	0.93	0.61	1.26	1.01
		160	1	0.238	0.77	1.01	0.76	1.02	0.98
			2	0.224	0.57	0.75	0.57	1.09	0.96
			3	0.192	0.53	0.69	0.52	1.27	1.06
0.10	0.35	100	3	0.171	0.69	0.84	0.76	1.21	0.94
		130	3	0.157	0.45	0.55	0.61	1.26	1.01
		160	1	0.189	0.47	0.60	0.76	1.02	0.99
			2	0.175	0.35	0.45	0.58	1.10	0.98
			3	0.151	0.32	0.41	0.53	1.27	1.07
	0.50	100	3	0.241	0.91	1.13	0.75	1.19	0.93
		130	3	0.222	0.59	0.74	0.60	1.24	0.99
		160	1	0.267	0.61	0.81	0.75	1.01	0.97
			2	0.149	0.46	0.59	0.57	1.09	0.97
			3	0.215	0.42	0.55	0.52	1.25	1.05
High				0.374	1.17	1.43	0.77	1.29	1.08
Low				0.080	0.32	0.41	0.45	0.72	0.56

[1] Values in bold italic font indicate specimens in which the failure is dominated by lateral bending.

Table C.2.2. Maximum V/M data, specimens with $D/b_f = 2.75$ and $b_f/t_f = 15$.

L_b/R	Target f_ℓ/f_b	D/t_w	d_o/D	$\frac{f_\ell}{f_b}$	$\frac{M_{FEA}}{M_y}$	$\frac{M_{FEA}}{M_{n(1/3\,rule)}}$	$\frac{V_{FEA}}{V_p}$	$\frac{V_{FEA}}{V_{n(AASHTO)}}$	$\frac{V_{FEA}}{V_{n(mod\ AASHTO)}}$
0.05	0.35	100	3	0.149	0.88	0.92	0.79	1.25	0.94
		130	3	0.142	0.55	0.57	0.62	1.27	1.02
		160	1	0.157	0.62	0.66	0.84	1.12	1.08
			2	0.148	0.46	0.49	0.62	1.19	1.06
			3	0.129	0.42	0.44	0.56	1.36	1.14
	0.50	100	***3***[(1)]	***0.265***	***1.09***	***1.18***	***0.65***	***1.03***	***0.78***
		130	3	0.211	0.81	0.87	0.61	1.25	1.00
		160	***1***	***0.257***	***0.83***	***0.91***	***0.75***	***1.00***	***0.97***
			2	0.223	0.67	0.72	0.60	1.16	1.03
			3	0.196	0.60	0.65	0.55	1.32	1.10
0.075	0.35	100	3	0.17	0.66	0.69	0.78	1.24	0.94
		130	3	0.162	0.41	0.43	0.61	1.26	1.01
		160	1	0.179	0.46	0.49	0.83	1.11	1.08
			2	0.173	0.34	0.36	0.61	1.18	1.05
			3	0.148	0.31	0.33	0.56	1.34	1.12
	0.50	100	3	0.225	0.87	0.94	0.78	1.24	0.94
		130	3	0.217	0.54	0.57	0.60	1.24	0.99
		160	1	0.241	0.60	0.66	0.82	1.10	1.06
			2	0.229	0.44	0.48	0.60	1.15	1.02
			3	0.202	0.40	0.43	0.54	1.31	1.09
0.10	0.35	100	2	0.172	0.44	0.47	0.80	1.10	0.90
		130	2	0.173	0.28	0.29	0.62	1.06	0.90
		160	1	0.161	0.31	0.33	0.83	1.11	1.07
			2	0.153	0.22	0.24	0.61	1.17	1.04
	0.50	100	3	0.229	0.65	0.70	0.78	1.23	0.93
		130	3	0.221	0.40	0.43	0.60	1.23	0.98
		160	1	0.245	0.45	0.49	0.81	1.09	1.05
			2	0.234	0.33	0.36	0.59	1.14	1.01
			3	0.204	0.30	0.32	0.54	1.31	1.09
High				0.265	1.09	1.18	0.84	1.36	1.14
Low				0.129	0.22	0.24	0.54	1.00	0.78

[(1)] Values in bold italic font indicate specimens in which the failure is dominated by lateral bending.

Table C.2.3. Maximum V/M data, specimens with $D/b_f = 2.75$ and $b_f/t_f = 20$.

L_b/R	Target f_ℓ/f_b	D/t_w	d_o/D	$\frac{f_\ell}{f_b}$	$\frac{M_{FEA}}{M_y}$	$\frac{M_{FEA}}{M_{n(1/3\,rule)}}$	$\frac{V_{FEA}}{V_p}$	$\frac{V_{FEA}}{V_{n(AASHTO)}}$	$\frac{V_{FEA}}{V_{n(mod\,AASHTO)}}$
0.05	0.35	100	3	0.153	1.06	1.15	0.75	1.19	0.92
		130	3	0.143	0.67	0.73	0.59	1.22	0.97
		160	1	0.164	0.73	0.82	0.77	1.03	1.00
			2	0.152	0.55	0.61	0.58	1.11	0.99
			3	0.127	0.52	0.58	0.55	1.33	1.11
	0.50	100	***3***[(1)]	***0.319***	***1.13***	***1.29***	***0.53***	***0.85***	***0.66***
		130	3	0.213	1.00	1.11	0.59	1.21	0.97
		160	***1***	***0.274***	***0.98***	***1.13***	***0.69***	***0.92***	***0.89***
			2	0.227	0.82	0.93	0.58	1.10	0.98
			3	0.193	0.77	0.86	0.54	1.30	1.09
0.075	0.35	100	3	0.175	0.79	0.86	0.75	1.18	0.92
		130	3	0.163	0.50	0.55	0.59	1.21	0.97
		160	1	0.186	0.55	0.62	0.77	1.03	0.99
			2	0.174	0.41	0.46	0.57	1.10	0.98
			3	0.145	0.39	0.43	0.55	1.32	1.11
	0.50	100	3	0.242	1.04	1.15	0.73	1.16	0.90
		130	3	0.224	0.66	0.74	0.58	1.20	0.96
		160	1	0.257	0.72	0.83	0.76	1.02	0.98
			2	0.244	0.53	0.61	0.56	1.07	0.95
			3	0.204	0.50	0.57	0.53	1.28	1.07
0.10	0.35	100	2	0.177	0.54	0.59	0.76	1.05	0.87
		130	2	0.173	0.34	0.38	0.60	1.02	0.88
		160	1	0.167	0.36	0.41	0.77	1.02	0.99
			2	0.161	0.26	0.29	0.56	1.07	0.95
	0.50	100	3	0.239	0.77	0.86	0.73	1.16	0.90
		130	3	0.224	0.49	0.54	0.57	1.17	0.94
		160	1	0.254	0.54	0.62	0.75	1.01	0.97
			2	0.243	0.39	0.45	0.55	1.05	0.93
			3	0.203	0.37	0.42	0.52	1.26	1.05
High				0.319	1.13	1.29	0.77	1.33	1.11
Low				0.127	0.26	0.29	0.52	0.85	0.66

(1) Values in bold italic font indicate specimens in which the failure is dominated by lateral bending.

Table C.2.4. Maximum V/M data, specimens with $D/b_f = 2.75$ and $b_f/t_f = 25$.

L_b/R	Target f_ℓ/f_b	D/t_w	d_o/D	$\frac{f_\ell}{f_b}$	$\frac{M_{FEA}}{M_y}$	$\frac{M_{FEA}}{M_{n(1/3\ rule)}}$	$\frac{V_{FEA}}{V_p}$	$\frac{V_{FEA}}{V_{n(AASHTO)}}$	$\frac{V_{FEA}}{V_{n(mod\ AASHTO)}}$
0.05	0.35	100	3	0.157	1.21	1.46	0.72	1.15	0.94
		130	3	0.142	0.79	0.98	0.58	1.20	0.97
		160	1	0.164	0.86	1.10	0.75	1.00	0.97
			2	0.151	0.65	0.83	0.56	1.08	0.96
			3	0.128	0.61	0.77	0.53	1.28	1.07
	0.50	100	***3***[(1)]	0.376	1.13	1.46	0.45	0.71	0.59
		130	***3***	0.240	1.05	1.33	0.51	1.06	0.86
		160	***1***	0.311	1.02	1.37	0.59	0.79	0.76
			2	0.231	0.95	1.25	0.55	1.06	0.94
			3	0.196	0.89	1.16	0.52	1.25	1.05
0.075	0.35	100	3	0.180	0.90	1.10	0.72	1.14	0.94
		130	3	0.166	0.58	0.72	0.57	1.17	0.95
		160	1	0.187	0.64	0.83	0.75	1.00	0.96
			2	0.179	0.47	0.61	0.54	1.05	0.93
			3	0.152	0.44	0.56	0.51	1.23	1.03
	0.50	100	3	0.251	1.20	1.50	0.72	1.14	0.94
		130	3	0.233	0.77	0.97	0.56	1.16	0.94
		160	1	0.265	0.85	1.12	0.74	0.98	0.95
			2	0.250	0.63	0.83	0.54	1.05	0.93
			3	0.215	0.58	0.76	0.50	1.22	1.02
0.10	0.35	100	2	0.183	0.61	0.74	0.73	1.00	0.87
		130	2	0.174	0.40	0.50	0.59	1.00	0.86
		160	1	0.168	0.43	0.55	0.75	1.00	0.96
			2	0.162	0.31	0.40	0.54	1.04	0.92
	0.50	100	3	0.241	0.90	1.11	0.71	1.13	0.93
		130	3	0.223	0.57	0.72	0.56	1.16	0.94
		160	1	0.257	0.62	0.83	0.72	0.97	0.93
			2	0.245	0.46	0.60	0.53	1.01	0.90
			3	0.213	0.42	0.55	0.48	1.17	0.98
High				0.376	1.21	1.50	0.75	1.28	1.07
Low				0.128	0.31	0.40	0.45	0.71	0.59

(1) Values in bold italic font indicate specimens in which the failure is dominated by lateral bending.

Table C.2.5. Maximum V/M data, specimens with $D/b_f = 3.25$ and $b_f/t_f = 25$.

L_b/R	Target f_ℓ/f_b	D/t_w	d_c/D	$\frac{f_\ell}{f_b}$	$\frac{M_{FEA}}{M_y}$	$\frac{M_{FEA}}{M_{n(1/3\,rule)}}$	$\frac{V_{FEA}}{V_p}$	$\frac{V_{FEA}}{V_{n(AASHTO)}}$	$\frac{V_{FEA}}{V_{n(mod\ AASHTO)}}$
0.05	0.35	160	1	0.157	0.84	1.08	0.74	0.99	0.95
			2	0.147	0.62	0.80	0.55	1.06	0.94
			3	0.127	0.57	0.73	0.51	1.23	1.03
	0.50	160	1	0.359	1.03	1.42	0.55	0.73	0.71
			2	0.257	1.00	1.33	0.53	1.02	0.91
			3	0.219	0.94	1.23	0.50	1.20	1.01
0.075	0.35	160	1	0.201	0.69	0.91	0.74	0.98	0.95
			2	0.197	0.49	0.64	0.52	1.00	0.89
	0.50	160	1	0.247	0.80	1.07	0.71	0.95	0.92
			2	0.235	0.59	0.78	0.52	1.00	0.89
			3	0.201	0.55	0.72	0.48	1.17	0.98
0.10	0.35	160	1	0.216	0.55	0.72	0.73	0.97	0.94
			2	0.210	0.39	0.52	0.52	1.00	0.89
	0.50	160	1	0.341	0.78	1.06	0.69	0.92	0.89
			2	0.324	0.57	0.77	0.50	0.97	0.86
			3	0.282	0.52	0.70	0.46	1.11	0.93
High				0.359	1.03	1.42	0.74	1.23	1.03
Low				0.127	0.39	0.52	0.46	0.73	0.71

C.3 HIGH-SHEAR HIGH-MOMENT DATA, SYMMETRIC GIRDERS

Table C.3.1. High-shear high-moment data, specimens with $D/b_f = 2.25$ and $b_f/t_f = 25$.

L_b/R	Target f_ℓ/f_b	D/t_w	d_o/D	α	$\frac{M_3}{M_2}$	$\frac{f_\ell}{f_b}$	$\frac{M_{FEA}}{M_y}$	$\frac{M_{FEA}}{M_{n(1/3\,rule)}}$	$\frac{V_{FEA}}{V_p}$	$\frac{V_{FEA}}{V_{n(AASHTO)}}$	$\frac{V_{FEA}}{V_{n(mod\ AASHTO)}}$
0.05	0.35	100	3	$M_{n(FEA)}/0.8V_{n(FEA)}L_b < 0.55$							
		130	3	0.153	-0.362	0.208	0.99	1.25	0.56	1.14	0.91
		160	1	0.176	-0.426	0.199	0.92	1.20	0.65	0.87	0.84
			2	0.045	-0.095	0.284	0.94	1.25	0.51	0.97	0.86
			3	0.010	-0.020	0.290	0.96	1.28	0.48	1.17	0.98
	0.50	100	3	$M_{n(FEA)}/0.8V_{n(FEA)}L_b < 0.55$							
		130	3								
		160	1								
			2								
			3								
0.075	0.35	100	3	0.249	-0.663	0.241	1.00	1.24	0.68	1.08	0.84
		130	3	0.066	-0.141	0.270	1.01	1.30	0.59	1.22	0.98
		160	1	0.073	-0.158	0.262	0.92	1.21	0.65	0.87	0.85
			2	-0.047	0.090	0.279	0.93	1.24	0.52	1.00	0.89
			3	-0.088	0.162	0.284	0.98	1.31	0.51	1.23	1.03
	0.50	100	3	$M_{n(FEA)}/0.8V_{n(FEA)}L_b < 0.55$							
		130	3	0.181	-0.443	0.300	0.83	1.07	0.49	1.01	0.81
		160	1	0.200	-0.500	0.289	1.00	1.33	0.74	0.99	0.95
			2	0.060	-0.128	0.323	0.93	1.25	0.52	0.99	0.88
			3	0.030	-0.062	0.329	0.95	1.28	0.50	1.20	1.00
0.10	0.35	100	3	0.128	-0.294	0.262	0.92	1.15	0.65	1.04	0.81
		130	3	-0.076	0.141	0.285	0.90	1.16	0.53	1.09	0.87
		160	1	-0.064	0.120	0.276	0.91	1.21	0.66	0.88	0.85
			2	-0.184	0.311	0.290	0.93	1.24	0.53	1.01	0.90
			3	-0.222	0.363	0.294	0.88	1.17	0.46	1.10	0.92
	0.50	100	3	0.227[1]	-0.587	0.329	0.96	1.22	0.63	0.99	0.77
		130	3	0.024[1]	-0.049	0.368	0.95	1.25	0.51	1.05	0.84
		160	1	0.052[1]	-0.110	0.353	0.92	1.25	0.63	0.84	0.81
			2	-0.091[1]	0.167	0.380	0.91	1.24	0.47	0.89	0.79
			3	-0.132[1]	0.233	0.386	0.94	1.29	0.44	1.07	0.90
High				0.249	0.363	0.386	1.01	1.33	0.74	1.23	1.03
Low				-0.222	-0.663	0.199	0.83	1.07	0.44	0.84	0.77

[1] The α values for these tests differ slightly from the criterion associated with $M/V = M_{n(FEA)}/0.8V_{n(FEA)}$

Table C.3.2. High-shear high-moment data, specimens with $D/b_f = 2.75$ and $b_f/t_f = 15$.

L_b/R	Target f_ℓ/f_b	D/t_w	d_o/D	α	$\frac{M_3}{M_2}$	$\frac{f_\ell}{f_b}$	$\frac{M_{FEA}}{M_y}$	$\frac{M_{FEA}}{M_{n(1/3\,rule)}}$	$\frac{V_{FEA}}{V_p}$	$\frac{V_{FEA}}{V_{n(AASHTO)}}$	$\frac{V_{FEA}}{V_{n(mod\ AASHTO)}}$
0.05	0.35	100	3	0.194	-0.480	0.213	1.01	1.08	0.67	1.07	0.80
		130	3	-0.023	0.045	0.232	1.04	1.13	0.56	1.16	0.92
		160	1	0.030	-0.062	0.221	0.93	1.01	0.67	0.90	0.87
			2	-0.113	0.203	0.234	1.00	1.08	0.54	1.03	0.92
			3	-0.150	0.261	0.237	1.02	1.11	0.51	1.23	1.03
	0.50	100	3	$M_{n(FEA)}/0.8V_{n(FEA)}L_b < 0.55$							
		130	3	0.227	-0.587	0.295	0.98	1.07	0.58	1.20	0.96
		160	1	Failure dominated by lateral bending in maximum V/M test							
			2	0.257[1]	-0.690	0.281	0.81	0.89	0.61	1.18	1.05
			3	0.090	-0.198	0.316	0.98	1.10	0.53	1.28	1.07
0.075	0.35	100	3	0.059	-0.125	0.263	1.01	1.10	0.68	1.08	0.81
		130	3	-0.159	0.274	0.276	1.01	1.11	0.55	1.14	0.91
		160	1	-0.097	0.177	0.264	0.95	1.05	0.71	0.95	0.92
			2	-0.258	0.410	0.277	0.98	1.08	0.52	1.01	0.89
			3	-0.283	0.441	0.279	0.99	1.10	0.50	1.21	1.02
	0.50	100	3	0.206	-0.520	0.317	1.01	1.11	0.69	1.09	0.82
		130	3	-0.024	0.047	0.348	1.05	1.18	0.57	1.17	0.93
		160	1	Analysis not conducted							
			2	-0.122	0.217	0.352	1.00	1.12	0.53	1.01	0.90
			3	-0.168	0.288	0.358	1.02	1.15	0.49	1.18	0.99
0.10	0.35	100	2	-0.148	0.258	Significant distortion in web panel outside of the test length at the maximum moment location; significant distortion of bearing stiffener for $D/t_w = 160$ cases					
		130	2	-0.350	0.519						
		160	1	-0.280	0.438						
			2	-0.416	0.588						
	0.50	100	3	0.049	-0.102	0.352	0.99	1.10	0.65	1.03	0.78
		130	3	0.180[1]	-0.439	0.315	0.53	0.59	0.57	1.18	0.94
		160	1	-0.118	0.211	0.355	0.94	1.06	0.67	0.89	0.87
			2	-0.269	0.424	0.371	0.99	1.13	0.52	0.99	0.88
			3	-0.309	0.472	0.374	1.10	1.25	0.53	1.27	1.06
High				0.257	0.472	0.374	1.10	1.25	0.71	1.28	1.07
Low				-0.309	-0.690	0.213	0.53	0.59	0.49	0.89	0.78

[1] The α values for this test differs slightly from the criterion associated with $M/V = M_{n(FEA)}/0.8V_{n(FEA)}$

[2] The α values for this test differs significantly from the criterion associated with $M/V = M_{n(FEA)}/0.8V_{n(FEA)}$, causing the test to be a high-shear low-moment test.

Table C.3.3. High-shear high-moment data, specimens with $D/b_f = 2.75$ and $b_f/t_f = 20$.

L_b/R	Target f_ℓ/f_b	D/t_w	d_o/D	α	$\frac{M_3}{M_2}$	$\frac{f_\ell}{f_b}$	$\frac{M_{FEA}}{M_y}$	$\frac{M_{FEA}}{M_{n(1/3\,rule)}}$	$\frac{V_{FEA}}{V_p}$	$\frac{V_{FEA}}{V_{n(AASHTO)}}$	$\frac{V_{FEA}}{V_{n(mod\ AASHTO)}}$
0.05	0.35	100	3	$M_{n(FEA)}/0.8V_{n(FEA)}L_b < 0.55$							
		130	3	0.101	-0.225	0.219	1.01	1.12	0.54	1.12	0.89
		160	1	0.133	-0.306	0.208	0.94	1.07	0.65	0.87	0.84
			2	0.000	0.000	0.226	0.98	1.12	0.52	0.99	0.88
			3	-0.012	0.024	0.227	0.99	1.12	0.51	1.22	1.02
	0.50	100	3	$M_{n(FEA)}/0.8V_{n(FEA)}L_b < 0.55$							
		130	3								
		160	1								
			2	0.220	-0.564	0.288	0.99	1.15	0.54	1.05	0.93
			3	0.200	-0.500	0.294	0.97	1.13	0.51	1.24	1.03
0.075	0.35	100	3	0.153	-0.362	0.251	1.01	1.13	0.65	1.04	0.80
		130	3	-0.061	0.115	0.271	1.01	1.14	0.52	1.08	0.86
		160	1	-0.014	0.028	0.257	0.98	1.12	0.67	0.89	0.86
			2	-0.153	0.265	0.273	1.00	1.15	0.51	0.99	0.88
			3	-0.168	0.288	0.274	0.96	1.11	0.48	1.16	0.97
	0.50	100	3	0.290	-0.816	0.298	1.10	1.24	0.70	1.12	0.87
		130	3	0.090	-0.198	0.338	1.06	1.23	0.56	1.15	0.92
		160	1	0.130	-0.299	0.320	0.97	1.13	0.66	0.89	0.86
			2	-0.020	0.039	0.348	0.98	1.15	0.50	0.95	0.84
			3	-0.040	0.077	0.351	1.01	1.19	0.49	1.18	0.99
0.10	0.35	100	2	-0.036	0.069	0.251	0.93	1.04	0.61	0.85	0.70
		130	2	-0.248	0.397	0.260	0.93	1.05	0.50	0.84	0.72
		160	1	-0.220	0.361	Significant distortion in the web panel outside of the test length at the maximum moment location					
			2	-0.359	0.528	0.299	0.90	1.04	0.44	0.85	0.76
	0.50	100	3	0.138[1]	-0.320	0.338	1.00	1.15	0.62	0.99	0.77
		130	3	-0.081	0.150	0.364	0.99	1.15	0.49	1.02	0.81
		160	1	-0.024	0.047	0.345	0.93	1.10	0.62	0.83	0.81
			2	-0.183	0.309	0.367	0.98	1.16	0.47	0.91	0.81
			3	-0.200	0.333	0.369	0.96	1.13	0.45	1.08	0.90
High				0.290	0.528	0.369	1.10	1.24	0.70	1.24	1.03
Low				-0.359	-0.816	0.208	0.90	1.04	0.44	0.83	0.70

[1] The α values for these tests differ slightly from the criterion associated with $M/V = M_{n(FEA)}/0.8V_{n(FEA)}$

Table C.3.4. High-shear high-moment data, specimens with $D/b_f = 2.75$ and $b_f/t_f = 25$.

L_b/R	Target f_ℓ/f_b	D/t_w	d_o/D	α	$\frac{M_3}{M_2}$	$\frac{f_\ell}{f_b}$	$\frac{M_{FEA}}{M_y}$	$\frac{M_{FEA}}{M_{n(1/3\ rule)}}$	$\frac{V_{FEA}}{V_p}$	$\frac{V_{FEA}}{V_{n(AASHTO)}}$	$\frac{V_{FEA}}{V_{n(mod\ AASHTO)}}$
0.05	0.35	100	3	$M_{n(FEA)}/0.8V_{n(FEA)}L_b < 0.55$							
		130	3	0.194	-0.480	0.204	0.98	1.23	0.53	1.10	0.89
		160	1	0.220	-0.564	0.192	0.95	1.24	0.65	0.87	0.84
			2	0.097	-0.214	0.214	0.97	1.27	0.51	0.99	0.88
			3	0.069	-0.149	0.218	0.91	1.19	0.45	1.10	0.92
	0.50	100	3	$M_{n(FEA)}/0.8V_{n(FEA)}L_b < 0.55$							
		130	3								
		160	1								
			2								
			3								
0.075	0.35	100	3	0.273	-0.750	0.224	0.95	1.17	0.66	1.04	0.86
		130	3	0.070	-0.151	0.256	0.99	1.27	0.56	1.15	0.93
		160	1	Analysis not conducted							
			2	-0.045	0.086	0.264	0.95	1.26	0.50	0.97	0.86
			3	-0.059	0.111	0.266	0.90	1.20	0.47	1.13	0.94
	0.50	100	3	$M_{n(FEA)}/0.8V_{n(FEA)}L_b < 0.55$							
		130	3	0.200	-0.500	0.318	0.96	1.25	0.53	1.09	0.89
		160	1	0.249	-0.663	0.292	0.92	1.23	0.67	0.89	0.86
			2	0.100	-0.222	0.332	0.94	1.27	0.50	0.96	0.85
			3	0.070	-0.151	0.339	1.06	1.43	0.53	1.28	1.07
0.10	0.35	100	2	0.050	-0.105	0.246	0.93	1.16	0.61	0.85	0.74
		130	2	-0.141	0.247	0.256	0.91	1.15	0.50	0.85	0.73
		160	1	-0.087	0.160	0.241	0.86	1.13	0.63	0.84	0.81
			2	-0.236	0.382	0.255	0.87	1.15	0.47	0.90	0.80
	0.50	100	3	0.213[(1)]	-0.542	0.320	0.96	1.22	0.59	0.93	0.77
		130	3	0.008[(1)]	-0.015	0.355	0.93	1.22	0.46	0.95	0.77
		160	1	0.059[(1)]	-0.125	0.332	0.83	1.13	0.54	0.73	0.70
			2	-0.098[(1)]	0.179	0.361	0.88	1.20	0.42	0.81	0.72
			3	-0.139[(1)]	0.244	0.367	0.91	1.25	0.40	0.96	0.81
High				0.273	0.382	0.367	1.06	1.43	0.67	1.28	1.07
Low				-0.236	-0.750	0.192	0.83	1.13	0.40	0.73	0.70

[(1)] The α values for these tests differ slightly from the criterion associated with $M/V = M_{n(FEA)}/0.8V_{n(FEA)}$

Table C.3.5. High-shear high-moment data, specimens with $D/b_f = 3.25$ and $b_f/t_f = 25$.

L_b/R	Target f_ℓ/f_b	D/t_w	d_o/D	α	$\frac{M_3}{M_2}$	$\frac{f_\ell}{f_b}$	$\frac{M_{FEA}}{M_y}$	$\frac{M_{FEA}}{M_{n(1/3\,rule)}}$	$\frac{V_{FEA}}{V_p}$	$\frac{V_{FEA}}{V_{n(AASHTO)}}$	$\frac{V_{FEA}}{V_{n(mod\,AASHTO)}}$
0.05	0.35	160	1	0.153	-0.362	0.194	0.94	1.23	0.57	0.76	0.74
			2	0.105	-0.235	0.202	0.93	1.22	0.51	0.98	0.87
			3	0.080	-0.174	0.206	0.94	1.22	0.49	1.17	0.98
	0.50	160	1	$M_{n(FEA)}/0.8V_{n(FEA)}L_b < 0.55$							
			2								
			3								
0.075	0.35	160	1	Analysis not conducted							
			2								
	0.50	160	1	0.234	-0.611	0.270	0.91	1.21	0.65	0.86	0.84
			2	0.089	-0.194	0.307	1.03	1.39	0.54	1.04	0.93
			3	0.060	-0.128	0.313	0.93	1.26	0.47	1.12	0.94
0.10	0.35	160	1	0.060	-0.128	0.279	0.86	1.16	0.65	0.86	0.84
			2	-0.090	0.165	0.303	0.83	1.12	0.46	0.89	0.79
	0.50	160	1	0.188[1]	-0.462	0.378	0.89	1.22	0.57	0.77	0.74
			2	0.039[1]	-0.081	0.423	0.91	1.27	0.43	0.83	0.74
			3	-0.006[1]	0.012	0.434	0.92	1.28	0.40	0.97	0.81
High				0.234	0.165	0.434	1.03	1.39	0.65	1.17	0.98
Low				-0.090	-0.611	0.194	0.83	1.12	0.40	0.76	0.74

[1] The α values for these tests differ from the criterion associated with $M/V = M_{n(FEA)}/0.8V_{n(FEA)}$

C.4 MOMENT-SHEAR INTERACTION DATA, UNSYMMETRIC GIRDERS

Table C.4.1. Uniform vertical bending data, unsymmetric specimens.

D/b_{fc}	b_f/t_f	$2D_c/t_w$	L_b/R	Target f_ℓ/f_b	d_o/D	$\frac{f_\ell}{f_b}$	Ratio to 2nd-order shell FEA $\frac{f_\ell}{f_b}$	$\frac{M_{FEA}}{M_y}$	$\frac{M_{FEA}}{M_p}$	$\frac{M_{FEA}}{M_{n(1/3\,rule)}}$	Ratio to $\frac{M_{FEA}}{M_{n(1/3\,rule)}}$ based on 2nd-order shell FEA
4.77	20	208	0.05	0.35	2	0.260	0.81	0.75	0.53	1.00	1.02
				0.5	3	0.387	0.77	0.70	0.50	1.06	1.03
			0.10	0.35	1	0.273	0.68	0.81	0.57	1.08	1.03
				0.5	1.5	0.392	0.71	0.71	0.50	0.98	1.04
2.75	25	169	0.05	0.35	3	0.259	0.62	0.86	0.66	1.20	1.05
				0.5	3	0.386	0.67	0.71	0.55	1.03	1.05
			0.10	0.35	2	0.263	0.61	0.79	0.61	1.10	1.05
				0.5	3	0.390	0.67	0.76	0.59	1.10	1.05
Average							0.70			1.07	1.04
Standard Deviation							0.070			0.069	0.013
High						0.392	0.81	0.86	0.66	1.20	1.05
Low						0.259	0.61	0.70	0.50	0.98	1.02

Table C.4.2. Maximum V/M data, unsymmetric specimens.

D/b_{fc}	b_f/t_f	$2D_c/t_w$	L_b/R	Target f_ℓ/f_b	d_o/D	$\frac{f_\ell}{f_b}$	$\frac{M_{FEA}}{M_y}$	$\frac{M_{FEA}}{M_p}$	$\frac{M_{FEA}}{M_{n(1/3\,rule)}}$	$\frac{V_{FEA}}{V_p}$	$\frac{V_{FEA}}{V_{n(AASHTO)}}$	$\frac{V_{FEA}}{V_{n(mod\ AASHTO)}}$
4.77	20	208	0.05	0.35	2	0.159	0.51	0.36	0.66	0.52	1.00	0.90
				0.5	3	0.196	0.73	0.52	0.96	0.50	1.21	1.04
			0.10	0.35	1	0.167	0.37	0.26	0.47	0.75	1.00	0.98
				0.5	1.5	0.251	0.42	0.30	0.56	0.58	0.95	0.89
2.75	25	169	0.05	0.35	3	0.119	0.73	0.56	0.98	0.59	1.22	0.97
				0.5	3	0.197	0.99	0.76	1.35	0.53	1.09	0.88
			0.10	0.35	2	0.142	0.39	0.30	0.53	0.63	1.07	0.92
				0.5	3	0.187	0.53	0.41	0.72	0.57	1.17	0.94
High						0.251	0.99	0.76	1.35	0.75	1.22	1.04
Low						0.119	0.37	0.26	0.47	0.50	0.95	0.88

Table C.4.3. High-shear high-moment load parameters, unsymmetric specimens.

D/b_{fc}	b_f/t_f	$2D_c/t_w$	L_b/R	Target f_ℓ/f_b	d_o/D	α	$\frac{M_3}{M_2}$
4.77	20	208	0.05	0.35	2	0.039	-0.080
				0.5	3	0.250	-0.670
			0.10	0.35	1	-0.160	0.279
				0.5	1.5	-0.030	0.045
2.75	25	169	0.05	0.35	3	0.213	-0.363
				0.5	3	$M_{n(FEA)}/0.8V_{n(FEA)} < 0.55$	
			0.10	0.35	2	-0.140	0.208
				0.5	3	0.060	-0.118
High						0.250	0.279
Low						-0.160	-0.670

Table C.4.4. High-shear high-moment analysis results, unsymmetric specimens.

D/b_{fc}	b_f/t_f	$2D_c/t_w$	L_b/R	Target f_ℓ/f_b	d_o/D	$\frac{f_\ell}{f_b}$	$\frac{M_{FEA}}{M_y}$	$\frac{M_{FEA}}{M_p}$	$\frac{M_{FEA}}{M_{n(1/3\,rule)}}$	$\frac{V_{FEA}}{V_p}$	$\frac{V_{FEA}}{V_{n(AASHTO)}}$	$\frac{V_{FEA}}{V_{n(mod\,AASHTO)}}$
4.77	20	208	0.05	0.35	2	0.198	0.82	0.58	1.08	0.46	0.88	0.79
				0.5	3	0.258	0.81	0.57	1.08	0.46	1.12	0.96
			0.10	0.35	1	0.221	0.87	0.62	1.15	0.65	0.87	0.84
				0.5	1.5	0.306	0.78	0.56	1.06	0.51	0.83	0.77
2.75	25	169	0.05	0.35	3	0.168	0.98	0.75	1.33	0.61	1.25	1.00
				0.5	3	$M_{n(FEA)}/0.8V_{n(FEA)} < 0.55$						
			0.10	0.35	2	0.206	0.90	0.69	1.23	0.54	0.92	0.79
				0.5	3	0.285	0.88	0.67	1.23	0.53	1.09	0.88
High						0.306	0.98	0.75	1.33	0.65	1.25	1.00
Low						0.168	0.78	0.56	1.06	0.46	0.83	0.77

C.5 MOMENT-SHEAR INTERACTION STRENGTH PLOTS, DATA GROUPED BY CROSS-SECTION PROFILE

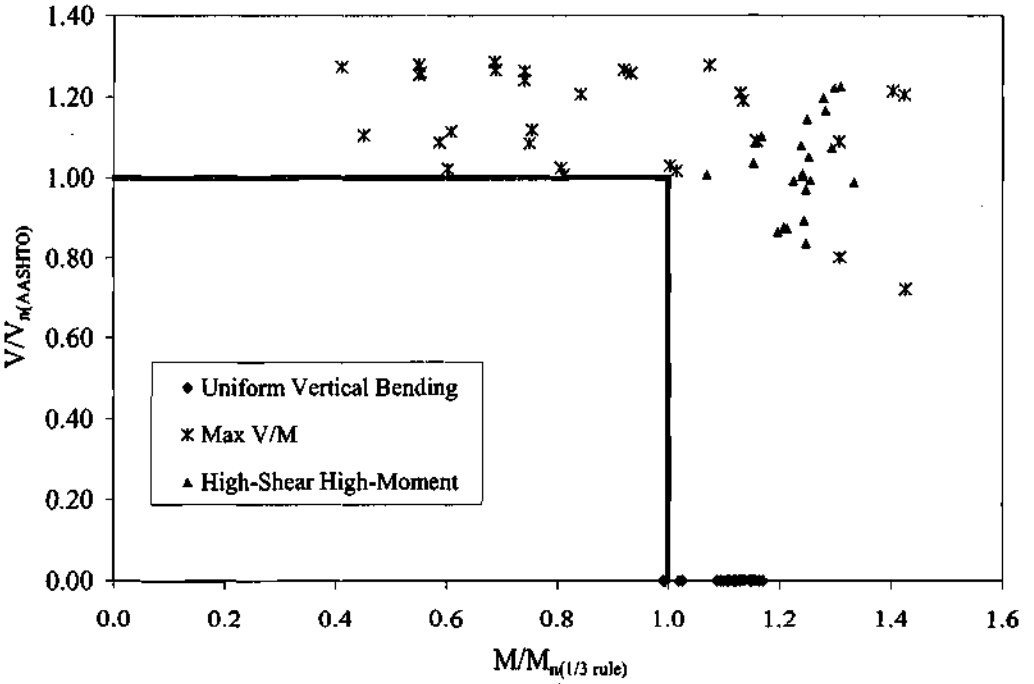

Figure C.5.1. Moment-shear interaction, normalized by $M_{n(1/3\ rule)}$ and $V_{n(AASHTO)}$, for symmetric specimens with $D/b_f = 2.25$ and $b_f/t_f = 25$.

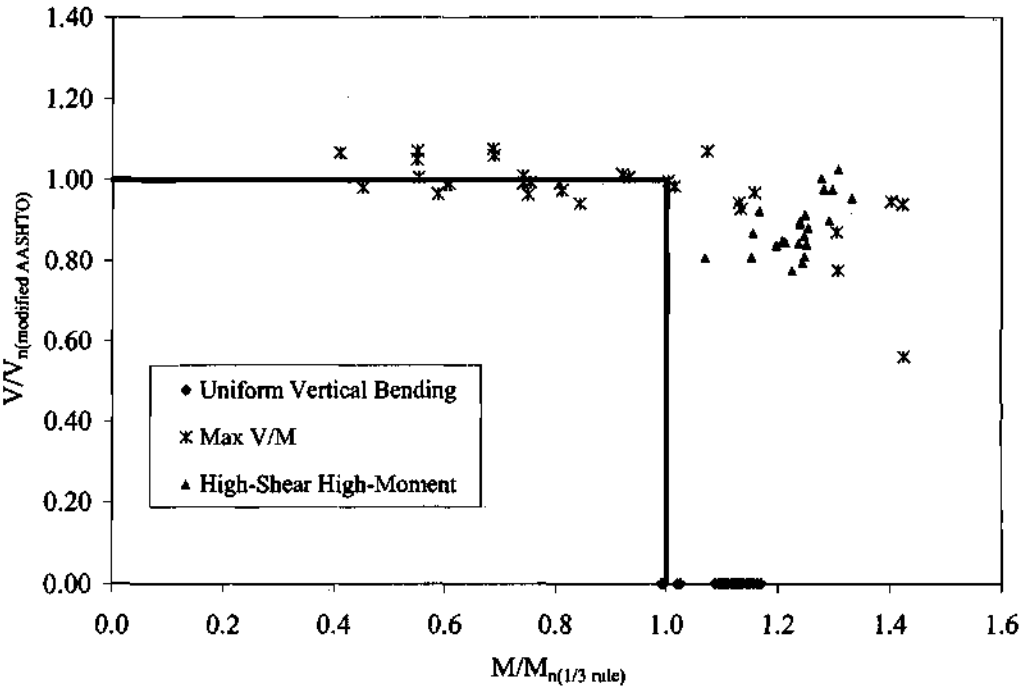

Figure C.5.2. Moment-shear interaction, normalized by $M_{n(1/3\ rule)}$ and $V_{n(modified\ AASHTO)}$, for symmetric specimens with $D/b_f = 2.25$ and $b_f/t_f = 25$.

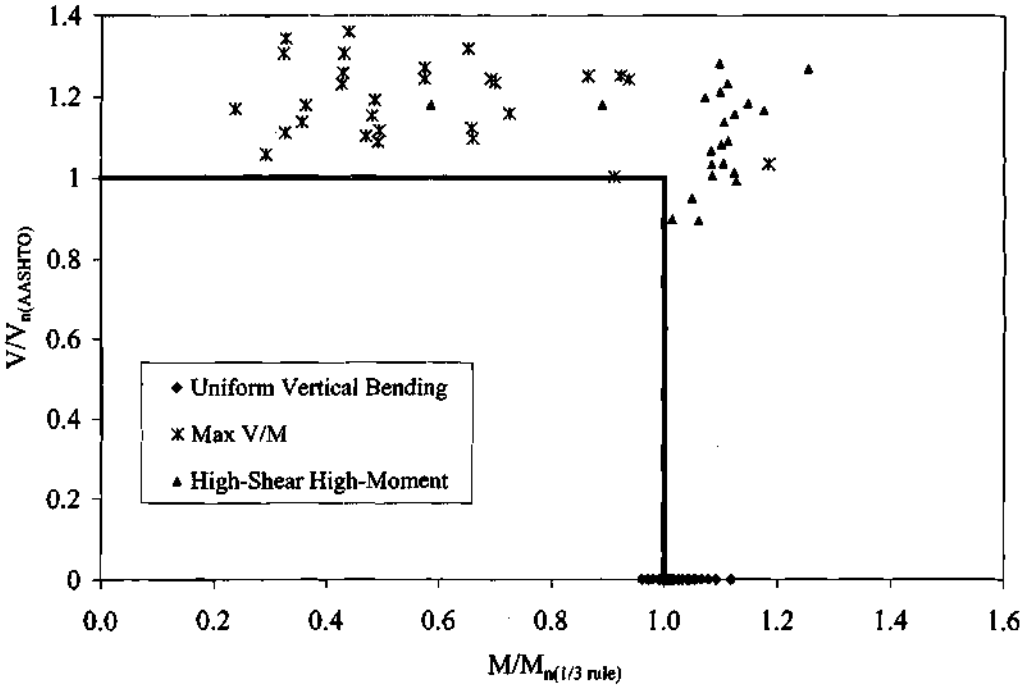

Figure C.5.3. Moment-shear interaction, normalized by $M_{n(1/3\ rule)}$ and $V_{n(AASHTO)}$, for symmetric specimens with $D/b_f = 2.75$ and $b_f/t_f = 15$.

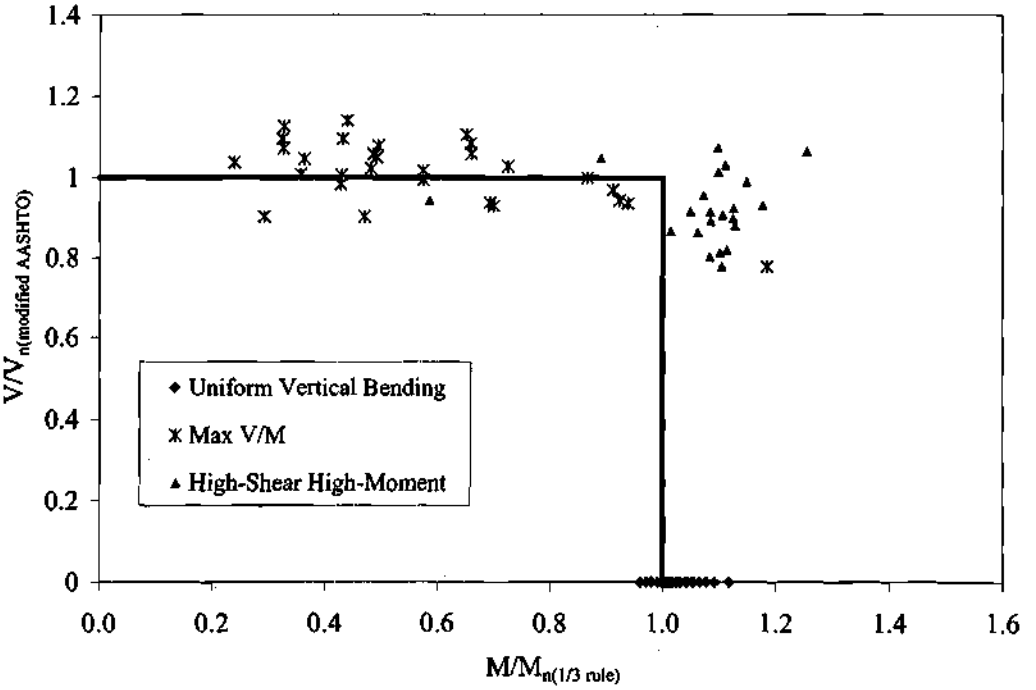

Figure C.5.4. Moment-shear interaction, normalized by $M_{n(1/3\ rule)}$ and $V_{n(modified\ AASHTO)}$, for symmetric specimens with $D/b_f = 2.75$ and $b_f/t_f = 15$.

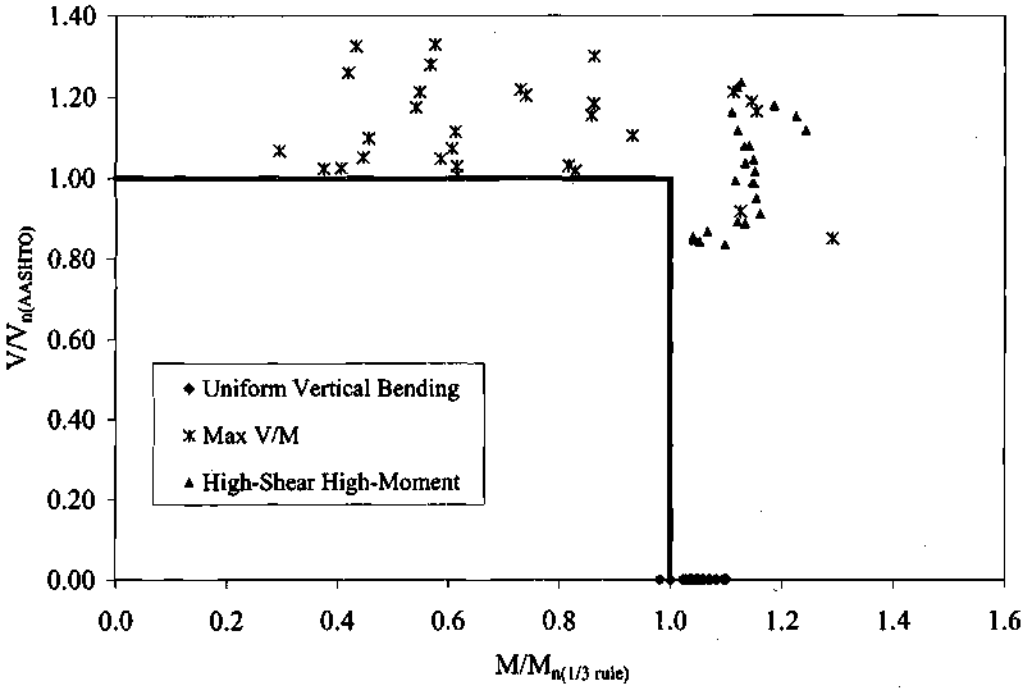

Figure C.5.5. Moment-shear interaction, normalized by $M_{n(1/3\ rule)}$ and $V_{n(AASHTO)}$, for symmetric specimens with $D/b_f = 2.75$ and $b_f/t_f = 20$.

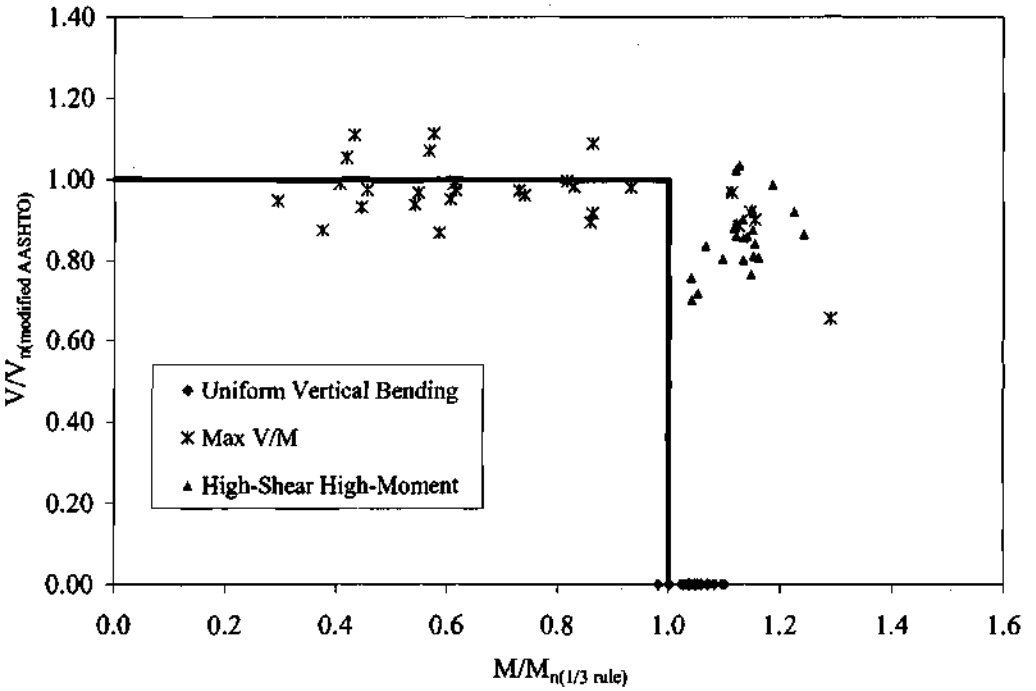

Figure C.5.6. Moment-shear interaction, normalized by $M_{n(1/3\ rule)}$ and $V_{n(modified\ AASHTO)}$, for symmetric specimens with $D/b_f = 2.75$ and $b_f/t_f = 20$.

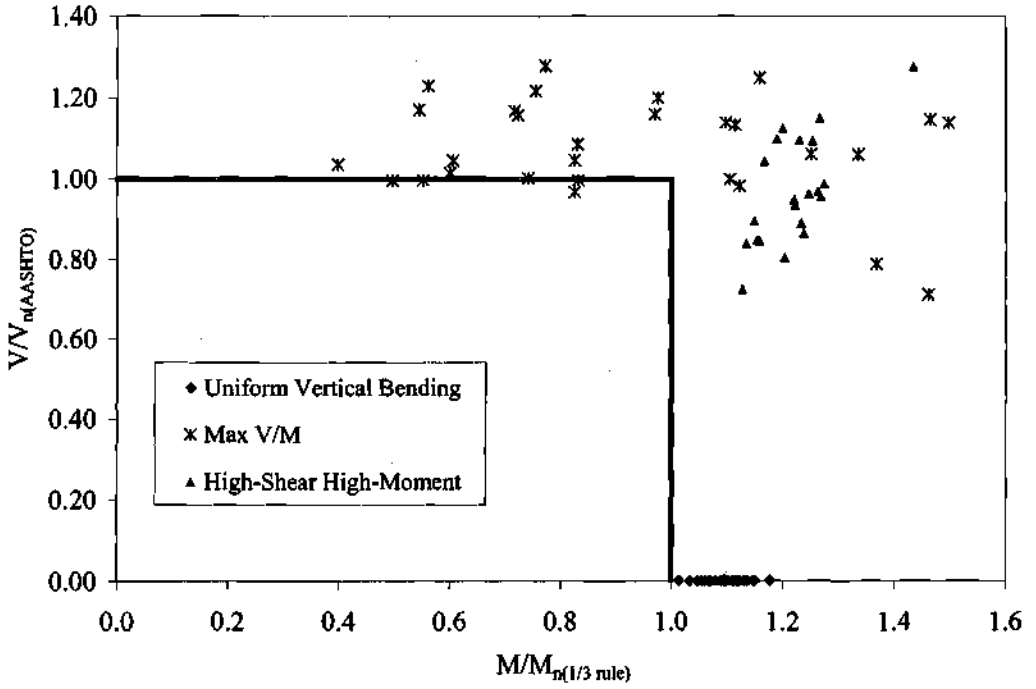

Figure C.5.7. Moment-shear interaction, normalized by $M_{n(1/3\ rule)}$ and $V_{n(AASHTO)}$, for symmetric specimens with $D/b_f = 2.75$ and $b_f/t_f = 25$.

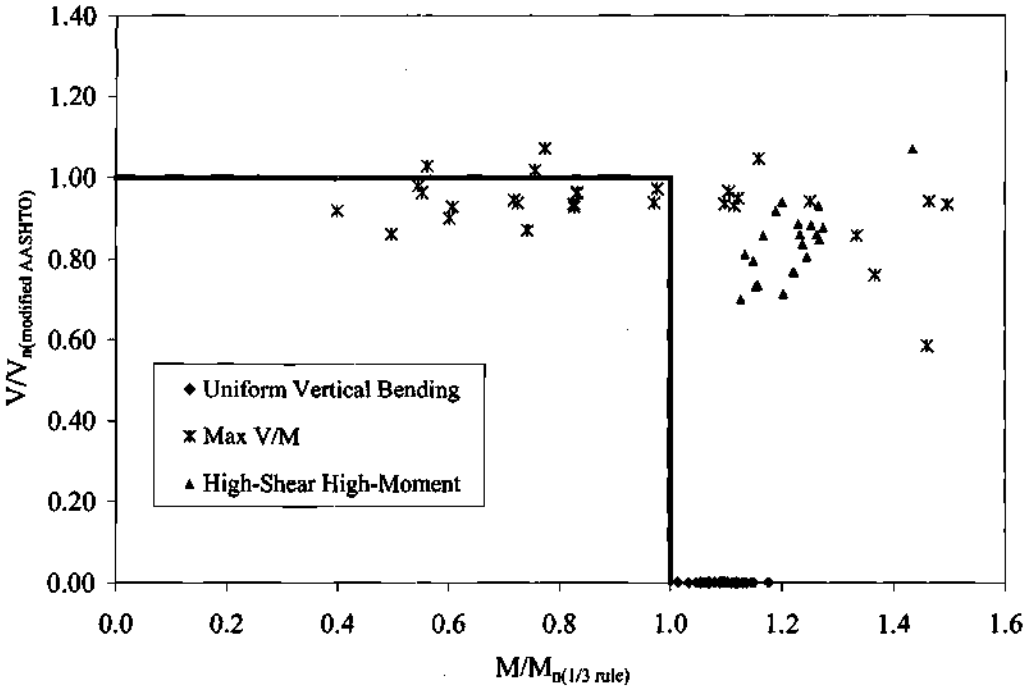

Figure C.5.8. Moment-shear interaction, normalized by $M_{n(1/3\ rule)}$ and $V_{n(modified\ AASHTO)}$, for symmetric specimens with $D/b_f = 2.75$ and $b_f/t_f = 25$.

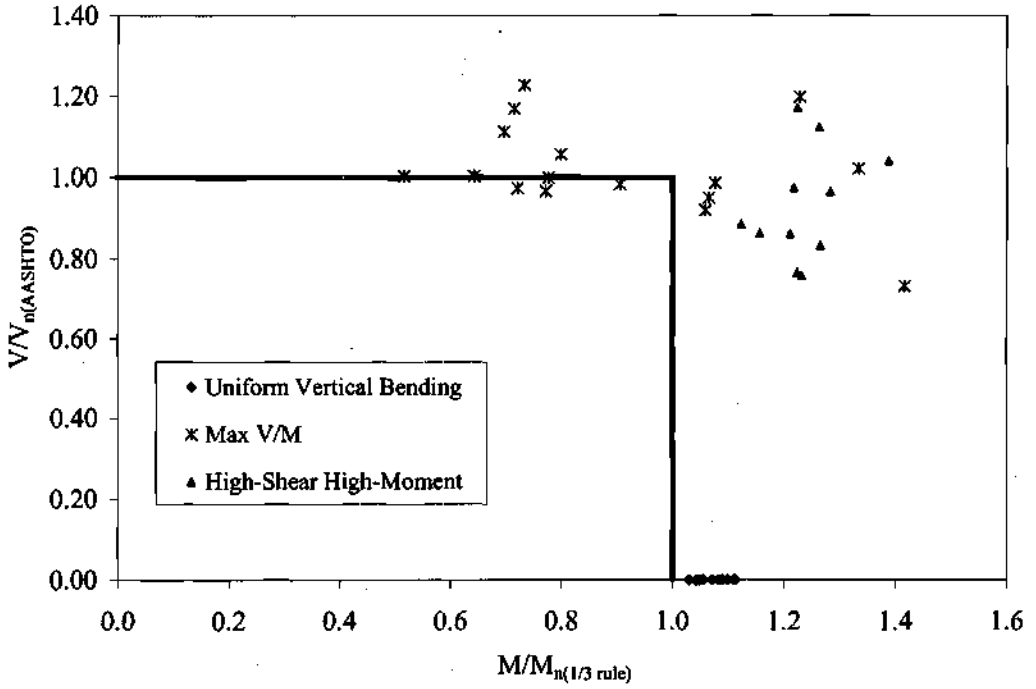

Figure C.5.9. Moment-shear interaction, normalized by $M_{n(1/3\ rule)}$ and $V_{n(AASHTO)}$, for symmetric specimens with $D/b_f = 3.25$ and $b_f/t_f = 25$.

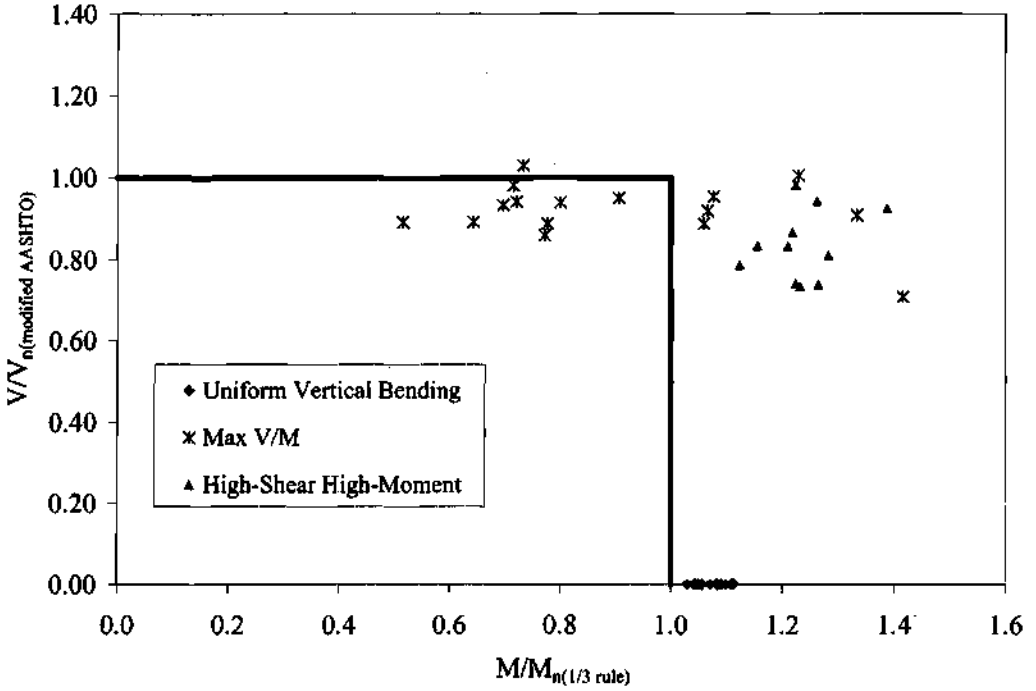

Figure C.5.10. Moment-shear interaction, normalized by $M_{n(1/3\ rule)}$ and $V_{n(modified\ AASHTO)}$, for symmetric specimens with $D/b_f = 3.25$ and $b_f/t_f = 25$.

APPENDIX D

INITIAL GEOMETRIC IMPERFECTION PARAMETERS

This appendix summarizes the initial geometric imperfection parameters specified for the primary test suite of the parametric studies conducted in this research. The overall approach used for definition of these imperfections is described in Section 3.4. This data is provided for the analyses of the experimental test girders in Section 4.3.

In the uniform vertical bending tests of the primary suite with $D/t_w = 130$ and 160, the web is artificially thickened to prevent web bend buckling from dominating, and an elastic linear buckling analysis is conducted to obtain a mode shape for application as an initial geometric imperfection. The web is thickened such that $D/t_w = 100$ is employed for all of these buckling analyses. The first (i.e., fundamental) buckling mode is scaled and applied as an initial displacement to the perfect horizontally curved geometry, with corresponding zero initial strain. Tables D1 through D5 list the scale factors (sf) applied to these fundamental buckling modes to obtain the nodal displacements associated with the specified initial imperfect geometry. The unscaled buckling mode has a maximum nodal displacement of 1.0. As described in Section 3.4, sf is set such that the dominant initial imperfection is at the AWS (1996) fabrication limit.

As described in Section 3.4, all of the maximum V/M tests of the primary suite are conducted with zero specified geometric imperfections. The perfect horizontally curved geometry in effect serves as an initial imperfection.

In the high-moment high-shear tests of the primary suite, a web thickness of $D/t_w = 100$ is again employed for the eigenanalysis in the majority of the studies, to obtain a mode shape for definition of the geometric imperfections. In a few cases the actual girder D/t_w is employed. Also, in a few cases, the second buckling mode is used for definition of the initial geometric imperfections instead of the first one. This is done to de-emphasize web bend buckling deformations. These cases are indicated in the tables. It should be noted that the high-shear high-moment loading is used for the linear buckling analyses of the high-shear high-moment specimens, whereas the loading producing uniform vertical bending is used for eigensolutions in the uniform vertical bending cases.

Similar procedures are employed to define the initial geometric imperfections in all of the other parametric study suites.

Table D1. Eigenmode scale factors (sf) used for generation of geometric imperfections, girders with $D/b_f = 2.25$ and $b_f/t_f = 25$.

D/t_w	d_o/D	L/R = 0.05				L/R = 0.075				L/R = 0.10			
		target $f_\ell/f_b = 0.35$		target $f_\ell/f_b = 0.50$		target $f_\ell/f_b = 0.35$		target $f_\ell/f_b = 0.50$		target $f_\ell/f_b = 0.35$		target $f_\ell/f_b = 0.50$	
		UVB[1]	HMS[2]	UVB	HMS	UVB	HMS	UVB	HMS	UVB	HMS	UVB	HMS
100	3	0.29	0.81[4]	0.30	NA[3]	0.29	0.82	0.29	0.82	0.29	0.84	0.29	0.88
130	3	0.29	0.83[4]	0.30		0.29	0.76	0.29	0.82	0.29	0.66	0.29	0.61
160	1	0.29	0.88	0.30		0.30	0.83	0.29	0.78	0.29	0.78	0.30	0.84
	2	0.30	0.51	0.29		0.30	0.53	0.29	0.64	0.29	0.64[4]	0.29	0.50
	3	0.29	0.54	0.30		0.29	0.53	0.29	0.52	0.29	0.52	0.29	0.49

[1] UVB denotes uniform vertical bending cases
[2] HMS denotes high-moment high-shear loading cases
[3] NA since $M_{n(FEA)}/0.8V_{n(FEA)}L_b < 0.55$
[4] Second mode used for generation of geometric imperfections

Table D2. Eigenmode scale factors (sf) used for generation of geometric imperfections, girders with $D/b_f = 2.75$ and $b_f/t_f = 15$.

D/t_w	d_o/D	L/R = 0.05				L/R = 0.075				L/R = 0.10			
		target $f_\ell/f_b = 0.35$		target $f_\ell/f_b = 0.50$		target $f_\ell/f_b = 0.35$		target $f_\ell/f_b = 0.50$		target $f_\ell/f_b = 0.35$		target $f_\ell/f_b = 0.50$	
		UVB	HMS	UVB	HMS	UVB	HMS	UVB	HMS	UVB	HMS	UVB	HMS
100	3	0.35	0.66	0.36	NA[1]	0.31	0.63	0.35	0.78	0.31	0.57	0.31	0.60
130	3	0.35	0.47	0.36	0.48	0.31	0.46	0.35	0.55	0.31	0.46	0.31	0.45
160	1	0.35	0.42	0.36	NA[2]	0.31	0.49	0.34	0.45	0.33	0.49[4]	0.30	0.47[4]
	2	0.35	0.46	0.36	0.42	0.31	0.39[4]	0.34	0.42	0.31	0.43[4]	0.32	0.41[4]
	3	0.35	0.44	0.36	0.41	0.31	0.43	0.35	0.40	NA[3]	NA[3]	0.35	0.41

[1] NA since $M_{n(FEA)}/0.8V_{n(FEA)}L_b < 0.55$
[2] NA since failure is dominated by lateral bending in corresponding maximum V/M test
[3] NA for target $L_b/R = 0.10$ and $f_\ell/f_b = 0.35$, since $L_b/D = 2$
[4] Second mode used for generation of geometric imperfections

Table D3. Eigenmode scale factors (sf) used for generation of geometric imperfections, girders with $D/b_f = 2.75$ and $b_f/t_f = 20$.

D/t_w	d_o/D	L/R = 0.05				L/R = 0.075				L/R = 0.10			
		target $f_\ell/f_b = 0.35$		target $f_\ell/f_b = 0.50$		target $f_\ell/f_b = 0.35$		target $f_\ell/f_b = 0.50$		target $f_\ell/f_b = 0.35$		target $f_\ell/f_b = 0.50$	
		UVB	HMS	UVB	HMS	UVB	HMS	UVB	HMS	UVB	HMS	UVB	HMS
100	3	0.35	0.85	0.35		0.33	0.79	0.34	0.90	0.31	0.65	0.31	0.74
130	3	0.35	0.52	0.35	NA[1]	0.33	0.50	0.34	0.69	0.31	0.50	0.31	0.48
160	1	0.32	0.62	0.32		0.31	0.547	0.31	0.54	0.31	0.52[4]	0.30	0.53
	2	0.34	0.46	0.36	0.81[3]	0.33	0.46[4]	0.33	0.45	0.31	0.45	0.31	0.44
	3	0.35	0.46	0.35	0.83[3]	0.33	0.45	0.34	0.51	NA[2]	NA[2]	0.31	0.44

[1] NA since $M_{n(FEA)}/0.8V_{n(FEA)}L_b < 0.55$

[2] NA for target $L_b/R = 0.10$ and $f_\ell/f_b = 0.35$, since $L_b/D = 2$

[3] $D/t_w = 160$ used for eigenanalysis.

[4] Second mode used for generation of geometric imperfections

Table D4. Eigenmode scale factors (sf) used for generation of geometric imperfections, girders with $D/b_f = 2.75$ and $b_f/t_f = 25$.

D/t_w	d_o/D	L/R = 0.05				L/R = 0.075				L/R = 0.10			
		target $f_\ell/f_b = 0.35$		target $f_\ell/f_b = 0.50$		target $f_\ell/f_b = 0.35$		target $f_\ell/f_b = 0.50$		target $f_\ell/f_b = 0.35$		target $f_\ell/f_b = 0.50$	
		UVB	HMS	UVB	HMS	UVB	HMS	UVB	HMS	UVB	HMS	UVB	HMS
100	3	0.35	0.81	0.35		0.33	0.85	0.34	1.0	0.31	0.73	0.31	0.92
130	3	0.35	0.64	0.35		0.33	0.61	0.34	0.75	0.31	0.57	0.31	0.53
160	1	0.32	0.65	0.32	NA[1]	0.31	0.67	0.31	0.67	0.31	0.63	0.30	0.61[4]
	2	0.34	0.50	0.36		0.33	0.60[4]	0.33	0.50	0.33	0.50	0.31	0.48[4]
	3	0.35	0.48	0.35		0.33	0.49	0.34	0.84[3]	NA[2]	NA[2]	0.31	0.46

[1] NA since $M_{n(FEA)}/0.8V_{n(FEA)}L_b < 0.55$

[2] NA for target $L_b/R = 0.10$ and $f_\ell/f_b = 0.35$, since $L_b/D = 2$

[3] $D/t_w = 160$ used for eigenanalysis.

[4] Second mode used for generation of geometric imperfections

Table D5. Eigenmode scale factors (sf) used for generation of geometric imperfections, girders with $D/b_f = 3.25$ and $b_f/t_f = 25$.

D/t_w	d_o/D	L/R = 0.05				L/R = 0.075				L/R = 0.10			
		target $f_\ell/f_b = 0.35$		target $f_\ell/f_b = 0.50$		target $f_\ell/f_b = 0.35$		target $f_\ell/f_b = 0.50$		target $f_\ell/f_b = 0.35$		target $f_\ell/f_b = 0.50$	
		UVB	HMS	UVB	HMS	UVB	HMS	UVB	HMS	UVB	HMS	UVB	HMS
160	1	0.37	0.58	0.36	NA[1]	0.36	NA[2]	0.35	0.64	0.34	0.62	0.35	0.58
	2	0.39	0.62	0.36		0.37		0.36	0.79	0.36	0.51	0.35	0.48
	3	0.39	0.62	0.38		0.37	NA[3]	0.38	0.57	NA[4]	NA[4]	0.36	0.45

[1] NA since $M_{n(FEA)}/0.8V_{n(FEA)}L_b < 0.55$

[2] NA, analysis not conducted

[3] NA for target $L_b/R = 0.10$ and $f_\ell/f_b = 0.35$, since $L_b/D = 2.5$

[4] NA for target $L_b/R = 0.10$ and $f_\ell/f_b = 0.35$, since $L_b/D = 2$

APPENDIX E

GAUSS POINT RESIDUAL STRESSES

The Gauss point residual stresses, specified as initial stresses in the full nonlinear analyses conducted in this research, are summarized in this appendix. These residual stresses are calculated based on the ECCS (1976) model for cut-curved girders and are calculated based on Culver-Nasir model (Culver and Nasir 1971) for heat-curved girders. The organization of this appendix is as follows. The Gauss point residual stresses specified for each of the single girder experimental test specimens, discussed in Chapter IV, are summarized in Section E.1. The values for the two-girder test system analyzed in Chapter IV are provided in Section E.2. Section E.3 presents values of Gauss point residual stresses for the three-girder test system analyzed in Chapter IV. Finally, the Gauss point residual stresses for all the parametric study specimens are presented in Section E.4.

E.1 SINGLE GIRDER TESTS

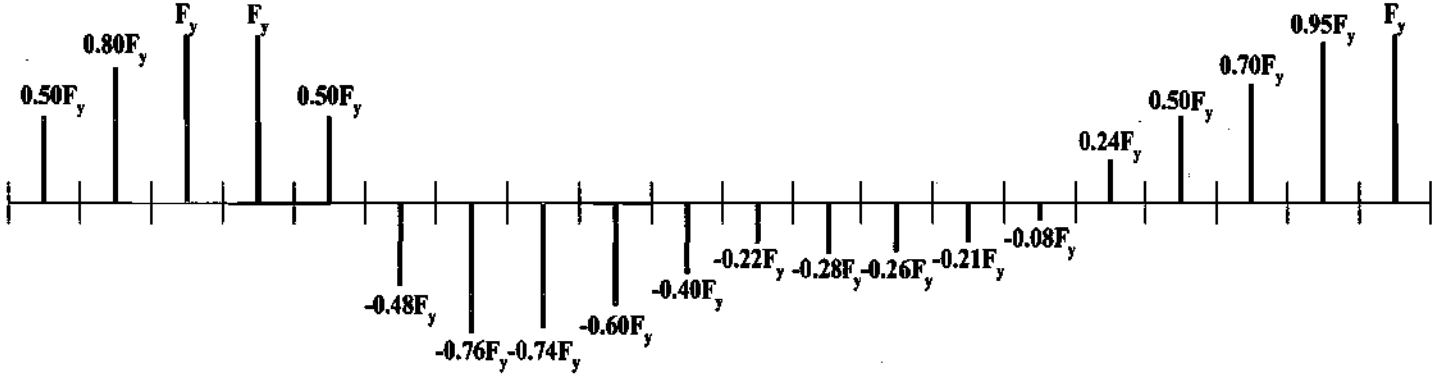

Figure E.1.1. Assumed Gauss point residual stresses in flanges for test C8-2 (Mozer et al. 1973) (web residual stresses are assumed to be zero).

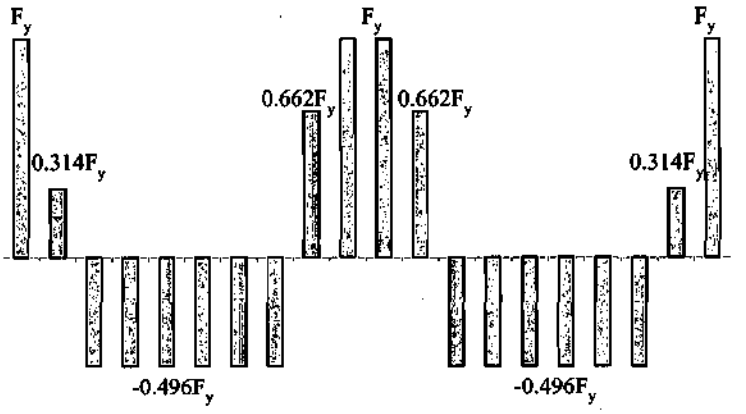

(a) Top and bottom flanges

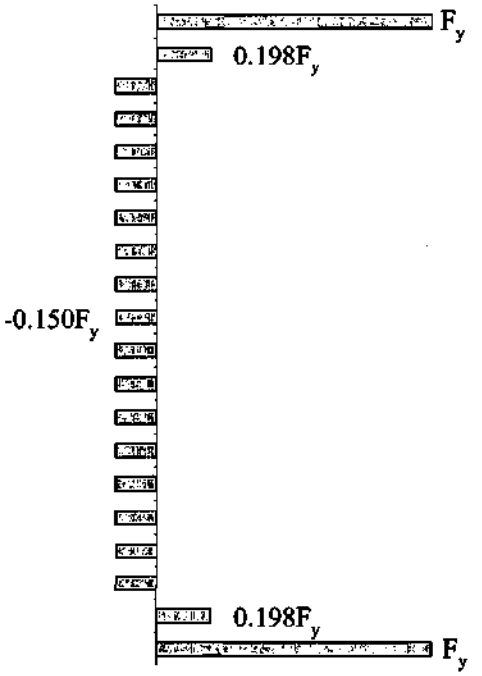

(b) Web

Figure E.1.2. Assumed Gauss point residual stresses for test C9-2 (Mozer et al. 1970).

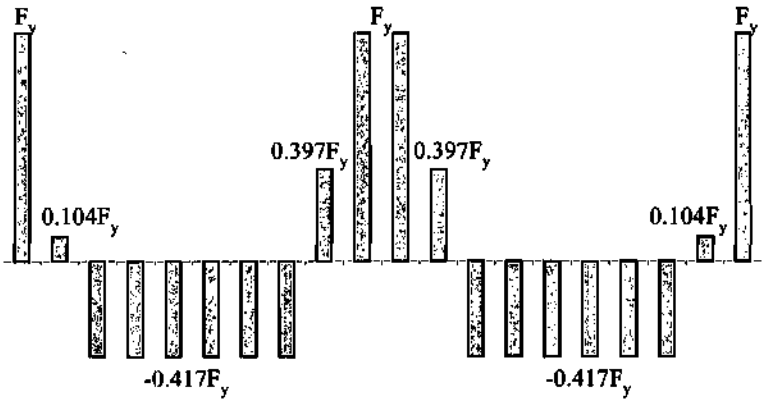

(a) Top and bottom flanges

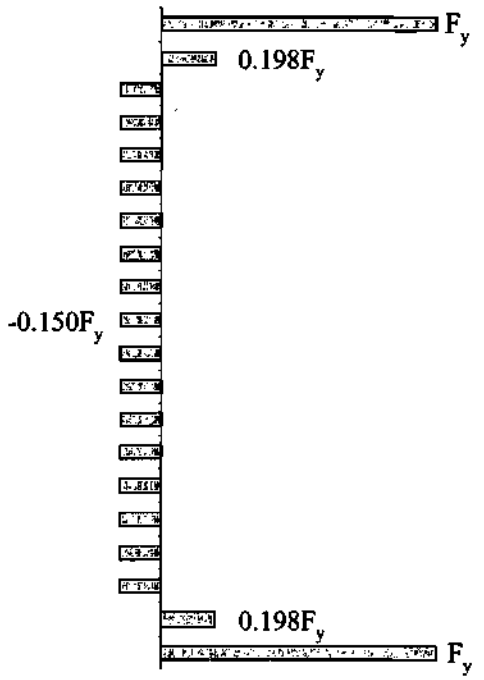

(b) Web

Figure E.1.3. Assumed Gauss point residual stresses for tests D13 and D14 (Mozer et al. 1970).

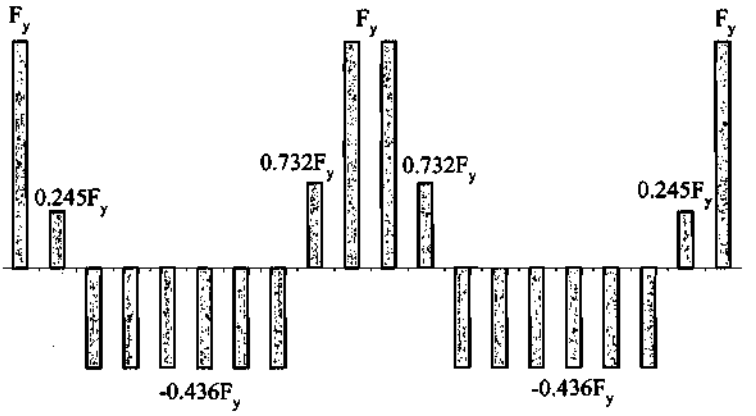

(a) Top and bottom flanges

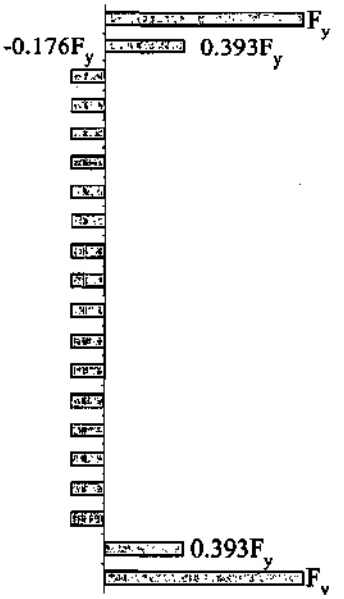

(b) Web

Figure E.1.4. Assumed Gauss point residual stresses for test L1-A (Mozer et al. 1971).

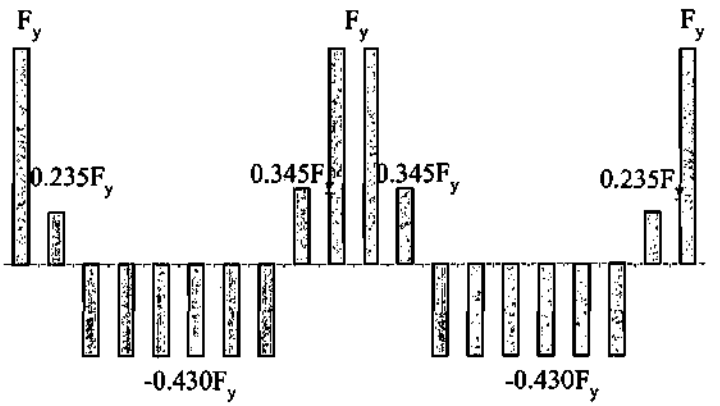

(a) Top and bottom flanges

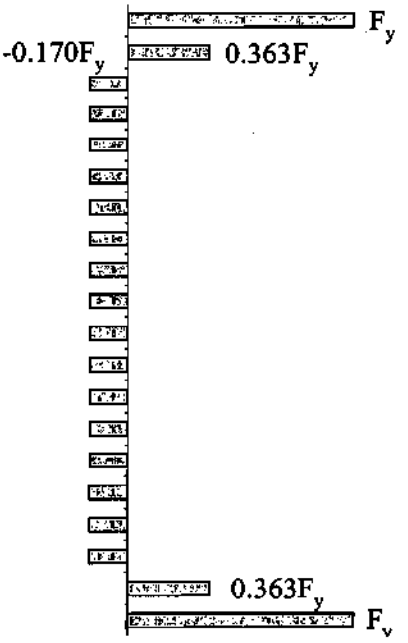

(b) Web

Figure E.1.5. Assumed Gauss point residual stresses for tests L2-A, B and C (Mozer et al. 1971) .

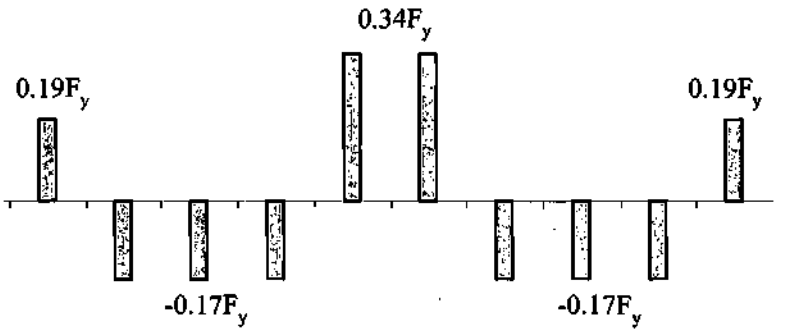

(a) Top and bottom flanges

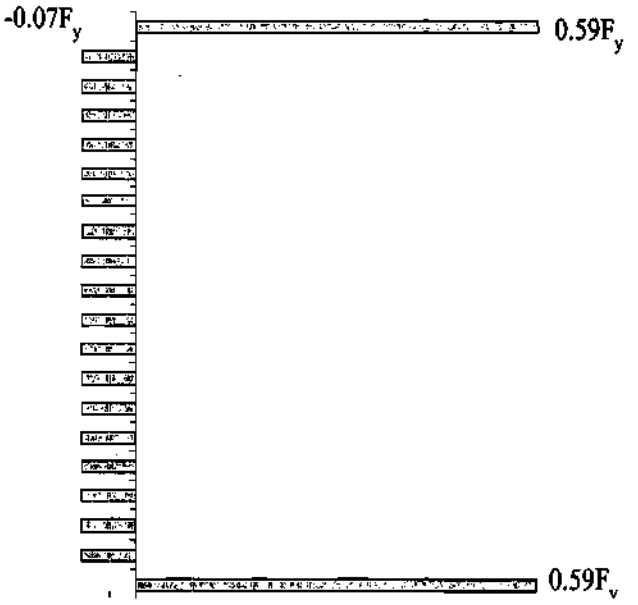

(b) Web

Figure E.1.6. Assumed Gauss point residual stresses for tests S1-0.10 and S1S-0.10.

E.2 TWO-GIRDER TEST SYSTEM

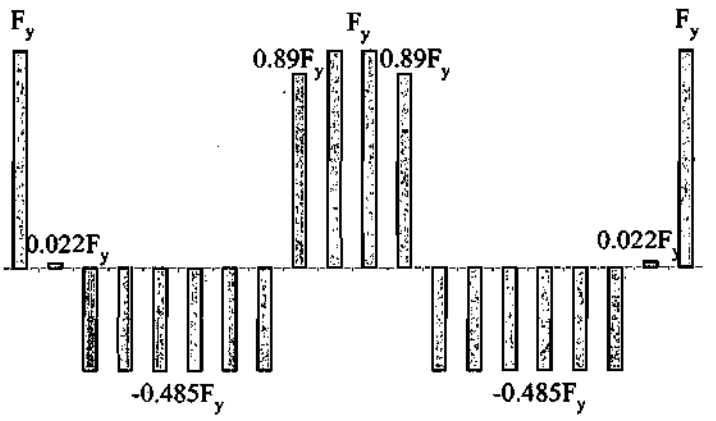

(a) Top and bottom flanges

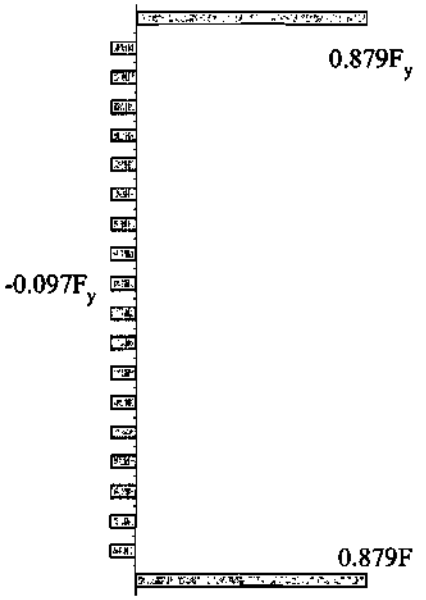

(b) Web

Figure E.2.1. Assumed Gauss point residual stresses for tests GI-2, GI-3, and GI-4 (Mozer et al. 1973).

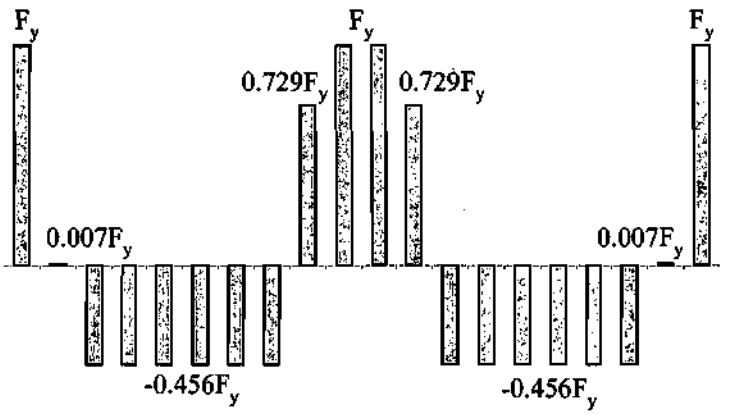

(a) Top and bottom flanges

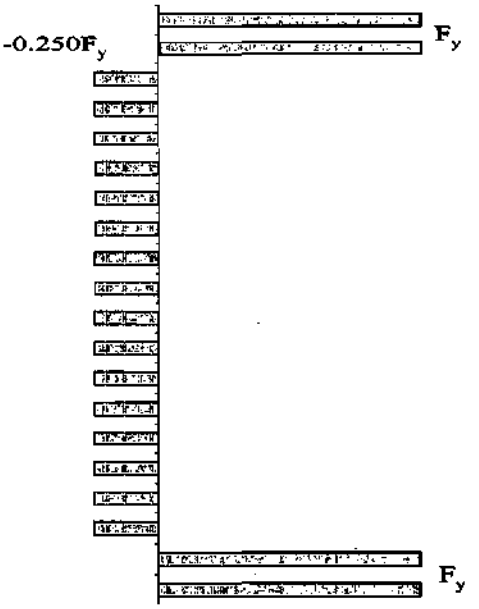

(b) Web

Figure E.2.2. Assumed Gauss point residual stresses for test GO-8 (Mozer et al. 1973).

E.3 THREE-GIRDER TEST SYSTEM

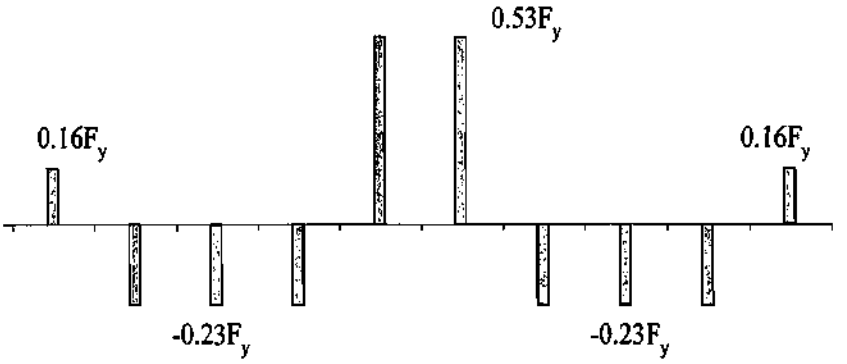

(a) Top and bottom flanges

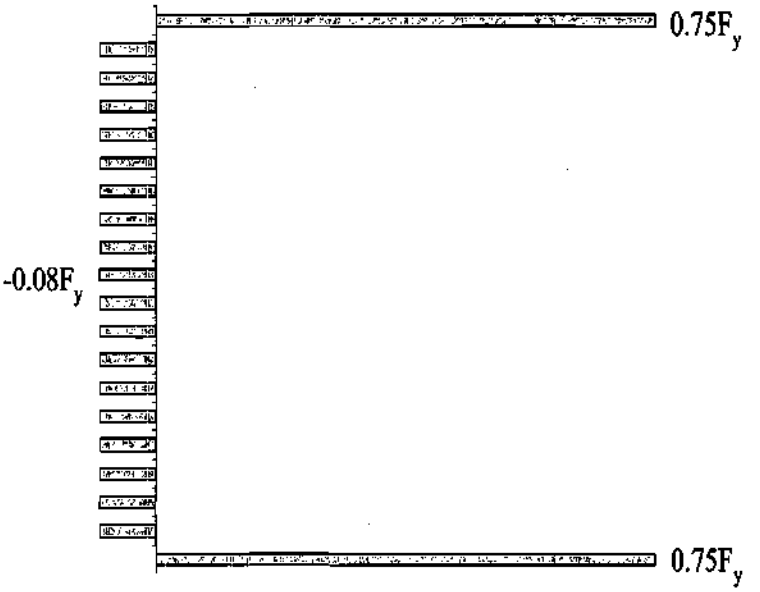

(b) Web

Figure E.3.1. Assumed Gauss point residual stresses for bending test B1 (Hartmann and Wright 2001).

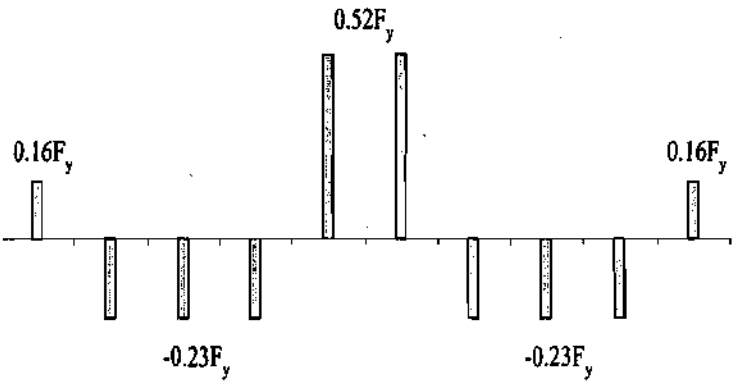

(a) Top and bottom flanges

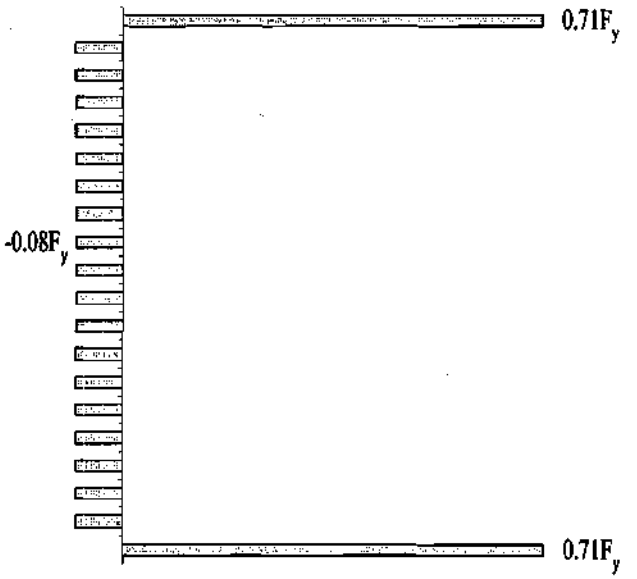

(b) Web

Figure E.3.2. Assumed Gauss point residual stresses for bending test B2 (Hartmann and Wright 2001).

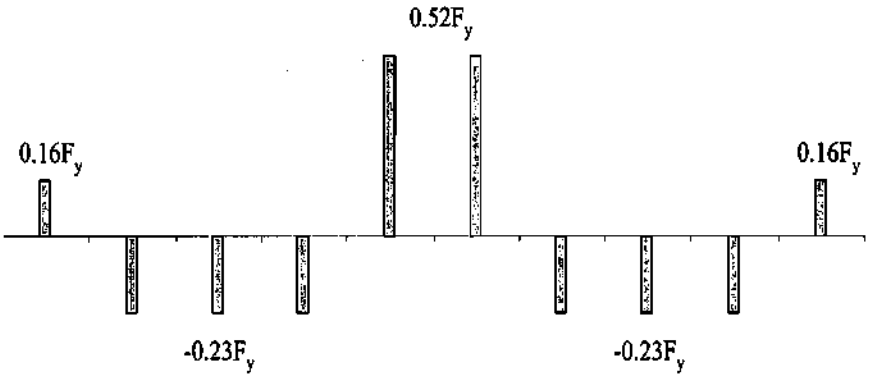

(a) Top and bottom flanges

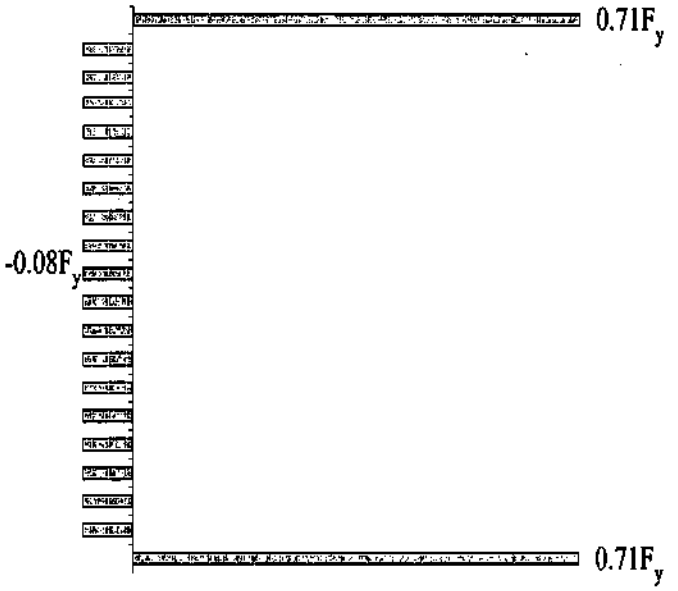

(b) Web

Figure E.3.3. Assumed Gauss point residual stresses for bending test B3 (Hartmann and Wright 2001).

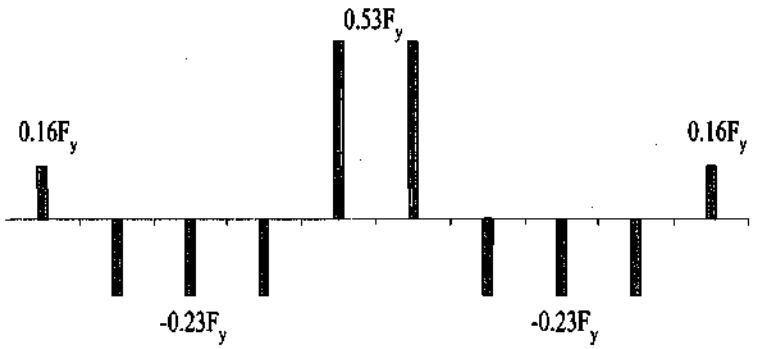

(a) Top flange

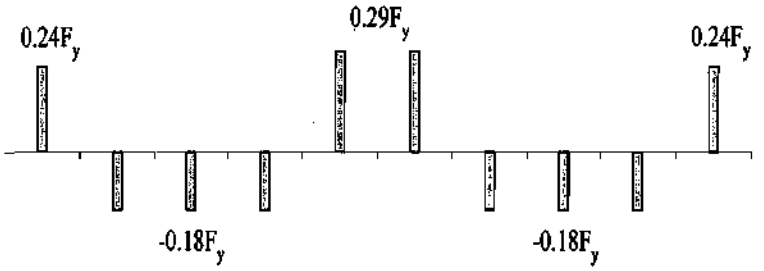

(b) Bottom flange

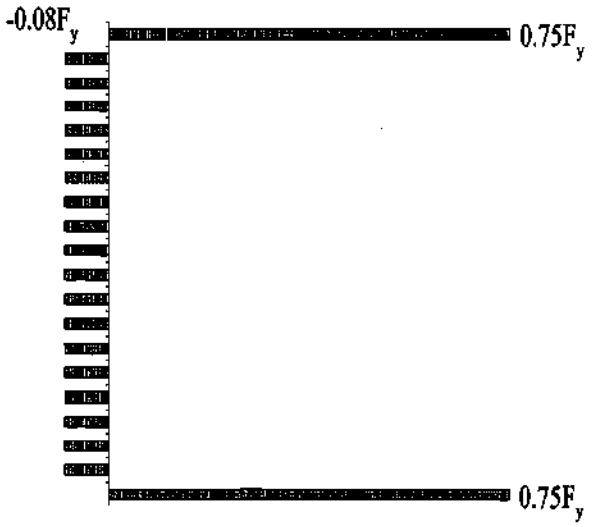

(c) Web

Figure E.3.4. Assumed Gauss point residual stresses for bending test B4 (Hartmann and Wright 2001).

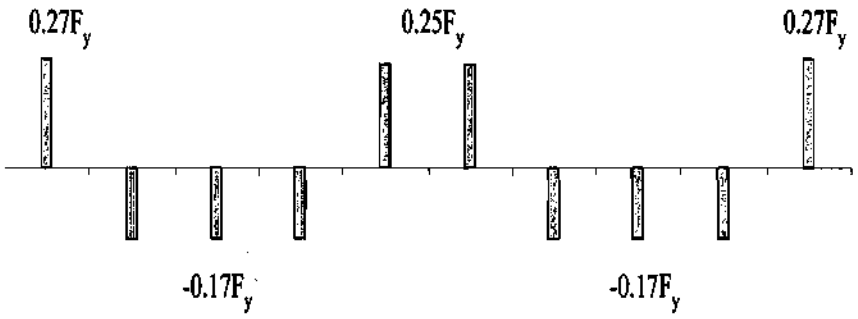

(a) Top and bottom flanges

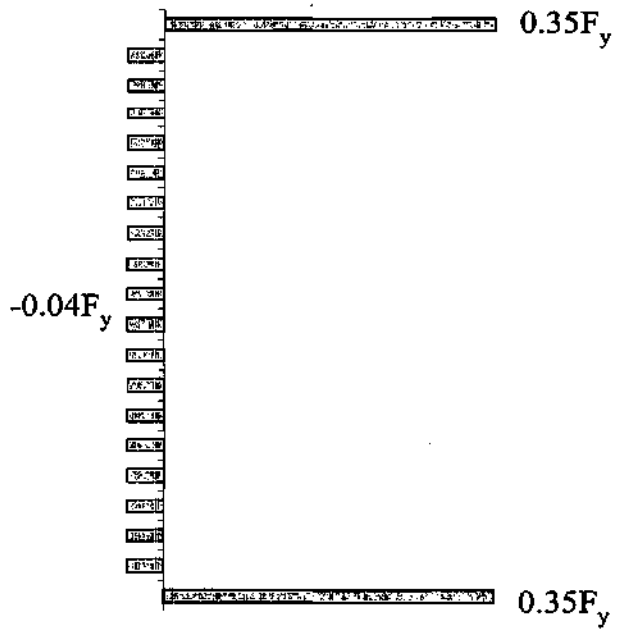

(b) Web

Figure E.3.5. Assumed Gauss point residual stresses for bending test B5 (Hartmann and Wright 2001).

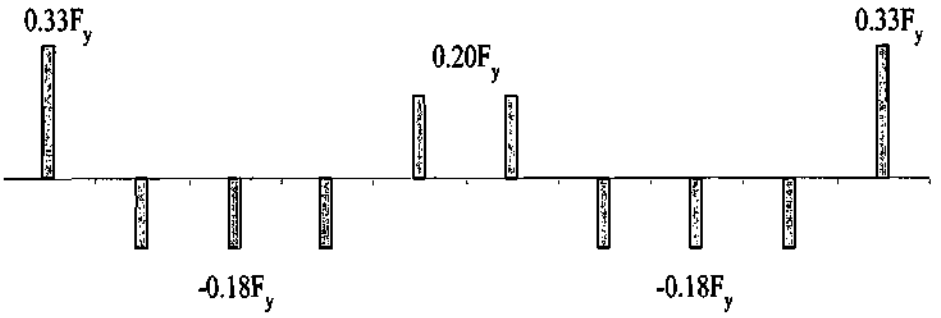

(a) Top and bottom flanges

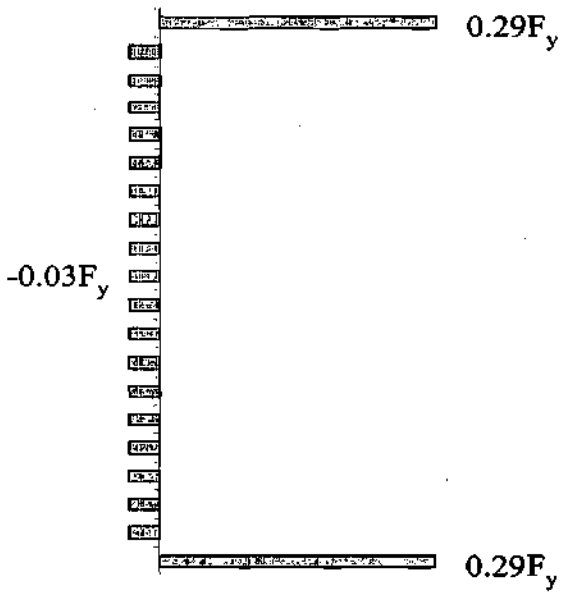

(b) Web

Figure E.3.6. Assumed Gauss point residual stresses for bending test B6 (Hartmann and Wright 2001).

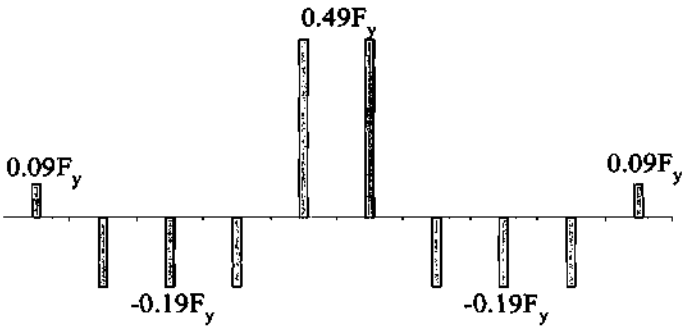

(a) Top flange

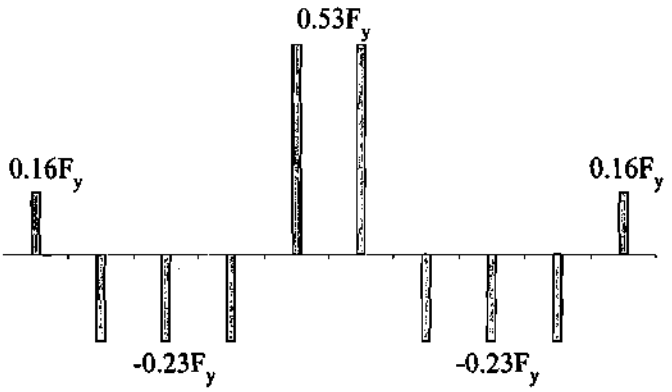

(b) Bottom flange

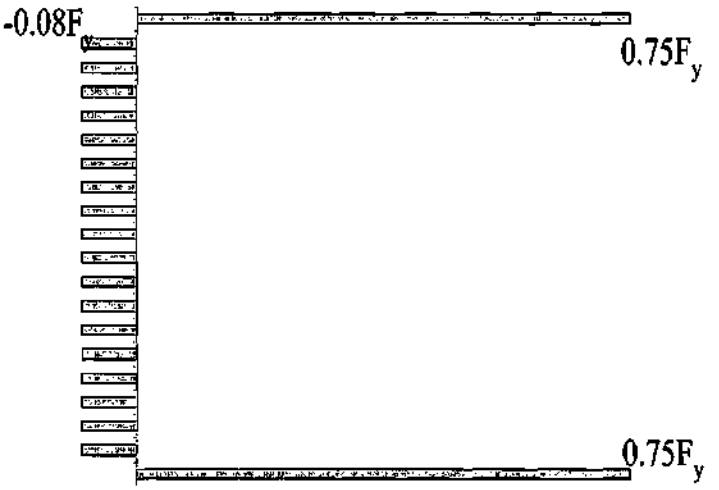

(c) Web

Figure E.3.7. Assumed Gauss point residual stresses for bending test B7 (Hartmann and Wright 2001).

E.4 PARAMETRIC STUDY SPECIMENS

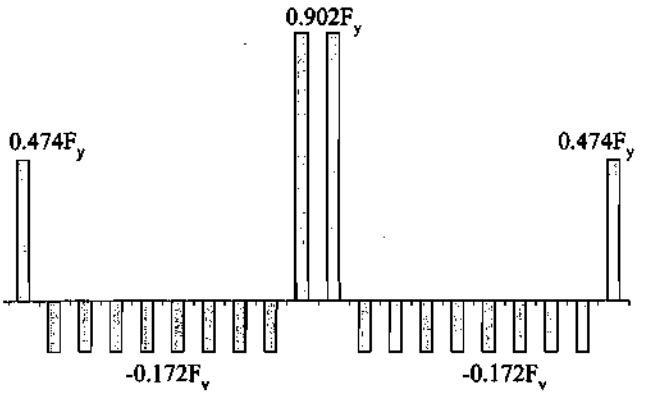

(a) Top and bottom flanges

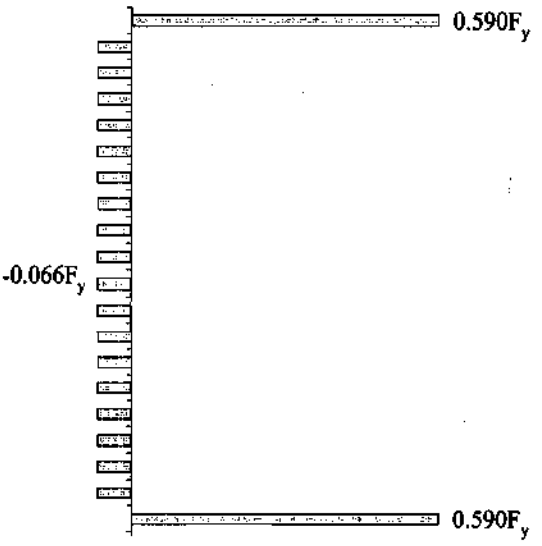

(b) Web

Figure E.4.1. Gauss point residual stresses for specimens with $D/b_f = 2.25$, $b_f/t_f = 25$ and $D/t_w = 100$.

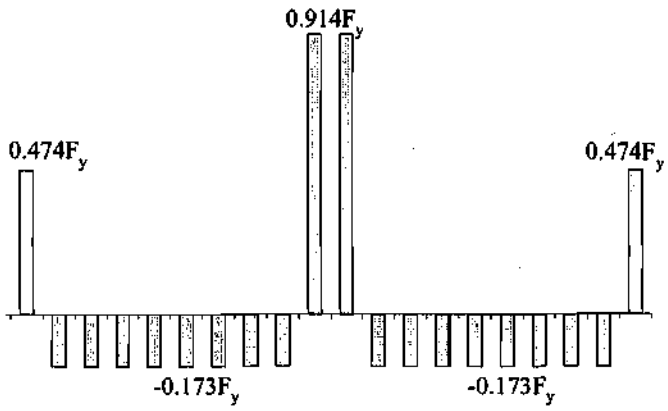

(a) Top and bottom flanges

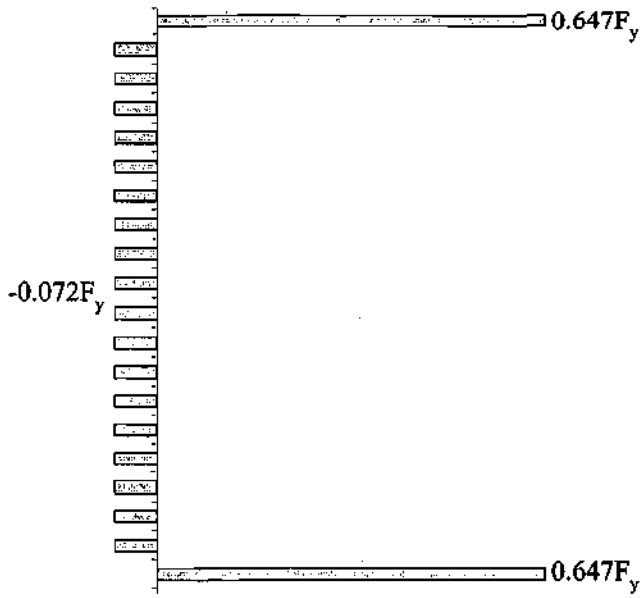

(b) Web

Figure E.4.2. Gauss point residual stresses for specimens with $D/b_f = 2.25$, $b_f/t_f = 25$ and $D/t_w = 130$.

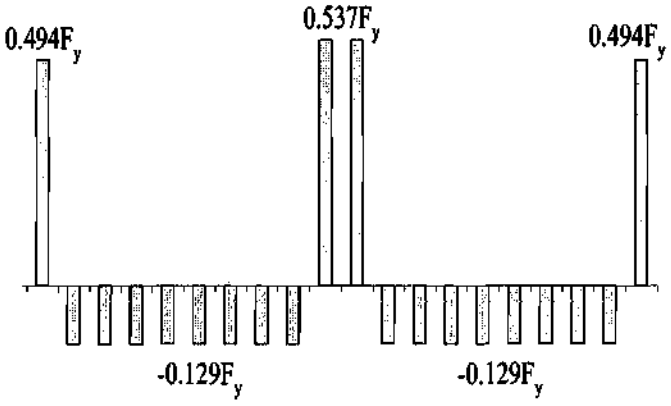

(a) Top and bottom flanges

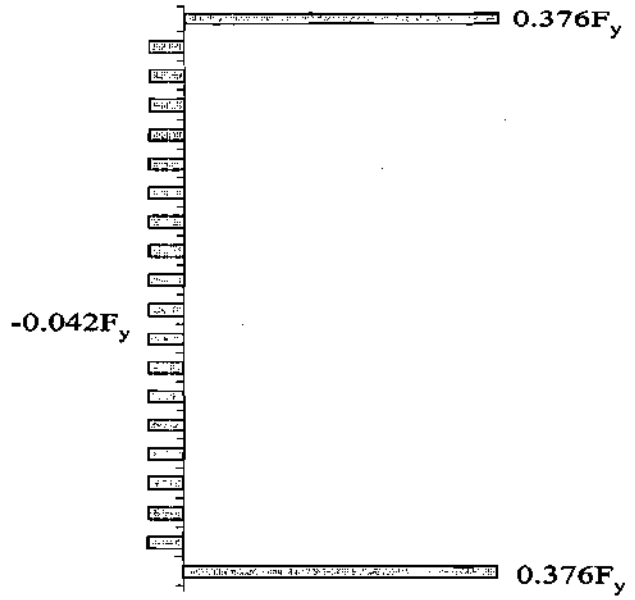

(b) Web

Figure E.4.3. Gauss point residual stresses for specimens with $D/b_f = 2.25$, $b_f/t_f = 25$ and $D/t_w = 160$.

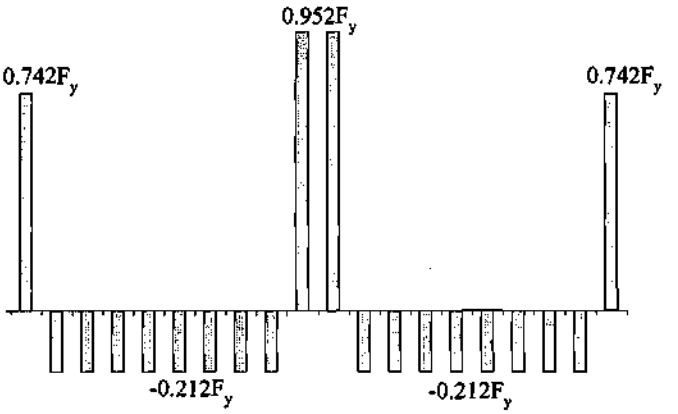

(a) Top and bottom flanges

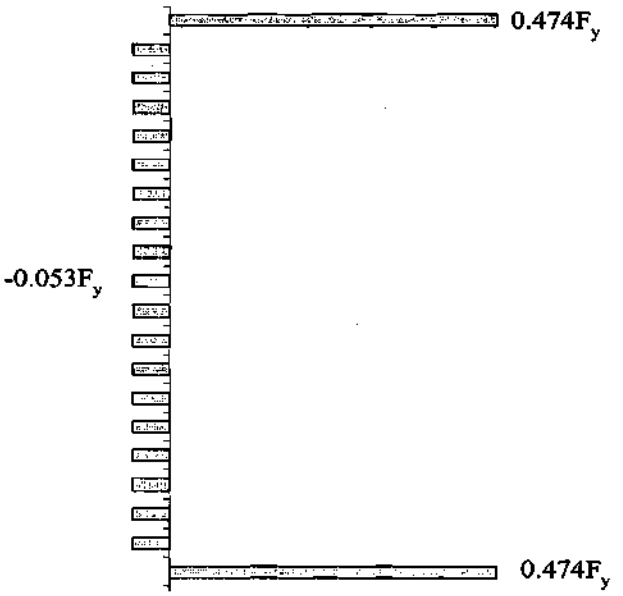

(b) Web

Figure E.4.4. Gauss point residual stresses for specimens with $D/b_f = 2.75$, $b_f/t_f = 15$ and $D/t_w = 100$.

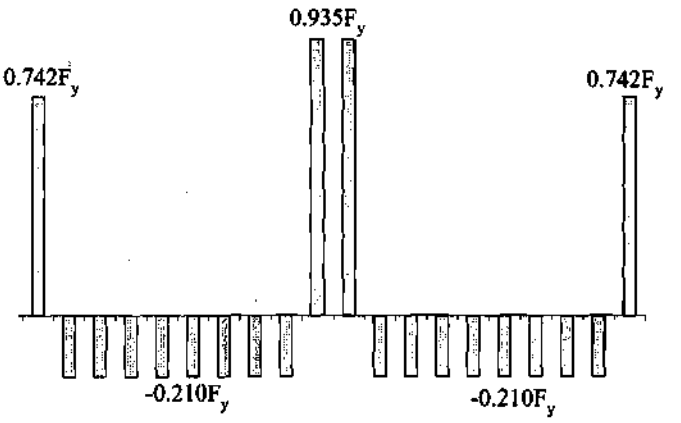

(a) Top and bottom flanges

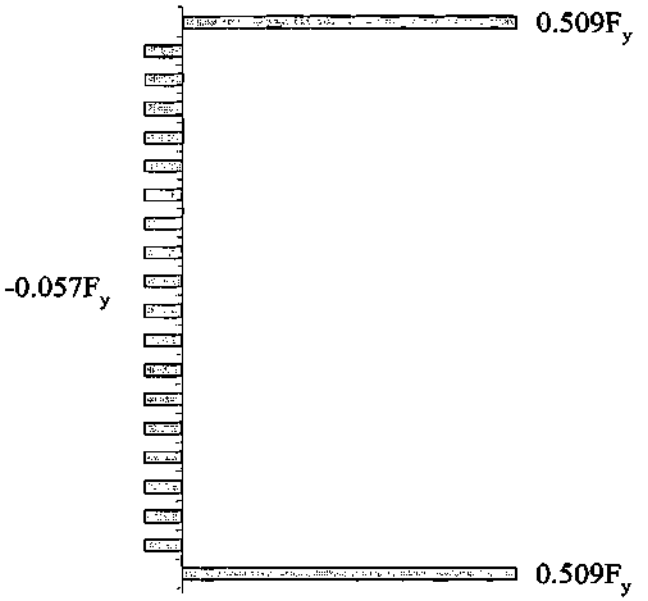

(b) Web

Figure E.4.5. Gauss point residual stresses for specimens with $D/b_f = 2.75$, $b_f/t_f = 15$ and $D/t_w = 130$.

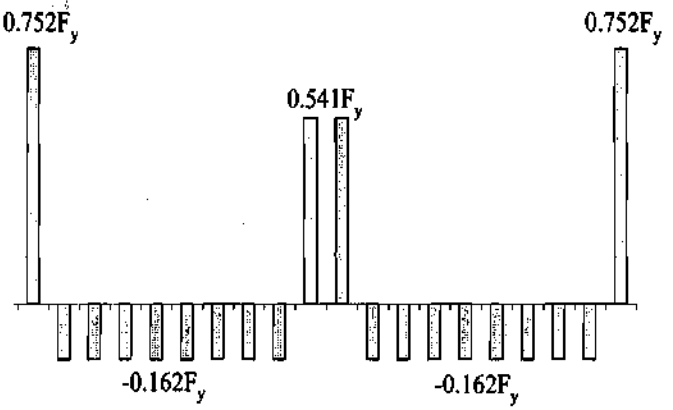

(a) Top and bottom flanges

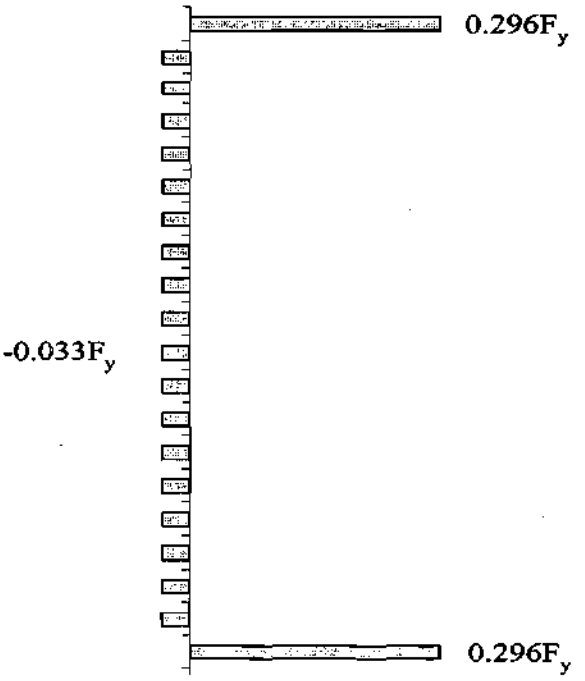

(b) Web

Figure E.4.6. Gauss point residual stresses for specimens with $D/b_f = 2.75$, $b_f/t_f = 15$ and $D/t_w = 160$.

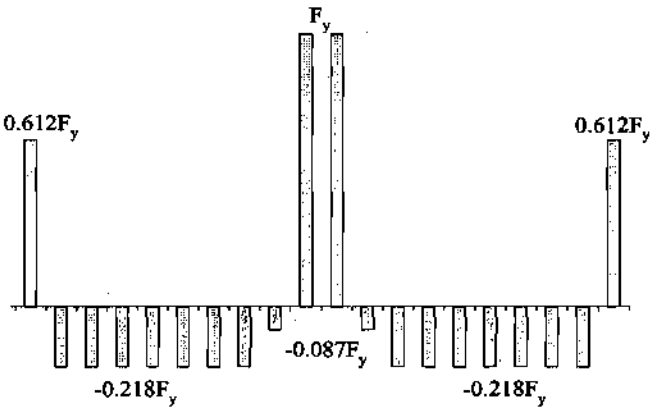

(a) Top and bottom flanges

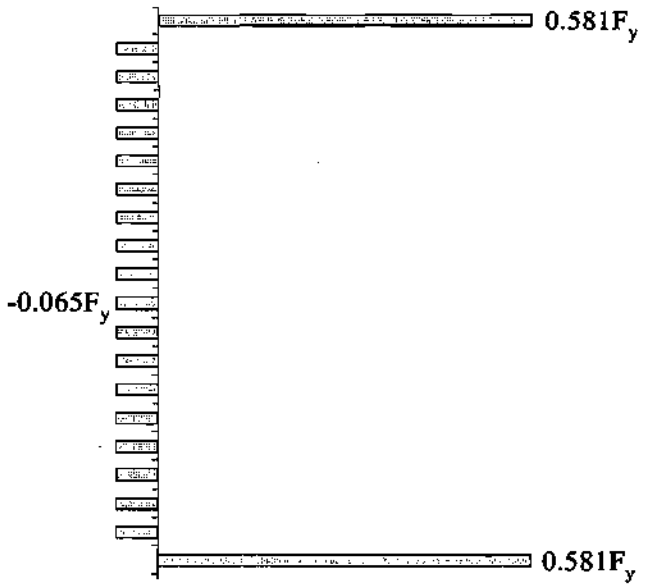

(b) Web

Figure E.4.7. Gauss point residual stresses for specimens with $D/b_f = 2.75$, $b_f/t_f = 20$ and $D/t_w = 100$.

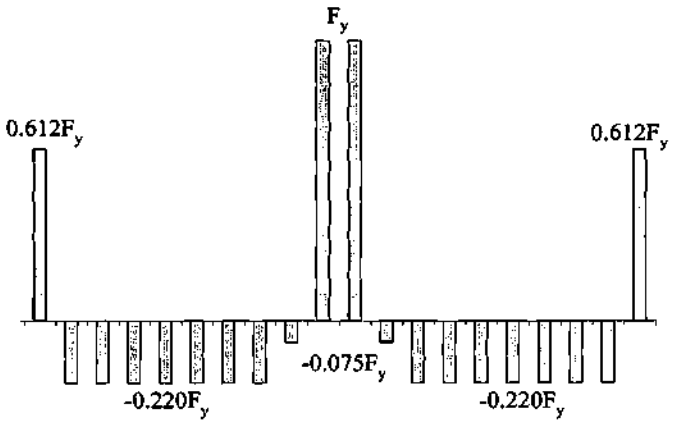

(a) Top and bottom flanges

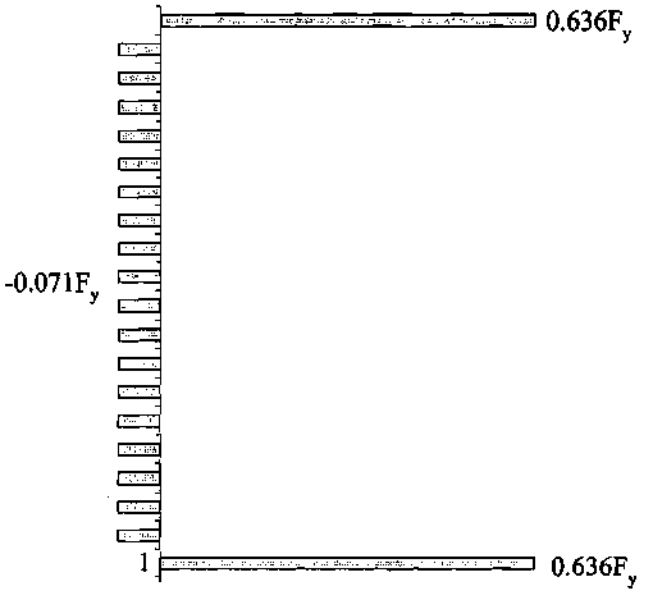

(b) Web

Figure E.4.8. Gauss point residual stresses for specimens with $D/b_f = 2.75$, $b_f/t_f = 20$ and $D/t_w = 130$.

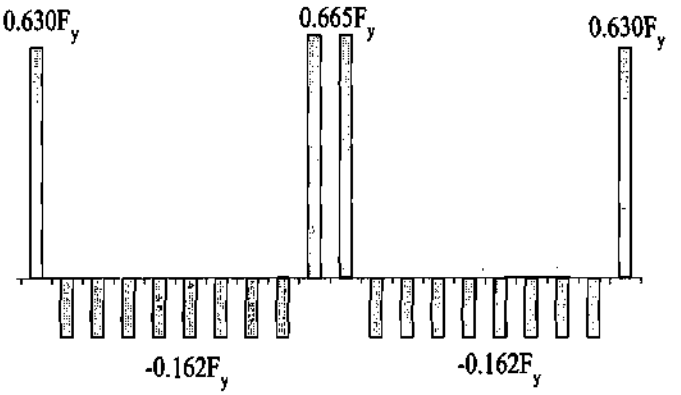

(a) Top and bottom flanges

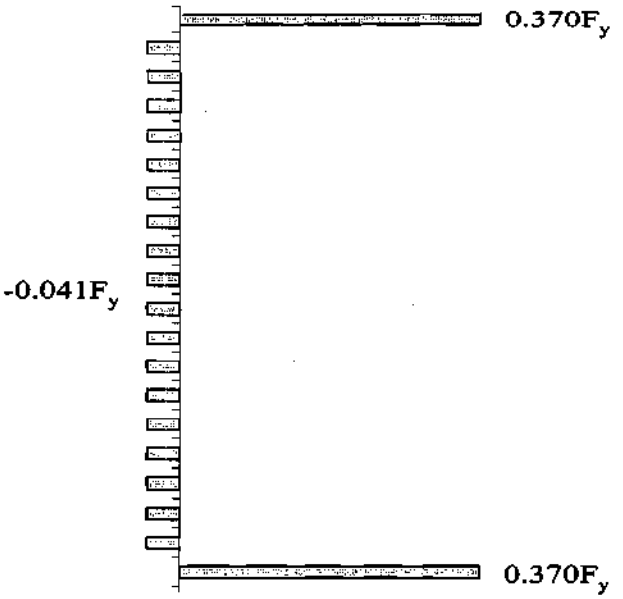

(b) Web

Figure E.4.9. Gauss point residual stresses for specimens with $D/b_f = 2.75$, $b_f/t_f = 20$ and $D/t_w = 160$.

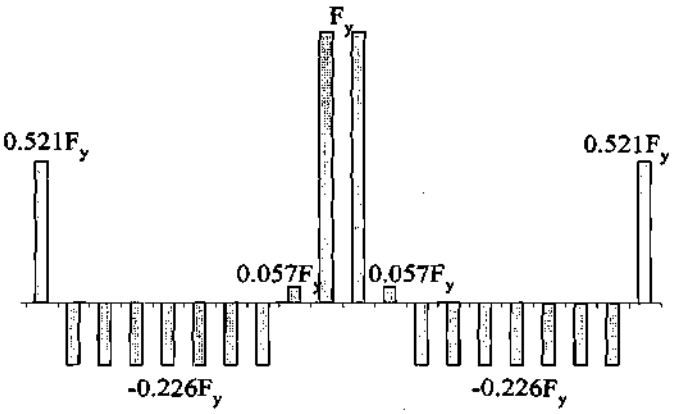

(a) Top and bottom flanges

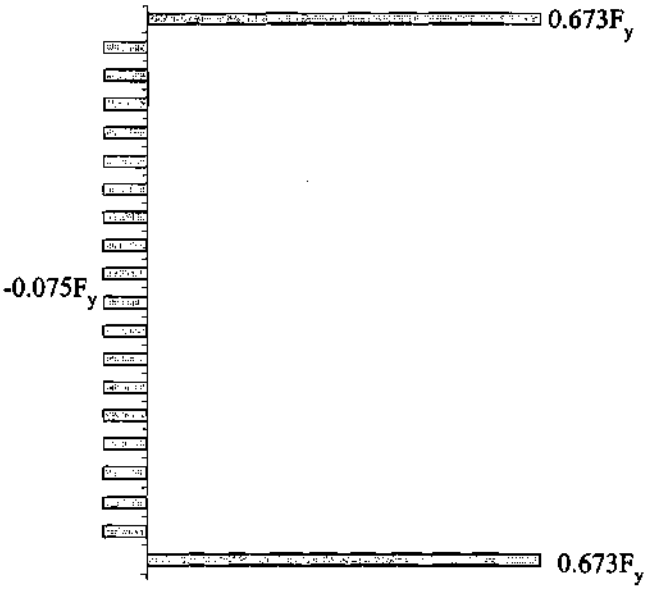

(b) Web

Figure E.4.10. Gauss point residual stresses for specimens with $D/b_f = 2.75$, $b_f/t_f = 25$ and $D/t_w = 100$.

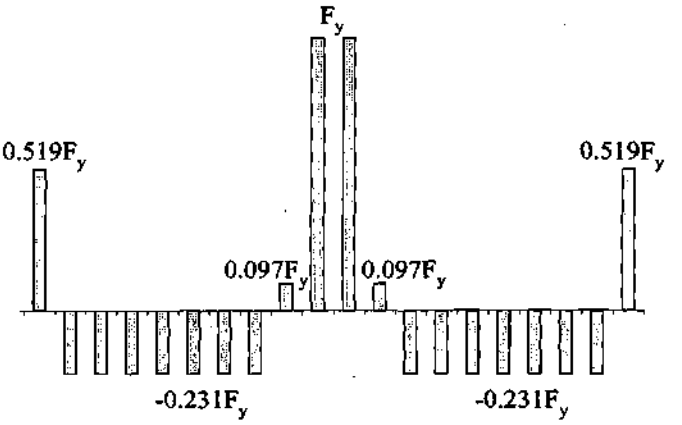

(a) Top and bottom flanges

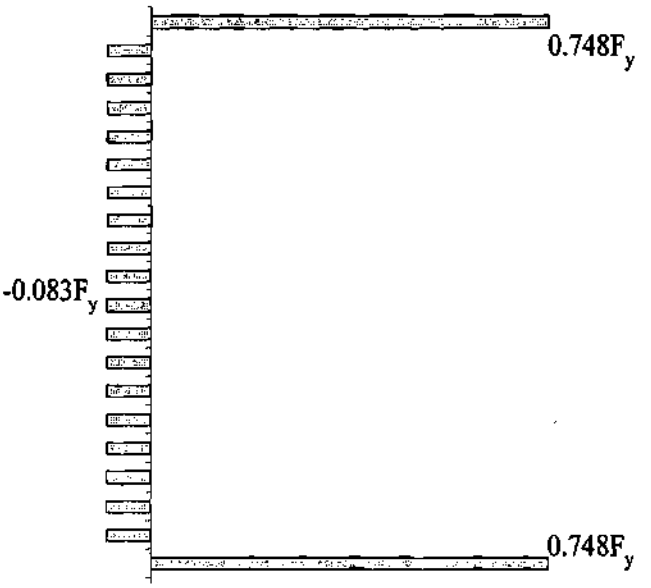

(b) Web

Figure E.4.11. Gauss point residual stresses for specimens with $D/b_f = 2.75$, $b_f/t_f = 25$ and $D/t_w = 130$.

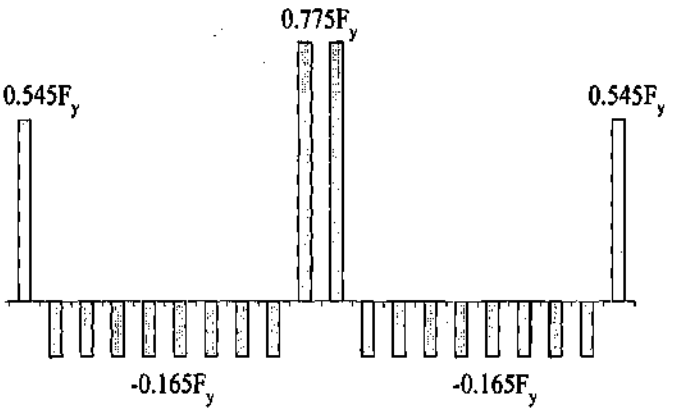

(a) Top and bottom flanges

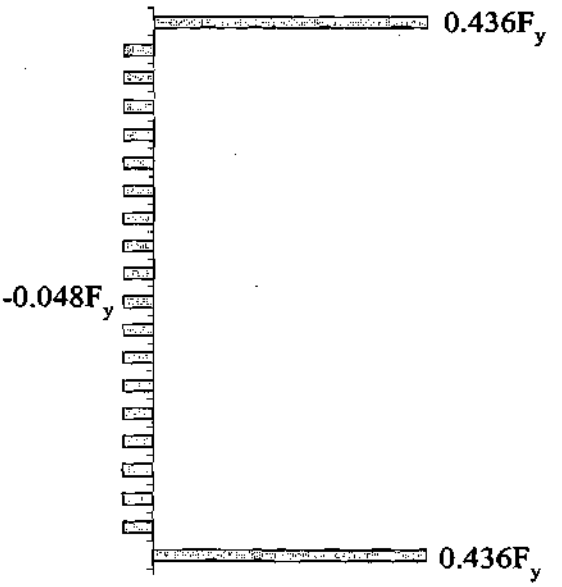

(b) Web

Figure E.4.12. Gauss point residual stresses for specimens with $D/b_f = 2.75$, $b_f/t_f = 25$ and $D/t_w = 160$.

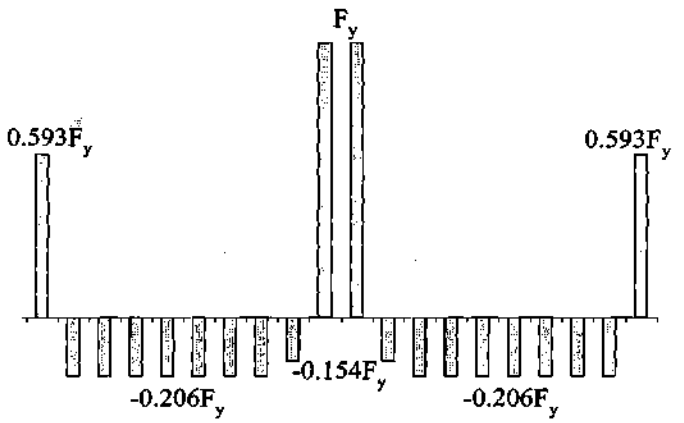

(a) Top and bottom flanges

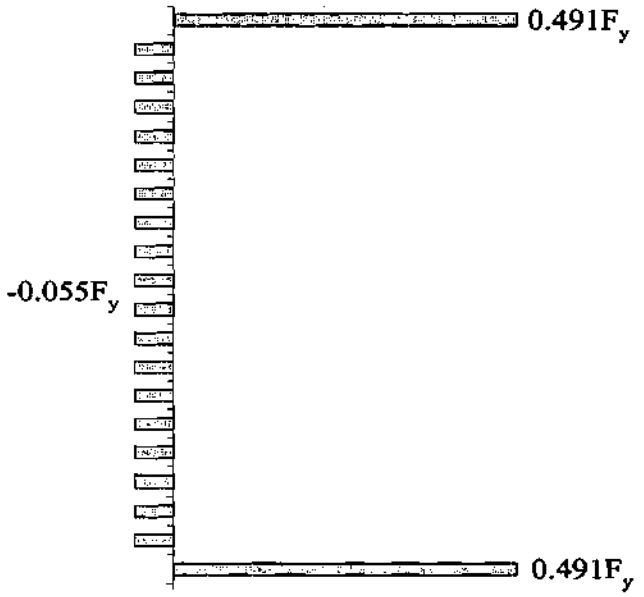

(b) Web

Figure E.4.13. Gauss point residual stresses for specimens with $D/b_f = 3.25$, $b_f/t_f = 25$ and $D/t_w = 160$.

Page missing from document.

APPENDIX F

CROSS-SECTION PLATE LENGTHS AND THICKNESSES OF PRIMARY PARAMETRIC STUDY GIRDERS

A summary of cross-section plate lengths and thicknesses of the parametric study girders within the primary test suite is presented in this appendix. The dimensions for the girders with $D/b_f = 2.25$ and $b_f/t_f = 25$ are presented in Fig. F1 and Table F1. This is followed by the data for the girders with $D/b_f = 2.75$ and $b_f/t_f = 15$ in Fig. F2 and Table F2, $D/b_f = 2.75$ and $b_f/t_f = 20$ in Fig. F3 and Table F3, $D/b_f = 2.75$ and $b_f/t_f = 25$ in Fig. F4 and Table F4, and $D/b_f = 3.25$ and $b_f/t_f = 25$ in Fig. F5 and Table F5.

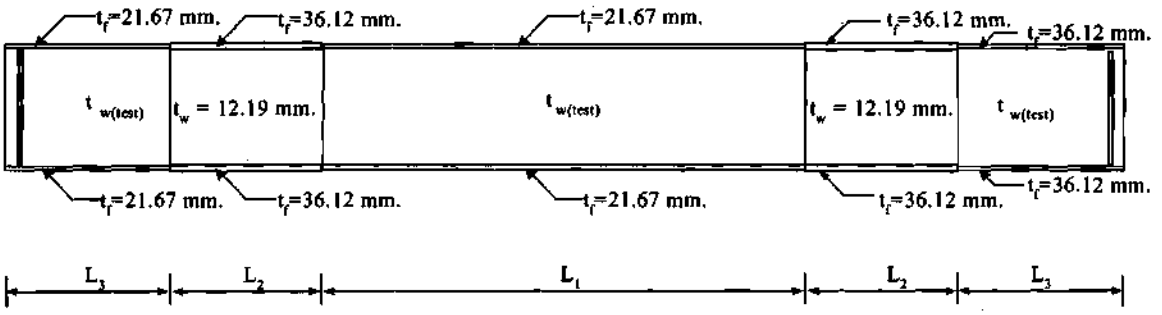

Figure F1. Cross-section plate lengths and thicknesses of the primary parametric-study girders with $D/b_f = 2.25$ and $b_f/t_f = 25$.

Table F1. Cross-section plate lengths and thickness for primary parametric-study girders with $D/b_f = 2.25$ and $b_f/t_f = 25$ (D = 1.22 m (48 in)).

L_b/R	Target f_t/f_b	D/t_w	$t_{w(test)}$ (mm)	L_1 (m)	L_2 (m)	L_3 (m)
0.05	0.35	100	12.19	7.32	2.74	3.05
		130	9.37	7.32	2.74	3.05
		160	7.62	7.32	2.74	3.05
	0.50	100	12.19	10.97	5.49	3.96
		130	9.37	10.97	5.49	3.96
		160	7.62	10.97	5.49	3.96
0.075	0.35	100	12.19	6.10	1.83	2.74
		130	9.37	6.10	1.83	2.74
		160	7.62	6.10	1.83	2.74
	0.50	100	12.19	7.32	3.05	2.74
		130	9.37	7.32	3.05	2.74
		160	7.62	7.32	3.05	2.74
0.10	0.35	100	12.19	4.88	1.83	1.52
		130	9.37	4.88	1.83	1.52
		160	7.62	4.88	1.83	1.52
	0.50	100	12.19	6.10	1.83	2.74
		130	9.37	6.10	1.83	2.74
		160	7.62	6.10	1.83	2.74

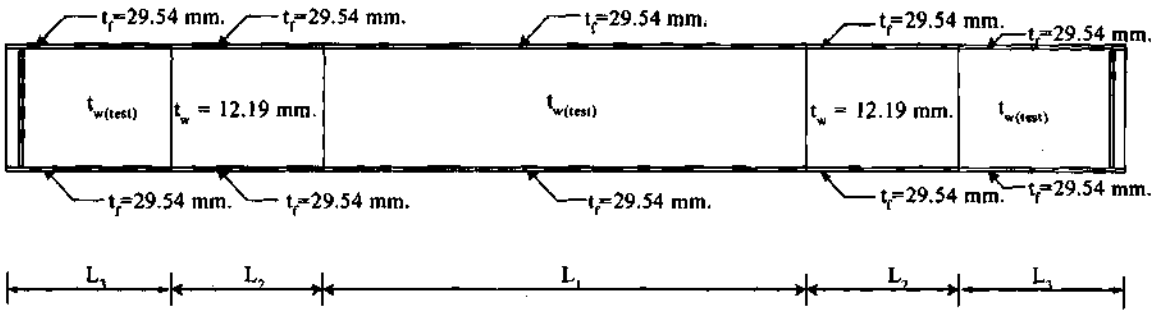

Figure F2. Cross-section plate lengths and thicknesses of the primary parametric-study girders with $D/b_f = 2.75$ and $b_f/t_f = 15$.

Table F2. Cross-section plate lengths and thickness for primary parametric-study girders with $D/b_f = 2.75$ and $b_f/t_f = 15$. (D = 1.22 m (48 in))

L_b/R	Target f_r/f_b	D/t_w	$t_{w(test)}$ (mm)	L_1 (m)	L_2 (m)	L_3 (m)
0.05	0.35	100	12.19	6.10	2.74	1.83
		130	9.37	6.10	2.74	1.83
		160	7.62	6.10	2.74	1.83
	0.50	100	12.19	8.53	4.27	2.74
		130	9.37	8.53	4.27	2.74
		160	7.62	8.53	4.27	2.74
0.075	0.35	100	12.19	4.88	1.83	1.52
		130	9.37	4.88	1.83	1.52
		160	7.62	4.88	1.83	1.52
	0.50	100	12.19	6.10	1.83	2.74
		130	9.37	6.10	1.83	2.74
		160	7.62	6.10	1.83	2.74
0.10	0.35	100	12.19	3.66	1.22	0.91
		130	9.37	3.66	1.22	0.91
		160	7.62	3.66	1.22	0.91
	0.50	100	12.19	4.88	1.83	1.52
		130	9.37	4.88	1.83	1.52
		160	7.62	4.88	1.83	1.52

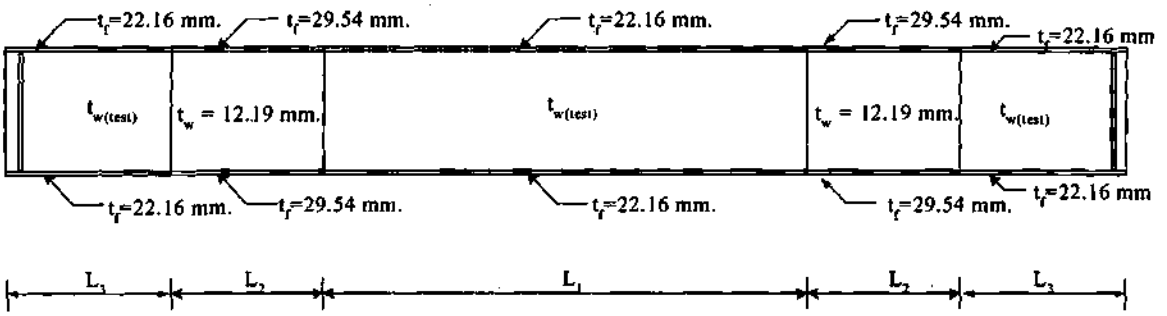

Figure F3. Cross-section plate lengths and thicknesses of the primary parametric-study girders with $D/b_f = 2.75$ and $b_f/t_f = 20$.

Table F3. Cross-section plate lengths and thickness for primary parametric-study girders with $D/b_f = 2.75$ and $b_f/t_f = 20$. (D = 1.22 m (48 in))

L_b/R	Target f_f/f_b	D/t_w	$t_{w(test)}$ (mm)	L_1 (m)	L_2 (m)	L_3 (m)
0.05	0.35	100	12.19	6.10	2.74	1.83
		130	9.37	6.10	2.74	1.83
		160	7.62	6.10	2.74	1.83
	0.50	100	12.19	8.53	4.27	2.74
		130	9.37	8.53	4.27	2.74
		160	7.62	8.53	4.27	2.74
0.075	0.35	100	12.19	4.88	1.83	1.52
		130	9.37	4.88	1.83	1.52
		160	7.62	4.88	1.83	1.52
	0.50	100	12.19	6.10	1.83	2.74
		130	9.37	6.10	1.83	2.74
		160	7.62	6.10	1.83	2.74
0.10	0.35	100	12.19	3.66	1.22	0.91
		130	9.37	3.66	1.22	0.91
		160	7.62	3.66	1.22	0.91
	0.50	100	12.19	4.88	1.83	1.52
		130	9.37	4.88	1.83	1.52
		160	7.62	4.88	1.83	1.52

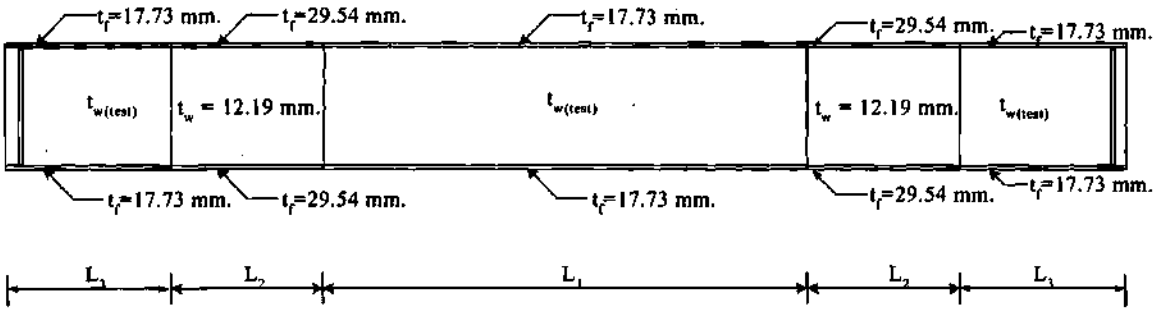

Figure F4. Cross-section plate lengths and thicknesses of the primary parametric-study girders with $D/b_f = 2.75$ and $b_f/t_f = 25$.

Table F4. Cross-section plate lengths and thickness for primary parametric-study girders with $D/b_f = 2.75$ and $b_f/t_f = 25$. (D = 1.22 m (48 in))

L_b/R	Target f_t/f_b	D/t_w	$t_{w(test)}$ (mm)	L_1 (m)	L_2 (m)	L_3 (m)
0.05	0.35	100	12.19	6.10	2.74	1.83
		130	9.37	6.10	2.74	1.83
		160	7.62	6.10	2.74	1.83
	0.50	100	12.19	8.53	4.27	2.74
		130	9.37	8.53	4.27	2.74
		160	7.62	8.53	4.27	2.74
0.075	0.35	100	12.19	4.88	1.83	1.52
		130	9.37	4.88	1.83	1.52
		160	7.62	4.88	1.83	1.52
	0.50	100	12.19	6.10	1.83	2.74
		130	9.37	6.10	1.83	2.74
		160	7.62	6.10	1.83	2.74
0.10	0.35	100	12.19	3.66	1.22	0.91
		130	9.37	3.66	1.22	0.91
		160	7.62	3.66	1.22	0.91
	0.50	100	12.19	4.88	1.83	1.52
		130	9.37	4.88	1.83	1.52
		160	7.62	4.88	1.83	1.52

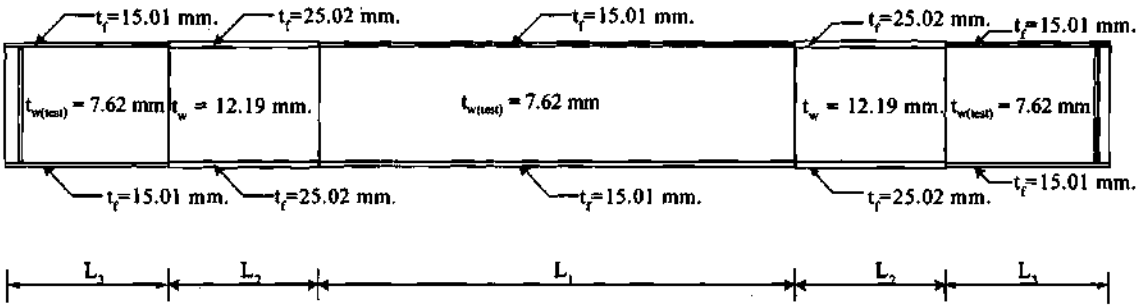

Figure F5. Cross-section plate lengths and thicknesses of the primary parametric-study girders with $D/b_f = 3.25$ and $b_f/t_f = 25$.

Table F5. Cross-section plate lengths and thickness for primary parametric-study girders with $D/b_f = 3.25$ and $b_f/t_f = 25$ (D = 1.22 m (48 in) and $t_{w(test)} = 7.62$ mm).

L_b/R	Target f_t/f_b	D/t_w	L_1 (m)	L_2 (m)	L_3 (m)
0.05	0.35	160	4.88	1.83	1.52
	0.50	160	7.32	3.05	2.74
0.075	0.35	160	4.27	1.83	0.61
	0.50	160	4.88	1.83	1.52
0.10	0.35	160	3.66	1.22	0.91
	0.50	160	4.88	1.83	1.52

APPENDIX G

STIFFENER DIMENSIONS

This appendix summarizes the dimensions of the bearing and transverse stiffeners utilized in the parametric study girders. Section G.1 summarizes the bearing stiffener dimensions whereas Section G.2 provides the dimensions of the transverse stiffeners. With the exception of the cases noted otherwise, all the transverse stiffeners in Section G.2 are sized based on the AISC LRFD (2001) straight-girder provisions. The design of the transverse stiffeners is discussed in Section 5.7.

G.1 BEARING STIFFENER DIMENSIONS

Table G.1.1. Bearing stiffener dimensions for primary parametric-study girders with $D/b_f = 2.25$ and $b_f/t_f = 25$.

Width b ($b = 0.40b_f$) (mm)	D/t_w	d_o/D	Thickness t (mm)					
			$L_b/R = 0.05$		$L_b/R = 0.075$		$L_b/R = 0.10$	
			target $f_t/f_b = 0.35$	target $f_t/f_b = 0.50$	target $f_t/f_b = 0.35$	target $f_t/f_b = 0.50$	target $f_t/f_b = 0.35$	target $f_t/f_b = 0.50$
217	100	3	22.23	16.51	22.23	22.23	22.23	22.23
	130	3	22.23	16.51	22.23	22.23	22.23	22.23
	160	1	22.23	16.51	22.23	22.23	22.23	22.23
		2	22.23	16.51	22.23	22.23	22.23	22.23
		3	22.23	16.51	22.23	22.23	22.23	22.23

Table G.1.2. Bearing stiffener dimensions for primary parametric-study girders with $D/b_f = 2.75$ and $b_f/t_f = 15$.

Width b ($b = 0.40b_f$) (mm)	D/t_w	d_o/D	Thickness t (mm)					
			$L_b/R = 0.05$		$L_b/R = 0.075$		$L_b/R = 0.10$	
			target $f_t/f_b = 0.35$	target $f_t/f_b = 0.50$	target $f_t/f_b = 0.35$	target $f_t/f_b = 0.50$	target $f_t/f_b = 0.35$	target $f_t/f_b = 0.50$
177	100	3[(1)]	25.40	19.05	25.40	25.40	34.93	25.40
	130	3[(1)]	25.40	19.05	25.40	25.40	34.93	25.40
	160	1	25.40	19.05	25.40	25.40	34.93	25.40
		2	25.40	19.05	25.40	25.40	34.93	25.40
		3	25.40	19.05	25.40	25.40	NA[(2)]	25.40

[(1)] $d_o/D = 2$ for $L_b/R = 0.10$ and target $f_t/f_b = 0.35$, since $L_b/D = 2$

[(2)] NA for target $L_b/R = 0.10$ and target $f_t/f_b = 0.35$, since $L_b/D = 2$

Table G.1.3. Bearing stiffener dimensions for primary parametric-study girders with $D/b_f = 2.75$ and $b_f/t_f = 20$.

Width b ($b = 0.40b_f$) (mm)	D/t_w	d_o/D	Thickness t (mm)					
			$L_b/R = 0.05$		$L_b/R = 0.075$		$L_b/R = 0.10$	
			target $f_\ell/f_b = 0.35$	target $f_\ell/f_b = 0.50$	target $f_\ell/f_b = 0.35$	target $f_\ell/f_b = 0.50$	target $f_\ell/f_b = 0.35$	target $f_\ell/f_b = 0.50$
177	100	3[1]	25.40	16.51	25.40	25.40	31.75	22.23
	130	3[1]	25.40	16.51	25.40	22.23	31.75	22.23
	160	1	25.40	16.51	25.40	22.23	31.75	22.23
		2	25.40	16.51	25.40	22.23	31.75	22.23
		3	25.40	16.51	25.40	22.23	NA[2]	22.23

[1] $d_o/D = 2$ for $L_b/R = 0.10$ and target $f_\ell/f_b = 0.35$, since $L_b/D = 2$

[2] NA for target $L_b/R = 0.10$ and target $f_\ell/f_b = 0.35$, since $L_b/D = 2$

Table G.1.4. Bearing stiffener dimensions for primary parametric-study girders with $D/b_f = 2.75$ and $b_f/t_f = 25$.

Width b ($b = 0.40b_f$) (mm)	D/t_w	d_o/D	Thickness t (mm)					
			$L_b/R = 0.05$		$L_b/R = 0.075$		$L_b/R = 0.10$	
			target $f_\ell/f_b = 0.35$	target $f_\ell/f_b = 0.50$	target $f_\ell/f_b = 0.35$	target $f_\ell/f_b = 0.50$	target $f_\ell/f_b = 0.35$	target $f_\ell/f_b = 0.50$
177	100	3[1]	25.40	15.24	25.40	22.23	22.23	22.23
	130	3[1]	25.40	15.24	25.40	22.23	22.23	22.23
	160	1	25.40	15.24	25.40	22.23	22.23	22.23
		2	25.40	15.24	25.40	22.23	22.23	22.23
		3	25.40	15.24	25.40	22.23	NA[2]	22.23

[1] $d_o/D = 2$ for $L_b/R = 0.10$ and target $f_\ell/f_b = 0.35$, since $L_b/D = 2$

[2] NA for target $L_b/R = 0.10$ and target $f_\ell/f_b = 0.35$, since $L_b/D = 2$

Table G.1.5. Bearing stiffener dimensions for primary parametric-study girders with $D/b_f = 3.25$ and $b_f/t_f = 25$.

Width b ($b = 0.40b_f$) (mm)	D/t_w	d_o/D	Thickness t (mm)					
			$L_b/R = 0.05$		$L_b/R = 0.075$		$L_b/R = 0.10$	
			target $f_\ell/f_b = 0.35$	target $f_\ell/f_b = 0.50$	target $f_\ell/f_b = 0.35$	target $f_\ell/f_b = 0.50$	target $f_\ell/f_b = 0.35$	target $f_\ell/f_b = 0.50$
150	160	1	22.23	16.51	22.23	22.23	22.23	22.23
		2	22.23	16.51	22.23	22.23	22.23	22.23
		3	22.23	16.51	NA[1]	22.23	NA[2]	22.23

[1] NA for target $L_b/R = 0.075$ and target $f_\ell/f_b = 0.35$, since $L_b/D = 2.5$

[2] NA for target $L_b/R = 0.10$ and target $f_\ell/f_b = 0.35$, since $L_b/D = 2$

G.2 TRANSVERSE STIFFENER DIMENSIONS

Table G.2.1. Transverse stiffener dimensions for primary parametric-study girders with $D/b_f = 2.25$ and $b_f/t_f = 25$.

Width b ($b = 0.30b_f$) (mm)	D/t_w	d_o/D	Thickness t (mm)					
			$L_b/R = 0.05$		$L_b/R = 0.075$		$L_b/R = 0.10$	
			target $f_t/f_b = 0.35$	target $f_t/f_b = 0.50$	target $f_t/f_b = 0.35$	target $f_t/f_b = 0.50$	target $f_t/f_b = 0.35$	target $f_t/f_b = 0.50$
163	100	3	15.24	15.24	15.24	15.24	NA[1]	15.24
	130	3	15.24	15.24	15.24	15.24	NA[1]	15.24
	160	1	15.24	15.24	15.24	15.24	16.51[2]	15.24
		2	15.24	15.24	15.24	15.24	16.51[2]	15.24
		3	15.24	15.24	15.24	15.24	NA[1]	15.24

[1] NA since $L_b/D = 3$
[2] Stiffener sized larger than the AASHTO LRFD minimum

Table G.2.2. Transverse stiffener dimensions for primary parametric-study girders with $D/b_f = 2.75$ and $b_f/t_f = 15$.

Width b ($b = 0.30b_f$) (mm)	D/t_w	d_o/D	Thickness t (mm)					
			$L_b/R = 0.05$		$L_b/R = 0.075$		$L_b/R = 0.10$	
			target $f_t/f_b = 0.35$	target $f_t/f_b = 0.50$	target $f_t/f_b = 0.35$	target $f_t/f_b = 0.50$	target $f_t/f_b = 0.35$	target $f_t/f_b = 0.50$
133	100	3	12.70	12.70	NA[1]	12.70	NA[2]	NA[1]
	130	3	12.70	12.70	NA[1]	16.51	NA[2]	NA[1]
	160	1	12.70	12.70	12.70	12.70	13.34[3]	13.97[3]
		2	12.70	12.70	12.70	12.70	NA[2]	13.97[3]
		3	16.51	16.51	NA[1]	17.78	NA[2]	NA[1]

[1] NA since $L_b/D = 3$
[2] NA since $L_b/D = 2$
[3] Stiffener sized larger than the AASHTO LRFD minimum

Table G.2.3. Transverse stiffener dimensions for primary parametric-study girders with $D/b_f = 2.75$ and $b_f/t_f = 20$.

Width b ($b = 0.30b_f$) (mm)	D/t_w	d_0/D	Thickness t (mm)					
			$L_b/R = 0.05$		$L_b/R = 0.075$		$L_b/R = 0.10$	
			target $f_t/f_b = 0.35$	target $f_t/f_b = 0.50$	target $f_t/f_b = 0.35$	target $f_t/f_b = 0.50$	target $f_t/f_b = 0.35$	target $f_t/f_b = 0.50$
133	100	3	12.70	12.70	NA[1]	12.70	NA[2]	NA[1]
	130	3	12.70	12.70	NA[1]	12.70	NA[2]	NA[1]
	160	1	12.70	12.70	12.70	12.70	13.34[3]	13.97[3]
		2	12.70	12.70	12.70	12.70	NA[2]	13.97[3]
		3	15.24	15.24	NA[1]	17.15	NA[2]	NA[1]

[1] NA since $L_b/D = 3$
[2] NA since $L_b/D = 2$
[3] Stiffener sized larger than the AASHTO LRFD minimum

Table G.2.4. Transverse stiffener dimensions for primary parametric-study girders with $D/b_f = 2.75$ and $b_f/t_f = 25$.

Width b ($b = 0.30b_f$) (mm)	D/t_w	d_0/D	Thickness t (mm)					
			$L_b/R = 0.05$		$L_b/R = 0.075$		$L_b/R = 0.10$	
			target $f_t/f_b = 0.35$	target $f_t/f_b = 0.50$	target $f_t/f_b = 0.35$	target $f_t/f_b = 0.50$	target $f_t/f_b = 0.35$	target $f_t/f_b = 0.50$
133	100	3	12.70	12.70	NA[1]	12.70	NA[2]	NA[1]
	130	3	12.70	12.70	NA[1]	12.70	NA[2]	NA[1]
	160	1	12.70	12.70	12.70	12.70	13.34[3]	13.97[3]
		2	12.70	12.70	12.70	12.70	NA[2]	13.97[3]
		3	15.24	15.24	NA[1]	17.15	NA[2]	NA[1]

[1] NA since $L_b/D = 3$
[2] NA since $L_b/D = 2$
[3] Stiffener sized larger than the AASHTO LRFD minimum

Table G.2.5. Transverse stiffener dimensions for primary parametric-study girders with $D/b_f = 3.25$ and $b_f/t_f = 25$.

Width b ($b = 0.30b_f$) (mm)	D/t_w	d_0/D	Thickness t (mm)					
			$L_b/R = 0.05$		$L_b/R = 0.075$		$L_b/R = 0.10$	
			target $f_t/f_b = 0.35$	target $f_t/f_b = 0.50$	target $f_t/f_b = 0.35$	target $f_t/f_b = 0.50$	target $f_t/f_b = 0.35$	target $f_t/f_b = 0.50$
113	160	1	12.70	12.70	12.70	12.70	12.70	12.70
		2	12.70	12.70	12.70	16.51	12.70	12.70
		3	NA[1]	16.51	NA[1]	NA[1]	NA[1]	NA[1]

[1] NA since $L_b/D \leq 3$

REFERENCES

AASHTO (1969). *Standard Specifications for Highway Bridges, 10th Edition*, American Association of State and Highway Transportation Officials, Washington D.C.

AASHTO (1993). *AASHTO Guide Specifications for Horizontally Curved Highway Bridges*, American Association of State and Highway Transportation Officials, Washington D.C.

AASHTO (2001). *AASHTO LRFD Bridge Design Specifications 2nd Edition with 1999, 2000 and 2001 Interims*, American Association of State and Highway Transportation Officials, Washington D.C.

AASHTO-AWS (1996). *Bridge Welding Code*, Joint Publication of American Associate of State Highway and Transportation Officials and American Welding Society, Inc. Washington, D.C.

AISC (1993). *Manual of Steel Construction, Load and Resistance Factor Design, Volume I – Structural Members, Specifications and Codes*, 2nd Ed., American Institute of Steel Constuction, Chicago, IL, 1280 pp.

AISC (1999). *Load and Resistance Factor Design Specification for Structural Steel Buildings*, American Institute of Steel Construction, Chicago, IL, 292 pp.

AISI (2000). Bridge Task Force Meeting Report, Sacramento, CA, August 9-10.

Ajam, W. and Marsh, C. (1991). "Simple Model for Shear Capacity of Webs," *Journal of Structural Engineering*, ASCE, 117(2), 410-422.

ASCE-WRC (1971). *Plastic Design in Steel: A Guide and Commentary (2nd Edition)*, Joint Committee of American Society of Civil Engineers and Welding Research Council ASCE Manual and Reports on Engineering Practice No. 41, New York, 336 pp.

ASCE Task Group on Effective Length (1997). *Effective Length and Notional Load Approaches for Assessing Frame Stability: Implications for American Steel Design*, Committee on Load and Resistance Factor Design, American Society of Civil Engineers, New York.

AWS (1996). *Bridge Welding Code*, ANSI/AASHTO/AWS D1.5-95, joint publication of American Association of State Highway and Transportation Officials and American Welding Society.

Abdel-Sayed, G. (1973). "Curved Webs Under Combined Shear and Normal Stresses," *Journal of the Structural Division*, ASCE, 99 (ST3), 511-525.

Aydemir, M. (2000). "Moment Shear Interaction in HPS Hybrid Plate Girder" M.S. thesis, School of Civil and Environmental Engineering, Georgia Institute of Technology, Atlanta, GA, 208 pp.

Barth, K.E. and White, D.W. (1997). "Finite Element Evaluation of Pier Moment-Rotation Characteristics in Continuous-Span Steel I Girders," *Engineering Structures*, 20(8), 761-777.

Barth, K.E., White, D.W., and Bobb, B. (2000). "Negative Bending Resistance of HPS 70 W Girders," *Journal of Constructional Steel Research*, 53(1), 1-31.

Basler, K., Yen, B.T., Mueller, J.A., and Thurlimann, B. (1960). "Web Buckling Tests on Welded Plate Girders," WRC Bulletin No. 64, Welding Research Council, New York, NY, 63 pp.

Basler, K. and Thurlimann, B. (1961). " Strength of Plate Girders in Bending," *Journal of Structural Division*, ASCE, 87(ST6), 153-181.

Basler, K. (1961b). " Strength of Plate Girders in Shear," *Journal of Structural Division*, ASCE, 87(ST7), 151-180.

Basler, K. (1961c). " Strength of Plate Girders Under Combined Bending and Shear," *Journal of Structural Division*, ASCE, 87(ST7), 181-197.

Basler, K. (1963). "Discussion of K. Basler 'Strength of Plate Girders in Shear,'" *Transaction ASCE*, 128(II), 712-719.

Bergmann, S. and Reissner, H (1932). "Uber die Knickung von, rechteckigen Platten bei Schubbeanspruchung," *Z. Flugtech Motorluftschiffahrt* Vol. 23, 6-

Bleich, F. (1952). *Buckling Strength of Metal Structures*, McGraw-Hill, New York, 508 pp.

Bradford, M.A. (1996). "Improved Shear Strength of Webs Designed in Accordance with the LRFD Specification," *Engineering Journal*, AISC, 33(3), 95-100.

Brockenbrough, R.L. and Johnston, B.G. (1968). *Steel Design Manual*, United States Steel Corporation, Pittsburgh, PA (Chapter 1).

Brockenbrough, R.L. (1970a). "Theoretical Stresses and Strains from Heat-Curving," *Journal of the Structural Division*, 96(ST 7), 1421-1444.

Brockenbrough, R.L. (1970b). "Criteria for Heat-Curving Steel Beams and Girders," *Journal of the Structural Division,* ASCE, 96(ST 10), 2209-2226.

Brockenbrough, R.L. and Ives, K.D. (1970). "Experimental Stresses and Strains from Heat Curving," *Journal of the Structural Division,* ASCE, 96(ST 7), 1305-1331.

CSA (1994). *Limit States Design of Steel Structures CAN/CSA-S16.1-94*, Canadian Standards Association, December.

Culver, C.G. (1969). "Instability of Horizontally Curved Members: Bending Behavior of Cylindrical Web Panels," *Research Report*, Department of Civil Engineering, Carnegie-Mellon University, November.

Culver, C.G. and Frampton, R.E. (1970). "Local Instability of Horizontally Curved Members," *Journal of the Structural Division*, ASCE, 96(ST 2), 245-265.

Culver, C.G. and Nasir, G. (1970). "Instability of Horizontally Curved Members: Buckling of Unstiffened Curved Plate," *Research Report,* Department of Civil Engineering, Carnegie-Mellon University, April.

Culver, C.G. and McManus, P.F. (1971). "Instability of Horizontally Curved Members: Lateral Buckling of Curved Plate Girders," *Research Report*, Department of Civil Engineering, Carnegie-Mellon University, September.

Culver, C.G. and Nasir, G. (1971). "Inelastic Flange Buckling of Curved Plate Girders," *Journal of the Structural Division*, ASCE, 97(4), 1239-1257.

Culver, C.G. (1972). "Design Recommendations for Curved Highway Bridges," *Project Report*, Carnegie-Mellon University, Report submitted to Pennsylvania Department of Transportation, June.

Culver, C.G., Dym, C. and Brogan, D. (1972a). "*Instability of Horizontally Curved Members-Bending Behavior of Cylindrical Web Panels,*" Carnegie-Mellon University, Report submitted to Pennsylvania Department of Transportation, January, 31 pp.

Culver, C.G., Dym, C. and Brogan, D. (1972b). "*Instability of Horizontally Curved Members-Shear Buckling of Cylindrical Web Panels,*" Carnegie-Mellon University, Report submitted to Pennsylvania Department of Transportation, June.

Culver, C.G., Dym, C. and Brogan, D. (1972c). "Bending Behavior of Cylindrical Web Panels," *Journal of the Structural Division*, ASCE, 98(ST 10), 2291-2308.

Culver, C.G., Dym, C.L. and Uddin, T. (1973). "Web Slenderness Requirements for Curved Girders," *Journal of the Structural Division*, ASCE, 99(ST3), 417-430.

CURT (1975). "Tentative Design Specifications for Horizontally Curved Highway Bridges, Part of Final Report, Research Project HPR2-(111), Horizontally Curved Highway Bridges, prepared for USDOT by CURT, March.

Daniels, J.H. and Herbein, W.C. (1980). "*Fatigue of Curved Steel Bridge Elements – Fatigue Tests of Curved Plate Girder Assemblies.*" Lehigh University, Bethlehem, PA, FHWA-RD-79-132 (1980), 91 pp.

Daniels, J.H., Fisher, J.W. and Yen, B.T. (1980). "Fatigue of Curved Steel Bridge Elements, Design Recommendations for Fatigue of Curved Plate Girder and Box Girder Bridges." Report No. FHWA-RD-79-138, Federal Highway Administration, Washington, D.C., 54 pp.

Davidson, J.S. (1996). "Nominal Bending and Shear Strength of Curved Steel I-Girder Bridge Systems," Ph.D. dissertation, Auburn University, Auburn, AL.

Davidson, J.S., Keller, M.A. and Yoo, C.H. (1996). "Cross-Frame Spacing and Parametric Effects in Horizontally Curved I-Girder Bridges," *Journal of Structural Engineering*, ASCE, 122(9), 1089-1096.

Davidson, J.S. and Yoo, C.H. (1996). "Local Buckling of Curved I-Girder Flanges," *Journal of Structural Engineering*, ASCE, 122(8), 936-947.

Davidson, J.S. and Yoo, C.H. (1999a). "Analytical Model of Curved I-Girder Web Panels Subjected to Bending," *Journal of Bridge Engineering*, ASCE, 4(3), 204-212.

Davidson, J.S. and Yoo, C.H. (1999b). "Finite Displacement Behavior of Curved I-Girder Webs Subjected to Bending," *Journal of Bridge Engineering*, ASCE, 4(3), 213-220.

Davidson, J.S. and Yoo, C.H. (2000a). "Behavior of Curved I-Girder Webs Subjected to Combined Bending and Shear," *Journal of Bridge Engineering*, ASCE, 5(2), 165-170.

Davidson, J.S. and Yoo, C.H. (2000b). "Effects of Longitudinal Stiffeners on Curved I-Girder Webs," *Journal of Bridge Engineering*, ASCE, 5(2), 171-178.

Davidson, J.S. and Yoo, C.H. (2000c). "Evaluation of Strength Formulations for Horizontally Curved Flexural Members," *Journal of Bridge Engineering*, ASCE, 5(3), 200-207.

Duwadi, S.R., Yadlosky, J.M. and Yoo, C.H. (1994). "Horizontally Curved Steel Bridge Research-Update," *Proceedings, Structures Congress XII*, ASCE, 1071-1076.

ECCS-Committee 8-Stability (1976). "*Manual on Stability of Steel Structures 2nd Edition,*" European Convention for Constructional Steelwork, Publication No. 22, 328 pp.

Fiechtl, A.L., Fenves, G.L. and Frank, K.H. (1987). "Approximate Analysis of Horizontally Curved Girder Bridges," *Research Report 360-2F*, Center for Transportation Research, University of Texas at Austin, November 1997, 80 pp.

Fisher, J. W., Yen, B.T. and Frank, K.H. (1979). "Minimizing Fatigue and Fracture in Steel Bridges," *Structural Integrity Technology,* 1979 ASME Conference, New York, 155-161.

Fujii, T. (1968b). "On an Improved Theory for Dr. Basler's Theory," IABSE 8th Congress, Final Report, New York.

Fukumoto, Y. and Nishida, S. (1981). "Ultimate Load Behavior of Curved I-Beams," *Journal of Engineering Mechanics Division,* ASCE, 107(EM2), 367-385.

Galambos, T.V., Frank, K. H. and McGogney, C.H. (1977). "Effect of Yielding on the Fatigue Strength of Steel Beams," *Public Roads,* 41(1), 10-17.

Galambos, T.V. (1978). "Tentative Load Factor Design Criteria for Curved Steel Bridges," *Research Report No. 50,* School of Engineering and Applied Science, Civil Engineering Department, Washington University, St. Louis, MO, May.

Galambos, T.V., Hajjar, J. F., Huang, W.H., Pulver, B. E. Leon, R. T. and Rudie, B. J. (2000). "Comparison of Measured and Computed Stresses in a Steel Curved Girder Bridge," Journal of Bridge Engineering, ASCE, 5(3), 191-199.

Gaylord, E.H. (1963). "Discussion of K. Basler 'Strength of Plate Girders in Shear,'" *Transaction ASCE*, 128(II), 712-719.

Grubb, M.A., Yadlosky, J.M., Herrmann, A.W. (1993). "Behavior of Horizontally Curved Steel Highway Bridges," *Structural Engineering in Natural Hazards Mitigation 1993,* ASCE, NY, 858-863.

Grubb, M.A. and Hall, D.H. (2001). "Chapter 2 -- Philosophy and Design of the I-Girder Bending Component Tests," *Volume II -- I-Girder Bending Component Tests*, FHWA Curved Steel Bridge Research Project, (in preparation).

Grubb, M.A. and Ibrahim, F.S. (2001). "Item #1: Proposed Replacement of Article C.2.3 in Appendix C of the AASHTO Manual for Condition Evaluation of Bridges," *Presentation to the February 2001 Meeting of the AASHTO T14 Technical Committee for Steel Design*, Sacramento, CA, 10 pp.

Hajjar, J.F., Galambos, T.V., Huang, W.H., Pulver, B.E. Leon, R.T. Rudie, B. J. (1999). "Measured vs. Computed Stresses in a Curved Steel Bridge," *Proceedings, Structures Congress XVII*, ASCE, 231-234.

Hall, D.H. (1994). "Curved Girders are Special," *Link Between Research and Practice*, Structural Stability Research Council, Bethlehem, P.A., 101-117.

Hall, D.H. and Yoo, C.H. (1995). *A Unified Approach for Designing and Constructing Horizontally Curved Girder Bridges Proposed AASHTO Specification (Highlights of Major Changes)*, Prepared for National Cooperative Highway Research Program, Transportation Research Board, National Research Council, April, 16 pp.

Hall, D.H. and Yoo, C.H. (1998). *Recommended Specifications for Steel Curved-Girder Bridge*, Prepared for National Cooperative Highway Research Program, Transportation Research Board, National Research Council, July 1998, 103 pp.

Hall, D.H., Grubb, M.A. and Yoo, C.H. (1999). "Improved Design Specifications for Horizontally Curved Steel Girder Highway Bridges," *NCHRP Report 424*, NCHRP, Washington, D.C.

Hall, D.H. (2000a). *Personal Communication.*

Hall, D.H. (2000b). The Effect of Material Properties on the Stability of Steel Girder Bridges, *Proceedings, Annual Technical Session*, Structural Stability Research Council.

Hall, D.H. (2001). *Personal Communication.*

Hanshin Highway Public Corporation (1988). *Guidelines for the Design of Horizontally Curved Girder Bridges (Draft)*, Steel Structures Committee, October, 179 pp.

Hartmann, J. (2000). *Personal Communication.*

Hartmann, J. and Wright, W. (2001). "An Experimental Investigation of the Bending Strength of Horizontally Curved Steel I-Girders," *To be published*

HKS (1998a). *ABAQUS/Standard Version 5.8-14*, Hibbitt, Karlsson & Sorensen, Inc., Pawtucket, RI.

HKS (1998b). *Getting Started with ABAQUS/Standard*, Hibbitt, Karlsson & Sorensen, Inc., Pawtucket, RI.

HKS (1998c). *ABAQUS/Standard User's Manual Volume II version 5.8*, Hibbitt, Karlsson & Sorensen, Inc., Pawtucket, RI.

Huang, W.H. (1996). "Curved I-Girder Systems," Ph.D. Dissertation, Department of Civil Engineering, University of Minnesota, Minneapolis, MN.

Johnson, D.L. (1985). "An Investigation into the Interaction of Flanges and Webs in Wide Flange Shapes," *Proceedings, Annual Technical Session*, Structural Stability Research Council, 395-405.

Kang, Y.J., Yoo, C.H. (1994a). "Thin-Walled Curved Beams I: Formulation of Nonlinear Equations," *Journal of Engineering Mechanics*, ASCE, 120(10), 2072-2101.

Kang, Y.J., Yoo, C.H. (1994b). "Thin-Walled Curved Beams II: Analytical Solutions for Buckling of Arches," *Journal of Engineering Mechanics*, 120(10), 2102-2125.

Kitipornchai, S. and Trahair, N.S. (1980). "Buckling Properties of Monosymmetric I-Beams," *Journal of Structural Division*, ASCE, 98(5), 941-957.

Kitada, T., Nakai, H. and Murayama, Y. (1993). "State-of-the-Art on Research, Design, and Construction of Horizontally Curved Bridges in Japan," *Proceeding, Annual Technical Session*, Structural Stability Research Council, Milwaukee, WI.

Lay, M.G. and Galambos, T.V. (1967). "Inelastic Beams Under Moment Gradient," *Journal of the Structural Division*, ASCE, 93(1), 381-399.

Lee, S.C., Davidson, J.S. and Yoo, C.H. (1996). "Shear Buckling Coefficients of Plate Girder Web Panels," *Computers & Structures*, 59(5), 789-795.

Lee, S.C. and Yoo, C.H. (1998). "Strength of Plate Girder Web Panels Under Pure Shear," *Journal of Structural Engineering*, ASCE, 124(2), 184-194.

Lee, S.C. and Yoo, C.H. (1999a). "Experimental Study on Ultimate Shear Strength of Web panels," *Journal of Structural Engineering*, ASCE, 125(8), 838-846.

Lee, S.C. and Yoo, C.H. (1999b). "Strength of Curved I-Girder Web Panels under Pure Shear," *Journal of Structural Engineering*, ASCE, 125(8), 847-853.

Linzell, D.G. (1999). "Studies of a Full-Scale Horizontally Curved Steel I-Girder Bridge System Under Self-Weight," Ph.D. thesis, School of Civil and Environmental Engineering, Georgia Institute of Technology, Atlanta, GA, 709 pp.

Linzell, D.G., Zureick, A.H. and Leon, R.T. (1999). "FHWA Experimental Studies of Curved Steel Bridge Behavior during Construction," *Proceedings, Structures Congress XVII*, ASCE, NY, 239-

Lukey, A.F. and Adams, P.F. (1969). "Rotation Capacity of Beams Under Moment Gradient," *Journal of Structural Division*, ASCE, 95(ST6).

Mariani, N, Mozer, J.D., Dym, C.L. and Culver, C.G. (1973). "Transverse Stiffener Requirements for Curved Webs," *Journal of Structural Division*, ASCE, 99(ST4), 757-771.

Marsh, C. and Ajam, W. (1987). "Post-Buckling Strength of Shear Webs without Diagonal Tension," unpublished paper, 10 pp.

Marsh, C., Ajam, W. and Ha, H.-K. (1988). "Finite Element Analysis of Postbuckled Shear Webs," *Journal of Structural Engineering*, 114(7), 1571-1587.

McManus, P.F. (1971). "Lateral Buckling of Curved Plate Girders," Ph.D. dissertation, Carnegie-Mellon University, Pittsburgh, PA, 189 pp.

Montgomery, S.L. (1987). "Fatigue And Ultimate Strength of A Transversely Stiffened Plate Girder" M.S. thesis, University of Texas at Austin, Austin, TX, 1987.

Mozer, J. and Culver, C.G. (1970). " Horizontally Curved Highway Bridges: Stability of Curved Plate Girders," *Report No. P1,* Prepared for U.S. Department of Transportation, Federal Highway Administration, August, 95 pp.

Mozer, J., Ohlson, R. and Culver, C.G. (1971). " Horizontally Curved Highway Bridges: Stability of Curved Plate Girders," *Report No. P2*, Prepared for U.S. Department of Transportation, Federal Highway Administration, September, 121 pp.

Mozer, J., Cook, J. and Culver, C.G. (1973). " Horizontally Curved Highway Bridges: Stability of Curved Plate Girders," *Report No. P3*, Prepared for U.S. Department of Transportation, Federal Highway Administration, January, 111 pp.

Nakai, H., Kitada, T. and Ohminami, R. (1984a). "Experimental Study on Ultimate Strength of Web Panels in Horizontally Curved Girder Bridges Subjected to Bending, Shear, and their Combinations," *Proceeding, Annual Technical Session Meeting*, Structural Stability Research Council, San Francisco, CA, 91-102.

Nakai, H., Kitada, T., Ohminami, R. and Fukumoto, K. (1984b). "A Proposition for Designing Transverse Stiffeners of Horizontally Curved Girders in Ultimate State," *Memoirs of the Faculty of Engineering*, Osaka University, Japan, Vol. 25, December, 111-131.

Nakai, H. and Yoo, C.H. (1988). *Analysis and Design of Curved Steel Bridges*, McGraw-Hill, NY, 673 pp.

Nowak, A.S., Nassif, H. and Frank, K.H. (1993). "Fatigue Load Spectra for a Steel Girder Bridge," *Transportation Research Record* No. 1393, 154-161.

Patterson, P.J., Corrado, J.A., Huang, J.S. and Yen, B.T. (1970). "Fatigue and Static Tests of Two Welded Plate Girders," *Welding Research Council Bulletin No. 155*, October.

Poellot, W.N. (1987). "Computer-Aided Design of Horizontally Curved Girders by the V-Load Method," *Engineering Journal*, AISC, 24(1), 42-50.

Phoawanich, N., White, D.W. and Zureick, A.H. (1999a). "Evaluation of Shear Test Specimens," Internal Project Report, Curved Steel Bridge Research Project, FHWA, July, 25 pp.

Phoawanich, N., White, D.W. and Zureick, A.H. (1999b). "Evaluation of Moment-Shear Test Specimens," Internal Project Report, Curved Steel Bridge Research Project, FHWA, July, 43 pp.

Phoawanich, N., White, D.W. and Zureick, A.H. (1999c). "Evaluation of Residual Stress Effects on Strengths of Test Specimens," Internal Project Report, Curved Steel Bridge Research Project, FHWA, July, 28 pp.

Porter, D.M., Rockey, K.C. and Evans, H.R. (1975). " The Ultimate Load Behavior of Plate Girders Loaded in Shear," *The Structural Engineer*, 53(8), 313-325.

Rudie, B.J. (1997). "A Study of the Deflections of Curved Steel Girder Bridge," M.S. thesis, Department of Civil Engineering, University of Minnesota, Minnepolis, MN.

Salmon C.G. and Johnson, J.E. (1996). *Steel Structures: Design and Behavior 4th Edition.* New York: HarperCollins College Publishers 1996, 1024 pp.

Seydel, E. (1933). "Uber das Ausbeulen von rechteckigen isotropen oder orthogonalanisotropen Platten bei Schubbeanspruchung," *Ing. Arch*, Vol. 4, 169-

Schilling, C.G. (1996). "Yield-Interaction Relationships for Curved I-Girders," *Journal of Bridge Engineering*, ASCE, 1(1), 26-33.

Selberg, A. (1973). "On the Shear Capacity of Girder Webs," University Trondheim Report.

Shanmugam, N.E., Thevendran, V, Liew, J.Y.R. and Tan, L.O. (1995). "Experimental Study on Steel Beams Curved in Plan," *Journal of Structural Engineering*, ASCE, 121(2), 249-259.

Simpson, M.D. and Birkemoe, P.C. (1997a). "Nonlinear Finite Element Modeling of Curved Girder Experiments," *Proceedings*, Annual Conference, Canadian Society of Civil Engineering, 319-328.

Simpson, M.D. and Birkemoe, P.C. (1997b). "Nonlinear Finite Element Modeling of Curved Girders: An Ultimate Strength Investigation," *Proceedings, Annual Technical Session*, Structural Stability Research Council, 325-337.

Simpson, M.D. (2000). "Analytical Investigation of Curved Steel Girder Behavior," Ph.D. Dissertation, University of Toronto, Toronto, Canada, 361 pp.

SSRC Task Group 14 (1991). "A Look to the Future," *Report of Workshop on Horizontally Curved Girders*, Structural Stability Research Council, 18 pp.

SSRC (1998). *Guide to Stability Design Criteria for Metal Structures 5th Edition*. Structural Stability Research Council, T.V. Galambos (ed.), McGraw-Hill, New York, 910 pp.

Thevendran, V., Shanmugam, N.E. and Liew, J.Y.R. (1997). "Experimental Techniques to Study the Ultimate Load Behavior of Beams Curved in Plan," *Proceedings of SPIE - The International Society for Optical Engineering*, Vol. 2921, 376-381.

Thevendran, V., Shanmugam, N.E., Chen, S. and Liew, J.Y.R. (1998). "Flexural Torsional Behaviour of Steel I-Beams Curved in Plan," *Journal of Constructional Steel Research*, 46(1-3), 79-80.

Thevendran, V., Chen, S., Shanmugam, N.E. and Liew, J.Y.R. (1999). "Nonlinear analysis of steel-concrete composite beams curved in plan," *Finite Element in Analysis and Design*, 32(3), 125-139.

Thevendran, V., Shanmugam, N.E., Chen, S. and Liew, J.Y.R. (2000). "Experimental Study on Steel-Concrete Composite Beams Curved in Plan," *Engineering Structures*, Vol. 22, No. 8, 877-889.

Timoshenko, S.P. (1910). "Einge Stabilitatsprobleme der Elastizitatstheorie," *Z. Math Phys.*, Vol. 58, 337.

Wasserman, E.P. (2000). "Study of Erection Issues and Composite System Behavior of the Full Scale Curved Girder Bridge Currently Under Test at the Turner-Fairbank Highway Research Center," *Federal Highway Administration Pooled Fund Proposal*, August 2000, 7 pp.

Yoo, C.H., Hall, D.H. and Schilling, C.G. (1993). "Improved Design Specifications for Horizontally Curved Steel Girder Highway Bridges", *NCHRP Interim Report on Project 12-38*, August.

Yoo, C.H., Hall, D.H. and Sabol, S.A. (1995). "Improved Design Specifications for Horizontally Curved Steel Girder Highway Bridges," *Proceedings of Structures Congress XIII*, ASCE, N.Y., 1699-1702

Yoo, C.H. (1996). "Ultimate Bending Strength Equations for Horizontally Curved I-Girders," Task D - Curved Steel Bridge Research Project, *Interim Report to FHWA (DTFH 61-92-C-00136)*, August.

Yoo, C.H., Kang, Y.J. and Davidson, J.S. (1996). "Buckling Analysis of Curved Beams by Finite Element Discretization," *Journal of Engineering Mechanics*, ASCE, 122(8), 760-770.

Yoo, C.H. and Davidson, J.S. (1997). "Yield Interaction Equations for Nominal Bending Strength of Curved I-Girders," *Journal of Bridge Engineering*, ASCE, 2(2), 37-44.

Yoo, C.H. (2000). *Personal Communication.*

Yura, J.A. (1988). "Elements for Teaching Load and Resistance Factor Design, Combined Bending and Axial Load," AISC, Chicago, IL 1988.

Zureick, A.H., Naqib, R. and Yadlosky, J.M. (1993). "Curved Steel Bridge Research Project: Interim Report I, Synthesis," *Publication No. FHWA-RD-93-129*, Federal Highway Administration, Washington, D.C., 103 pp.

Zureick, A.H. and Shih, B. (1995). "Local Buckling of Fiber-Reinforced Polymeric Structural Members under Linearly-Varying Edge Loading," *Publication No. FHWA-RD-*, May, 106 pp.

Zureick, A.H. and Shih, B. (1998). "Local Buckling of Fiber-Reinforced Polymeric Structural Members under Linearly-Varying Edge Loading-Part 1. Theoretical Formulation," *Composite Structures*, 41(1998), 79-86.

Zureick, A.H. and Naqib, R. (1999). "Horizontally Curved Steel I-Girders State-of-the-Art Analysis Methods," *Journal of Bridge Engineering*, ASCE, 4(1), 38-47.

Zureick, A., Linzell, D. Leon, R.T. and Burrell, J. (2000). "Curved Steel I-Girder Bridges: Experimental and Analytical Studies," *Engineering Structures*, 22(2), 180-190.

Zureick, A.H. and Kim, Y.S. (2000). "Synthesis on Bending Test Components of Curved Steel Bridge Research Project," *Unpublished Report.*

Zureick, A.H., White, D.W., Park, J.Y. and Phoawanich, N. (2001). "Shear Strength of Curved Bridge I Girders, Experimental Tests," Project Report, Curved Steel Bridge Research Project, FHWA, (in preparation).